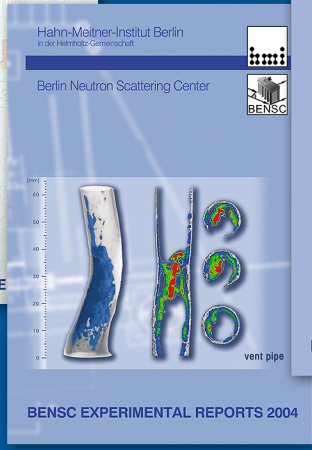
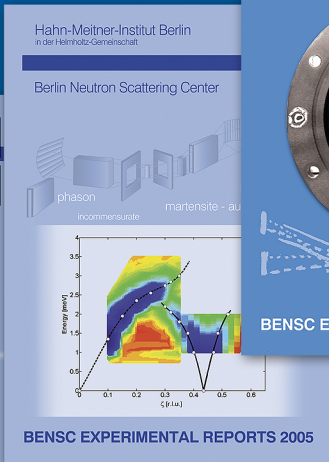
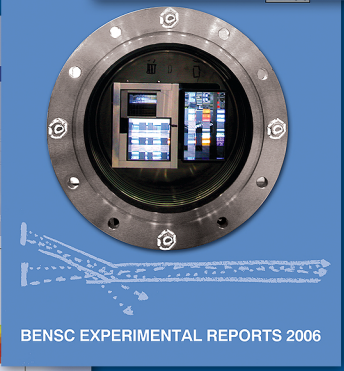
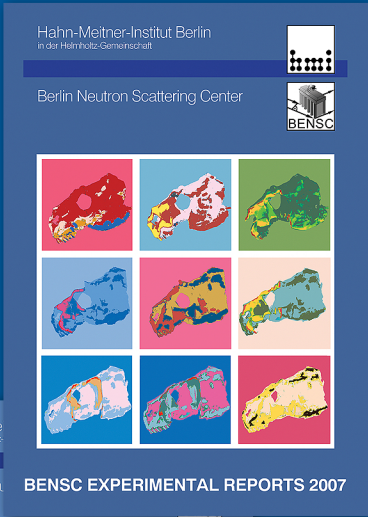




16 years BENS  
1993 - 2008



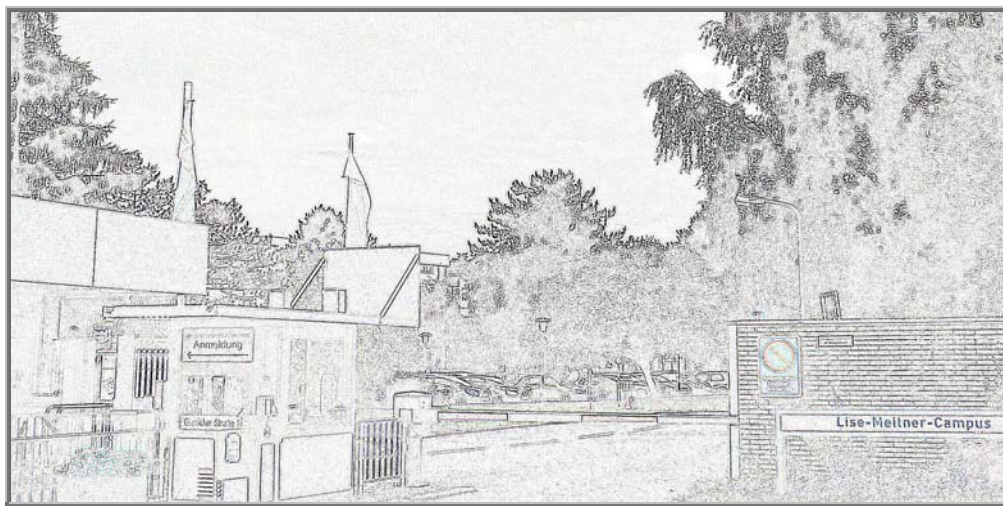
# HELMHOLTZ ZENTRUM BERLIN für Materialien und Energie



# BENSC

## EXPERIMENTAL REPORTS

### 2008



Entrance to the Lise-Meitner-Campus

edited by

A. Rödiger, A. Brandt  
and H.A. Graf

Berlin Neutron Scattering Center  
Helmholtz-Zentrum Berlin für Materialien und Energie GmbH  
(formerly Hahn-Meitner-Institut)  
in der Helmholtz Gemeinschaft

July 2009

---

Berichte des Helmholtz-Zentrums Berlin

**HMI – B 622**

ISSN 0936 - 0891

Picture on front cover:

Retrospective of all the covers used for the BENSCH Experimental Reports since 1993.

In November 1992, a Scientific Panel allocated for the first time neutron beam time for external users at the Berlin research reactor BER II of Hahn-Meitner Institute GmbH (HMI). The newly founded Berlin Neutron Scattering Center BENSCH took over the responsibility to organize the user service at BER II and to overlook the maintenance and improvement of the increasing number of neutron instruments. Since the start of the user service in 1993, the annual BENSCH Experimental Report has been published to give an overview on the experimental work that had been done during the respective year. In July 2008, HMI changed its name to Helmholtz-Zentrum für Materialien und Energie (HZB). This was the first step towards the upcoming merger with another large scale research facility located in Berlin: BESSY.

With 1 January 2009, the former Hahn-Meitner Institute GmbH (HMI) has finally merged with the Berliner Elektronenspeicherring-Gesellschaft für Synchrotronstrahlung m.b.H. (BESSY) to form the new Helmholtz Zentrum für Materialien und Energie (HZB).

HZB is now operating the neutron source BER II at the Lise-Meitner-Campus in Berlin Wannsee and the 3<sup>rd</sup> generation synchrotron source BESSY II at the Wilhelm-Conrad-Röntgen-Campus in Berlin Adlershof. The HZB User Service – with its two outposts in Wannsee (neutrons) and Adlershof (photons) – is ready to help scientists from all over the world with their beam time applications and everything connected with the resulting experiments.

Picture on back cover:

Retrospective of all the covers used for the BENSCH Experimental Reports since 1993, including the one for 2008.

The cover was designed by *screenworks*, Leibnizstraße 59, 10629 Berlin, [www.screenworks.de](http://www.screenworks.de)

---

**Editorial:**

The *Berlin Neutron Scattering Center* (BENSCH) was a department of the former *Hahn-Meitner-Institut Berlin GmbH*, now *Helmholtz-Zentrum Berlin für Materialien und Energie GmbH*. BENSCH was developing and running the Neutron Scattering Instruments at the Berlin Research Reactor BER II and was responsible for the service to external users.

The *Helmholtz-Zentrum Berlin für Materialien und Energie GmbH* is a member of the Helmholtz Association of German Research Centres and is financed by the Federal Republic of Germany and the City State of Berlin.

**Address:**

HZB User Coordination - Neutrons  
Helmholtz-Zentrum Berlin  
für Materialien und Energie GmbH  
Lise-Meitner-Campus  
Glienicke Strasse 100  
D – 14109 Berlin

Phone: +49-30-8062 2778, - 2169, -2304, -3153

FAX: +49-30-8062 2523

Email: [neutrons@helmholtz-berlin.de](mailto:neutrons@helmholtz-berlin.de)

Net: <http://www.helmholtz-berlin.de/userservice/neutrons>

## CONTENTS

Introduction	IV
List of BENSFC Instruments	VII
How to apply for BENSFC Beam Time	XI
Acknowledgement for Support by the European Commission	XIII
List of Contributed Reports	XVI

### Part I: EXPERIMENTAL REPORTS 2008

<b>Development of Instruments and Methods</b>	<b>1</b>
<b>Magnetism</b>	<b>31</b>
Magnetic Structures and Phase Transitions	
Magnetic Excitations	
Magnetic Thin Films	
<b>Structure</b>	<b>109</b>
Chemical Structure	
Structural Excitation	
Geology	
<b>Biology &amp; Soft Matter</b>	<b>145</b>
Biology	
Soft Matter	
<b>Material Science</b>	<b>201</b>
Structure and Phases	
Strain and Stress	
<b>Cultural Heritage</b>	<b>249</b>
<b>Fundamental Physics and Others</b>	<b>257</b>

### Part II: LIST OF BENSFC PUBLICATIONS

Theses	265
Publications 2008	266
Conference Contributions	284
Seminar Talks	290
Posters	299

<b>AUTHOR INDEX</b>	<b>309</b>
---------------------	------------

## Introduction

The present volume of the BENSCH Experimental Reports is the last one published in a format familiar to our users since 1993 when the first of these annual reports was issued. End of 2008 two of Berlin's largest research centres, the Helmholtz-Zentrum Berlin (former Hahn-Meitner-Institut) and the Berlin synchrotron radiation source BESSY, have merged to form the new Helmholtz-Zentrum Berlin für Materialien und Energie (HZB). With this merger, a new era dawns in the user facilities of the joint institute. HZB is now one of the few centres worldwide that are able to offer the whole range of instruments for neutron and synchrotron radiation experiments in one laboratory structure. Promoting the synergistic use of neutron and synchrotron radiation will be a major focus of the new institute. A common user entry point, a unified proposal procedure and one common Scientific Selection Panel for both facilities will be established to facilitate joint experiments with both probes.

The present report gives an overview on the research with neutrons carried out at BENSCH in 2008. The reactor BER-II delivered neutrons for experiments on 224 days. Fourteen instruments were fully scheduled for external user operation, one instrument was only partly on schedule. The experiments performed at BENSCH are described by 241 reports, 172 from external users and 69 from BENSCH scientists.

### BENSCH User Service

BENSCH is open to the national and international scientific community. About 70% of the available beam time at the scheduled instruments are given to external users, 30% to in-house researchers. A fraction of the beam time for external users (up to 20% of the total beam time of an instrument) can be assigned to long-term collaborating groups from German universities and other national and international research institutions, the rest (at least 50% of the total beam time) is allocated to short term projects via a peer-review selection process.

BENSCH has an outstanding tradition in providing sample environment for extreme conditions. A special emphasis is put on high magnetic fields and low and ultra low temperatures. Sample environment for high pressures up to 10 kbar and high temperatures is equally available.

More recently, a further focus in sample environment was put on the development of equipment for neutron scattering experiments under controlled gas pressure to serve a growing user community from the fields of material science and soft condensed matter. This new "Dedicated Environment for Combined Gas Adsorption and Scattering Experiments" (DEGAS) includes

humidity chambers for investigating biological samples as well as equipment for in-situ adsorption experiments on e.g. metal-organic framework systems.

A detailed technical handbook describing the existent equipment has been published by the BENSCH sample environment group. It is continuously updated. This handbook as well as a detailed description of the neutron instruments is available on the internet under:

<http://www.helmholtz-berlin.de/userservice>

### Scientific Selection Panel

The beam-time allocation for the short-term projects is decided by the Scientific Selection Panel of BENSCH, which meets twice a year, in May and in November. In 2008 the Selection panel consisted of the following ten external and two in-house members:

#### External members:

**Dr. G. Auffermann**

MPI CPfS Dresden, Germany

**Dr. K. Clausen**

Paul-Scherrer-Institute, Switzerland

**Prof. Dr. R. von Klitzing**

TU Berlin, Germany

**Prof. Dr. K. McEwen**

University College of London, U.K.

**Dr. H. Mutka**

ILL, France

**Dr. Th. Steriotis**

NCSR Democritos, Greece

**Dr. O. Stockert**

MPI CPfS Dresden, Germany

**Dr. P. Strunz**

Academy of Sciences of the Czech Republic

**Prof. Dr. R. Triolo**

University of Palermo, Italy

**Prof. Dr. J. Webster**

Rutherford Appleton Laboratory, U.K.

#### Internal members:

**Prof. Dr. A. Tennant**

HZB Berlin

**Dr. C. Pappas,**

HZB Berlin

From 2009 onwards a new Scientific Selection Panel for reviewing neutron and synchrotron radiation proposals in joint sessions will be installed. To facilitate in-depth scientific discussions this panel will consist of six sub-groups (colleges), each focussed on a particular scientific field.

## Support for European Access to BENSC

BENSC is a major partner in the European Access programme “*Integrated Infrastructure Initiative for Neutron Scattering and Muon Spectroscopy (NMI3)*” under the 6<sup>th</sup> EU Framework Programme (FP6). The most important branch of NMI3 includes 12 different access activities offering European users approximately 5000 beam days of access to more than 150 instruments at European neutron and muon facilities with support for travel and subsistence. The programme started in January 2004 and ended in June 2008. BENSC had committed itself to provide a minimum of 1040 instrument days for European users over this period of 4.5 years.

In 2008, 92 projects of 68 different European groups using 668 instrument days have been supported by BENSC. A total of 138 users out of 17 countries were involved. A list of the respective experimental reports included in this volume can be found on page XVII. Over the whole validity period of the NMI3 programme 371 European groups have been supported. They used 2055 instrument days, i.e. almost twice as much as originally contracted.

## Major Instrumental Developments

Detailed studies have been performed in 2008 to find the optimal configuration for the planned new supermirror guide system replacing the old neutron guides in the Neutron Guide Hall I (NGH-I). In parallel to the exchange of the guide system the present cold source will be replaced by a new cold source using a focusing type moderator cell. These activities will take place between October 2010 and April 2011. In addition, extensive upgrade plans have been worked out for two highly demanded user instruments in the NGH-I, the three-axes spectrometer FLEX (V2) and the TOF spectrometer NEAT (V3). An increase of performance by an order of magnitude can be expected by these upgrades.

The construction of two new instruments in the NGH-I has also been started in 2008. They were designed by university groups and are funded by

the German Ministry of Education and Research. These instruments are (i) BioRef, a TOF reflectometer with a focus on the characterisation of bio-functional interfaces (University of Heidelberg in cooperation with BENSC) and (ii) PONTO, a tomography station with a focus on the use of polarised monochromatic neutrons (Beuth Technical Highschool Berlin in cooperation with BENSC). Both instruments will strongly profit by the new guide system.

In the new Neutron Guide Hall II (NGH-II) the final two instruments designated for this hall have been built up in a basic version: the extreme-environment diffractometer EXED and the high resolution SANS machine VSANS. Both instruments entered the commissioning phase.

The thermal neutron scattering instruments E1 and E4 have been upgraded by installing a large doubly bent graphite monochromator (E1) and a large doubly bent Ge monochromator (E4) while E6 was equipped with a second area detector.

## BENSC Instruments at BESSY II

In 1998 HMI-BENSC started to build and operate three beamlines with four instruments at the Berlin 3<sup>rd</sup> generation synchrotron radiation source BESSY II in order to promote the complementary use of neutrons and synchrotron photons. With the merger of HMI and BESSY to form the new Helmholtz-Zentrum Berlin end of 2008 any distinction between the former HMI instruments at BESSY and the other BESSY instruments has become meaningless. All users of the Helmholtz-Zentrum Berlin are offered the whole range of instruments at the research reactor BER II and at the synchrotron radiation source BESSY II under equal conditions. The access will furthermore be facilitated by establishing a common user portal – GATE – for submitting proposals for both probes.

Basic statistical information on the experiments performed at these four BENSC-operated BESSY instruments in 2008 is given in the table below together with a short description of the characteristic features of the instruments.

## Short User Statistics for HMI-BENSC Instruments at BESSY in 2008

	Main instrument characteristics	External projects		In-house projects	
		Number of projects	Beam time (in weeks)	Number of projects	Beam time (in weeks)
UE46-PGM	Spectroscopy / Reflectometry	12	21	8	14
7T-MPW-MagS	Res. Magn. Scatt. / High-Resol. Diffract.	6	7	8	9
7T-MPW-SAXS	ASAXS/GISAXS	12	11	6	6
7T-MPW-EDDI	Materials Science / Stress Analysis	20	22	9	13

## Special Events

### 50 Years Research with Neutrons at HZB

In July 2008 the Helmholtz-Zentrum Berlin celebrated the 50th anniversary of the first criticality of the first research reactor BER I on the site of the Helmholtz-Zentrum Berlin in Wannsee. This first reactor was shut down in 1972 and replaced by the present facility BER II, which first became critical in December 1973. The BER II was shut down in 1985 and almost completely renewed between 1985 and 1991: The thermal power has been increased from 5 to 10 MW, a Cold Source has been installed and a Neutron Guide Hall (NGH-I) with innovative and highly competitive instruments has been put up.

Numerous neutron scientists from other centres, users and retired employees joined the staff of the Helmholtz-Zentrum Berlin in their celebration of the anniversary and enjoyed two days with a varied programme of talks on neutron science – in the past, the present and the future, in Berlin and elsewhere.

### 29<sup>th</sup> Berlin School on Neutron Scattering

The 29th Berlin School on Neutron Scattering was held at HZB from 3 - 7 March 2008. It was attended by 27 students and young postdoctoral scientists. 15 students/postdoctoral scientists were from German universities or research institutes, 9 students came from member countries of the European Union, while three came from beyond Europe (Russia, China and Taiwan).

The participants were selected from a total of 60 applicants. The school is part of the curriculum of the Faculty of Mathematics and Sciences of the Technical University Berlin and was sponsored by the European Union under its NMI3 Program.

The school started with a one day theoretical introduction to methods of neutron scattering, which comprised the basic principles of neutron scattering, an introduction to neutron sources, the different types of neutron instrument and sample environment. However, the main emphasis was on hands-on experience of the neutron scattering techniques at BENSC, including triple-axis spectroscopy, powder diffraction, small angle neutron scattering, reflectometry, time-of-flight spectroscopy and tomography.

The students were divided into streamed groups of 4 or 5 people and spent three hours on each instrument over a period of three days doing experiments. On the last day a series of lectures were given to provide an overview of how neutron scattering is contributing in the subject areas of biology, chemistry, engineering and physics. Altogether, the school involved a total of 30 hours of practical and theoretical training.

### Conferences and Workshops

The **German Neutron Scattering Conference 2008** was held at the Technical University of Munich in Garching from 15 – 17 September 2008 with a strong participation by BENSC users and HZB scientists.

The **16th International Conference on Ternary and Multinary Compounds (ICTMC16)** took place in Berlin from 15 - 19 September 2008. The HZB was significantly involved in the organisation of this conference besides the Department of Geosciences of the Free University Berlin. 157 scientists from 17 countries, amongst them 27 participants from the HZB and many BENSC users, have met in Berlin to present and discuss their recent scientific results.

The **3rd BENSC Adsorption Workshop** was held from 1 – 2 October 2008. It was attended by 43 participants, most of them experts in the field. 34 participants were external scientist of which 13 came from abroad. 17 talks on instrumental and scientific topics were given, almost all of them (16) by the external experts.

This new workshop series has been launched in order to get a feedback from the “adsorption community” on existing DEGAS equipment and suggestions for new developments. DEGAS stands for **Dedicated Environment for combined Gas Adsorption and Scattering Experiments** and consists of an ensemble of sophisticated but user-friendly instrumentation allowing neutron scattering experiments under controlled gas pressure. In parallel standard commercial laboratory equipment for adsorption experiments has been installed which is also offered to users either for complementing neutron measurements or for stand-alone experiments. Building up this second sample environment focus beside the high-magnetic field equipment has brought many new users from diverse fields to BENSC.

## List of BENS-Neutrons Instruments

### Instruments in the BER II Experiment Hall (thermal neutrons) *Telefon numbers: +49(0)30/8062-*

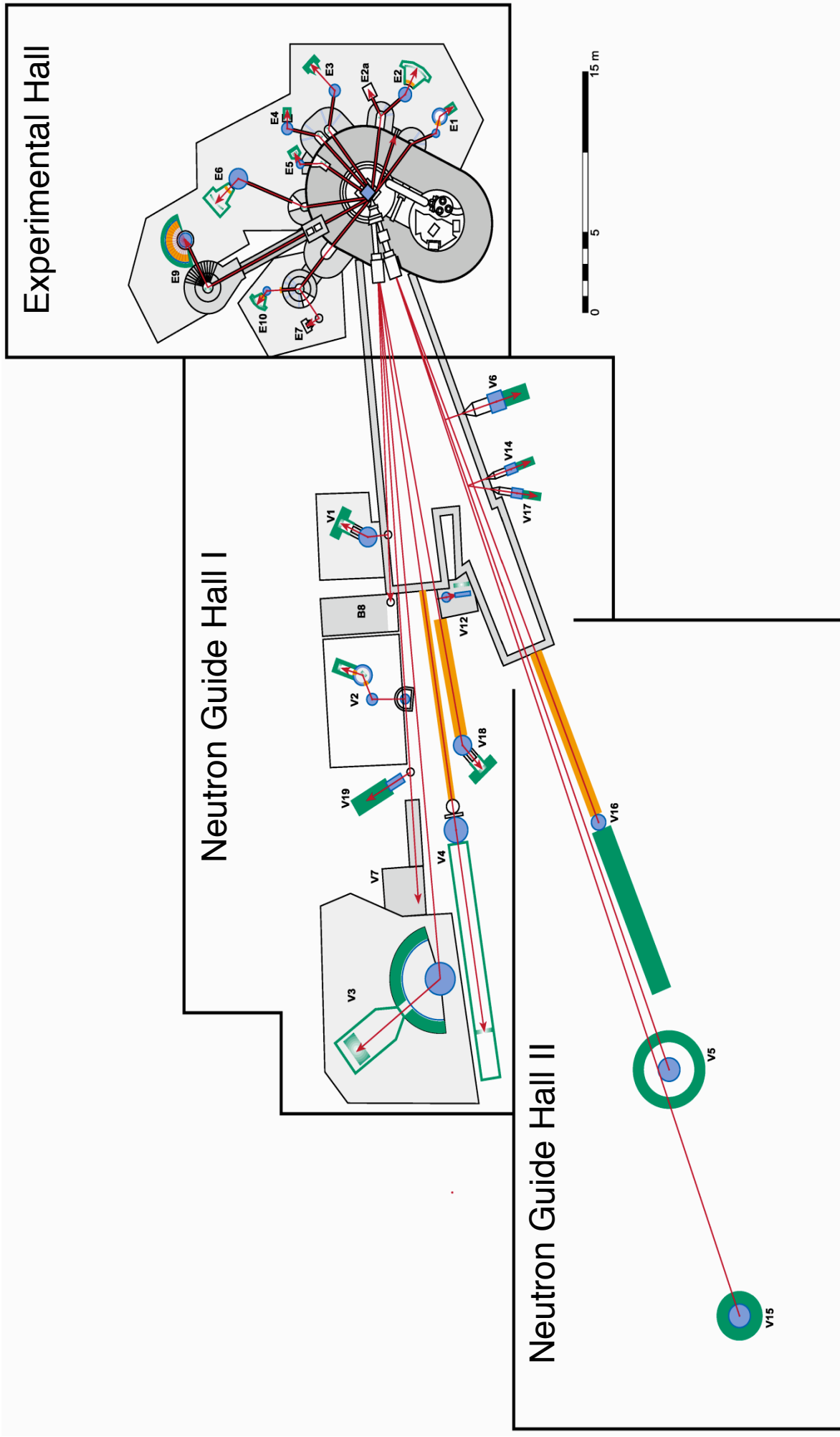
	Instrument	ext.	Inst. Scientists	ext.
<b>E1</b>	3-Axis Spectrometer with Polarisation Analysis (limited access only in close co-operation with local staff members)	3101	A. Hoser M. Mihalik	2847 2793
<b>E2</b>	Flat-Cone Single Crystal Diffractometer (E2a: Crystal-Test Diffractometer)	3102	J. Hoffmann A. Hoser	2185 2847
<b>E3</b>	Residual Stress Analysis and Texture Diffractometer	3103	R. Wimpory	3097
<b>E4</b>	2-Axis-Diffractometer (E4b: Position for Single Crystal Orientation)	3104	K. Prokes S. Matas	2804 2804
<b>E5</b>	4-Circle Diffractometer	3104	M. Reehuis	2692
<b>E6</b>	Focusing Single Crystal Diffractometer	3105	N. Stüßer A. Hoser	3171 2847
<b>E7</b>	Residual Stress Analysis Diffractometer (limited access only in close co-operation with local staff members)	3107	R. Wimpory	3097
<b>E9</b>	Fine Resolution Powder Diffractometer (FIREPOD)	3106	D. Argyriou P. Henry F. Yokaichiya S. Kimber M. Tovar	3016 2686 3177 3079 2768
<b>E10</b>	HELIX, 3He-Diffractometer	3106	K. Siemensmeyer	2757

### Instruments in the BER II Cold Neutron Guide Halls *Telefon numbers: +49(0)30/8062-*

	Instrument	ext.	Inst. Scientists	ext.
<b>V1</b>	Membrane Diffractometer	3121	T. Hauß A. Buchsteiner	2071 2071
<b>V2</b>	I: 3-Axis Spectrometer (FLEX) II: FLEX with NRSE opt.	3122	K. Habicht K. Rule M. Skoulatos D. Le	2807 3067 2171 2803
<b>V3</b>	Time-of-Flight Spectrometer (NEAT)	3123	M. Russina E. Kemner Z. Izaola	3159 3073 3179
<b>V4</b>	Small Angle Scattering Instrument (SANS)	3124	U. Keiderling S. Prévost V. Ryukhtin A. Brandt D. Clemens K. Vogtt	2339 2339 3099 2169 2280 3022
<b>V5</b>	Spin-Echo Spectrometer with ToF Option (SPAN)	3125	S. Wellert	2046 3072 3174
<b>V6</b>	Reflectometer	2806	R. Steitz R. Köhler A. Teichert	2149 3077 2044
<b>V7</b>	Cold Neutron Tomography and Radiography (CONRAD)	3327	N. Kardjilov A. Hilger M. Dawson	2298 2298
<b>B8</b>	Neutron-Autoradiography (limited access only in close co-operation with local staff members)	3121	A. Denker	3000
<b>V12a</b>	Bent-crystal Diffractometer (USANS) / Tomography	3131	W. Treimer S. Seidel	2221 3298
<b>V14</b>	Mirror Test Device	2284	T. Krist	2045
<b>V15</b>	Extreme Environment Diffractometer (EXED) (commissioning)	3283	O. Prokhnenko H. Bleif	3068 2758

	<b>Instrument</b>	<b>ext.</b>	<b>Inst. Scientists</b>	<b>ext.</b>
<b>V16</b>	Very Small Angle Neutron Scattering (VSANS) <i>(commissioning)</i>	3281	D. Clemens K. Vogtt	2280 3022
<b>V17</b>	Detector Test Station	3284	T. Wilpert C. Schulz S. Alimov	2743 2675 2675
<b>V18</b>	Reflectometer for biological applications (BioRef) <i>(under construction)</i>	****	R. Steitz M. Strobl A. Paul	2149 2490 2925
<b>V19</b>	Polarized Neutron Tomography (PONTO) <i>(under construction)</i>	****	W. Treimer O. Ebrahimi	2221 3076
<b>X2</b>	X-ray Reflectometer <i>(Sample Preparation V6, only in close co-operation with local staff members)</i>	3112	H. Bleif	2758

# Floor Plan of the Neutron Instruments at the BER II



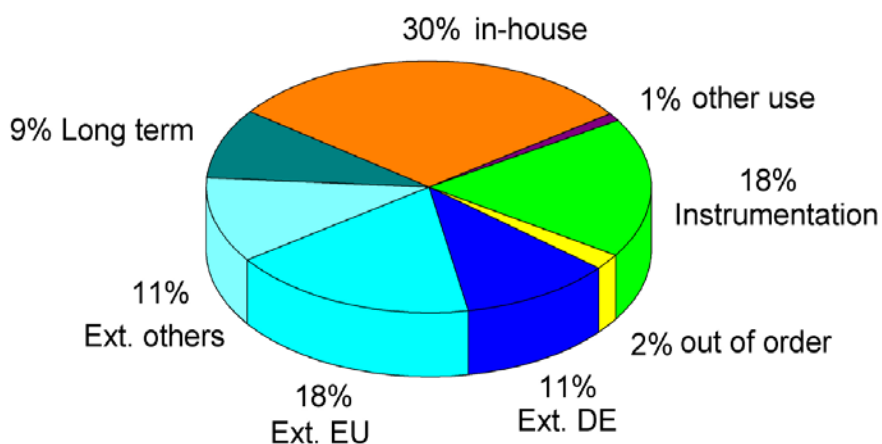
## Instrument Statistics 2008

**Table: Detailed statistical data on the use of the scheduled instruments**

Instr.	Inst. days	EXT (DE) in %	EXT (EU) in %	EXT (other) in %	LT in %	EF in %	other use in %	Inst. in %	OOO in %
E1*	224	10	4	0	0	12	2	64	8
E2	224	24	14	7	3	26	2	25	0
E3	224	11	22	2	15	40	0	9	0
E4	224	0	31	19	0	42	0	8	0
E5	224	0	0	15	36	48	0	1	0
E6	224	11	0	13	0	32	0	3	0
E9	224	19	35	4	0	35	1	6	0
V1	222,5	28	19	7	23	13	0	9	0
V2	222,5	6	27	26	0	37	0	4	0
V3	222,5	2	22	28	0	37	0	11	0
V4*	222,5	16	9	5	5	18	2	18	29
V5	222,5	7	22	23	5	36	0	8	0
V6	222,5	17	10	6	20	27	2	20	0
V7	222,5	18	12	10	7	42	1	9	0
V12	222,5	0	8	5	18	0	0	68	0

Note: The table gives detailed statistical data on the use of the scheduled instruments. The pie chart shows the statistical data given in the table, summarized over all instruments. The meaning of the individual entries is explained in the legend below. EXT (DE), EXT (EU) and EXT (other) refer to projects performed by external users from Germany, EU or other countries via accepted "normal" short-term proposals submitted to BENSCH. Please note that the long-term projects are also projects performed by external user groups, where instrument time is either given on the basis of an accepted long-term proposal or on the basis of a cooperation agreement with BENSCH.

### Overall Statistics on Instrument Use in 2008



<b>Inst.-days</b>	Neutron days per Instrument
<b>EXT (DE)</b>	German Universities, Research institutes
<b>EXT (EU)</b>	Universities and Research Institutes from the EU and associated states
<b>EXT (other)</b>	Non-EU Universities and Research Institutes
<b>LT</b>	Long term projects
<b>EF</b>	In-house projects
<b>other use</b>	e.g. industry, teaching (neutron school)
<b>Inst.</b>	Instrument time (tests, developments ...)
<b>OOO</b>	out of operation
<b>E1*</b>	under construction in 2008
<b>V4*</b>	technical problems in 2008

## **How to apply for beam time at BER II (HZB-Neutrons) and BESSY II (HZB-Photons)**

The research reactor BER II is a major European neutron scattering facility with exceptional capabilities to conduct complex experiments under extreme conditions. Outstanding sample environment provides high static magnetic fields up to 17 T, high, low, and ultra-low temperatures and controlled gas pressures up to 10 kbar. The advanced and partly unique neutron scattering instrumentation and the quality of the user service attract researchers worldwide.

The storage ring BESSY II is a leading third-generation synchrotron-radiation source providing ultrabright photon beams from the long wavelength Terahertz region to hard X-rays with complete control of the polarization of the radiation and energy range. More than 50 beamlines offer a multi-faceted mixture of experimental opportunities at undulator, wiggler and dipole sources with excellent energy resolutions.

Details on the instrumentation at both sources are available on the WEB:

<http://www.helmholtz-berlin.de/userservice>

BER II and BESSY II are open to both the national and the international user community. The main fraction of the beam time is reserved for external short-term research proposals. All applications are reviewed by an international Scientific Selection Panel (SSP) twice a year. Beamtime is granted on the basis of scientific merit. To promote the synergetic use of neutron and synchrotron radiation, the Scientific Selection Panel is dealing with proposals for neutrons and synchrotron photons in joint sessions. To this purpose the Panel is divided in 6 sub-groups (colleges) each being focussed on a particular scientific field in order to facilitate in-depth discussions.

**Deadlines for the submission of proposals are**

**1 March and 1 September.**

The instrument responsables of HZB are asked to advise potential users and comment on the technical feasibility of the proposed experiments. For these tasks this limited class of HZB-scientists has access to the submitted proposals.

Requests for urgent or confidential experiments (Director's Discretionary Time) and for industrial use may be submitted at any time.

Applications for HZB-Neutrons as well as HZB-Photons beam time should be made by using GATE, the common user entry point for both neutron and synchrotron radiation applications

[http://www.helmholtz-berlin.de/userservice/gate\\_en.html](http://www.helmholtz-berlin.de/userservice/gate_en.html)

Research projects for the complementary use of HZB-Neutrons and HZB-Photons are strongly encouraged.

For further information please contact:

### **Helmholtz-Zentrum Berlin für Materialien und Energie GmbH**

HZB User Office – Neutrons  
Lise-Meitner-Campus  
Glienicke Str. 100  
D-14109 Berlin (Wannsee)  
Germany

HZB User Office – Photons  
Wilhelm-Conrad-Röntgen Campus  
Albert-Einstein-Str. 15  
D-12489 Berlin (Adlershof)  
Germany

Phone: +49 - 30 - 8062 2304 / 3153  
Fax: +49 - 30 - 8062 2523  
Email: neutrons@helmholtz-berlin.de

Phone: +49 - 30 - 6392-2931  
Fax: +49 - 30 - 6392-2931  
Email: photons@helmholtz-berlin.de

The BENSIC Experimental Reports are intended as interim summaries. In view of the short time available between the termination of certain experiments and the deadline for this report, the results presented here have to be considered as preliminary. The inclusion of reports in this volume does not constitute a publication in the usual sense. Final results will be submitted for publication in regular scientific journals.

## Acknowledgement for Support by the European Commission

The access of BENSC users from European Community Member States and Associated States to BENSC has been substantially supported by the European Community under the Framework Programs FP5 and FP6.

**FP6:** BENSC is a partner in the EU supported network of European neutron facilities – the **Neutron and Muon Integrated Infrastructure Initiative (NMI3)**, an action within the EU FP6 activity ‘Structuring the European Research Area: Research Infrastructures Action’.

The access contract under NMI3 has been effective for 4 • years, from 01/2004 until 6/2008, the relevant EU contract number for acknowledgements is **RII3-CT-2003-505925**. In order to bridge the gap between this program and a new access program under FP7 BENSC continued to support all eligible EU users until the end of 2008 by HZB funds.

Results of EU supported groups are contained in 67 reports of this volume.

<b>NMI3-Nº.</b>	<b>Page</b>	<b>Authors</b>	<b>Affiliation</b>
1235	38	Coldea et al.	Univ. Bristol, UK
1252	251	Triolo et al.	Univ. of Palermo, I
1265	228	Zawisky et al.	TU – ATI Wien, AT
1266	231	Schöbel et al.	TU Wien, AT
1270	46	Kamarad et al.	ASCR IP Prague, CZ
1297	140	Pavese et al.	Univ. Milano, I
1299	253	Triolo et al.	Univ. of Palermo, I
1301	40	Gondek et al.	AGH-UST, Krakow, PL
1310	234	Schöbel et al.	TU Wien, AT
1311	229	Tatlisu et al.	ATI Wien, AT
1314	205	Remhof et al.	EMPA, CH
1317	166	Klößgen et al.	Univ. Odense, DK
1318	73	Salazar-Alvarez et al.	Institut Català de Nanotecnologia, E
1320	61	Paul-Boncour et al.	CNRS, F
1322	143	Sobolev et al.	LGIT, CNRS & UJF, Grenoble, F
1323	184	Eibl et al.	ILL Grenoble, F
1326	151	Bradshaw et al.	Univ. of Edinburgh, UK
1328	84	McEwen et al.	Univ. College, London, UK
1332	192	Zarbaksh et al.	QM UCL, UK

<b>NMI3-Nº.</b>	<b>Page</b>	<b>Authors</b>	<b>Affiliation</b>
1333	206	Steriotis et al.	NCRS Demokritos, GR
1334	212	Katsaros et al.	NCSR Demokritos, GR
1335	153	Garab et al.	HAS BRC Szeged, H
1336	152	Berti et al.	Univ. Of Florence & CSGI, I
1337	235	Fiori et al.	UPM Ancona, I
1338	236	Manescu et al.	UPM Ancona, I
1339	169	Deriu et al.	Univ. Parma, I
1340	176	Gerelli et al.	Univ. Parma, I
1342	259	Raitman et al.	L.A.S., LV
1343	48	Mufti et al.	Univ. Groningen, NL
1344	123	Jalarvo et al.	FERMIO, Oslo, NO
1345	124	Nowicki et al.	AMU, Poznań, PL
1347	125	Kopcewicz et al.	Inst. of Electronic Mat. Technology, PL
1348	62	Penc et al.	JU Krakow, PL
1349	97	Gondek et al.	AGH-UST, Krakow, PL
1350	63	Orendáčová et al.	PJSU Košice, SK
1351	217	Strunz et al.	ASCR NPI Řež, CZ
1352	90	Lefmann et al.	Univ. of Copenhagen, DK
1354	260	Tamaki et al.	TAMAKI MI, JP
1354	224	Josic et al.	PSI, CH
1355	207	Remhof et al.	EMPA, CH

<b>NMI3-Nº.</b>	<b>Page</b>	<b>Authors</b>	<b>Affiliation</b>
1357	51	Kamarad et al.	ASCR IP Prague, CZ
1358	65	Mihalik et al.	Charles Univ. Prague, CZ
1360	75	Vestergaard Jensen et al.	DTU - Risø, DK
1361	128	Climent-Pascual et al.	UC Madrid, E
1365	185	Eibl et al.	ILL Grenoble, F
1367	157	Russo et al.	ILL+ INFM OGG & CRS-SOFT, F
1369	170, 186	Saboungi et al.	CNRS Orleans, F
1370	35	Sainctavit et al.	UPMC Paris, F
1371	35	Sainctavit et al.	UPMC Paris, F
1372	180	Bauduin	CEA Saclay, F
1373	66	Paul-Boncour et al.	CNRS, F
1375	76	Hill et al.	Univ. of Edinburgh, UK
1374	113	Fennell et al.	UC London, UK

<b>NMI3-Nº.</b>	<b>Page</b>	<b>Authors</b>	<b>Affiliation</b>
1378	241	Robinson et al.	Univ. of Limerick, IE
1379	242	Fiori et al.	UPM Ancona, I
1383	243	Manescu et al.	UPM Ancona, I
1384	181, 182	Milioto et al.	Univ. Palermo, I
1385	155	Ranieri et al.	Univ. of Genova, I
1390	198	van Heijkamp et al.	TU Delft, NL
1391	135	Jalarvo et al.	FERMIO, Oslo, NO
1392	67	Baran et al.	JU Krakow, PL
1393	68	Baran et al.	JU Krakow, PL
1394	69	Gondek et al.	AGH-UST, Krakow, PL
1395	99	Gondek et al.	AGH-UST, Krakow, PL
1397	59	Szlawska et al.	PAS ILTSR Wroclaw, PL
1399	136	Pérez-Hernández et al.	CSIC Sevilla, E

Notice:

The quality of figures in the electronic versions, CD and WEB ([http://www.helmholtz-berlin.de/userservice/neutrons/reports\\_en.html](http://www.helmholtz-berlin.de/userservice/neutrons/reports_en.html)) – especially in colour presentation – is remarkably higher than in the print version

## List of Contributed Experimental Reports

PAGE	TITLE	TEAM	PROPOSAL		
<b><i>Development of Instruments and Methods</i></b>					
3	<b>Larmor phase topology with NRSE – experimental test of correction devices</b>	K. Habicht <sup>1</sup>	<sup>1</sup> HZB	V2	<b>PHY-02-630-EF</b>
4	<b>Specular and Off-specular Scattering with Polarization and Polarization analysis on Reflectometer V6</b>	P. Amitesh <sup>1</sup> R. Steitz <sup>1</sup>	<sup>1</sup> HZB	V6	<b>PHY-04-1723-EF</b>
5	<b>Test of solid state polarizer for imaging</b>	A. Hilger <sup>1</sup> N. Kardjilov <sup>1</sup> I. Manke <sup>1</sup> M. Strobl <sup>1</sup> M. Dawson <sup>1</sup>	<sup>1</sup> HZB	V7	<b>PHY-04-1444-EF</b>
6	<b>Dark-field contrast – a new imaging signal for neutron tomography</b>	M. Strobl <sup>1+2</sup> A. Hilger <sup>1</sup> N. Kardjilov <sup>1</sup> I. Manke <sup>1</sup> Ch. Grünzweig <sup>3</sup> O. Ebrahimi <sup>4</sup>	<sup>1</sup> HZB <sup>2</sup> Uni Heidelberg <sup>3</sup> PSI, CH <sup>4</sup> TFH, Berlin	V7	<b>PHY-04-1514-DT</b>
7	<b>Visualisation of flux-pinning in superconductors</b>	A. Hilger <sup>1</sup> N. Kardjilov <sup>1</sup> I. Manke <sup>1</sup> M. Dawson <sup>1</sup>	<sup>1</sup> HZB	V7	<b>PHY-04-1534-EF</b>
8	<b>Radiography with polarized neutrons</b>	A. Hilger <sup>1</sup> N. Kardjilov <sup>1</sup> I. Manke <sup>1</sup> M. Dawson <sup>1</sup> M. Strobl <sup>1</sup> D. Wallacher <sup>1</sup>	<sup>1</sup> HZB	V7	<b>OTH-04-1538-EF</b>
9	<b>Polarimetric magnetic field tomography</b>	M. Strobl <sup>1+2</sup> A. Hilger <sup>1</sup> N. Kardjilov <sup>1</sup> I. Manke <sup>1</sup> E. Jericha <sup>3</sup> G. Badurek <sup>3</sup>	<sup>1</sup> HZB <sup>2</sup> Uni Heidelberg <sup>3</sup> TU – ATI, AT	V7	<b>PHY-04-1628-EF</b>
10	<b>Spin-polarised neutron radiography on electric conductors</b>	I. Manke <sup>1</sup> N. Kardjilov <sup>1</sup> A. Hilger <sup>1</sup> M. Dawson <sup>1</sup>	<sup>1</sup> HZB	V7	<b>PHY-04-1629-EF</b>
11	<b>Visualization of local textures using Bragg Edge Radio- and Tomography</b>	M. Boin <sup>1</sup> N. Kardjilov <sup>1</sup>	<sup>1</sup> HZB	V7	<b>MAT-04-1632-EF/ MAT-04-1633-EF</b>
12	<b>Test of New Scintillating Screens</b>	I. Manke <sup>1</sup> N. Kardjilov <sup>1</sup> A. Hilger <sup>1</sup> M. Dawson <sup>1</sup>	<sup>1</sup> HZB	V7	<b>PHY-04-1637-IT</b>
13	<b>Test of He3 polarisators for imaging</b>	I. Manke <sup>1</sup> N. Kardjilov <sup>1</sup> A. Hilger <sup>1</sup> M. Dawson <sup>1</sup> M. Strobl <sup>1</sup> K. Anderson <sup>2</sup> F. Bordenave <sup>2</sup> D. Julian <sup>2</sup>	<sup>1</sup> HZB <sup>2</sup> ILL, F	V7	<b>PHY-04-1638-IT</b>
14	<b>Spin-echo-like neutron imaging</b>	M. Strobl <sup>1+2</sup> A. Hilger <sup>1</sup> N. Kardjilov <sup>1</sup> I. Manke <sup>1</sup>	<sup>1</sup> HZB <sup>2</sup> Uni Heidelberg	V7	<b>ART-04-1728-EF</b>
15	<b>Using neutrons for non-destructive testing at the surface Part 1</b>	Ch. Genzel <sup>1</sup> I. Denks <sup>1</sup> R. Wimpory <sup>1</sup>	<sup>1</sup> HZB	E3	<b>EF/BESSY</b>

## List of Contributed Experimental Reports

PAGE	TITLE	TEAM	PROPOSAL
16	Using neutrons for non-destructive testing at the surface Part 2	R. Wimpory <sup>1</sup> A. Venter <sup>2</sup>	<sup>1</sup> HZB <sup>2</sup> NECSA, SA E3 EF
17	Installation of the new double chopper at the SANS instrument	U. Keiderling <sup>1</sup> S. Prévost <sup>2</sup>	<sup>1</sup> HZB <sup>2</sup> TU Berlin V4 EF
18	Neutron imaging in a spin-echo instrument	M. Strobl <sup>1+2</sup> A. Hilger <sup>1</sup> P. Wellert <sup>1</sup> S. O. Seidl <sup>1</sup> C. Pappas <sup>1</sup>	<sup>1</sup> HZB <sup>2</sup> Uni Heidelberg V5 EF
19	High resolution investigations of edge effects in neutron imaging	M. Strobl <sup>1+2</sup> A. Hilger <sup>1</sup> I. Manke <sup>1</sup> N. Kardjilov <sup>1</sup>	<sup>1</sup> HZB <sup>2</sup> Uni Heidelberg V7 EF
20	Application of neutron dark-field contrast imaging	M. Strobl <sup>1+2</sup> A. Hilger <sup>1</sup> I. Manke <sup>1</sup> N. Kardjilov <sup>1</sup> D. Penumadu <sup>3</sup>	<sup>1</sup> HZB <sup>2</sup> Uni Heidelberg <sup>3</sup> Univ. of Tennessee, USA V7 EF
21	V12a DCD equipped with polarizing devices	S. O. Seidel <sup>1</sup> W. Treimer <sup>1+2</sup> R. Monka <sup>1</sup> O. Ebrahimi <sup>1</sup>	<sup>1</sup> TFH Berlin <sup>2</sup> HZB V12a EF
22	Installation and the implantation of an area detector dedicated to small angle scattering	S. O. Seidel <sup>1</sup> W. Treimer <sup>1+2</sup> R. Monka <sup>1</sup> O. Ebrahimi <sup>1</sup>	<sup>1</sup> TFH Berlin <sup>2</sup> HZB V12a EF
23	Influence of Beam Divergence on Coherent Neutron Diffraction	S. O. Seidel <sup>1</sup> W. Treimer <sup>1</sup> O. Ebrahimi <sup>1</sup> N. Beul <sup>2</sup> M. Strobl <sup>3</sup>	<sup>1</sup> TFH Berlin <sup>2</sup> HZB <sup>3</sup> Uni Heidelberg V12b EF
24	Neutron diffraction by Cu-wires	S. O. Seidel <sup>1</sup> W. Treimer <sup>1</sup> O. Ebrahimi <sup>1</sup> E. Rudolf <sup>1</sup> N. Beul <sup>2</sup> M. Strobl <sup>3</sup>	<sup>1</sup> TFH Berlin <sup>2</sup> HZB <sup>3</sup> Uni Heidelberg V12b EF
25	Single slit neutron diffraction	S. O. Seidel <sup>1</sup> W. Treimer <sup>1</sup> O. Ebrahimi <sup>1</sup>	<sup>1</sup> TFH Berlin V12b EF
26	2 dimensional spin analyzer and Ni/Ti supermirrors	Th. Krist <sup>1</sup> J.-E. Hoffmann <sup>1</sup> G. Heldt <sup>1</sup>	<sup>1</sup> HZB V14 EF
27	Time-of-flight Bragg edge imaging at a continuous neutron source	M. Strobl <sup>1+2</sup> A. Hilger <sup>1</sup> I. Manke <sup>1</sup> N. Kardjilov <sup>1</sup> T. Kandemir <sup>1</sup>	<sup>1</sup> HZB <sup>2</sup> Uni Heidelberg V17 EF
28	Flux and Spectrum at the V18 position at NL3b	M. Strobl <sup>1+2</sup> H.-J. Bleif <sup>1</sup>	<sup>1</sup> HZB <sup>2</sup> Uni Heidelberg V18 EF
29	A new tomography for polarized neutrons	W. Treimer <sup>1</sup> O. Ebrahimi <sup>1</sup> S. O. Seidl <sup>1</sup> N. Karakas <sup>1</sup>	<sup>1</sup> TFH Berlin V19 EF

## List of Contributed Experimental Reports

PAGE	TITLE	TEAM	PROPOSAL
30	First neutron tomography with the new experiment V19 "PONTO"	O. Ebrahimi <sup>1</sup> S. O. Seidl <sup>1</sup> W. Treimer <sup>1</sup> N. Karakas <sup>1</sup>	<sup>1</sup> TFH Berlin V19 EF

### Magnetism

#### Magnetic Structure and Phase Transitions

33	High field magnetic state transition in the frustrated kagome lattice antiferromagnets	K. Matan <sup>1</sup> Y. S. Lee <sup>1</sup> D. Grohol <sup>1</sup> V. Sikolenko <sup>2</sup>	<sup>1</sup> MIT, USA <sup>2</sup> HZB E1 PHY-02-498
34	Magnetic Structure of Li <sub>2</sub> ZrCuO <sub>4</sub>	W. Lorenz <sup>1</sup> W. D. Stein <sup>1</sup> R. Schedler <sup>2</sup>	<sup>1</sup> IFW Dresden <sup>2</sup> HZB E1 PHY-02-640
35	Neutron diffraction study of the magnetic structure transformation in the Y <sub>0.22</sub> Sr <sub>0.78</sub> CoO <sub>3</sub>	P. Sainctavit <sup>1</sup> V. Sikolenko <sup>2+3</sup> V. Efimov <sup>4</sup>	<sup>1</sup> UPMC Paris, F <sup>2</sup> PSI, CH <sup>3</sup> ETHZ, CH <sup>4</sup> JINR, RU E1/E9 PHY-02-660/ PHY-01-2366
36	Bulk moduli of molecule based magnets: (5MAP) <sub>2</sub> CuBr <sub>4</sub> and Cu Pyrimidine	S. Süllow <sup>1</sup> D. Schulze Grachtrup <sup>1</sup> K. Prokes <sup>2</sup> N. Stüßer <sup>2</sup>	<sup>1</sup> TU Braunschweig <sup>2</sup> HZB E1 PHY-02-687
37	Static magnetic and structural properties of the diamond spin chain azurite	S. Süllow <sup>1</sup> C. Gibson <sup>2</sup> J. U. Hoffmann <sup>2</sup>	<sup>1</sup> TU Braunschweig <sup>2</sup> HZB E2 PHY-01-2025
38	Field-dependence of magnetic order in an Ising magnet in transverse field	R. Coldea <sup>1</sup> G. L. Pascut <sup>1</sup> J. U. Hoffmann <sup>2</sup> B. Kemke <sup>2</sup> K. Kiefer <sup>2</sup> S. Gerischer <sup>2</sup>	<sup>1</sup> Univ. of Bristol, UK <sup>2</sup> HZB E2 PHY-01-2030
39	Crystalline and magnetic structure of mixed Tb <sub>{1-x}</sub> Bi <sub>x</sub> MnO <sub>{3+Δ}</sub> multiferroic material	I. Golosovskiy <sup>1</sup> S. Vakhrushev <sup>2</sup> J. U. Hoffmann <sup>3</sup>	<sup>1</sup> PNPI RAS, RU <sup>2</sup> PTI RAS Ioffe, RU <sup>3</sup> HZB E2 PHY-01-2100
40	Magnetic and crystal structure of Ho <sub>3</sub> Pd <sub>4</sub> Ge <sub>4</sub>	L. Gondek <sup>1</sup> O. Prokhnenko <sup>2</sup> J. U. Hoffmann <sup>2</sup>	<sup>1</sup> AGH-UST, PL <sup>2</sup> HZB E2 PHY-01-2110
41	Diffuse scattering in the paramagnetic regime of CeRhIn <sub>5</sub>	O. Stockert <sup>1</sup> J. U. Hoffmann <sup>2</sup>	<sup>1</sup> MPI CPfS, Dresden <sup>2</sup> HZB E2 PHY-01-2190
42	Magnetoelectric correlations in multiferroic ErMnO <sub>3</sub>	D. Meier <sup>1</sup> M. Fiebig <sup>1</sup> J. U. Hoffmann <sup>2</sup>	<sup>1</sup> Uni Bonn, HISKP <sup>2</sup> HZB E2 PHY-01-2341
43	Magnetic structure of Ce <sub>2</sub> PdSi <sub>3</sub> and Dy <sub>2</sub> PdSi <sub>3</sub>	M. Frontzek <sup>1</sup> W.-D. Stein <sup>1</sup> J. U. Hoffmann <sup>2</sup> A. Hoser <sup>2</sup>	<sup>1</sup> TU, Dresden <sup>2</sup> HZB E2 PHY-01-2342
44	Satellite scattering in multiferroic LuFe <sub>2</sub> O <sub>4</sub>	A. Mulders <sup>1</sup> S. Lawrence <sup>1</sup> J. U. Hoffmann <sup>2</sup> K. Kiefer <sup>2</sup>	<sup>1</sup> Curtin Univ., AUS <sup>2</sup> HZB E2 PHY-01-2350
45	Temperature evolution of the crystal and magnetic structures in the Ni-Mn-Ga-(Fe, Cu) ferromagnetic shape memory alloys	I. Glavatskyi <sup>1</sup> J. U. Hoffmann <sup>2</sup>	<sup>1</sup> IMP, UA <sup>2</sup> HZB E2 PHY-01-2353

## List of Contributed Experimental Reports

PAGE	TITLE	TEAM	PROPOSAL
46	<b>Magnetic ordering in multiferroic TbMnO<sub>3</sub> under pressure</b>	J. Kamarad <sup>1</sup> O. Prokhnenko <sup>2</sup> N. Aliouane <sup>2</sup> K. Prokes <sup>2</sup> D. Argyriou <sup>2</sup>	<sup>1</sup> ASCR IP, CZ <sup>2</sup> HZB E4 <b>PHY-01-2122</b>
47	<b>Nonmagnetic impurity effect on ferroelectric phase of multiferroic CuFeO<sub>2</sub></b>	S. Mitsuda <sup>1</sup> T. Nakajima <sup>1</sup> M. Yamano <sup>1</sup> K. Prokes <sup>2</sup> K. Kiefer <sup>2</sup> S. Gerischer <sup>2</sup>	<sup>1</sup> Tokyo US, JP <sup>2</sup> HZB E4 <b>PHY-01-2126</b>
48	<b>Magnetic field dependence of the magnetic modulation in the relaxor ferroelectric (Tb,Ca)MnO<sub>3</sub></b>	N. Mufti <sup>1</sup> G. Blake <sup>1</sup> S. Riyadi <sup>1</sup>	<sup>1</sup> Univ. Groningen, NL E4 <b>PHY-01-2221</b>
49	<b>Unconventional metallic magnetism in RCrSb<sub>3</sub> (R = Ce, and Pr): A neutron diffraction study on single crystals</b>	M. Inamdar <sup>1</sup> K. Prokes <sup>2</sup>	<sup>1</sup> Tata Inst., IND <sup>2</sup> HZB E4 <b>PHY-01-2222</b>
50	<b>Microscopic spin-polarization coupling in multiferroic CuFeO<sub>2</sub></b>	S. Mitsuda <sup>1</sup> T. Nakajima <sup>1</sup> K. Prokes <sup>2</sup> A. Podlesnyak <sup>2</sup>	<sup>1</sup> Tokyo US, JP <sup>2</sup> HZB E4 <b>PHY-01-2285-DT</b>
51	<b>Magnetic structures in NdRhSn under uniaxial and hydrostatic pressures</b>	J. Kamarad <sup>1</sup> M. Mihalik <sup>2</sup> V. Sechovsky <sup>2</sup> K. Prokes <sup>3</sup>	<sup>1</sup> ASCR IP, CZ <sup>2</sup> CU Prague, CZ <sup>3</sup> HZB E4 <b>PHY-01-2381</b>
52	<b>Er<sub>2</sub>Ni<sub>2</sub>Pb single crystal in magnetic fields</b>	K. Prokes <sup>1</sup>	<sup>1</sup> HZB E4 <b>PHY-01-2445-EF</b>
53	<b>Magnetic order of the Pr<sup>3+</sup>- and V<sup>3+</sup>-ions in Pr<sub>0.90</sub>Ca<sub>0.10</sub>VO<sub>3</sub></b>	C. Ulrich <sup>1</sup> B. Keimer <sup>1</sup> J. Fujioka <sup>2</sup> S. Miyasaka <sup>2</sup> Y. Tokura <sup>2</sup> M. Reehuis <sup>1+3</sup>	<sup>1</sup> MPI, Stuttgart <sup>2</sup> Univ. of Tokyo, JP <sup>3</sup> HZB E5 <b>PHY-01-1724-LT</b>
54	<b>Structural and magnetic phase transitions in PrVO<sub>3</sub> and Pr<sub>0.90</sub>Ca<sub>0.10</sub>VO<sub>3</sub></b>	C. Ulrich <sup>1</sup> B. Keimer <sup>1</sup> J. Fujioka <sup>2</sup> S. Miyasaka <sup>2</sup> Y. Tokura <sup>2</sup> M. Reehuis <sup>1+3</sup>	<sup>1</sup> MPI, Stuttgart <sup>2</sup> Univ. of Tokyo, JP <sup>3</sup> HZB E5 <b>PHY-01-1724-LT</b>
55	<b>Magnetic order and phase transitions in HoVO<sub>3</sub></b>	C. Ulrich <sup>1</sup> B. Keimer <sup>1</sup> J. Fujioka <sup>2</sup> S. Miyasaka <sup>2</sup> Y. Tokura <sup>2</sup> M. Reehuis <sup>1+3</sup>	<sup>1</sup> MPI, Stuttgart <sup>2</sup> Univ. of Tokyo, JP <sup>3</sup> HZB E5 <b>PHY-01-1724-LT</b>
56	<b>Structural and magnetic phase transitions in HoVO<sub>3</sub></b>	C. Ulrich <sup>1</sup> B. Keimer <sup>1</sup> J. Fujioka <sup>2</sup> S. Miyasaka <sup>2</sup> Y. Tokura <sup>2</sup> M. Reehuis <sup>1+3</sup>	<sup>1</sup> MPI, Stuttgart <sup>2</sup> Univ. of Tokyo, JP <sup>3</sup> HZB E5 <b>PHY-01-1724-LT</b>
57	<b>Magnetic ordering in the hole-doped vanadate Ca<sub>0.10</sub>Y<sub>0.90</sub>VO<sub>3</sub></b>	C. Ulrich <sup>1</sup> B. Keimer <sup>1</sup> J. Fujioka <sup>2</sup> S. Miyasaka <sup>2</sup> Y. Tokura <sup>2</sup> M. Reehuis <sup>1+3</sup>	<sup>1</sup> MPI, Stuttgart <sup>2</sup> Univ. of Tokyo, JP <sup>3</sup> HZB E5 <b>PHY-01-1724-LT</b>
58	<b>Structural and magnetic phase transitions in LuVO<sub>3</sub></b>	M. Skoulatos <sup>1</sup> J. Morris <sup>2</sup> M. Reehuis <sup>1+3</sup>	<sup>1</sup> HZB <sup>2</sup> Univ. of Liverpool, UK <sup>3</sup> MPI, Stuttgart E5 <b>PHY-01-2291-EF</b>

## List of Contributed Experimental Reports

PAGE	TITLE	TEAM	PROPOSAL
59	Neutron diffraction study of the magnetic ordering in U <sub>2</sub> NiSi <sub>3</sub>	M. Szlawska <sup>1</sup> D. Kaczorowski <sup>1</sup> M. Reehuis <sup>2</sup>	<sup>1</sup> PAS ILTSR, PL <sup>2</sup> HZB E5 <b>PHY-01-2404</b>
60	Magnetic structure of the (Dy <sub>1-x</sub> Y <sub>x</sub> ) <sub>3</sub> Co compounds	A. Pirogov <sup>1</sup> A. Gubkin <sup>2</sup>	<sup>1</sup> IMP, RU <sup>2</sup> USU, RU E6 <b>PHY-01-1558</b>
61	Metamagnetic transitions in Y <sub>1-x</sub> R <sub>x</sub> Fe <sub>2</sub> D <sub>4.2</sub> compounds (R= Tb)	V. Paul-Boncour <sup>1</sup> A. Hoser <sup>2</sup> N. Stüßer <sup>2</sup>	<sup>1</sup> CNRS, F <sup>2</sup> HZB E6 <b>PHY-01-2235</b>
62	Neutron diffraction studies of the hexagonal TbNi <sub>1-x</sub> AuxIn compounds for 0 < x < 1	B. Penc <sup>1</sup> S. Baran <sup>1</sup> A. Arulraj <sup>2</sup>	<sup>1</sup> JU Krakow, PL <sup>2</sup> HZB E6 <b>PHY-01-2238</b>
63	Investigation of magnetic order induced by magnetic field in the quantum magnet Cu(tn)Cl <sub>2</sub>	A. Orendáčová <sup>1</sup> M. Orendáč <sup>1</sup> A. Buchsteiner <sup>2</sup> K. Siemensmeyer <sup>2</sup>	<sup>1</sup> PJSU, SK <sup>2</sup> HZB E6 <b>PHY-01-2240</b>
64	Neutron Diffraction Studies on RuSr <sub>2</sub> Y <sub>1.5</sub> Ce <sub>0.5</sub> Cu <sub>2</sub> O <sub>10</sub> (Ru-1222) and Ru <sub>0.9</sub> Sr <sub>2</sub> YCu <sub>2.1</sub> O <sub>7.9</sub> (Ru-1212)	R. Nigam <sup>1</sup> A. Pan <sup>1</sup> S. Dou <sup>1</sup> N. Stüßer <sup>2</sup>	<sup>1</sup> Univ. Wollongong, AUS <sup>2</sup> HZB E6 <b>MAT-01-2241</b>
65	Study of the magnetic phase transitions of PrIr <sub>2</sub> Si <sub>2</sub> compound	M. Mihalik <sup>1</sup> N. Stüßer <sup>2</sup>	<sup>1</sup> CU Prague, CZ <sup>2</sup> HZB E6 <b>PHY-01-2396</b>
66	Metamagnetic transitions in Y <sub>0.5</sub> Er <sub>0.5</sub> Fe <sub>2</sub> D <sub>4.2</sub> compound	V. Paul-Boncour <sup>1</sup> A. Hoser <sup>2</sup> N. Stüßer <sup>2</sup>	<sup>1</sup> CNRS, F <sup>2</sup> HZB E6 <b>PHY-01-2397</b>
67	Investigation of frustrated magnetism in the hexagonal TmTX intermetallics (T = Ag, Pt; X = Si, Ge, In)	S. Baran <sup>1</sup> B. Penc <sup>1</sup> A. Arulraj <sup>2</sup>	<sup>1</sup> JU Krakow, PL <sup>2</sup> HZB E6 <b>PHY-01-2400</b>
68	Neutron diffraction studies of tetragonal TmT <sub>2</sub> X <sub>2</sub> intermetallics	B. Penc <sup>1</sup> S. Baran <sup>1</sup> A. Hoser <sup>2</sup> K. Kiefer <sup>2</sup>	<sup>1</sup> JU Krakow, PL <sup>2</sup> HZB E6 <b>PHY-01-2401</b>
69	Low temperature magnetic structures of CePdIn and PrPdIn	J. Czub <sup>1</sup> L. Gondek <sup>2</sup> N. Stüßer <sup>3</sup>	<sup>1</sup> JU Krakow, PL <sup>2</sup> AGH-UST, PL <sup>3</sup> HZB E6 <b>PHY-01-2402</b>
70	Magnetic Phase Transitions in PrMn <sub>2</sub> Ge <sub>2-x</sub> Si <sub>x</sub>	J. L. Wang <sup>1</sup> S. J. Campbell <sup>1</sup> M. Hoffmann <sup>2</sup> N. Stüßer <sup>3</sup> A. Arulraj <sup>3</sup>	<sup>1</sup> UNSW@ADFA, AUS <sup>2</sup> TU München <sup>3</sup> HZB E6 <b>PHY-01-2405</b>
71	Magnetic structure and the magnetoelectrical coupling mechanism in La doped multiferroic BiFeO <sub>3</sub>	J. L. Wang <sup>1</sup> Z. X. Cheng <sup>2</sup> X. L. Wang <sup>2</sup>	<sup>1</sup> UNSW@ADFA, AUS <sup>2</sup> Univ. Wollongong, AUS E6 <b>MAT-01-2406</b>
72	Study of magnetic correlation in the quasi-1-D spin-chain compound Sr <sub>3</sub> NiPtO <sub>6</sub> using neutron	S. M. Yusuf <sup>1</sup> E. V. Sampathkumaran <sup>2</sup> S. Rayaprol <sup>3</sup> A. Jain <sup>4</sup> N. Stüßer <sup>5</sup>	<sup>1</sup> BARC, IND <sup>2</sup> Tata Inst., IND <sup>3</sup> CSR, IND <sup>4</sup> PU Chandigarh, IND <sup>5</sup> HZB E6 <b>PHY-01-2408</b>
73	Determining of the magnetic structure of metastable nanomaterials: CoO würtzite, CoO blende and Ni hcp	G. Salazar-Alvarez <sup>1</sup> A. Lopez-Ortega <sup>1</sup> J. Nogues <sup>1</sup> J. Sort <sup>2</sup> M. Tovar <sup>3</sup> F. Yokaichiya <sup>3</sup>	<sup>1</sup> ICN, E <sup>2</sup> UAB-ICREA, E <sup>3</sup> HZB E9 <b>CHE-01-2194</b>

## List of Contributed Experimental Reports

PAGE	TITLE	TEAM	PROPOSAL
74	<b>Magnetic structure of Li<sub>2</sub>ZrCuO<sub>4</sub></b>	W. Lorenz <sup>1</sup> W.-D. Stein <sup>2</sup> O. Prokhnenko <sup>3</sup>	<sup>1</sup> IFW Dresden <sup>2</sup> TU Dresden <sup>3</sup> HZB E9 <b>PHY-01-2204</b>
75	<b>Phase separation in manganites</b>	N. Vestergaard Jensen <sup>1</sup> S. Kimber <sup>2</sup>	<sup>1</sup> DTU, DK <sup>2</sup> HZB E9 <b>PHY-01-2360</b>
76	<b>Neutron diffraction of mesoporous Mn<sub>3</sub>O<sub>4</sub> and Mn<sub>2</sub>O<sub>3</sub></b>	A. Hill <sup>1</sup> M. Tovar <sup>2</sup> A. Harrison <sup>1+3</sup>	<sup>1</sup> Univ. of Edinburgh, UK <sup>2</sup> HZB <sup>3</sup> ILL, F E9 <b>CHE-01-2367</b>
77	<b>Nuclear and Magnetic structure of the Orbital Ordered Spinel MgV<sub>2</sub>O<sub>4</sub></b>	B. Lake <sup>1</sup> E. Wheeler <sup>1</sup> N. Islam <sup>1</sup> M. Reehuis <sup>1</sup>	<sup>1</sup> HZB E9 <b>PHY-01-2457-EF</b>
78	<b>Time resolved measurements of the VL dynamics in ultra pure bulk Niobium</b>	S. Mühlbauer <sup>1</sup> A. Wiedenmann <sup>2</sup> U. Keiderling <sup>2</sup>	<sup>1</sup> TU München <sup>2</sup> HZB V4 <b>PHY-04-1551</b>
79	<b>Search for the FFLO phase in a heavy-fermion superconductor CeCoIn<sub>5</sub></b>	H. Furukawa <sup>1</sup> S. Kawamura <sup>1</sup> H. Shishido <sup>2</sup> T. Shibauchi <sup>2</sup> Y. Matsuda <sup>2</sup> B. Lake <sup>3</sup>	<sup>1</sup> Ochanomizu Univ., JP <sup>2</sup> Kyoto Univ., JP <sup>3</sup> HZB V4 <b>PHY-04-1572</b>
80	<b>Symmetry breaking vortex lattice structures in ultra pure Niobium</b>	A. Wiedenmann <sup>1</sup> S. Mühlbauer <sup>2</sup> P. Böni <sup>2</sup> C. Pfleiderer <sup>2</sup> E. M. Forgan <sup>3</sup> M. Laver <sup>3</sup> G. Behr <sup>4</sup>	<sup>1</sup> HZB <sup>2</sup> TU München <sup>3</sup> Univ. of Birmingham, UK <sup>4</sup> IFW, Dresden V4 <b>PHY-04-1604</b>
81	<b>The critical dynamics of the weak itinerant ferromagnets Mn<sub>1-y</sub>Fe<sub>y</sub>Si, y = 0.06, 0.08, 0.10</b>	S. Grigoriev <sup>1</sup> V. Dyadkin <sup>1</sup> E. Moskvina <sup>2</sup>	<sup>1</sup> PNPI RAS, Gatchina, RU <sup>2</sup> HZB V5 <b>PHY-03-563</b>
82	<b>The quantum dynamic of the helix structure in Mn<sub>0.87</sub>Fe<sub>0.13</sub>Si</b>	E. Moskvina <sup>1</sup> V. Dyadkin <sup>1</sup> V. Piyadov <sup>1</sup>	<sup>1</sup> PNPI RAS, Gatchina, RU V5 <b>PHY-03-599-LT</b>
83	<b>Antiferromagnetic structure in UNiAl at dilution temperature</b>	K. Prokes <sup>1</sup>	<sup>1</sup> HZB E4 <b>EF</b>

### Magnetic Excitations

84	<b>Spin waves in the single domain magnetic phases of PrB<sub>6</sub></b>	K. A. McEwen <sup>1</sup> M. D. Le <sup>1</sup> K. Rule <sup>2</sup>	<sup>1</sup> UC, London, UK <sup>2</sup> HZB V2 <b>PHY-02-645</b>
85	<b>Magnetic excitations of the geometrically frustrated antiferromagnet CuFeO<sub>2</sub> under magnetic field</b>	F. Ye <sup>1</sup> J. Fernandez-Baca <sup>1</sup> K. Rule <sup>2</sup>	<sup>1</sup> ORNL, USA <sup>2</sup> HZB V2 <b>PHY-02-648</b>
87	<b>Polarisation analysis of the frustrated pyrochlore Tb<sub>2</sub>Ti<sub>2</sub>O<sub>7</sub></b>	K. Rule <sup>1</sup> K. Habicht <sup>1</sup> M. Skoulatos <sup>1</sup> K. Kiefer <sup>1</sup>	<sup>1</sup> HZB V2 <b>PHY-02-652-EF</b>
88	<b>Spin dispersion along the c axis in the diamond chain compound azurite</b>	S. Süllo <sup>1</sup> C. Gibson <sup>2</sup> K. Rule <sup>2</sup>	<sup>1</sup> TU Braunschweig <sup>2</sup> HZB V2 <b>PHY-02-664-DT</b>

## List of Contributed Experimental Reports

PAGE	TITLE	TEAM	PROPOSAL
89	<b>Peculiar Field Response of Antiferromagnetism in non-centrosymmetric superconductor CePt3Si</b>	K. Kaneko <sup>1</sup> O. Stockert <sup>1</sup> K. Habicht <sup>2</sup> M. Skoulatos <sup>2</sup> K. Kiefer <sup>2</sup> S. Gerischer <sup>2</sup>	<sup>1</sup> MPI CPfS Dresden <sup>2</sup> HZB V2 <b>PHY-02-665</b>
90	<b>Approaching the high magnetic field quantum phase transition of CoCl2.2D2O</b>	K. Lefmann <sup>1</sup> J. Larsen <sup>1</sup> S. U. H. Eisenhardt <sup>1</sup> K. Habicht <sup>2</sup> M. Reehuis <sup>2</sup>	<sup>1</sup> Univ. of Copenhagen, DK <sup>2</sup> HZB V2 <b>PHY-02-667</b>
91	<b>Magnetic excitation of XXZ spin model in magnetic field</b>	T. Masuda <sup>1</sup> S. Hondo <sup>1</sup> K. Kaneko <sup>2</sup> K. Rule <sup>3</sup>	<sup>1</sup> Univ. Yakohama City, JP <sup>2</sup> MPI CPfS, Dresden <sup>3</sup> HZB V2 <b>PHY-02-671</b>
92	<b>Field induced ordered phase in a quantum dimer system Ba3Cr2O8</b>	M. Kofu <sup>1</sup> S. H. Lee <sup>1</sup> K. Rule <sup>2</sup> B. Lake <sup>2</sup> S. Gerischer <sup>2</sup>	<sup>1</sup> Univ. of Virginia, USA <sup>2</sup> HZB V2 <b>PHY-02-672</b>
93	<b>Search for Spin-Density Waves in Pb</b>	T. Keller <sup>1</sup> P. Aynajian <sup>1</sup> K. Habicht <sup>2</sup>	<sup>1</sup> MPI-FKF. Stuttgart <sup>2</sup> HZB V2 <b>PHY-02-681-EF</b>
94	<b>Magnetic Excitation Spectrum of the Frustrated Quantum Dimer Antiferromagnet Strontium Chromate</b>	D. L. Quintero Castro <sup>1</sup> B. Lake <sup>1</sup> N. Islam <sup>1</sup> E. Wheeler <sup>1</sup>	<sup>1</sup> HZB V2 <b>PHY-02-682-EF</b>
95	<b>Combined spin- and dimensionality crossover upon magnetic saturation of iron</b>	A. Hoser <sup>1</sup> K. Habicht <sup>1</sup> U. Köbler <sup>2</sup>	<sup>1</sup> HZB <sup>2</sup> FZ, Jülich V2 <b>PHY-02-684-EF</b>
96	<b>Spin excitations in the [V30Mo72] Kagome Molecular Cluster</b>	J. van Slageren <sup>1</sup> T. Guidi <sup>2</sup> B. Lake <sup>2</sup> O. Pieper <sup>2</sup>	<sup>1</sup> Univ. of Nottingham, UK <sup>2</sup> HZB V3 <b>PHY-03-530-EF</b>
97	<b>INS studies of crystal field in RPdIn (R=Ce, Pr, Nd) compounds</b>	L. Gondek <sup>1</sup> Z. Izaola <sup>2</sup> M. Russina <sup>2</sup>	<sup>1</sup> AGH-UST, PL <sup>2</sup> HZB V3 <b>PHY-03-552</b>
98	<b>Determination of crystal field parameters for the intermetallic compound ErCr2Si2</b>	B. Saensunon <sup>1</sup> G. A. Stewart <sup>1</sup> P. C. M. Gubbens <sup>2</sup> M. Russina <sup>3</sup> E. Kemner <sup>3</sup>	<sup>1</sup> UNSW@ADFA, AUS <sup>2</sup> TU Delft, NL <sup>3</sup> HZB V3 <b>MAT-03-553</b>
99	<b>INS studies of crystal field in RPdIn (R=Ce, Nd) compounds</b>	L. Gondek <sup>1</sup> Z. Izaola <sup>2</sup> M. Russina <sup>2</sup> J. Czub <sup>3</sup>	<sup>1</sup> AGH-UST, PL <sup>2</sup> HZB <sup>3</sup> JU Krakow, PL V3 <b>PHY-03-589</b>
100	<b>Spin excitations in the novel two-leg spin-ladder compound BiCu2PO6</b>	M. Skoulatos <sup>1</sup> K. Habicht <sup>1</sup> E. Kemner <sup>1</sup> B. Lake <sup>1</sup> J. Goff <sup>2</sup> C. Geibel <sup>3</sup> R. Nath <sup>3</sup>	<sup>1</sup> HZB <sup>2</sup> Royal Holloway, London, UK <sup>3</sup> MPI-CPfS, Dresden V3 <b>PHY-03-610-EF</b>
101	<b>Spin excitations in LuVO3</b>	M. Skoulatos <sup>1</sup> K. Habicht <sup>1</sup> J. Goff <sup>2</sup> L. D. Tung <sup>3</sup>	<sup>1</sup> HZB <sup>2</sup> Royal Holloway, London, UK <sup>3</sup> Dept. of Physics, Liverpool, UK V2 <b>EF/ Instrument time</b>

## List of Contributed Experimental Reports

PAGE	TITLE	TEAM	PROPOSAL
102	<b>Magnetic Excitation Spectrum of the Frustrated Quantum Dimer Antiferromagnet Strontium Chromate</b>	B. Lake <sup>1</sup> D. L. Quintero Castro <sup>1</sup> E. Wheeler <sup>1</sup> M. Russina <sup>1</sup> N. Islam <sup>1</sup>	<sup>1</sup> HZB V3 EF
<b>Magnetic Thin Films</b>			
103	<b>PNR study of Co/CoO exchange bias system by ion implantation</b>	K. Temst <sup>1</sup> J. Demeter <sup>1</sup> A. Teichert <sup>1+2</sup> R. Steitz <sup>2</sup>	<sup>1</sup> KU Leuven, B <sup>2</sup> HZB V6 PHY-04-1618-LT
104	<b>Probing noncollinear spin structure in oppositely exchange-biased NiFe/FeMn/CoFe trilayers</b>	K.-Y. Kim <sup>1</sup> J. S. Lee <sup>1</sup> H. C. Choi <sup>2</sup> C. Y. You <sup>2</sup> A. Teichert <sup>3</sup> R. Steitz <sup>3</sup>	<sup>1</sup> KAERI, HANARO, KR <sup>2</sup> Inha Univ., KR <sup>3</sup> HZB V6 PHY-04-1704
105	<b>PNR study of epitaxial Co/CoO exchange bias system formed by ion implantation</b>	J. Demeter <sup>1</sup> A. Schrauwen <sup>1</sup> A. Teichert <sup>1+2</sup> R. Steitz <sup>2</sup>	<sup>1</sup> KU Leuven, B <sup>2</sup> HZB V6 PHY-04-1720-LT
106	<b>PNR study of a BiFeO<sub>3</sub> multiferroic film</b>	K. Temst <sup>1</sup> M. J. van Bael <sup>1</sup> J. Demeter <sup>1</sup> A. Teichert <sup>1+2</sup> R. Steitz <sup>2</sup>	<sup>1</sup> KU Leuven, B <sup>2</sup> HZB V6 PHY-04-1721-LT
107	<b>Influence of bias voltage on structure and reflectivity of Si/Fe multilayers</b>	A. Teichert <sup>1+2</sup> R. Steitz <sup>2</sup> T. Krist <sup>2</sup> J. E. Hoffmann <sup>2</sup>	<sup>1</sup> KU Leuven, B <sup>2</sup> HZB V6 PHY-04-1722-LT
<b>Structure</b>			
<b>Chemical Structure</b>			
111	<b>Structure of (PbFe<sub>2</sub>/3W<sub>1</sub>/3O<sub>3</sub>)<sub>1-x</sub>-(PbTiO<sub>3</sub>)<sub>x</sub> solid solutions</b>	A. Naberezhnov <sup>1</sup> J. U. Hoffmann <sup>2</sup>	<sup>1</sup> RAS Ioffe PTI, RU <sup>2</sup> HZB E2 MAT-01-2033
112	<b>Neutron scattering study on rattling in filled skutterudite compounds</b>	K. Kaneko <sup>1</sup> A. Hoser <sup>2</sup>	<sup>1</sup> MPI CPfS Dresden <sup>2</sup> HZB E2 PHY-01-2343
113	<b>2<sup>nd</sup> to 3<sup>rd</sup> cross over in CFTD</b>	T. Fennell <sup>1</sup> A. Hoser <sup>2</sup>	<sup>1</sup> ILL, F <sup>2</sup> HZB E2 PHY-01-2348
114	<b>Crystal structure of UIrGe</b>	K. Prokes <sup>1</sup> M. Reehuis <sup>1</sup>	<sup>1</sup> HZB E5 PHY-01-2184-EF
115	<b>Crystal structure of YFe<sub>0.13</sub>Mn<sub>1.87</sub>O<sub>5</sub></b>	N. Aliouane <sup>1</sup> D. Argyriou <sup>1</sup> A. Malyuk <sup>1</sup> M. Reehuis <sup>1+2</sup>	<sup>1</sup> HZB <sup>2</sup> MPI Stuttgart E5 PHY-01-2287-EF
116	<b>Crystal structure of MgV<sub>2</sub>O<sub>4</sub></b>	B. Lake <sup>1</sup> E. Wheeler <sup>1</sup> N. Islam <sup>1</sup> M. Reehuis <sup>1</sup>	<sup>1</sup> HZB E5 PHY-01-2459-EF

## List of Contributed Experimental Reports

PAGE	TITLE	TEAM	PROPOSAL
117	Phase transitions of the spinel $MgV_2O_4$	B. Lake <sup>1</sup> E. Wheeler <sup>1</sup> N. Islam <sup>1</sup> M. Reehuis <sup>1</sup> H. J. Bleif <sup>1</sup>	<sup>1</sup> HZB E5 <b>PHY-01-2459-EF</b>
118	Crystal structure, vacancy order and cation distribution in $CuGaSe_2$ -related semiconductors	S. Lehmann <sup>1</sup> M. Tovar <sup>1</sup> D. Fuertes-Marrón <sup>2</sup>	<sup>1</sup> HZB <sup>2</sup> ETSIT, E E9 <b>MAT-01-1858/ MAT-01-1953</b>
119	Crystal structure of the $CuIn_3Se_5$ - $CuGa_3Se_5$ solid solution series	J. Friedrich <sup>1</sup> J. M. Merino <sup>1</sup> M. León <sup>1</sup> S. Schorr <sup>2</sup> M. Tovar <sup>3</sup> S. Lehmann <sup>3</sup>	<sup>1</sup> UA, Madrid, E <sup>2</sup> FU Berlin <sup>3</sup> HZB E9 <b>PHY-01-2201</b>
120	Neutron Diffraction of “real” $Cu/ZnO/Al_2O_3$ Catalysts for Methanol Synthesis	A. Furche <sup>1</sup> M. Behrens <sup>1</sup> S. Kühl <sup>1</sup> M. Tovar <sup>2</sup> D. Wallacher <sup>2</sup>	<sup>1</sup> FHI, Berlin <sup>2</sup> HZB E9 <b>CHE-01-2202</b>
121	Proton Mobility in Solid Super Proton Conductors	C. A. C. Dreismann <sup>1</sup> M. Lerch <sup>1</sup> T. Abdul-Redah <sup>1</sup> M. Tovar <sup>2</sup> S. Kimber <sup>2</sup> F. Yokaichiya <sup>2</sup>	<sup>1</sup> TU Berlin <sup>2</sup> HZB E9 <b>CHE-01-2203</b>
122	In situ Neutron Powder Diffraction Study of $CD_4$ Adsorption in $Cu_3(1,3,5\text{-benzenetricarboxylate})_2$	S. Kaskel <sup>1</sup> M. Tovar <sup>2</sup> D. Wallacher <sup>2</sup>	<sup>1</sup> TU Dresden <sup>2</sup> HZB E9 <b>CHE-01-2205</b>
123	Structural and order-disorder effects of water uptake in proton conducting perovskites	N. Jalarvo <sup>1</sup> T. Norby <sup>1</sup> N. Aliouane <sup>2</sup> D. Wallacher <sup>3</sup>	<sup>1</sup> FERMIO, NO <sup>2</sup> IFE, NO <sup>3</sup> HZB E9 <b>CHE-01-2211</b>
124	High-resolution neutron diffraction study on the phase transitions in $Cu_{1-x}Zn_xFe_2O_4$	W. Nowicki <sup>1</sup> F. Yokaichiya <sup>2</sup>	<sup>1</sup> AMU Poznan, PL <sup>2</sup> HZB E9 <b>MAT-01-2213</b>
125	Crystal structure phase transition in $Bi_{1-x}R_xFeO_3$ (R=La,Nd)	M. Kopcewicz <sup>1</sup> D. Karpinsky <sup>2</sup>	<sup>1</sup> IEMT, PL <sup>2</sup> JISSSP, NAS, BY E9 <b>PHY-01-2216</b>
126	In-situ Neutron Diffraction Investigation of Methanol Synthesis over $Cu/ZnO/Al_2O_3$ Catalysts	M. Behrens <sup>1</sup> R. Naumann <sup>1</sup> S. Kißner <sup>1</sup> S. Kühl <sup>1</sup> M. Tovar <sup>2</sup> D. Wallacher <sup>2</sup>	<sup>1</sup> FHI Berlin <sup>2</sup> HZB E9 <b>CHE-01-2357</b>
127	Investigation of $MoVTeNb$ oxide catalysts for selective oxidation of propane	A. Trunschke <sup>1</sup> R. Naumann <sup>1</sup> Y. Kolen'ko <sup>1</sup> F. Girgsdies <sup>1</sup> M. Behrens <sup>1</sup> M. Tovar <sup>2</sup>	<sup>1</sup> FHI Berlin <sup>2</sup> HZB E9 <b>CHE-01-2358</b>
128	Neutron diffraction study of ultramarine-type pigments	E. Climent-Pascual <sup>1</sup> J. Hernandez-Velasco <sup>2</sup> A. Hoser <sup>3</sup>	<sup>1</sup> UC, Madrid, E <sup>2</sup> CSIC, Madrid, E <sup>3</sup> HZB E9 <b>CHE-01-2363</b>
129	Structure of $NaMgAl(oxalate)_3 \cdot 9H_2O$ – an Extraordinary Spectral Hole-Burning Host	H. Riesen <sup>1</sup> S. J. Campbell <sup>1</sup> D. Kearley <sup>2</sup> F. Yokaichiya <sup>3</sup> M. Tovar <sup>3</sup>	<sup>1</sup> UNSW@ADFA, AU <sup>2</sup> ANSTO, AU <sup>3</sup> HZB E9 <b>PHY-01-2377</b>

## List of Contributed Experimental Reports

PAGE	TITLE	TEAM	PROPOSAL
130	Determination of the site occupancy fractions of the Ti <sub>2</sub> AlNb-based intermetallics by NS	B. Wu <sup>1</sup> Q. Li <sup>1</sup> F. Yokaichiya <sup>2</sup> M. Tovar <sup>2</sup>	<sup>1</sup> Fuzhou Univ. CN <sup>2</sup> HZB E9 <b>MAT-01-2378</b>
131	Evidence for the formation of cross-linked chloroperoxidase in mesopores	M. Hartmann <sup>1</sup> D. Jung <sup>1</sup> M. Paradiso <sup>1</sup> D. Wallacher <sup>2</sup> A. Brandt <sup>2</sup>	<sup>1</sup> Uni Augsburg <sup>2</sup> HZB V4 <b>CHE-04-1549</b>
132	CaFe <sub>2</sub> As <sub>2</sub> under hydrostatic pressure	D. Argyriou <sup>1</sup> K. Prokes <sup>1</sup> S. Kimber <sup>1</sup> A. Goldman <sup>2</sup>	<sup>1</sup> HZB <sup>2</sup> Ames Lab, ISU, USA E4 <b>EF</b>

### Structural Excitations

133	Inelastic Neutron Scattering from hydrogen clathrate-hydrates	M. Russina <sup>1</sup> E. Kemner <sup>1</sup> L. Ulivi <sup>2</sup> M. Celli <sup>2</sup>	<sup>1</sup> HZB <sup>2</sup> CNR, IT V3 <b>PHY-03-483-EF</b>
134	QENS study of diffusion in Cu-Se superionic conductor	S. Danilkin <sup>1</sup> C. Ling <sup>2</sup> R. Macquart <sup>2</sup> M. Russina <sup>3</sup> Z. Izaola <sup>3</sup>	<sup>1</sup> ANSTO, AU <sup>2</sup> Univ. of Sydney, AU <sup>3</sup> HZB V3 <b>PHY-03-554</b>
135	Hydrogen dynamics in complex proton conducting perovskites	N. Jalarvo <sup>1</sup> D. Wallacher <sup>2</sup>	<sup>1</sup> FERMIO, NO <sup>2</sup> HZB V3 <b>PHY-03-588</b>
136	Distinct Dynamic Behaviour of Water Molecules in Hydrated Pores	N. Pérez-Hernández <sup>1</sup> D. Fort <sup>1</sup> J. Eckert <sup>2</sup> N. Tsapatsaris <sup>3</sup>	<sup>1</sup> CSIC Sevilla, E <sup>2</sup> UOC, USA <sup>3</sup> HZB V3 <b>CHE-03-596</b>
137	Phason Dynamics in the Icosahedral Quasicrystal i-AlCuFe	R. Brand <sup>1</sup> C. Pappas <sup>2</sup> P. Bentley <sup>2</sup>	<sup>1</sup> Uni Duisburg-Essen <sup>2</sup> HZB V5 <b>PHY-03-526</b>
138	Phason Dynamics in the Icosahedral Quasicrystal i-AlCuFe	R. Brand <sup>1</sup> C. Pappas <sup>2</sup> E. Moskvina <sup>2</sup>	<sup>1</sup> Uni Duisburg-Essen <sup>2</sup> HZB V5 <b>PHY-03-600</b>
139	Spectral Hole-Burning – Neutron Spin-Echo Studies of Water Flips in NaMgAl(oxalate) <sub>3</sub> ·9H <sub>2</sub> O	H. Riesen <sup>1</sup> S. J. Campbell <sup>1</sup> D. Kearley <sup>2</sup> C. Pappas <sup>3</sup> S. Wellert <sup>3</sup>	<sup>1</sup> UNSW@ADFA, AU <sup>2</sup> ANSTO, AU <sup>3</sup> HZB V5 <b>PHY-03-605</b>

### Geology

140	Cation partitioning in Zn(AlFe) <sub>2</sub> O <sub>4</sub> spinels as a function of temperature, by neutron powder diffraction	A. Pavese <sup>1</sup> E. Ferrari <sup>1</sup> N. Marinoni <sup>1</sup> A. Hoser <sup>2</sup>	<sup>1</sup> Univ. Milano, IT <sup>2</sup> HZB E2 <b>GEO-01-2035</b>
141	Investigation of the Al/Si distribution in sanidine	S. Schorr <sup>1</sup> A. Hoser <sup>2</sup>	<sup>1</sup> FU Berlin <sup>2</sup> HZB E2 <b>GEO-01-2340</b>
142	Hydrogen bonds evaluation in the crystal structure of mineral catapleiite	O. Karimova M. Reehuis <sup>2</sup>	<sup>1</sup> RAS IGEM Moscow, RU <sup>2</sup> HZB E5 <b>CHE-01-2244</b>
143	Hydration of Sm <sup>3+</sup> , Ni <sup>2+</sup> and Na <sup>+</sup> in Clay Interlayer: Quasielastic Neutron Study	O. Sobolev <sup>1</sup> L. Charlet <sup>1</sup> C. J. Cuello <sup>2</sup>	<sup>1</sup> Univ. Grenoble, LGIT, F <sup>2</sup> ILL, F V3 <b>GEO-03-0547</b>

## List of Contributed Experimental Reports

PAGE	TITLE	TEAM	PROPOSAL
<b>Biology &amp; Soft Matter</b>			
<b>Biology</b>			
147	Determination of the crystal structure of L and DL-Serine under pressure	H. Nunes Bordallo <sup>1</sup> A. Buchsteiner <sup>1</sup> W. Kalceff <sup>2</sup> E. V. Boldyreva <sup>3</sup>	<sup>1</sup> HZB <sup>2</sup> UTS, Sydney, AU <sup>3</sup> NSU, Novosibirsk, RU E6 <b>BIO-01-2294-EF</b>
148	Structural Anomalies in Valine	H. Nunes Bordallo <sup>1</sup> D. Argyriou <sup>1</sup>	<sup>1</sup> HZB E9 <b>BIO-01-1822-EF</b>
149	Structural Organization of Photosystem II Membranes of Green Plants	J. Pieper <sup>1</sup> M. Weiß <sup>1</sup> G. Renger <sup>1</sup> T. Hauß <sup>2</sup> S. Dante <sup>2</sup>	<sup>1</sup> TU Berlin <sup>2</sup> HZB V1 <b>BIO-01-2247</b>
150	Role of ceramide [AP] and ceramide [EOS] in the structural assembly of stratum corneum model membrane	A. Schröter <sup>1</sup> T. Engelbrecht <sup>1</sup> R. Neubert <sup>1</sup> T. Hauß <sup>2</sup>	<sup>1</sup> MLU Halle (Saale) <sup>2</sup> HZB V1 <b>BIO-01-2249</b>
151	Membrane Interactions of an Anthelmintic Drug	J. Bradshaw <sup>1</sup> F. Sa'adedin <sup>1</sup> L. Ke <sup>1</sup> T. Hauß <sup>2</sup>	<sup>1</sup> Univ. of Edinburgh, UK <sup>2</sup> HZB V1 <b>BIO-01-2251</b>
152	Mixed POPN bilayers for the confinement of ss-DNA	D. Berti <sup>1</sup> S. Milani <sup>1</sup> S. Dante <sup>2+3</sup> T. Hauß <sup>2</sup>	<sup>1</sup> Univ of Florence CSGI, IT <sup>2</sup> HZB <sup>3</sup> ITT Genova, IT V1 <b>BIO-01-2253</b>
153	Diffraction by magnetically aligned lamellar aggregates of LHCII	G. Garab <sup>1</sup> G. Nagy <sup>2</sup> T. Hauß <sup>3</sup>	<sup>1</sup> BRC, Szeged, HU <sup>2</sup> ILL, F <sup>3</sup> HZB V1 <b>BIO-01-2254</b>
154	Nanostructures and hydration of phospholipids/lysopholipids multilamellar membrane	E. Ermakova <sup>1</sup> M. A. Kiselev <sup>1</sup> S. Dante <sup>2</sup> T. Hauß <sup>2</sup>	<sup>1</sup> JINR Dubna, RU <sup>2</sup> HZB V1 <b>BIO-01-2255</b>
155	Amyloid aggregates in lipid membranes	R. Ranieri <sup>1</sup> A. Relini <sup>1</sup> T. Hauß <sup>2</sup>	<sup>1</sup> Univ. of Genova, IT <sup>2</sup> HZB V1 <b>BIO-01-2420</b>
156	Moving towards the understanding of each functional group in proteins	E. Boldyreva <sup>1</sup> B. Kolesov <sup>2</sup> H. Nunes Bordallo <sup>3</sup> E. Kemner <sup>3</sup>	<sup>1</sup> NSU, Novosibirsk, RU <sup>2</sup> RAS SB, Novosibirsk, RU <sup>3</sup> HZB V3 <b>BIO-03-557</b>
157	Investigation of the hydration water and internal dynamics of biocompatible and not biocompatible polymer	D. Russo <sup>1</sup> A. De Francesco <sup>1</sup> M. Russina <sup>2</sup>	<sup>1</sup> ILL – INFM - OGG, F <sup>2</sup> HZB V3 <b>BIO-03-582</b>
158	Concentration fluctuations and microdomain formation in lipid membranes	R. Winter <sup>1</sup> K. Czeslik <sup>1</sup> C. Jeworrek <sup>1</sup> K. Vogtt <sup>2</sup>	<sup>1</sup> TU Dortmund <sup>2</sup> HZB V4 <b>CHE-04-1635-EF</b>
159	Influence of Temperature and Co-solvents on the Large Scale Structure of $\beta$ -Lactoglobulin	M. C. Bellissent-Funel <sup>1</sup> K. Vogtt <sup>1</sup>	<sup>1</sup> HZB V4 <b>BIO-04-1710-EF</b>
160	Contrast Matched SANS on Small Unilamellar Vesicles : The Lateral Distribution of Lipid Rafts	K. Vogtt <sup>1</sup> C. Jeworrek <sup>2</sup>	<sup>1</sup> HZB <sup>2</sup> TU Dortmund V4 <b>BIO-04-1711-EF</b>
161	3-dimensional water flow imaging using cold neutron CT and D2O tracer – Studies on rose bent-neck	U. Matsushima <sup>1</sup> W. Graf <sup>2</sup> N. Kardjilov <sup>3</sup> W. Herppich <sup>4</sup>	<sup>1</sup> Iwate Univ., JP <sup>2</sup> HU, Berlin <sup>3</sup> HZB <sup>4</sup> ATB Potsdam V7 <b>BIO-04-1498</b>

## List of Contributed Experimental Reports

PAGE	TITLE	TEAM	PROPOSAL	
162	Neutron tomography of wet teeth	P. Zaslansky <sup>1</sup> N. Kardjilov <sup>2</sup>	<sup>1</sup> MPI, Potsdam <sup>2</sup> HZB	V7 BIO-04-1533-EF
163	In-situ observation of pressure induced phase changes in cellular food materials	O. Schlüter <sup>1</sup> S. Boguslawski <sup>2</sup> N. Kardjilov <sup>3</sup>	<sup>1</sup> ATB, Potsdam <sup>2</sup> TU, Berlin <sup>3</sup> HZB	V7 BIO-04-1586
164	Role of water in human teeth: neutron tomography of in-situ dehydration and rehydration	P. Zaslansky <sup>1</sup> N. Kardjilov <sup>2</sup> A. Hilger <sup>2</sup>	<sup>1</sup> MPI, Potsdam <sup>2</sup> HZB	V7 BIO-04-1587
165	Kinetics of hemolysis of red blood cells $\alpha$ -hemolysin studied by very small angle neutron scattering	C. Garvey <sup>1</sup> P. Kuchel <sup>2</sup> P. Walter <sup>3</sup> M. Strobl <sup>3</sup>	<sup>1</sup> ANSTO, AU <sup>2</sup> Univ. of Sydney, AU <sup>3</sup> HZB	V12a BIO-04-1581
<b>Soft Matter</b>				
166	Structure and Dynamics of Mesoporous Materials	B. Klösgen <sup>1</sup> N. V. Reichhardt <sup>2</sup> A. Carnerup <sup>2</sup> T. Hauß <sup>3</sup>	<sup>1</sup> Univ. Odense, DK <sup>2</sup> Univ. Lund, S <sup>3</sup> HZB	V1 PHY-01-2250
167	Characterization of mixed fluorocarbon and hydrocarbon surfactant crystals	M. Gradzielski <sup>1</sup> K. Bressel <sup>1</sup> S. Prévost <sup>2</sup>	<sup>1</sup> TU, Berlin <sup>2</sup> HZB	V1 CHE-01-2412
168	Structural anomalies in strongly supercooled confined water	O. Paris <sup>1</sup> M. Erko <sup>1</sup> D. Wallacher <sup>2</sup> T. Hauß <sup>2</sup>	<sup>1</sup> MPI, Potsdam <sup>2</sup> HZB	V1 PHY-01-2418
169	Dynamics of confined water in polysaccharide gels of pharmaceutical interest	A. Deriu <sup>1</sup> C. Chiapponi <sup>1</sup> I. Finelli <sup>2</sup> G. Paradossi <sup>2</sup>	<sup>1</sup> Univ. of Parma <sup>2</sup> Univ. of Rome	V3 BIO-03-551
170	Effects of cation asymmetry in the dynamics of two room temperature ionic liquids	M. L. Saboungi <sup>1</sup> D. Price <sup>1</sup> M. A. Gonzalez <sup>2</sup> Z. Izaola <sup>3</sup> M. Russina <sup>3</sup>	<sup>1</sup> CNRS, Orleans, F <sup>2</sup> ILL, Grenoble, F <sup>3</sup> HZB	V3 MAT-03-583
171	Proton Motions in Water-Saturated Plasma-Produced Membranes	V. Peterson <sup>1</sup> G. Kearley <sup>1</sup> C. Corr <sup>2</sup> Z. Izaola <sup>3</sup>	<sup>1</sup> ANSTO, AU <sup>2</sup> ANU Canberra, AU <sup>3</sup> HZB	V3 CHE-03-591
172	Conformational characteristics of PHA in solution	R. Russell <sup>1</sup> S. Yun <sup>1</sup>	<sup>1</sup> ANSTO, AU	V4 BIO-04-1391
173	Desorption study mechanism in hierarchical mesoporous silica followed by C5F12 in-situ SANS	B. Smarsly <sup>1</sup> S. Mascotto <sup>1</sup> D. Wallacher <sup>2</sup> A. Brandt <sup>2</sup>	<sup>1</sup> Uni Gießen <sup>2</sup> HZB	V4 PHY-04-1459
174	Surface Aggregate structure of a Binary Surfactant Mixture on Colloidal Silicas	D. Lugo <sup>1</sup> G. H. Findenegg <sup>1</sup> S. Prévost <sup>2</sup>	<sup>1</sup> TU Berlin <sup>2</sup> HZB	V4 CHE-04-1546
175	The Role of the Water Shell and Counterion Distribution around Charged Proteins Studied by SANS	F. Schreiber <sup>1</sup> F. Zhang <sup>1</sup> L. Ianeselli <sup>1</sup> R. Martin <sup>2</sup> S. Prévost <sup>3</sup>	<sup>1</sup> Uni Tübingen <sup>2</sup> Univ. of Kent, UK <sup>3</sup> HZB	V4 PHY-04-1556
176	Structural investigation of phospholipid/polysaccharide nanocapsules	Y. Gerelli <sup>1</sup> A. Deriu <sup>1</sup> S. Barberi <sup>1</sup> D. Clemens <sup>2</sup>	<sup>1</sup> Univ. of Parma <sup>2</sup> HZB	V4 BIO-04-1568

## List of Contributed Experimental Reports

PAGE	TITLE	TEAM	PROPOSAL
177	Phase behaviour mixtures of anionic perfluoro surfactants and nonionic TDMAO	M. Gradzielski <sup>1</sup> K. Bressel <sup>1</sup> S. Prévost <sup>2</sup>	<sup>1</sup> TU, Berlin <sup>2</sup> HZB V4 <b>CHE-04-1610-EF</b>
178	Temperature-induced microemulsion-to-vesicle transition followed by SANS	M. Gradzielski <sup>1</sup> A. Barth <sup>1</sup> S. Prévost <sup>1+2</sup>	<sup>1</sup> TU, Berlin <sup>2</sup> HZB V4 <b>CHE-04-1610EF</b>
179	Scaling-behaviour of PNIPAM microgels with different crosslinker densities	Matthias Karg <sup>1</sup> A. Brandt <sup>2</sup> D. Wallacher <sup>2</sup> S. Prévost <sup>2</sup>	<sup>1</sup> TU Berlin <sup>2</sup> HZB V4 <b>CHE-04-1642</b>
180	Study of the supramolecular structure of $\mu$ E used as host medium for lanthanide ion separation	P. Bauduin <sup>1</sup> C. Bauer <sup>1</sup>	<sup>1</sup> ICSM CEA, F V4 <b>CHE-04-1660</b>
181	Effects on the block copolymer self-assembling in water of block selective cyclodextrin addition	S. Milioto <sup>1</sup> G. Lazzara <sup>1</sup> M. Gradzielski <sup>2</sup> S. Prévost <sup>2+3</sup>	<sup>1</sup> Univ. of Palermo, IT <sup>2</sup> TU, Berlin <sup>3</sup> HZB V4 <b>CHE-04-1667</b>
182	Nanocomposites based on clay nanoparticles and block copolymer	S. Milioto <sup>1</sup> G. Lazzara <sup>1</sup> M. Gradzielski <sup>2</sup> S. Prévost <sup>2+3</sup>	<sup>1</sup> Univ. of Palermo, IT <sup>2</sup> TU, Berlin <sup>3</sup> HZB V4 <b>CHE-04-1667</b>
183	Micellar-Size effect on the Catalytic Hydrogenation of Dimethyl Itaconate in TX-100 Microemulsions	M. Gradzielski <sup>1</sup> J. Milano <sup>1</sup> R. Schomäcker <sup>1</sup> S. Prévost <sup>2</sup>	<sup>1</sup> TU, Berlin <sup>2</sup> HZB V4 <b>MAT-04-1714-LT</b>
184	Structural relaxation in the ultra fragile glass former Decalin	S. Eibl <sup>1</sup> M. Plazanet <sup>1</sup> C. Pappas <sup>2</sup> E. Moskvin <sup>2</sup>	<sup>1</sup> ILL, F <sup>2</sup> HZB V5 <b>PHY-03-561</b>
185	Fast structural relaxation in the ultra fragile glass former Decalin	S. Eibl <sup>1</sup> S. Wellert <sup>2</sup> C. Pappas <sup>2</sup> E. Moskvin <sup>2</sup>	<sup>1</sup> ILL, F <sup>2</sup> HZB V5 <b>PHY-03-601</b>
186	Effects of cation asymmetry in the dynamics of two room temperature ionic liquids	M. L. Saboungi <sup>1</sup> B. Aoun <sup>1+2</sup> M. A. Gonzalez <sup>2</sup> S. Wellert <sup>3</sup> C. Pappas <sup>3</sup>	<sup>1</sup> CNRS, F <sup>2</sup> ILL, F <sup>3</sup> HZB V5 <b>MAT-03-603</b>
187	Asymmetric lipid bilayer sandwiched in polyelectrolyte multilayer films by layer-by-layer assembly	R. Köhler <sup>1</sup> J. Chen <sup>2</sup> R. Krastev <sup>3</sup>	<sup>1</sup> HU, Berlin <sup>2</sup> MPI, Potsdam <sup>3</sup> NMI, Reutlingen V6 <b>PHY-04-1531-EF</b>
188	Polyelectrolyte based nanocomposites	R. Köhler <sup>1+2</sup> M. Kolasinska <sup>2</sup> R. Krastev <sup>3</sup>	<sup>1</sup> HZB <sup>2</sup> MPI, Potsdam <sup>3</sup> NMI, Reutlingen V6 <b>PHY-04-1531-EF</b>
189	Water content of polyelectrolyte multilayers: Influence of type of degree of polymer charge and ion specific effects	S. Doodoo <sup>1</sup> R. v. Klitzing <sup>1</sup> R. Steitz <sup>2</sup>	<sup>1</sup> TU, Berlin <sup>2</sup> HZB V6 <b>CHE-04-1594</b>
190	In-situ – SRSANS investigations of gas condensation in mesoporous metaloxide thin films	B. Smarsly <sup>1</sup> S. Mascotto <sup>1</sup> D. Wallacher <sup>2</sup> R. Steitz <sup>2</sup>	<sup>1</sup> Uni Gießen <sup>2</sup> HZB V6 <b>PHY-04-1596</b>
191	Immobile Light Water and Proton-Deuterium Exchange in Polyelectrolyte Multilayers	C. A. Helm <sup>1</sup> O. Ivanova <sup>1</sup> O. Soltwedel <sup>1</sup> M. Gopinadhan <sup>1</sup> R. Steitz <sup>2</sup>	<sup>1</sup> EMAU, Greifswald <sup>2</sup> HZB V6 <b>PHY-04-1597</b>
192	Critical and multilayer adsorption from alkane + perfluoroalkane mixtures to chemically modified and bare silicone substrates	A. Zarbakhsh <sup>1</sup> J. Webster <sup>2</sup> A. Teicher <sup>3</sup>	<sup>1</sup> QM UCL, UK <sup>2</sup> RAL, ISIS, UK <sup>3</sup> HZB V6 <b>PHY-04-1601</b>

## List of Contributed Experimental Reports

PAGE	TITLE	TEAM	PROPOSAL	
193	<b>The solid-liquid interface of sheared micellar solutions</b>	R. Steitz <sup>1</sup> M. Wolff <sup>2</sup> P. Gutfreund <sup>2</sup> S. Gerth <sup>3</sup>	<sup>1</sup> HZB <sup>2</sup> Uni Ruhr, Bochum <sup>3</sup> Uni Erlangen	V6 <b>PHY-04-1617-EF</b>
194	<b>Influence of thermal treatment on thin polyelectrolyte multilayers of varying charge density</b>	R. Köhler <sup>1</sup> I. Dönch <sup>2</sup> R. Krastev <sup>2</sup> A. Laschewsky <sup>3</sup> A. Fery <sup>4</sup>	<sup>1</sup> HZB <sup>2</sup> MPI, Potsdam <sup>3</sup> IAP, Potsdam <sup>4</sup> Uni Bayreuth	V6 <b>PHY-04-1622</b>
195	<b>Water content of polyelectrolyte multilayers: Influence of type of degree of polymer charge and ion specific effects</b>	S. Doodoo <sup>1</sup> R. v. Klitzing <sup>1</sup> R. Steitz <sup>2</sup>	<sup>1</sup> TU, Berlin <sup>2</sup> HZB	V6 <b>PHY-04-1698</b>
196	<b>Hofmeister effects on the structure of protein adsorbates</b>	C. Czeslik <sup>1</sup> F. Evers <sup>1</sup> M. Tolan <sup>1</sup> R. Steitz <sup>2</sup> R. Köhler <sup>2</sup>	<sup>1</sup> TU Dortmund <sup>2</sup> HZB	V6 <b>CHE-04-1699</b>
197	<b>Water at a Hydrophobic Substrate and the Effect of Pressure, continued</b>	R. Steitz <sup>1</sup> M. Kreuzer <sup>2</sup> R. Dahint <sup>2</sup>	<sup>1</sup> HZB <sup>2</sup> RKU Heidelberg	V6 <b>PHY-04-1718-EF</b>
198	<b>Determination of kinetics of structural growth in coagulating milk</b>	L. F. van Heijkamp <sup>1</sup> P. Walter <sup>2</sup> M. Strobl <sup>2</sup> S. O. Seidel <sup>2</sup> R. Monka <sup>2</sup>	<sup>1</sup> Univ. of Delft, B <sup>2</sup> HZB	V12a <b>PHY-04-1678</b>
199	<b>USANS of magnetite sphere suspensions in ferrofluids</b>	A. G. Wagh <sup>1</sup> S. Abbas <sup>1</sup> S. O. Seidel <sup>2</sup> R. Monka <sup>2</sup> W. Treimer <sup>3</sup>	<sup>1</sup> BARC, IND <sup>2</sup> TFH, Berlin <sup>3</sup> HZB	V12a <b>PHY-04-1679</b>

### *Material Science*

#### **Structure and Phases**

203	<b>Hydration kinetics of cement with PCE superplasticizers</b>	G. Kloess <sup>1</sup> M. Ende <sup>1</sup> A. König <sup>1</sup> S. Schorr <sup>2</sup> J. U. Hoffmann <sup>3</sup> A. Hoser <sup>3</sup>	<sup>1</sup> Uni Leipzig <sup>2</sup> FU Berlin <sup>3</sup> HZB	E2 <b>MAT-01-2027</b>
204	<b>In-situ neutron diffraction studies of complex aluminium hydride material at high deuterium pressure</b>	C. Weidenthaler <sup>1</sup> A. Pommerin <sup>1</sup> W. Schmidt <sup>1</sup> M. Felderhoff <sup>1</sup> A. Buchsteiner <sup>2</sup> D. Wallacher <sup>2</sup>	<sup>1</sup> MPI, Mülheim <sup>2</sup> HZB	E6 <b>MAT-01-2233</b>
205	<b>On the synthesis of LiBD4 via AIB2</b>	A. Remhof <sup>1</sup> F. Buchter <sup>1</sup> O. Friederichs <sup>1</sup> D. Wallacher <sup>2</sup>	<sup>1</sup> EMPA, CH <sup>2</sup> HZB	E6 <b>MAT-01-2234</b>
206	<b>Study of hydrogen storage in metal doped carbon by neutron diffraction</b>	T. Steriotis <sup>1</sup> G. Charalambopoulou <sup>1</sup> J. Hernandez-Velasco <sup>2</sup> D. Wallacher <sup>3</sup>	<sup>1</sup> NCSR Demokritos, GR <sup>2</sup> ICM, Madrid, E <sup>3</sup> HZB	E6 <b>CHE-01-2236</b>

## List of Contributed Experimental Reports

PAGE	TITLE	TEAM	PROPOSAL
207	On the cycling behaviour of LiBD4	A. Remhof <sup>1</sup> J. W. Kim <sup>1</sup> O. Friederichs <sup>1</sup> D. Wallacher <sup>2</sup>	<sup>1</sup> EMPA, CH <sup>2</sup> HZB E6 <b>MAT-01-2395</b>
208	Effect of restricted geometry on stability of ferroelectric phase in confined KNO3 and NaNO2	A. Naberezhnov <sup>1</sup> E. Resjakiewicz-Pasek <sup>2</sup>	<sup>1</sup> RAS Ioffe PTI, RU <sup>2</sup> Univ. of Wroclaw, PL E9 <b>MAT-01-2117</b>
209	Phase transition on shape memory NiTi wires	M. Tovar <sup>1</sup>	<sup>1</sup> HZB E9 <b>MAT-01-2314-EF</b>
210	Investigation of phase transitions of 4 mol% yttria stabilized zirconia using neutron scattering	V. Ryukhtin <sup>1+3</sup> R. Ochrombel <sup>2</sup> S. Bilge <sup>2</sup> O. Prokhenko <sup>3</sup> A. Wiedemann <sup>3</sup>	<sup>1</sup> TU Berlin <sup>2</sup> DRL, Köln <sup>3</sup> HZB E9 <b>MAT-01-2318</b>
211	Investigation of the structural changes of the crystalline metal organic framework (MOFs) MIL-88B up	R. Köhn <sup>1</sup> C. Scherb <sup>1</sup> F. Yokaichiya <sup>2</sup> D. Wallacher <sup>2</sup>	<sup>1</sup> LMU, München <sup>2</sup> HZB E9 <b>MAT-01-2359</b>
212	Neutron Diffraction Studies of Polymer/Clay Nanocomposites	F. K. Katsaros <sup>1</sup> T. Steriotis <sup>1</sup> A. A. Sapalidis <sup>1</sup> E. P. Favvas <sup>1</sup>	<sup>1</sup> NCSR Demokritos, GR V1 <b>MAT-01-2252</b>
213	Analysis of sorption strains in SBA-15 by in-situ neutron diffraction using zero contrast water	O. Paris <sup>1</sup> J. Prass <sup>1</sup> D. Wallacher <sup>2</sup> A. Brandt <sup>2</sup> S. Dante <sup>2</sup>	<sup>1</sup> MPI, Potsdam <sup>2</sup> HZB V1 <b>PHY-01-2317-EF</b>
214	Functional groups and pore geometry in proton-conducting mesoporous SO3H-MCM-41	M. Wark <sup>1</sup> R. Marshall <sup>1</sup> D. Wallacher <sup>2</sup> T. Hauß <sup>2</sup>	<sup>1</sup> Uni Leibniz, Hannover <sup>2</sup> HZB V1 <b>MAT-01-2417</b>
215	Understanding the Water Transport between the Gel and Capillary Pores in cement pastes	L. Alridge <sup>1</sup> H. Bordallo-Nunes <sup>2</sup>	<sup>1</sup> ANSTO, AU <sup>2</sup> HZB V3 <b>MAT-03-520</b>
216	In-situ monitoring of the deformation of nanopores due to capillary forces upon vapour sorption	G. Reichenauer <sup>1</sup> M. Wiener <sup>1</sup> D. Wallacher <sup>2</sup> A. Brandt <sup>2</sup>	<sup>1</sup> ZAE, München <sup>2</sup> HZB V4 <b>MAT-04-706</b>
217	In-situ observation of diffusion in porous membrane produced from single crystal superalloy	P. Strunz <sup>1</sup> J. Šaroun <sup>1</sup> D. Mukherji <sup>2</sup> U. Keiderling <sup>3</sup>	<sup>1</sup> NPI, CZ <sup>2</sup> TU Braunschweig <sup>3</sup> HZB V4 <b>MAT-04-1559</b>
218	Characterization of porosity microstructure in PYSZ-based TBC coatings using SANS	V. Ryukhtin <sup>1+3</sup> R. Ochrombel <sup>2</sup> S. Bilge <sup>2</sup> D. Wallacher <sup>3</sup> A. Wiedemann <sup>3</sup>	<sup>1</sup> TU Berlin <sup>2</sup> DRL, Köln <sup>3</sup> HZB V4 <b>MAT-04-1607-EF</b>
219	SANS investigations of porosity structure in thermal barrier coatings	V. Ryukhtin <sup>1+3</sup> R. Ochrombel <sup>2</sup> S. Bilge <sup>2</sup> S. Prévost <sup>3</sup> A. Wiedemann <sup>3</sup>	<sup>1</sup> TU Berlin <sup>2</sup> DRL, Köln <sup>3</sup> HZB V4 <b>MAT-04-1712-EF</b>
220	An investigation of water propagation at membrane on PEMFC using Neutron Imaging Technique	T. J. Kim <sup>1</sup> C. M. Sim <sup>1</sup> N. Kardjilov <sup>2</sup>	<sup>1</sup> KAERI, KR <sup>2</sup> HZB V7 <b>OTH-04-1223</b>

## List of Contributed Experimental Reports

PAGE	TITLE	TEAM	PROPOSAL
221	<b>Combined local current distribution measurements and neutron radiography of operating DMFCs</b>	A. Schröder <sup>1</sup> K. Wippermann <sup>1</sup> I. Manke <sup>2</sup> N. Kardjilov <sup>2</sup> A. Hilger <sup>2</sup> J. Schloesser <sup>2</sup> S. Petrov <sup>2</sup>	<sup>1</sup> FZ, Jülich <sup>2</sup> HZB V7 <b>MAT-04-1492</b>
222	<b>Transmission analysis on strong absorbing boron alloyed steels</b>	M. Zawisky <sup>1</sup> E. Dyrnjaja <sup>1</sup> N. Kardjilov <sup>2</sup>	<sup>1</sup> TU – ATI, AT <sup>2</sup> HZB V7 <b>MAT-04-1493</b>
223	<b>Combined neutron and impedance spectroscopy measurements for water detection in a PEM fuel cell</b>	R. Kuhn <sup>1</sup> P. Krüger <sup>1</sup> J. Kacerowski <sup>1</sup> C. Hartnig <sup>1</sup> A. Hilger <sup>2</sup> N. Kardjilov <sup>2</sup> I. Manke <sup>2</sup>	<sup>1</sup> ZSW, Ulm <sup>2</sup> HZB V7 <b>MAT-04-1588-LT</b>
224	<b>Energy selective imaging of structural materials</b>	L. Josic <sup>1</sup> E. Lehmann <sup>1</sup> M. Tamaki <sup>2</sup> A. Hilger <sup>3</sup> N. Kardjilov <sup>3</sup> M. Dawson <sup>3</sup>	<sup>1</sup> PSI, CH <sup>2</sup> Tamaki MI, JP <sup>3</sup> HZB V7 <b>MAT-04-1685</b>
225	<b>Fracture of a mechanically constrained Ni-Mn-Ga single crystal after extended magnetic cycling</b>	M. Chmielus <sup>1</sup> R. Schneider <sup>1</sup> K. Rolfs <sup>1</sup> A. Hilger <sup>1</sup> A. Paulke <sup>1</sup> P. Müllner <sup>2</sup>	<sup>1</sup> HZB <sup>2</sup> Boise State Univ., USA V7 <b>MAT-04-1724-EF</b>
226	<b>Influence of thermo-mechanical training of Ni-Mn-Ga single crystals on crack initialization</b>	M. Chmielus <sup>1</sup> R. Schneider <sup>1</sup> K. Rolfs <sup>1</sup> A. Hilger <sup>1</sup> A. Paulke <sup>1</sup>	<sup>1</sup> HZB V7 <b>MAT-04-1724-EF</b>
227	<b>Quantitative mapping of <math>\alpha</math>-FE, <math>\gamma</math>-FE- and Fe<sub>3</sub>C phases in steels using Bragg-edge tomography</b>	T. Kandemir <sup>1</sup> U. Gerling <sup>1</sup> N. Kardjilov <sup>2</sup> A. Hilger <sup>2</sup> I. Manke <sup>2</sup>	<sup>1</sup> FH Aachen <sup>2</sup> HZB V7 <b>MAT-04-1776</b>
228	<b>Transmission analysis on strong absorbing boron alloyed steels</b>	M. Zawisky <sup>1</sup> E. Dyrnjaja <sup>1</sup> M. Strobl <sup>2</sup>	<sup>1</sup> ATI, AT <sup>2</sup> HZB V12a <b>MAT-04-1480</b>
229	<b>Investigation of the Fusion Relevant Material by USANS</b>	H. Tatlisu <sup>1</sup> P. Walter <sup>2</sup> M. Strobl <sup>2</sup>	<sup>1</sup> TU – ATI, AT <sup>2</sup> HZB V12a <b>MAT-04-1582</b>

### Strain and Stress

230	<b>Residual stress states in machine components, comparison of calculation, neutron- and x-ray diffraction</b>	T. Hirsch <sup>1</sup> J. Epp <sup>1</sup> T. Poeste <sup>2</sup> R. Schneider <sup>3</sup>	<sup>1</sup> Uni Bremen <sup>2</sup> Uni Kassel <sup>3</sup> HZB E3 <b>MAT-01-1987</b>
231	<b>Residual stresses in monofilament reinforced composites</b>	M. Schöbel <sup>1</sup> G. Fiedler <sup>1</sup> G. Requena <sup>1</sup> H. Kaminski <sup>1</sup>	<sup>1</sup> TU Wien, AT E3 <b>MAT-01-2148</b>
232	<b>Micro stress accumulation in multiphase superalloys</b>	J. Repper <sup>1</sup> M. Hoffmann <sup>1</sup> R. Wimpory <sup>2</sup>	<sup>1</sup> TU München <sup>2</sup> HZB E3 <b>MAT-01-2260</b>

## List of Contributed Experimental Reports

PAGE	TITLE	TEAM	PROPOSAL
233	<b>Residual stress distribution in composite castings</b>	U. Wasmuth <sup>1</sup> M. Reihle <sup>1</sup> R. Wimpory <sup>2</sup>	<sup>1</sup> TU München <sup>2</sup> HZB E3 <b>MAT-01-2261</b>
234	<b>Residual stresses in diamond reinforced MMC for heat sink applions</b>	M. Schöbel <sup>1</sup> G. Fiedler <sup>1</sup> W. Altendorfer <sup>1</sup> J. Jonke <sup>1</sup>	<sup>1</sup> TU Wien, AT E3 <b>MAT-01-2262</b>
235	<b>Residual stresses in CFC-Cu joining brazed to CuCrZr alloy for nuclear fusion technology</b>	F. Fiori <sup>1</sup> V. Calbucci <sup>1</sup> R. Wimpory <sup>2</sup>	<sup>1</sup> UPM Ancona, IT <sup>2</sup> HZB E3 <b>MAT-01-2263</b>
236	<b>Residual stress distribution: a key to understand the interfacial bonding mechanisms of high-velocity oxy-fuel (HVOF) thermally sprayed coating/substrate system</b>	A. Manescu <sup>1</sup> R. Wimpory <sup>2</sup>	<sup>1</sup> UPM Ancona, IT <sup>2</sup> HZB E3 <b>MAT-01-2264</b>
237	<b>Stresses in built-up welding stainless steel on ferrite</b>	V. Sumin <sup>1</sup> S. Sheverev <sup>1</sup> R. Wimpory <sup>2</sup>	<sup>1</sup> JINR, RU <sup>2</sup> HZB E3 <b>MAT-01-2265</b>
238	<b>Quantifying residual stress in welding CT specimens</b>	R. Wimpory <sup>1</sup> S. Kamel <sup>2</sup> N. Nikbin <sup>2</sup>	<sup>1</sup> HZB <sup>2</sup> IC, London, UK E3 <b>MAT-01-2275-EF</b>
239	<b>Visualization of local textures using neutron diffraction</b>	M. Boin <sup>1</sup> R. Schneider <sup>1</sup> R. Wimpory <sup>1</sup> T. Poeste <sup>1</sup> C. Randau <sup>2</sup>	<sup>1</sup> HZB <sup>2</sup> TU Clausthal E3 <b>MAT-01-2277-EF</b>
240	<b>Residual stress states in hardened components, analysis of case hardened 20MnCr5 discs</b>	T. Hirsch <sup>1</sup> J. Epp <sup>1</sup> T. Poeste <sup>2</sup> R. Schneider <sup>3</sup> R. Wimpory <sup>3</sup>	<sup>1</sup> Uni Bremen <sup>2</sup> Uni Kassel <sup>3</sup> HZB E3 <b>MAT-01-2429</b>
241	<b>Measurement of reference d0 samples for improved residual stress characterisation of Al alloys</b>	J. S. Robinson <sup>1</sup> R. Wimpory <sup>2</sup>	<sup>1</sup> Univ. of Limerick, IE <sup>2</sup> HZB E3 <b>MAT-01-2432</b>
242	<b>Residual strain/stress distribution in friction stir welded aluminium plates</b>	F. Fiori <sup>1</sup> V. Calbucci <sup>1</sup> A. Manescu <sup>1</sup> R. Wimpory <sup>2</sup>	<sup>1</sup> UPM Ancona, IT <sup>2</sup> HZB E3 <b>MAT-01-2434</b>
243	<b>Strain/stress analysis in Nb3Sn/metal matrix composite superconducting cables for nuclear fusion technology</b>	V. Calbucci <sup>1</sup> A. Manescu <sup>1</sup> R. Wimpory <sup>2</sup>	<sup>1</sup> UPM Ancona, IT <sup>2</sup> HZB E3 <b>MAT-01-2435</b>
244	<b>Measurement of residual stress in draw wires</b>	R. Wimpory <sup>1</sup> N. O'Dowd <sup>2</sup> P. Tierman <sup>2</sup>	<sup>1</sup> HZB <sup>2</sup> Univ. of Limerick, IE E3 <b>MAT-01-2440-EF</b>
245	<b>Mosaic width as indicator of crystal quality during the life of Ni-Mn-Ga single crystals</b>	M. Chmielus <sup>1</sup> R. Schneider <sup>1</sup> K. Rolfs <sup>1</sup> T. Poeste <sup>1</sup> R. Wimpory <sup>1</sup> P. Müllner <sup>2</sup>	<sup>1</sup> HZB <sup>2</sup> Boise State Univ., USA E3 <b>MAT-01-2442-EF</b>
246	<b>Martensitic Structure of Co-alloyed Ni-Mn-Ga</b>	K. Rolfs <sup>1</sup> R. Wimpory <sup>1</sup>	<sup>1</sup> HZB E3/E7 <b>MAT-01-2443-EF</b>
247	<b>Residual strain-stress in anisotropic cold-rolled Zr-alloy</b>	V. Sumin <sup>1</sup> S. Sheverev <sup>1</sup> R. Wimpory <sup>2</sup>	<sup>1</sup> JINR. RU <sup>2</sup> HZB E7 <b>MAT-01-2266</b>

## List of Contributed Experimental Reports

PAGE	TITLE	TEAM	PROPOSAL	
248	<b>TG4 Stress Relieved Specimen Measurements and grain size effect</b>	R. Wimpory <sup>1</sup>	<sup>1</sup> HZB	E3 EF

### *Cultural Heritage*

251	<b>Identification of Hidden Objects of Archaeological Interest</b>	R. Triolo <sup>1</sup> V. Benfante <sup>1</sup> I. Sciacca <sup>1</sup> I. Ruffo <sup>1</sup>	<sup>1</sup> Univ. of Palermo, IT	V7	<b>ART-04-1408</b>
252	<b>Endosymbionts of fossil Echinodermata using neutron and X-ray computed tomography</b>	C. Neumann <sup>1</sup> N. Kardjilov <sup>2</sup> A. Hilger <sup>2</sup>	<sup>1</sup> HU Berlin <sup>2</sup> HZB	V7	<b>GEO-04-1489</b>
253	<b>Preservation and Conservation of waterlogged wood</b>	R. Triolo <sup>1</sup> V. Benfante <sup>1</sup> G. Giambona <sup>1</sup> I. Ruffo <sup>1</sup>	<sup>1</sup> Univ. of Palermo, IT	V7	<b>ART-04-1299</b>
254	<b>Investigating Wood Conservation Procedures by Neutron Tomography</b>	R. Triolo <sup>1</sup> E. Fertitta <sup>1</sup> L. Chiappisi <sup>1</sup> I. Ruffo <sup>2</sup>	<sup>1</sup> Univ. of Palermo, IT <sup>2</sup> ITC "L. Sturzo", IT	V7	<b>ART-04-1688</b>
255	<b>Neutron autoradiographs of Paris Bordone: The two Chess Players</b>	C. Laurenze-Landsberg <sup>1</sup> C. Schmidt <sup>1</sup> B. Schröder-Smeibidl <sup>2</sup>	<sup>1</sup> SMB, Berlin <sup>2</sup> HZB	B8	<b>ART-05-0030</b>

### *Fundamental Physics and Others*

259	<b>Spatial Distribution of Neutrons Scattered by Vibrating Crystals</b>	E. Raitman <sup>1</sup> V. Gavrilovs <sup>1</sup> N. Stüßer <sup>2</sup>	<sup>1</sup> LAS, LV <sup>2</sup> HZB	E6	<b>PHY-01-2237</b>
260	<b>Coherent Scattering Neutron Imaging of Nickel Single Crystal</b>	M. B. Tamaki <sup>1</sup> L. Josic <sup>2</sup> G. Frei <sup>2</sup> E. H. Lehmann <sup>2</sup> A. Hilger <sup>3</sup> N. Kardjilov <sup>3</sup>	<sup>1</sup> TAMAKI MI, JP <sup>2</sup> PSI, CH <sup>3</sup> HZB	V7	<b>MAT-04-1685</b>



# **Development of Instruments and Methods**





## EXPERIMENTAL REPORT

### Larmor phase topology with NRSE – experimental test of correction devices

Proposal N°  
PHY-02-630-EF  
Instrument **V2-NRSE**  
Local Contact  
K. Habicht

Principal Proposer: K. Habicht – HMI Berlin  
Experimental Team: K. Habicht – HMI Berlin

Date(s) of Experiment  
06/02/2008 -11/02/2008

Date of Report: 15/01/2009

This experiment is part of the NMI3-JRA-PNT project with the aim to manipulate the Larmor phase topology within the resolution volume of a triple-axis spectrometer with spin-echo. The state-of-the-art design of NRSE apparatus allows matching planes of constant Larmor phase with the slope of the dispersion. Theoretical analysis has however identified sample properties, e.g. curvature of the dispersion surface, to be crucial to resolution. The aim here is to overcome this effect by a set of correction elements providing small additional Larmor precession as a function of beam divergence and thus surfaces of constant Larmor phase distinct from planar.

Numerical analysis and previous experiments carried out at V2/FLEX have shown that a combination of current sheets and flippers, inserted between the two bootstrap coils of the first NRSE arm, can be used to provide an effective tilt angle. However mapping the Larmor phase topology with an active current sheet setup showed that the linear modulation dominates and a substantial second order modification towards curved Larmor surfaces was not evident.

During the present experiment a simpler setup was therefore installed in the first NRSE arm consisting of 3 solenoid coils only (Fig. 1). FLEX was operated in a configuration with scattering senses (SM=-1, SS=-1, SA=+1) at  $k_i = k_f = 2.4 \text{ \AA}^{-1}$  where second-order contamination is substantially suppressed by the curved neutron guide. No additional collimators were used besides a transmission polarizer after the PG monochromator and a bender after the PG analyzer. The NRSE option was operated in bootstrap-mode with an effective frequency  $f_{\text{eff}} = 1 \text{ MHz}$ . Data sets have been collected under conditions slightly offset from the standard Larmor diffraction conditions, i.e. with tilt angles of the RF-coils set to  $\theta_1 = +34.9^\circ$  and  $\theta_2 = -44.9^\circ$ . This rotates the Larmor phase map in the (hkk) wavevector plane while the polarization is still good enough to provide sufficient modulation contrast. The topology of the Larmor phase inside the resolution ellipsoid of the TAS was measured by TAS-scanning the (200) Bragg peak along the longitudinal and transverse directions in Q-space keeping the NRSE parameters fixed and without operating the additional solenoid coils (Fig. 2). As expected, the Bragg peak appears intensity modulated in a direction slightly offset from the longitudinal direction in Q-space.

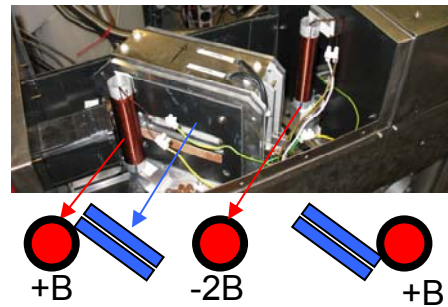


Fig. 1: Experimental setup: NRSE arm 1 with solenoid coils.

A second set of measurements has been performed with operating the solenoid coils providing a field integral which is sensitive to divergence. In this case the linear modulation is modified and curved Larmor surfaces are observed for the first time for Q-regions located off the central region (Fig. 3).

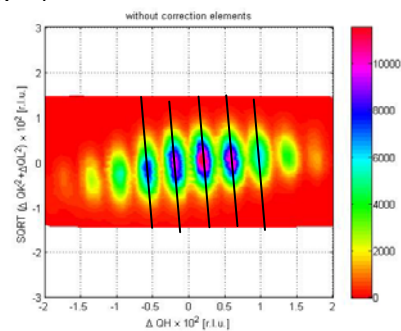


Fig. 1: Larmor phase map measured *without* operating solenoid coils in first NRSE arm

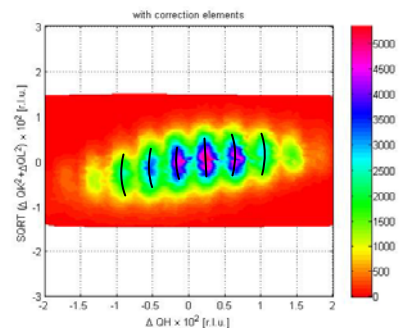


Fig. 2: Larmor phase map measured *with* operating solenoid coils in first NRSE arm. Lines are guide to the eye.

	<b>EXPERIMENTAL REPORT</b> <b>Specular and Off-specular Scattering with Polarization and Polarization analysis on Reflectometer V6</b>	Proposal N° PHY-04-1723-EF Instrument <b>V6</b> Local Contact A. Teichert
	Principal Proposer: Amitesh Paul, HZB Experimental Team: R. Steitz, HZB	Date(s) of Experiment 17/12/2008 – 21/12/2008

Date of Report: 14/01/2009

We investigate the magnetization configuration of CoO/Co/Au polycrystalline ML for two different applied fields. This experiment demonstrates that V6 is now fully equipped for off-specular measurements with polarization and polarization analysis in investigating magnetic thin films and multilayers.

While polarization is provided by a supermirror in front of the sample, polarization analysis is done by a stack of supermirrors turned 90° with respect to the polarizing supermirror in order to get a larger angular acceptance that is relevant of observing diffuse scattering. The detector is a 2-dimensional position sensitive one and two Mezei flippers are used to reverse the spin projection. An optimization of the flipper currents and the analyzer tilt could achieve a flipping ratio of about 16-20.

All four channels are measured at a remanent applied field which are shown in Figure 1. All measurements are, however, done at room temperature for this exchange coupled system and therefore no exchange biasing phenomena is expected. The intensity in the non-spin-flip channels show superlattice peaks (up to 5 orders) due to the chemical periodicity in the multilayer. The presence of off-specular scattering in the spin-flip channels, around the critical angle of total reflection, when measured at remanence, is due to the presence of buried domains in the multilayer. They are found to disappear when measured at saturation. A typically observed asymmetry in the two SF channels is also observed which is due different critical angles of total reflection for incident or exit angle neutrons with respect to the magnetization direction of the Co layer.

We extract the specular scattering by selecting a window along the region where incident angle ( $\alpha_i$ ) is equal to the exit angle ( $\alpha_f$ ). We also present the specular data for this measurement in Figure 2. The SF data when compared to that measured at saturation, it

shows some true SF signal. This SF signal is due to the coherent rotation of the Co magnetization that is expected at remanence. At saturation all the SF signal (not shown) are owed to the inefficiencies of the polarizer and analyzer devices.

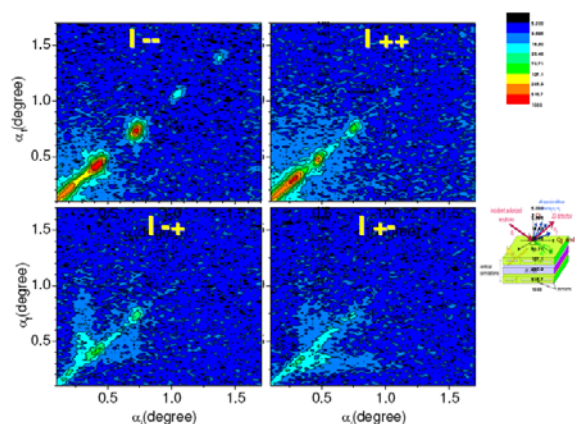


Fig. 1. Intensity maps for four different neutron scattering cross-sections for a [Co/CoO/Au] $\times$ 16 multilayer. The colour encodes the scattered intensity on a logarithmic scale.

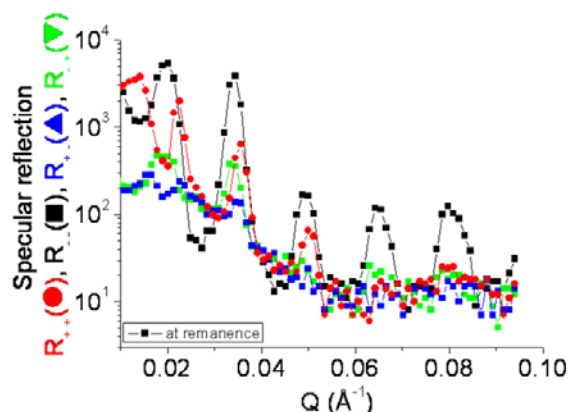


Fig. 2. Specular reflectivity patterns for NSF and SF channels for a [Co/CoO/Au] $\times$ 16 multilayer.

In future, we plan to investigate the specimen for different field cooling conditions in its exchange biased state.

	<b>EXPERIMENTAL REPORT</b>	Proposal N° PHY-04-1444-EF
	<b>Test of solid state polarizer for imaging</b>	Instrument <b>V7</b>  Local Contact N. Kardjilov
Principal Proposer: A. Hilger, (HZB) Experimental Team: N. Kardjilov, (HZB) I. Manke, (HZB) M. Strobl, (HZB) M. Dawson, (HZB)		Date(s) of Experiment  07/05/2007 – 13/05/2007

Date of Report: January 2009

Polarized neutron radiography is based on the spatially resolved measurement of the final precession angles of a collimated and polarized monochromatic neutron beam that passes through a magnetic field present inside and/or outside of a sample. Experiments using polarized neutrons were carried out at the neutron imaging beam line CONRAD at HZB [1]. For this purpose the instrument was equipped with solid state polarizing benders [2] providing a beam with a cross-section of 15 mm width and 45 mm height, Fig. 1. For larger samples a scanning arrangement was adopted for investigating samples of up to 20 cm width. A double crystal monochromator device was used to select a defined wavelength from the cold neutron spectrum. The achieved spatial resolution in the radiography images was around 500  $\mu\text{m}$  for the given experimental geometry.

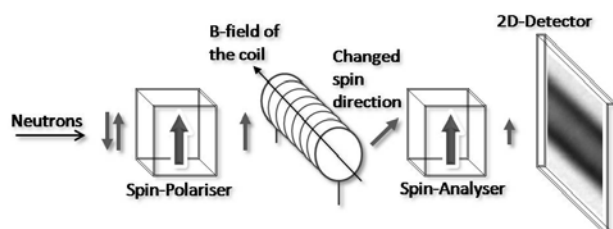


Fig.1. Spin-polarized neutron imaging: The neutron spin rotates in the magnetic field of a sample and hence approaches the spin analyzer typically in a non-parallel orientation. The angle of the final spin rotation  $\varphi$  depends on the magnetic field integral along the beam path.

The potential of the method was demonstrated by the visualization of magnetic fields around a cylindrical coil at different current values, Fig. 2.

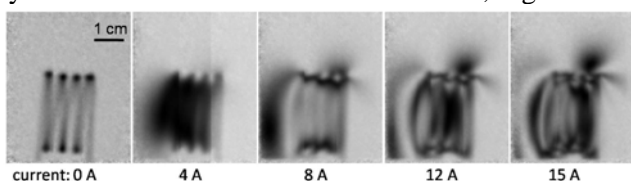


Fig. 2 Cylindrical coil investigated with polarized neutron radiography at different current values: The spin of the neutrons is rotated due to the coil's

magnetic field which is perpendicular to the original spin orientation defined by the polarizer. The resultant spin orientation is converted by transmission through the spin analyzer into gray levels between white for parallel and black for anti-parallel spin orientation with respect to the analyzer.

The spin polarized radiography was also successfully used for imaging the expelled and pinned magnetic field in superconductors. An example of this is shown in Fig. 3

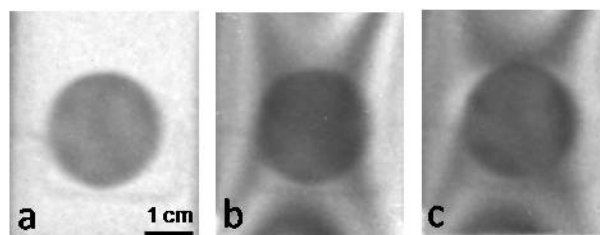


Fig. 3 Visualization of the Meissner effect by polarized neutron radiography: YBCO superconductor pellet (20 mm diameter, 5 mm thickness) at: a)  $T > T_c$ ,  $B = 0 \text{ mT}$ , b)  $T > T_c$ ,  $B = 2 \text{ mT}$ , c)  $T < T_c$ ,  $B = 2 \text{ mT}$ . The external magnetic field  $B$  is expelled from the sample volume at  $T < T_c$ . The critical temperature for YBCO ( $T_c$ ) is 94 K.

This new technique can be used to investigate many other physical effects of magnetism in the bulk of materials. In particular, the ability of neutrons to penetrate large volumes of many materials of up to several centimeters promises interesting applications in materials science.

## References

- [1] N. Kardjilov et al., Nature Physics **4**, 399 (2008)
- [2] Th. Kris et al., Physica B **241-243**, 82-85 (1998)



## EXPERIMENTAL REPORT

### Dark-field contrast – a new imaging signal for neutron tomography

Proposal N°  
PHY-04-1514-DT  
Instrument **V7**

Local Contact  
N. Kardjilov

Principal Proposer: M. Strobl, HZB & Uni Heidelberg  
Experimental Team: A. Hilger and N. Kardjilov, HZB  
I. Manke, HZB  
Ch. Grünzweig, PSI  
O. Ebrahimi, TFH

Date(s) of Experiment  
  
02/07/2007 – 09/07/2007

Date of Report: 14/01/2009

Differential neutron phase contrast has been explored with double crystal diffractometers (DCD) [1]. However, only the recent development of a grating interferometer for imaging [2] for this technique enabled through high efficiency a broad application of the method. The high angular resolution of a DCD provides additional contrast for ultra small angle scattering [3] which is referred to as dark-field contrast. Consequently measurements using a grating interferometer were conducted at the CONRAD instrument in order to investigate the potential to achieve dark-field contrast images and to perform corresponding tomographies one reasonable time scales. An Al matrix with a number of different holes that has been measured earlier at the V12a DCD has been used as a reference sample. Fig. 1 displays the radiographic images of the three contrast signals that can be extracted from the grating interferometer data.

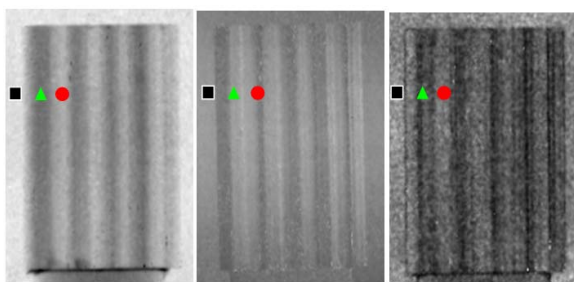


Fig. 1 Radiographic images from a radiographic measurement corresponding to attenuation, differential phase and dark field contrast.

The images are extracted from a single scan in which the so called source grating is moved through the beam in several steps resulting in a sinusoidal response in every detector pixel (compare Fig. 2). These curves can be described by the three parameters of the offset, a phase and the amplitude corresponding to attenuation, refraction (i.e. differential phase contrast) and dark field

scattering, respectively [4] as could be demonstrated by the results of the measurements.

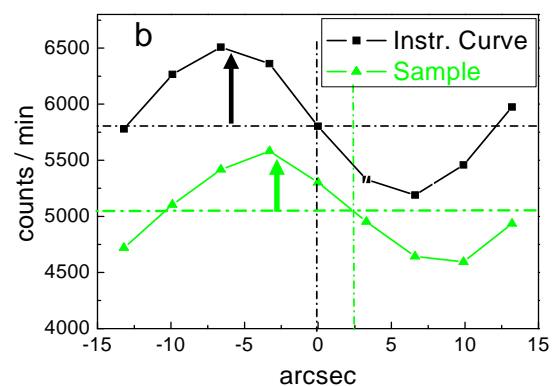


Fig. 2 Response functions from grating measurements for single pixel

With data recorded in a tomographic measurement it could be shown that the dark-field data can be reconstructed (compare Fig. 3) in analogy to such from a DCD but the data can be recorded with an efficiency about 2 orders of magnitude higher.

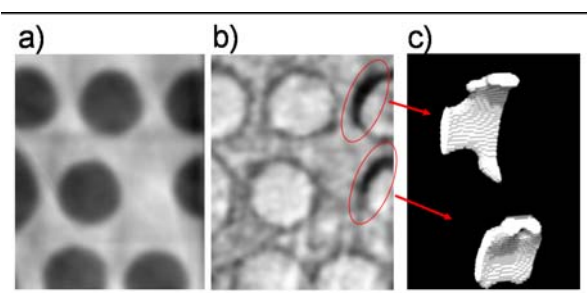


Fig. 3 Details of reconstruction from differential phase (a) and dark field contrast (b), sediments only found in dark field reconstruction

#### References

- [1] M. Strobl et al. NIMB 222 3-4 (2004)
- [2] F. Pfeiffer et al. PRL 96, 215505 (2006)
- [3] M. Strobl et al. APL 85, 3 (2004)
- [4] M. Strobl et al. PRL 101, 123902 (2008)



## EXPERIMENTAL REPORT

# Visualisation of flux-pinning in superconductors

Proposal N°  
PHY-04-1534-EF  
Instrument **V7**  
Local Contact  
N. Kardjilov

Principal Proposer: A. Hilger, (HZB)  
Experimental Team: N. Kardjilov, (HZB)  
I. Manke, (HZB)  
M. Dawson, (HZB)

Date(s) of Experiment  
  
04/08/2007 – 10/08/2007

Date of Report: January 2009

The experimental setup contains two solid-state polarisers; one is situated in front of the sample position and the other one (the so-called analyser) is located between the sample position and the imaging detector. The analyser is aligned parallel to the polariser in order to guarantee the passage of neutrons carrying a spin parallel to the initial polarisation and to absorb neutrons with anti-parallel spin. The image of a sample detected behind the polarisation analyser is determined by a superposition of conventional attenuation contrast  $I_a(x,y)$  and the contrast variations due to spin rotation  $I_m(x,y)$

$$I(x,y) = \underbrace{I_0(x,y)}_{I_a(x,y)} \cdot \exp\left(-\int_{\text{path}} \Sigma(s) ds\right) \cdot \underbrace{\frac{1}{2}(1 + \cos\varphi(x,y))}_{I_m(x,y)}$$

where  $I_0(x,y)$  is the incident beam intensity,  $\Sigma$  is the linear attenuation coefficient of the sample and  $(x,y)$  are the co-ordinates in the detector plane.

The technique was applied to study flux trapping effects in lead, a type-I superconductor. The sample, a polycrystalline lead cylinder, was cooled down to  $T_0=6.8$  K (below the critical temperature for superconductivity,  $T_c=7.2$  K). During cooling a homogenous magnetic field of 10 mT was applied parallel to the cylinder axis and perpendicular to the magnetic moment of the incident neutron beam. After this, the magnetic field was switched off. Magnetic fields are partially trapped in the superconductor due to grain boundaries and other defects. The temperature dependence of the residual field distribution inside the sample was visualised by recording radiographic images during step heating from  $T_0$  to  $T_c$  with  $\Delta T=0.1$  K. The images (Fig. 1) show an inhomogeneous residual field which decreases during heating and vanishes completely when the critical temperature  $T_c$  is reached and superconductivity breaks down. For the case (shown in Fig. 1 – 7.0 K) of a weak trapped residual field, a tomographic investigation was performed by rotating the sample around the vertical axis. The measurement consisted of 60 radiographic images recorded at equidistant projection angles over a range of 180°. For the reconstruction of the volumetric data set from the

collected two-dimensional images a numerical reconstruction algorithm (filtered back projection) was applied resulting in a three-dimensional representation of the flux trapped in the sample at 7.0 K (Fig. 2).

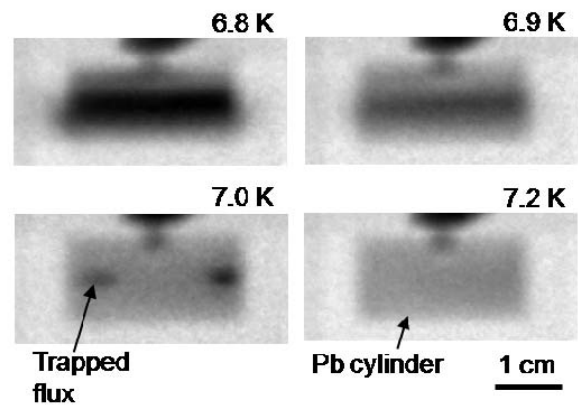


Fig. 1. Radiographic projections of trapped flux in a polycrystalline lead cylinder at different temperatures below  $T_c = 7.2$  K.

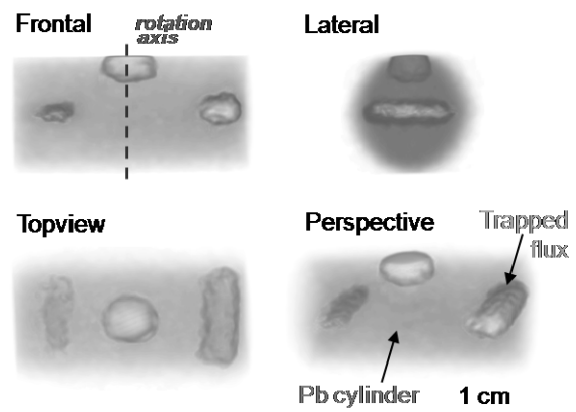


Fig. 2 Trapped flux at 7.0 K (yellow) visualised in different tomographic views.

### References

- [1] N. Kardjilov et al., Nature Physics **4**, 399 (2008)

	<b>EXPERIMENTAL REPORT</b>  <b>Radiography with polarized neutrons</b>	Proposal N° OTH-04-1538-EF  Instrument <b>V7</b>  Local Contact N. Kardjilov
	Principal Proposer: A. Hilger, (HZB), N. Kardjilov, (HZB) Experimental Team: I. Manke, (HZB) M. Dawson, (HZB) M. Strobl, (HZB) D. Wallacher, (HZB)	Date(s) of Experiment  09/07/2008 – 14/07/2008

Date of Report: January 2009

## Introduction

In addition to conventional tomography at the CONRAD-beamline it is feasible to use a new device for the polarisation of the neutron beam. This setup consists of two solid state benders, one for the polarisation of the beam and the other to analyse one component of the spin state. This experimental equipment allows for an investigation of magnetic fields outside a sample and also in bulk materials[1]. In comparison to these measurements the field distributions were calculated using Biot-Savart's law.

## Experimental description

A double-crystal monochromator consisting of two adjustable C(002) crystals with a mosaic spread of  $3.5^\circ$  was used to choose a wavelength of  $\lambda=0.35\text{nm}$  with a bandwidth  $\Delta\lambda/\lambda=0.12$ . The flux density at the sample position for an unpolarized monochromatic beam was about  $5 \times 10^5 \text{ neutrons} \cdot \text{cm}^{-2} \cdot \text{s}^{-1}$ . The 400  $\mu\text{m}$  thick Li6F scintillator screen was used for neutron detection. The light was deflected by a mirror into the 50-mm-focus Nikon camera lens and was recorded by an Andor DW436N-BV CCD camera with  $2048 \times 2048$  pixels. The CCD was cooled down to  $-50^\circ\text{C}$  to minimize electronic noise. The spatial resolution were 300  $\mu\text{m}$  in the vertical and 500  $\mu\text{m}$  in the horizontal direction for a sample-to-detector distance of 50 cm. To enable the investigation of samples wider than the beam width of 15 mm, a scan technique was applied. The samples together with the detector were scanned through the beam defined by the fixed polarizing benders. Exposure times of the order of 15 min were necessary for a single image on a scan path of 6 cm. The beam height was 50 mm and for investigation of taller fields only the sample was displaced in horizontal direction.

## Results

In the case of the levitating dipole magnet over a superconducting  $\text{YBa}_2\text{Cu}_3\text{O}_7$  pellet a closed cycle refrigerator was utilized to cool down the pellet to 60 K ( $T_c = 90 \text{ K}$ ). The field strength at surface of the dipole was approx. 100 mT. The radiogram of the permanent magnet is shown in Fig. 1a. Fig 1b shows the comparison between the simulation of the final spin state and measured image. In the outer part the compliance is satisfactorily. The difference in the inner parts is caused by a varying resolution in the calculation and measurement.

Fig. 2 shows the measured superposition of two magnetic fields generated by perfect dipoles. The fields are rectified and the positions were fixed by an aluminium slat between the magnets

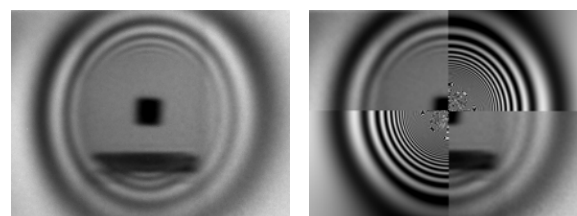


Fig 1: Levitating dipole, a: Experimental result, b: Comparison to the calculated field

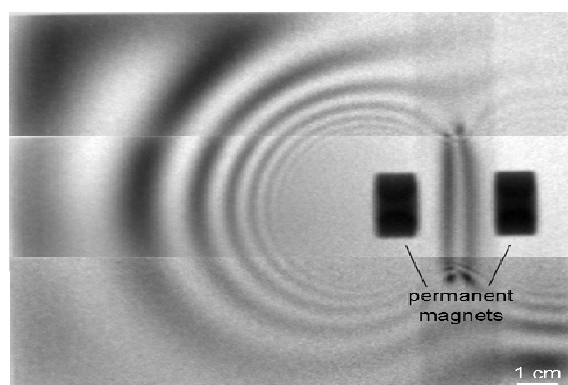


Fig.2: Superposition of the magnetic field of two dipole magnets

[1] N. Kardjilov et al, Nature Physics 4 399 (2008)

	<b>EXPERIMENTAL REPORT</b>  <b>Polarimetric magnetic field tomography</b>	Proposal N° PHY-04-1628-EF  Instrument <b>V7</b>  Local Contact N. Kardjilov
	Principal Proposer: M. Strobl, HZB & Uni Heidelberg Experimental Team: A. Hilger and N. Kardjilov, HZB E. Jericha, ATI Manke, HZB G. Badurek, ATI	Date(s) of Experiment  11/02/2008 – 16/02/2008

Date of Report: 14/01/2009

Only recently the potential of polarised neutrons for imaging could be demonstrated in several experiments carried out at the cold neutron radiography and tomography instrument CONRAD [1,2]. However, in contrast to proposed methods of tensorial neutron tomography in perfect crystal interferometers [3,4], the method has been limited to distinct magnetic field geometries that could be investigated.

For the presented measurements a combined approach of polarised neutron imaging in a conventional pinhole set-up with polarimetric spin analyses [5] was chosen in order to perform a tomographic measurement of an arbitrary magnetic field to achieve data for tensorial reconstruction [3,4] of the 3-dimensional field.

For that purpose the polarised imaging set-up at CONRAD [1,2] has been equipped with two crossed  $\pi/2$  spin flipping coils both before and behind the sample position (compare Fig. 1).

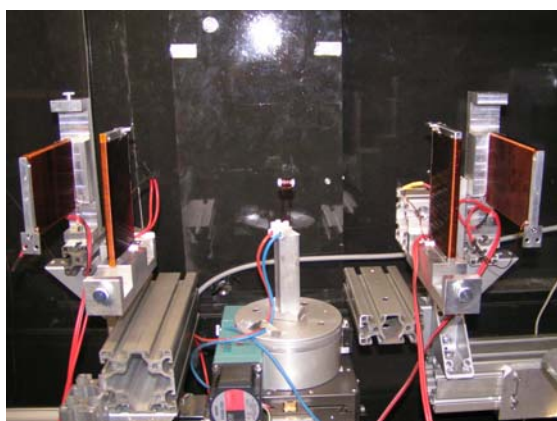


Fig. 1 Set-up for polarimetric imaging at CONRAD; in the centre of the image is the sample position (here the sample is a small electric coil producing an inhomogeneous magnetic sample field) Before and behind the sample position crossed  $\pi/2$  spin flipping coils are installed.

For the measurements the sample position had to be shielded against external stray fields by an iron case (30 x 30 x 30 cm<sup>3</sup>) with holes

only for the incoming and outgoing beam as well as for the sample holder. As a reference sample a simple coil made of Al wire with a few windings with a diameter of 1 cm has been used in order to achieve an inhomogeneous field for investigations. 10 tomographic runs have been recorded including all combinations of incoming and analysed spin directions (x,y,z) and a conventional attenuation tomography with the field free sample coil (in order to separate attenuation from spin analyses based contrast. The achieved spatial resolution was dominated by the geometric conditions of the order of a few hundred micrometers. For every tomographic run 100 projection images have been recorded, each with an exposure time of 30 sec.

Fig. 2 shows the nine images of a polarimetric radiography. The analyses of the tomographic data, i.e. efforts to reconstruct the magnetic field from the recorded data are ongoing.

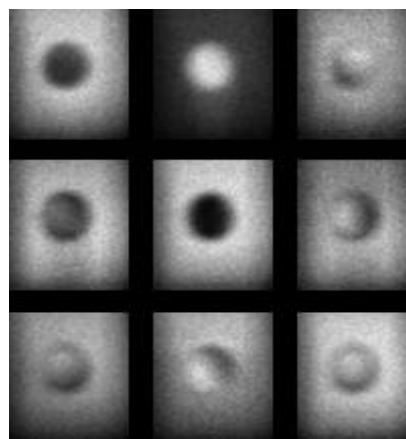


Fig. 2 Polarimetric radiographies corresponding to xx,xy, xz, yx, yy, yz, zx, zy, zz combination of incoming respectively analysed spin orientation (top left to bottom right).

- [1] N. Kardjilov et al., Nat. Phys. 4 (2008)
- [2] I. Manke et al. JAP 104, 1 (2008)
- [3] G. Badurek et al. Phys. B 234–236 (1997)
- [4] E. Jericha et al. Phys B 397 (2007)
- [5] M. Strobl et al. Phys B, accepted

	<b>EXPERIMENTAL REPORT</b>  <b>Spin-polarised neutron radiography on electric conductors</b>	Proposal N° PHY-04-1629-EF  Instrument <b>V7</b>  Local Contact N. Kardjilov
	Principal Proposer: I. Manke, (HZB) Experimental Team: N. Kardjilov, (HZB) A. Hilger, (HZB) M. Dawson, (HZB)	Date(s) of Experiment  26/05/2008 – 31/05/2008

Date of Report: January 2009

The skin effect in the bulk of an electrical conductor, i.e., the displacement of the current density from the inner part to the edges, has been investigated with spatial resolution using spin-polarized neutron imaging [1].

Measurements were performed at the neutron imaging facility CONRAD at HZB. A schematic drawing of the experimental setup is shown in Fig.1. The monochromatic neutron beam was polarized by a solid-state spin-polarizing bender and passed through the sample. The beam polarization was then analyzed by a second polarizing bender, the so-called spin analyzer, and transmitted neutrons were detected by a spatially-resolving detector.

In such a polarized neutron imaging setup the magnetic field of a sample provides image contrast due to changes in the previously defined neutron spin state that occurs in a magnetic field. In the ideal case, the magnetic field to be visualized in and around a conductor is aligned perpendicular to the (initial) neutron spin polarization direction and the overall rotation of the neutron spin is not more than  $\pi$ .

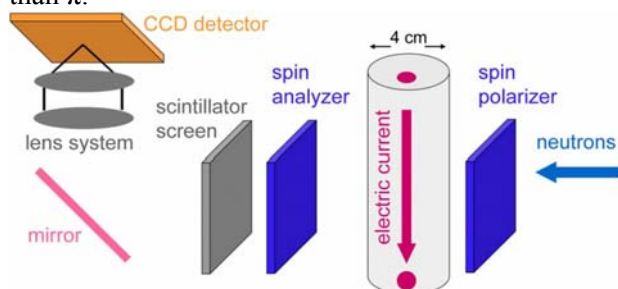


Fig. 1. Schematic drawing of the experimental setup. An aluminum rod of 4 cm thickness with applied asymmetrical electric contact (top: 1 cm offset, bottom: contact at the side).

The current distribution in a conducting cylindrical aluminum rod with 4 cm diameter was investigated. Two electrical contacts were fixed to the rod at the top and bottom surfaces such that the magnetic field of the sample was perpendicular to the vertically oriented magnetic moment of the neutrons. For the first measurements the contacts were placed at different positions off-center of the circular cross section in order to simulate a realistic nontrivial case (Fig. 1). Images were taken with

different applied currents. The exposure time for a single image was up to 120 s. The field of view was  $8 \times 3 \text{ cm}^2$  and the spatial resolution was approximately  $300 \mu\text{m}$  in the vertical and  $500 \mu\text{m}$  in the horizontal direction, mainly limited by the beam divergence

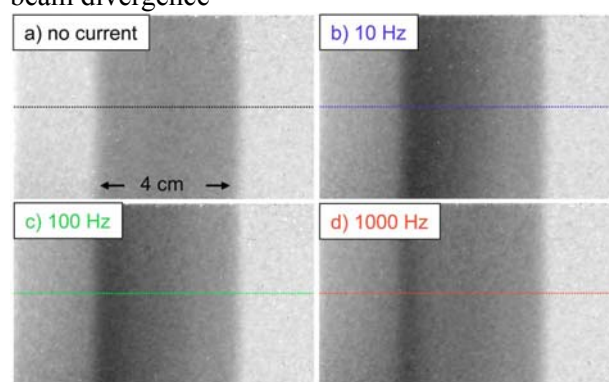


Fig. 2 (a) Spin-polarized neutron radiograms of a 4 cm thick aluminum rod without applied current and with 25 A alternating current at (b) 10 Hz, (c) 100 Hz, and (d) 1000 Hz. Due to the asymmetric electric contact and the skin effect the current is shifted to the left side at increased frequencies resulting in a corresponding shift of the magnetic field.

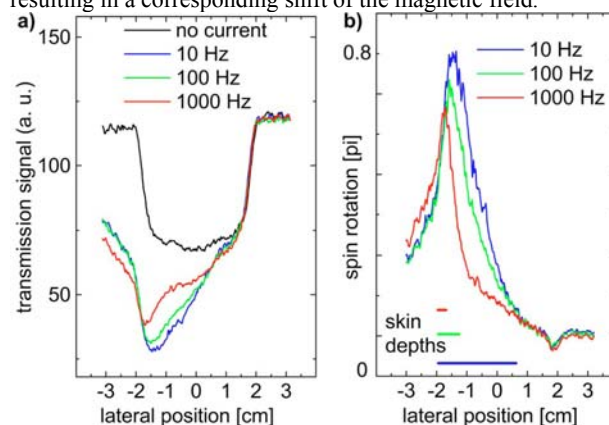


Fig. 3 (a) Cross sections along the marked lines in Fig. 2. With applied current the transmission signal is decreased due to the neutron spin rotation. The gray shaded area marks the extensions of the aluminum rod. (b) The graphs in (a) were normalized and reveal the beam polarization. The values for the skin depth are shown for the three frequencies applied.

## References

- [1] I. Manke et al., J. Appl. Phys. **104**, 076109 (2008)



## EXPERIMENTAL REPORT

### Visualization of local textures using Bragg Edge Radio- and Tomography

Proposal N°  
MAT-04-1632-EF  
MAT-04-1633-EF

Instrument **V7**

Local Contact M. Boin

Principal Proposer: M. Boin, Helmholtz Centre Berlin  
Experimental Team: N. Kardjilov, Helmholtz Centre Berlin

Date(s) of Experiment  
17/01/2008 – 21/01/2008

Date of Report: 13/01/2009

A textured Mg AZ31 specimen was investigated on CONRAD (V7) using Bragg edge transmission. The sample was expected to have local changes which was verified before on E3 as well as on STRESS-SPEC (FRM-II) using the conventional diffraction method [1]. Three local sample positions were compared with the reference data (see pole figure in figure 1) from the diffraction measurements.

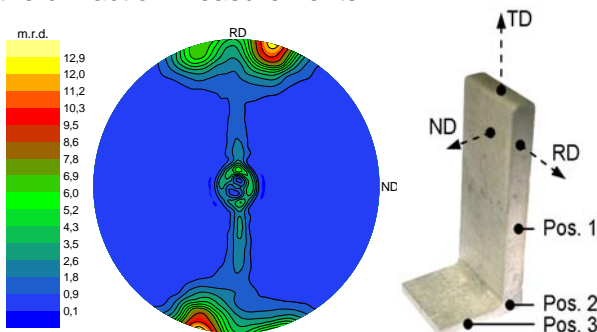


Figure 1: Extruded Mg AZ31 sample - RD, TD and ND represent the rolling, transverse and normal direction. The left graphic shows the pole figure for sample position 1.

The first step towards the texture analysis using Bragg edge neutron transmission was to perform a wavelength scan to determine the sample specific Bragg edge positions. Therefore, we used the monochromatic option to setup well defined neutron energies and capture radiographic images for each setting. The detected transmission intensities have been used to set the wavelength position close to a Bragg edge (in our case: 5.55 Å). The diagram in figure 2 shows the energy-dependent intensity changes, known as Bragg edges.

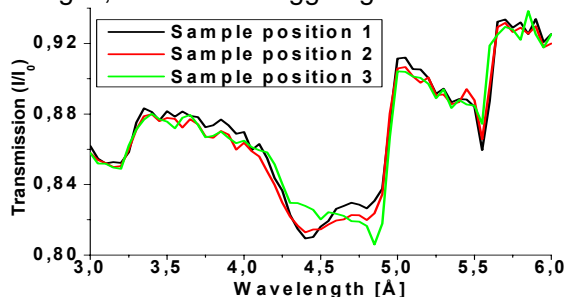


Figure 2: Wavelength scan showing Bragg edges.

After setting the neutron energy, such that the intensity changes close to the first Bragg edge

can be detected, the second step of the experiment was performed. The sample was rotated around 90° in 1° steps and tilted by 0°, 5°, 10°, 15° and 18°. For each position radiographic images were captured as shown in figure 3 as well as reference pictures with a wavelength outside the Bragg edge area.

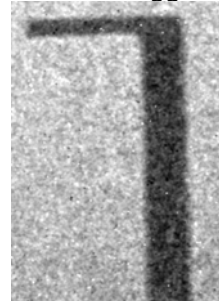


Figure 3: Radiographic image from the Mg AZ31 sample.

Finally, the detected intensities have been normalized by the reference pictures and compared with the dataset from the diffraction analysis.

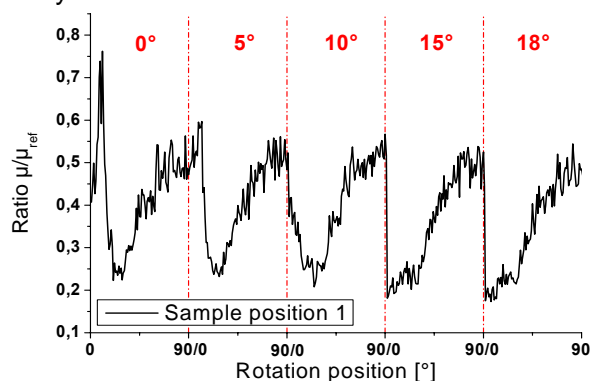


Figure 3: Intensity analysis for sample position 1.

Although only the ratio between the captured absorption coefficients is plotted it is clearly visible that the neutron cross section changes due to the texture effect, i.e. the number of crystallites with preferred orientation to RD changes with rotation likewise the intensities in the pole figure.

[2] M. Boin, BENSC report, MAT-01-2277-EF



## EXPERIMENTAL REPORT

### Test of New Scintillating Screens

Proposal N°  
PHY-04-1637-IT  
Instrument **V7**  
Local Contact  
N. Kardjilov

Principal Proposer: N. Kardjilov, (HZB), I. Manke, (HZB)  
Experimental Team: N. Kardjilov, (HZB)  
A. Hilger, (HZB)  
M. Dawson, (HZB)

Date(s) of Experiment  
08/01/2008 – 10/01/2008

Date of Report:

#### Introduction

A limiting factor for the spatial resolution in imaging experiments is the detector system. Recently two different micro-set-ups with a field-of-view of about 25-30 mm and a resolution better than 50  $\mu\text{m}$  have been realized [1,2]. The disadvantage of these set-ups is the high-cost of the detector systems. A conventional low-cost upgrade of the standard CCD-based detector systems can provide comparable results. The use of a commercially available high-resolution lens system optimized for high-end digital cameras provides a 1:1 projection ratio without big losses of light intensity and image distortions. In this way the limiting factor is the pixel size of the CCD camera. Improvement of the scintillator screen can increase the resolution further.

#### Experiment and results

Using a cold neutron beam with a negligible gamma content is a precondition for applying scintillator screens based on Gadox ( $\text{Gd}_2\text{O}_2\text{S}(\text{Tb})$ ) active layers. The scintillating layer can be very thin in comparison to the standard  $^6\text{LiF}$  based scintillators due to the higher cross-section of Gd for cold neutrons. Fig. 1a presents the result of a resolution test of a CCD-camera-based detector system using a 10  $\mu\text{m}$  thick Gadox screen, 200 mm Nikon lens (AF Micro-Nikkor 200 mm f/4D) and 2048x2048 pixel CCD camera (Andor DW436N-BV).

The pixel size for the presented image was 13.5  $\mu\text{m}$  resulting in a field of view of 28 x 28  $\text{mm}^2$ . The achieved spatial resolution as seen in Fig. 1a was 50  $\mu\text{m}$ . The effect of the scintillator screen on the achieved resolution was studied by performing a tomographic investigation on a stainless steel piece with a standard 200  $\mu\text{m}$   $^6\text{LiFZnS:Ag}$  screen, Fig. 1b, and 10  $\mu\text{m}$  Gadox scintillator, Fig. 1c. The improvement of the resolution can be seen clearly in Fig. 1c where the 80  $\mu\text{m}$  crack and the remains of a contrast agent therein are resolved in detail.

The high resolution tomography can be used for investigations of fine details in industrial parts, e.g. fuel distribution in the channels (350  $\mu\text{m}$  diameter) of diesel fuel injector, Fig. 2

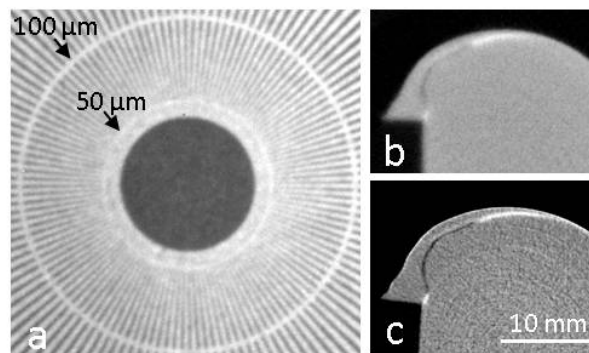


Fig. 1. a) Resolution test of a detector system based on 2048x2048 pixel CCD camera with 10  $\mu\text{m}$  Gadox scintillator screen using a standard Gd test pattern; tomographic slice of a stainless steel piece with a crack using b) 200  $\mu\text{m}$   $^6\text{LiFZnS:Ag}$  screen and c) 10  $\mu\text{m}$  Gadox screen for the measurement.

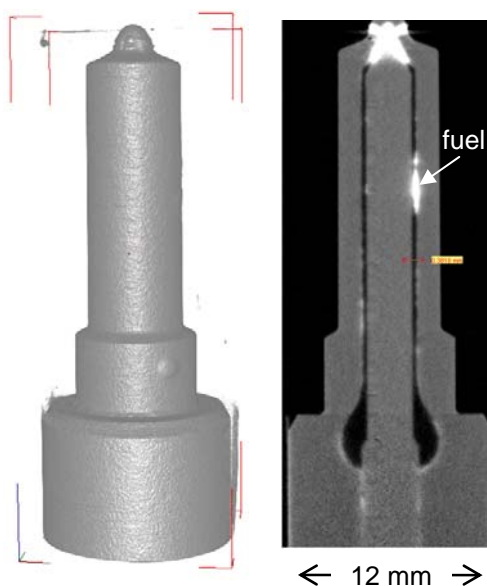


Fig. 2 High resolution neutron tomography of a fuel injector.

#### References

- [1] E. H. Lehmann et al., Nucl. Instr. and Meth. A **576**, 389-396 (2007).
- [2] O. H.W. Siegmund et al., Nucl. Instr. and Meth. A **579**, 188-191 (2007).

	<b>EXPERIMENTAL REPORT</b>  <b>Test of He3 polarisators for imaging</b>	Proposal N° PHY-04-1638-IT Instrument <b>V7</b> Local Contact Nikolay Kardjilov
	Principal Proposer: Nikolay Kardjilov, Ingo Manke, (HZB), Ken Anderson (ILL) Experimental Team: Martin Dawson, Ingo Manke, André Hilger, Nikolay Kardjilov, Markus Strobl, (HZB) Florian Bordenave, David Julian, (ILL)	Date(s) of Experiment  18/03/2008 – 20/03/2008

Date of Report: January 2009

By integrating neutron polarisers with a neutron imaging system it is possible to achieve direct, real-space visualisation of magnetic field distributions both in and around matter. One polariser (the polariser) is used to polarise the neutron beam and a second (the analyser) is used to analyse the cumulative rotation of the polarisation resulting from precession around the magnetic field.

In initial experiments on CONRAD [1] a pair of magnetised solid state benders [2,3], were utilised as polarisers since they have several advantages: they are compact, self-contained and simple to implement. However, they also have the disadvantages that the structure of the benders attenuates the beam, the polarisation is not uniform across the beam, the field of view is limited (1×4cm) and the polarised beam is deflected from straight-through propagation. Recently, new devices (<sup>3</sup>He polarising cells) that overcome these problems have been successfully tested.

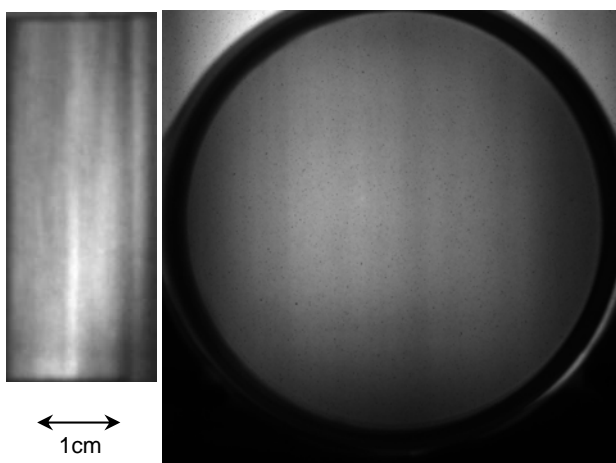


**Figure 1:** Flat field images measured using the bender (left) and the new device (right).

Figure 1 compares flat field images measured using the bender and the <sup>3</sup>He cell. The faint striping pattern in the cell image is caused by beam profile inhomogeneities produced by the

neutron guide. The strong striping pattern in the bender image is caused by beam attenuation produced by the vertical blade structure of the bender.

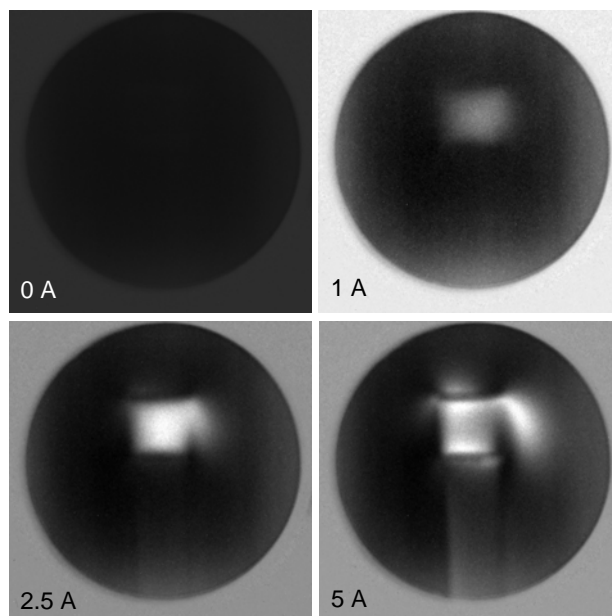


**Figure 2:** Polarised neutron images of a current-carrying solenoid.

Figure 2 shows polarised neutron images of a solenoid carrying alternating currents of varying magnitude. These images were formed by dividing the images measured when the polariser and analyser are aligned anti-parallel and parallel. Brighter regions indicate where there is polarisation rotation caused by the magnetic field around the coil.

### References

- [1] N Kardjilov et al, *Nat. Phys.* **4** pp 399-403 (2008)
- [2] Th Krist et al, *Physica B* **241-243** pp 82-5 (1998)
- [3] Th Krist et al, *Physica B* **356** pp 197–200 (2005)

	<b>EXPERIMENTAL REPORT</b>  <b>Spin-echo-like neutron imaging</b>	Proposal N° ART-04-1728-EF  Instrument <b>V7</b>  Local Contact N. Kardjilov
	Principal Proposer: M. Strobl, HZB & Uni Heidelberg Experimental Team: A. Hilger, HZB I. Manke, HZB N. Kardjilov, HZB	Date(s) of Experiment  22/07/2008 – 29/07/2008

Date of Report: 14/01/2009

Imaging with polarised neutrons provides the opportunity to investigate magnetic fields even in the bulk of massive samples. This has been demonstrated recently with measurements at the cold neutron radiography and tomography instrument CONRAD [1]. It could be shown that even tomographic investigations to derive volumetric reconstructions of magnetic fields are feasible. However, difficulties arise for quantification and reconstruction, when spin rotations bigger than  $\pi$  are induced by the sample. This drawback can be overcome by measurements with different wavelengths in order to retrieve the magnetic field integral along the path of the neutron beam. Here another approach was used, i.e. to apply a spin-echo like technique which has the advantage, that a broad energy spectrum of the incoming beam can be utilised. For that purpose a reference or spin echo field has been introduced in the set-up before the sample position. This precession field has a defined length and can be controlled by an electric current supply. In Figure 1 the response function in a detector pixel is shown when the current was increased from 0 A to 5 A in 500 steps.

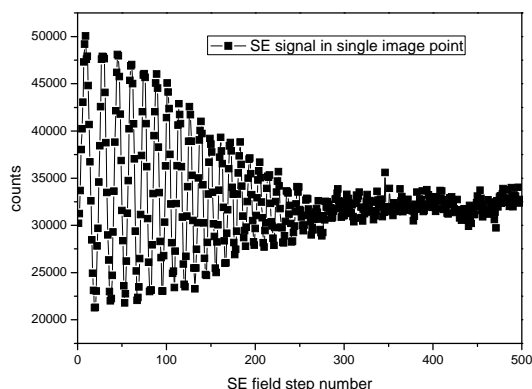


Fig. 1 Response function in the detector for increasing precession field.

As a reference sample the field of a dipole magnet was used, which was directed parallel

to the precession field. However, a  $\pi$  flipper has been installed after the precession field. Hence, in an image position where the spin rotation i.e. the magnetic field integral of the sample matches the one of the first precession field a spin echo should be found. A typical echo function should be found when varying the precession field (as well as spatially along lines of increasing respectively decreasing field integrals of the projection). However, the results of corresponding measurements did not display corresponding echo functions (compare Fig. 2).

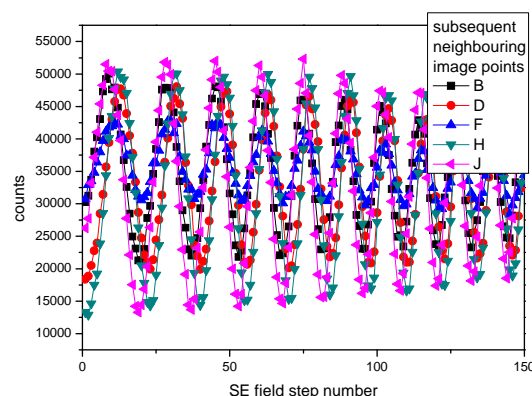


Fig. 2 Results of spin-echo-like measurements of a dipole field for neighbouring image points

The reason might be found in improper magnetic shielding of the preliminary set-up used.

#### References

- [1] N. Kardjilov et al. Nat. Phys. 4 (2008)



## EXPERIMENTAL REPORT

### Using neutrons for non-destructive testing at the surface Part 1

Proposal N° EF/BESSY  
Collaboration  
Instrument **E3**  
Local Contact  
Robert C. Wimpory

Principal Proposer: Christoph Genzel, HZB; Ingwer Denks, HZB;  
Robert C. Wimpory, HZB  
Experimental Team: Robert C. Wimpory, HZB

Date(s) of Experiment  
30/04/2008 – 03/05/2008

Date of Report: 05/01/2009

The new instrument up-grade of E3 in May 2007 [1] has provided a significant boost to the efficiency and number of measurements that can be performed. This not only leads to increase in speed of measurement but also minimises edge effect contributions that normally result from partially submerged gauge volumes rendering strain determination at surfaces more feasible.

These measurements show that for ferritic steel (using the hkl 211 reflection on a Specimen a 10mm thick, specimen previously measured on EDDI [2]), the surface effect appears to be very small in both reflection and transmission geometries at its normal optimal conditions (i.e. without adjusting the optimal bending radius of the monochromator). Normally the bending radius for the optimal operation and the suppression of the surface effect is different [3].

Table 1 shows the strain values obtained for the normal direction. The first two points have a high uncertainty and possibly the first point suffers from 'peak clipping' however it can be seen from 0.098 mm onwards the strain determination is good. With adjustments this can be improved in the future.

Table. 1 Surface strain measurements in normal direction

Position (mm)	Strain (um/m)	Error (um/m)	FWHM (deg)	Time (s)
0.031	-615	180	0.178	7200
0.065	-640	147	0.270	7200
0.098	-184	80	0.273	7200
0.131	-132	71	0.320	7200
0.165	-148	70	0.341	7200
0.198	-158	63	0.352	7200
0.231	-13	62	0.332	7200
0.265	-104	63	0.352	7200
0.298	-42	66	0.358	3600

A gauge volume of  $1.5 \times 1.5 \times 1.5 \text{ mm}^3$  was used, which may seem large but the accuracy of the surface measurements relies on two things a) exact knowledge of where the surface is b) knowledge of the size and shape of the gauge volume. Results indicate that the gauge volume is extremely sharp and determining the surface was possible to about  $\pm 0.01\text{mm}$ . Figure 1 shows the normal and transverse strains from 0.1mm to 2mm showing that the strain more or less zero, as is expected, without need to correct for surface effect.

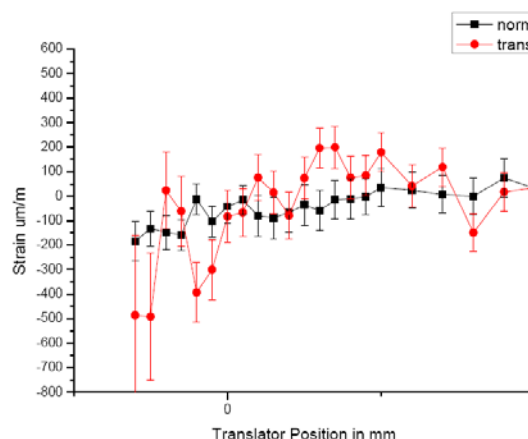


Figure 1. Strain in Normal and Transverse direction in strain-free Fe sample

#### References

- [1] R.C. Wimpory et al, 'Efficiency Boost of the Materials Science Diffractometer E3 at BENSC: One Order of Magnitude Due to a Horizontally and Vertically Focusing Monochromator', Neutron News, Volume 19, Issue 1 January 2008, pages 16 – 19
- [2] I.A. Denks and Ch. Genzel 'Enhancement of energy dispersive residual stress analysis by consideration of detector electronic effects, Nuclear Instruments and Methods in Physics Research B 262 (2007) 87–94
- [3] Miroslav Vrána, P. Mikula 'Suppression of Surface Effect by Using Bent-Perfect-Crystal Monochromator in Residual Strain Scanning' Material Science Forum Vols. 490-491 (2005) pp 234-238



## EXPERIMENTAL REPORT

### Using neutrons for non-destructive testing at the surface Part 2

Proposal N° EF

Instrument **E3**

Local Contact  
Robert C. Wimpory

Principal Proposer: Robert C. Wimpory, HZB, Andrew Venter (NECSA, South Africa)  
Experimental Team: Robert C. Wimpory, HZB

Date(s) of Experiment

31/10/2008 – 03/1/2008

Date of Report: 13/01/2009

The new instrument up-grade of E3 in May 2007 [1] has provided a significant boost to the efficiency and number of measurements that can be performed. This not only leads to increase in speed of measurement but also minimises edge effect contributions that normally result from partially submerged gauge volumes rendering strain determination at surfaces more feasible.

A previous measurement on a strain free sample showed that there was no surface effect on E3 for the Fe (211) peak, the optimal resolution bending radius of the monochromator coinciding with the bending radius where the surface effect is suppressed [2].

In this measurement a sample with a distinctive non-zero residual strain and stress distribution was chosen to see how well one can measure near to the surface. The sample chosen was a 8mm thick two laser pass bent metal plate (from high-energy laser beams) [3].

Neutron diffraction strain measurements have been performed using the (211) Bragg reflection with a scattering angle of  $\sim 78.8^\circ$  and a neutron wavelength of 1.486 Å. A gauge volume of  $1.5 \times 1.5 \times 1.5 \text{ mm}^3$  was employed. The strain components, longitudinal (parallel to the laser path), transverse (in-plate normal to the laser path) and normal (perpendicular to plate surface, i.e. parallel to the laser direction).

Figure 1 shows that the strain could be determined to 0.1mm from the treated surface (0mm) in all directions. The strain gradients were not steep and so de-convolution was not necessary. The stresses in figure 2 are compared to previous E3 measurements. The normal stress, i.e. perpendicular to the sample surface, is flat at around 0 MPa and is 0MPa perpendicular to the surface as expected, showing that near surface measurements are feasible.

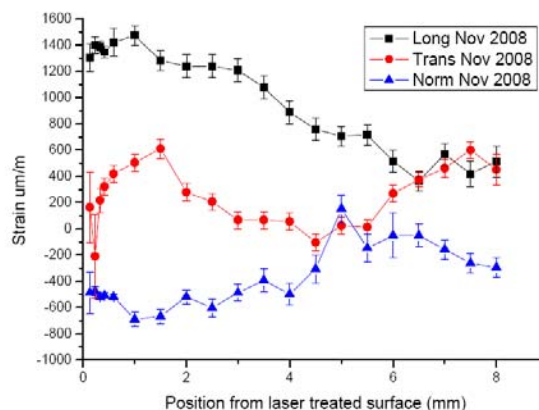


Figure 1. Strain distribution in LS2 sample

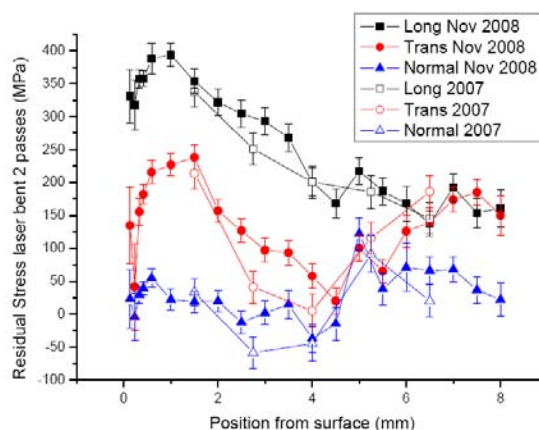


Figure 2. Stress distribution in LS2 sample

## References

- [1] R.C. Wimpory et al, 'Efficiency Boost of the Materials Science Diffractometer E3 at BENSC: One Order of Magnitude Due to a Horizontally and Vertically Focusing Monochromator', Neutron News, Volume 19, Issue 1 January 2008, pages 16 – 19
- [2] Miroslav Vrána, P. Mikula 'Suppression of Surface Effect by Using Bent-Perfect-Crystal Monochromator in Residual Strain Scanning' Material Science Forum Vols. 490-491 (2005) pp 234-238
- [3] Venter, A.M., van der Watt, M.W., Wimpory, R.C., Schneider, R., McGrath, P.J., Topic, M.: Neutron strain investigations of laser bent samples. Materials Science Forum 571-572 (2008), p. 63-68



	<b>EXPERIMENTAL REPORT</b>	Proposal N° EF Instrument <b>V5</b>
	<b>Neutron imaging in a spin-echo instrument</b>	Local Contact C. Pappas
Principal Proposer: M. Strobl, HZB & Uni Heidelberg Experimental Team: A. Hilger, HZB P. Wellert, HZB O. Seidl C. Pappas	Date(s) of Experiment 15/10/2008 – 19/10/2008	

Date of Report: 14/01/2009

Soon after imaging with polarised neutrons has been demonstrated to be a valuable tool for investigations of the spatial distribution of magnetic fields even in bulk samples [1] spin-echo set-ups based on RF-flippers have been utilised for imaging experiments as well [2,3]. All these approaches have been based on polarised monochromatic incoming beams and required measurements with different wavelengths in order to provide quantitative results in cases of spin phase changes bigger than  $\pi$  induced in the field of the sample. Here a different approach similar to a preliminary test at the CONRAD facility described elsewhere in this issue. Imaging experiments on a reference field of a magnetic dipole have been carried out in the spin-echo instrument SPAN. For that purpose a pinhole of  $1 \times 1 \text{ cm}^2$  has been inserted before the first arm of the set-up and a sample position at the end but inside the second spin echo field has been introduced while a polarisation analyser (solid state bender) and a scintillator CCD camera detector have been installed right behind it. This way a spatial resolution of approximately  $200 \mu\text{m}$  could be achieved and images like in Fig. 1 where the main field component is parallel to the spin echo field have been recorded. The typical annular image structure caused by different numbers of multiple spin rotations is clearly visible. The magnet itself is only visible as a black area (nearly no transmission) in the lower right corner. Other structures are due to the attenuation of the sample holder.

Conventional multiple spin-echo scans varying the precession field in the first arm of the spectrometer have been performed for different orientations of the sample. The wavelength chosen was  $0.4 \text{ nm}$ , however, with a loose resolution of app. 10% in order to achieve a performance superior to comparable earlier polarised neutron imaging experiments. Typically scans conveyed 60 steps on a range of about  $12 \text{ A}$  of the spin echo field coil. Three

images are recorded for each step with an exposure time of normally 5 min each. The three images per step allowed for filtering of white spots contaminating the images owed to background radiation.

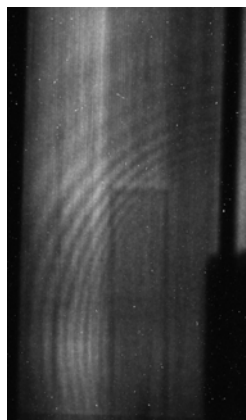


Fig. 1 Typical image ( $3 \times 5 \text{ cm}^2$ ) of magnetic field of dipole

In Fig. 2 the spin echo-signal as scanned for the constellation according to Fig. 1 is displayed for two image points with a spin phase difference of  $\pi$ . Further data analyses are still ongoing.

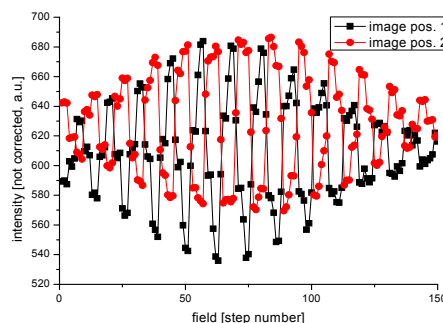


Fig. 2 Spin echo signal in two image point

#### References

- [1] N. Kardjilov et al. Nat. Phys. 4 (2008)
- [2] F. Piegsa et al. NIMA 586 (2008)
- [3] M. Kageyama et al. submitted to NIMA (2008)



## EXPERIMENTAL REPORT

### High resolution investigation on edge effects in neutron imaging

Proposal N° EF  
Instrument **V7**  
Local Contact  
N. Kardjilov

Principal Proposer: M. Strobl, HZB & Uni Heidelberg  
Experimental Team: A. Hilger, HZB  
I. Manke, HZB  
N. Kardjilov

Date(s) of Experiment  
31/08/2008 – 07/09/2008

Date of Report: 14/01/2009

For some time Fresnel diffraction has been accounted responsible for edge enhancement found in neutron imaging and high coherence has been suggested to be needed to achieve such additional contrast [1]. In analogy to results in x-ray imaging the effects have been referred to as phase contrast. However, doubts concerning this explanation arose due to actually achieved coherence conditions and not corresponding results [2]. In order to finally falsify above explanations and to verify that refraction and total reflection effects – which do not require high coherence - can be hold responsible for the measured edge effects a series of systematic measurements has been conducted at the CONRAD instrument. For the purpose a recently developed high resolution detector that allowed for intrinsic spatial resolutions of up to 40  $\mu\text{m}$  could be employed. Several measurements with different samples of round and rectangular cross sections made of Al and Fe have been used and measured under various geometric conditions (Tab. 1).

The results prove clearly that high coherence is not a precondition but corresponding spatial resolution and geometries [2,3] (Fig.1 and 2). Additionally measurements at long straight edges could clarify the role of total reflection (Fig. 3) [3].

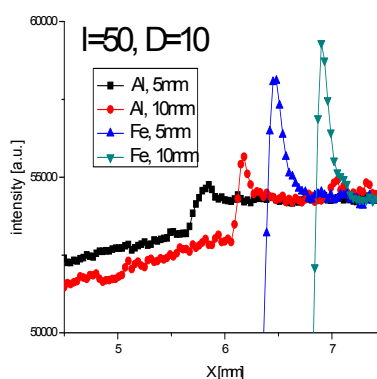


Fig. 2 line profiles of measurements at different cylindrical samples ( $L/D=450$ )

D [mm]	L/D	l [mm]	d [ $\mu\text{m}$ ]
5	900	5, 50, 100	5, 50, 100
10	450	5, 50, 100	10, 100, 200
20	225	5, 50, 100	20, 200, 400
30	150	5, 50, 100	30, 300, 600

Tab. 1 Geometric conditions of conducted radiographic measurements

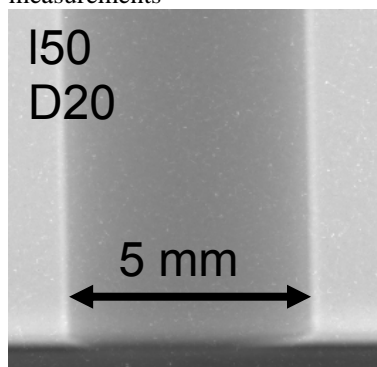


Fig. 1 Example image of a cylinder displaying strong edge effects despite an  $L/D$  of only 225

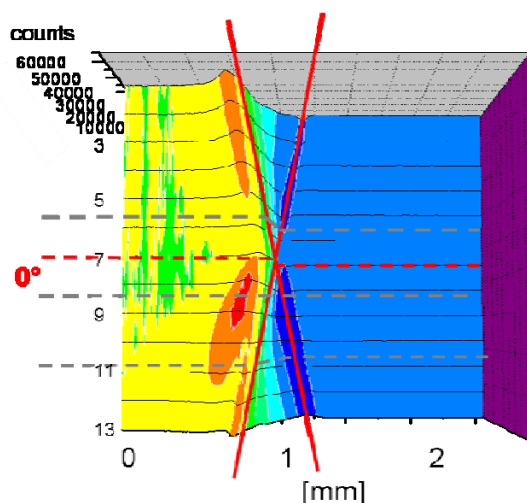


Fig. 3 13 line profiles of measurements at a long straight edge at different angles (increment  $0.05^\circ$ )

### References

- [1] B.E. Allmann et al. Nat. 408 (2000)
- [2] Strobl et al. NIMB 266 (2008)
- [3] Strobl et al. submitted to NIMA

	<b>EXPERIMENTAL REPORT</b>  <b>Application of neutron dark-field contrast imaging</b>	Proposal N° EF Instrument <b>V7</b>  Local Contact N. Kardjilov
	Principal Proposer: M. Strobl, HZB & Uni Heidelberg Experimental Team: A. Hilger, HZB I. Manke, HZB D. Penumadu, Uni Tennessee N. Kardjilov, HZB	Date(s) of Experiment  30/07/2008 – 04/08/2008

Date of Report: 14/01/2009

Recent measurements carried out at the cold neutron radiography and tomography instrument CONRAD utilizing a grating interferometer demonstrated the feasibility of efficient dark field radiography and tomography measurements [1]. This technique enables the detection and 3-dimensional visualisation of regions with altered scattering i.e. microscopic structure not amenable to conventional imaging. Consequently the method has a high potential of applications in many fields including material sciences.

Measurements have been conducted at the CONRAD instrument equipped with the grating interferometer investigating several samples. The kind of samples exposed have been fatigue test specimens made of Al and Fe. Due to the fact that applied strain alters the microstructure - conventionally investigated in scattering experiments with no respectively limited spatial resolution - until material failure e.g. cracks occur such samples seem to be well suited for dark field contrast imaging investigations. An example of radiographic results on a 2024-T3 Al alloy fatigue test sample is presented in Fig. 1. Although no broad regions of altered structure around the designated crack region could be identified – most probably due to too low scattering in the relatively thin (5 mm) Al, microcracks in the corresponding area could be visualised (only) in the dark field image.

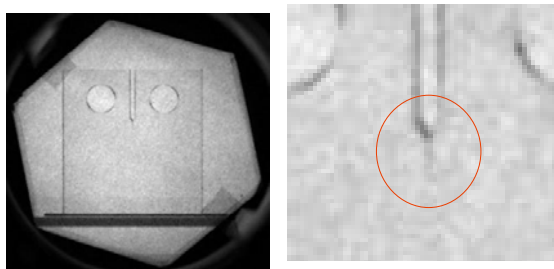


Fig. 1 Dark field image of a 0.5 mm thick Al fatigue test sample. Right side detail displaying microcrack not detected with attenuation and phase contrast

Other samples have been e.g. Al-Si binary metallic alloys castings with varying levels of hydrogen concentrations in the initial melts. Fig. 2 displays radiographies due to the three contrast parameters and it is obvious that certain structures in the sample are revealed only in the dark field contrast images.

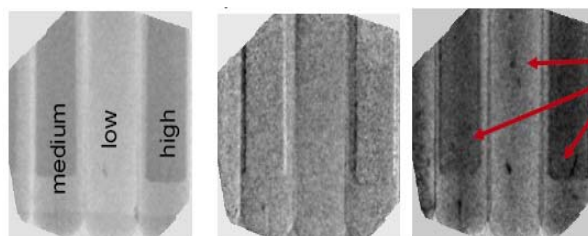


Fig. 2 Attenuation, phase and dark-field images of Al-Si binary castings

These structures also found in the volumetric tomography data (Fig. 3) are assumed to be related to microscopic porosity which shall be verified by further investigations, e.g. by USANS.

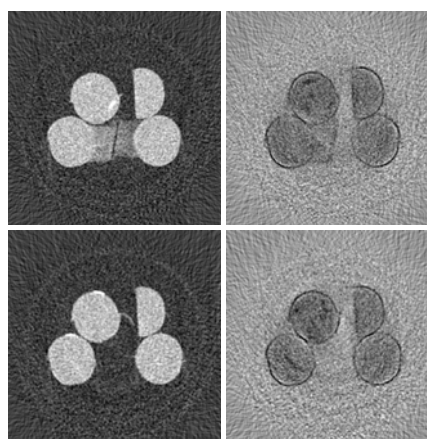


Fig. 3 Tomographic cross sections of attenuation contrast (left) and dark-field contrast (right)

#### References

[1] M. Strobl et al. PRL 101, 123902 (2008)



## EXPERIMENTAL REPORT

### V12a DCD equipped with polarizing devices

Proposal N° EF  
Instrument **V12a**  
Local Contact  
W. Treimer

Principal Proposer: S.O. Seidel, W. Treimer, University of Applied Sciences  
Experimental Team: S.O. Seidel, University of Applied Sciences - FBII  
Robert Monka, University of Applied Sciences  
O. Ebrahimi, University of Applied Sciences – FB II  
W. Treimer, University of Applied Sciences – FB II  
and HZB

Date(s) of Experiment  
  
November 2008

Date of Report: January 2009

In order to use the V12a for USANS with polarized neutrons we performed test measurements using polarizing benders and super mirrors.

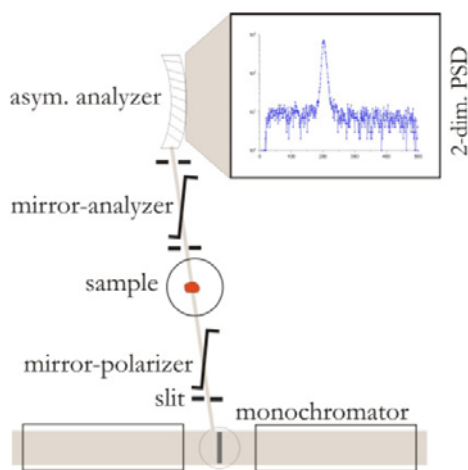


Fig. 1: Schematic drawing of the setup

Fig.1 shows the basic geometry realized by super mirrors, which required shifting the detector unit around 30 cm to the end of the optical bench. Then it was possible to place both mirrors sufficiently apart from each other, leaving enough space for the sample. Additionally we placed two slits in front of both mirrors. The produced plateau-effect due to improved beam geometry can be seen in Fig.2.

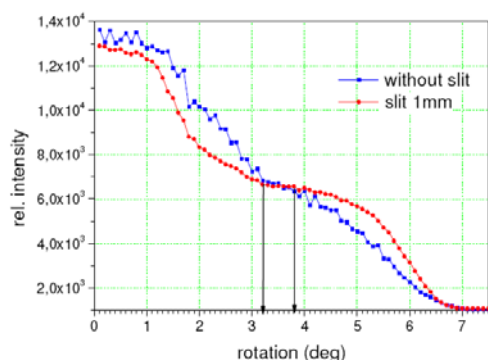


Fig. 2: Sum profile polarizer

After this adjustment the first plateau of polarization was defined around 0.7 deg. We analyzed the polarization with the downstream installed mirror. Due to the lack of space we used only a depolarizing iron plate and measured the intensity between and behind both mirrors.

Figure 3 depicts the sum profile for all rotation steps with polarized and unpolarized neutrons. Clearly, the influence of the iron plate position (in-between and behind the mirrors) can be seen in the shifts of the intensity curves. Additionally, we have illustrated the polarization ratio dependency on the degree of rotation of the analyzer.

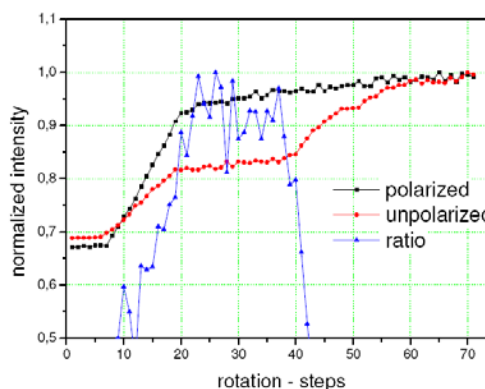


Fig. 3: Sum profile - Shim test with iron plate

In a further measurement, with orientation angle placed in the center of the first plateau (Fig. 2), the degree of polarization  $P$  was determined as

$$P = \left[ \left( \frac{\varphi_{pol} - \varphi_{background}}{\varphi_{depol} - \varphi_{background}} \right) - 1 \right] * 100$$

Using the specified formula above, we defined an average polarization of about 85 percent.

*This work was financed by the BMBF project 03TR7TFH*



## EXPERIMENTAL REPORT

### Installation and the implantation of an area detector dedicated to small angle scattering

Proposal N° EF  
Instrument **V12a**  
Local Contact  
W. Treimer

Principal Proposer: Robert Monka, W. Treimer, University of Applied Sciences  
Experimental Team: Robert Monka, University of Applied Sciences  
Sven-Oliver Seidel, University of Applied Sciences – FB II  
Omid Ebrahimi, University of Applied Sciences  
W. Treimer, University of Applied Sciences and HZB

Date(s) of Experiment  
  
April, May 2008

Date of Report: January 2009

The installation and start-up of the area detector for the V12 Instrument made it necessary to improve the existing detector system shielding, and to equip the steering computer with an appropriate measuring map as well as with the control card for the motor control and configuration panel. First of all the detector was positioned on adjustment devices (rotation, translation, tilting) and attached to the computer-aided measuring system. Subsequently, the curved analyzer crystal was adapted, so that the characterization of the detector characteristics could be performed.

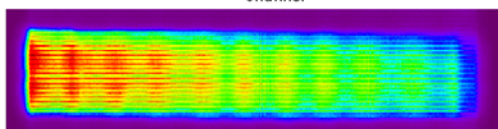
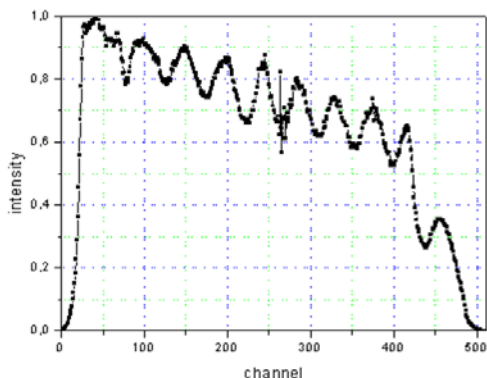


**Fig. 1:** Sum profile for the correction curve as a function of the rotation of the analyzer

Due to the new configuration it was necessary to detect a correction curve (Fig1). The following test measurements (Table1) and adjusting measurements for the motor control analyzer crystal by means of a LabView surface served at the same time for the test the reliability of the entire measuring system as well as the determination of the device-specific parameters.

Figure 2 depict the curves for the bending of the analyser to determine the q- values.

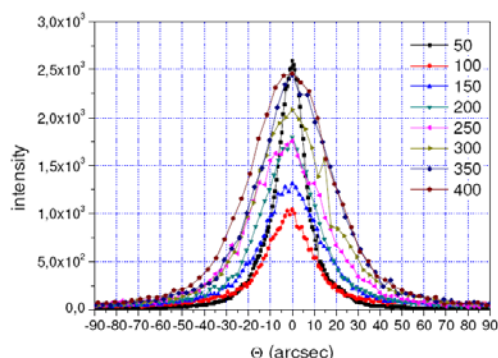


**Fig. 2:** V12a rocking curves depending on the bending of the analyzer

Tables 1 show the results e.g. the horizontal and vertical spatial resolution, the determination of the momentum transfer (Q-range and q-resolution) and the neutron flux in front of the sample position.

**Table 1:** Results of test measurements with the new 2- dimensional detector

Neutron guide	NL3B, curved R = 500
Monochromator crystal	perfect Si single crystal (111), edged, asymmetric alpha
Wavelength	0.4758 nm
Diffract. analyser crystals	perfect Si single crystal (111), edged, completely asymmetric
Neutron flux at sample position (bending 100µm)	$\Phi=2300 \text{ n/s} \cdot \text{cm}^2$
Resolution	hor.: 382µm / Pixel vert.: 770µm / Pixel
$\Delta q$ - resolution	$(0,069-0,237) \cdot 10^{-3} \text{ nm}^{-1}$
Detector	He3 Denex 200TN active area: 190x190 mm <sup>2</sup> yield of neutrons: up to 90%

*This work was financed by the BMBF project 03TR7TFH*



## EXPERIMENTAL REPORT

### Influence of Beam Divergence on Coherent Neutron Diffraction

Proposal N° EF  
Instrument **V12b**  
Local Contact  
W. Treimer

Principal Proposer: O. Ebrahimi, W. Treimer, University of Applied Science  
Experimental Team: O. Ebrahimi, University of Applied Science  
W. Treimer, University of Applied Science  
S.-O. Seidel, University of Applied Science  
N. Beul, HZB for Materials and Energy  
M. Strobl, University of Heidelberg

Date(s) of Experiment  
  
February 2008 – July 2008

Date of Report: 05/01/2009

In previous experiments (see report) the lateral coherence width in a high resolution double crystal diffractometer (DCD) was investigated by means of diffraction of cold neutrons ( $\lambda = 0.533\text{nm}$ ) by increasing thick Cu wires ( $40\mu\text{m} - 180\mu\text{m}$ ). Loss of interference fringes in the intensity distribution should give a hint about the lateral extent of the coherent neutron wave in the DCD. Earlier experiments have shown that a decrease of FWHM of the rocking curve (RC) did not lead to an enlargement of the lateral coherence width [1]–[2]. The decrease of the Darwin width from  $5.8''$  down to  $1.6''$  was done with special seven-fold reflecting monochromator and analyzer crystals [3]. It is of principle interest to ascertain to what extent a decrease of the incident beam collimation (corresponding to a decrease of  $\Delta\lambda/\lambda$ ) leads to a change (enlargement) of the (lateral) coherence length. For this purpose a soller collimator was placed in front of the Si monochromator which reduced the beam collimation from  $0.5^\circ$  down to  $0.11^\circ$ . A theoretical description for these experiments will be published soon. Here a short (and surprising) summary is given. Fig.1 shows the results for diffraction patterns, having a FWHM of the RC =  $2.2''$  and a beam collimation of  $0.5^\circ$ . The intensity pattern did not show remarkable interference fringes for  $180\mu\text{m}$  wire thickness.

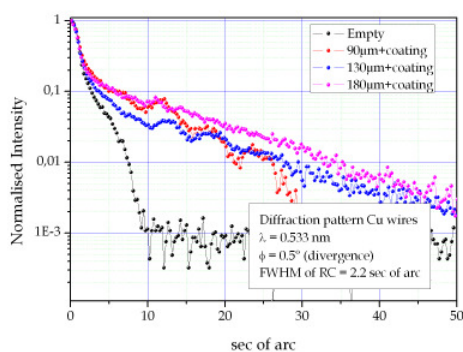


Fig.1 Diffraction pattern of Cu wires divergence =  $0.5^\circ$ .

Small fringes can be seen for  $90\mu\text{m}$  and  $130\mu\text{m}$  wire thickness (+ coatings). Fig.2 shows the same experiments with a reduction of the incident beam collimation in front of the Si monochromator from  $0.5^\circ$  to  $0.11^\circ$ . Interference fringes could be observed for  $130\mu\text{m} + 16\mu\text{m}$  coating, and for the  $180\mu\text{m}$  thick wire (+  $32\mu\text{m}$  coating) some remarkable and unique interference fringes could be observed. However, if the beam collimation alone would determine the coherence properties of the neutron wave then one should have observed much more pronounced interference fringes for  $180\mu\text{m}$  thickness. Having a nearly four-fold better collimation, because the lateral coherence width should be of enlarged of the same order.

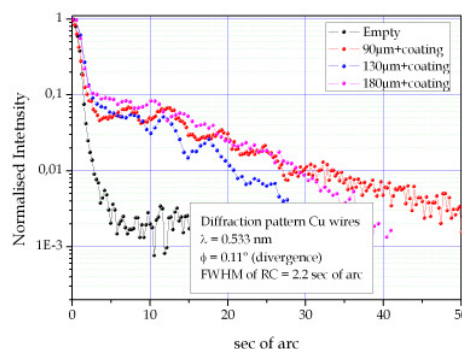


Fig.2 Interference pattern due to different beam collimation  $0.11^\circ$ .

#### Acknowledgement

*This research project has been supported by the BMBF project 03TR6TFH and 03TR7TFH*

#### References

- [1] W. Treimer, M. Strobl, A. Hilger, Phys. Lett. A 305 (2002) 87
- [2] W. Treimer, A. Hilger, M. Strobl, Physica B 385–386 (2006) 1388–1391
- [3] W. Treimer, M. Strobl, A. Hilger, Physics Letters A 289 (2001) 151–154



## EXPERIMENTAL REPORT

### Neutron diffraction by Cu-wires

Proposal N° EF  
Instrument **V12b**  
Local Contact  
W. Treimer

Principal Proposer: O. Ebrahimi, W. Treimer, University of Applied Science  
Experimental Team: O. Ebrahimi, University of Applied Science  
W. Treimer, University of Applied Science  
S.-O. Seidel, University of Applied Science  
E. Rudolf, University of Applied Science  
N. Beul, HZB for Materials and Energy  
M. Strobl, University of Heidelberg

Date(s) of Experiment

February 2008 – July 2008

Date of Report: 05/01/2008

In SAS experiments it is assumed that the whole structure under investigation is coherently illuminated by radiation (neutron or x-rays). The use of a DCD as an (ultra) small angle scattering instrument involves the knowledge of the coherence properties of neutrons in such an instrument and is so of principle interest. Earlier experiments with Si gratings have shown for the V12b DCD a lateral coherence width of about  $80(20) \mu\text{m}$  [1]-[3]. Similar experiments have been performed by the Austrian group in Vienna and Grenoble, using shorter wave lengths and smaller Darwin widths due to different reflections [4]. At the HZB a series of diffraction experiments have been performed with cold neutrons ( $\lambda = 0.533\text{nm}$ ) with the V12b instrument using the tuneable high angular resolution of this set up. In order to determine the lateral coherence length the interference fringes were measured caused by different thick Cu wires. To enhance the diffraction effect a whole set of Cu wires, arranged parallel to each other, were put between the Si monochromator and the Si analyser. We used wire thickness from  $40\mu\text{m}$  up to  $180 \mu\text{m}$ , each of them was coated with a  $\text{NHCO}_2$  compound having different thickness and compositions. A detailed characterization for the index of refraction of this coating could not be found due to lack of information however, a nearly, for all wires, constant value for its index of refraction could be determined. A graphite monochromator (002) reflected neutrons to the Si monochromator (seven-fold (111)-reflection) which served as coherent source for the investigations. The measured intensity with the Si analyser crystal is the convolution of the resolution function of the DCD with the Cu wire diffraction pattern. For the first diffraction series we used an incident beam collimation of  $0.5^\circ$  and a FWHM of  $1.6 \text{ sec of arc}$ . Fig.1 and Fig.2 shows the results:

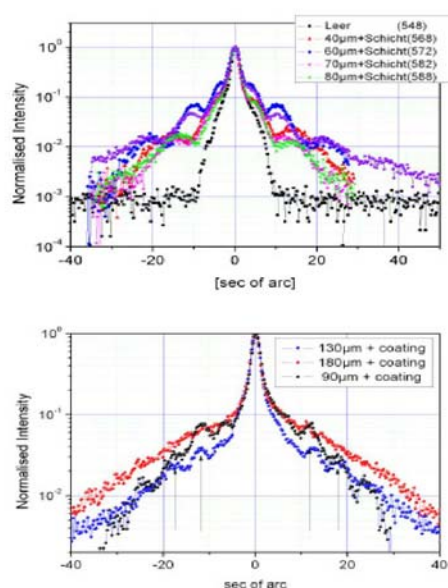


Fig.1 (top) and Fig. 2: Diffraction pattern of different thick Cu wires, see text.

Using thicker wires ( $90\mu\text{m}$ ,  $130\mu\text{m}$  and  $180\mu\text{m}$ ) (small) interference fringes could be observed until a diameter of  $130\mu\text{m} + \text{coating}$ . For a wire thickness of  $180\mu\text{m}$  only usual small angle scattering could be observed. From these measurements a lateral coherent width  $w_{c,l}$  for this set up and collimation could be determined as  $w_{c,l} > 100(30)\mu\text{m}$ .

#### Acknowledgement:

This research project has been supported by the BMBF project 03TR6TFH and 03TR7TFH

#### References

- [1] W. Treimer, M. Strobl, A. Hilger, Physics Letters A 289 (2001) 151–154
- [2] W. Treimer, M. Strobl, A. Hilger, Phys. Lett. A 305 (2002) 87
- [3] W. Treimer, A. Hilger, M. Strobl, Physica B 385–386 (2006) 1388–1391
- [4] E. Jericha, M. Baron, M. Hainbuchner, R. Loidl, M. Villa, H. Rauch, J. Appl. Cryst. (2003). 36, 778-782



## EXPERIMENTAL REPORT

### Single slit neutron diffraction

Proposal N° EF  
Instrument **V12b**

Local Contact  
W. Treimer

Principal Proposer: W. Treimer, O. Ebrahimi, S.-O. Seidel  
Experimental Team: W. Treimer, TFH Berlin, FB II  
O. Ebrahimi, TFH Berlin, FB II  
S.-O. Seidel, TFH Berlin, FB II

Date(s) of Experiment  
May 2008 – July 2008

Date of Report: 12/01/2009

Coherence properties in a DCD (V12a) instrument have been investigated by means of the measurement of the diffraction of cold neutrons ( $\lambda = 0.522\text{nm}$ ) by different thick Cu wires (thickness ranging from  $40\mu\text{m}$  up to  $180\mu\text{m}$ ) that were coated by an electric isolating compound (see reports). In order to validate these results and/or to verify the observed diffraction pattern we used the classical single slit diffraction, which was first done by C. G. Shull [1], and other people [2]. In earlier experiments [3], with the V12b DCD we measured a lateral coherence width of  $80(20)\mu\text{m}$ , assuming a Gaussian wave front incident on the slit. The decrease of the Darwin width of the monochromator and analyser crystal by a factor more than three did not lead to a corresponding enlargement of the lateral coherence width. The beam divergence was  $0.5^\circ$ .

For a series of slit diffraction experiments the beam divergence was reduced down to  $0.11^\circ$  using a solid state soller-collimator in front of the monochromator crystal of the DCD. Figures 1 – 4 show the pattern, assuming different lateral coherence widths.

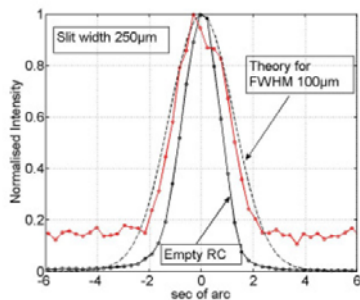


Fig. 1: Single slit diffraction, red experimental points, assumed lateral coherence width:  $100\mu\text{m}$

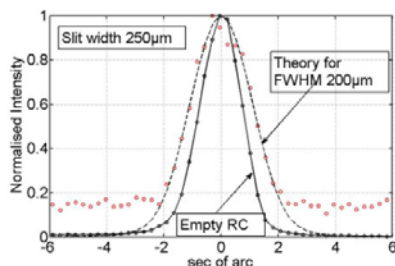


Fig. 2: As Fig.1, assumed lateral coherence width:  $200\mu\text{m}$ , empty RC means not slit in the DCD.

These experiments have been repeated with a  $450\mu\text{m}$  wide slit (Fig.3 and Fig.4)

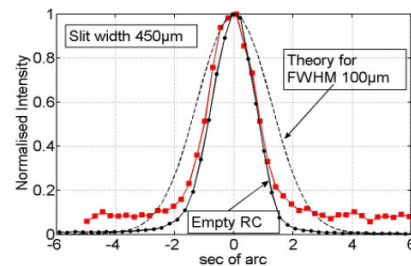


Fig.3: Slit diffraction shows a broadening of the RC, assumed coherence width:  $100\mu\text{m}$

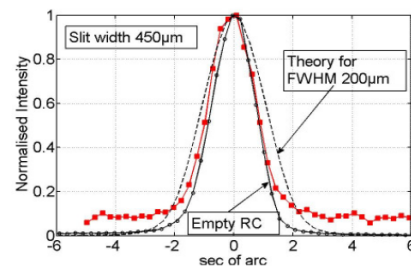


Fig.4: As Fig.3, assumed coherence width:  $200\mu\text{m}$

One has to note two things: Firstly the diffraction data could be fitted well by increasing the lateral coherence width from  $100\mu\text{m}$  (coarse divergence) up to app.  $200\mu\text{m}$  for the slit opening of  $250\mu\text{m}$ , however, a good agreement could already be seen for a  $\text{FWHM} = 180\mu\text{m}$ , secondly, this behaviour could also be observed for a  $450\mu\text{m}$  slit opening, but not satisfying data fit could be found. Increasing to Gaussian wave shape up to plane wave could not fit the data. So other effects (edge diffraction) apparently cause the broadening of the RC as can be seen in Fig.3 and Fig.4.

#### References

- [1] C. G. Shull, Phys. Rev. **179**, 4 752-754 (1969)
- [2] A. Zeilinger, R. Gähler, C.G. Shull, W. Treimer, W. Mampe, Rev. Mod. Physics, Vol 60, 4, October 1988
- [3] W. Treimer, A. Hilger, M. Strobl, Physica B 385–386 (2006) 1388–1391

#### Acknowledgement:

*This research project has been supported by the BMBF project 03TR6TFH and 03TR7TFH*



## EXPERIMENTAL REPORT

### 2 dimensional spin analyzer and Ni/Ti supermirrors

Proposal N° EF  
Instrument **V 14**  
Local Contact  
Th. Krist

Principal Proposer: Th. Krist – HZB, Berlin  
Experimental Team: J.-E. Hoffmann – HZB, Berlin  
G. Heldt – HZB, Berlin  
Th. Krist – HZB, Berlin

Date(s) of Experiment  
2008

Date of Report: 15/01/2009

For the spin analysis of diffusely scattered neutrons at the reflectometer V6 a two dimensional analyzer was built. The cross section is 50mm x 120mm and the length is 600mm. Placed at a distance of 500mm behind the sample it covers an angular range of 6°. The transmitted intensity is recorded at a two-dimensional detector directly behind the analyzer. V6 works at a wavelength of 4.7Å.

The analyzer is made up of six parallel cavities. Each of them consists of two parallel glass plates covered with a nickel layer and a diagonally inserted line of wafers coated with polarizing Fe-Si supermirrors with  $m=2.5$ .

For a test the analyzer was measured at V14 with neutrons with a wavelength of 4.9Å and a polarization of 98.6%, which corresponds to a flipping ratio of 140. The analyzer was shifted through the beam over the full width. Thus all six cavities are examined.

Fig. 1 shows the neutron intensity for both spin components transmitted through the analyzer together with the flipping ratio. The data are raw data without any correction. We find values for the flipping ratio between 40 and 80. A correction to the incoming polarisation of 98.6% leads to values of 55 to 185.

The analyzer was delivered to V6 and is presently being integrated in the experimental set up.

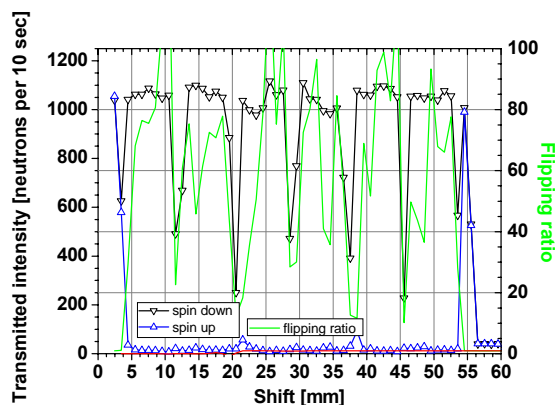


Fig. 1. Neutron intensity for both spin components transmitted through the analyzer described in the text together with the flipping ratio, showing values between 40 and 80 for the raw data.

The investigations in neutron optical devices employing Ni-Ti layers were continued. The research was concerned with optimizing interfacial roughness, stress and neutron reflectivity of Ni -Ti supermirrors by variation of sputter parameters like pressure and flux of the working gas Ar as well as additional gases like nitrogen and air.

At the beginning experiments were carried out with monochromators to characterize the basic structure of these multilayers. The samples were prepared using an in-house DC magnetron sputtering system. To calculate the layer thickness the supermirror-algorithm invented by F. Mezei was used. Subsequently  $m=2$  Ni-Ti supermirrors were produced. Measurements performed at V14 showed a strong dependence of the injected sputtering gas and the used flux. Fig 2. shows the result for an  $m=2$  Ni/Ti supermirror with a reflection of approx. 93% at the edge.

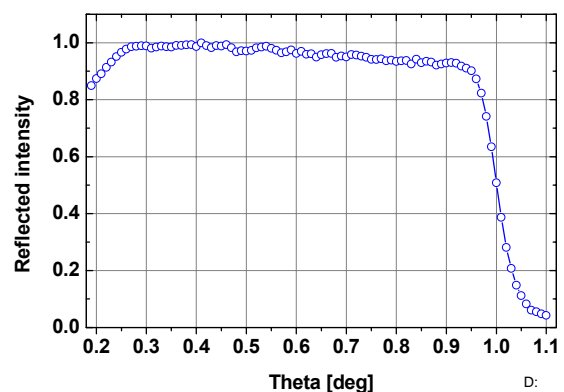


Fig 2: Intensity of the reflected neutron beam from a Ni-Ti supermirror with  $m=2$  relative to the direct beam.

#### Reference:

- [1] F. Mezei, Commun. Phys., 1 (1976), 81



## EXPERIMENTAL REPORT

### Time-of-flight Bragg edge imaging at a continuous neutron source

Proposal N° EF

Instrument **V17**

Local Contact  
D. Clemens

Principal Proposer: M. Strobl, HZB and Uni Heidelberg

Experimental Team:  
A. Hilger, HZB  
N. Kardjilov, HZB  
I. Manke, HZB  
T. Kandemir, HZB

Date(s) of Experiment

15/12/2008 – 16/12/2008  
19/12/2008 – 21/12/2008

Date of Report: 15/01/2009

Energy dispersive imaging provides spatially resolved information on the internal crystalline structure of bulk samples [1,2,3]. Up to now efficient measurements with state-of-the-art spatial resolution were only possible using monochromatic beams achieved either by crystal monochromators [2] or by energy selectors at continuous neutron sources. However, with the advent of high flux pulsed sources and new developments in the field of fast imaging detectors [4] a huge efficiency gain of such measurements in time-of-flight (TOF) mode become feasible. Corresponding prove of principle experiments have been performed e.g. at ISIS [3] which were however due to conventional detectors not yet able to exploit the potential of spectroscopic measurements because only one wavelength could be recorded at a time. Due to a lack of a suitable detector still the same approach has been used in test experiments at the chopper spectrometer VSANS. A fast intensified scintillator CCD imaging detector [5] has been installed for that purpose at the very end of the VSANS detector tank approximately 30 m downstream the pulse shaping choppers. Only chopper 1, 3 and 4 have been utilised running at a frequency of 50 Hz and phased to achieve a constant wavelength resolution of about 1.5% on a wavelength band from 3.2 to 4.8 Å containing the significant Bragg edge of Fe corresponding to the used samples.

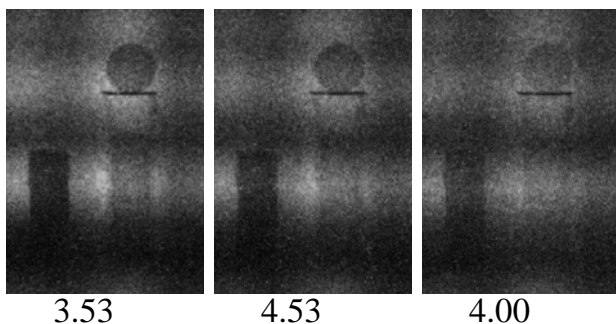


Fig. 1 Radiographic images of different Fe samples at different wavelengths measured in TOF mode (image area is about 5.2 x 7.5 cm<sup>2</sup>)

Due to the limited time for this preliminary test measurements the exposure time of 40 min per wavelength and the wavelength resolution of the detection have been rather limited. However, the results – even as they provide no sufficient signal to noise hindering high spatial resolution and no satisfying wavelength sampling increments (app. 3 %) – demonstrate the feasibility of such measurements at the beam line (Fig. 1 and Fig. 2) and can be the basis of considerations for chopper based TOF imaging allowing in contrast to pulsed sources for variable optimised wavelength resolution for specific measurements.

Further measurements on the basis of the achieved results are foreseen.

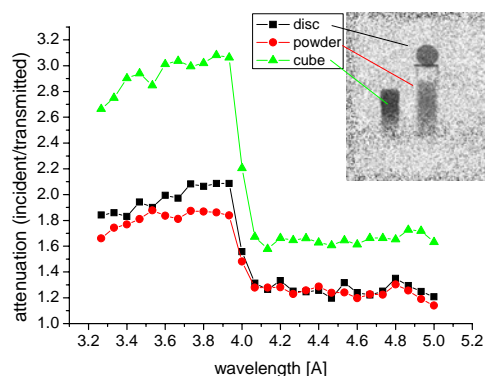


Fig. 2 Attenuation spectra of different samples measured. Resolution and signal are not yet sufficient for spatial resolved Bragg edge analyses (values are mean values of areas corresponding to app 1000 pixels i.e. app. 32 mm<sup>2</sup>)

We would like to acknowledge B. Schillinger for providing the fast intensified CCD camera system

#### References

- [1] J.R. Santisteban et al. J. Appl. Cryst. 34 (2001)
- [2] W. Treimer et al. APL **89** (2006) 203504
- [3] W. Kockelmann et al. NIMA 578 (2007)
- [4] A.S. Tremsin et al., NIMA 592 (2008)
- [5] B. Schillinger et al. Phys. B **385-386** (2006)

	<b>EXPERIMENTAL REPORT</b>  <b>Flux and Spectrum at the V18 position at NL3b</b>	Proposal N° EF Instrument <b>V18</b>  Local Contact M. Strobl
	Principal Proposer: M. Strobl, Uni Heidelberg and HZB Experimental Team: H.-J. Bleif, HZB	Date(s) of Experiment  March 2008

Date of Report: 15/01/2009

A new time-of-flight reflectometer (V18) is currently under construction at the end of the cold neutron guide NL3b in the V-hall. The instrumental design is based on simulations carried out using the VITNESS software package [1,2]. The basis of the instrument simulations are previously carried out simulations of the existing guide system up to the position of the future instrument and a proper definition of the source itself. The guide which starts with the extraction part at app. 1.5 m from the cold source and continues through the rotary shutter is split from about 5 m from the source. The guide NL3b is the lower part of the guide that deviates from the upper part (NL3a) with a curvature (R=500m) 5m and ends at 27m. At that position a flux measurement has been conducted using an Au foil. Subsequently a chopper with a frequency of 50 Hz and a duty cycle of 1% has been placed at the end of the guide. Time-of-flight spectra have been recorded utilizing He3 detectors 3.35m downstream with corresponding data acquisition electronics. In Fig. 1 a measured spectrum is displayed. It clearly shows a local minimum which corresponds to a monochromator further upstream in the beam supplying the V12b double crystal diffractometer with the peak wavelength of 5.2 Å.

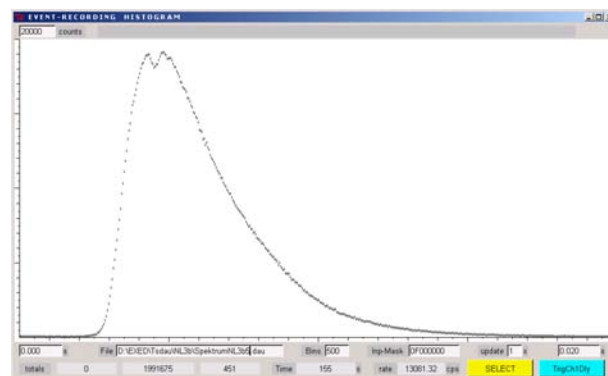


Fig. 1 Time-of-flight spectrum as recorded at the end of the NL3b

The data of both kind of measurements have been evaluated carefully. A total flux density of  $6 \times 10^7 \text{ cm}^{-2}\text{s}^{-1}$  could be found from the gold foil measurement when taking into account the spectrum. The spectrum has been corrected for the efficiency at different wavelengths and then has been scaled with the result of the flux measurement. The resulting spectrum is given in Fig. 2 together with the result from a simulation (scaled to the same total flux). The obvious deviations – except for the dump caused by the monochromator, which has not been simulated - might be due to disalignments of guide pieces. However, the results of the simulations have been downscaled by nearly an order of magnitude.

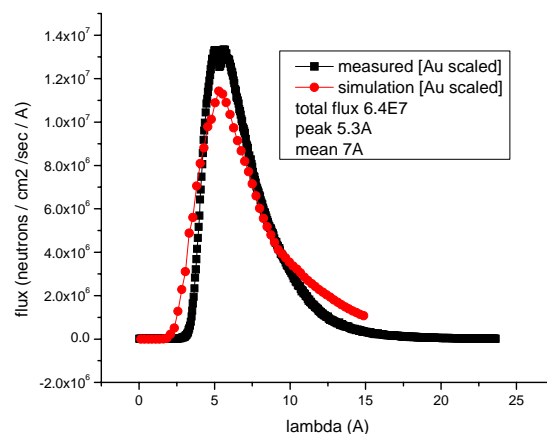


Fig. 2 Comparison of measured and simulated spectra scaled to the measured integral flux density

### References

- [1] G. Zsigmond, K. Lieutenant, F. Mezei Neutron News, 13, 4 (2002)
- [2] <http://www.hmi.de/projects/ess/vitess/>



## EXPERIMENTAL REPORT

### A new tomography for polarized neutrons

Proposal N° EF  
Instrument **V19 (PONTO)**  
Local Contact  
W. Treimer

Principal Proposer: W. Treimer, O. Ebrahimi, S.-O. Seidel, N. Karakas  
Experimental Team: O. Ebrahimi, TFH Berlin, FB II  
N. Karakas, TFH Berlin, FB II  
S.-O. Seidel, TFH Berlin, FB II  
W. Treimer, TFH Berlin, FB II

Date(s) of Experiment  
  
December 2008

Date of Report: 12/01/2009

In the frame of the BMBF financed project 03TRE7TFH a tomography instrument for polarized neutrons is built up and established at the HZB at the neutron guide NL1b at the BERII reactor (Fig.1). This instrument is dedicated to sophisticated experiments with polarized neutrons and neutron tomography.

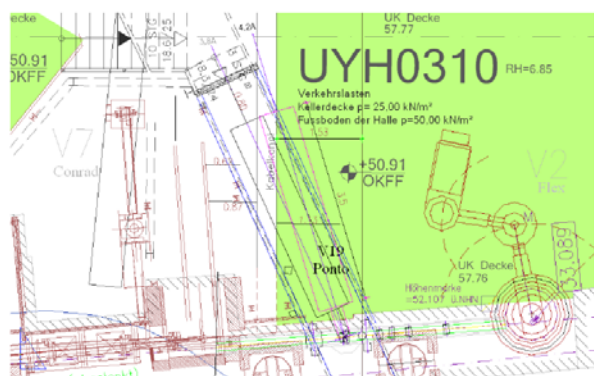


Fig.1 'PONTO' (POLARIZED Neutron TOMography), the new V19 instrument, situated at the N11a BER II at Helmholtz-Centre Berlin

This instrument works with monochromatic neutrons coming from a graphite monochromator (mosaic spread  $0.4^\circ - 0.8^\circ$ ) using a wavelength ( $3.8\text{Å} < \lambda < 4.3\text{Å}$ ), and it will be equipped with a polarizing and analyzing device. The rather short flight path to the 2D detector is app. 3.2m apart from the monochromator. Sample holder and optical devices can be moved on an optical bench and adjusted to the experiment. The field of view (FOV) is determined by the effective reflecting crystal surface of the C monochromator which is app.  $30 \times 30 \text{ mm}^2$ . To change the mean wavelength the instrument can be rotated around the monochromator, moving on air cushions (Fig.2).

A very first test run showed a neutron flux of  $5 \times 10^5 \text{ cm}^2 \text{ sec}^{-1}$ , keeping in mind that the C-monochromator could not be optimized with respect to its Bragg-reflection. This means a gain of a factor five compared to the old V12c instrument which was used as a tomography set up. It was measured by determining the saturation intensity as a function of exposure time of the 2D detector

using diaphragm of  $1 \text{ cm}^2$ , quite in the middle of the sensitive area, for three different distances of the detector from the monochromator (Fig.3). More detailed measurements will be performed if the C-monochromator can be operated automatically. Another quick test with this set up was the investigation of the spatial resolution using a "Siemens star". The spatial resolution with a scintillator thickness of  $400 \mu\text{m}$  was about  $200 \mu\text{m}$ , however, it will be repeated in more detail after the reactor shut down in April 2009.

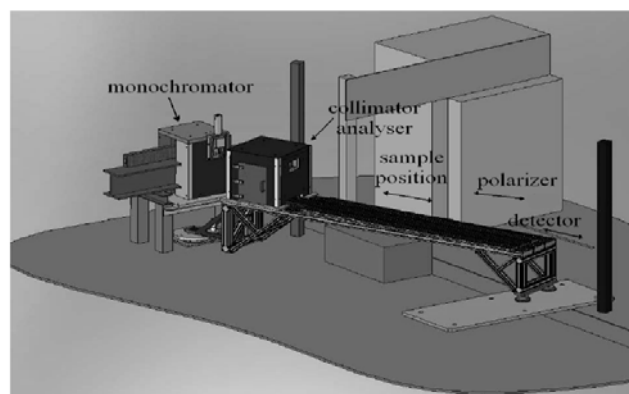


Fig. 2 Sketch of the layout of PONTO.

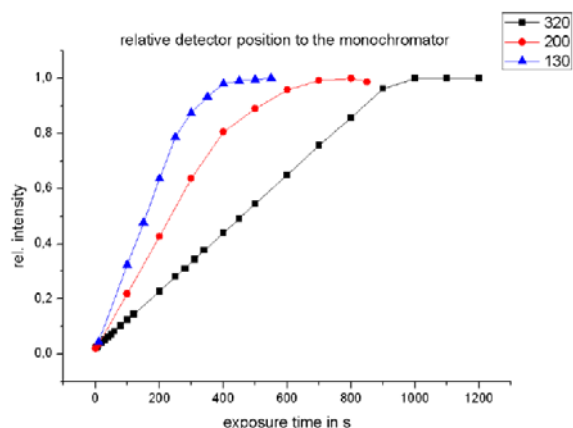


Fig.3 Saturation measurement for the 2D-detector as a function of exposure time for three different detector distances from the monochromator. Area= $1 \text{ cm}^2$

#### Acknowledgement

This research project has been supported by the BMBF project 03TR7TFH

	<b>EXPERIMENTAL REPORT</b>  <b>First neutron tomography with the new experiment V19 "PONTO"</b>	Proposal N° EF Instrument <b>V19 (PONTO)</b>  Local Contact W. Treimer
	Principal Proposer: S.-O. Seidel, O. Ebrahimi, W. Treimer, N. Karakas Experimental Team: S.-O. Seidel, TFH Berlin, FB II O. Ebrahimi, TFH Berlin, FB II N. Karakas, TFH Berlin, FB II W. Treimer, TFH Berlin, FB II and HZB	Date(s) of Experiment  December 2008

Date of Report: 13/01/2009

The new set up V19 (Polarized Neutron Tomography = PONTO) is an instrument dedicated to neutron tomography with polarized neutrons and other sophisticated experiments on neutron scattering and neutron optics. It is situated at the NI1b neutron guide and operates with wave length from 0.38 nm up to 0.43nm served from a graphite crystal which has a reflectivity of app. 80%. The instrument can be rotated around the monochromator and can use a small wavelength band around the Fe Bragg edge and this small rotation option opens the possibility to use the attenuation behavior of Fe around its Bragg edge. Furthermore one can adjust the position of the detector and sample in a distance from 1m to 3.4m to the monochromator crystal. In the first operating position of the monochromator and the optical bench a wavelength  $\lambda = 0.41$  nm was used. After the determination of spatial resolution and flux intensity (see report) we started with a tomography of some teeth that have been already investigated with the small tomography set up V12c (that has been removed). To get a consistent comparison we have taken the same 2D detector facility from V12c. This consisted of a LiZnS scintillator (thickness 400  $\mu$ m), a mirror, a Nikon objective and a CCD-camera with a pixel area of 1k\*1k pixels. The teeth were recorded at two sample positions, 1.7m and 3.2m to get an information about the exposure times/view and resolution. Therefore two different exposure times, 6min and 14min, respectively, per projection (view) were chosen. The tomography contains 451 / 277 projections, dark fields and flat fields with the same exposure time were recorded. The reconstruction of the slices was performed with the program Octopus<sup>®</sup>, the reconstruction of the volume data with VGStudio2.0<sup>®</sup>. Fig.1-Fig.4 shows the results which all were quite promising. The much shorter distance did not lead automatically to a much worse volume reconstruction, which can be partially compensated if more projection were measured.

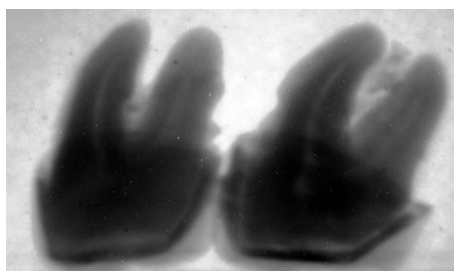


Fig. 1 Radiogram of a couple of teeth

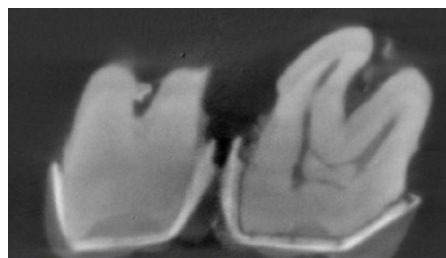


Fig. 2 Reconstructed slice in x-z direction

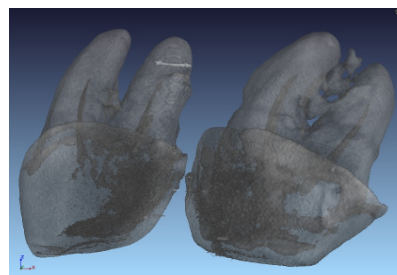


Fig. 3: Reconstructed volume, sample position 320 cm

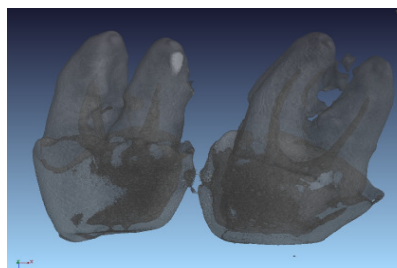


Fig. 4: Reconstructed volume, sample position 170 cm

*Acknowledgement This research project has been financed by the BMBF project 03TR7TFH*

# Magnetism

Magnetic Structure and Phase Transitions	33
Magnetic Excitations	84
Magnetic Thin Films	103





## EXPERIMENTAL REPORT

### High field magnetic state transition in the frustrated kagome lattice antiferromagnets

Proposal N° PHY-02-498

Instrument **E1**

Local Contact  
V. Sikolenko

Principal Proposer: K. Matan, Massachusetts Institute of Technology, MA, USA  
 Experimental Team: Y.S. Lee, Massachusetts Institute of Technology, MA, USA  
 D. Grohol, Massachusetts Institute of Technology, MA, USA  
 V. Sikolenko, Hahn-Meitner- Institute, Germany

Date(s) of Experiment

27/11/2005 – 07/12/2005

Date of Report: January 2009

Neutron scattering measurements in high fields were performed at E1 using VM1 magnet to study  $\text{Fe}_3(\text{OD})_6(\text{SO}_4)_2$ , where  $A = \text{Ag}$  and  $\text{K}$ , a spin  $-5/2$  kagome lattice antiferromagnet. Ag and K jarosites show three-dimensional long-range order for temperature below  $T_N \sim 60$  K and 65 K, respectively.

We have investigated the spin canting due to the Dzyaloshinskii-Moriya (DM) interaction in jarosite using neutron scattering measurements. The in-plane component of the DM interaction forces the spins on a triangle to cant out of the kagome planes to form an “umbrella” structure of ferromagnetically aligned moments within the layers. However, in zero field, the weak ferromagnetic interplane coupling forces the spins on the adjacent plane to align in such an arrangement that the canted moments on any two adjacent layers cancel out each other. In high field, the Zeeman energy overcomes the ferromagnetic inter-plane coupling causing the spins on the alternating layers to rotate  $180^\circ$ . This  $180^\circ$  spin rotation flips the direction of the canted moment on the alternating layers causing the sudden increase in the magnetization at the critical field. This field-induced spin-canting transition corresponds to the non-trivial change in the spin-texture. In particular, the transition yields a net, non-zero value for the scalar chirality. Our elastic neutron scattering measurements in high magnetic field provide the first direct evidence of the  $180^\circ$  spin rotation that gives rise to the magnetic transition at high field in the kagome lattice antiferromagnet.

This work was supported by the NSF under Grant No. DMR 0239377, and in part by the MRSEC program under Grant No. DMR 02-13282

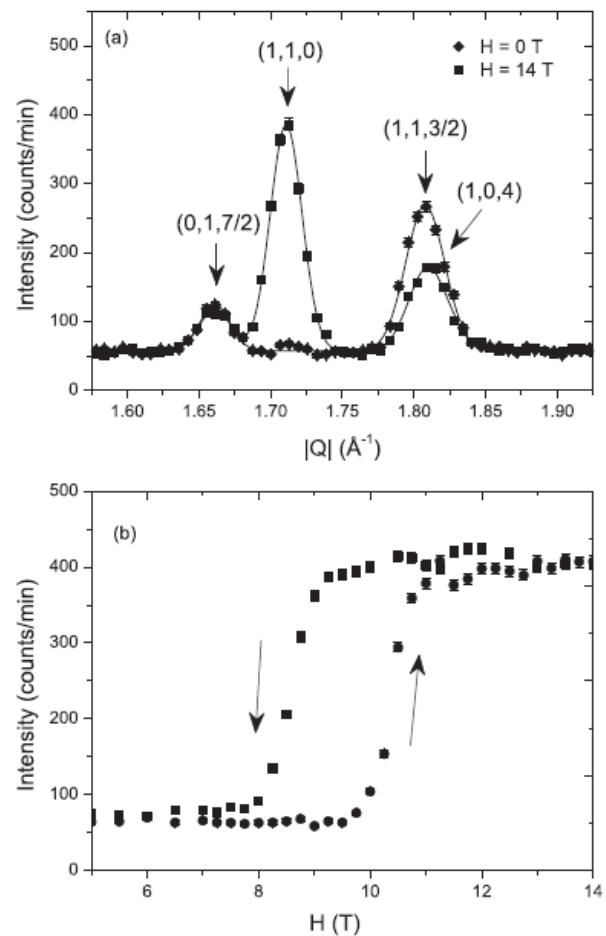


FIG. 1. Elastic neutron scattering measurements were performed using the triple-axis spectrometer E1 at BENSC.

(a) The  $2\theta$  scans at  $T = 3$  K show two magnetic Bragg peaks in zero field (diamonds) at  $(1\ 1\ 3/2)$  and  $(0\ 1\ 7/2)$ , and one magnetic peak in  $H = 14$  T (squares) at  $(1\ 1\ 0)$ . The structural peak at  $(1\ 0\ 4)$  is also denoted by the green arrow.

(b) The field dependence of the  $(1\ 1\ 0)$  peak intensity shows the transition to the ferromagnetic state at high field. The inset shows the derivative of the intensity.



## EXPERIMENTAL REPORT

### Magnetic Structure of Li<sub>2</sub>ZrCuO<sub>4</sub>

Proposal N° PHY-02-640

Instrument **E1**

Local Contact  
Roland Schedler

Principal Proposer:

Wolfram Lorenz

Date(s) of Experiment

Experimental Team:

Wolfram Lorenz, Leibnitz-Institute for Solid State and Materials Research (IFW) Dresden  
Wolf-Dieter Stein, Institute for Solid State Physics, Technical University Dresden  
Roland Schedler, The Berlin Neutron Scattering Centre (BENS), Hahn-Meitner-Institute, Berlin

18/01/2008 – 21/01/2008

Date of Report: 15/01/2009

From the structure of spin-chains of the  $\gamma$ -polymorph of Li<sub>2</sub>ZrCuO<sub>4</sub> frustrated magnetic interactions are expected to be introduced by competing interactions of the nearestneighbour ferromagnetic coupling and nextnearest neighbour antiferromagnetic coupling. For such coupling scheme the ratio of both interactions determines the ground state to be either ferromagnetic or helical separated by a quantum critical point. Our macroscopic studies of Li<sub>2</sub>ZrCuO<sub>4</sub> are well described by helically ordered spin-chain very close to the quantum critical point. The magnetic properties of critical systems provide sensitive testing ground for theories of low-dimensional magnetism. To verify the expectation of helical ordering of this system, we have performed neutron powder diffraction experiments at E9 / BENS. We are grateful to have been able to have been conceded additional beam time at the E1. Li<sub>2</sub>ZrCuO<sub>4</sub> itself and helical magnetic structures in general are highly sensitive to temperature and magnetic fields. To investigate the behaviour of the expected helical structure we examined the dependence of the most intense magnetic structure reflex elastically in the 12 T cryomagnet (VM-2). The experiment was performed on a sample of compressed polycrystalline pallets (~ 10 g) in an aluminium container with a neutron wavelength of  $\lambda = 2.458 \text{ \AA}$ . Data have been collected in zero magnetic field at temperatures of  $T = 3\text{-}15 \text{ K}$  ( $T_N = 6.9 \text{ K}$ ). Within error bars the observed magnetic reflex does show no shift in temperature below the ordering temperature, in accord with comparable data taken at TOFTOF / FRM II. In contrast to this, at E1 we observed broad, but non-vanishing intensity even outside the magnetically ordered phase at for slightly lowered  $q$ -transfer. This observation is surprising, but can not be attributed to a background signal. At  $T = 3\text{K}$  and at  $6.7\text{K}$  – just below the ordering temperature -the magnetic field dependence of

the reflex was examined in an applied magnetic field of  $\mu_0 H = 0\text{-}9 \text{ T}$  (c.f. 1). The observed shift of the reflex in magnetic field supports our expectation of incommensurate magnetic ordering. The sharpening and change in intensity is found to not be due to field induced reorientation of the crystallites.

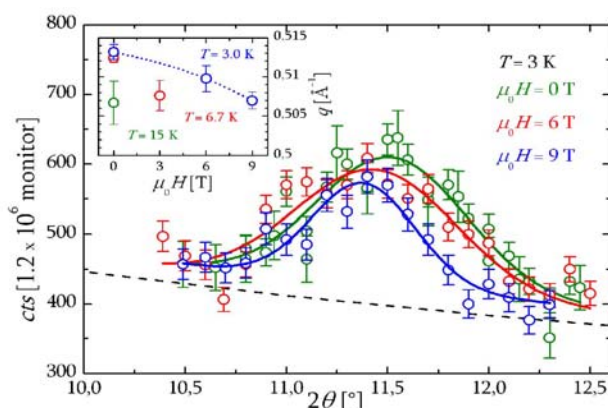


Fig. 1: Magnetic field dependence of the observed magnetic reflex shows shifting and sharpening for higher fields. The background is taken  $\sim (1+1/\sin(2\theta))$ . The inset shows the field dependence of the reflex at 3 K. The reflex showed non-vanishing intensity even outside the magnetically ordered phase.

Altogether, we can conclude from the magnetic field dependence of the magnetic structure, that the compound is indeed likely to show helical magnetic ordering. To reduce the significant neutron absorption by the sample, utilization of isotope enriched <sup>7</sup>Li is recommended for further experiments.



## EXPERIMENTAL REPORT

### Neutron diffraction study of the magnetic structure transformation in the $Y_{0.22}Sr_{0.78}CoO_3$

Proposal N° PHY-02-660  
PHY-01-2366

Instrument **E1, E9**

Local Contact  
F. Yokaichiya

Principal Proposer: P. Saintavit, Université Pierre et Marie Curie  
Experimental Team: Vadim Sikolenko, ETH Zürich and Paul Scherrer Institut  
Vadim Efimov, Joint Institute for Nuclear Research

Date(s) of Experiment

26/11/2008 – 03/12/2008

Date of Report: 12/01/2009

Complex cobalt oxides with perovskite-like structure  $LnCoO_3$  attract a great interest because of unusual magnetic and magnetoresistive properties. Trivalent cobalt exhibit unique electronic phases characterized by interplay between nearly degenerate spin states. Recently cobaltites  $Y_{1-x}(Ca,Sr)_xCoO_3$  with a new type of layer ordering have been synthesized [1-4]. Substitution Sr by Y leads to decreasing of Co-O distances and to formation a new structure. We chose the concentration of yttrium 0.22 because this composition exhibits the highest ferromagnetic moment and the Curie temperature within  $Y_{1-x}Sr_xCoO_3$  series. Doping with calcium ions stabilizes the ferromagnetic component and then suppress it.

We used E9 diffractometer in order to refine the structure and E1 spectrometer to detail study of the temperature dependence of magnetic contribution in some particular reflexions.

The neutron diffraction spectra are preferable described in the frame of orthorhombic, than a tetragonal structure (space group  $Pnma$ ) as a double perovskite ( $a \sim 2 \times 2^{1/2} \times a_p$ ,  $b \sim 2 \times b_p$  and  $c \sim 2^{1/2} \times a_p$ ) At the temperatures close to Curie point a monoclinic distortions have been observed (see Fig.1).

Both samples (with calcium concentration 0.1 and without calcium) exhibit ferromagnetic components. The temperature behaviour of reflexions with magnetic contribution are similar to those observed in [5,6] in the samples with neodymium substitution. The magnetic moment of cobalt directs along c-axis.

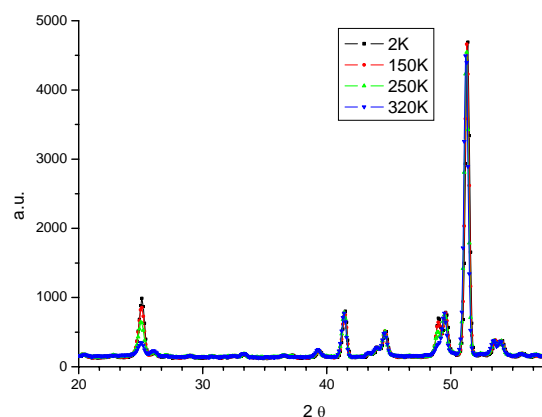


Fig.1. Part of the diffraction pattern, collected at the E9 spectrometer at different temperatures. The reflexion at 25 degree has a magnetic contribution

#### Acknowledgement

*This research project has been supported by the European Commission under the 6<sup>th</sup> Framework Programme through the Key Action: Strengthening the European Research Infrastructures.*

*Contract n°: RII3-CT-2003-505925 (NMI 3).*

*This project has been also partly supported by RFBR, project 08-09-90053-Bel\_a.*

#### References

1. R. Withers et al. *J.Solid State Chem* 174, 198 (2003)
2. M.James et al *J.Solid State Chem* 177, 1886 (2004)
3. S.Istomin et al *Solid State Sci* 6, 539 (2004)
4. S. Istomin et al *Chem Mater* 15, 4012 (2003)
5. V.Sikolenko et al *J.Phys.:Cond.Mat.* 16, 7313 (2004)
6. A.Sazonov et al *J.Phys.:Cond.Mat.* 17, 4181 (2005)



## EXPERIMENTAL REPORT

### Bulk moduli of molecule based magnets: (5MAP)<sub>2</sub>CuBr<sub>4</sub> and Cu Pyrimidine

Proposal N° PHY-02-687

Instrument **E1**

Local Contact  
Karel Prokes

Principal Proposer: Stefan Süllo, TU Braunschweig  
Experimental Team: Dirk Schulze Grachtrup, TU Braunschweig  
Karel Prokes, BENSC  
Norbert Stüßer, BENSC

Date(s) of Experiment

11/12/2008 – 15/12/2008

Date of Report: 14/01/2009

Recently, it was demonstrated that the pressure dependence of the structural and magnetic properties of molecule based magnetic materials can be predicted by state-of-the-art ab-initio electronic structure calculations with good accuracy [1]. Based on these studies additional calculations have been carried out for related materials and which now should be checked by experiment [2].

One of the materials under consideration, Cu Pyrimidine  $\text{Cu}(\text{C}_4\text{N}_2\text{H}_4)(\text{NO}_3)_2(\text{H}_2\text{O})_2$ , previously has been characterized as S=1/2 staggered antiferromagnetic Heisenberg chain crystallizing in a monoclinic structure (space group C2/c, lattice parameters  $a=12.14\text{\AA}$ ,  $b=11.44\text{\AA}$ ,  $c=7.46\text{\AA}$ ,  $\beta=113.8^\circ$  at 10K) [3]. For this material corresponding calculations regarding structural pressure effects have been carried out. These calculations predict a bulk modulus of 9.1GPa and a reduction of the lattice constants between 2% and 9%, depending on the crystallographic axis [2].

Originally, the scope of the experiment was to verify the calculations for bulk modulus and reduction of lattice constants for two materials,  $\text{Cu}(\text{C}_4\text{N}_2\text{H}_4)(\text{NO}_3)_2(\text{H}_2\text{O})_2$  and  $(5\text{MAP})_2\text{CuBr}_4$ , using the E6 spectrometer to measure the lattice constants at ambient pressure and an applied pressure of ~10kbar. For technical reasons, the experiment had to be shifted to the E1 spectrometer and limited to measurements for only Cu Pyrimidine. As a result, the experiment represents a feasibility study for such kind of experiments at E1.

The main result of the study is the neutron diffraction spectrum shown in Fig. 1. This spectrum was taken in a pressure cell filled with ~90mm<sup>3</sup> of Cu Pyrimidine powder at a pressure of 7kbar and a temperature of 2K (diameter of sample space in pressure cell ~2.7mm). The measured angles were chosen in such a way that at least 6 Bragg peaks should be accessible to allow a lattice parameter refinement. The measurement time was about 40 minutes per point for 3 different rotation angles (OMGS) of the cryostat,

summing up to a total measurement time of 2h per point.

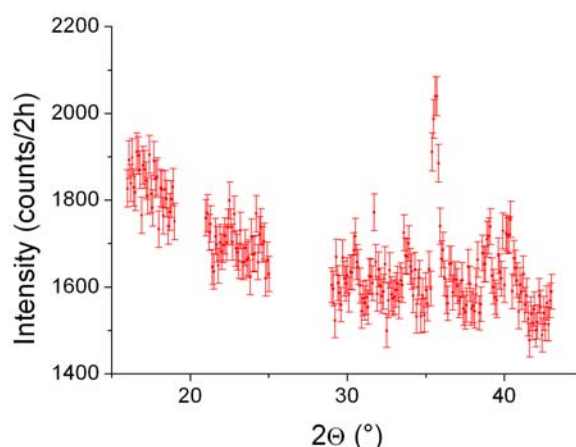


Fig. 1: Neutron diffraction spectrum for Cu Pyrimidine at 2K measured in a pressure cell with an applied pressure of 7kbar.

The spectrum in Fig. 1 shows one peak at ~36° (expected to be the [-1 1 2] and [3 1 0] peaks). At additional peaks can be guessed at ~30°, ~34°, ~39° and ~40°. Only, the low signal-to-noise ratio prevents a lattice parameter refinement of the data. Therefore, up to this point the predictions of the ab-initio calculations could not be verified.

Concerning the issue of feasibility of such kind of experiments at the E1, increasing the sample volume (pressure cell with 6 mm sample space) appears necessary.

#### References:

- [1] J. Kreitlow *et al.*, Phys. Rev. B **72** (2005) 134418
- [2] M. Neef, K. Doll, private comm. (2008)
- [3] R. Feyerherm *et al.*, J. Phys. Condens. Matter **12** (2000) 8495

	<b>EXPERIMENTAL REPORT</b>  <b>Static magnetic and structural properties of the diamond spin chain azurite</b>	Proposal N° PHY-01-2025 Instrument <b>E2</b>  Local Contact Jens-Uwe-Hoffmann
	Principal Proposer: Steffan Süllow, TU Braunschweig Experimental Team: Steffan Süllow, TU Braunschweig Clare Gibson, HMI Jens-Uwe-Hoffmann, HMI	Date(s) of Experiment  28/04/2008 – 04/05/2008

Date of Report: 14/01/2009

Recently, the observation of a  $1/3$  magnetization plateau in azurite  $\text{Cu}_3(\text{CO}_3)_2(\text{OH})_2$  led to the proposal, that this material represents the first realization of a diamond chain of coupled  $S = 1/2$  spins [1]. In its most general form, the distorted diamond chain, the model consists of spin triangles arranged in chain structures, with a magnetic coupling of the diamond backbone  $J_2$ , and the monomer couplings  $J_1$  and  $J_3$  along the chain, with  $J_1 \neq J_2 \neq J_3$ . Key aspects of recent investigations on azurite concerned size and type of these magnetic exchange couplings, and the nature of the plateau phase [1-3]. Surprisingly, a seemingly more trivial aspect, the nature of the phase transition occurring at  $T_N = 1.9\text{K}$  in zero magnetic field, has been studied only superficially. In this situation, we have started an investigation of the second order phase transition of azurite by means of single crystal neutron diffraction.

The experiment was carried out using the flat-cone diffractometer, E2, at BENSC. The single crystal of azurite was aligned in the  $a^*b^*$ -plane and inserted into an orange cryostat. Measurements were taken at 1.4 K and 2.5 K to be certain that the sample was either below or above  $T_N$ , respectively. The neutron wavelength was fixed at  $2.40\text{\AA}$  to ensure greatest resolution from the thermal neutrons.

Sharp reflections were observed at each of the expected structural reciprocal lattice vectors for azurite. Furthermore, additional weak reflections were also observed in the low temperature data set and can be seen in Fig. 1 (highlighted by the red circle). These low temperature peaks confirm the long range antiferromagnetic order of azurite, and which has previously not been observed with neutrons scattering. The propagation vector that best describes these magnetic reflections is  $(\frac{1}{2} \frac{1}{2} \frac{1}{4})$ . Presently, based on these data further analysis is underway to fully refine the magnetic structure of azurite.

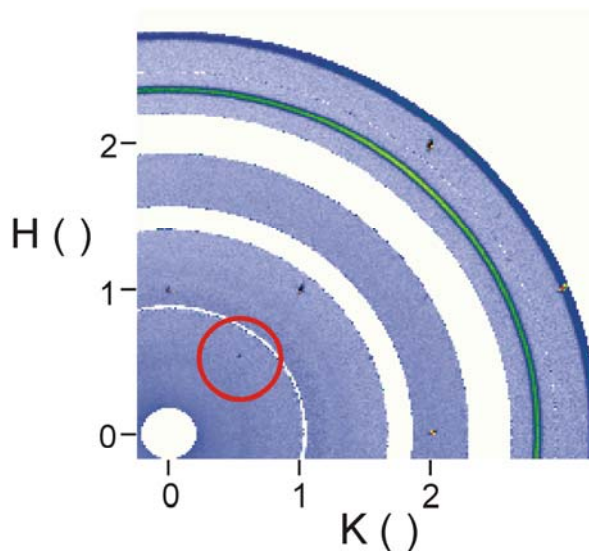


Fig. 1: The diffraction pattern of azurite, measured at 1.4K using the flat cone diffractometer E2 at BENSC. Due to the 2D position sensitive detectors of E2 we were also able to observe scattering in the  $c^*$  direction. A magnetic peak with a propagation vector  $(\frac{1}{2} \frac{1}{2} \frac{1}{4})$ , highlighted by the red circle, is clearly visible.

- [1] H. Kikuchi et al., Phys. Rev. Lett. **94**, 227201 (2005).
- [2] B. Gu, and G. Su, Phys. Rev. Lett. **97**, 089701 (2006).
- [3] K.C. Rule et al., Phys. Rev. Lett. **100**, 117202 (2008).



## EXPERIMENTAL REPORT

### Field-dependence of magnetic order in an Ising magnet in transverse field

Proposal N° PHY-01-2030

Instrument **E2**

Local Contact  
Jens-Uwe Hoffmann

Principal Proposer: R. Coldea, University of Bristol, UK  
 Experimental Team: G.L. Pascut, University of Bristol, UK  
 R. Coldea, University of Bristol, UK  
 J.U. Hoffmann, B. Kemke, K. Kiefer,  
 S. Gerischer, BENSC

Date(s) of Experiment

30/06/2008 – 10/07/2008

Date of Report: 15/01/2008

This experiment was part of our research programme to investigate novel field-induced phase transitions in quantum magnets. Here we apply transverse fields to an Ising magnet to introduce quantum fluctuations and drive a transition from long-range magnetic order to a gapped quantum paramagnetic phase.  $\text{CoNb}_2\text{O}_6$  has ferromagnetic Ising chains running along the  $c$ -axis, and the chains are weakly coupled by frustrated antiferromagnetic interactions in a triangular lattice in the basal  $ab$  plane. The purpose of this experiment was to use the highly-pixelated 2D area detectors of E2 to measure the magnetic Bragg peaks (which all occur out-of the horizontal scattering plane) and determine how the magnetic order evolves with the applied field, in particular find the structure just below the critical field.

A large single crystal of  $\text{CoNb}_2\text{O}_6$  of 6.7 g was mounted with the  $a$ - and  $c$ - axes in the horizontal scattering plane, and vertical magnetic fields up to 5.7 T were applied along the  $b$ -axis, transverse to the Ising direction. The crystal was placed in a dilution insert with a base temperature of 40 mK. An important requirement of the experiment was to have the crystal aligned as precisely as possible with the  $b$ -axis vertical to have the magnetic field transverse to the Ising axes. We initially tried with the attocube goniometer but the torques above 2 T proved to be too large and the goniometer arcs moved. The crystal mount was then replaced with a mechanical copper support that allowed continuous tilting in two direction with locking and this proved rigid in field.

The instrument was operated with an incident neutron wavelength  $\lambda=0.91\text{\AA}$  (Cu) to compress reciprocal space and be able to access Bragg peaks with a vertical component in the range  $-0.8 < K \text{ (rlu)} < 0.2$  using the 2D pixelated area detectors. Typical 2D maps of magnetic Bragg peaks at 0 and 5.2 T are shown in Fig. 1a-b) indicating a change in the ordering wavevector from  $K=1/2$  at low field to a value close to  $1/3$  at high field. Diffraction peaks were measured by collecting 2D images for various sample rotation angles  $\omega$  to cover the peak extent in all 3 directions. Counting times were typically of order 20 to 60 mins for a full rocking curve scan for magnetic

Bragg peaks at high field when the intensities are weak.

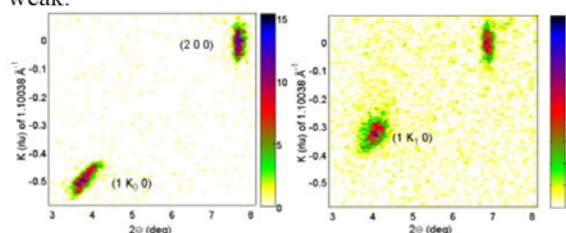


**Fig 1.** Map of the nuclear (2,0,0) and magnetic (1,K,0) Bragg peaks in (a) zero magnetic field and (b) 5.2 T, indicating a shift in the ordering wavevector with field. Data was collected with the 2D area detector and colour is intensity in counts per monitor.

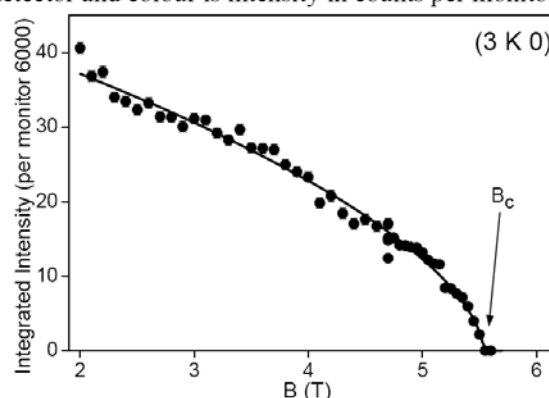


**Fig 2.** Integrated intensity of the (3,K,0) magnetic Bragg peak vs. field, solid line is a power-law fit.

To determine the order parameter and test for possible changes in the magnetic structure upon approaching the critical field we monitored several non-equivalent magnetic Bragg peaks including (1,K,0), (2,K,0) and (3,K,0) and the order parameter for the latter is shown in Fig 2. Complete sets of over 10 magnetic Bragg peaks were collected at 0, 4.4 and 5.2 T to determine the magnetic structure. A quantitative analysis of the data is currently in progress.

*This research project has been supported by the European Commission under the 6<sup>th</sup> Framework Programme through the Key Action: Strengthening the European Research Infrastructures. Contract n°: RII3-CT-2003-505925 (NMI 3).*



## EXPERIMENTAL REPORT

### Crystalline and magnetic structure of mixed $Tb_{1-x}Bi_xMnO_{3+\delta}$ multiferroic material

Proposal N° PHY-01-2100

Instrument **E2**

Local Contact  
Jens-Uwe Hoffmann

Principal Proposer:

Golosovskiy Igor, Petersburg Nuclear Physics  
Institute RAS, 188300 Gatchina, St. Petersburg,  
Russia

Experimental Team:

Vakhrushev Sergey, Ioffe PTI RAS, St. Petersburg,  
Russia  
Jens-Uwe Hoffmann, HMI, Berlin

Date(s) of Experiment

26/06/2008 – 30/06/2008

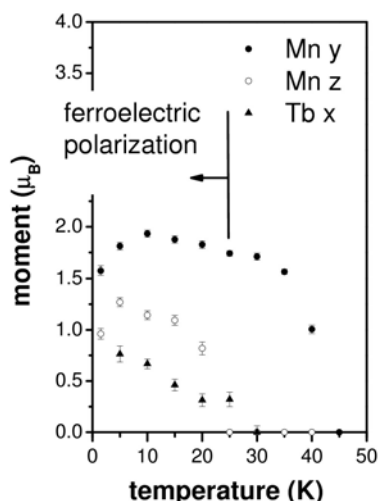
Date of Report: 14/01/2009

Neutron diffraction experiments with the doped multiferroic  $Tb_{0.95}Bi_{0.05}MnO_3$  showed the next principal results:

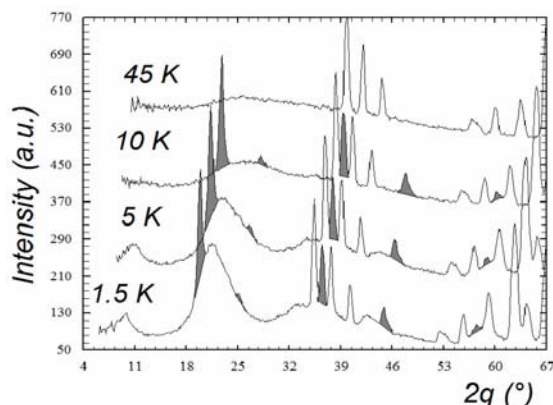
1. In contrast with undoped  $TbMnO_3$  starting from room temperature the ferromagnetic moments with components:  $Tb_x$ ,  $Tb_z$  and  $Mn_x$  (with opposite direction of  $Tb_x$ ) was observed down to 5 K. The initial magnetisation leads to strong texture at the application of the external magnetic field 5T. About 10% of material remains non-textured. Magnetic behaviour in this part differs from the dominant portion.

2. At about 43 K the spiral component of  $Mn_y$  with the propagation vector  $\mathbf{k} = [0 \ 0.283 \ 0]$  appears, the latter weakly changes with temperature.

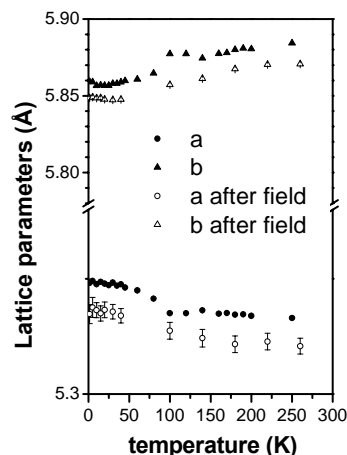
3. At about 28 K (temperature of ferroelectric transition) the magnetic components  $Mn_z$  and  $Tb_x$  (the latter is induced) appears (see figure below). Total magnetic structure corresponds to the A antiferromagnetic mode.



4. The intrinsic helical order of Tb with a new propagation vector  $[0 \ 0.431(5) \ 0]$  appears below about 10 K via a strong short ordering, simultaneously with "ordered moment" within G antiferromagnetic structure (see figure below). The last one has a correlation length of about  $90(10) \text{ \AA}$ .



5. The structural instability was observed in the temperature dependence of the unit cell parameters in the range of 100-150 K. (see figure below: lattice parameters  $a$  and  $b$ ). This instability disappeared after an application of the magnetic field of 5T. Helix parameters remain unchanged; however ferrimagnetic moments appeared aligned along  $y$ -axis.



These results are fully consistent with the results of the magnetic resonant scattering experiments at the single crystal sample conducted at BESSY. The paper combining results from BENSC and BESSY is in progress.



## EXPERIMENTAL REPORT

### Magnetic and crystal structure of $\text{Ho}_3\text{Pd}_4\text{Ge}_4$

Proposal N° PHY-01-2110

Instrument **E2**

Local Contact  
O. Prokhnenko  
J. Hoffmann

Principal Proposer:

L. Gondek, AGH. University of Science and Technology

Experimental Team:

O. Prokhnenko, BENSC  
J. Hoffmann, BENSC

Date(s) of Experiment

18/06/2008 – 24/06/2008

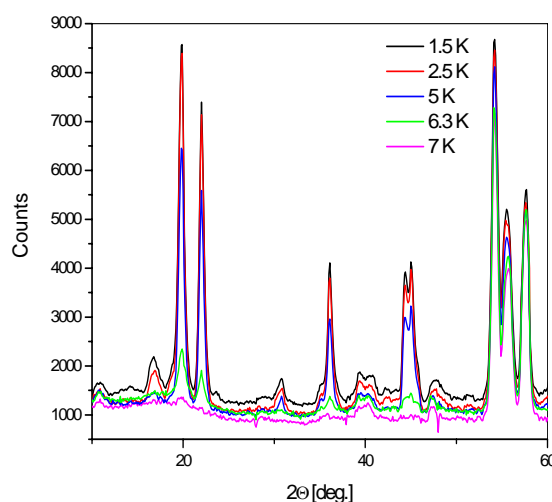
Date of Report: 14/01/2009

The performed experiment on  $\text{Ho}_3\text{Pd}_4\text{Ge}_4$  is a continuation of our previous studies on 344 compounds.

The experiment was intended to be performed on E9 diffractometer, however due to its overloading; it was shifted to E2 apparatus. Measurements performed during experiment revealed that both rare earth sublattices exhibit complicated magnetic ordering resulting with a large number of magnetic reflections below the ordering temperature. The ordering temperature was estimated to be about 6.8 K. Additional transitions can be recognised at temperatures of 2 and 6 K.

In those temperatures additional reflections of magnetic origin vanishes. From this point of view the performed experiment was successful; it was possible to evidence multiple magnetic transitions. However, the low resolution of the E2 diffractometer as well as problems with detectors and soft ware make numerical analyse of the collected data very difficult.

It must be emphasised, that this experiment was the first one running after rebuilding of the E2 detector, so the problems encountered during processing the data are hardly solvable. In present, according to preliminary data taken at E6 diffractometer an effort is made to make some rescaling of the collected data in order to enable reliable numerical refinements.



*I would like to express my gratitude to dr. Jens-Uwe Hoffmann for his assistance in overcoming the technical problems.*

*This research project has been supported by the European Commission under the 6<sup>th</sup> Framework Programme through the Key Action: Strengthening the European Research Infrastructures.*

*Contract n°: RII3-CT-2003-505925 (NMI 3).*



## EXPERIMENTAL REPORT

### Diffuse scattering in the paramagnetic regime of CeRhIn<sub>5</sub>

Proposal N° PHY-01-2190

Instrument **E2**

Local Contact  
J.-U. Hoffmann

Principal Proposer: O. Stockert, Max-Planck-Institut CPfS Dresden  
 Experimental Team: O. Stockert, Max-Planck-Institut CPfS Dresden  
 J.-U. Hoffmann, HMI Berlin

Date(s) of Experiment

03/03/2008 – 12/03/2008

Date of Report: 09/01/2009

The ground states in the heavy-fermion system CeMIn<sub>5</sub> (M = Co, Rh, Ir) are antiferromagnetically ordered or superconducting depending on the composition and/or the application of hydrostatic pressure. Common to all antiferromagnetically ordered CeMIn<sub>5</sub> is the fact that the magnetic structure is quite similar with a propagation vector  $\tau = (1/2 \ 1/2 \ \tau_c)$  and  $\tau_c \approx 0.3-0.5$ . Nesting properties of the Fermi surface seem to be responsible for the magnetic order and already tiny changes in chemical composition or pressure are sufficient to tune the Fermi surface. Within the CeMIn<sub>5</sub> family of compounds CeRhIn<sub>5</sub> has the highest antiferromagnetic ordering temperature  $T_N = 3.8\text{K}$  and orders in an incommensurate magnetic structure with a propagation vector close to  $\tau \approx (1/2 \ 1/2 \ 0.3)$ . The aim of the present proposal was to measure the diffuse scattering on paramagnetic CeRhIn<sub>5</sub> above  $T_N$  in order to extract information about the Fermi surface and possible nesting properties intrinsic in the CeMIn<sub>5</sub> system.

Therefore we investigated the antiferromagnetic order and the diffuse scattering above  $T_N$  in a CeRhIn<sub>5</sub> single crystal. We performed a neutron diffraction experiment on E2 using  $\lambda = 2.4\text{\AA}$ . The crystal was mounted with the  $[1\bar{1}0]$  axis vertical to give a  $[110] - [001]$  scattering plane. Intensity maps were recorded between  $T = 2\text{K}$  and  $10\text{K}$ .

As shown in Figs. 1 and 2 antiferromagnetic Bragg peaks could clearly be observed at incommensurate positions  $\approx (1/2 \ 1/2 \ -0.3)$  and  $\approx (1/2 \ 1/2 \ -0.7)$  confirming the known propagation vector  $\tau \approx (1/2 \ 1/2 \ 0.3)$  of CeRhIn<sub>5</sub>. Around  $T_N = 3.8\text{K}$  the magnetic intensity vanishes. Unfortunately, despite long counting times no diffuse scattering could be detected just above  $T_N$  in the paramagnetic regime (cf. Fig. 2).

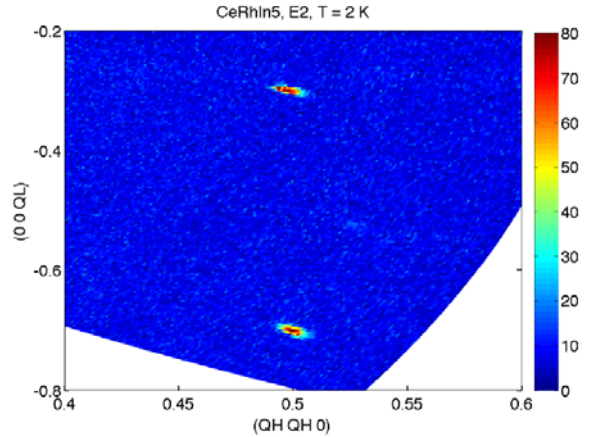


Fig. 1: Intensity map of the reciprocal  $(QH \ QH \ QL)$  plane around  $(1/2 \ 1/2 \ 1/2)$  in CeRhIn<sub>5</sub> at  $T = 2\text{K}$  measured on E2 with  $\lambda = 2.4\text{\AA}$ .

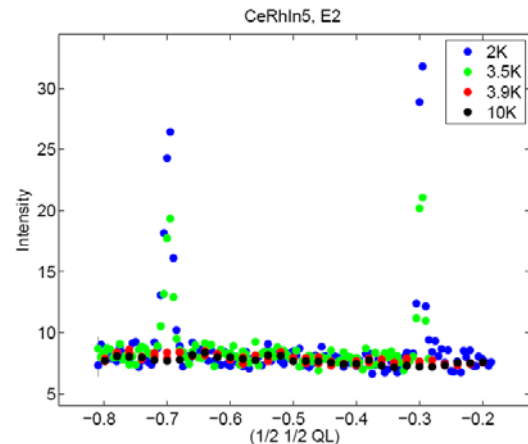


Fig. 2: Intensity cuts along  $[001]$  through  $(1/2 \ 1/2 \ 1/2)$  in CeRhIn<sub>5</sub> at different temperatures below and above  $T_N$ .

Most likely, the diffuse scattering is hidden in the background. At the time of the experiment the diffractometer E2 was not fully optimized with respect to the background. Measurements with energy analysis to enhance the signal-to-background ratio are in progress to study with higher sensitivity.



## EXPERIMENTAL REPORT

### Magnetolectric correlations in multiferroic ErMnO<sub>3</sub>

Proposal N° PHY-01-2341

Instrument **E2**

Local Contact  
Jens Uwe Hoffmann

Principal Proposer: Manfred Fiebig, Uni Bonn, HISKP  
 Experimental Team: M. Fiebig, Uni Bonn, HISKP  
 D. Meier, Uni Bonn, HISKP  
 J.- U. Hoffmann, HZ Berlin

Date(s) of Experiment

18/08/2008 – 25/08/2008

Date of Report: January 2009

In our experiment the competition of the magnetic 3d and 4f sublattices of hexagonal ErMnO<sub>3</sub> and their impact on the microscopy of magnetolectric interactions in this system were investigated. For this purpose, measurements were performed using an Orange Cryostat in combination with a He<sup>3</sup>/He<sup>4</sup> dilution stick at E2. This enabled measurements down to 30 mK, where ErMnO<sub>3</sub> is fully ordered, exhibiting ferroelectricity, antiferromagnetic Mn<sup>3+</sup> ordering and magnetic ordering at the two Er<sup>3+</sup> sites.

Use of the flat cone geometry allowed full scans of the (h0l)-plane at different temperatures, which reveals the symmetry of the different ordered phases. In addition, the intensity of certain reflexes giving access to specific aspects of the multiple order, was traced between 3 mK and 80 K.

A detailed quantitative analysis of the data is still in progress. However, important questions about the rare-earth ordering in hexagonal RMnO<sub>3</sub> can already be answered: Figure 1 shows the intensity of the (301)-reflex probing the rare-earth ordering on the 2a-site as function of temperature. In ErMnO<sub>3</sub> as a representative for all RMnO<sub>3</sub> compounds with a R-ion smaller than Ho<sup>3+</sup> (Er, Tm, Yb), this reflex appears below the Néel temperature T<sub>N</sub> and saturates (figure 1, left panel). Thus the onset of ferromagnetic order on the 2a-site coincides with T<sub>N</sub>. For HoMnO<sub>3</sub> a completely different behaviour was observed by T. Lonkai [1]. Here the 2a-ordering evolves far below T<sub>N</sub>=76 K and discontinuities due to reordering are detected as the temperature is lowered (figure 2, right panel).

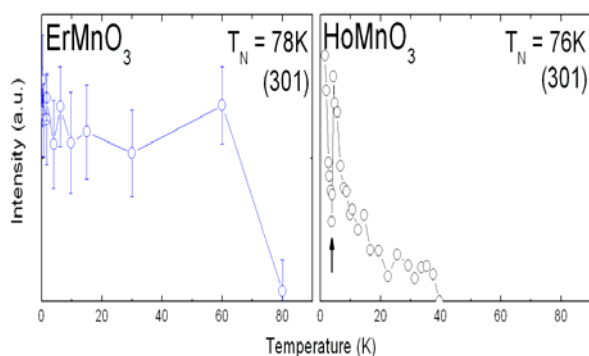


Figure 1: Temperature dependence of the (301)-reflex in ErMnO<sub>3</sub> and HoMnO<sub>3</sub>. The reflex probes the ordering of the rare-earth moments at the 2a-site. HoMnO<sub>3</sub> data from [1].

Furthermore, observation of an upcoming (001)-reflex below T<sub>N</sub> points to a z-component supplementing the Mn<sup>3+</sup> order in the basal xy-plane (presented in figure 2).

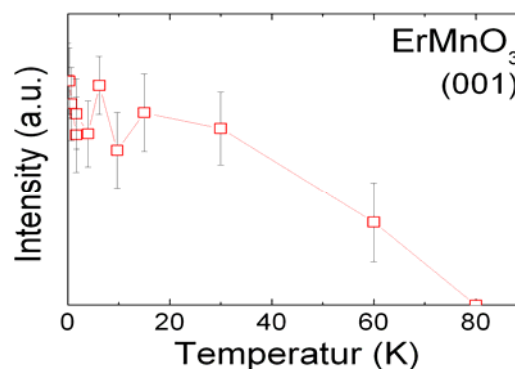


Figure 2: I<sub>001</sub>(T), indicating a z-component of the Mn<sup>3+</sup> order below T<sub>N</sub>.

This observation of a Mn(z) component and a tendency for ferromagnetic Er<sup>3+</sup> order right below T<sub>N</sub> are incompatible with the previously assumed P<sub>6<sub>3</sub>cm</sub> symmetry of the system and indicates symmetry reduction due to unexpectedly pronounced coupling between Mn<sup>3+</sup>, Er<sup>3+</sup> and ferroelectric order.

Further experiments on hexagonal DyMnO<sub>3</sub> will allow to extend our model about the magnetolectric behaviour of hexagonal rare-earth manganites to cases with larger R-ions than Ho<sup>3+</sup>. With HoMnO<sub>3</sub> playing the role of a borderline compound of the series, DyMnO<sub>3</sub> is a key compound to further expand investigations on the competing interactions in hexagonal RMnO<sub>3</sub>.

#### Reference

1. T. Lonkai: *Electric and Magnetic Order Parameters in the Multiferroic Hexagonal RMnO<sub>3</sub> System*, PhD thesis (Universität of Tübingen, 2003)



**EXPERIMENTAL REPORT**  
**Magnetic structure of Ce<sub>2</sub>PdSi<sub>3</sub> and Dy<sub>2</sub>PdSi<sub>3</sub>**

Proposal N° PHY-01-2342

Instrument **E2**

Local Contact  
 J.-U. Hoffmann

Principal Proposer: W.-D. Stein, IFP, TU Dresden  
 Experimental Team: M. Frontzek, IFP, TU Dresden  
 J.-U. Hoffmann, BENSC  
 A. Hoser, BENSC

Date(s) of Experiment

08/07/2008 – 13/07/2008  
 22/07/2008 – 28/07/2008

Date of Report: 03/12/2008

The magnetic structures of the hexagonal  $R_2\text{PdSi}_3$  ( $R = \text{Ho}, \text{Tb}, \text{Er}, \text{Tm}$ ) have been successfully determined on the “old” E2 spectrometer which had been shown to be ideally suited for this task (see for instance [1, 2]). Here, the determination of the zero field magnetic structure on two other  $R_2\text{PdSi}_3$  ( $R = \text{Ce}, \text{Dy}$ ) compounds in a diffraction experiment on the “new” E2 is presented. Single crystals of these compounds became available recently and we conducted the experiment on a  $\text{Ce}_2\text{PdSi}_3$  ( $T_N = 3 \text{ K}$ ) crystal and two  $\text{Dy}_2\text{PdSi}_3$  ( $T_N = 8 \text{ K}$ ) single crystals. The  $\text{Dy}_2\text{PdSi}_3$  single crystals were prepared as small rods and mounted with their respective axis perpendicular to the scattering plane to minimize absorption effects.

The experiment used a standard orange type cryostat, the PG monochromator, additional graphite filters and 15 min collimation. Each sample was measured both in  $(HK0)$  and  $(HHL)$  scattering geometry.

The measurement on  $\text{Dy}_2\text{PdSi}_3$  yielded a commensurate antiferromagnetic structure. The magnetic reflections can be indexed  $(1/6, 1/6, 1/24)$  and  $(1/6, 1/6, 1/12)$ . Reflections are found also on two times of these values.

The measurement on  $\text{Ce}_2\text{PdSi}_3$  at base temperature had very low intensity due to magnetic scattering, due to a small ordered moment and the vicinity to the Néel temperature. Figure 1 shows the reciprocal  $(HK0)$ -plane of  $\text{Ce}_2\text{PdSi}_3$ . The nuclear reflection (2) at the position  $(1.25, 0.75, 0.125)$  originates from a crystallographic superstructure which is found in the whole series [2]. The magnetic reflections are not located in the scattering plane but have an additional  $L$ -component. The values of the direction perpendicular to the scattering plane (i. e.  $L$  values in  $(HK0)$  geometry) could be retrieved directly from the position on the area

detector. The reflections are found on positions  $(0.22, 0, 0.2)$  (A),  $(0.025, 0.15, 0.2)$  (B) and  $(-0.35, 1, 0.1)$  (C). The six-fold symmetry generates intensity on equivalent positions as well.

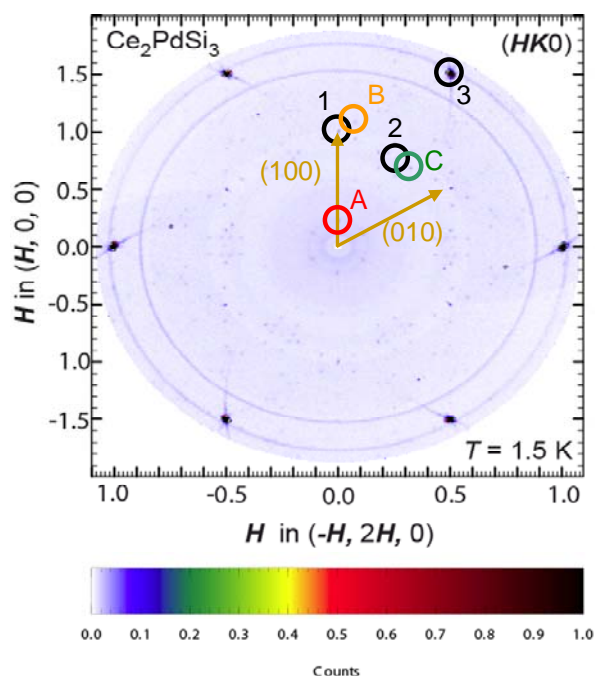


Figure 1: Reciprocal  $(HK0)$ -plane of  $\text{Ce}_2\text{PdSi}_3$  at  $T=2 \text{ K}$ . The plane is derived from the integration of the whole detector height. Two arrows indicate  $1/6$  of the plane defined by reciprocal lattice directions. Within three black circles (1-3) mark intensity due to nuclear scattering. The coloured circles (A-C) mark intensity due to magnetic scattering (see text).

The added resolution in the out-of scattering plane component on the “new” E2 simplified the characterisation of these complex multi- $\tau$  structures. We gratefully acknowledge the financial and technical support from the HZ, Berlin.

[1] M. Frontzek, A. Kreyssig, E. Faulhaber, J.-U. Hoffmann, HMI Exp. Report PHY-01-1747 (2005)

[2] M. Frontzek, S. Raasch, T. Lonkai, HMI Exp. Report PHY-01-1548 (2004)



## EXPERIMENTAL REPORT

### Satellite scattering in multiferroic LuFe<sub>2</sub>O<sub>4</sub>

Proposal N° PHY-01-2350

Instrument **E2**

Local Contact  
Jens-Uwe Hoffmann

Principal Proposer: Annemieke Mulders, Curtin University of Technology  
 Experimental Team: Shane Lawrence, Curtin University of Technology  
 Annemieke Mulders, Curtin University of Technology  
 Jens-Uwe Hoffmann, BENSC  
 Klaus Kiefer, BENSC

Date(s) of Experiment

15/12/2008 – 21/12/2008

Date of Report: 14/01/2009

Magnetoelectric multiferroics are of significant interest as they are materials with simultaneous electric and magnetic order. Within this class of materials there is the potential for strong coupling between the electric and magnetic degrees of freedom. LuFe<sub>2</sub>O<sub>4</sub> is an electronic ferroelectric that has a hexagonal layered structure composed of FeO bilayers separated by single layers of LuO, with the Fe occupying the sites of a triangular lattice within each bilayer. A simultaneously frustrated ferroelectric and ferrimagnetic phase exists below ~250 K [1]. This frustrated order is characterised by both diffuse rods along the  $c^*$ -axis at  $(H/3, H/3, L)$  and discrete diffraction spots characterized by the incommensurate propagation vector  $(1/3 + \delta, 1/3 + \delta, 3/2)$ . Recent work suggests that LuFe<sub>2</sub>O<sub>4</sub> becomes ferroelectric under an applied electric field and is antiferroelectric without an applied electric field [2]. This contradicts results from resonant x-ray diffraction [3]. Latest calculations suggest that under an applied electric field the charge order propagation vector becomes commensurate [4]. In such a case the magnetic structure is also expected to become commensurate.

In this experiment we record the magnetic structure as a function of applied electric field. A crystal of LuFe<sub>2</sub>O<sub>4</sub> was aligned with the (110) and (001) directions oriented in the horizontal plane and mounted between electrodes such that the applied electric field was parallel to the  $c$ -axis. Regions of the (HHL) plane containing portions of the  $(1/3, 1/3, L)$  and  $(2/3, 2/3, L)$  rods were collected as a function of applied electric field and temperature.

Figure 1 compares the magnetic neutron scattering at 180 K integrated along the  $(1 -1 0)$  direction after cooling in zero electric field (Fig 1a), and after cooling in an applied electric field of 4kV/cm (Fig 1b). A difference in intensity due to a change in domain population is observed. Additional data was collected in zero field as well as instantaneous positive and negative fields at temperatures below the magnetic transition temperature. Further analysis of these datasets is required in order to determine the influence of the applied electric field.

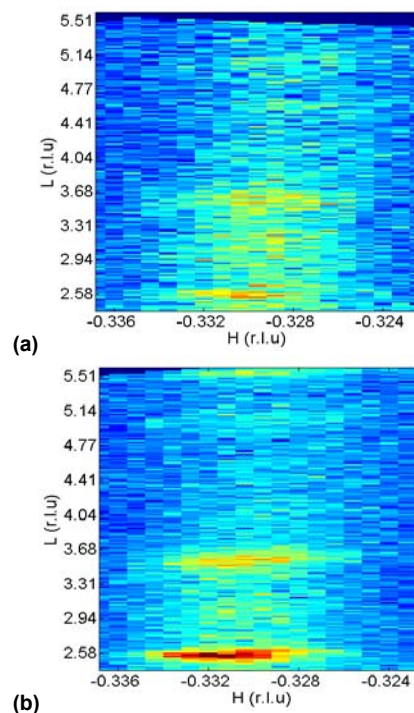


**Figure 1: Preliminary plots of scattering intensity along the  $(1/3, 1/3, L)$  rod at 180 K after being cooled in (a) zero applied field and, (b) an applied electric field of 4 kV/cm.**

#### References

- Ikeda, N.; Ohsumi, H.; Ohwada, K.; Ishii, K.; Inami, T.; Kakurai, K.; Murakami, Y.; Yoshii, K.; Mori, S.; Horibe, Y.; Kito, H., **2005**, *Ferroelectricity from iron valence ordering in the charge-frustrated system LuFe<sub>2</sub>O<sub>4</sub>*, Nature, 436, 1136-1138.
- Angst, M.; Hermann, R. P.; Christianson, A. D.; Lumsden, M. D.; Lee, C.; Whangbo, M. H.; Kim, J. W.; Ryan, P. J.; Nagler, S. E.; Tian, W.; Jin, R.; Sales, B. C.; Mandrus, D., **2008**, *Charge Order in LuFe<sub>2</sub>O<sub>4</sub>: Antiferroelectric Ground State and Coupling to Magnetism*, Physical Review Letters, 101, 227601.
- Mulders, A.M.; Lawrence, S.M.; Staub, U; Garcia-Fernandez, M.; Scagnoli, V; Mazzoli, C; Pomjakushina, E.; Conder, K.; Wang, Y., **2008**, *Direct observation of charge order and orbital glass state in multiferroic LuFe<sub>2</sub>O<sub>4</sub>*, arXiv:0812.3094v1 [cond-mat.str-el].
- Harris, A.B.; Yildirim, T., **2008**, *Charge and Spin Ordering in the Mixed Valence Compound LuFe<sub>2</sub>O<sub>4</sub>*, arXiv:0812.3575v1 [cond-mat.str-el].



## EXPERIMENTAL REPORT

### Temperature evolution of the crystal and magnetic structures in the Ni-Mn-Ga-(Fe,Cu) ferromagnetic shape memory alloys

Proposal N° PHY-01-2353

Instrument **E2**

Local Contact  
J.-U. Hoffmann

Principal Proposer: I. Glavatskyy, Institute for Metal Physics, UA  
Experimental Team: I. Glavatskyy, Institute for Metal Physics, UA  
J.-U. Hoffmann, HMI BENSCH

Date(s) of Experiment

01/12/2008 – 03/12/2008

Date of Report: 20/12/2008

The temperature evolution of the crystal structure of the Ni-Mn-Ga based magnetic shape memory alloys had been a topic of severe discussion over the last years, producing a bunch of publications based on the experimental and ab-initio theoretical studies, often with contradictory results. However, this subject is of particular importance, both for the fundamental and applied points, due to high technological potential of such multifunctional alloys. Thus, we aimed our studies to resolve the conflicts and clarify the crystal structure of the martensite in Ni<sub>2</sub>-Mn-Ga-(Cu, Fe) alloys [1,2] by means of neutron powder thermodiffractometry.

**Experiment:** For the experimental studies with E2 diffractometer at  $\lambda=0.24\text{nm}$ , powder specimens were prepared from highly homogeneous Ni-Mn-Ga-(Fe,Cu) alloys by high impact ball milling, followed with 800°C annealing in argon atmosphere to remove stresses and defects introduced to the material. Measurements were performed during cooling and heating cycles, using the Orange Cryofurnace.

**Results:** Even from the draft analysis and comparison of the obtained diffraction patterns vs. temperature (see e.g. Fig.1 for heating cycle from 20K) we conclude the notable changes in the peak profiles. Thus, while the crystal structure is conserved in general over the entire temperature interval of the martensite phase existence, the strong changes in the (020) and (211) and smaller satellite peaks are most probably caused by the stacking faults, forming the short range order along [010] direction. This is due to the anisotropic temperature dependence of the martensite lattice parameters [3], and thus – changes of the energy of the stacking faults, which is already very low in the martensite phase of the material. Such changes in the crystal structure affect the microstructure of the martensite as well, having the hierarchical twinning morphology from the nanometer up to millimeter scale. Such changes in the defect structure of the martensite, affecting the microstructural level, obviously bring up changes in the transport (magnetic, electric etc.) which are often mistakenly considered in literature as signs of the intermartensitic phase transitions [4].

The most notable changes for this alloy in the martensitic phase occur at  $T\sim 100\text{K}$  and  $\sim 260\text{K}$ , corresponding to the temperatures determined by low-field magnetic susceptibility methods in studies performed preliminary to this diffraction experiment.

Secondly, for the first time in this alloy system, the experimental evidence of the antiferromagnetic order is observed (Fig.1). The AFM phase co-exist with ferromagnetic order in below  $T\sim 100\text{K}$ .

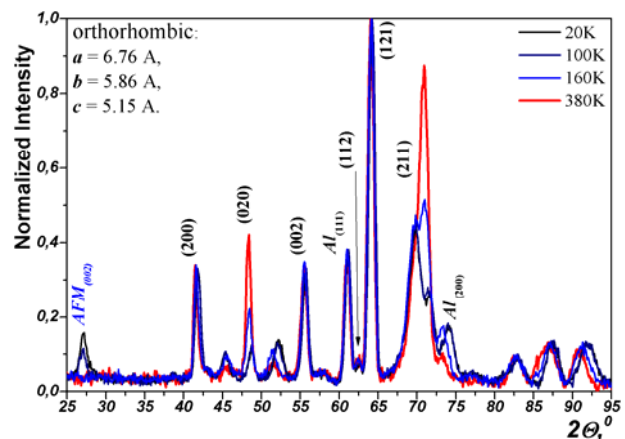


**Fig.1.** Powder diffraction pattern evolution of the Ni-Mn-Ga-Cu(2.7at.%) alloy with temperature.

- [1] I. Glavatskyy, N. Glavatska, Soderberg O., Hannula S.-P., Hoffmann J.-U. // Scripta Mater., 54 (2006), 1891-1895.
- [2] I. Glavatskyy, N. Glavatska, A. Dobrinsky, J.-U. Hoffmann, O. Söderberg, S.-P. Hannula // Scripta Mater. 56/7 (2007), 565-568.
- [3] I. Glavatskyy, N. Glavatska, I. Urubkov, J.-U. Hoffman, F. Bourdarot // Mat. Sci. Eng. A, 481-482 (2008), 298-301.
- [4] O. Heczko, N. Lanska, O. Soderberg, K. Ullakko // J. Magn. Magn. Mater. 242-245 (2002) 1446-1449.



## EXPERIMENTAL REPORT

### Magnetic ordering in multiferroic TbMnO<sub>3</sub> under pressure

Proposal N° PHY-01-2122

Instrument **E4**

Local Contact K. Prokes

Principal Proposer: J. Kamarad, Institute of Physics AS, CR, Prague, CR  
 Experimental Team: O. Prokhnenko, Hahn-Meitner-Institut, Berlin, DE  
 N. Aliouane, Hahn-Meitner-Institut, Berlin, DE  
 K. Prokes, Hahn-Meitner-Institut, Berlin, DE  
 D. Argyriou, Hahn-Meitner-Institut, Berlin, DE

Date(s) of Experiment

04/12/2007 – 14/12/2007

Date of Report: 17/3/2008

The spin frustration in perovskite manganites RMnO<sub>3</sub> leads to complex arrangements of magnetic moments that can break inversion symmetry and cause the coexistence and coupling between ferroelectricity and magnetism [1]. The magnetic ordering of TbMnO<sub>3</sub> exhibits three transitions. The Mn-spins order occurs at  $T_{\text{Mn}} = 41$  K like a longitudinal spin density wave with propagation vector  $\tau$  along crystal  $b$ -direction,  $\tau_{\text{Mn}} = 0.27 b^*$ . The ferroelectric transition occurs at  $T_{\text{FE}} = 28$  K when the Mn-spins develop a cycloidal order. The Tb-spins order independently with  $\tau_{\text{Tb}} = 0.42 b^*$  at  $T_{\text{Tb}} = 7$  K [2]. The transitions are detected by a set of  $(0 k \pm \tau_{\text{Mn}}, \tau_{\text{Tb}})$  neutron reflections satellites below the transition temperatures.

Recently, the bulk magnetic properties of TbMnO<sub>3</sub> were studied under pressure. The critical fields of metamagnetic transitions at 5 K observed with field along  $b$ -axis are affected by external pressure, Fig. 1, showing that the reversals of the Tb-moments and the accompanied flop of electric polarization between  $c$ - and  $a$ -axis are volume sensitive [3].

The E4 diffractometer with the HM3 cryo-magnet and the CuBe pressure cells were used to determine a volume sensitivity of the Tb- and Mn-spins arrangements in TbMnO<sub>3</sub>. The single crystal was compressed in the pressure cell up to 10 kbar at horizontal magnetic field along the  $b$ -axis up to 6.5 T at temperatures from 60 K down to 2 K.

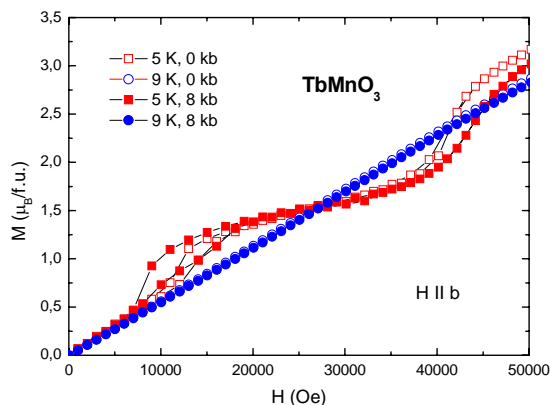


Fig.1: Magnetization isotherms of TbMnO<sub>3</sub> with  $H // b$ -axis under hydrostatic pressure.

The experiment configuration (with the crystal  $a$ -axis parallel to the axis of the E4 diffractometer and the  $b$ -axis along the horizontal field) allows to detect magnetic reflections with the lowest index  $(0 0 \pm \tau_{\text{Mn}} 1)$  and  $(0 0 \pm \tau_{\text{Tb}} 1)$  only. The propagation of both, the Tb- and the Mn-spins order, along the  $b$ -direction showing the most pronounced effects in the bulk magnetization was clearly confirmed with  $\tau_{\text{Mn}} = 0.28 b^*$  and  $\tau_{\text{Tb}} = 0.42 b^*$ .

The magnetic field evolution of the reflections up to 6.5 T at 2 K has revealed a stability of the Mn-spins arrangement with the field insensitive propagation vector  $\tau_{\text{Mn}}$  in this temperature range. However, the propagation vector  $\tau_{\text{Tb}}$  decreases substantially from the value  $\tau_{\text{Tb}} = 0.42 b^*$  to the value  $\tau_{\text{Tb}} = 0.33 b^*$  at magnetic fields where a magnetization plateau was observed in the bulk magnetic measurement (see Fig.1). The further decrease of  $\tau_{\text{Tb}}$  to the value  $\tau_{\text{Tb}} = 0.25 b^*$  was observed at fields above the second metamagnetic transition. This seems to be a tangible evidence of the dominant role of the Tb-spins order in the metamagnetic transitions at temperatures below  $T_{\text{Tb}}$ .

In agreement with the mentioned bulk magnetization measurements under high pressures, the pressure induced changes of both the propagation vectors have been revealed.

The further analysis of the received diffraction data is running.

*This project has been supported by EC under 6<sup>th</sup> FP, Contract n°: RII3-CT-2003-505925 (NMI 3).*

- [1] T. Kimura et al., Nature **426** (2003) 55 and Phys. Rev. **B 71** (2005) 224425
- [2] D. Meier al., New J. Phys. **9** (2007) 100
- [3] J. Kamarád et al., Joint 21<sup>st</sup> AIRAPT and 45<sup>th</sup> EHPRG Conference, Catania 2007



## EXPERIMENTAL REPORT

### Nonmagnetic impurity effect on ferroelectric phase of multiferroic $\text{CuFeO}_2$

Proposal N° PHY-01-2126

Instrument **E4**

Local Contact  
K. Prokes

Principal Proposer: S. Mitsuda, Tokyo Univ. of Science  
Experimental Team: T.Nakajima, S.Mitsuda, M.Yamano; Tokyo  
K. Prokes, K. Kiefer, S. Gerischer; HCB Berlin

Date(s) of Experiment  
18/06/2008 – 27/06/2008

Date of Report: 8. 1. 2009

Delafossite compound  $\text{CuFeO}_2$  (CFO) has attracted increasing interest as a new class of magnetoelectric (ME) multiferroic, because of the recent discovery of the ferroelectricity in the first magnetic-field-induced phase.[1] Unlike the well-studied ME-multiferroics with the ‘cycloid-type’ magnetic orderings (such as  $\text{TbMnO}_3$ ), CFO shows a ‘proper-screw type’ magnetic order with an incommensurate wave vector  $(q, q, 3/2)$  where  $q \sim 0.203$  in the ferroelectric phase.[2] In addition, the previous polarized neutron diffraction study on  $\text{CFAO}(x=0.02)$  have revealed that there is a one-to-one correspondence between the spin helicity, right-handed (RH) or left-handed (LH) helical arrangement of the spins, and the polarity of the induced ferroelectric polarization. This suggests that the origin of the ferroelectricity in this system is not the ‘spin-current model’,[3] but the ‘ $d$ - $p$  hybridization model’ proposed by Arima.[4]

One of the unsolved problems of the multiferroic property in this system is the magnitude of the macroscopic ferroelectric polarization ( $P$ ); the previously reported values of  $P$  in CFO,[1]  $\text{CFAO}$ [5] and  $\text{CFGO}$ [6] are rather different from each other (these values span the range from  $40 \mu\text{C}/\text{m}^2$  in  $\text{CFAO}$  to  $400 \mu\text{C}/\text{m}^2$  in pure CFO). In order to completely elucidate the spin-polarization coupling in CFO system, it is critical to answer the following question: "What determines the magnitude of  $P$  in this system?"

In the present study, we performed polarized neutron diffraction measurements and in-situ pyroelectric measurements on  $\text{CFGO}(x=0.035)$ , which undergoes the ferroelectric transition at  $T_c \sim 8\text{K}$  under zero magnetic field, at the two-axis neutron diffractometer E4 installed at the Berlin Neutron Scattering Center. Spin polarized incident neutrons with wavelength of  $2.44 \text{ \AA}$  were obtained by a pyrolytic graphite (002) monochromator and a supermirror polarizer. The flipping ratio of the polarized neutron beam was  $\sim 8.3$ . The polarization vector of the incident neutron was set to be parallel or antiparallel to the scattering vector by a guide-field of a helmholtz coil and a spin flipper. The sample was cut into a thin plate shape ( $6 \times 10 \times 1 \text{ mm}^3$ ) with the widest surfaces normal to the hexagonal  $[110]$  axis, and was mounted in a pumped  $^4\text{He}$  cryostat with a hexagonal  $(H, H, L)$  scattering plane.

Figures 1(a)-1(b) show the poling electric field ( $E_p$ ) dependence of the asymmetry in the fractions of the LH and RH helical orderings,  $D_{(110)} = (V_{\text{LH}} - V_{\text{RH}}) / (V_{\text{LH}} + V_{\text{RH}})$  deduced from the results of the polarized neutron diffraction measurements, and  $P$  obtained the pyroelectric measurements, respectively. Taking account of the existence of the three magnetic domains originated from the

three-fold rotational symmetry of the crystal, (see the inset of Fig. 1(b)) we performed a least-square fitting analysis of the  $E_p$ -dependence of  $P$ , using the observed values of  $D_{(110)}$ . As shown in Fig. 1(b), the calculated and observed values of  $P$  show a good agreement. From the result of the analysis, the magnitude of the local ferroelectric polarization ( $P_0$ ) in  $\text{CFGO}(x=0.035)$  was determined to be  $\sim 550 \mu\text{C}/\text{m}^2$ . This indicates that  $\text{CFGO}(x=0.035)$  can achieve the ferroelectric polarization comparable to the typical values of  $P$  in pure CFO.

From these results, we conclude that the substitution of a small amount of nonmagnetic  $\text{Ga}^{3+}$  (or  $\text{Al}^{3+}$ ) ions does not largely change the magnitude of the local ferroelectric polarization, but reduces the sensitivity of  $P$  to  $E_p$ .

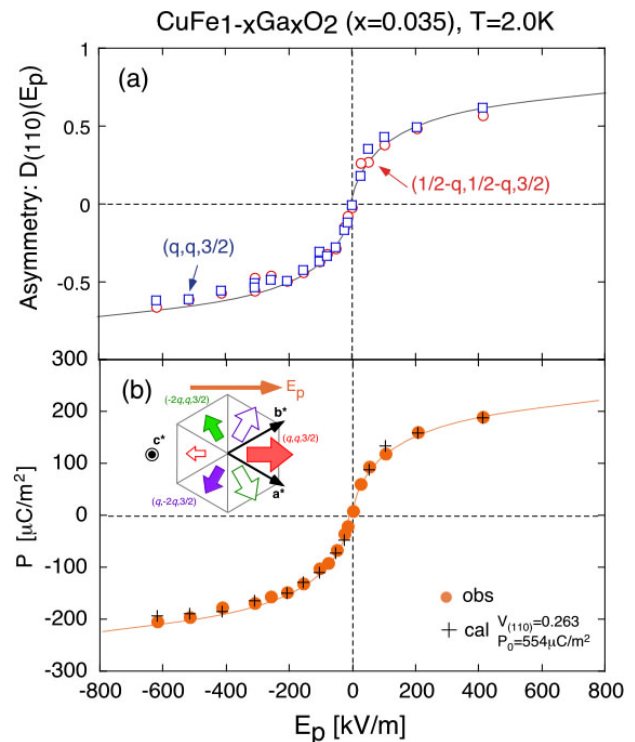


Fig. 1: The  $E_p$ -dependences of (a)  $D_{(110)}$  in the  $(110)$ -domain, (b) the observed and calculated values of  $P$  in  $\text{CFGO}(x=0.035)$  at  $T=2.0\text{K}$ . The solid lines are guides to the eyes, which are drawn so as to be symmetric. The inset shows the schematic drawing of the distributions of the three magnetic domains.

- [1] T. Kimura *et al.*, Phys. Rev. B **73** 220401 (2006)
- [2] T. Nakajima *et al.*, J. Phys. Soc. Jpn. **76** 043709 (2007).
- [3] H. Katsura *et al.*, Phys. Rev. Lett **95**, 057205(2005)
- [4] T. Arima, J. Phys. Soc. Jpn., **76** 073702 (2007).
- [5] S. Seki *et al.*, Phys. Rev. B, **75** 100403 (2007).
- [6] N. Terada *et al.*, Phys. Rev. B **78** 014101 (2008).



## EXPERIMENTAL REPORT

### Magnetic field dependence of the magnetic modulation in the relaxor ferroelectric (Tb,Ca)MnO<sub>3</sub>

Proposal N° PHY-01-2221

Instrument E4

Local Contact  
Karel Prokeš

Principal Proposer: N. Mufti – Univ. Groningen, NL  
Experimental Team: N. Mufti, G. Blake, S. Riyadi – Univ. Groningen, NL

Date(s) of Experiment

06/02/2008 – 12/02/2008

Date of Report: 08/01/2009

In a previous experiment we investigated the magnetic, dielectric and ferroelectric properties of low-doped Tb<sub>1-x</sub>Ca<sub>x</sub>MnO<sub>3</sub>. We demonstrated that on increasing the level of Ca doping, the ferroelectricity is gradually suppressed via an intermediate state at  $x = 0.05$ . The intermediate state exhibits the universal signature of a relaxor ferroelectric state: a broad frequency-dependent peak in the real part of the temperature dependence of the dielectric susceptibility. Our previous neutron scattering study at BENSC showed that the relaxor behaviour in this system is associated with a decreased coherence length of the Mn spin-spiral structure, without any change in the modulation wave vector [1]. In TbMnO<sub>3</sub> when magnetic field is applied along the  $b$ -axis, the polarization is flopped from the  $c$ -axis to the  $a$ -axis. This polarization flop is associated with a transformation from an incommensurate (IC) to commensurate Mn spin configuration with propagation vector  $(0, \frac{1}{4}, 0)$  [2], whereas in DyMnO<sub>3</sub> no change in wave-vector occurs with the same polarization flop [3]. The aim of the present experiment was to study the evolution of the magnetic structure of Tb<sub>1-x</sub>Ca<sub>x</sub>MnO<sub>3</sub> with magnetic field.

The measurements on E4 were performed using single crystals of Tb<sub>1-x</sub>Ca<sub>x</sub>MnO<sub>3</sub> with  $x = 0.02$  (dimensions 5 mm x 5 mm x 1 mm) mounted in a horizontal magnet cryostat (HM1, manufactured by RMC Cryosystems). This cryostat can operate in the temperature range 1.5 K to 300 K and at magnetic fields of up to 6T applied in the horizontal plane. The main difficulty in this experiment was to find the magnetic reflections of interest; large volumes of reciprocal space were blocked by the magnet and the tilt of the cryomagnet was limited to only a few degrees out of the horizontal plane.

In Figure 1(a) we plot the temperature dependence of the wave vector  $q_{Mn}$ , and the integrated intensity and peak width of the  $(0, -q_{Mn}, 1)$  reflection at various magnetic fields, obtained by fitting the peaks with a Gaussian function. We find that the wave vector  $q_{Mn} \sim 0.28$  does not change when magnetic fields of up to 6 T are applied along the  $b$ -direction. This behavior is in contrast to undoped TbMnO<sub>3</sub>, in which the polarization flop is accompanied by a first order

transition where  $q_{Mn}$  changes from 0.28 to 0.25 for both  $H//b$  and  $H//a$ . [2] The polarization flop in our  $x = 0.02$  sample takes place at approximately  $H = 6$  T from our dielectric and polarization measurements. In Figure 1(b) and (c) we observe that the integrated intensity decreases at  $H = 6$ T while the peak width increases. This behavior indicates that the coherence length of the Mn spin spiral structure begins to decrease at 6 T, which is the maximum magnetic field obtainable with the horizontal-field magnet.

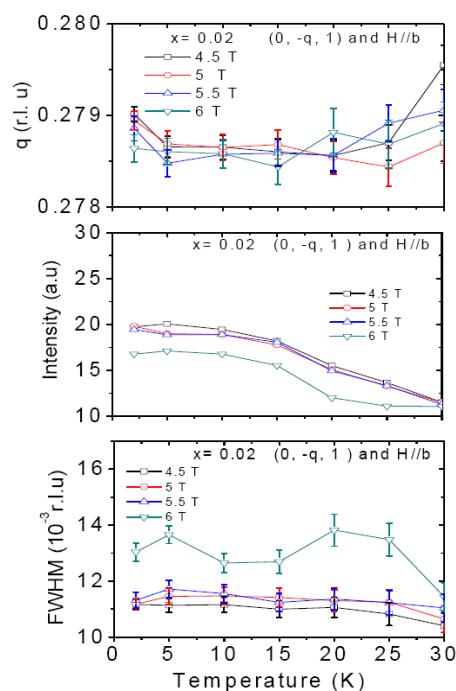


Figure 1. Temperature dependence of (a) Mn spin wavevector ( $q_{Mn}$ ), (b) integrated intensity, and (c) FWHM of the  $(0, -q_{Mn}, 1)$  reflection of Tb<sub>0.98</sub>Ca<sub>0.02</sub>MnO<sub>3</sub> in magnetic fields applied along the  $b$ -axis.

#### References:

- [1]. N. Mufti, et. al, Phys. Rev. B 78, 024109 (2008).
- [2] N. Aliouane et. al, Phys. Rev. B 73, 020102 (R) (2006).
- [3] J. Stremper, et. al., Phys. Rev. B 75, 212402 (2007).

	<b>EXPERIMENTAL REPORT</b> <b>Unconventional metallic magnetism in RCrSb<sub>3</sub></b> <b>(R = Ce, and Pr) : A neutron diffraction study on</b> <b>single crystals</b>	Proposal N° PHY-01-2222 Instrument <b>E4</b> Local Contact K. Prokes
	Principal Proposer: Inamdar Manjusha, Tata Inst. Mumbai, Ind Experimental Team: Inamdar Manjusha, Tata Inst. Mumbai, Ind K. Prokes, Hahn-Meitner-Institut, Berlin	Date(s) of Experiment 21/04/2008 – 30/04/2008

Date of Report: January 2009

RCrSb<sub>3</sub> has a quasi 2 D structure, space group Pbcm, with layers of RSb and CrSb<sub>2</sub> stacked along a axis. It displays variety of interesting magnetic phenomenon due to interaction of 4f moments of rare earth ion and 3d moments of Cr ions. The neutron diffraction work on LaCrSb<sub>3</sub> [1] shows enhancement in intensities for (100), (020) and (002) reflections indicating ferromagnetic (FM) nature of ordering. The temperature dependence of (100) reflection gives T<sub>C</sub> of 126 K in LaCrSb<sub>3</sub> identified with FM ordering of Cr spins. Also there's coexistence of orthogonal FM and antiferromagnetic (AFM) spin sublattices. A spin reorientation transition in bc plane for both sublattices is seen at T<sub>Sr</sub> = 95 K The FM moment on Cr is 1.64 μ<sub>B</sub>/f.u. at 10 K which is in fair agreement with the magnetization data.

The next member of the series, CeCrSb<sub>3</sub> offers an opportunity to study the above unusual magnetism of Cr in presence of a correlated ion Ce. We grew single crystals of CeCrSb<sub>3</sub> by flux method. Cr orders FM at 115 K in CeCrSb<sub>3</sub> but we don't observe any further sharp changes in magnetization to indicate ordering for Ce moments. The isothermal magnetization measurements show higher value of saturation moments at 2 K as that compared to of LaCrSb<sub>3</sub>.

This suggests a possibility that Ce may be carrying some moment, but the nature of ordering of Ce moments was not clear by any of the bulk measurements [2].

The neutron diffraction experiment was done at HMI on CeCrSb<sub>3</sub> single crystal sample. The (100) reflection shows large enhancement in intensity on lowering of temperature. The temperature dependence of (100) shown in Fig.1 indicate T<sub>C</sub> of 117 K, which is in agreement with the magnetization data. (002) and (020) show marginal increase in intensity with lowering of temperature indicating that orientation of moments is in bc plane. The data at 20K was refined with moment on the Cr site alone. Figure 2 shows the reasonable agreement between observed and calculated intensities. We obtain M<sub>B</sub> = 1.6 μ<sub>B</sub> and M<sub>C</sub> = .6 μ<sub>B</sub>. The values are close to that obtained from isothermal magnetization measurements for 20 K. The FM moments and their orientations obtained for CeCrSb<sub>3</sub> is similar to that reported for LaCrSb<sub>3</sub>. From this we infer that down to 20K Cr moments on CeCrSb<sub>3</sub> and LaCrSb<sub>3</sub> behave identically. On lowering the temperature further below 20K, we expect the Ce moments to order. This part of analysis with Ce and Cr moments together and further measurements are in progress.

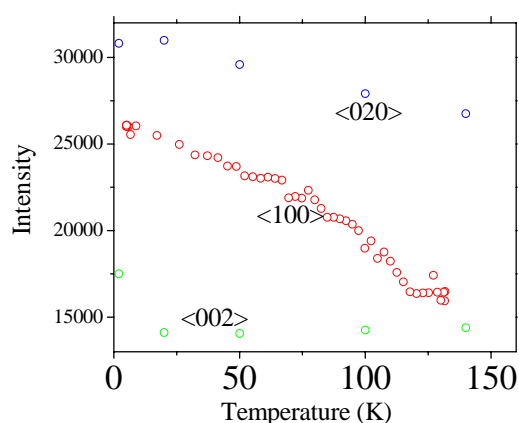


Fig. 1

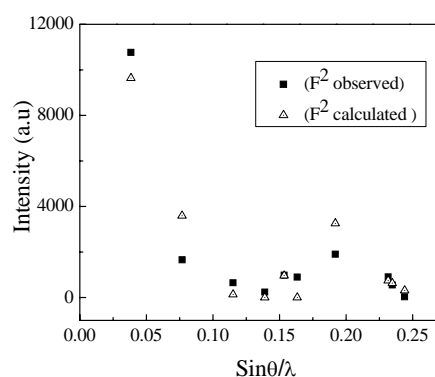


Fig. 2

**References:**

- [1] Granado et. al., PRL, vol. **89**, 10 (2002).
- [2] Manjusha I., A. Thamizhavel, S. Ramakrishnan, JMMM, vol. **320**, 21 (2008).



## EXPERIMENTAL REPORT

### Microscopic spin-polarization coupling in multiferroic $\text{CuFeO}_2$

Proposal N°  
PHY-01-2285-DT

Instrument **E4**

Local Contact  
K. Prokes

Principal Proposer:  
Experimental Team:

S. Mitsuda, Tokyo Univ. of Science  
T. Nakajima, S. Mitsuda; Tokyo Univ. of Sci.  
K. Prokes, A. Podlesnyak; HCB Berlin

Date(s) of Experiment

16/01/2008 – 21/01/2008

Date of Report: 08/01/2009

Delafossite compound  $\text{CuFeO}_2$  (CFO) has attracted increasing interest as a new class of magnetoelectric (ME) multiferroic, because of the recent discovery of the ferroelectricity in the first magnetic-field-induced phase.[1] The magnetic structure in the ferroelectric phase was determined to be a ‘proper-screw type’ magnetic structure with a incommensurate wave vector  $(q, q, 3/2)$  where  $q \sim 0.207$ . [2] This suggests that the origin of the ferroelectricity in this system is not the ‘spin-current model’, [3] which successfully explains the ferroelectricity in ‘cyclind type’ ferroelectric helimagnets, such as  $\text{TbMnO}_3$ .

Recently, Arima has proposed that the variation in the  $d$ - $p$  hybridization with spin-orbit coupling is relevant to the ferroelectricity in CFO system. [4] Applying a microscopic theory derived by Jia *et al.* [5] to a cluster model with a proper helical spin arrangement, Arima has predicted that the ferroelectric phase of CFO system must have spatial modulations with wave numbers of  $2q$  and  $4q$  (where  $q$  is the magnetic modulation wave number) in the helical-axis components of the local electric polarization vectors. Spatial modulations of the local polarization must result in lattice modulations, which can be observed by x-ray diffraction measurements. Therefore, we investigated the lattice modulations in the ferroelectric phase in order to confirm that the origin of the ferroelectricity in CFO system is the  $d$ - $p$  hybridization model.

We performed x-ray diffraction measurements on  $\text{CuFe}_{1-x}\text{Al}_x\text{O}_2$  with  $x=0.015$ , in which the ferroelectric phase shows up under zero field. We found satellite reflections identified as  $(0, 3-2q, 0)$  under zero field. This indicates that the FEIC phase is accompanied by  $2q$ -lattice modulations. We also investigated the magnetic field dependence of the intensity of the  $2q$  satellite reflection. As shown in Fig. 1(a), the intensity of the  $2q$  reflection slightly increases with increasing magnetic field along the helical axis of the magnetic structure. In order to deduce the magnetic field dependence of the ‘amplitude’ of the  $2q$  lattice modulation from the result of the x-ray measurement, we must determine the magnetic field dependence of the magnetic domain distribution. This is because the CFO system has the three magnetic domains, whose propagation wave vectors are assigned as  $(q, q, 3/2)$ ,  $(q, -2q, 3/2)$  and  $(-2q, q, 3/2)$ , owing to the threefold rotational symmetry of the crystal, as shown in Fig. 1(e).

Therefore, we performed neutron diffraction measurements under applied magnetic fields along the helical axis, at the two-axis neutron diffractometer E4 installed at the Berlin Neutron Scattering Center. The details of the experiments are described in Ref. 6. As shown in Fig.

1(b) the magnetic Bragg reflections corresponding to the FEIC magnetic ordering increase with increasing magnetic field. This indicates that the fraction of the magnetic domains with a wave vector  $(q, q, 3/2)$  is enhanced by the magnetic field along the  $[110]$  axis, as shown in Fig. 1(f). Taking account of the result of the neutron measurement, we conclude that the amplitude of the  $2q$ -lattice modulation does not exhibit remarkable change, and it decreases slightly above  $H=3$  T (see Fig. 1(c)). This result is consistent with our calculation based on the Arima’s theory, and support that the origin of the ferroelectricity in this system is the  $d$ - $p$  hybridization model. These works have been published as Phys. Rev. B **78** 024106 (2008).

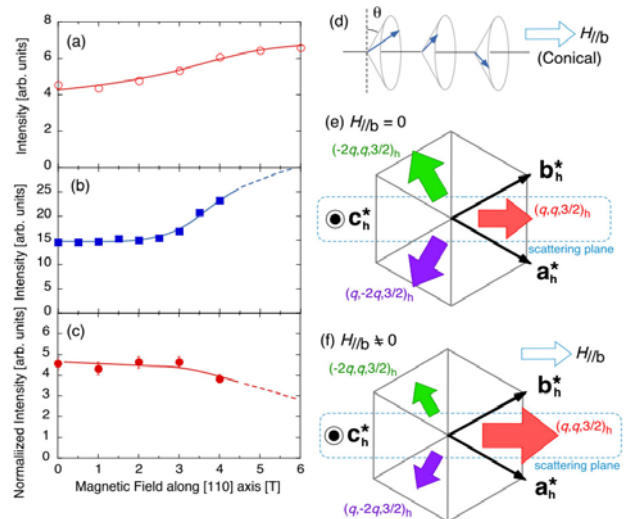


Fig. 1: The magnetic field dependence of (a) the integrated intensity of  $(0, 3-2q, 0)$  reflection observed in the X-ray diffraction measurements, (b)  $(1/2-q, 1/2-q, 3/2)$  magnetic Bragg reflection observed in the neutron diffraction measurements at  $T=4.5$  K, and (d) the integrated intensity of  $(0, 3-2q, 0)$  reflection normalized by the data of the neutron diffraction measurements. (d) Schematic drawings of a conical structure with uniform magnetization component along the helical axis. [(e)-(f)] Schematic drawings of the fractions of three magnetic domains (e) under zero field, and (f) under applied field along the helical axis ( $[110]$  axis). The directions of the filled arrows denote the  $[001]$  projections of the propagation wave vectors. The sizes of arrows qualitatively show the fractions of each domain.

- [1] T. Kimura *et al.*, Phys. Rev. B **73** 220401 (2006)
- [2] T. Nakajima *et al.*, J. Phys. Soc. Jpn. **76** 043709 (2007).
- [3] H. Katsura *et al.*, Phys. Rev. Lett **95**, 057205(2005)
- [4] T. Arima, J. Phys. Soc. Jpn., **76** 073702 (2007).
- [5] C. Jia *et al.*, Phys. Rev. B, **76** 144424 (2007).
- [6] T. Nakajima *et al.*, Phys. Rev. B **78** 024106 (2008).

	<b>EXPERIMENTAL REPORT</b>  <b>Magnetic structure in NdRhSn under uniaxial and hydrostatic pressures</b>	Proposal N° PHY-01-2381 Instrument <b>E4</b>  Local Contact K. Prokes
	Principal Proposer: J. Kamarad, Institute of Physics AS CR, v.v.i., Prague, CR Experimental Team: M. Mihalik, FMP, Charles University, Prague, CR K. Prokes, Helmholtz Zentrum Berlin, Berlin, DE V. Sechovský, FMP, Charles University, Prague, CR	Date(s) of Experiment  29/09/2008 – 13/10/2008

Date of Report: 14/01/2009

The ground state of the hexagonal NdRhSn compound is characterized by strong magneto-crystalline anisotropy with EMD along  $c$ -axis and by spontaneous magnetization that corresponds to  $2/3$  of the  $\text{Nd}^{3+}$  free-ion moment. At temperatures from 7.6 K up to 9.8 K, the compound exhibits AF ordering that is strongly suppressed by uniaxial compression along  $c$ -axis, but, it is supported by hydrostatic pressure.

To uncover an evolution of the magnetic structures in NdRhSn, we performed series of the neutron diffraction experiments on NdRhSn single crystals using the diffractometer E4 at BENSC with horizontal HM2 magnet and two high pressure CuBe cells - uniaxial (Fig.1) and hydrostatic.



Fig.1 : Uniaxial CuBe pressure cell

The crystals were oriented with  $b$ -axis parallel to the axis of the diffractometer E4 and compressed along  $c$ -axis in the uniaxial pressure CuBe cells to search for the non-collinear incommensurate structures with the propagation along  $c$ -axis. The temperature evolution of the nuclear and magnetic reflections found was followed from 2 K up to 15 K in magnetic fields up to 4 T at several distinct pressure conditions: besides ambient pressure, under hydrostatic pressure of 0.98 GPa and under uniaxial compression of 0.1 GPa and 0.18 GPa.

The incommensurate AF structure with the propagation vector  $(00t)$ ,  $t = 0.092 \pm 0.002$  at 8 K, was verified by a detection of satellites of the (200) (Fig.2) and (201) reflections in a narrow range of temperature from  $T_N = 9.8$  K down to  $T_C = 7.6$  K. The F-AF transition has been detected by a sharp decrease of magnetic contribution to the (200) nuclear reflection (Fig.3).

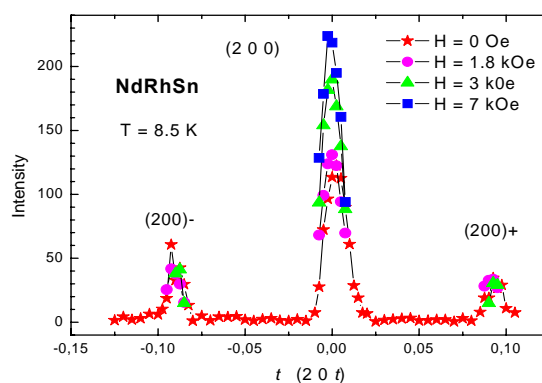


Fig.2: Effect of field on nuclear and satellite reflections

Despite of an expected difference in an evolution of the magnetic structures in NdRhSn, no detectable changes of the propagation vector were revealed under hydrostatic and uniaxial pressures!

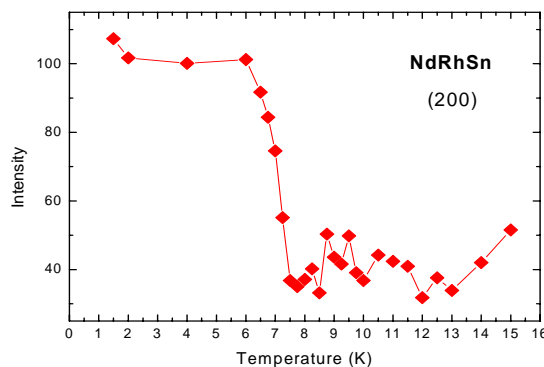


Fig.3: Ferromagnetic contribution to (200) reflection under hydrostatic pressure 0.73 GPa.

This pressure behavior points to a very complex competition of the magnetic interactions that can be discussed within a scenario assuming the RKKY-type interaction dominating the ordering of the localized Nd  $4f$ -moments along the crystal  $c$ -axis.

*This research project has been supported by the EC under the 6<sup>th</sup> FP through the Key Action: Strengthening the European Research Infrastructures. Contract n°: RII3-CT-2003-505925 (NMI 3-1357).*

	<b>EXPERIMENTAL REPORT</b>  <b>Er<sub>2</sub>Ni<sub>2</sub>Pb single crystal in magnetic fields</b>	Proposal N° PHY-01-2445-EF  Instrument <b>E4</b>  Local Contact K. Prokes
	Principal Proposer:      K. Prokes, HZB Experimental Team:        K. Prokes, HZB	Date(s) of Experiment  <p style="text-align: center;">October 2008</p>

Date of Report: 18/01/2009

Er<sub>2</sub>Ni<sub>2</sub>Pb crystallizes in the orthorhombic Mn<sub>2</sub>AlB<sub>2</sub> type crystal structure [1]. All the Er atoms occupy the same crystallographic position and are equivalent in the crystal structure. However, due to competing magnetic interactions along various links connecting the R ions a significant frustration exists leading in Er<sub>2</sub>Ni<sub>2</sub>Pb to a large variety of different antiferromagnetic structures. Previous bulk magnetic measurements (for references see [2]) suggested three magnetic phase transitions at T<sub>N1</sub> = 3.4 K, T<sub>N2</sub> = 3.2 K and T<sub>N3</sub> = 2.0 K to exist in Er<sub>2</sub>Ni<sub>2</sub>Pb. Neutron diffraction experiments down to 1.5 K and to 460 mK [2] proved all the magnetic phases to be antiferromagnetic and coexisting over extended temperature range. Striking is that the two experiments revealed different phase transition temperature values. Moreover, it seems that at the low temperature limit (even at 460 mK) the Er moments are not fully developed. The primary question is then whether the full moment can be recovered by an application of magnetic field. Previously we have performed an experiment on a fixed powder sample (see page 67 in BENSC Reports from 2002). The analysis showed that at least two irreducible groups have to be mixed in order to explain the observed field dependences. The magnetic moment, however, attained full Er<sup>3+</sup> magnitude. In the present experiment we have used a 1.18 mg small single crystal extracted from the bulk piece prepared by arc melting of constituent elements.

The crystal has been oriented with its b axis along the magnetic field up to 6.5 T generated by the vertical VM-2 cryomagnet. Due to a limited angular range we have followed only a small number of reflections and performed few typical reciprocal space scans. Individual reflection have been measured for typically one hour, integrated using computer code LAMP, fitted to a Gaussian profile, corrected for the Lorentz factor and analyzed using the Er<sup>3+</sup> magnetic form factor. The analysis of the zero-field intensities obtained above the T<sub>N</sub> and at 1.7 K, the lowest temperature of the present experiment were fully in agreement with published crystallographic and magnetic structure information. In Fig. 1 we show the field

dependence of two nuclear reflections exhibiting the strongest magnetic contribution. As can be seen, the (001) reflection increases by a factor of eight or so. This increase is in rather good agreement with previous powder studies. Striking result is, however, that a small intensity has been also observed on top of the crystallographically forbidden (100) reflection indicating a loss of a symmetry element caused by a small tilt of Er magnetic moments.

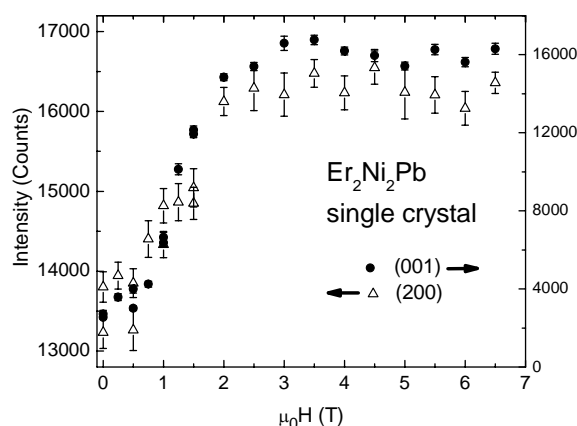


**Fig. 1:** The field dependence of the integrated intensities of (001) and (200) reflections that exhibit the strongest increase in intensity due to field-induced ferromagnetic ordering.

Due to the size of the crystal used (1.18 mg !) the details of the anticipated canting could not be studied in detail. Equally we could not study the intermediate magnetic structure that appears in intermediate magnetic fields as suggested by magnetic bulk measurements and observed by neutron powder diffraction [2] either. Larger crystal is needed. Neglecting the intensity seen on the (100) reflection we could determine the main component of the Er moments that lie along the b axis and attains 8.8 μ<sub>B</sub>/Er.

#### References

- [1] L.D. Gulay, Y.M. Kalychak, M. Wolczyk, J. Alloys Compd. **311**, 228 (2000)
- [2] K. Prokeš, and J.A. Mydosh, Eur. Phys. J. B **67**, 1 (2009)



## EXPERIMENTAL REPORT

### Magnetic order of the Pr<sup>3+</sup>- and V<sup>3+</sup>-ions in Pr<sub>0.90</sub>Ca<sub>0.10</sub>VO<sub>3</sub>

Proposal N°  
PHY-01-1724-LT

Instrument **E5**

Local Contact  
M. Reehuis

Principal Proposer:

C. Ulrich, B. Keimer – MPI Stuttgart  
J. Fujioka, S. Miyasaka, Y. Tokura –  
Department of Applied Physics, University of  
Tokyo, Japan

Date(s) of Experiment

Experimental Team:

M. Reehuis – MPI Stuttgart, HZB, Berlin

07/10/2008 – 14/10/2008

Date of Report: 07/01/2008

A detailed description of the magnetic order of the vanadium and cerium moments CeVO<sub>3</sub> was given recently [1]. In the low-temperature monoclinic phase (setting in *P2<sub>1</sub>/b*) the magnetic moments of the vanadium ions were found to be purely *C*-type ordered in the *ab*-plane. Antiferromagnetic interactions between magnetic moments on vanadium and cerium ions induce a progressive magnetic polarization of the cerium sublattice at lower temperatures, resulting in a ferrimagnetic structure.

In the present single-crystal neutron diffraction study carried out on the E5 experiment ( $\lambda = 2.38$  Å, PG-monochromator) we have shown that the magnetic ordering in PrVO<sub>3</sub> as well as in the Ca-doped compound Pr<sub>0.90</sub>Ca<sub>0.10</sub>VO<sub>3</sub> is very similar to that observed earlier for CeVO<sub>3</sub> [1]. In contrast to PrVO<sub>3</sub> the investigated crystal of the Ca-doped sample was only slightly twinned. Therefore the coupling of the magnetic moments of the Pr- and V-atoms could be deduced in more detail for Pr<sub>0.90</sub>Ca<sub>0.10</sub>VO<sub>3</sub> from the temperature dependence of the magnetic intensities of particular reflections. As shown in Fig. 1 the spontaneous increase of the magnetic intensities of the reflections 100, 010, 102 and 012 at  $T_N = 117$  K clearly shows the onset of antiferromagnetic order of the V-moments. At lower temperatures it can be seen that the intensity of 102 is still increasing, whereas the intensities of 012, 100, and 010 are decreasing. This indicates the onset of the induced antiferromagnetic

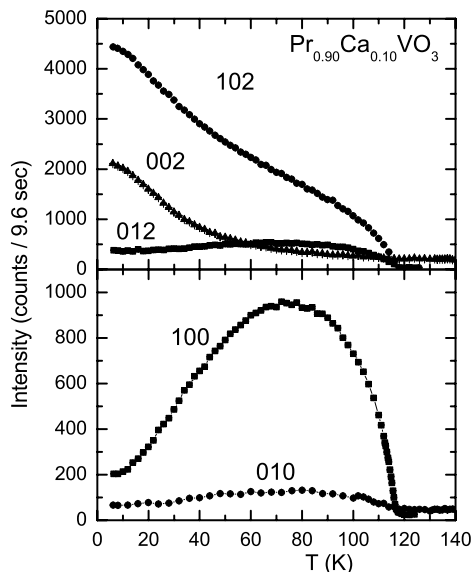


Fig 1. *T*-dependence of the magnetic intensities of particular Bragg reflections of Pr<sub>0.90</sub>Ca<sub>0.10</sub>VO<sub>3</sub>.

order of the Pr-moments. Further, the increase of the 002 indicates the ferromagnetic order of the Pr-moments.

From our structure refinements using the FullProf program we were able to determine the magnetic moments of both the cerium and the vanadium moments along the *x*- and *y*-directions. We found that the magnetic moments of the V-atoms are aligned predominantly along the *b*-axis, reaching a moment  $\mu_y = 1.13(3)$   $\mu_B$ . The moment along the *a*-axis is  $\mu_x = 0.32(3)$   $\mu_B$  and the total moment is  $\mu_{\text{exp}} = 1.17(3)$   $\mu_B$ . The ration  $\mu_y / \mu_x = 3.53$  is very similar to that of CeVO<sub>3</sub>  $\mu_y / \mu_x = 3.44$  [1].

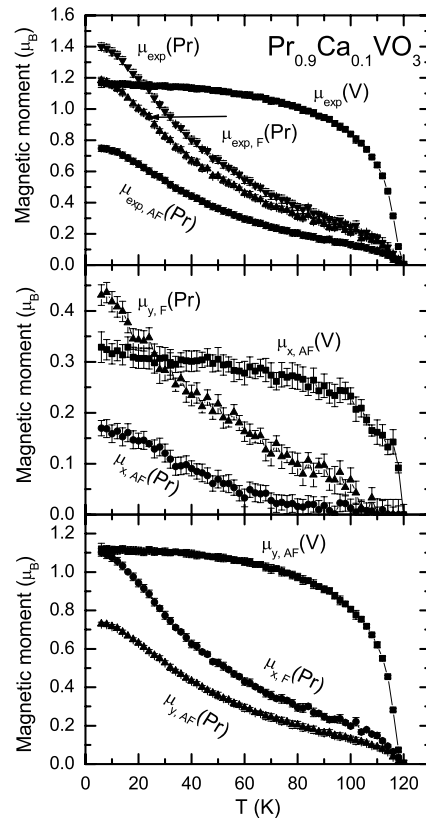


Fig 2. *T*-dependence of the magnetic moments of the V-atoms in Pr<sub>0.90</sub>Ca<sub>0.10</sub>VO<sub>3</sub>. The *C<sub>y</sub>*-component of the vanadium induces a ferrimagnetic order of the Pr-moments with the modes *C<sub>y</sub>* and *F<sub>x</sub>*; accordingly the *C<sub>x</sub>*-component of the vanadium induces a ferrimagnetic order of the Pr-moments with the modes *C<sub>x</sub>* and *F<sub>y</sub>*.

#### Reference

- [1] M. Reehuis, C. Ulrich, P. Pattison, M. Miyasaka, Y. Tokura, B. Keimer, Eur. Phys. J. B. **64** (2008) 27.



## EXPERIMENTAL REPORT

### Structural and magnetic phase transitions in $\text{PrVO}_3$ and $\text{Pr}_{0.90}\text{Ca}_{0.10}\text{VO}_3$

Proposal N°  
PHY-01-1724-LT

Instrument **E5**

Local Contact  
M. Reehuis

Principal Proposer: C. Ulrich, B. Keimer – MPI Stuttgart  
J. Fujioka, S. Miyasaka, Y. Tokura –  
Department of Applied Physics, University of  
Tokyo, Japan

Experimental Team: M. Reehuis – MPI Stuttgart, HZB, Berlin

Date(s) of Experiment

07/10/2008 – 14/10/2008  
17/10/2008 – 19/10/2008  
27/10/2008 – 02/11/2008

Date of Report: 07/01/2008

Recently we gave an account on the structural and magnetic properties of the prototypical Mott-Hubbard insulators  $\text{YVO}_3$ ,  $\text{NdVO}_3$  and  $\text{TbVO}_3$  [1, 2]. Each vanadate shows a structural phase transition ( $T_S$  at 200 K, 187 K and 191 K) from an orthorhombic ( $Pbnm$ ) to a monoclinic structure ( $P2_1/b$ ), where a G-type orbital ordering sets in. At lower temperature ( $T_N$  at 116 K, 138 K and 113 K) the magnetic moments of the  $\text{V}^{3+}$ -ions show an antiferromagnetic C-type ordering in the  $ab$ -plane. It could be seen that the ionic radii of the rare-earth ions  $R^{3+}$  strongly influence the transition temperatures  $T_N$  and  $T_S$  [2, 3]. A change of the valence by a substitution of the trivalent  $R^{3+}$ -ions by the divalent ions  $\text{Ca}^{2+}$  and  $\text{Sr}^{2+}$  gives rise to a further change of  $T_S$  and  $T_N$ . The same tendency was found recently for  $\text{CeVO}_3$ , where cerium occurs in an intermediate-valent state [4].

In the present work we have investigated the phase transitions of  $\text{PrVO}_3$  and the  $\text{Ca}^{2+}$ -doped vanadate  $\text{Pr}_{0.90}\text{Ca}_{0.10}\text{VO}_3$  by single-crystal neutron diffraction. Cylindrical single crystals with the dimensions  $d = 3$  mm and  $h = 6$  mm were measured on the instrument E5 ( $\lambda = 2.38$  Å, PG-monochromator). For both samples we found Bragg intensities on the forbidden positions (203), (013) or (031) indicating a crystal twinning. The twinning of the Ca-doped samples is only 8 %, while it is strongly pronounced (of about 37 %) for pure  $\text{PrVO}_3$ . In order to observe the structural and magnetic phase transitions we have measured the temperature dependence of the intensities of the pure magnetic reflection 100 and of the strongest nuclear reflections 202 and 022, where the magnetic intensity is negligible. In Fig. 1 it can be seen for the reflection 100 of  $\text{PrVO}_3$  that magnetic intensity spontaneously appears at  $T_N = 140(1)$  K, whereas it was found to be significantly reduced [ $T_N = 117(1)$  K] for  $\text{Pr}_{0.90}\text{Ca}_{0.10}\text{VO}_3$  (Fig. 2). The same tendency we found for the structural phase transitions. Figs. 1 and 2 show that the reflections 202 and 022 of  $\text{PrVO}_3$  and  $\text{Pr}_{0.90}\text{Ca}_{0.10}\text{VO}_3$  show a strong increase of their intensities at 180(2) K and 135(2) K, respectively. In agreement with Ref. 3 we were able to show that an increase of a Ca-doping level with  $x = 0.10$  causes a strong destabilization of both the G-type orbital and the C-type spin order.

#### References

- [1] C. Ulrich, G. Khaliullin, J. Sirker, M. Reehuis, M. Ohl, M. Miyasaka, Y. Tokura, B. Keimer, Phys. Rev. Lett. **91** (2003) 257202.  
[2] M. Reehuis, C. Ulrich, P. Pattison, B. Ouladdiaf, M.C. Rheinstädter, M. Ohl, L.P. Regnault, M. Miyasaka, Y. Tokura, B. Keimer, Phys. Rev. B. **73** (2006) 094440.

- [3] J. Fujioka, S. Miyasaka, Y. Tokura, Phys. Rev. B. **72** (2005) 024460.  
[4] M. Reehuis, C. Ulrich, P. Pattison, M. Miyasaka, Y. Tokura, B. Keimer, Eur. Phys. J. B. **64** (2008) 27.

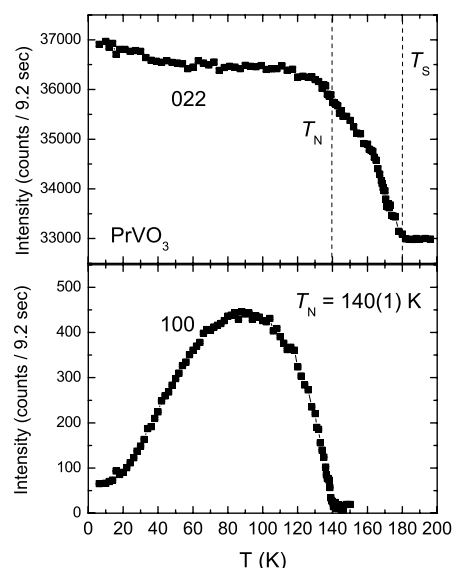


Fig 1.  $T$ -dependence of the intensities of the Bragg reflections 100 and 022 of  $\text{PrVO}_3$ . Due to crystal twinings these reflections contain 37(1) % of the reflections 010 and 202.

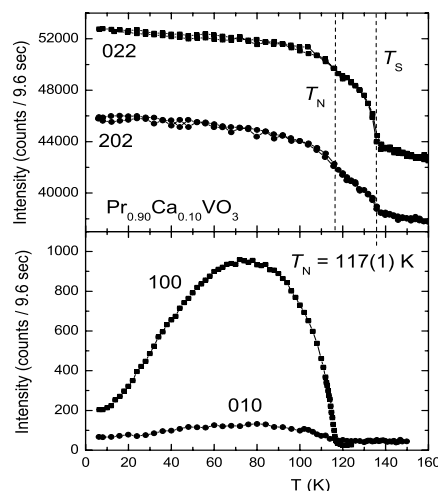


Fig 2.  $T$ -dependence of the intensity of the reflections 100, 010, 022 and 202 of  $\text{Pr}_{0.90}\text{Ca}_{0.10}\text{VO}_3$ .



## EXPERIMENTAL REPORT

# Magnetic order and phase transitions in $\text{HoVO}_3$

Proposal N°  
PHY-01-1724-LT  
Instrument **E5**  
Local Contact  
M. Reehuis

Principal Proposer: C. Ulrich, B. Keimer – MPI Stuttgart  
S. Miyasaka, J. Fujioka, Y. Tokura – University of Tokyo, Japan  
Experimental Team: M. Reehuis – MPI Stuttgart, HZB Berlin

Date(s) of Experiment  
03/03/2008 – 16/03/2008

Date of Report: 01/04/2008

In the present report we have given an account on the magnetic order of the vanadium and holmium moments in  $\text{HoVO}_3$ . A single-crystal neutron diffraction study has been carried out on the four-circle diffractometer E5 using a PG-monochromator selecting the neutron wavelength  $\lambda = 2.38 \text{ \AA}$ .

In Fig. 1 it can be seen that magnetic intensity appears at  $T_N = 113(3) \text{ K}$  on the positions of the reflections 010 and 100, indicating a C-type ordering of the V-atoms in the  $ab$ -plane. With decreasing temperature the reflection 010 shows a spontaneous decrease at 26 K, where the C-type order changes into a pure G-type order along the  $c$ -axis. This structure type was clearly evidenced for the isotopic compound  $\text{YVO}_3$  [1], where the  $\text{Y}^{3+}$ -ion is diamagnetic. Assuming the same magnetic structure for the V-sublattice in  $\text{HoVO}_3$  the  $T$ -dependence of the 100 is expected to be very similar to that of the 010. But Fig. 1 shows that the magnetic intensity of the 100 is still increasing down to 6 K. Further an anomaly could be found just below 26 K during the cooling down process starting from 120 K. Consequently this magnetic intensity can be ascribed to a C-type order of the Ho-moments along the  $b$ -axis. At about 26 K a spontaneous increase of magnetic intensity has been found for the reflection 020. This indicates a ferromagnetic order of the Ho-moments along the  $a$ -axis. Our data analysis showed that the Ho-moments are also G-type ordered along the  $c$ -axis, resulting finally in a magnetic structure with the modes  $F_x$ ,  $C_y$  and  $G_z$ , respectively. For the space group  $Pbnm$  the irreducible representations with the basis functions  $[F_x, C_y, -]$  and  $[-, -, G_z]$  could be deduced from Bertaut's representation analysis [2]. The total magnetic structure finally can be presented by a reducible representation with the basis function  $[F_x, C_y, G_z]$ . Using this model the magnetic structure was successfully refined. The obtained magnetic structure of  $\text{HoVO}_3$  is presented in Fig. 2. At 6 K the refined magnetic moments reach the value  $\mu_{\text{exp}} = 6.9(3) \mu_B$ . This is considerably smaller than the theoretical value  $\mu_{\text{eff}} = g \cdot J = 10.0 \mu_B$  for the free  $\text{Ho}^{3+}$ -ion. The components along the three different axes are  $\mu_x = 2.3(2) \mu_B$ ,  $\mu_y = 6.1(2) \mu_B$  and  $\mu_z = 2.1(2) \mu_B$ , respectively. For the V-atoms we found for the G-type ordered V-atoms a moment value  $\mu_z = 1.25(3) \mu_B$  at 6 K.

### References

- [1] C. Ulrich, G. Khaliullin, J. Sirker, M. Reehuis, M. Ohl, S. Miyasaka, Y. Tokura, B. Keimer, Phys. Rev. Lett. **91**, 257202 (2003).  
[2] E. F. Bertaut, Acta Cryst. A **24** (1968) 217.

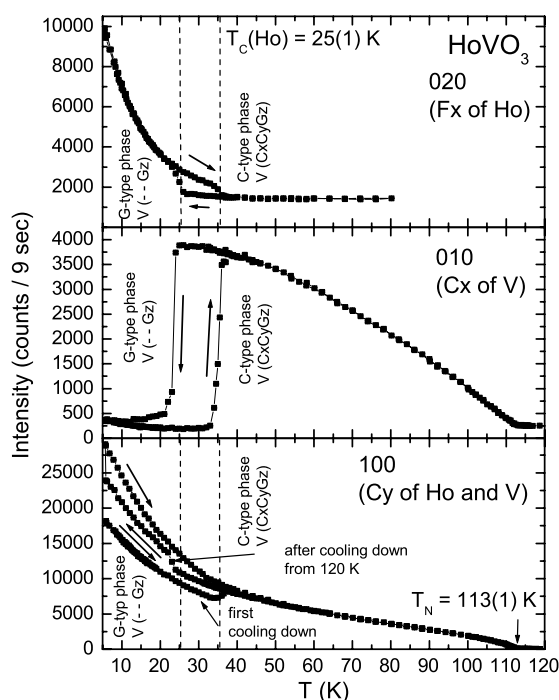


Fig 1.  $T$ -dependence of the magnetic intensity of the Bragg reflections 020, 010 and 100 of  $\text{HoVO}_3$ .

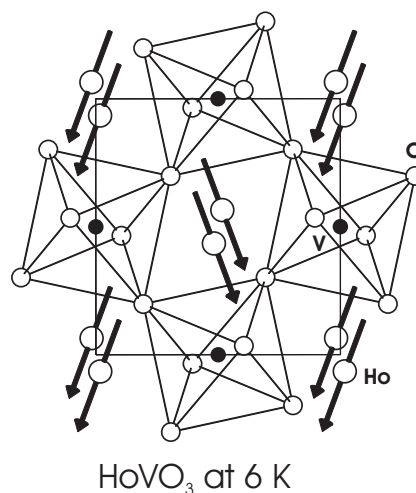


Fig 2. Magnetic structure of  $\text{HoVO}_3$ . The magnetic structure of the Ho-sublattice can be described with the basis function  $(F_x, C_y, G_z)$ . The V-moments are G-type ordered along the  $z$ -direction.



## EXPERIMENTAL REPORT

### Structural and magnetic phase transitions in HoVO<sub>3</sub>

Proposal N°  
PHY-01-1724-LT  
Instrument **E5**  
Local Contact  
M. Reehuis

Principal Proposer: C. Ulrich, B. Keimer – MPI Stuttgart  
S. Miyasaka, J. Fujioka, Y. Tokura –  
Department of Applied Physics, University of  
Tokyo, Japan  
Experimental Team: M. Reehuis, MPI Stuttgart – HZB, Berlin

Date(s) of Experiment

03/03/2008 – 16/03/2008

Date of Report: 11/01/2009

Vanadates with the formula  $RVO_3$  ( $R = Y$  or rare-earth element) exhibit many exciting properties which can be related to orbital or spin rearrangements. Recently we were able to explain the unusual properties of  $YVO_3$  by novel orbital fluctuations [1]. A phase transition from an orthorhombic to a monoclinic structure sets in at 200 K. Below  $T_N = 116$  K the vanadium moments show antiferromagnetic ordering with the modes  $C_x$ ,  $C_y$  and  $G_z$ , where the z-component is the weakest [1, 2]. At 77 K  $YVO_3$  exhibits an additional structural phase transition. Here the crystal structure changes again to the orthorhombic structure, where the vanadium moments are purely G-type ordered along z [1, 2]. This additional structural phase transition can only be observed for the vanadates with smaller  $R^{3+}$ -ions ( $R^{3+} = Ho^{3+} - Lu^{3+}$ ) [3].

In the present study we have investigated the structural and magnetic phase transitions of  $HoVO_3$ . A single-crystal neutron diffraction study has been performed on the four-circle diffractometer E5 (PG-monochromator:  $\lambda = 2.38$  Å). The used cylindrical single-domain crystal of  $HoVO_3$  with dimensions  $d = 3$  mm and  $h = 6$  mm was grown by the floating zone technique [3].

The presence of structural phase transition could be identified by the measurement of the  $T$ -dependence of the strong nuclear reflection 022 (Fig. 1). The spontaneous change of the intensity at 200 K can be ascribed to the transition from the high-temperature orthorhombic ( $Pbnm$ ) to the monoclinic ( $P2_1/b$ ) phase. The same transition temperature was found for  $YVO_3$  [1-3]. This is not surprising, since the ionic radii of the  $Ho^{3+}$ - and the  $Y^{3+}$ -ions are very similar. Fig. 2 shows that magnetic intensity was observed at  $T_N = 113(1)$  K on the position of the reflection 011. This clearly suggests the onset of the G-type ordering of the V-atoms. This temperature is slightly smaller than  $T_N = 116(1)$  K observed for  $YVO_3$ . At  $T_{S2} = 26$  K finally (cooling down process), we have found the structural transition back to the orthorhombic symmetry ( $Pbnm$ ). With increasing temperature this transition sets in at much higher temperature at 36 K, indicating strong hysteresis effects. Recently a slightly higher temperature ( $T_{S2} = 38$  K) was observed by Sikora et al. [4]. It is interesting to note that no hysteresis could be observed for the first phase transition at  $T_{S2} = 200$  K (Fig. 1). Surprisingly the second structural phase transition of  $HoVO_3$  sets in at much lower temperature than that of the yttrium compound ( $T_{S2} = 77$  K). Probably the high magnetic moment of the Ho-moments as well as its magnetocrystalline anisotropy may show a strong influence on the magnetic order of the vanadium sublattice.

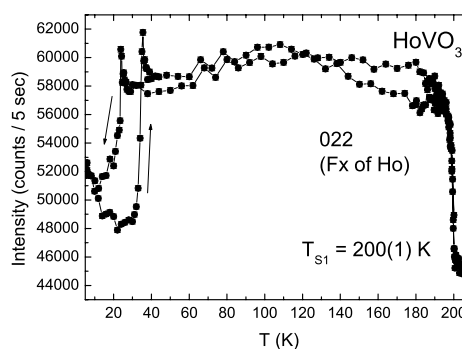


Fig 1.  $T$ -dependence of the magnetic intensity of the Bragg reflections 012 of  $HoVO_3$ .

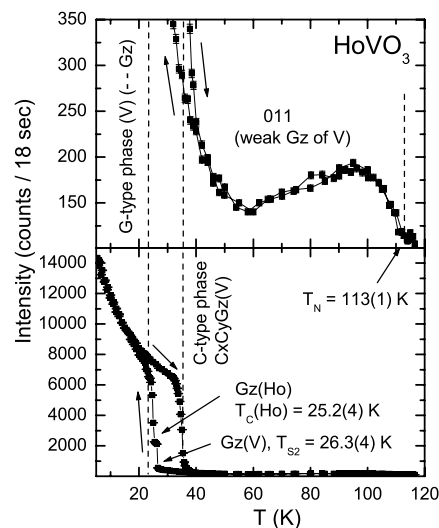


Fig 2.  $T$ -dependence of the reflections 101 and 011 of  $HoVO_3$  indicating G-type ordering.

#### References

- [1] C. Ulrich, G. Khaliullin, J. Sirker, M. Reehuis, M. Ohl, S. Miyasaka, Y. Tokura, B. Keimer, Phys. Rev. Lett. **91**, 257202 (2003).
- [2] M. Reehuis, C. Ulrich, P. Pattison, B. Ouladdiaf, M.C. Rheinstädter, M. Ohl, L.P. Regnault, S. Miyasaka, Y. Tokura, B. Keimer, Phys. Rev. B **73**, 094440 (2006).
- [3] S. Miyasaka, Y. Okimoto, M. Iwama, Y. Tokura, Phys. Rev. B **68**, 100406(R) (2003).
- [4] M. Sikora, C. Marquina, M.R. Ibarra, A.A. Nugroho, T.T.M. Palstra, J. Magn. Magn. Mater. **316**, e692 (2007).



**EXPERIMENTAL REPORT**  
**Magnetic ordering in the hole-doped**  
**vanadate  $\text{Ca}_{0.10}\text{Y}_{0.90}\text{VO}_3$**

Proposal N°  
 PHY-01-1724-LT  
 Instrument **E5**  
 Local Contact  
 M. Reehuis

Principal Proposer: C. Ulrich, B. Keimer – MPI Stuttgart  
 M. Reehuis – MPI Stuttgart, HZB, Berlin  
 J. Fujioka, S. Miyasaka, Y. Tokura –  
 University of Tokyo, Japan  
 Experimental Team: M. Reehuis – MPI Stuttgart, HZB, Berlin

Date(s) of Experiment

17/03/2008 – 20/03/2008

Date of Report: 14/01/2009

Our neutron scattering investigations on insulating  $\text{YVO}_3$  led to the discovery of unusual magnetic ground states and excitations due to the interplay of spin and orbital degrees of freedom [1].  $\text{YVO}_3$  exhibits two magnetic phases, a C-type phase between 116 K and 77 K and a G-type phase below 77 K. While the magnetic properties of the G-type phase are in accordance with standard theoretical descriptions, the C-type phase shows highly unusual static and dynamic spin correlations. The V-moment is strongly reduced and the spin structure is highly non-collinear. This can be ascribed to the presence of an additional G-type component in the so-called C-type phase. In the present report we show how the structural and magnetic properties as well as the magnetic moments of  $\text{Ca}_x\text{Y}_{1-x}\text{VO}_3$  are influenced with an increasing doping level up to  $x = 0.10$ , where the correlation of the G-type orbital becomes much weaker than in pure  $\text{YVO}_3$  [2]. A cylindrical single crystal of  $\text{Ca}_{0.10}\text{Y}_{0.90}\text{VO}_3$  with the dimensions  $d = h = 3$  mm has been measured on the four-circle diffractometer E5 (neutron wavelength  $\lambda = 2.38$  Å). In order to identify structural phase transitions of this vanadate we have measured the  $T$ -dependence of the strong Bragg reflection 202. In agreement with the results given in Ref. [2] we found that the first-order transition from the C-type to the G-type phase is quenched. We only found the onset of a continuous increase at 149(1) K, which indicates the structural phase transition from the orthorhombic to the monoclinic phase. This temperature is considerably smaller than those observed for the doped vanadates  $\text{Ca}_x\text{Y}_{1-x}\text{VO}_3$  between  $x = 0.01$  and  $x = 0.05$  (see Table 1). In order to investigate the magnetic structure of  $\text{Ca}_{0.10}\text{Y}_{0.90}\text{VO}_3$  we have measured the  $T$ -dependence of the reflections 100, 010 and 011 (Fig. 1). It can be seen that the reflections 100 and 010 show magnetic intensity at  $T_N = 98(1)$  K, indicating a collinear C-type ordering in the  $ab$ -plane. The observation of the weak magnetic reflection 011 finally suggests the presence of the additional component  $G_z$ , resulting practically in the same non-collinear spin structure as observed for  $\text{YVO}_3$  [1]. It is interesting to see in Table 1 that a doping level up to  $x = 0.10$  causes a considerable

reduction of both the structural and the magnetic transitions, whereas the magnetic moments of the V-atoms are not significantly changed (Table 1). Further details of the structural and magnetic properties of hole-doped vanadates  $\text{Ca}_x\text{Y}_{1-x}\text{VO}_3$  were reported recently [3].

Table 1. Phase transition temperatures and magnetic moments of the V-atoms (at 10 K) in  $\text{Ca}_x\text{Y}_{1-x}\text{VO}_3$ .

$x(\text{Ca})$	0.01	0.02	0.05	0.10
$\mu(C_x)$ ( $\mu_B$ )	0.82(4)	0.92(4)	0.92(4)	0.73(4)
$\mu(C_y)$ ( $\mu_B$ )	1.28(3)	1.17(3)	1.35(3)	1.34(3)
$\mu(G_z)$ ( $\mu_B$ )	0.10(2)	0.09(2)	0.09(2)	0.14(3)
$\mu_{\text{exp}}$ ( $\mu_B$ )	1.53(2)	1.49(2)	1.64(5)	1.53(5)
$T_{S1}$ (K)	189(1)	184(1)	162(1)	149(1)
$T_N$ (K)	114(1)	114(1)	103(1)	98(1)

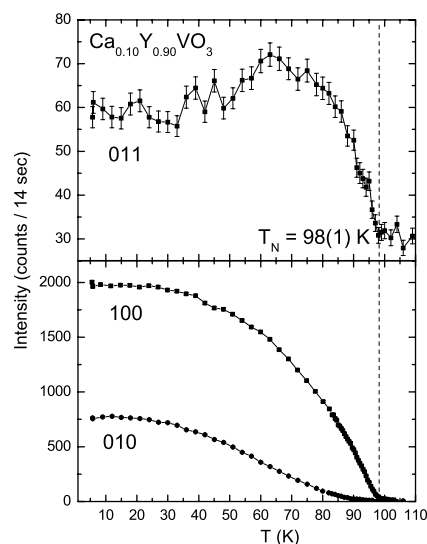


Fig. 1. Temperature dependence of the intensity of the Bragg reflections 100, 010 and 011 for  $\text{Ca}_{0.10}\text{Y}_{0.90}\text{VO}_3$ .

## References

- [1] C. Ulrich, G. Khaliullin, J. Sirker, M. Reehuis, M. Ohl, S. Miyasaka, Y. Tokura, B. Keimer, Phys. Rev. Letters **91** (2003) 257202.
- [2] J. Fujioka, S. Miyasaka, Y. Tokura, Phys. Rev. B **72** (2005) 024460.
- [3] M. Reehuis, C. Ulrich, J. Fujioka, S. Miyasaka, Y. Tokura, B. Keimer, ICTMC16, Berlin 2008, Book of Abstracts, ID 108.



## EXPERIMENTAL REPORT

# Structural and magnetic phase transitions in LuVO<sub>3</sub>

Proposal N°  
PHY-01-2291-EF  
Instrument **E5**

Local Contact M. Reehuis

Principal Proposer: M. Skoulatos – HZB, Berlin  
J. Morris – University of Liverpool, UK  
Experimental Team: M. Reehuis, MPI Stuttgart – HZB, Berlin  
M. Skoulatos – HZB, Berlin

Date(s) of Experiment

17/06/2008 – 13/07/2008

Date of Report: 11/01/2009

Perovskite distorted vanadates  $RVO_3$  ( $R = Y$  or rare-earth element) exhibit interesting physical properties. A variety of phenomena observed in  $YVO_3$  have pointed the scientific community in looking for new models, that try to incorporate both spin and orbital physics, i.e. magnetic and lattice degrees of freedom [1, 2]. A very interesting vanadate is  $LuVO_3$ , since lutetium is the end member of the rare-earth elements and due to the well-known lanthanide contraction its ionic radius is the smallest. Therefore the “ionic-size effect” leads to a strong tilting of the  $VO_6$ -octahedra. Further the  $Lu^{3+}$ -ions are diamagnetic like  $La^{3+}$  and  $Y^{3+}$ . Therefore a change of the structural and magnetic properties cannot be influenced by unpaired  $4f$ -electrons, which are strongly localized in the other  $R^{3+}$ -ions.

A single-crystal neutron diffraction study of  $LuVO_3$  has been carried out on the four-circle diffractometer E5, using the neutron wavelength  $\lambda = 2.38 \text{ \AA}$  (PG-monochromator). For our experiment a crystal of  $LuVO_3$  with the dimensions  $2 \times 4 \times 5 \text{ mm}^3$  was used. In order to investigate the structural and magnetic phase transitions we have measured the  $T$ -dependence of particular Bragg reflection (Fig. 1). During the cooling down process we found that the intensity of the reflection 202 starts increasing at about 175 K. This can be ascribed to the transition from the high-temperature orthorhombic ( $Pbnm$ ) to the monoclinic ( $P2_1/b$ ) phase. From specific heat and susceptibility measurements this transition could be identified at  $T_{S1} = 170 \text{ K}$  [3]. This is in fact much smaller than  $T_{S1} = 200 \text{ K}$  as observed for  $YVO_3$ . [1 – 3]. Fig. 1 shows that magnetic intensity has been observed at the positions of the symmetrically forbidden reflections 100, 010 and 011 below the Néel temperature  $T_N = 108 \text{ K}$ . This value is also smaller than  $T_N = 116 \text{ K}$  observed for  $YVO_3$ . Further cooling leads to a strong change of intensity of the 101 and 202, indicating the second structural phase transition  $T_{S2}$ , where the monoclinic changes back to the orthorhombic structure ( $Pbnm$ ). In contrast, the second structural phase transition of  $LuVO_3$  has been observed (with increasing temperature) at a slightly higher temperature ( $T_{S2} = 81 \text{ K}$ ) than for  $YVO_3$  ( $T_{S2} = 77 \text{ K}$ ). It is interesting to see that hysteresis loops could be observed during the cooling and heating processes.

The magnetic moments of the  $V^{3+}$ -ions could be deduced from data sets of  $LuVO_3$  collected at 6 K in the orthorhombic and at 81 K in the monoclinic phase. At the lowest temperature the V-moments are purely G-type ordered parallel to the  $c$ -axis with a moment value  $\mu_{exp} = 1.41(4) \mu_B$ . In the monoclinic phase the moments are predominantly C-type ordered in the  $ab$ -plane ( $\mu_x = 0.60(3) \mu_B$ ,  $\mu_y = 0.87(4) \mu_B$ ). As found earlier for  $YVO_3$  [1, 2] an additional G-type component [ $\mu_z = 0.31(3) \mu_B$ ]

could be identified, resulting finally in a total moment  $\mu_{exp} = 1.41(4) \mu_B$ .

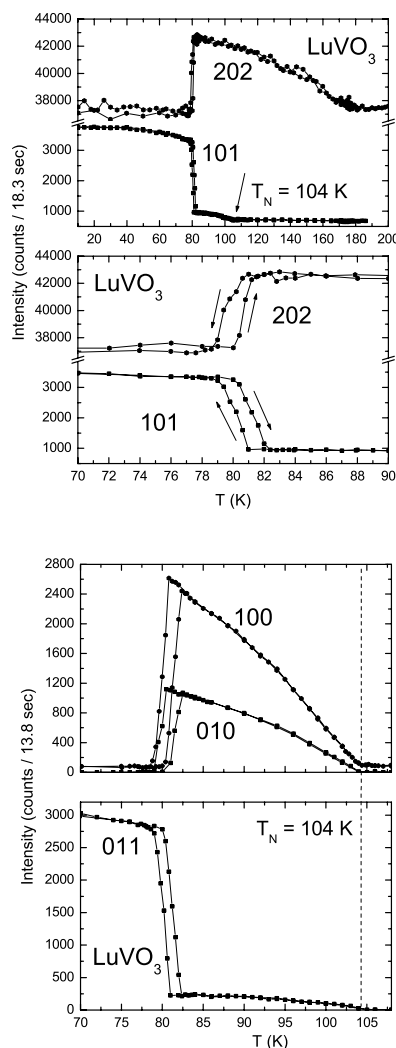


Fig 1.  $T$ -dependence of the Bragg reflections 202, 101, 011, 100 and 010 of  $LuVO_3$ .

## References

- [1] C. Ulrich, G. Khaliullin, J. Sirker, M. Reehuis, M. Ohl, S. Miyasaka, Y. Tokura, B. Keimer, Phys. Rev. Lett. **91**, 257202 (2003).
- [2] M. Reehuis, C. Ulrich, P. Pattison, B. Ouladdiaf, M.C. Rheinstädter, M. Ohl, L.P. Regnault, S. Miyasaka, Y. Tokura, B. Keimer, Phys. Rev. B **73**, 094440 (2006).
- [3] S. Miyasaka, Y. Okimoto, M. Iwama, Y. Tokura, Phys. Rev. B **68**, 100406(R) (2003).



## EXPERIMENTAL REPORT

### Neutron diffraction study of the magnetic ordering in U<sub>2</sub>NiSi<sub>3</sub>

Proposal N° PHY-01-2404

Instrument **E5**

Local Contact  
Manfred Reehuis

Principal Proposer: Maria Szlawska – PAS ILTSR, Wroclaw, PL  
Experimental Team: Dariusz Kaczorowski - PAS ILTSR, Wroclaw, PL  
Manfred Reehuis – Helmholtz Centre, Berlin

Date(s) of Experiment  
03/11/2008 – 10/11/2008

Date of Report: 25/11/2008

The U-based compound U<sub>2</sub>NiSi<sub>3</sub> crystallizes with disordered AlB<sub>2</sub>-type structure. It reveals rather unusual magnetic properties due to inherent non-magnetic atomic disorder and topological frustration in the uranium sublattice. While DC magnetic measurements indicate strongly anisotropic ferromagnetism, the AC magnetic susceptibility and isothermal remanent magnetisation data show behaviour typical of spin-glasses. It seems that long-range magnetic ordering coexists in this compound with spin-glass state with the Curie temperature close to the freezing temperature [1-4].

In order to get direct evidence for the ferromagnetic order we carried out the neutron diffraction measurements on single-crystalline specimen using the E5 Diffractometer installed at BENS (Helmholtz Centre Berlin for Materials and Energy). The neutron spectra were taken in a wide 2θ-range at 6 K and 40 K. Furthermore, the intensity of several Bragg peaks (0 0 1), (-1 1 0), (1 0 0) and (0 1 0) was studied as a function of temperature from 6 to 30 K (see Fig.1).

The obtained results unambiguously proved the long range magnetic ordering. U<sub>2</sub>NiSi<sub>3</sub> is ferromagnetic below the Curie temperature of 24 K. From comparison of the magnetic and structural peak intensities the ordered moment was estimated to be 1.05(3)μ<sub>B</sub> per uranium atom, which well corresponds to the bulk magnetisation value in high magnetic fields. The ordered moment lies perpendicular to the c-axis of the hexagonal unit cell. Because of twinning of the single crystal used there was no possibility to determine the direction of the magnetic moment within the basal plane.

*This research project has been supported by the European Commission under the 6<sup>th</sup> Framework Programme through the Key Action: Strengthening the European Research*

*Infrastructures Contract n° RII3-CT-2003-505925 (NMI 3).*

#### References:

- [1] D. Kaczorowski et al., J. Phys.: Condens. Matter **5** (1993) 9185
- [2] A. Schröder et al., J. Magn. Magn. Mater. **140-144** (1995) 1407
- [3] B. Chevalier et al., J. Alloys Comp. **233** (1996) 150
- [4] M. Szlawska et al., Materials Science **25** (2007) 1267

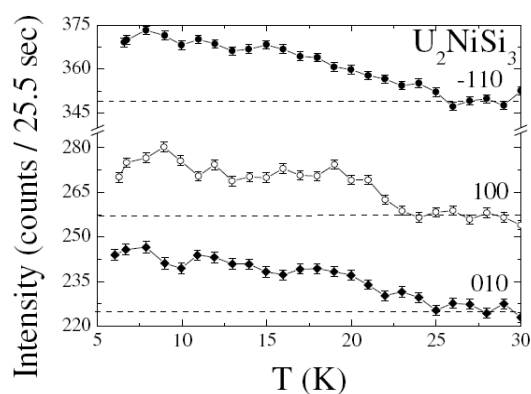
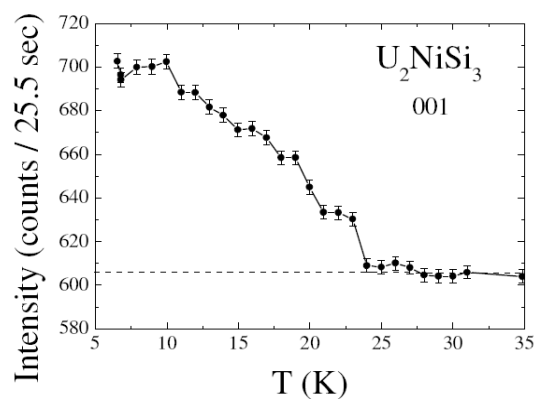


Fig.1: Integrated neutron intensities of the (0 0 1), (-1 1 0), (1 0 0) and (0 1 0) Bragg peaks as a function of temperature.



## EXPERIMENTAL REPORT

### Magnetic structure of the $(\text{Dy}_{1-x}\text{Y}_x)_3\text{Co}$ compounds

Proposal N° PHY-01-1558

Instrument **E6**

Local Contact  
Norbert Stüßer

Principal Proposer: Dr. Pirogov, Alexander, IMP, Ekaterinburg, RU  
Experimental Team: Gubkin Andrew F., USU Ekaterinburg, RU

Date(s) of Experiment

04/12/2007 – 09/12/2007

Date of Report: 02/10/2008

Rare earth intermetallic compounds  $\text{R}_3\text{T}$  ( $\text{T}=\text{Co}, \text{Ni}, \text{Rh}$ ) crystallize in the low symmetry orthorhombic crystal structure of  $\text{Fe}_3\text{C}$  type (space group  $\text{Pnma}$ ). The magnetic moments of R ions form the complex noncollinear antiferromagnetic (AF) or ferromagnetic (F) structures, which can be ascribed to the competition between the RKKY exchange interaction and low symmetry crystal-field effects. The 3d metal atoms do not have ordered magnetic moments in  $\text{R}_3\text{T}$ , therefore the compounds with  $\text{R} = \text{La}$  and  $\text{Y}$  are Pauli paramagnets. According to previous studies  $\text{Dy}_3\text{Co}$  compound exhibits an antiferromagnetic behavior below the Neel temperature  $T_N=44$  K, the magnetic structure of  $\text{Dy}_3\text{Co}$  can be described by two wave vectors  $\mathbf{k}_1=0$  and  $\mathbf{k}_2=2\pi(1/2a, 0, 1/2c)$  at 4.2 K [1,2]. This magnetic structure changes to another AF structure with increasing temperature above  $T_1 \sim 32$  K. In the temperature interval  $T_1 < T < T_2$  the AF structure is suggested to be described by the wave vector  $\mathbf{k}_1$ .

Our preliminary studies of the magnetization behavior of the  $(\text{Y}_{1-x}\text{Dy}_x)_3\text{Co}$  pseudo-binaries allowed us to assume that the magnetic structures of the compounds with  $0.2 < x < 0.8$  can be described only one wave vector in the whole temperature range below  $T_N$ . In the present project carried out the neutron diffraction study of  $(\text{Y}_{1-x}\text{Dy}_x)_3\text{Co}$  compounds in order to reveal the evolution of the magnetic state with increasing Dy concentration starting from  $\text{Y}_3\text{Co}$ . According to previous investigations [4,5] the  $\text{Y}_3\text{Co}$  compound is observed to exhibit some anomalies in the behavior of the electrical resistivity, specific heat and elastic constants around 150 K. In the present project, we have measured powder neutron diffraction patterns for  $\text{Y}_3\text{Co}$  in the temperature interval 1.5 K – 300 K at the wavelength  $\lambda=2.452\text{\AA}$  (shown in Fig.1). We did not find any magnetic contributions to the Bragg reflections in this temperature interval, which is indicative of a non-magnetic origin of the anomalies. An unusual behavior with temperature of the integral intensity of some Bragg reflections (see inset in the fig. 1) can be attributed to the changes of the crystal structure in the vicinity of 150 K.

In order to study the temperature transformation of the crystal structure of  $\text{Y}_3\text{Co}$  in detail the additional experiments on a single crystalline sample with synchrotron radiation are needed.

Because of the high absorption cross section of dysprosium atoms in the Dy containing  $(\text{Y}_{1-x}\text{Dy}_x)_3\text{Co}$  compounds we couldn't get high quality neutron diffraction patterns which are necessary to analyze the magnetic structure.

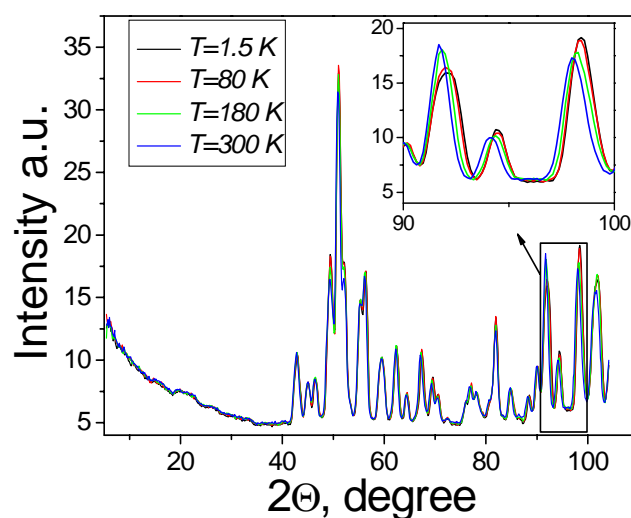


Fig. 1 Neutron diffraction patterns for a powder sample of  $\text{Y}_3\text{Co}$  measured at  $T=1.5\text{K}, 80\text{K}, 180\text{K}, 300\text{K}$  ( $\lambda= 2.452 \text{\AA}$ ). Inset shows neutron diffraction patterns in detail.

#### References:

1. N. V. Baranov, A. N. Pirogov, A. E. Teplykh., J. Alloys and Compounds, 226 (1995) 70.
2. A. E. Teplykh, A. N. Pirogov and N. V. Baranov. Materials science forum. 321-324 (2000) 653.
3. E. Talik et al. J. Less-Common Metals, 138 (1988) 129.
4. G. M. Kvashnin, O. P. Kvashnina, Solid State Physics, v. 38, N 4, 1996.
5. N. V. Baranov et al., J. Alloys and Comp., 329 (2001) 22.



## EXPERIMENTAL REPORT

### Metamagnetic transitions in $Y_{1-x}R_xFe_2D_{4.2}$ compounds ( $R = Tb$ )

Proposal N° PHY-01-2235

Instrument **E6**

Local Contact  
Norbert Stüßer

Principal Proposer: Valérie Paul-Boncour, CNRS, France  
Experimental Team: Andreas Hoser, HMI, Berlin  
Norbert Stüßer, HMI, Berlin

Date(s) of Experiment

18/02/2008 – 24/02/2008

Date of Report: 20/05/2008

From 18 to 24 February, neutron diffraction experiments have been performed on  $YFe_2D_{4.2}$  and  $Y_{0.5}Tb_{0.5}Fe_2D_{4.2}$  versus temperature and applied field on E6 instrument.

$YFe_2D_{4.2}$  undergoes a first order transition from ferromagnetic (F) to antiferromagnetic (AF) structure at 84 K. Above the transition the magnetization curves display a metamagnetic behaviour. Neutron powder diffraction (NPD) patterns were measured at 90, 100 and 125 K for field variation between 0 and 10 T. As the field increases a progressive change from AF to F structure is observed (Fig. 1). The transition field is shifted to larger values as T increases.

$Y_{0.5}Tb_{0.5}Fe_2D_{4.2}$  shows a magnetic transition at 129 K. This higher temperature compared to  $YFe_2D_{4.2}$  can be explained only partially by its larger volume. Measurements were performed without field from 5 to 180 K, in order to determine the evolution of the magnetic structure versus temperature. We observe only a change of nuclear line intensities which indicates that the compound remains ferrimagnetic without AF structure. For heavy rare earth like Tb, an antiparallel coupling is expected between Tb and Fe. This is confirmed for this compound as a compensation point is observed at 50 K. The data analysis at zero field and versus temperature shows a progressive decrease of the magnetic line intensities with a sharp decrease at 140 K. Field dependent measurements between 0 and 13 T were performed at 135 K (Fig. 2), 140, 145 and 150 K. The NPD pattern refinement indicates a growing of the ferrimagnetic line intensities, which reach saturation at a larger field as the temperature increases.

The difference of magnetic behaviour, as well as the larger transition temperature of  $Y_{0.5}Tb_{0.5}Fe_2D_{4.2}$  compared to  $YFe_2D_{4.2}$  can be

explained by the influence of the molecular field of Tb on the Fe moments.

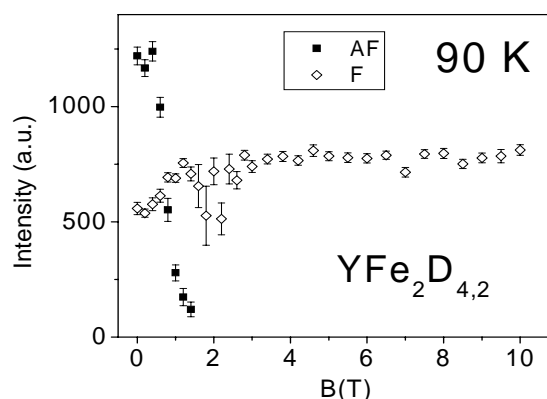


Fig. 1: Evolution of the AF and F magnetic line intensities of  $YFe_2D_{4.2}$  at 90 K.

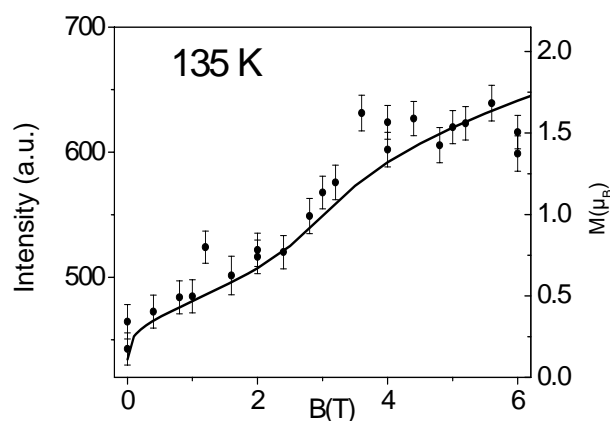


Fig. 2: Evolution of the ferrimagnetic line intensities of  $Y_{0.5}Tb_{0.5}Fe_2D_{4.2}$  at 135 K compared to the magnetization curve.

#### Acknowledgement

*This research project has been supported by the European Commission under the 6<sup>th</sup> Framework Programme through the Key Action: Strengthening the European Research Infrastructures. Contract n°: RII3-CT-2003-505925 (NMI 3).*



## EXPERIMENTAL REPORT

### Neutron diffraction studies of the hexagonal TbNi<sub>1-x</sub>Au<sub>x</sub>In compounds for 0 < x < 1

Proposal N° PHY-01-2238

Instrument **E6**

Local Contact  
Norbert Stüßer

Principal Proposer: Penc B., Jagiellonian University, Kraków, PL  
Experimental Team: Penc B., Jagiellonian University, Kraków, PL  
Baran S., Jagiellonian University, Kraków, PL  
Arulraj A., HMI, Berlin

Date(s) of Experiment

10/03/2008 – 16/03/2008

Date of Report: 15/01/2009

Polycrystalline samples of the TbNi<sub>1-x</sub>Au<sub>x</sub>In ( $x = 0.1, 0.2, 0.4, 0.6$  and  $0.8$ ) intermetallics were studied by magnetometric, X-ray and neutron diffraction methods. All of the samples crystallize in the hexagonal ZrNiAl-type structure ( $P\bar{6}2m$  space group, No. 189).

The investigated compounds crystallize in the hexagonal ZrNiAl-type structure. The  $a$  and  $c$  lattice constants and the unit cell volume  $V$  increase with increasing Au content  $x$  while the  $a/c$  ratio shows an anomalous dependence with the maximum for  $x = 0.4$ . The Au atoms preferentially occupy the 2(c) position.

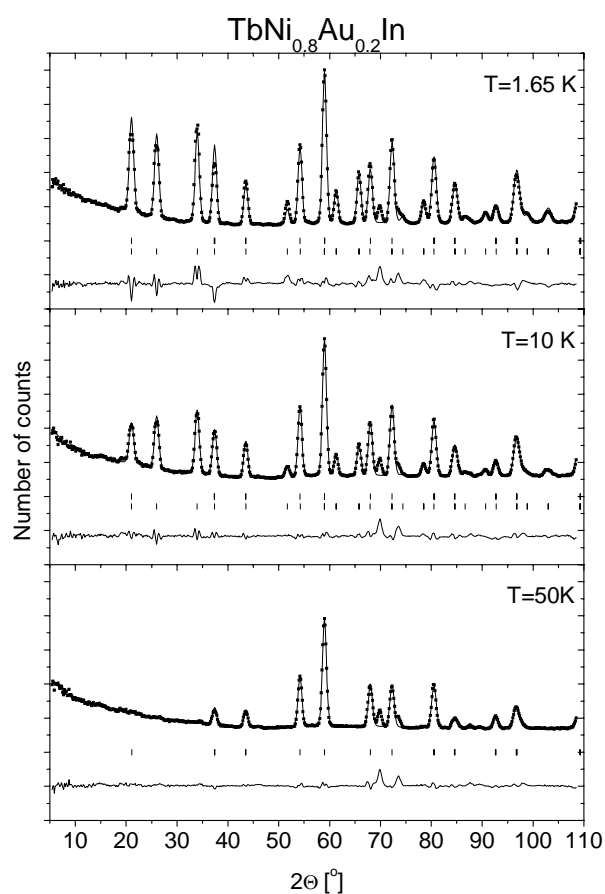
The hexagonal arrangement of the rare earth atoms introduces geometrical frustration in case of antiferromagnetic coupling in the  $a-b$  plane. TbNiIn and TbAuIn have different magnetic structures. TbNiIn has two magnetic phases described by the propagation vector  $\mathbf{k} = (\frac{1}{2}, 0, \frac{1}{2})$  [1]. In TbAuIn a noncollinear antiferromagnetic ordering of the  $120^\circ$ -type described by the propagation vector  $\mathbf{k} = (0, 0, \frac{1}{2})$  was found below  $T_N = 35$  K [2].

Magnetic data indicate that all compounds are antiferromagnets. The value of the Néel temperature decreases with increasing the Au content  $x$ . For the compounds with  $x$  equal to 0.1, 0.2 and 0.4 an additional phase transition in the ordered state is observed. Neutron diffraction data collected for the samples with  $x = 0.1, 0.2$  and  $0.4$  indicate similar magnetic ordering to those observed in TbNiIn. Tb magnetic moments form a noncollinear structure in the  $a-b$  plane. This order is described by the propagation vector  $\mathbf{k} = (\frac{1}{2}, 0, \frac{1}{2})$ . For  $x = 0.8$  the magnetic order is described by the propagation vector  $\mathbf{k} = (0, 0, \frac{1}{2})$ , similarly to TbAuIn. The Tb moments lie in the  $a-b$  plane and form a noncollinear structure of the  $120^\circ$ -type.

The results of these investigations were presented at The European Conference "Physics of Magnetism 2008", Poznań, 24-27.06. 2008 and were published in Acta Physica Polonica A.

[1] Ł. Gondek et al., J. Magn. Magn. Mater., 272-276 (2004) e443.

[2] A. Szytuła et al., J. Alloys Comp. 336 (2002) 11



Neutron diffraction patterns of TbNi<sub>0.8</sub>Au<sub>0.2</sub>In compound.

Acknowledgements: This research project has been supported by the European Commission under the 6<sup>th</sup> Framework Programme through the Key Action: Strengthening the European Research Infrastructures. Contract n°: RII3-CT-2003-505925 (NMI 3)



## EXPERIMENTAL REPORT

### Investigation of magnetic order induced by magnetic field in the quantum magnet $\text{Cu}(\text{tn})\text{Cl}_2$

Proposal N° PHY-01-2240

Instrument **E6**

Local Contact  
Alexandra Buchsteiner

Principal Proposer:

Alžbeta Orendáčová, P. J. Šafárik University, Košice, Slovakia

Experimental Team:

Martin Orendáč, P. J. Šafárik University, Košice, Slovakia

Alexandra Buchsteiner, Helmholtz Zentrum Berlin, Germany

Konrad Siemensmeyer, Helmholtz Zentrum Berlin, Germany

Date(s) of Experiment

17/06/2008 – 24/06/2008

Date of Report: 16/12/2008

Previous studies revealed  $\text{Cu}(\text{N}_2\text{C}_3\text{H}_6\text{D}_4)\text{Cl}_2$  can be treated as a two-dimensional (2d) magnet with dominant square-lattice like interactions,  $J/k_B \approx 3$  K. Phase transition to the ordered state was not indicated in zero magnetic field down to 60 mK [1]. Elastic neutron scattering experiment was performed at temperatures from 0.5 to 2 K and magnetic field up to 4 T to enlighten the origin of a specific heat anomaly appearing at 0.8 K in nonzero magnetic field.

The polycrystalline sample with mass 1g has been studied. The first powder diffraction spectrum was recorded in the angular range between 5 and 109 degree at 100 K in order to compare with former X-ray studies. For the investigation of the magnetic properties of the sample the angular range was limited to 5 to 34 degree which allows also for a higher statistics in the available experiment time. Comparative runs were performed in the magnetic field  $B = 0$  and 4 T at temperatures 0.5 K, 0.8 K, 2 K and 20 K. The runs in zero field were performed twice; before and after the application of magnetic field to check the possible effects of the sample reorientation induced by magnetic field and/or remanency effects introduced by a potential magnetic phase transition. Each run lasted 8 hours. Within the used statistics, the spectra did not change significantly with temperature (Fig.1). We found a slight change in intensity only for the Bragg peak (002) at 15 degree indicating some ferromagnetic order or magnetic field induced uniform magnetization (Fig.2). The change of the intensity does not depend on the temperature. In order to explain the origin of the found ferromagnetic contribution, additional measurements of isothermal ac susceptibility at temperatures below 1K and magnetic fields up to 10 T have been performed [2]. In coincidence with neutron data, preliminary analysis suggests only slight temperature dependence of uniform magnetization. In conclusion, further experiments are necessary to decide about the existence of a

field induced real phase transition to the 3d ordered state at 0.8 K.

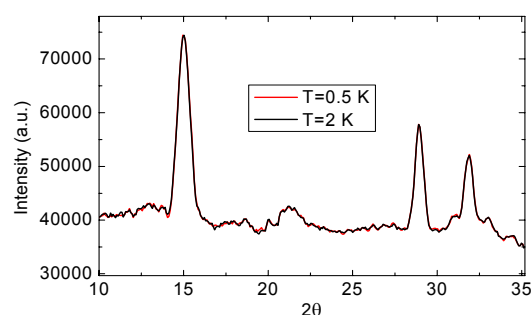


Fig.1: Comparison of powder spectra in  $B=0$ .

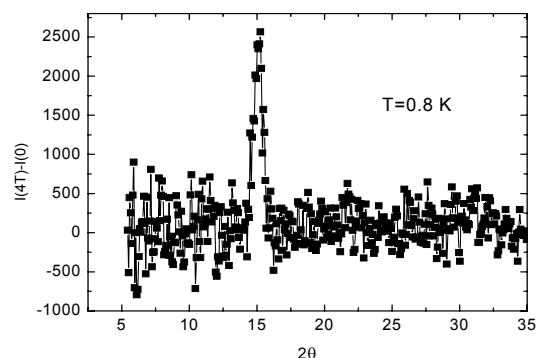


Fig.2: Difference of powder spectra measured in  $B=4\text{T}$  and 0.

*This research project has been supported by the European Commission under the 6<sup>th</sup> Framework Programme through the Key Action: Strengthening the European Research Infrastructures. Contract n°: RII3-CT-2003-505925 (NMI 3). M. Orendáč acknowledges financial support of VEGA 1/3027/06.*

[1] V. Zeleňák et al. Inorg. Chem. 45 (2006) 1774.

[2] A. Orendáčová et al. NHMFL 2008 research report.



**EXPERIMENTAL REPORT**  
**Neutron Diffraction Studies on**  
**RuSr<sub>2</sub>Y<sub>1.5</sub>Ce<sub>0.5</sub>Cu<sub>2</sub>O<sub>10</sub> (Ru1222) and**  
**Ru<sub>0.9</sub>Sr<sub>2</sub>YCu<sub>2.1</sub>O<sub>7.9</sub> (Ru1212)**

Proposal N° MAT-01-2241  
 Instrument **E6**  
 Local Contact  
 Dr. Norbert Stuesser

Principal Proposer: Ms. Rashmi Nigam, Institute for Superconducting and Electronic Materials, University of Wollongong, NSW, Australia  
 Experimental Team: A/Prof. Alexey Pan, Institute for Superconducting and Electronic Materials, University of Wollongong, NSW, Australia  
 Prof. ShiXue Dou, Institute for Superconducting and Electronic Materials, University of Wollongong, NSW, Australia  
 Dr. Norbert Stuesser, BENSC, Hahn Meitner Institut, Berlin

Date(s) of Experiment

25/04/2008 – 04/05/2008

Date of Report: 18/12/2008

Neutron diffraction (ND) measurement was carried out on two samples namely, RuSr<sub>2</sub>Y<sub>1.5</sub>Ce<sub>0.5</sub>Cu<sub>2</sub>O<sub>10</sub> (Ru1222) and Ru<sub>0.9</sub>Sr<sub>2</sub>YCu<sub>2.1</sub>O<sub>7.9</sub> (Ru-1212) using Focussing diffractometer (E6).

Ru1212 sample:

- i) Full spectra was measured from  $2\theta = 13^\circ$  to  $101^\circ$  with step size = 21 and at various temperatures ( $T = 1.5$  K, 10 K, 25 K, 30 K, 60 K, 90 K, 120 K, 140 K, 150 K, 180 K and 200 K).  $(\frac{1}{2}, \frac{1}{2}, \frac{1}{2})$ ,  $(\frac{1}{2}, \frac{1}{2}, \frac{3}{2})$  and  $(\frac{1}{2}, \frac{1}{2}, \frac{5}{2})$  magnetic peaks were obtained at  $2\theta = 26.26^\circ$ ,  $31.6^\circ$  and  $40.25^\circ$  respectively (see Fig.1).
- ii) Half spectra was measured from  $2\theta = 13^\circ$  to  $52.6^\circ$  at same temperatures as mentioned above with step size = 11 to obtain better statistics for magnetic peak intensities. With increasing temperature magnetic peak intensity reduces and magnetic peak disappears at  $T = 140$  K, indicating the magnetic transition.
- iii) ND data was obtained under applied magnetic field  $H \geq 5$  T using VM3. Full spectra was obtained at  $T = 1.5$  K for applied fields of 0T, 2.5 T and 5 T in the first run. With increasing field the magnetic peak intensity reduces and peak almost disappears at applied field of 5 T. In the second run ND data was obtained for  $H = 0$  T, 0.5 T, 1 T, 1.5 T, 2 T, 2.5 T, 3 T, 5T. Measurement at each field took 3 hrs.

Ru-1222 sample:

Unlike Ru1212 sample not enough time was left for the sequential measurement of Ru1222 sample. However following measurements were carried out to get some idea about the magnetic behaviour of Ru1222 sample:-

- i) Full spectra was measured from  $2\theta = 13^\circ$  to  $101^\circ$  while the system was cooling from

250 K down to 1.5 K. Weak magnetic peaks were obtained.

- ii) Full spectrum was again measured at 1.5 K for 20 hrs at applied field of 0 T in order to increase the intensity of magnetic peaks. Following this, ND data was obtained at 1.5 K for 20 hrs at 5 T and then again at 0 T. Magnetic peak does not completely vanish at 5 T. The intensities of ND pattern obtained at 0 T after the measurement of 5 T does not match with the 0 T data obtained first, reason of which is still not clear. More careful and detailed measurement of Ru1222 sample is needed.

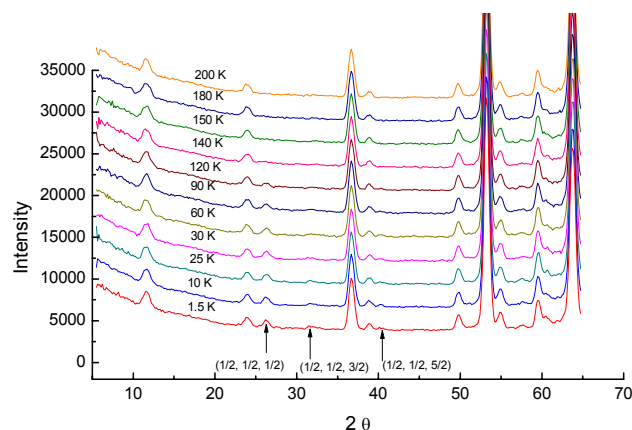


Fig. 1 Neutron diffraction pattern of Ru1212 sample obtained at different temperatures and at applied field of 0 T.

	<b>EXPERIMENTAL REPORT</b>  <b>Study of the magnetic phase transitions of PrIr<sub>2</sub>Si<sub>2</sub> compound</b>	Proposal N° PHY-01-2396 Instrument <b>E6</b> Local Contact Norbert Stüßer
	Principal Proposer: M. Mihalik, Faculty of Mathematics and Physics, Charles University, Prague, Czech Republic Experimental Team: N. Stüßer, Helmholtz-Zentrum Berlin, Berlin, Germany	Date(s) of Experiment  03/11/2008 – 06/11/2008

Date of Report: 14/01/2009

The PrIr<sub>2</sub>Si<sub>2</sub> compound belongs to the family of a polymorphic compounds, which can crystallize in a ThCr<sub>2</sub>Si<sub>2</sub>-type (LT-phase) and CaBe<sub>2</sub>Ge<sub>2</sub>-type (HT-phase) crystallographic modification. The HT-phase of this compound was found to be paramagnetic down to 2 K, however the LT-phase was found to undergo two magnetic phase transitions at T<sub>N</sub> = 45.5(1) and T<sub>i</sub> = 23.7(2) K. The magnetization measurements performed on this phase revealed that the *c*-axis is the easy axis of the magnetization. To better understand the magnetic structure in the LT-phase of PrIr<sub>2</sub>Si<sub>2</sub> we have performed the powder neutron experiment on the E6 diffractometer at BENSCH.

We have collected a powder neutron patterns for 10° < 2θ < 100° at several temperatures in the both magnetic phases and also at the paramagnetic region (Fig. 1). Additionally to this we have performed short scans from 33 degrees up to 48 degrees around T<sub>i</sub> to see how the magnetic phase transition evolves in the temperature.

We have successfully fitted all obtained powder patterns and found the magnetic structure for this compound. At temperatures below T<sub>i</sub> (Fig. 2) we have found the simple antiferromagnetic phase (+-stacking along the *c*-axis) with the magnetic propagation vector *k* = (0 0 1). We have found that only the Pr ions possess the stable magnetic moment of 3.2 μ<sub>B</sub>, which equals to the theoretical magnetic moment of free Pr<sup>3+</sup> ion.

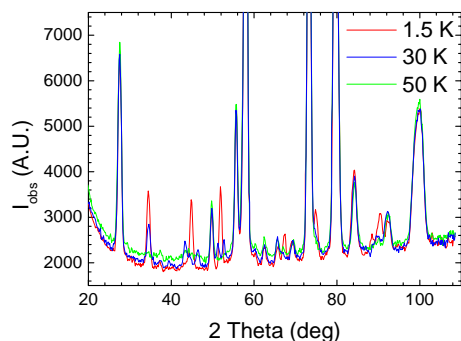


Fig. 1: The comparison of the obtained powder neutron diffraction patterns for different temperatures.

At temperature region T<sub>i</sub> < T < T<sub>N</sub> (Fig. 3) we have found more complex antiferromagnetic structure with the magnetic propagation vector *k* = (0 0 5/6). Also in this case the stable magnetic moments were found only on the Pr<sup>3+</sup> ions amounting 3.2 μ<sub>B</sub>/Pr. All magnetic moments in this antiferromagnetic phase were aligned along the *c*-axis.

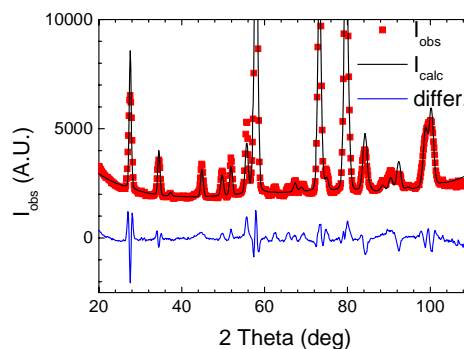


Fig. 2: The comparison of the observed pattern at T = 1.5 K with the calculated pattern according to our model.

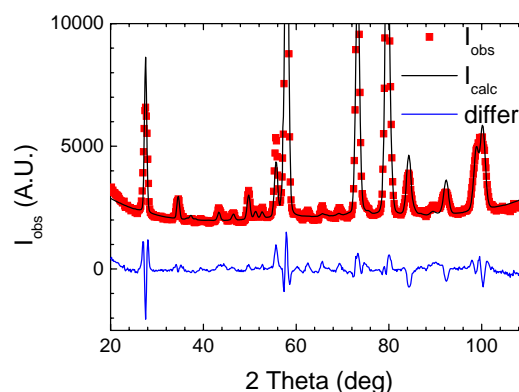


Fig. 3: The comparison of the observed pattern at T = 30 K with the calculated pattern according to our model.

*This research project has been supported by the European Commission under the 6<sup>th</sup> Framework Programme through the Key Action: Strengthening the European Research Infrastructures. Contract n°: RII3-CT-2003-505925 (NMI 3).*



## EXPERIMENTAL REPORT

### Metamagnetic transitions in $Y_{0.5}Er_{0.5}Fe_2D_{4.2}$ compound

Proposal N° PHY-01-2397

Instrument **E6**

Local Contact  
Norbert Stüsser

Principal Proposer: Valérie Paul-Boncour, CNRS, France  
Experimental Team: Andreas Hoser, HMI, Berlin  
Norbert Stüsser, HMI, Berlin

Date(s) of Experiment

03/12/2008 – 08/12/2008

Date of Report: 08/01/2009

$Y_{1-x}R_xFe_2(H,D)_{4.2}$  ( $R = Er, Tb$ ) compounds display a magnetovolumic transition which temperature depends on the nature and the concentration of the rare earth as well as the nature of the (H, D) isotope. This transition temperature  $T_M$  is also very sensitive to external parameters like pressure or magnetic field. The purpose of this work was to study the evolution of the magnetic structure of  $Y_{0.5}Er_{0.5}Fe_2D_{4.2}$  and  $Y_{0.9}Tb_{0.1}Fe_2D_{4.2}$  versus field at different temperatures in order to understand more clearly the influence of the rare earth on the metamagnetic behaviour.

The neutron diffraction experiment was performed on  $Y_{0.5}Er_{0.5}Fe_2D_{4.2}$  at different temperatures between 2 and 120 K and for increasing field between 0 and 12 T on the E6 spectrometer and with a vertical magnet. We have measured only this compound in order to collect several data with good statistics.

The results on  $Y_{0.5}Er_{0.5}Fe_2D_{4.2}$  show that at 2 K, the Er moment undergoes a spin reorientation as the magnetic field increases. Then above the transition at 55 K, the antiferromagnetic line ( $2\theta = 6^\circ$ ) progressively disappears whereas the ferromagnetic line ( $2\theta = 30^\circ$ ) increases as the magnetic field increases (Figures 1 and 2), reaching a maximum at 5 T. The cell volume increases to larger values as it was observed in  $YFe_2D_{4.2}$ , confirming the magnetostrictif character of the metamagnetic transition.

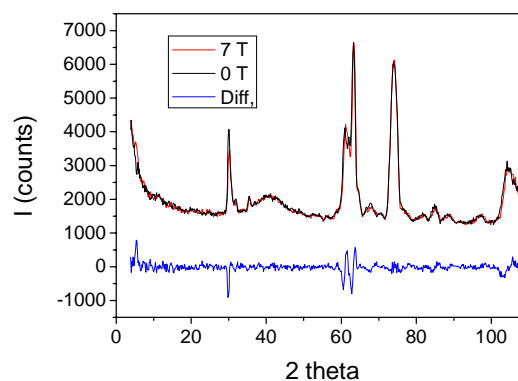


Figure 1: Comparison of the NPD patterns measured at 55 K without field and at 7 T.

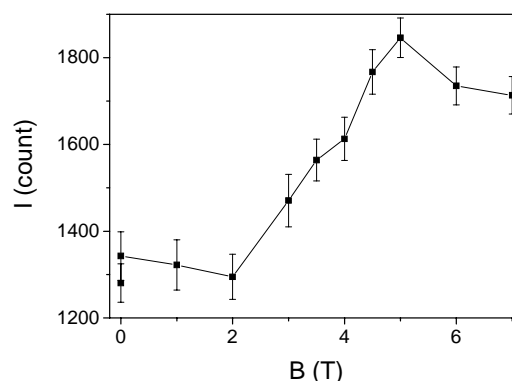


Figure 2: Evolution of the ferromagnetic line intensity ( $2\theta = 30^\circ$ ).

#### Acknowledgement

This research project has been supported by the European Commission under the 6<sup>th</sup> Framework Programme through the Key Action: Strengthening the European Research Infrastructures.

Contract n°: RII3-CT-2003-505925 (NMI3-1373).

	<b>EXPERIMENTAL REPORT</b> <b>Investigation of frustrated magnetism in the hexagonal TmTX intermetallics (T = Ag, Pt; X = Si, Ge, In)</b>	Proposal N° PHY-01-2400 Instrument <b>E6</b> Local Contact A. Arulraj
	Principal Proposer: S. Baran, Jagiellonian University, Kraków, Poland Experimental Team: A. Arulraj, BENSC, Helmholtz-Zentrum, Berlin, Germany B. Penc, Jagiellonian University, Kraków, Poland	Date(s) of Experiment 06/11/2008 – 09/11/2008

Date of Report: 15/01/2009

Three powder samples were investigated by neutron diffractometry under this project: TmNiIn, TmAgGe and TmPtIn. The experiment was performed on the E6 diffractometer equipped with the standard orange cryostat. The samples were cool down to 1.5 K.

The TmTX (T -transition metal, X -p-electron element) intermetallics crystallize in the hexagonal ZrNiAl-type crystal structure.

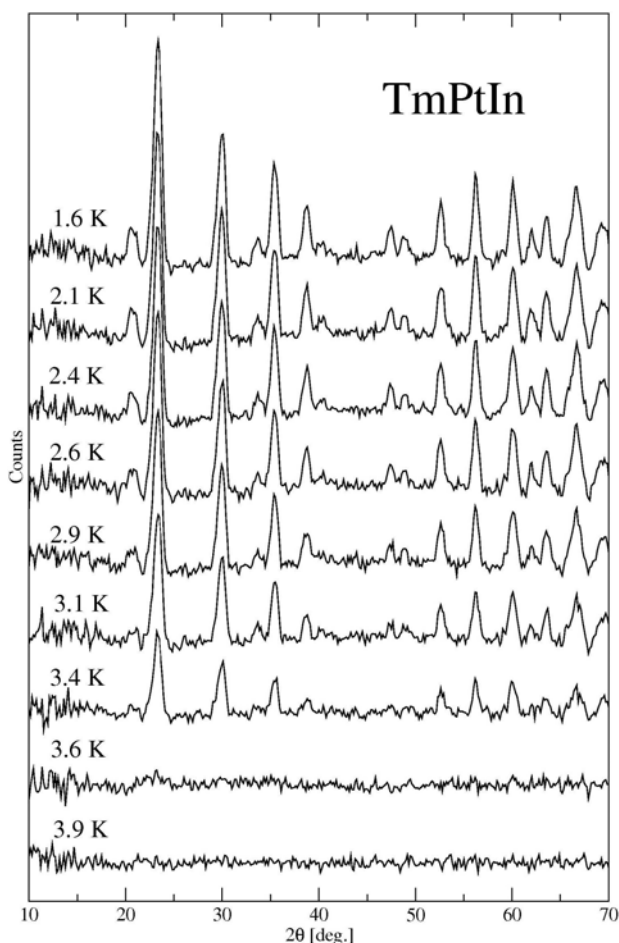


**Figure 1.** Temperature dependence of the TmPtIn neutron diffraction pattern. The patterns were obtained by making a difference between particular low-temperature pattern and the paramagnetic pattern obtained at 4.1 K.

In case of all investigated compounds the Bragg reflections of magnetic origin are present in the neutron diffraction patterns collected at low temperature (see fig. 1).

The temperature of transition to magnetically ordered state was found to be approximately 2.7, 4.4 and 3.5 K for TmNiIn, TmAgGe and TmPtIn, respectively.

The preliminary analysis of the low temperature neutron diffraction patterns suggests that all investigated compounds are antiferromagnets but the propagation vectors which describe the magnetic structures are different. In case of TmAgGe it is  $k = [1/2, 0, 0]$  (magnetic unit cell is doubled when compared to the crystallographic one). A commensurate magnetic structure was also found in TmPtIn ( $k = [1/4, 1/4, 1/2]$ ). The case of TmNiIn is the most complicated one. The low temperature neutron diffraction pattern is similar to that of TmPtIn, however, the reflections of magnetic origin are slightly shifted and they are significantly broadened. This broadening may be caused by short-range character of magnetic ordering and/or by overlapping of magnetic reflections. In order to explain the broadening phenomenon an experiment at lower temperature and with better angle resolution is required.

## Acknowledgements

This research project has been supported by the European Commission under the 6<sup>th</sup> Framework Programme through the Key Action: Strengthening the European Research Infrastructures. Contract n°: RII3-CT-2003-505925 (NMI 3).



## EXPERIMENTAL REPORT

### Neutron diffraction studies of tetragonal $TmT_2X_2$ intermetallics

Proposal N° PHY-01-2401

Instrument **E6**

Local Contact A. Hoser

Principal Proposer: S. Baran, Jagiellonian University, Kraków, Poland  
Experimental Team: A. Hoser, BENSC, Helmholtz-Zentrum, Berlin, Germany  
K. Kiefer, BENSC, Helmholtz-Zentrum, Berlin, Germany  
B. Penc, Jagiellonian University, Kraków, Poland

Date(s) of Experiment

09/11/2008 – 16/11/2008

Date of Report: 15/01/2009

Three powder samples were investigated by neutron diffractometry under this project:  $TmRu_2Si_2$ ,  $ErCu_2Si_2$  and  $HoFe_2Ge_2$ . The experiment was performed on the E6 diffractometer equipped with the standard orange cryostat and  $^3He$  insert in it. The samples were cool down to 0.47 K.

The  $RT_2X_2$  (R - rare earth element, T - transition metal, X - p-electron element) crystallize in the tetragonal  $ThCr_2Si_2$ -type crystal structure.

No magnetic ordering was found in  $TmRu_2Si_2$ . This fact leads to the conclusion that the specific heat anomaly observed at 0.9 K is of a non-magnetic origin.

The Bragg reflections of magnetic origin are present in the neutron diffraction pattern of  $ErCu_2Si_2$  (see fig. 1). With increasing temperature satellite reflections appear at 1.00 K. All magnetic reflections disappear at 1.50 K.

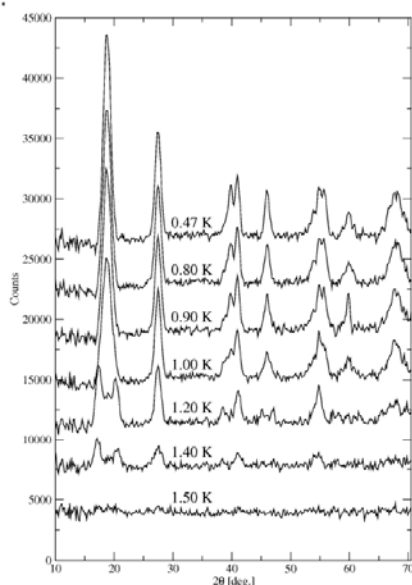


**Figure 1.** Temperature dependence of the  $ErCu_2Si_2$  neutron diffraction pattern. The patterns were obtained by making a difference between particular low-temperature pattern and the paramagnetic pattern obtained at 1.60 K.

$ErCu_2Si_2$  is an antiferromagnet described by the propagation vector  $\mathbf{k} = [1/2, 0, 1/2]$  at low temperature. The magnetic moments form ferromagnetic (101) layers stacked antiferromagnetically. The magnetic order may be described equivalently by a monoclinic magnetic unit cell (see fig. 2).

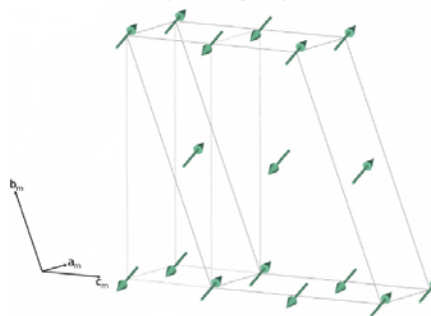


**Figure 2.** The antiferromagnetic low-temperature magnetic structure of  $ErCu_2Si_2$  described by the monoclinic magnetic unit cell. The crystallographic tetragonal unit cell is marked by dotted lines.

The satellite reflections are due to an incommensurate modulated structure described by the propagation vector  $\mathbf{k} = [0, 0, k_z]$  (the monoclinic unit cell is taken into account) where  $k_z$  increases with temperature from 0.048(1) at 1.00 K upto 0.086(1) at 1.40 K.

The preliminary analysis of the  $HoFe_2Ge_2$  neutron diffraction patterns reveals the presence of an antiferromagnetic order below 1.50 K. Another group of weak Bragg reflections of magnetic origin appears below 0.8 K. This low-temperature magnetic structure has not yet been resolved.

### Acknowledgements

*This research project has been supported by the European Commission under the 6<sup>th</sup> Framework Programme through the Key Action: Strengthening the European Research Infrastructures. Contract n°: RII3-CT-2003-505925 (NMI 3).*

	<b>EXPERIMENTAL REPORT</b>  <b>Low temperature magnetic structures of CePdIn and PrPdIn</b>	Proposal N° PHY-01-2402 Instrument <b>E6</b> Local Contact Norbert Stüßer
	Principal Proposer: L. Gondek, AGH Univ. of Science and Technology Experimental Team: J. Czub, Jabiellonian University Norbert Stüßer, BENS	Date(s) of Experiment  06/08/2008 – 10/08/2008

Date of Report: 15/01/2009

The RPdIn compounds exhibit interesting magnetic properties, which were widely investigated, especially in CePdIn case. In our group a systematic studies of this family including a great variety of complementary techniques are carried out. The performed experiment was aimed at determining of magnetic structures of CePdIn and PrPdIn samples at low temperatures (<1K). In case of CePdIn an antiferromagnetic ordering below 1.65 K was reported. The CePdIn compound exhibit heavy fermion behaviour with extremely large Sommerfeld coefficient.

Our experiment was performed on polycrystalline CePdIn sample. The sample was single phased without impurities. The neutron diffraction patterns were collected in two temperatures of 0.6 K and 3 K. Measurements revealed that the sample exhibit desired ZrNiAl-crystal structure, however no reflections of magnetic origin were found in neutron diffraction pattern collected at 0.6 K. It turned out, that the granted beamtime, that was reduced with respect to time we applied did not allowed to get satisfactory statistic. As the predicted Ce magnetic moment was some tenth of Bohr magnetons, the time we could spend on measurements was not sufficient. The collected data show no trace of magnetic contribution even in differential spectra between 0.6 and 3 K. Taking into account reduced beamtime measurements for PrPdIn sample were not performed.

*This research project has been supported by the European Commission under the 6<sup>th</sup> Framework Programme through the Key Action: Strengthening the European Research Infrastructures.*

*Contract n°: RII3-CT-2003-505925 (NMI 3).*



## EXPERIMENTAL REPORT

### Magnetic Phase Transitions in PrMn<sub>2</sub>Ge<sub>2-x</sub>Si<sub>x</sub>

Proposal N° PHY-01-2405

Instrument **E6**

Local Contact  
Norbert Stüßer

Principal Proposer: J L Wang, School of PEMS, UNSW@ADFA, CANBERRA ACT 2600 Australia  
 Experimental Team: J L Wang, S J Campbell, UNSW@ADFA, Australia  
 M Hoffmann, Technische Universität München, Germany  
 Norbert Stüßer and Anthony Arulray, BENSC

Date(s) of Experiment

08/10/2008 – 13/10/2008

Date of Report: 09/01/2009

The magnetic states of PrMn<sub>2</sub>Ge<sub>2-x</sub>Si<sub>x</sub> can be varied from the predominant ferromagnetic ordering of Ge-rich compounds to antiferromagnetic ordering for Si-rich compounds by controlling Mn-Mn distances via Si substitution for Ge [1]. Using E6, we have obtained neutron diffraction patterns for PrMn<sub>2</sub>Ge<sub>2-x</sub>Si<sub>x</sub> (x=0.4, 1.2, 1.6) from 10-480 K in 100 K steps and PrMn<sub>2</sub>Ge<sub>1</sub>Si<sub>1</sub> from 5-460 K in 25 K steps. This has allowed us to determine the magnetic structures and magnetovolume effects at the critical transition temperatures.

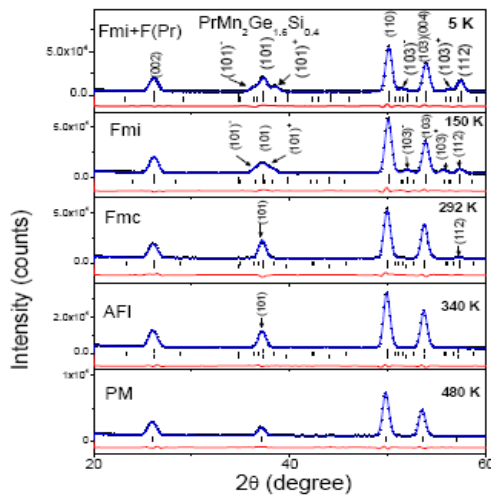


Fig. 1 Representative neutron diffraction patterns for PrMn<sub>2</sub>Ge<sub>1.6</sub>Si<sub>0.4</sub> from 5-480 K.

We have confirmed and characterized the transformation in PrMn<sub>2</sub>Ge<sub>1.6</sub>Si<sub>0.4</sub> [1] from a canted ferromagnetic (Fmc) to a conical configuration (Fmi) around  $T_{c/c} \sim 167$  K. This is indicated by the occurrence of satellite peaks of  $hkl$  reflections with  $h + k = 2n + 1$  - such as  $(101)^+$  and  $(101)^-$  - as shown in Fig.1.

As demonstrated in Fig. 2, our investigations reveal co-existence of canted ferromagnetism (characterized by the (112) peak) and antiferromagnetism (characterized by the (111) peak) for PrMn<sub>2</sub>Ge<sub>2-x</sub>Si<sub>x</sub> with x=1 and 1.2. This new information extends our understanding of the

relationship between lattice parameters and magnetic states for the Mn-sublattice in this system. Magnetovolume effects have been detected at the first order transition  $T_C^{Pr}$  for both PrMn<sub>2</sub>Ge<sub>1</sub>Si<sub>1</sub> and PrMn<sub>2</sub>Ge<sub>0.8</sub>Si<sub>1.2</sub>. In addition, below room temperature PrMn<sub>2</sub>Ge<sub>0.4</sub>Si<sub>1.6</sub> is found to exhibit canted antiferromagnetism (AFmc) rather than AFI [1].

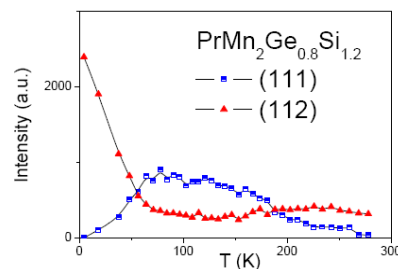
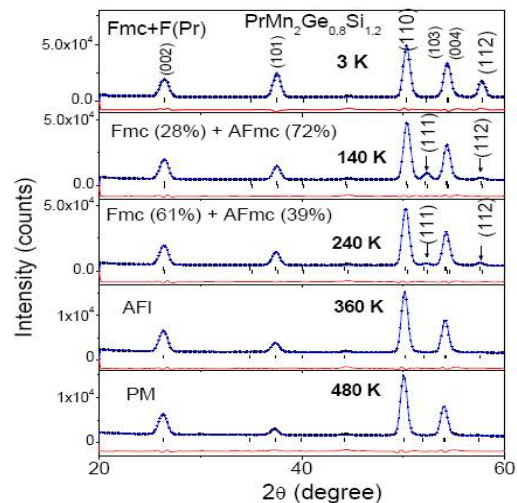


Fig. 2 (upper): Representative neutron diffraction patterns for PrMn<sub>2</sub>Ge<sub>0.8</sub>Si<sub>1.2</sub> from 3-480 K; (lower): Temperature dependences of: (111) and (112) peak intensities.

Combined with our magnetisation data, we are now able to establish a definitive phase diagram for PrMn<sub>2</sub>Ge<sub>2-x</sub>Si<sub>x</sub> as functions of temperature and composition. Our findings will extend and modify the current diagram reported in the literature [1].

[1] S Kervan, AKılıc and A Gencer, J. Phys.: Condens. Matter **16** (2004) 4955–4962.



## EXPERIMENTAL REPORT

### Magnetic structure and the magnetoelectrical coupling mechanism in La doped multiferroic BiFeO<sub>3</sub>

Proposal N° MAT-01-2406

Instrument **E6**

Local Contact  
Norbert Stüßer

Principal Proposer: Z.X. Cheng, ISEM, University of Wollongong, NSW 2522, Australia  
 Experimental Team: Prof. X.L. Wang, ISEM, University of Wollongong, NSW 2522, Australia  
 Dr. J.L. Wang, School of PEMS, UNSW@ADFA, Canberra, Australia

Date(s) of Experiment

04/10/2008 – 08/10/2008

Date of Report: 15/01/2009

La doping has been proved to be able to significantly improve the magnetic moment and reduce the electrical leakage in multiferroic BiFeO<sub>3</sub>. How La doping in BiFeO<sub>3</sub> changes its magnetic structure and magnetic ordering temperature is very important from the point of views of both practical application and basic research. Using E6, we have obtained the diffraction pattern of pure and La doped BiFeO<sub>3</sub> in wide temperature ranges.

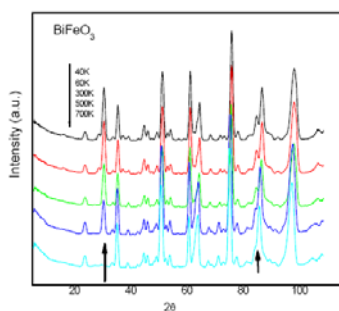


Fig.1 Neutron diffraction pattern of the undoped BiFeO<sub>3</sub> recorded at different temperatures

Figure 1 shows that the magnetic peak in pure BiFeO<sub>3</sub> disappears at a temperature of 700K. So the magnetic transition happens at between 500K and 700K, which is in accordance with the reported value of T<sub>N</sub>=643K. From the pattern recorded at 40K and 60K, no any detectable change was found. It means the observed abnormality from magnetic measurement is not from the magnetic transition.

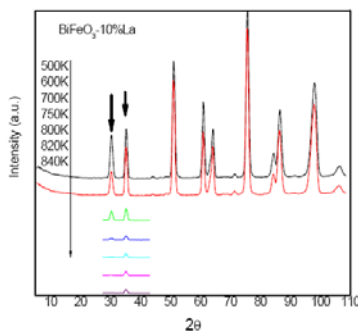


Fig.2 Neutron diffraction pattern of the 10% La doped BiFeO<sub>3</sub> recorded at different temperatures

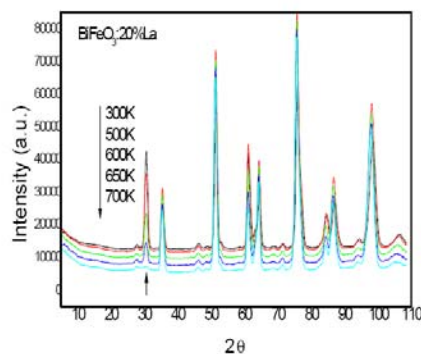


Fig.3 Neutron diffraction pattern of the 10% La doped BiFeO<sub>3</sub> recorded at different temperatures

Figure 2 shows the magnetic transition of 10% La doped BiFeO<sub>3</sub> happens between 820K and 800K. Figure 3 shows that magnetic transition of 20% La doped BiFeO<sub>3</sub> happens around 700K.

It is observed that all the doping result in a increase of the magnetic ordering temperature. However, there is no rule has been found for the transition temperature. The doping did not change the crystal structure of the BiFeO<sub>3</sub>. This result is meaningful for practical applications due to the evidence that magnetoelectric coupling can happen at much higher temperature in La doped BiFeO<sub>3</sub>.

The reason for La doping enhancing the interaction between magnetic irons should be further studied. Detailed magnetic structure will be determined by Rietveld refinement soon.



## EXPERIMENTAL REPORT

### Study of magnetic correlation in the quasi-1-D spin-chain compound Sr<sub>3</sub>NiPtO<sub>6</sub> using neutron

Proposal N° PHY-01-2408

Instrument **E6**

Local Contact  
Dr. N. Stüßer

Principal Proposer: Dr. S. M. Yusuf  
Experimental Team: Prof. E.V. Sampathkumaran  
Dr. S. Rayaprol  
Dr. N. Stüßer  
Mr. A. Jain

Date(s) of Experiment

18/08/2008 – 20/08/2008

Date of Report: 15/01/2009

The compound Sr<sub>3</sub>NiPtO<sub>6</sub>, crystallizing in the rhombohedral structure (space group  $R\bar{3}c$ ), belongs to the family of A<sub>3</sub>MXO<sub>6</sub>-type (A = Ca, Sr, and M/X= alkali or transition metal ions) quasi 1-D spin-chain compounds. The crystal structure of the compound Sr<sub>3</sub>NiPtO<sub>6</sub> consists of spin-chains made up of alternating face sharing RhO<sub>6</sub> octahedra and NiO<sub>6</sub> trigonal prism running along the crystallographic *c* axis. These chains are arranged on a triangular lattice in the *ab* plane. The temperature dependent magnetic susceptibility curve exhibits a Curie-Weiss behavior above 150 K, below which there is a gradual deviation from this behavior which may be due to the presence of a short-range spin-spin correlation [1]. The negative value of  $\theta_p$  indicates the antiferromagnetic nature of magnetic interaction. The observed values of *C/T* and susceptibility are large and constant at low temperature [1]. On the basis of these magnetic behaviors, the compound has been labeled as “spin liquid” [1].

In order to understand the nature of magnetic ordering, we have carried out the neutron diffraction experiments on the powder sample of Sr<sub>3</sub>NiPtO<sub>6</sub> using the E6 diffractometer at BENSC, using the wavelength of 2.44 Å, at different temperatures over 1.5 K - 200 K.

Figure 1 depicts the Rietveld refined neutron diffraction patterns at different temperature over 1.5 - 200K. No extra Bragg peak as well as no observable enhancement in the intensity of the fundamental (nuclear) Bragg peaks has been found down to 1.5 K. These observations rule out the possibility of a long-range-magnetic-ordering in this compound down to 1.5 K. We believe that neutron powder diffraction experiments down to ~ 10 mK temperature may shed more light on the spin ordering process for this “spin liquid” compound.

1. N. Mohapatra, K. K. Iyer, S. Rayaprol, and E. V. Sampathkumaran, Phys. Rev B **75**, 214422 (2007).

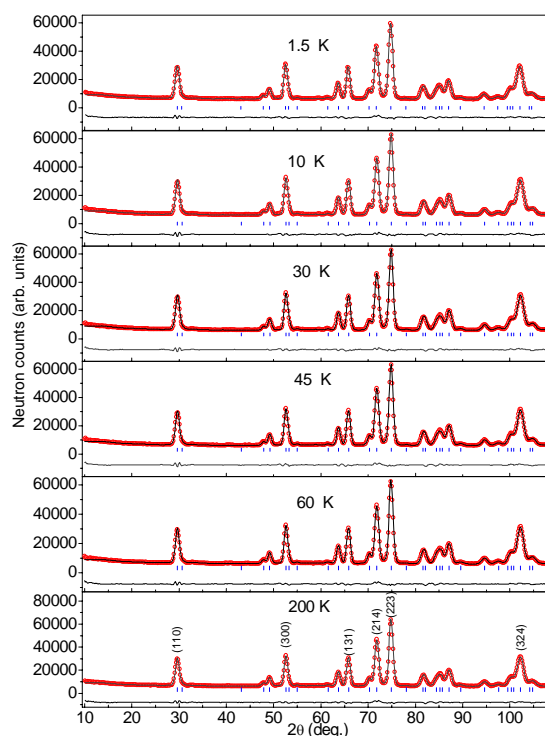


Figure. 1. Observed (open circles) and Rietveld calculated (solid lines) neutron diffraction patterns for Sr<sub>3</sub>NiPtO<sub>6</sub> using a wavelength of 2.44 Å. Solid line at the bottom of each panel shows the difference between the observed and the calculated patterns.



## EXPERIMENTAL REPORT

**Determining of the magn. structure of metastable nanomaterials: CoO würtzite, CoO blende and Ni hcp**

Proposal N° CHE-01-2194

Instrument **E9**

Local Contact  
Michael Tovar

Principal Proposer: German Salazar-Alvarez, Institut Català de Nanotecnologia

Experimental Team: Alberto Lopez-Ortega, ICN  
Jordi Sort, UAB-ICREA  
Josep Nogues, ICN-ICREA  
Michael Tovar, HMI  
Fabiano Yokaichiya, HMI

Date(s) of Experiment

14/03/2008 – 20/03/2008

Date of Report: 15.01.2009

Powder neutron diffraction experiments to elucidate the magnetic structure of divers Ni and CoO polymorphs were carried out at the instrument E9 using the standard “orange” cryostat and neutrons with a wavelength of 1.79803 Å at T = 2 K and 298 K. About 200 mg of sample were mounted in Vanadium cylinders of about 5 mm diameter. Three different samples were measured (only two samples shown).

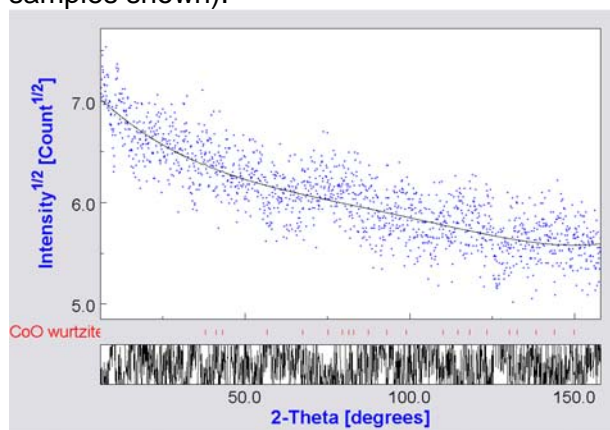


**Figure 1.** Diffractogram corresponding to sample 1 (CoO würtzite) measured at 2 K.

Figure 1 shows the signal measured on sample 1 composed of a CoO polymorph isostructural with the würtzite crystal. The data was obtained after ca. 24 h of acquisition time. It is believed that the low amount of powder combined with the relatively large absorption cross section of cobalt and the relative low neutron flux of the instrument (two to three orders of magnitude lower than D20 at ILL) rendered the measurement impossible. Moreover, the acquisition of data in serial mode extended the integration time needed to obtain useful data.

Figure 2 shows the spectra obtained for sample 2 at two different temperatures using an acquisition time of 34 h/spectrum. In agreement with the laboratory X-ray diffraction

patterns, the sample is shown to be composed of both fcc and hcp nickel nanoparticles. Regardless of the lengthy acquisition times noisy data was obtained. However, there seem to be small temperature-dependent reflections at lower angles (17 ° and 32 °). However, due to the noisy spectra no conclusions can be draw. To be able to get any meaningful results we would need to use a diffractometer with higher neutron flux or more sample.

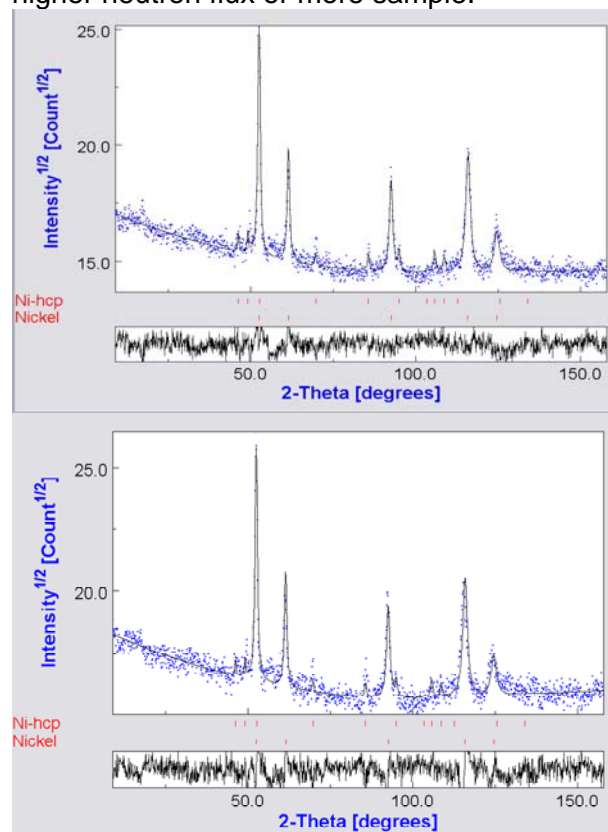


**Figure 2.** Diffractogram corresponding to sample 2 (Ni fcc and Ni hcp) measured at (top) 2 K and (bottom) 298 K.

*This research project has been supported by the European Commission under the 6<sup>th</sup> Framework Programme through the Key Action: Strengthening the European Research Infrastructures. Contract N°: RII3-CT-2003-505925 (NMI 3).*



## EXPERIMENTAL REPORT

### Magnetic structure of Li<sub>2</sub>ZrCuO<sub>4</sub>

Proposal N° PHY-01-2204

Instrument **E9**

Local Contact  
Oleksandr Prokhnenko

Principal Proposer: Wolfram Lorenz  
Experimental Team: Wolfram Lorenz, Leibnitz-Institute for Solid State and Materials Research, (IFW) Dresden  
Wolf-Dieter Stein, Institute for Solid State Physics, Technical University, Dresden  
Oleksandr Prokhnenko, The Berlin Neutron Scattering Centre (BENSC) Hahn-Meitner-Institute Berlin

Date(s) of Experiment

16/01/2008 – 18/01/2008

Date of Report: 15/01/2009

From the structure of spin-chains of the  $\gamma$ -polymorph of Li<sub>2</sub>ZrCuO<sub>4</sub> frustrated magnetic interactions are expected to be introduced by competing interactions of the nearestneighbour ferromagnetic coupling and nextnearest neighbour antiferromagnetic coupling. For such coupling scheme the ratio of both interactions determines the ground state to be either ferromagnetic or helical separated by a quantum critical point. Our macroscopic studies of Li<sub>2</sub>ZrCuO<sub>4</sub> are well described by helically ordered spin-chains very close to the quantum critical point. The magnetic properties of critical systems provide sensitive testing ground for theories of low-dimensional magnetism. To verify the expectation of helical ordering of this system, we have performed neutron powder diffraction experiments at E9 / BENSC in magnetic fields up to 5 T. Li<sub>2</sub>ZrCuO<sub>4</sub> itself and helical magnetic structures in general are highly sensitive to temperature and magnetic fields. The experiment was performed on a sample of compressed polycrystalline pallets (~ 10 g) in a vanadium container with a neutron wavelength of  $\lambda = 1.798$  Å. Powder diffraction data have been collected in zero magnetic field at  $T = 2$  K and  $T = 10$  K, below and above the ordering temperature ( $T_N = 6.9$  K), respectively. A third measurement was done at  $T = 2$  K in an applied magnetic field of  $\mu_0 H = 5$  T. With lower statistics the empty container was measured. From an earlier experiment at TOFTOF / FRM II two magnetic reflections were known before. Expecting ~ 12 h of beam-time for a single measurement we used altogether 30 h for measurement at 2 K in zero field (c.f. 1). Yet, no further magnetic reflections could be clearly identified. Though weak, altogether 5 magnetic reflexes have been identified by comparison of these data with the measurements at 5 T and at 10 K. Their positions show a slight deviation from a magnetic structure given by a magnetic

propagation vector  $\tau = (0 \ 0.5 \ 0)$  as would be appropriate for ferromagnetically ordered chains. Indeed, very small pitch angles are expected for a helical magnet close to ferromagnetic order. However, to refine the propagation vector statistics is insufficient. In  $\mu_0 H = 5$  T a shift of the reflexes was observed.

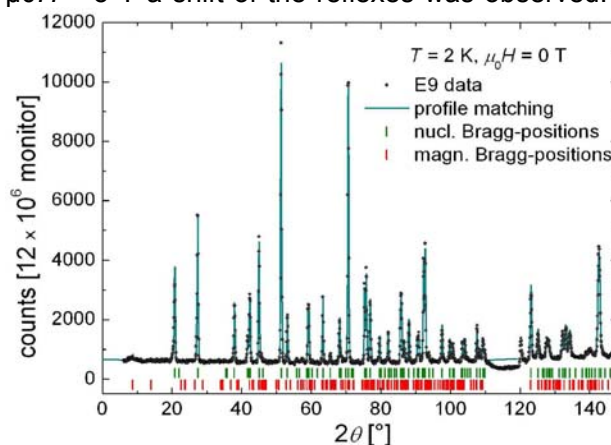


Fig. 1: Diffraction pattern as collected in zero field at  $T = 2$  K. The nuclear structure is in good accord to literature. The magnetic intensity found indicates helical ordering with small pitch angles.

As single crystals of this interesting compound are still not available, neutron powder diffraction remains the most promising method to determine its magnetic structure. For further experiments a high intensity diffractometer appears the appropriate instrument, even at the cost of lowered resolution. Moreover, to reduce the significant neutron absorption by the sample, utilization of isotope enriched Li is recommended to further increase statistics.



## EXPERIMENTAL REPORT

### Phase separation in manganites

Proposal N° PHY-01-2360

Instrument **E9**

Local Contact  
Dimitri Argyriou

Principal Proposer: Niels Vestergaard Jensen, Risø DTU  
Experimental Team: Niels Vestergaard Jensen, Risø DTU  
Simon Kimber, HME SF2

Date(s) of Experiment  
30/10/2008 – 02/11/2008

Date of Report: 15/01/2009

## INTRODUCTION

The perovskite manganites are notable for their extremely rich phase diagram in the charge, spin and lattice degrees of freedom. They have the general formula  $AMnO_3$  with the Mn ions occupying the centers of oxygen octahedra. They form a magnetic lattice where

antiferromagnetic (AFM) superexchange competes with ferromagnetic (FM) double exchange mediated by eg electrons forming Mn-O-Mn bonds. These couplings are dependent on the orbital arrangement, and interact with the lattice through the Jahn-Teller (JT) effect. This explains why many of the observed phase transitions couple all three degrees of freedom. The corresponding free-energy landscape is highly complex, with very different phases often having very similar free energies.

Where phases are in close competition they may coexist, and the choice of phase can be extremely sensitive to the external magnetic field, leading to focus on the manganites for applications such as colossal magnetoresistive sensors and magnetic refrigerants.

## EXPERIMENT

We investigated the influence of Ga and Sc doping (respectively) on the Mn-site of  $La_{0.67}Ca_{0.33}MnO_3$  after having characterized the materials magnetically. We looked for signs of AFM/FM coexistence above and below the FM/PM transition.

We intended to study the effect of magnetic field on any phase separation. Unfortunately the magnet control electronics failed, leaving the experiment to be performed in zero field.

## RESULTS

No antiferromagnetic peaks were found, see fig. 1. The data analysis is still in progress.

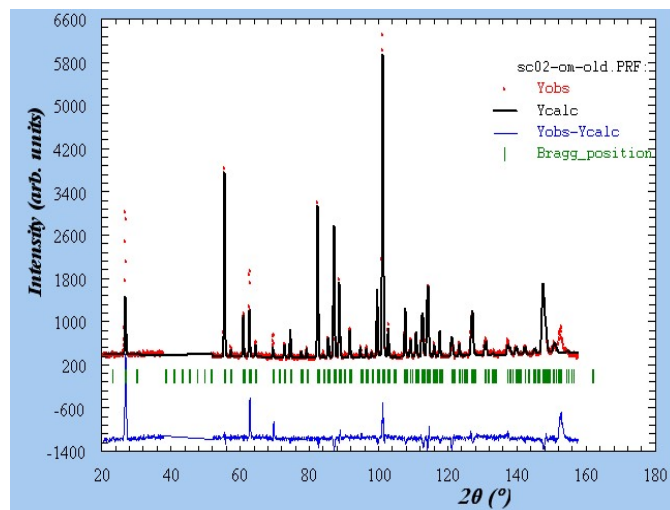


Fig 1: Rietveld fit to data for  $La_{0.67}Ca_{0.33}Mn_{0.98}Sc_{0.02}O_3$  (purely structural contribution). The ferromagnetic component is obvious on several peaks, but no antiferromagnetic component is apparent.

This research project has been supported by the European Commission under the 6<sup>th</sup> Framework Programme through the Key Action: Strengthening the European Research Infrastructures. Contract n°: RII3-CT-2003-505925 (NMI 3).



## EXPERIMENTAL REPORT

### Neutron diffraction of mesoporous Mn<sub>3</sub>O<sub>4</sub> and Mn<sub>2</sub>O<sub>3</sub>

Proposal N° CHE-01-2367

Instrument **E9**

Local Contact  
Dr Michael Tovar

Principal Proposer:

Mr Adrian Hill, The University of Edinburgh

Date(s) of Experiment

Experimental Team:

Dr Michael Tovar, Helmholtz Zentrum Berlin für  
Materialien und Energie  
Professor Andrew Harrison, Institut Laue-Langevin  
and the University of Edinburgh

25/07/2008 – 29/07/2008

Date of Report: 06/08/2008

Mesoporous forms of Mn<sub>3</sub>O<sub>4</sub> (hausmannite) and  $\alpha$ -Mn<sub>2</sub>O<sub>3</sub> have recently been prepared with highly crystalline walls. The pore sizes and surface areas are 3.75 nm and 100 m<sup>2</sup> g<sup>-1</sup> for Mn<sub>3</sub>O<sub>4</sub> and 3.56 nm and 139 m<sup>2</sup> g<sup>-1</sup> for Mn<sub>2</sub>O<sub>3</sub>, [Jiao, F., *et al.*, *Adv. Mater.*, **2007**, 19, 4063]. We have performed high resolution powder diffraction studies upon these materials with the E9 diffractometer at key temperatures.

#### Mesoporous Mn<sub>3</sub>O<sub>4</sub>.

Scans were taken at 6 different temperatures, 2, 25, 35, 40, 60 and 100 K (**Figure 1**).

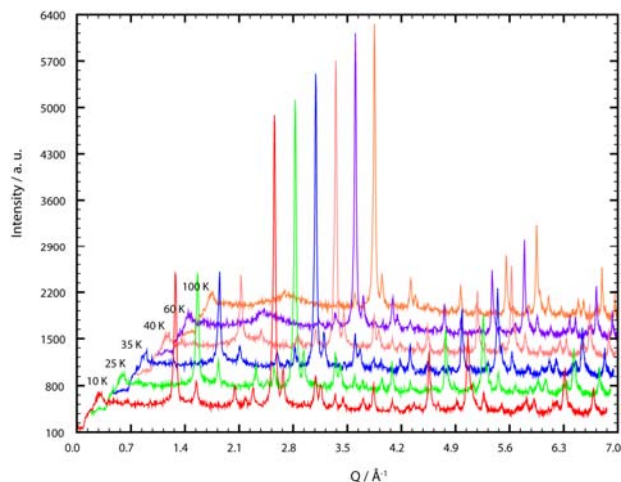


**Figure 1.** Diffraction patterns of mesoporous Mn<sub>3</sub>O<sub>4</sub>.

A clear onset of magnetic ordering can be seen to occur between 40 and 60 K ( $T_C = 41$  K in bulk material Mn<sub>3</sub>O<sub>4</sub>). The material has the crystallographic space group  $I4_1/amd$ . The magnetic cell has a doubling of the lattice dimension along  $b$ . The Bragg peaks which change dramatically in intensity (**Figure 2**) over this transition are the (110) and (120) peaks, (indexed with the magnetic cell).

Diffuse scattering can be observed above  $T_C$ , where the (110) and (101) magnetic Bragg peaks are expected. This has been seen in bulk material, [Kuriki, A., *et al.*, *J. Phys. Soc. Jpn.*, **2003**, 72, 458].

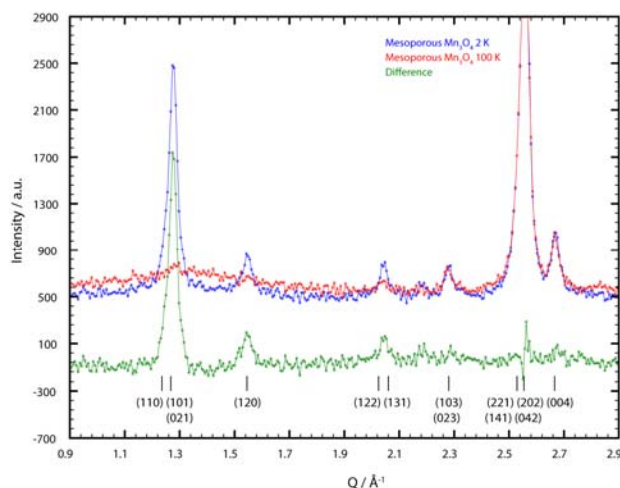


**Figure 2.** 2 K – 100 K difference plot for Mn<sub>3</sub>O<sub>4</sub>.

#### Mesoporous Mn<sub>2</sub>O<sub>3</sub>.

Scans were taken at 2, 20, 50, 70, 100 and 200 K. A difference curve between the 2 and 200 K data is shown below (**Figure 3**).

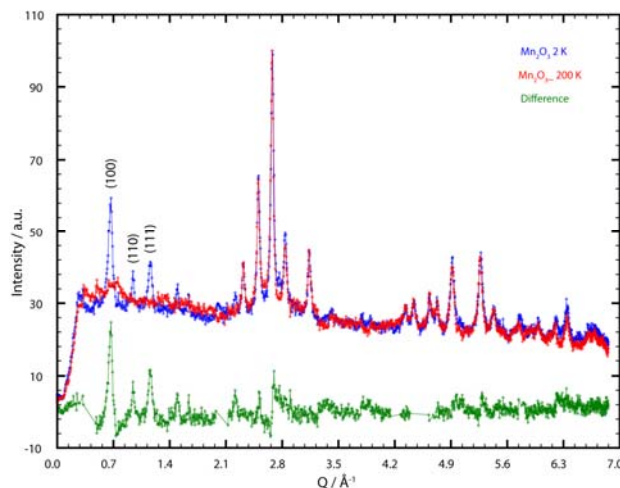


**Figure 3.** 2 K – 200 K difference plot for Mn<sub>2</sub>O<sub>3</sub>.

The first 3 magnetic peaks, (100), (110), and (111) can clearly be seen at 2 K. Showing similar magnetic structure to bulk Mn<sub>2</sub>O<sub>3</sub>.

*This research project has been supported by the European Commission under the 6<sup>th</sup> Framework Programme through the Key Action: Strengthening the European Research Infrastructures.*

Contract n°: RII3-CT-2003-505925 (NMI 3).



## EXPERIMENTAL REPORT

### Nuclear and Magnetic structure of the Orbital Ordered Spinel $MgV_2O_4$

Proposal N° PHY-01-2457-EF

Instrument E9

Local Contact M. Tovar

Principal Proposer: B. Lake – HZB, Berlin, TU-Berlin

Experimental Team: E. Wheeler – HZB, Berlin,  
N. Islam – HZB, Berlin,  
M. Reehuis – HZB, Berlin

Date(s) of Experiment

22/07/2008 – 25/07/2008

Date of Report: 14/01/2009

The vanadium spinel material  $MgV_2O_4$  has both spin and orbital degrees of freedom at low temperature. In order to understand any ordering of the orbitals and their effect on the spin interactions we have investigated the crystal structure of  $MgV_2O_4$  in the tetragonal low-temperature phase and the magnetic order of the vanadium sublattice.

A neutron diffraction experiment was performed on the fine-resolution powder diffractometer E9. This instrument uses a Ge(511)-monochromator giving an incident wavelength of  $\lambda = 1.79 \text{ \AA}$ . We mounted a vanadium cylinder containing 3g of powdered  $MgV_2O_4$  in an orange cryostat reaching a base temperature of 2 K. We have measured diffraction patterns at 10 different temperatures between 2 K and 70 K. For all measurements the powder patterns were recorded in the 2-theta range from  $5^\circ$  to  $150^\circ$ , which took approximately 5 hours for each temperature to reach satisfactory statistics.

From our measurements we confirmed the presence of the cubic to tetragonal transition which was seen by the splitting of particular cubic reflections as shown in Fig. 1b. The whole powder did not have the same transition temperature and we observed phase co-existence giving a range over which the transition occurred. At 42 K the whole powder was in a single tetragonal phase. The fit shows a tetragonal distortion  $c/a = 0.9937$ .

We fitted the data of the cubic phase (at 70K) with the spinel structure using the space group  $Fd\bar{3}m$ , as found earlier for  $ZnV_2O_4$  [1]. A summary of the results is given in Table 1. Although, later measurements on E5 indicated that cubic  $MgV_2O_4$  crystallizes in the lower-symmetric space group  $F\bar{4}3m$ , where the  $d$ -glide plane is violated.

But in the neutron powder patterns the superstructure reflections (as the 200 or 420) observed in our single-crystal experiment, could not be detected, since they were found to be rather weak. Therefore it seems not surprising, that the refinements in the lower symmetric space group  $F\bar{4}3m$  did not show any improvement. Finally the refinements were carried out in the higher symmetry space groups  $I4_1/amd$  and  $Fd\bar{3}m$  for the data collected at 2 K and 70 K, respectively. At 2 K we observed additional primitive Bragg reflections, which could be generated with the rule  $(hkl)_M = (hkl)_N \pm \mathbf{k}$ , where the wave vector is  $\mathbf{k} = (001)$ . The refinement of the magnetic structure resulted in a highly reduced magnetic moment of  $0.35(5)\mu_B$  per  $V^{3+}$  ion.

**Table 1:** Fitting parameters for crystal structure of  $MgV_2O_4$ . For  $Fd\bar{3}m$  (at 2 K) Zn is at the Wyckoff position  $8a$  (1/8,1/8,1/8), V at  $16d$  (1/2,1/2,1/2) and O at  $2e$  ( $x,x,x$ ); for  $I4_1/amd$  (at 70 K) Zn is at  $4a$ (0,3/4,1/8), V at  $8d$  (0,0,1/2) and O at  $16h$  (0, $x,x,z$ ), respectively

T (K)	2	70
a (Å)	5.9585(1)	8.40856 (13)
c (Å)	8.37562 (14)	
V (Å <sup>3</sup> )	297.44(1)	594.51(3)
x(O)	-	0.26057(8)
x(O)	0.02021(16)	-
z(O)	0.26156(12)	-
$\chi^2$	2.786	4.431

### Reference

[1] M. Reehuis et al., Eur. Phys. J. B **35** 311 (2003).

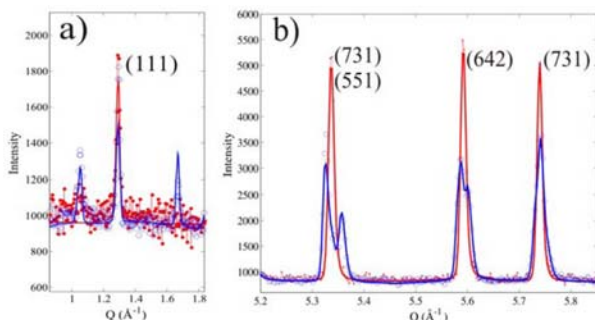


Figure 1:

Neutron powder diffraction pattern at 2 and 70 K. a) shows the magnetic peaks which appear at lower Q below  $T_N = 37 \text{ K}$ . At high Q-values the particular structural Bragg peaks show a splitting at lower temperature indicating the tetragonal distortion. All the given indices correspond to the cubic cell.



## EXPERIMENTAL REPORT

### Time resolved measurements of the VL dynamics in ultra pure bulk Niobium

Proposal N° PHY-04-1551

Instrument **V4**

Local Contact  
A. Wiedenmann

Principal Proposer: Sebastian Mühlbauer, TU München  
Experimental Team: Sebastian Mühlbauer, TU München  
Albrecht Wiedenmann, HZ Berlin  
Uwe Keiderling, HZ Berlin

Date(s) of Experiment

09/01/2008 – 12/01/2008  
16/02/2008 – 19/02/2008

Date of Report: January 2009

#### Introduction:

By SANS, the 2D magnetic field distribution of bulk vortex lattices (VL) may be studied in great detail. SANS offers access for measuring the coherence length and penetration depth, VL symmetry and pinning potentials as function of applied magnetic field and temperature. But until nowadays, this was limited to the static properties of VLs. Microscopic measurements of vortex dynamics are only possible for thin film, where surface effects and pinning play a dominant role. Therefore, the intrinsic properties of VL dynamics are only accessible by macroscopic techniques as i.e. transport measurements. By using time resolved stroboscopic SANS we now succeeded in microscopically measuring the dynamic properties of bulk undisturbed VLs.

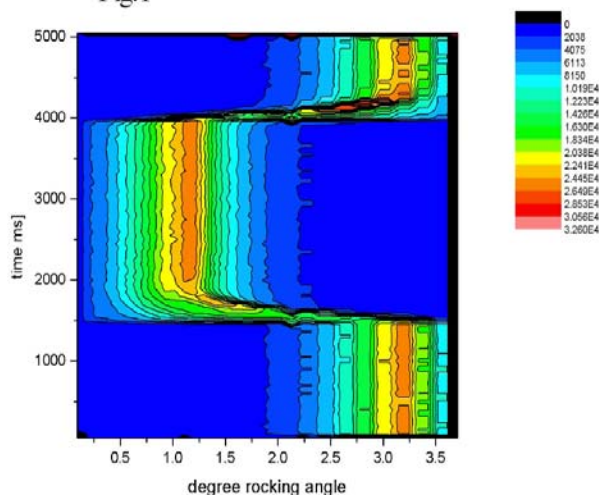
#### Setup:

A static magnetic field  $B_{\text{stat}}$  was applied parallel to the incident neutron beam as well as parallel to the (110) axis of the bulk Niobium single crystal. By applying a small magnetic field  $B_{\text{osc}}$  in the scattering plane perpendicular to  $B_{\text{stat}}$ , the magnetic field direction may be moved due to vector addition of the two fields.  $B_{\text{osc}}$  was driven with rectangular pulses, generating two equilibrium positions for  $B$  – and therefore also for the VL in the sample. The dynamic response of the VL, especially its relaxation processes have been recorded by time resolved stroboscopic SANS at V4 at HMI. The time resolution of this setup is defined by the used sample detector distance and the used wavelength, caused by smearing due to the finite wavelength resolution of the selector. At 11 Å, a time resolution of about 20ms is observed. The measurement is

performed in a stroboscopic manner adding many cycles.

Rockingscan performed at 4K and  $B_{\text{stat}} = 100$  mT, timescale in ms.  $B_{\text{osc}} = 4$  mT. The repetition cycle of the oscillating field was 2 Hz.

Fig.1



The shifting of the VL between the two equilibrium positions is visible. Switching the field  $B_{\text{osc}}$  on or off is a symmetric process. The equilibrium is reached after about 600ms after the magnetic field direction is changed. As the VL firstly reacts on the changed field at the surface of the sample, the propagation of the VL into the bulk sample may be described as strongly dampened wave.

#### Results:

By performing rocking scans, we were able to observe in detail the switching of the VL between the two different equilibrium positions, as shown in fig.1. A detailed analysis of the involved relaxation processes concerning flux creeping and flux flow will follow.

	<b>EXPERIMENTAL REPORT</b>  <b>Search for the FFLO phase in a heavy-fermion superconductor CeCoIn<sub>5</sub></b>	Proposal N° PHY-04-1572 Instrument <b>V4</b>  Local Contact Dr. Uwe Keiderling
	Principal Proposer: H. Furukawa, Ochanomizu University Experimental Team: S. Kawamura, Ochanomizu University H. Shishido, Kyoto University T. Shibauchi, Kyoto University Y. Matsuda, Kyoto University B. Lake, HMI	Date(s) of Experiment  30/05/2008 – 02/06/2008

Date of Report: 15/03/2008

Novel superconductivity in a heavy fermion compound CeCoIn<sub>5</sub> with  $T_c = 2.3$  K has been studied extensively. In particular, various experimental results have recently suggested that “FFLO state” appears at low- $T$  and high- $H$  corner in the  $H$ - $T$  phase diagram in this system [1]. In order to directly detect the FFLO state in CeCoIn<sub>5</sub>, we have performed SANS experiments, which is the only technique to bare an evidence of the FFLO state.

The measurements were carried out at V4. Neutrons with wavelength of 4.5 Å were used, and PSD was set at 4 m position from the sample. A <sup>3</sup>He-<sup>4</sup>He dilution refrigerator with a vertical-field magnet was used to cool the sample down to 0.05 K. Single crystals of CeCoIn<sub>5</sub> were aligned on an Al<sub>2</sub>O<sub>3</sub> plate so that the  $c$ -axis is parallel to the vertical magnetic field and the  $a$ -axis is parallel to the incident neutron beam. The crystals cover the area of 16mm $\phi$ . The total mass of the crystals is about 0.4g. We had 3days beamtime. We used about 1.5 days for the measurement, since we spent the rest for experimental setup and recovery from some setup problem

In this configuration, diffractions from the vortex lattice should appear on the horizontal line in the image. In addition to them, in the FFLO phase, weaker superlattice spots are expected to appear on the vertical lines, reflecting periodic nodal planes originating from the spatial modulations of the superconducting order parameter along the flux line.

Continuing to the previous measurement performed in February 2008, we carried out  $\omega$  scans to search the signals from the superlattice in a wider  $Q$  region at 0.05 K and 4.8 T, where the FFLO phase is expected to exist. However, clear evidence of the FFLO phase was not bared.

At 4.8 T, we did not observed the original spots from the vortex lattice, too. Therefore, we performed the measurement at 3 T to estimate intensity by observing the original signals from the vortex lattice, because more intense signals are expected at 3 T because of the multiplicity. However, we did not detect the diffractions. Based on the present measurement, it was concluded that we need to increase the sample amount to detect the weak signals from the superlattice in the FFLO phase. We are planning the continuation to this study after preparing enough amount of the sample.

[1] For example, K. Kumagai et al., Phys. Rev. Lett. 97 (2006) 227002.



## EXPERIMENTAL REPORT

### Symmetry breaking vortex lattice structures in ultra pure Niobium

Proposal N° PHY-04-1604

Instrument **V4**

Local Contact  
A. Wiedenmann

Principal Proposer: Albrecht Wiedenmann, HZB  
 Experimental Team: S. Mühlbauer, P. Böni, C. Pfeiderer, TU München  
 E.M. Forgan, University of Birmingham  
 M. Laver, University of Birmingham  
 G. Behr, IFW Dresden

Date(s) of Experiment

12/01/2008 – 15/01/2008

Date of Report: January 2009

#### Introduction:

The symmetry of vortex lattices (VL) is strongly influenced by so called non local corrections to the Ginzburg-Landau (GL) theory, extending its applicability to medium inductions and temperatures. But also the topology of the Fermi surface of the underlying superconducting material can play an important role. By applying the magnetic field along a four-fold (100) crystal symmetry direction, frustration between the six-fold VL symmetry is induced, thus leading to a rich VL phase diagram in Niobium. An isosceles phase at high temperatures is followed by an scalene phase at medium fields, surrounded by a high field and low field square VL phase [1]. Typical data for the scalene phase, obtained on V4 is shown in fig.1. Furthermore, these VL structures have the surprising property to break crystal symmetry. The origin of the symmetry breaking transition nevertheless remains unclear. In order to further examine the VL topology of Niobium with the magnetic field applied along the (100) axis, we have performed high resolution SANS on V4.

#### Results:

The instrument was used in conventional SANS geometry, the resolution was improved by adding a further slit at 12m collimation length, defining a L/D ratio of 600. A horizontal cryo-magnet was used for the studies. The VL symmetry was measured as a function of the angle  $\beta$ , defining the angle between the (100) symmetry direction and the direction of the applied magnetic field in an (110) plane. The results may be summarized as follows: The symmetry breaking transition of the VL in Niobium vanishes for all four phases at a characteristic angle  $\beta$  at roughly  $19^\circ$  away from the (100) axis. The scalene phase shows an additional characteristic angle  $\alpha$  at  $6^\circ$ , where VL symmetry changes from scalene to isosceles. Both  $\alpha$  and  $\beta$  only show a weak temperature dependence which is given in fig.2 and 3 for  $\beta$ . As non local corrections

to GL are supposed to show a pronounced field and temperature dependence and as furthermore magnetoresistance, mapping the Fermi topology, shows characteristic features at  $17^\circ$  off the (100) axis, we state that the reason for the mentioned symmetry breaking transition may be due to Fermi topology effects.

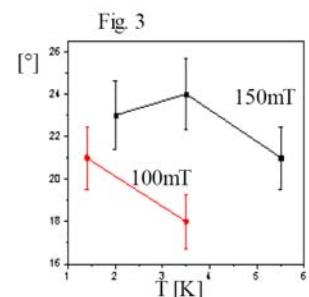
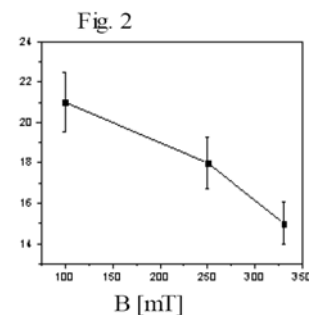
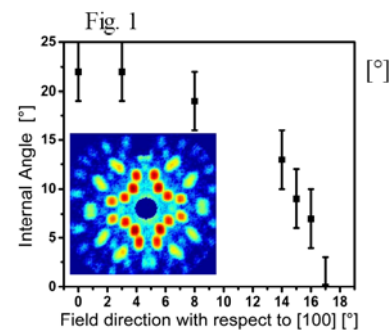


Fig. 1: The inset shows typical data for the scalene phase at 2K and 150mT for B parallel (100). The graph displays the internal angle of two VL domains as a function of the rotation angle of B. The characteristic angle  $\beta$  at  $17^\circ$  is visible. Fig. 2 and 3: Temperature and field dependence of the characteristic angle  $\beta$ .

[1] Laver et al PRL 96, 167002 (2006)



## EXPERIMENTAL REPORT

### The critical dynamics of the weak itinerant ferromagnets $Mn_{1-y}Fe_ySi$ , $y = 0.06, 0.08, 0.10$ .

Proposal N° PHY-03-563

Instrument **V5**

Local Contact  
Evgeny Moskvina

Principal Proposer: S. Grigoriev, PNPI RAS, Gatchina, St.-Petersburg, 188300, Russia

Experimental Team: V. Dyadkin, PNPI RAS, Gatchina, RU  
E. Moskvina HMI, Berlin, DE

Date(s) of Experiment

13/05/2008 – 26/05/2008

Date of Report: 15.01.2009

Magnetic properties of MnSi are intensively studied in recent years. One of the reasons is the ability of this system to reach the quantum critical point (QCP), i.e. zero-temperature second-order phase transition – quantum phase transition (QPT) between magnetic and non-magnetic state driven by external parameter. This parameter could be applied pressure [1], magnetic field and so on. Replacing small amount of magnetic ions ( $Mn^{2+}$ ) by the ones of different type gives rise to QCP. In this case the concentration of doping ions is an external parameter driving QPT.

The weak itinerant ferromagnet MnSi has the space group  $P2_13$  with the lattice constant  $a = 0.456$  nm. The magnetic structure is a left-handed ferromagnetic spiral along the  $\langle 111 \rangle$  direction with a propagation vector  $k = (2\pi/a) \times (\xi\xi\xi)$ , where  $\xi = 0.017$ . This spiral structure is the result of hierarchy of three main interactions [2]: ferromagnetic exchange interaction responsible for the ferromagnetic ordering, Dzyaloshinskii-Moriya (DM) interaction responsible for the spiral arrangement and weak anisotropic exchange (AE) interaction fixing the direction of the magnetic spiral along one of the cube diagonals. As it was found in [1],  $T_c$  decreases with increasing pressure and the critical pressure is  $p_c \approx 14.6$  kbar.

The PPMS and SANS experiments have shown that the substitution of Mn by Fe changes the critical temperature  $T_c$ . The critical temperature decreases linearly with the concentration  $y$ . By linear interpolating we have got critical value  $y = 0.14$ , where  $T_c$  vanishes to zero. Our estimates show that it is the isotropic exchange interaction that is related to and responsible for the decrease of  $T_c$ , while the DM interaction is changed with the Fe concentration insignificantly.

Paramagnetic neutron spin echo (NSE) was used to investigate the critical dynamics in these compounds. The experiments were performed with a wavelength of  $6.5\text{\AA}$ .

The intermediate scattering function  $I(Q, t)$  was measured at different temperatures in the critical region near  $T_c$  ( $T_c \approx 16, 9.5$ , and  $6.6$  K for  $y = 0.06, 0.08$  and  $0.10$  respectively) and for different scattering vectors  $q = |\mathbf{q}| = |\mathbf{k} - \mathbf{Q}|$ .

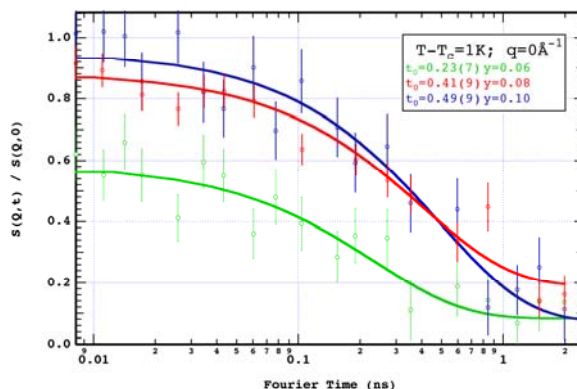


Figure: Normalized scattering function in  $Mn_{1-y}Fe_ySi$  for different Fe doping at the same  $T - T_c = 1$ ,  $q = 0 \text{ \AA}^{-1}$ .

The normalized scattering functions for three crystals are shown on the picture for two different temperatures at the magnetic Bragg position. The solid lines show the best least square fit to an exponential decay:

$$I(q, t) \sim y_0 + A \exp(-t/t_0).$$

This exponential law Fourier transforms to the scattering function:

$$S(q, \omega) = 2/\pi \Gamma / (\Gamma^2 + \omega^2)$$

with the HWHM linewidth  $\Gamma [\mu\text{eV}] = \hbar/t_0 = 0.658/t_0$  [ns]. The dependence of the magnetic relaxation on the temperature and scattering vector is as weak as in pure MnSi (see PHY-03-471 report), indicating, obviously, the same origin of behavior during the phase transition. But the relaxation slows down relatively with increasing the doping Fe.

[1] C. Pfleiderer *et al*, Nature **427** (2004) 227.

[2] P. Bak and M. Jensen J.Phys. C **13**, (1980) L881.

[3] S.V. Grigoriev *et al* Phys.Rev. B **72** (2005) 134420.



## EXPERIMENTAL REPORT

### The quantum dynamic of the helix structure in $\text{Mn}_{0.87}\text{Fe}_{0.13}\text{Si}$ .

Proposal N°  
PHY-03-599-LT

Instrument **V5**

Local Contact  
Catherine Pappas

Principal Proposer: E. Moskvina, PNPI RAS, Gatchina, St. Petersburg, 188300, Russia  
Experimental Team: V. Dyadkin, PNPI RAS, Gatchina, RU  
V. Piyadov, PNPI RAS, Gatchina, RU

Date(s) of Experiment

08/12/2008 – 21/12/2008

Date of Report: 15/01/2009

Magnetic properties of MnSi are intensively studied in recent years. One of the reasons is the ability of this system to reach the quantum critical point (QCP), i.e. zero-temperature second-order phase transition – quantum phase transition (QPT) between magnetic and non-magnetic state driven by external parameter. This parameter could be applied pressure [1], magnetic field and so on. Replacing small amount of magnetic ions ( $\text{Mn}^{2+}$ ) by the ones of different type gives rise to QCP. In this case the concentration of doping ions is an external parameter driving QPT.

The weak itinerant ferromagnet MnSi has the space group  $P2_13$  with the lattice constant  $a = 0.456$  nm. The magnetic structure is a left-handed ferromagnetic spiral along the  $\langle 111 \rangle$  direction with a propagation vector  $\mathbf{k} = (2\pi/a)\mathbf{x}(\xi\xi\xi)$ , where  $\xi = 0.017$ . This spiral structure is the result of hierarchy of three main interactions [2]: ferromagnetic exchange interaction responsible for the ferromagnetic ordering, Dzyaloshinskii-Moriya (DM) interaction responsible for the spiral arrangement and weak anisotropic exchange (AE) interaction fixing the direction of the magnetic spiral along one of the cube diagonals.

The PPMS and SANS experiments have shown that the substitution of Mn by Fe changes the critical temperature  $T_c$ . The critical temperature decreases linearly with the concentration  $y$ . By linear interpolating we have got critical value  $y = 0.13$ , where  $T_c$  vanishes to zero.

We could not obtain single crystals with concentration  $y = 0.13$  up to the experiment time. We used two crystals with  $y = 0.09$  and  $0.11$  instead. We checked these samples with magnetization measurements (see fig.). As it can be clearly seen from the picture, the  $y = 0.09$  sample still behaves as a pure MnSi and lower concentration samples: it exhibit two critical fields  $H_{C1}$  and  $H_{C2}$ , responsible for the helix domain reorientation and field-induced phase transition from conical to ferromagnetic state respectively [4]. For the second sample  $H_{C1}$  is shifted to almost zero, while  $H_{C2}$  and then the associated with it phase transition still exist.

We tried to use paramagnetic spin echo to study spin dynamics in both samples, but the magnetic scattering from these samples was too small to obtain pronounceable spin echo response. The possible reason is the crystals we used were too small (discs 3mm thick and 5mm diameter). For

the  $y = 0.09$  sample one needs about 0.15T field to orient spirals along  $\langle 111 \rangle$ , but it was not possible to obtain such a field on SPAN while the sample is in a cryostat on the beam. For the  $y = 0.11$  the reorientation field is very low, but the magnetic moment is as one order of magnitude less as for the first sample.

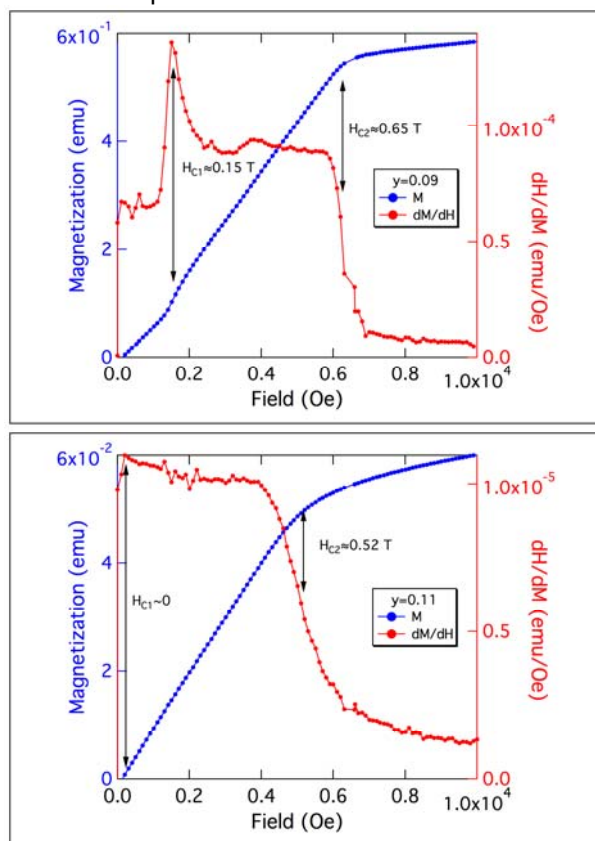


Figure: Magnetization curves for  $y=0.09$  and  $0.11$  with the field applied along  $\langle 111 \rangle$  at  $T = 3$  K.

- [1] C. Pfleiderer *et al*, Nature **427** (2004) 227.
- [2] P. Bak and M. Jensen J.Phys. C **13**, (1980) L881.
- [3] S.V. Grigoriev *et al* Phys.Rev. B **72** (2005) 134420.
- [4] S.V. Grigoriev *et al* to be published.

	<b>EXPERIMENTAL REPORT</b>  <b>Antiferromagnetic structure in UNiAl at dilution temperature</b>	Proposal N° EF Instrument <b>E4</b>  Local Contact K. Prokes
	Principal Proposer: K. Prokes, HZB Experimental Team: K. Prokes, HZB	Date(s) of Experiment  July 2008

Date of Report: January 2009

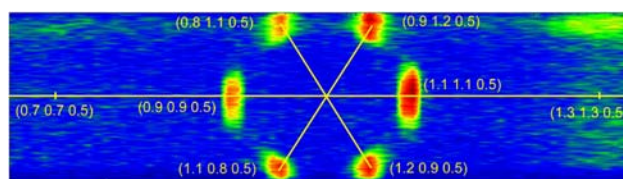
UNiAl is a member of the large group of hexagonal ternary compounds with ZrNiAl-type structure. It orders antiferromagnetically (AF) below  $T_N = 19.3$  K. There are three symmetry equivalent propagation vectors (three 1-k domains) that describe the AF order [1]. Uranium magnetic moments are within each domain modulated sinusoidally within the basal plane and coupled AF with U moments in the adjacent plane. The modulation has been reported not being even partially squared-up down to 1.7 K [1]. All the moments are oriented along the hexagonal axis and the maximum size amounts to  $1.25 \mu_B$ .

The single crystal sample used in the present study is the same one as used previously for neutron diffraction experiment [1] and measured in the temperature range between 150 mK and 30 K on the double-axis diffractometer E4. The incident-neutron wavelength was  $2.44 \text{ \AA}$  and an ILL orange-type cryostat combined with a dilution refrigerator insert has been employed to achieve low temperatures. The data were collected for about 12 h at 150 mK and 4 h at 30 K in the case of the single crystal. The crystal has been fixed with its  $(hh0)$ - $(00l)$  plane in the scattering plane. The E4 diffractometer is currently equipped with a  $200 \times 200 \text{ mm}^2$  PSD enabling to observe apart from the  $(hhl)^{+q1}$  reflections also those resulting from  $q_2$  and  $q_3$  propagation vectors that are few degrees above and below the scattering plane.

In Fig. 1 we show portion of the reciprocal scan on UNiAl single crystal recorded at 150 mK. The area shown in the figure starts on the left at  $(0.65 \ 0.65 \ 0.5)$  and finishes on the right at  $(1.35 \ 1.35 \ 0.5)$ . The two magnetic reflections situated along the long horizontal line are indexable as  $(1 \ 1 \ 0)^{+q1}$  and  $(1 \ 1 \ 0)^{-q1}$  with  $q_1 = (0.1 \ 0.1 \ 0.5)$ . Thanks to the large angular opening also reflections lying outside the scattering plane indexable by  $q_2 = (-0.1 \ 0.2 \ 0.5)$  and by  $q_3 = (-0.2 \ 0.1 \ 0.5)$  are visible. At the first glance, no clear diffracted signal is found at the positions of the expected third harmonics  $(0.7 \ 0.7 \ 0.5)$  and  $(1.3 \ 1.3 \ 0.5)$ .

Projections of small areas around the  $(0.9 \ 0.9 \ 0.5)$  and  $(0.7 \ 0.7 \ 0.5)$  reciprocal space positions onto the horizontal axis are shown in Fig. 2a and

2b, respectively. As can be seen, there is indeed a weak intensity at the  $(0.7 \ 0.7 \ 0.5)$  position. This results suggests that the AF structure in UNiAl starts indeed to square-up in the low-temperature limit. The ratio  $I_{3rd}/I_{1st}$  of their intensities amounts to 0.044. Model calculation with the assumption of a completed squaring-up of the sine wave leads to the ratio of 0.19. One possible explanation for a much smaller 3<sup>rd</sup> harmonics is that the uranium magnetic moments are to a certain extent frustrated due to competition of antiferromagnetic and ferromagnetic exchange interactions within the basal plane. As a consequence, moments cannot fully develop and significant fluctuations exist even



at such a low temperature.

Fig 1: The reciprocal space scan on UNiAl single crystal at 150 mK through the six magnetic reflections and positions where the third harmonics is to be expected.

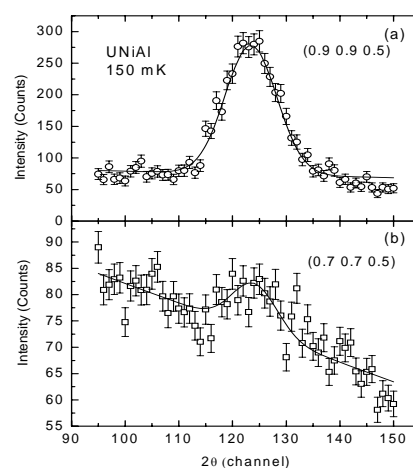


Fig 2: Scattering diffraction profiles recorded at 150 mK on UNiAl single crystal at (a) the position of the magnetic reflection  $(0.9 \ 0.9 \ 0.5)$  and (b) the position of the expected third harmonics  $(0.7 \ 0.7 \ 0.5)$ .

Reference:  
K. Prokeš, et al., Phys. Rev. B **58**, 2692 (1998).



## EXPERIMENTAL REPORT

### Spin waves in the single domain magnetic phases of PrB<sub>6</sub>

Proposal N° PHY-02-645  
Instrument **V2**  
Local Contact Kirrily Rule

Principal Proposer: Prof. K. A. McEwen – University College London  
Experimental Team: Mr. M. D. Le - University College London  
Dr. K. C. Rule – HMI, Berlin

Date(s) of Experiment  
22/05/2008 – 02/06/2008

Date of Report: 03/07/2008

Praseodymium Hexaboride exhibits a rich magnetic phase diagram with complex ordered structures which are thought to be stabilized by the  $Q_{xy}$  quadrupolar interactions [1]. At zero applied field, there are two antiferromagnetic phases with double- $q$  structures, whilst above 2T a spin flop transition occurs in the lower temperature commensurate (C) phase to a single- $q$  structure [2]. In addition, the applied magnetic field preferentially selects one of the three zero field domains, so that in principle the in-field dispersion is simpler as it arises from a single domain.

In this experiment we have investigated the magnetic excitations of PrB<sub>6</sub> in applied fields up to 6T. The FLEX spectrometer was operated with scattering sense (-1,-1,+1) at fixed  $k_F=1.55\text{\AA}^{-1}$  and  $k_F=1.3\text{\AA}^{-1}$ . 60° collimation was used between the monochromator and sample. The PG(002) monochromator and analyser were focused with no further collimation to maximise the flux. The crystal was mounted with ( $hh$ ) as the horizontal scattering plane and a vertical field was applied along [1 -1 0].

In a previous experiment [3] we found that the dispersion in the C-phase at 6T was unexpectedly asymmetric about the magnetic Brillouin zone centre (BZC) at  $Q = (\frac{1}{4} \frac{1}{4} \frac{1}{2})$ , along the [hh0] direction. We have now confirmed that this is also the case in zero field, but that the dispersion along [00l] is symmetric about the magnetic BZC. The dispersion along [hh0] is instead symmetric about  $Q = (\frac{1}{2} \frac{1}{2} \frac{1}{2})$ , in both zero field and in-field, as shown in Figure 1.

We have also observed and mapped the dispersion of a relatively weak lower energy mode which we had not been able to see before. This observation is important for the theoretical description of this

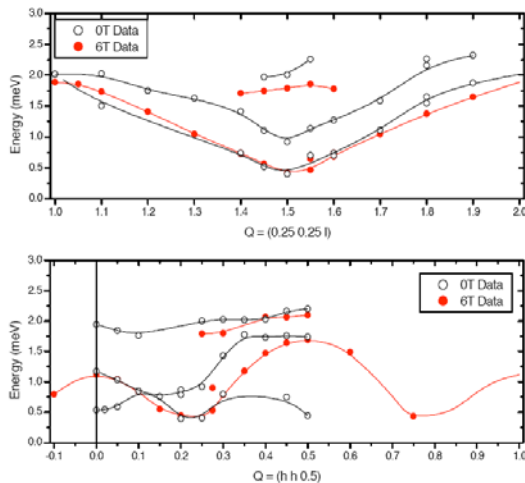


Figure 1. Dispersion along the principal symmetry directions in the C-phase at zero field and 6T.

system with the quadrupolar interactions because the energy of this mode ( $\sim 0.5\text{meV}$ ) is more consistent with the strength of the quadrupolar interaction observed from bulk measurements than the stronger, higher energy mode ( $\sim 1\text{meV}$ ). However, so far the theoretical model only gives qualitative agreement with the data (figure 2), and more importantly does not predict that the single- $q$  structure is stable in an applied field. Further calculations are in progress.

In addition, figure 1 shows that the dispersion of the lower mode along  $Q = (\frac{1}{4} \frac{1}{4} L)$  in 6T is almost the same as that of one of the modes in zero field. This suggests that the two sets of modes in zero field arise from different domains.

Finally, initial studies in the incommensurate (IC) phase at 5K and 6T shows that the excitations at the magnetic BZC and zone edge are qualitatively similar to the zero field case. This is expected as there is no metamagnetic transition in this phase.

#### References

- [1] S. Kobayashi et al., J. Phys. Soc. Jap. **70** (2001) 1721
- [2] P. Burlet et al., J. Phys (Paris) C, **8** (1988) 459
- [3] K.A. McEwen et. al., BENSC Report 2007, experiment. PHY-02-617.

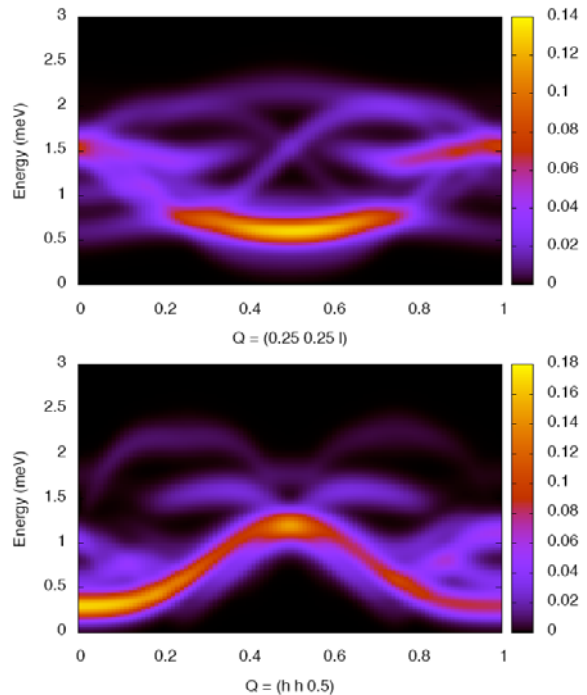


Figure 2. Calculated dispersion along the principal symmetry directions in the C-phase at zero field

	<b>EXPERIMENTAL REPORT</b> <b>Magnetic excitations of the geometrically frustrated antiferromagnet CuFeO<sub>2</sub> under magnetic field</b>	Proposal N° PHY-02-648 Instrument <b>V2</b> Local Contact Kirrily Rule
	Principal Proposer: Feng Ye, ORNL, USA Experimental Team: Feng Ye, ORNL, USA J. Fernandez-Baca, ORNL, USA Kirrily Rule, HZB	Date(s) of Experiment 15/04/2008 – 22/04/2008

Date of Report: January 2009

Using high resolution inelastic neutron scattering technique, we have investigated the evolution of the spin dynamics of the geometrically frustrated triangular lattice antiferromagnet (TLA) CuFeO<sub>2</sub> under application the magnetic field. A 6-Tesla horizontal field magnet is implemented to drive the system close to the phase boundary where electric polarization takes place. Such investigation of the elemental excitation will help to understand the underlying mechanism of multiferroic effects in the frustrated system.

Geometrically frustrated magnetic systems have received considerable attention in recent years due to the presence of extraordinary magnetic properties. The delafossite CuFeO<sub>2</sub> is of particular interest because of the discovery of multiferroic phenomena with either the application of a magnetic field or the substitution of nonmagnetic impurities [1-5]. As a model material of TLA, CuFeO<sub>2</sub> forms an Ising-like 4-sublattice antiferromagnet order at low temperature, with spin moment pointing along the *c* axis. Our recent inelastic neutron scattering (INS) studies [6] reveal that the quasi-Ising like spin order results from the delicate balance between competing interactions. Higher order (up to the third nearest neighbor) exchange interactions have to be included in order to characterize the dispersion relations in the hexagonal plane. We also found dispersive excitations perpendicular to the hexagonal plane indicative of a substantial inter-layer coupling. Most remarkably, we found that the spin wave dispersion has two dips at the wavevectors associated with the multiferroic phase. The dynamics precursory indicates the system could be transformed into a non-conventional spin structure that is intimately related to the polar state.

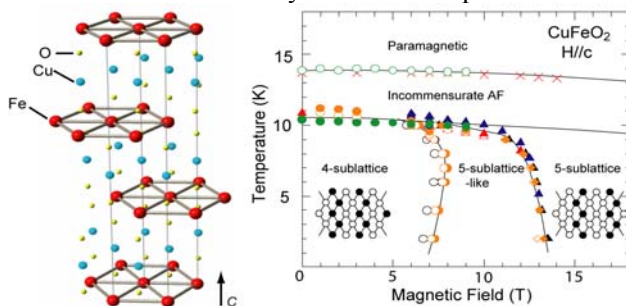


**Figure 1** Sketch of CuFeO<sub>2</sub> crystal structure and its H-T phase diagram. For magnetic field between 7 and 13 Tesla, the system exhibits electric polarization

The close correlation between the magnetic and electric properties demands a detailed characterization of the spin dynamics as the system is driven into the ferroelectric (FE) phase with magnetic field greater than 7 Tesla [Fig. 1]. Our earlier INS studies and model calculation show that a magnetic field around 7 Tesla would close the spin-gap (around 0.9 meV) as observed in the dispersion curves along  $[H,H,1.5]$  [Ref. 6]. However, the evolution of the spin dynamics remains unknown. Specifically, what is the relationship between the spin wave instability of the collinear magnetic structure and the appearance of the non-collinear magnetic phase when system is driven to the multiferroic phase under magnetic field?

A large single crystal of CuFeO<sub>2</sub> (mass around 4 g) was prepared by floating zone method for the INS measurement. Due to the 3D nature of the magnetic structure, the magnetic Bragg peaks occur at  $(1/4, 1/4, 3/2)$  and equivalent positions. The sample is aligned in the  $[H,H,L]$  scattering plane to study the spin dynamics near the magnetic Bragg peak. A horizontal field magnet is needed in order to apply field along the spin easy-axis. In addition, a cold neutron spectrometer is required due to the rather small energy scale of the magnetic interactions. The V2 triple-axis spectrometer at BENSC in combination with the horizontal-field magnetic makes such investigation feasible.

In order to get access to the desired the energy and momentum transfer, the sample is oriented such that the crystalline *c*-axis is slightly off the magnetic field direction. Figure 2 shows contour maps of the spin dynamics along two symmetric directions. Similar to our previous INS studies at  $H=0$ , the spin wave excitations are highly dispersive in both the  $[H, H, 1.5]$  and the  $[0, 0, L]$  directions with energies bound within 0.5 and 4 meV. The two energy dips (at  $q=0.205$  and  $0.295$ ) observed in the hexagonal plane are exact the wavevectors corresponding to incommensurate magnetic structure in the FE phase. With the field applied along the *c*-axis, one clearly observed the splitting of degenerate dispersion relations in both directions caused by the Zeeman energy. To quantify this field dependence, we have conducted *E*-scan at  $Q=(0.15, 0.15, 1.5)$  at several magnetic fields (Figure 3). The observed linear

dependence of the splitting is well characterized by the equation  $\Delta E=2g\mu_B H$ . It indicates that the spin wave of the collinear magnetic structure will be destroyed for  $\mu_0 H > 7.7$  Tesla, in accord with the data shown in Figure 1. Unfortunately, the available magnetic field (5.95 Tesla) is not sufficient to drive the system into the electric polarized state, where the corresponding spin dynamics deserves future study.

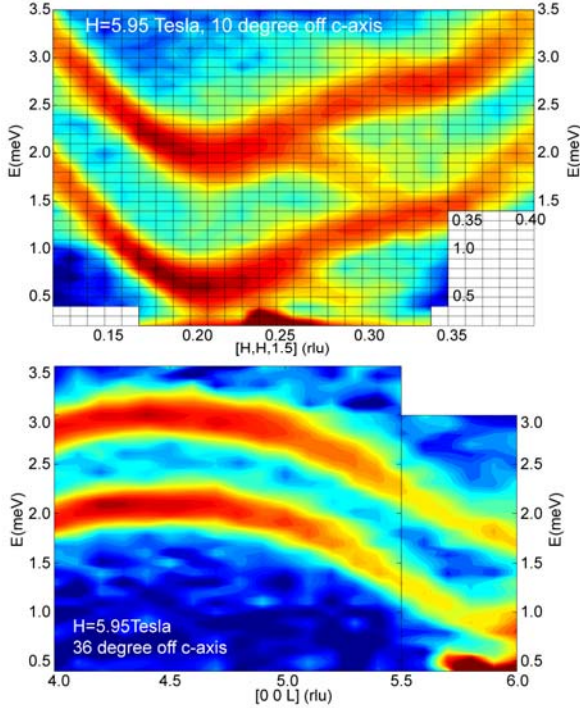


**Figure 2** Inelastic neutron scattering results obtained at V2 cold neutron scattering spectrometer at BENSNC.

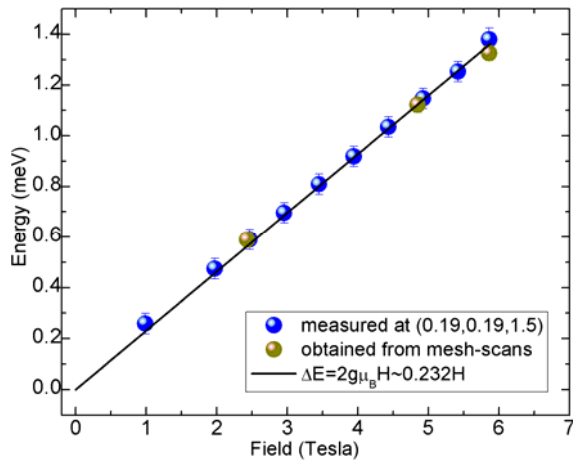


**Figure 3** Field dependence of the Zeeman splitting measured at the wavevector transfer  $Q=(0.19,0.19,1.5)$ .

## References

- [1] T. Kimura, J. C. Lashley, and A. P. Ramirez, Phys. Rev. B 73, 220401(R) (2006).
- [2] S. Seki, *et al.*, Phys. Rev. B 75, 100403(R) (2007).
- [3] T. Nakajima, *et al.*, J. Phys. Soc. Jpn. 76, 043709 (2007).
- [4] S. Kanetsuki, *et al.*, J. Phys.:Condens. Matter 19, 145244 (2007).
- [5] F. Ye, *et al.*, Phys. Rev. B, 73, 220404(R) (2006).
- [6] F. Ye, *et al.*, Phys. Rev. Lett. 99, 157201 (2007)

	<b>EXPERIMENTAL REPORT</b>  <b>Polarisation analysis of the frustrated pyrochlore</b> <b>Tb<sub>2</sub>Ti<sub>2</sub>O<sub>7</sub></b>	Proposal N° PHY-02-652-EF  Instrument <b>V2</b>  Local Contact Kirrily Rule
	Principal Proposer:      Kirrily Rule - HMI Experimental Team:      Klaus Habicht Markos Skoulatos, Klaus Kiefer	Date(s) of Experiment  03/11/2008 – 13/11/2008

Date of Report: 17/11/2008

V2, the triple axis spectrometer was used to investigate the magnetic contribution to the diffuse inelastic scattering observed in Tb<sub>2</sub>Ti<sub>2</sub>O<sub>7</sub>. In zero field and T = 0.4K, Tb<sub>2</sub>Ti<sub>2</sub>O<sub>7</sub> is a highly correlated cooperative paramagnet with disordered spins residing on a pyrochlore lattice of corner sharing tetrahedra. Broad, diffuse scattering was observed in previous time of flight measurements, characteristic of very short ranged spin correlations (Fig 1a)<sup>1</sup>. This diffuse scattering, which was also broad in energy (Fig 1d) was most obvious around the (002) position which is structurally forbidden in this system. In small applied fields (B<2T), sharp intensity was observed at the (002) position, while at the same time, the diffuse scattering intensity decreased (Fig 1b, Fig 2).

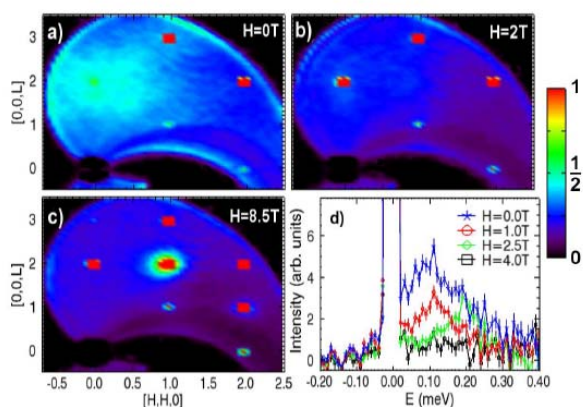


Fig 1: TOF data showing diffuse inelastic scattering around (0,0,2)

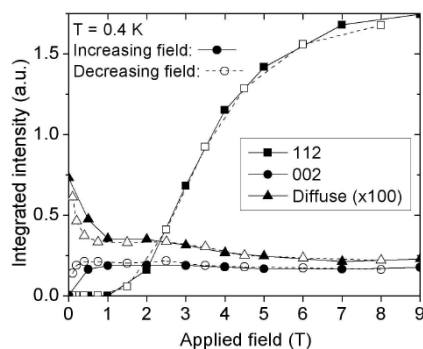


Fig 2: Field dependent behaviour of the integrated intensities of the diffuse and Bragg scattering.

By using polarised neutrons and separating the spin flip (SF) and non-spin flip (NSF) scattering, the

magnetic component of this diffuse scattering could be revealed. A single crystal of Tb<sub>2</sub>Ti<sub>2</sub>O<sub>7</sub> was mounted in a dilution stick within the asymmetric vertical field magnet VM2. FLEX was oriented with two cavity polarizers; one located within the monochromator shielding, the other within the detector shielding. A single spin flipper was located before the sample to control the direction of the neutron spin. The flipping ratio was around 10 for the zero field data. The final wave vector was fixed at 1.2 Å<sup>-1</sup> and a Be filter was placed in the scattered beam to reduce λ/2 reflections. The energy resolution of the instrument was 60 μeV full width half maximum.

The SF and NSF scattering was measured for a number of Bragg peaks (magnetic and structural) at temperatures between 0.035 – 30 K and for fields up to 2T. Constant Q, energy scans were also performed around the (0,0,2) position in SF and NSF. Although the application of a magnetic field reduces the intensity of the diffuse scattering, a small field of 0.25T was necessary to ensure a guide field was present in all space. The inelastic results can be seen in Fig. 3.

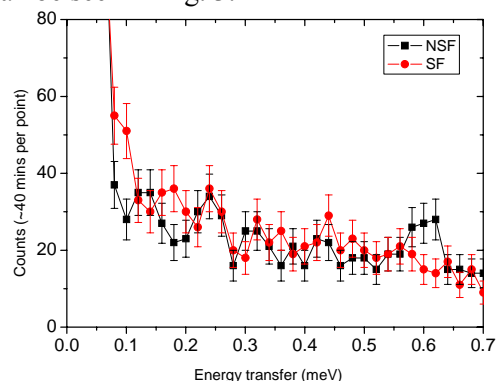


Fig. 3: SF and NSF results around the (002) position at 35mK and 0.25T

We observed almost no difference between the SF and NSF inelastic scattering around the (002) Bragg peak. In fact due to poor polarisation, low flux and stray fields from the magnet the diffuse inelastic scattering was not clearly resolved.

<sup>1</sup> Rule KC, Ruff JPC, Gaulin BD, et al. PRL **96** 177201 (2006)

	<b>EXPERIMENTAL REPORT</b>  <b>Spin dispersion along the c axis in the diamond chain compound azurite</b>	Proposal N° PHY-02-664-DT  Instrument <b>V2</b>  Local Contact Kirrily Rule
	Principal Proposer: Stefan Süllow, TU Braunschweig Experimental Team: Stefan Süllow, TU Braunschweig Clare Gibson, HMI Kirrily Rule, HMI	Date(s) of Experiment  03/11/2008 – 06/11/2008

Date of Report: 15/01/2008

Recently, the observation of a 1/3 magnetization plateau in azurite  $\text{Cu}_3(\text{CO}_3)_2(\text{OH})_2$  led to the proposal, that this material represents the first realization of a distorted diamond chain of coupled  $S = 1/2$  spins [1-3]. The model consists of spin triangles arranged in chain structures, with a magnetic coupling of the diamond backbone  $J_2$ , and the monomer couplings  $J_1$  and  $J_3$  along the chain, with  $J_1 \neq J_2 \neq J_3$ . From an inelastic neutron scattering study [3] we extracted the coupling parameters in the plateau phase, obtaining a dominant antiferromagnetic  $J_2 = 55\text{K}$ , monomer couplings  $J_1 = 1\text{K}$ ;  $J_3 = -20\text{K}$ , and an additional superexchange coupling  $J_{SE} = 6.5\text{K}$  between monomer sites. Along the  $a$  axis, the spin excitation spectrum was dispersionless, implying that for this direction the interchain coupling is 1K or less. In order to finalize our experiment, here we have studied the dispersion along the  $c$  axis, *viz.*, determine the interchain coupling in this direction.

The experiment was carried out using the V2 spectrometer FLEX at BENSC. The single crystal of azurite was aligned in a way that in reciprocal space the range  $(0\ K\ L)$ , with  $0 \leq K, L \leq 1$ , was accessible. Measurements were taken at 1.5 K in zero magnetic field, with an incident neutron wave vector  $k_i = 1.3\text{\AA}^{-1}$ . In the Figs. 1 and 2 we summarize the essential result of our experiment, the spin excitation spectra of azurite for measurements at  $(0\ 1\ L)$  and  $(0\ 0.75\ L)$  up to 5 meV. From both figures it is apparent that none of the excitation modes exhibits pronounced dispersion, putting an upper limit of about 1K to the effective interchain coupling along the  $c$  axis. Altogether, our data prove the 1D character of the magnetic behaviour of azurite.

- [1] H. Kikuchi et al., Phys. Rev. Lett. **94**, 227201 (2005).  
 [2] B. Gu, and G. Su, Phys. Rev. Lett. **97**, 089701 (2006).  
 [3] K.C. Rule et al., Phys. Rev. Lett. **100**, 117202 (2008).

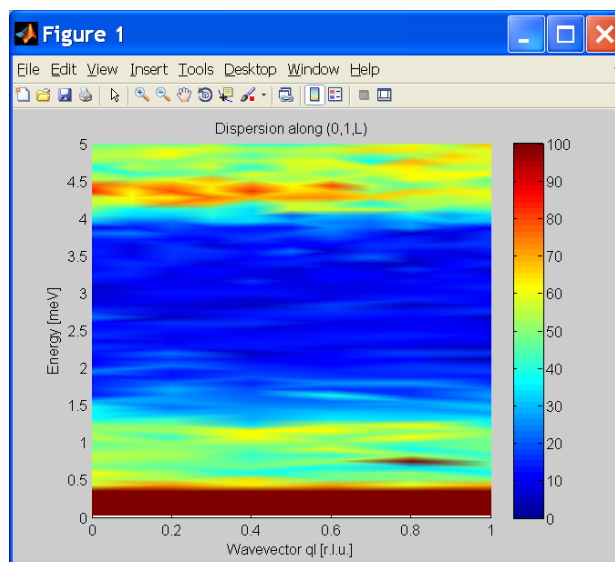


Fig. 1: The spin excitation spectrum of azurite at 1.5K along  $(0\ 1\ L)$ .

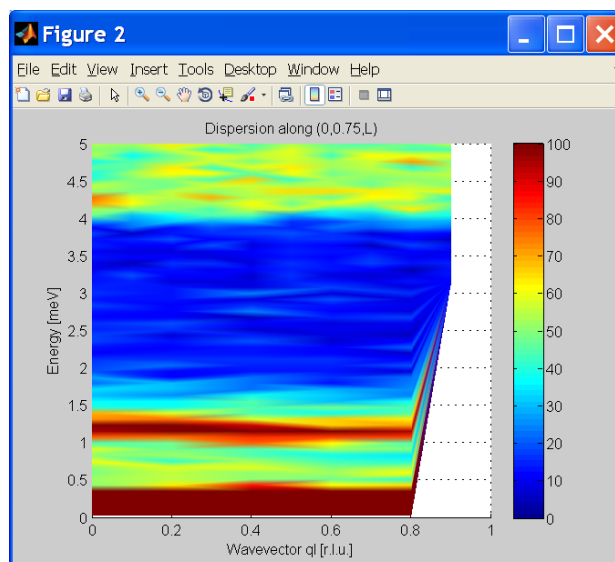


Fig. 2: The spin excitation spectrum of azurite at 1.5K along  $(0\ 0.75\ L)$ .



**EXPERIMENTAL REPORT**  
**Peculiar Field Response of**  
**Antiferromagnetism in non-centrosymmetric**  
**superconductor CePt<sub>3</sub>Si**

Proposal N° PHY-02-0665  
 Instrument **V2**  
 Local Contact  
 M. Skoulatos

Principal Proposer: K. Kaneko, ASRC, Japan Atomic Energy Agency, MPI-CPfS  
 Experimental Team: O. Stockert, MPI-CPfS, Dresden  
 M. Skoulatos, HZ-Berlin  
 K. Habicht, HZ-Berlin  
 K. Kiefer, HZ-Berlin  
 S. Gerischer, HZ-Berlin

Date(s) of Experiment  
 30/09/2008 – 12/10/2008

Date of Report: 14/01/2008

The recent discovery on the heavy-fermion superconductivity in a non-centrosymmetric compound CePt<sub>3</sub>Si attracts a lot of attention since novel superconducting properties are expected under this symmetry[1]. Another characteristic feature in CePt<sub>3</sub>Si is the coexistence of superconductivity with long range antiferromagnetic order[2]. Therefore the study of the antiferromagnetism and its interplay with superconductivity is of high importance. The antiferromagnetic structure of CePt<sub>3</sub>Si can be described with  $\mathbf{q} = (0\ 0\ 1/2)$ , in which the reduced magnetic moments of 0.17  $\mu_B$  orient parallel to the  $\langle 100 \rangle$  direction. The antiferromagnetic intensity does not exhibit a significant anomaly on passing through  $T_{sc} \sim 0.7$  K and persists well below  $T_{sc}$ [2,3]. On the other hand, we found that the antiferromagnetic peak intensity increases with applying fields, which is contrary to the usual case[3]. In order to clarify the overall field response and its possible relationship with superconductivity, we measured the detailed magnetic field response of the antiferromagnetic intensity in CePt<sub>3</sub>Si below  $T_{sc}$  and up to  $B=6.6$  T

Neutron scattering experiments were carried out on the cold triple-axis spectrometer V2. The horizontal magnetic field up to 6.6 T was applied along the  $[0\ 0\ 1]$  direction using the superconducting magnet HM-3. The sample was cooled down to 40 mK by a <sup>3</sup>He-<sup>4</sup>He dilution fridge.

The enhancement of the antiferromagnetic peak intensity when applying a field was clearly observed at 40 mK, i.e., well below  $T_{sc}$ . Figure 1 shows the  $0\ 0\ 1/2$  magnetic peak profile at 40 mK measured at several magnetic fields. The  $0\ 0\ 1/2$  antiferromagnetic intensity increases with field without substantial change in the peak profile, and the strongest intensity was observed at the maximum field of 6.6 T. We have clarified that the antiferromagnetic intensity keeps increasing even at the present maximum field. The intensity at 6.6 T becomes

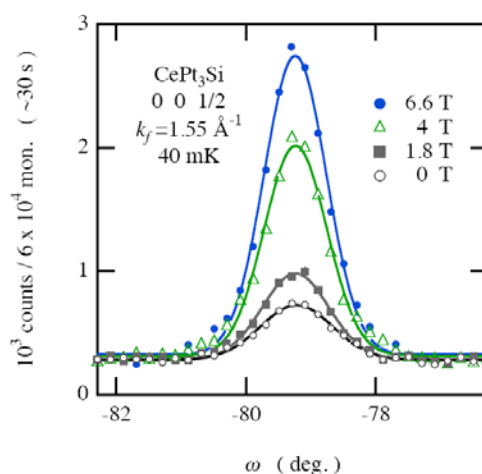


Fig. 1 The  $0\ 0\ 1/2$  magnetic reflection profile at 40 mK in CePt<sub>3</sub>Si measured at several magnetic field.

4.5 times stronger than that at zero field. Since the moment reorientation should give the decrease for the  $0\ 0\ 1/2$  intensity, the present intensity enhancement should originate from the increase of the ordered antiferromagnetic moment by a factor of more than 2.

In contrast, no clear anomaly was observed at around the upper critical field of the superconducting state, which is similar to the behavior in the temperature dependence[2,3]. Both results suggest a weak coupling of the static magnetism in CePt<sub>3</sub>Si to its superconductivity.

At present, there is no clear explanation for the observed field dependence. In order to get insights on the underlying origin of this phenomena, neutron inelastic experiments under fields are currently in progress.

### References

- [1] E. Bauer *et al.*, Phys. Rev. Lett. **92**, 027003 (2004).
- [2] N. Metoki *et al.*, J. Phys.: Condens. Matter **16**, L207 (2004).
- [3] K. Kaneko *et al.*, J. Phys. Soc. Jpn. **75**, Suppl. pp. 177 (2006).



## EXPERIMENTAL REPORT

### Approaching the high magnetic field quantum phase transition of $\text{CoCl}_2 \cdot 2\text{D}_2\text{O}$

Proposal N° PHY-02-667

Instrument **V2**

Local Contact  
Klaus Habicht

Principal Proposer: Kim Lefmann, University of Copenhagen  
 Experimental Team: Jacob Larsen, University of Copenhagen  
 Sara U. H. Eisenhardt, University of Copenhagen  
 Klaus Habicht, HMI  
 Manfred Reehuis, HMI

Date(s) of Experiment

25/11/2008 – 10/12/2008

Date of Report: 07/01/2009

An increasing interest in quantum criticality for the purpose of understanding phenomena such as high-temperature superconductivity and entanglement of electrons in solids calls for experimental investigations of quantum phase transitions. From the theoretical papers on the one-dimensional Ising models in a transverse magnetic field, it has been widely recognized, a textbook-example of a quantum phase transition (QPT) [1], a phase transition which occurs when the thermal fluctuations are negligible compared to the quantum fluctuations.

The monoclinic crystal  $\text{CoCl}_2 \cdot 2\text{D}_2\text{O}$  is well known as a quasi one-dimensional Ising system [2, 3]. When a magnetic field is applied along the easy axis (see fig. 1) the system undergoes a QPT at a critical field  $H_c = 16.2\text{T}$ , from being antiferromagnetically ordered perpendicular to the ferromagnetic Ising-chain direction ( $c$ -axis on fig. 1) to being completely paramagnetic. [1]

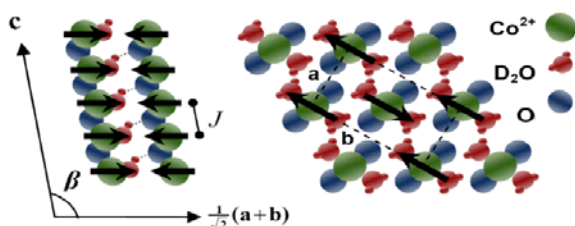


Figure 1: Left: the antiferromagnetically ordered state with the ferromagnetic Ising-chains which also is the crystal growth direction Right: the magnetic unit cell.

The larger sample was aligned at the instrument E5 and the smaller sample at the instrument E4. We used inelastic neutron scattering to measure the spin wave excitation from 0T to 14.8T and we intended to measure in even higher field using the Dy booster thereby completing the magnetic phase diagram of  $\text{CoCl}_2 \cdot 2\text{D}_2\text{O}$ . Figure 2 shows the measured excitation energy at  $q = (030)$  and  $q = (21-1)$ .

We encounter problems due to a large background already in the 0-14.8 T range where we had a large sample mass. Along with the high background, the small crystal which should go in the Dy booster was damaged due to unexpected

chemical reaction with the glue during the preparations, so we were forced to abandon the hope of reaching 17.8T during this beamtime. Instead we used elastic neutron scattering to investigate the order parameter at  $q = (21-1)$ . The magnetization (see fig. 3) clearly showed the onset of a phase transition at high field.

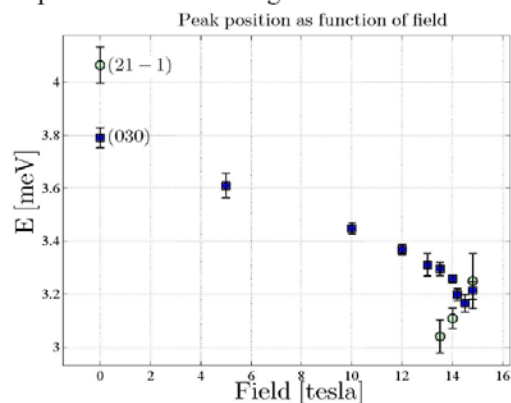


Figure 2: The measured excitation energy vs. field.

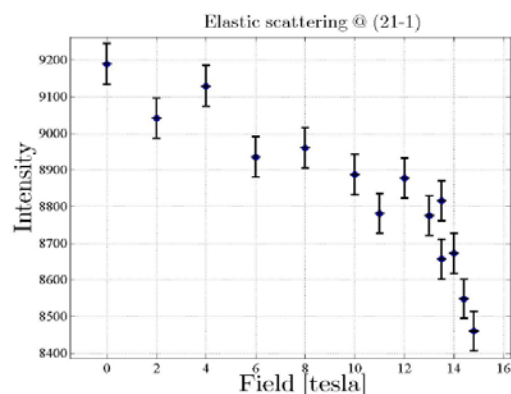


Figure 3: The magnetic order parameter vs. field.

- [1] S. Sachdev, Quantum Phase Transitions, Cambridge (1999).
- [2] N.B. Christensen, M.Sc. thesis, NBI (2000)
- [3] J. K. Kjems, J. Als-Nielsen and H. Fogedby, Phys. Rev. B **12**, 5190 (1975).

*This research project has been supported by the European Commission under the 6<sup>th</sup> Framework Programme through the Key Action: Strengthening the European Research Infrastructures.*

*Contract n°: RII3-CT-2003-505925 (NMI 3).*



## EXPERIMENTAL REPORT

### Magnetic excitation of XXZ spin model in magnetic field

Proposal N° PHY-02-671

Instrument **V2**

Local Contact K. Habicht

Principal Proposer: Masuda Takatsugu, Univ. Yakohama City, JP  
 Experimental Team: T. Masuda, Univ. Yakohama City, JP  
 S. Hondo, Univ. Yakohama City, JP  
 K. Kaneko, MPI CPfS Dresden  
 Kirrily Rule, HZ Berlin

Date(s) of Experiment

19/08/2008 – 26/08/2008

Date of Report: January 2009

Recent interest in quantum phenomena in 1D antiferromagnet (AFM) is focused on exotic behaviour of spins in magnetic field. Particularly the spin system with power decay in correlation known as Luttinger liquid [1] is one of challenging topics. In spinless fermion representation the dispersion of 1D AFM is half filled with the Fermi wave vector of  $k_f = \pi/2$ , and consequently the spin correlation is staggered. The magnetic excitation is characterized by gold stone mode from  $q = \pi$ . In applied field, on the other hand, the number of the fermion changes and the dispersion is no longer half filled. Consequently the spin correlation becomes incommensurate (IC) and soft mode at IC wave vector appears. Such behaviour was observed in ideal Heisenberg 1D AFM Cu benzoate and Cu pyrazine dinitrate [2,3]. Since both compounds are located quite close to quantum criticality, the long range order is not observed. In contrast in Ising-like XXZ model, the ground state in zero field is Néel ordered state. Applied field induces quantum phase transition and the spin liquid with IC spin correlation is predicted.

Experimental realization of such Ising-like  $S=1/2$  XXZ compound with ideal energy scale for inelastic neutron scattering (INS) experiment is found in  $\text{BaCo}_2\text{V}_2\text{O}_8$  [4,5,6]. From the magnetization and ESR measurements  $\varepsilon = 0.5$ ,  $J = 65\text{K}$  were identified [5]. Here  $\varepsilon$  is anisotropy parameter. Néel order appears at 5.4K and the ordered phase is suppressed when field is applied in easy axis. Surprisingly the Néel order does not simply disappear as in theoretical prediction but a novel magnetic order appears at low temperature and in high field [6]. The phase is ascribed to freezing of IC spin correlation characteristic of 1D AFM in field and indeed we observed the associated IC magnetic Bragg peak [7].

In the last proposal round we performed inelastic neutron scattering by using horizontal magnet (HM1) in V2/FLEX. In Fig. 1 (a) a set of constant  $q$  scans in  $H = 6\text{T}$  are shown. Well defined peak is observed at 0.9 meV in  $q = (-4\ 0\ 1)$  and the peak energy systematically shifts to lower energy with  $q$ . In Fig. 1 (b) the gapless

excitation from incommensurate wave vector at  $q_{IC} = (-4\ 0\ 1.175)$  is clearly obtained. The behaviour is totally consistent with longitudinal  $S^{ZZ}(q, \omega)$  calculated by exact diagonalization method with 28 sites. Similar results are obtained at  $H = 5\text{T}$  and 4.5 T.

At present we have a few problems: we did not observe any meaningful signal at  $l > l_C = 1.175$  and we have not observed any transverse excitation in high field. We think that this is because of short of counting time. We are planning continuation experiment to obtain publication quality data in the next proposal round.

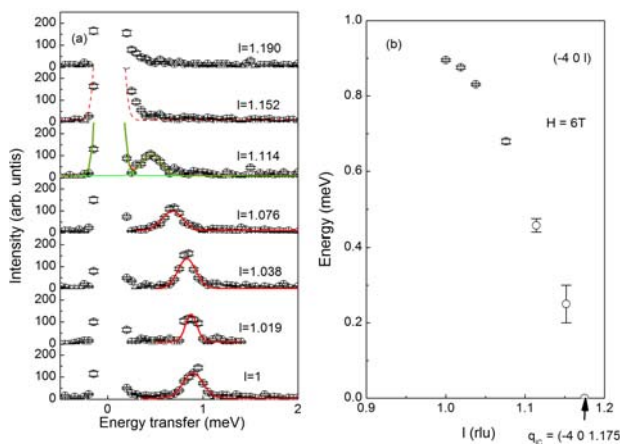


Figure 1: (a) Constant  $q$  scans at  $H = 6\text{T}$ .  
 (b) Magnetic dispersion at 6T.

## References

- [1] F. D. M. Haldane, PRL 45, 1358 (1980).
- [2] D.C. Dender et al., PRL 79, 1750 (1997).
- [3] M. B. Stone et al., PRL 91, 037205 (2003).
- [4] Z. He et al., PRB 72, 172403 (2005).
- [5] S. Kimura et al., PRL 99, 087602 (2007).
- [6] S. Kimura et al., PRL 100, 057202 (2008).
- [7] S. Kimura et al., cond-mat. arXiv:0808.4073.



## EXPERIMENTAL REPORT

### Field induced ordered phase in a quantum dimer system Ba<sub>3</sub>Cr<sub>2</sub>O<sub>8</sub>

Proposal N° PHY-02-672

Instrument **V2**

Local Contact Kirrily Rule

Principal Proposer: M. Kofu, University of Virginia, USA  
 Experimental Team: S.-H. Lee, University of Virginia, USA  
 K. Rule, Helmholtz Zentrum Berlin  
 B. Lake, Helmholtz Zentrum Berlin  
 S. Gerischer, Helmholtz Zentrum Berlin

Date(s) of Experiment

13/10/2008 – 19/10/2008

Date of Report:

Over the last decade, several exotic quantum phenomena have been observed in spin dimer systems. For instance, the field-induced Bose-Einstein condensation (BEC) of magnons [1] was observed in a quantum dimer system, TiCuCl<sub>3</sub>, and the field-induced Wigner crystallization of magnons [2] was observed in the Shastry-Sutherland orthogonal dimer system SrCu<sub>2</sub>(BO<sub>3</sub>)<sub>2</sub>. Recently, a new class of spin dimer systems has been reported with the general formula A<sub>3</sub>B<sub>2</sub>O<sub>8</sub> (A=Sr<sup>2+</sup>, Ba<sup>2+</sup>, B=Mn<sup>5+</sup>, Cr<sup>5+</sup>) [3], where the 5+ transition metal ion forms dimers along the *c* axis. Interestingly, a frustrating triangular lattice is formed by the dimers in the *ab* plane. For Ba<sub>3</sub>Mn<sub>2</sub>O<sub>8</sub> with orbitally nondegenerate Mn<sup>5+</sup>(3*d*<sup>2</sup>, *s*=1), specific heat measurements under *H* suggests a condensation of magnons. A recent inelastic neutron scattering study showed that the magnetic interactions between dimers are effectively two-dimensional in nature as a result of this interplane frustration [4]. On the other hand, a related chromate, Ba<sub>3</sub>Cr<sub>2</sub>O<sub>8</sub> has the quantum spin from the orbitally degenerate Cr<sup>5+</sup>(3*d*<sup>1</sup>, *s*=1/2) ion. Most recently, we have performed inelastic neutron scattering measurements for Ba<sub>3</sub>Cr<sub>2</sub>O<sub>8</sub>, and we found that there exist three singlet-triplet excitation modes. Our complete analysis shows that the three modes are due to spatially anisotropic interdimer interactions that are induced by the lattice distortion of the tetrahedron of oxygens surrounding the Jahn-Teller active Cr<sup>5+</sup> ion [5].

In order to investigate the BEC of magnons in the new quantum dimer based on non-Cu<sup>2+</sup> ion, Ba<sub>3</sub>Cr<sub>2</sub>O<sub>8</sub>, we carried out neutron scattering measurements using the V2 triple-axis spectrometer along with VM1B 15T vertical magnet and dilution refrigerator. Above H=12T, elastic magnetic scattering was observed at Q=(1/2, 1/2, 3). Figure 1(a) shows magnetic Bragg intensity as a function of magnetic field at various temperatures. From the power-law fitting, we determined critical field, *H<sub>c</sub>* (*T*), and obtained the phase diagram of ordered phase (Fig.1(b)). The BEC theory

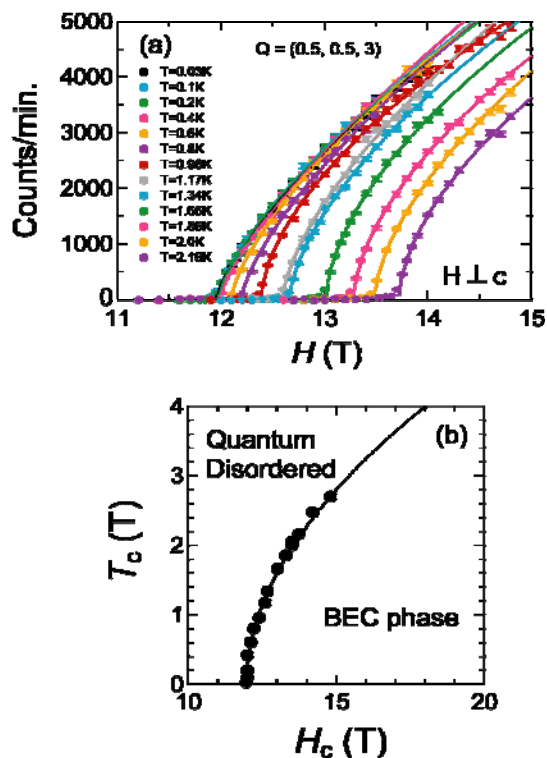


Fig1 : (a) Magnetic Bragg intensity as a function of magnetic field. (b) Phase diagram of BEC phase.

predicts that the critical temperature *T<sub>c</sub>* and *H<sub>c</sub>* are related in a power-law,  $T_c \sim [H_c(T) - H_c(0)]^\nu$  ( $\nu=2/d$ ), where *d* is dimensionality. The obtained value from our data is  $\nu=0.52(4)$  which is smaller than the theoretical value ( $d=2/3$ ).

## References

- [1] T. Nikuni *et al.*, Phys. Rev. Lett. **84**, 5868 (2000).
- [2] H. Kageyama *et al.*, Phys. Rev. Lett. **82**, 3168 (1999).
- [3] For example, M. Uchida *et al.*, J. Phys. Soc. Jpn. **70**, 1790 (2001) ; T. Nakajima *et al.*, J. Phys. Soc. Jpn. **75**, 054706 (2007).
- [4] M. B. Stone *et al.*, Phys. Rev. Lett. **100**, 237201 (2008).
- [5] M. Kofu *et al.*, Phys. Rev. Lett. in press (2009).



## EXPERIMENTAL REPORT

### Search for Spin-Density Waves in Pb

Proposal N°  
PHY-02-681-EF

Instrument **V2**

Local Contact  
K. Habicht

Principal Proposer: K. Habicht – HMI Berlin  
 Experimental Team: T. Keller – MPI-FKF Stuttgart  
 P. Aynajian – MPI-FKF Stuttgart  
 K. Habicht – HMI Berlin

Date(s) of Experiment  
 05/06/2008 – 08/06/2008  
 30/06/2008 – 05/07/2008  
 07/07/2008 – 08/07/2008

Date of Report: 15.01.2009

A recent detailed experimental study of the wave vector and temperature dependence of the lifetimes of transverse acoustic phonons in the elemental superconductors Pb and Nb found that the superconducting energy gap coincides with sharp Fermi-surface anomalies [1]. Here the phonon lifetime shows a pronounced peak at designated wavevectors which shows up as deviations from the linear behaviour of the dispersion. Despite known Kohn-anomalies a new energetically low-lying anomaly in the dispersion with reduced lifetime was found which is not reproduced by theoretical calculations based on functional perturbation theory and its origin remains unexplained. The aim of this experiment is to explore one possible scenario for the microscopic origin of the anomaly, which is based on the existence of spin-density waves (SDW) as predicted by Overhauser [2].

Originally SDWs in Pb were suggested by Overhauser and Daemen [3] to explain a low temperature residual electronic specific heat observed in Pb. The search for SDWs in elemental Pb has led to conflicting experimental results and has been discussed controversially since [4, 5, 6]. Early neutron scattering measurements searching for elastic satellites to the (210) Bragg peak in zero magnetic field were performed at NIST using the BT-9 spectrometer. These measurements gave a negative result at the  $5 \times 10^{-8}$  sensitivity level. Overhauser [6] explained this finding with a longitudinal polarization state of the SDW resulting in zero intensity for the (210) SDW-satellites. He also showed that it is possible that a magnetic field can rotate the polarization vector resulting in a transverse component which renders a SDW visible to neutrons and thus the SDW will show up as field-induced elastic scattering intensity. The optimum orientation of the field with respect to the total wavevector  $Q$  is at  $45^\circ$ .

In order to test the SDW scenario we performed a series of elastic Q-scans. FLEX was operated in a configuration with scattering senses (SM=-1, SS=-1, SA=+1) at  $k_i = k_f = 2.66 \text{ \AA}^{-1}$ . Two PG filters were installed in the first arm to suppress second order contamination. The same lead single crystal as used for the previous NRSE measurements was mounted in the (hk0) scattering plane in the new horizontal field magnet HM3. The accessible wavevector space close to the (210) Bragg peak

has been mapped out at zero field and  $B=5T$ . The magnetic field was oriented at  $45^\circ$  relative to the crystallographic (210) direction. The Figure shows the  $B=5T$  data as an example. The pronounced ring-like features could be attributed to either Al powder lines or double scattering involving scattering from a Pb Bragg peak and Al powder scattering. No field dependent elastic signal indicative of a SDW could be found within the accessible Q-range at  $45^\circ$  field angle. Additional elastic measurements were performed with the field at  $65^\circ$  relative to the (210) direction. However the corresponding zero field measurements could not be completed due to the reactor shutdown. Thus the region close to (1.25 1.25 0) still remains unexplored calling for further experiments.

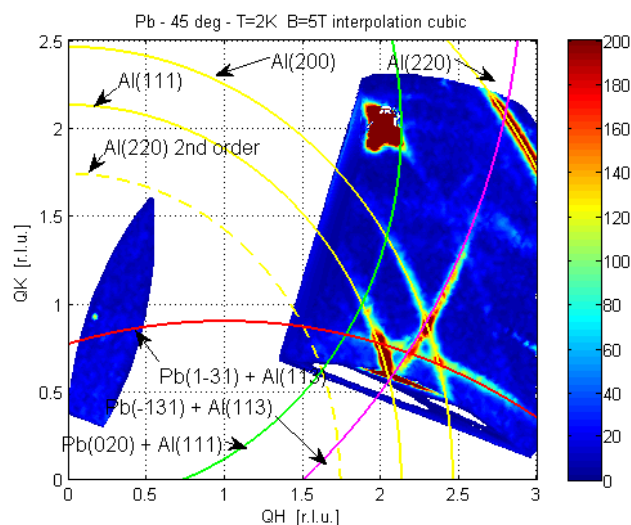


Fig.: Map of the accessible wavevector space close to the (210) Bragg peak measured at  $B=5T$ .

- [1] P. Aynajian, T. Keller, S.M. Shapiro, K. Habicht and B. Keimer, *Science* **319**, 1509 (2008).
- [2] A. W. Overhauser, *Phys. Rev.* **128**, 1437 (1962).
- [3] A. W. Overhauser, L. L. Daemen *Phys. Rev. Lett.* **61**, 1885 (1988).
- [4] A. W. Overhauser, T. M. Giebultowicz, *Phys. Rev. B* **47**, 14338 (1993).
- [5] J.D. Short, J. P. Wolfe, *Phys. Rev. Lett.* **24** (2000).
- [6] J. P. Wolfe, T. L. Head, *J. Phys. Conference Series* **92**, 012097 (2007)

	<b>EXPERIMENTAL REPORT</b> <b>Magnetic Excitation Spectrum of the Frustrated Quantum Dimer Antiferromagnet Strontium Chromate</b>	Proposal N° PHY-02-682-EF Instrument <b>V2</b> Local Contact Kirrily Rule
	Principal Proposer: Diana Lucia Quintero Castro, HZB Experimental Team: Bella Lake, HZB Nazmul Islam, HZB Elisa Wheeler, HZB	Date(s) of Experiment 04/08/2008 – 10/08/2008

Date of Report: 05/01/2009

We performed an inelastic neutron scattering experiment on the triple axis spectrometer FLEX at Neutron Cold Guide, BENSC, Helmholtz Zentrum Berlin. The aim of this experiment was to investigate the magnetic excitation spectrum of Sr<sub>3</sub>Cr<sub>2</sub>O<sub>8</sub> where the Cr<sup>5+</sup> ions have S=1/2.

For our investigations we used one single crystal of Sr<sub>3</sub>Cr<sub>2</sub>O<sub>8</sub> of length 2.7 cm, diameter 6.4 mm and mass around 3.8 g. FLEX was operated in the W configuration (+ - +). The collimation settings were guide-60'-open-open, meaning that the beam was collimated only after the monochromator. Most of the measurements were performed with a fixed final wavevector  $k_f = 1.2 \text{ \AA}^{-1}$  below 2 K.

The one-magnon excitations were measured by performing energy scans at constant wavevector in the QH-QL plane in the hexagonal coordinate system.

Along  $(0,0,L)$  and  $(1,0,L)$  we found one dispersion mode (see Figure 1), but there is a shift of one reciprocal lattice unit in the period of the sinusoidal mode for the  $(1,0,L)$  with respect to the  $(0,0,L)$ .

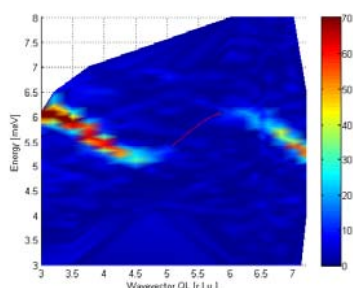


**Fig 1.** One-magnon excitation spectrum as a function of energy and wavevector in the  $(0,0,L)$  direction.

Along  $(h,0,1.5)$   $(h,0,4.5)$   $(0.5,0,l)$  and  $(h,0,3)$  we found three modes, which cover a bandwidth in energy from 3.5 meV to 7 meV (Figure 2). The three modes arise from the three domains which form below the hexagonal to monoclinic transition at around room temperature [1].

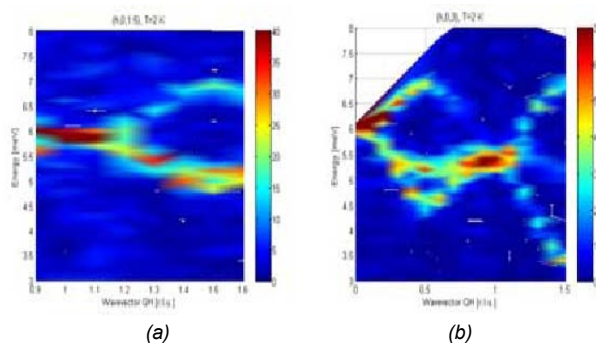


**Fig 2.** (a) One-magnon excitation spectrum as a function of energy and wavevector in the  $(h,0,1.5)$  direction. (b) One-magnon excitation spectrum as a function of energy and wavevector in the  $(h,0,3)$  direction

The experiment was completely successful and there were no complications or problems. Although, some more time was needed at the instrument to investigate the dispersion in the hexagonal plane  $(H, K, 0)$ . Data analysis is underway to determine the dominant exchange paths and compare them to the values suggested in [1].

**Reference:**

[1] L.C. Chapon, C. Stock, P.G. Radaelli, C. Martin LANL preprint server <http://xxx.lanl.gov/abs/0807.0877>



## EXPERIMENTAL REPORT

### Combined spin- and dimensionality crossover upon magnetic saturation of iron

Proposal N°  
PHY-02-684-EF

Instrument **V2**

Local Contact K. Habicht

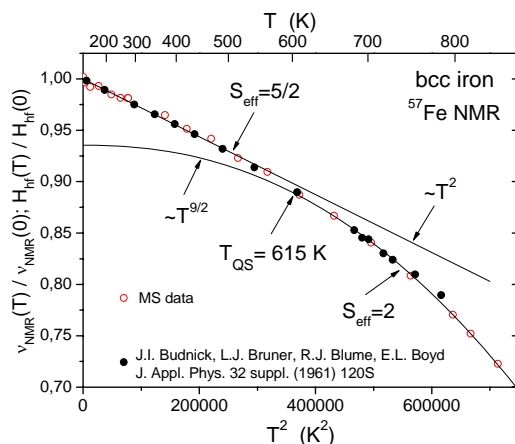
Principal Proposer: Andreas Hoser, Helmholtz-Zentrum Berlin  
Experimental Team: Klaus Habicht, Helmholtz-Zentrum Berlin  
U. Köbler, FZ Jülich

Date(s) of Experiment

17/06/2008 – 22/06/2008

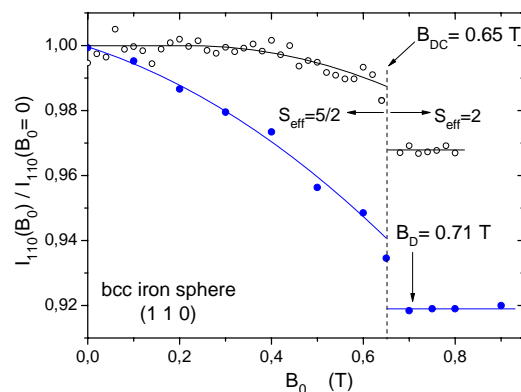
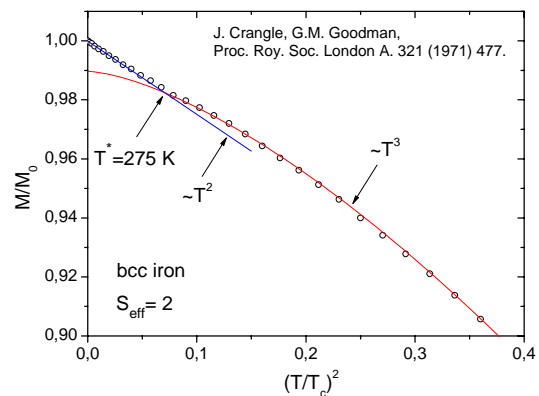
Date of Report: January 2009

Iron is known as a weak ferromagnet [1]. This means that due to particularities in the band structure there is some tendency to magnetic instability. For instance, it has been observed long ago [2] that the temperature dependence of the zero field spontaneous magnetization measured by  $^{57}\text{Fe}$  NMR does not agree with the macroscopic spontaneous magnetization [3]. In fact, upon magnetic saturation the properties of iron change fundamentally. Fig. 1 shows zero field  $^{57}\text{Fe}$  NMR and Mössbauer spectroscopic (MS) data of iron as a function of absolute temperature squared. These data reveal crossover from low temperature  $T^2$  function to high temperature  $T^{9/2}$  function at crossover temperature  $T_{\text{QS}}=615$  K. Since iron is cubic (isotropic) in zero field this crossover can be interpreted as quantum state crossover (QS) from half-integer effective spin  $S_{\text{eff}}=5/2$  to integer spin  $S_{\text{eff}}=2$  [4].



A completely different analysis is obtained for the macroscopic spontaneous magnetization [3]. Fig. 2 shows data after [3] as a function of  $(T/T_C)^2$ . Crossover from  $T^2$  to  $T^3$  function at crossover temperature  $T^*=275$  K is identified.  $T^3$  is the universality class of 1D magnets with integer spin [4]. This shows that upon magnetic saturation iron has assumed axial symmetry and is one-dimensional (1D). The effective spin is  $S_{\text{eff}}=2$ . Interpretation of low temperature  $T^2$  function also is by  $S_{\text{eff}}=2$  but now with 3D anisotropic (dynamic) symmetry. We have performed field dependent elastic neutron scattering studies on a single crystalline iron sphere in order to observe the spin- and dimensionality crossover upon magnetic saturation. Fig. 3 shows absolute intensity data of two independent experiments as a function of a vertical field. Instead of increasing the scattering intensities decrease. Reduced intensities are

typical for 1D symmetry. The sudden drop in intensity at  $B_{\text{DC}}=0.65$  T we identify as crossover. This crossover is below the demagnetization field and must be driven by magneto-elastic effects rather than by the field. From the fact that the anomaly at  $B_{\text{DC}}$  is observed only in neutron scattering but not in the macroscopic magnetization it can be concluded that the crossover from 3D to 1D symmetry involves mainly the transverse magnetization components.



- [1] A.P. Malozemoff et al. Phys. Rev. B 29 (1984) 1620.
- [2] M.A. Butler et al. Phys. Rev. B 5 (1972) 990.
- [3] J. Crangle, G.M. Goodman, Proc. Roy. Soc. (London) A.321 (1971) 477.
- [4] U. Köbler, A. Hoser, Physica B 362 (2005) 295.



## EXPERIMENTAL REPORT

### Spin excitations in the [V30Mo72] Kagome Molecular Cluster.

Proposal N°  
PHY-03-530-EF  
Instrument **V3**  
Local Contact  
E. Kemner  
M. Russina

Principal Proposer: T. Guidi, Hahn-Meitner-Institut, Berlin  
Experimental Team: J. van Slageren, University of Nottingham, UK  
B. Lake, Hahn-Meitner-Institut, Berlin  
O. Pieper, Hahn-Meitner-Institut, Berlin

Date(s) of Experiment  
02/07/2007 – 09/07/2007

Date of Report: 08/01/2009

We used NEAT time of flight spectrometer to investigate the low energy spin excitations in the Keplerate molecular cluster [V30Mo72]. The structure of the molecule consists of 30  $V^{IV}$  ions arranged in corner-sharing triangles that are grouped around pentagons to form an icosidodecahedron (Fig. 1) [1]. Each individual  $V^{IV}$  ion has  $s = \frac{1}{2}$  and the antiferromagnetic interaction within the triangles makes this system highly frustrated. Theoretical calculations predict an  $S=0$  ground state and a broad band of energy levels for the excited states [2]. Quantum Monte Carlo simulations of magnetic susceptibility data collected on [V30Mo72] predict a strong exchange interactions ( $J / k_B = 245$  K) [1] and the singlet to triplet excitation is expected at an energy transfer of about 4.5 meV. In the rotational band model the energies of the lowest states of each spin multiplicity are proportional to the square of the total spin quantum number. The lowest spin configurations are proposed to arise from the coupling of three parallel lattices of 10 spins each. A more detailed calculation for V30 cluster shows that instead of discrete levels, bands of states are formed (Fig. 2, ref [2]), and therefore very broad INS transitions are expected.

Preliminary inelastic neutron experiments in zero magnetic field revealed the presence of a broad inelastic peak centered at about 7 meV, but the temperature and Q dependence of the observed feature give an indication of the presence of phonon excitations that may mask the magnetic scattering.

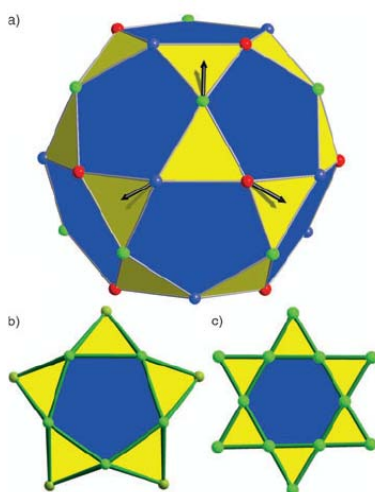


**Fig. 1** a) Structure of [V30Mo72]. The coloured balls are the vanadium ions.  
b) A fragment of the [V30Mo72] cluster showing the five linked triangles around the pentagon.  
c) A fragment of the Kagome lattice.

Here we used INS under an applied magnetic field to investigate the magnetic component of the broad excitation previously observed. Experiments were performed using a 5 T cryomagnet at a base temperature of 1.5 K. An incident wavelength of 2.1 Å was used to explore the energy transfer region up to 18 meV. Fig. 3 shows the INS intensity as a function of energy transfer, integrated over  $0 < Q < 5 \text{ \AA}^{-1}$ , and for two different magnetic fields,  $B = 0$  T and 5 T. The broad feature that extends from 4 to 11 meV is consistent with what previously observed on the IN5 spectrometer in zero field. The data at 5 T show little differences with respect to the data in zero field. The magnetic component is thus found to be very weak and masked by the dominant non magnetic background.

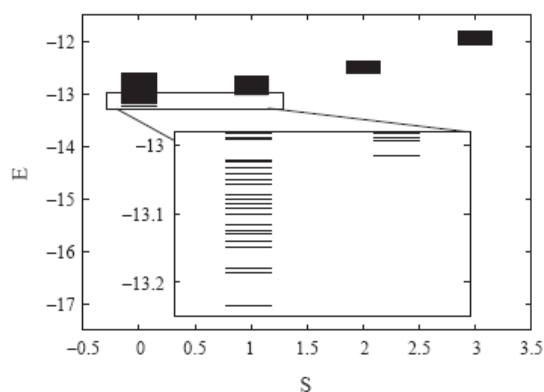


**Fig. 2** Energies (in units of J) of the low lying spin states of V30 as a function of total spin  $S$ . [2]

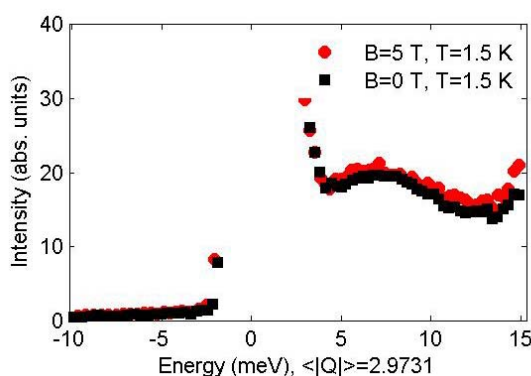


**Fig. 3** INS spectrum measured with  $\lambda = 2.1 \text{ \AA}$ ,  $T = 1.5$  K and two different magnetic field values,  $B = 0$  (black) and 5 T (red).

[1] A. Muller, A. M. Todea, J. van Slageren, M. Dressel, H. Bogge, M. Schmidmann, M. Luban, L. Engelhardt, M. Rusu, *Angew. Chem. Int. Ed.* **44**, 3857 (2005).

[2] R. Schmidt, J. Richter, J. Schnack, *J. Magn. Magn. Mater.* **295**, 164-167 (2005)



## EXPERIMENTAL REPORT

### INS studies of crystal field in RPdIn (R=Ce, Pr, Nd) compounds.

Proposal N° PHY-03-552

Instrument **V3**

Local Contact Z. Izaola

Principal Proposer: Łukasz Gondek, AGH University of Science and Technology  
Experimental Team: Zunbeltz Izaola, BENSC, HMI  
Margarita Russina

Date(s) of Experiment

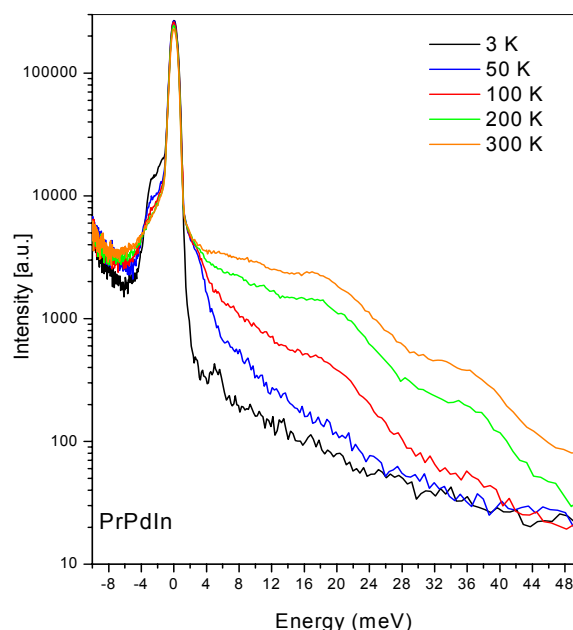
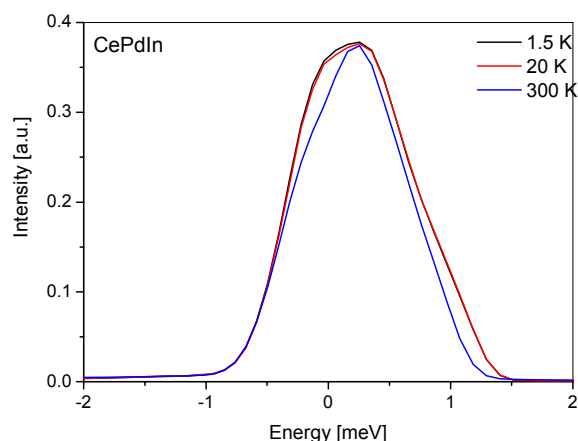
11/02/2008 – 16/02/2008

Date of Report: 21/05/2008

The RPdIn compounds exhibit interesting magnetic properties, which have been widely investigated in the past. The proposed experiment on RPdIn (R=Ce, Pr, Nd) was aimed to determine the crystal field levels scheme using the INS technique. In fact no reliable analysis of CEF effects on RPdIn family could be found in literature.

Experiment was performed for CePdIn and PrPdIn samples. Additionally LaPdIn sample was measured as a reference. Measurements for CePdIn sample revealed highly delocalised nature of the 4f electrons. No clearly visible crystal field (CF) effects were observed. However, some interesting asymmetry of the elastic line was evidenced. This asymmetry may be related to strong electronic correlation at least at low temperatures. In contradiction, for PrPdIn sample analysis of INS spectra confirm crystal field levels splitting estimated from specific heat data. It may be deduced, that the ground CF state is a singlet. The next singlet is 1.7 meV above the ground state. Third CF level is located at 2.8 meV above the ground state. The small energy between ground and first excited CF level explains non Curie-Weiss behaviour of magnetic susceptibility of PrPdIn.

On the other hand, in energy gain spectra there are visible transitions from higher CF levels, at about 33 meV (380 K), 25 meV (290 K) and 18 meV (210 K). All this transitions are in a good agreement with splitting estimated basing on specific heat data.



*This research project has been supported by the European Commission under the 6<sup>th</sup> Framework Programme through the Key Action: Strengthening the European Research Infrastructures. Contract n°: RII3-CT-2003-505925 (NMI 3).*



## EXPERIMENTAL REPORT

### Determination of crystal field parameters for the intermetallic compound $\text{ErCr}_2\text{Si}_2$

Proposal N° MAT-03-0553

Instrument **V3**

Local Contact M. Russina

Principal Proposer: G. A. Stewart, UNSW@ADFA, Canberra  
Experimental Team: B. Saensunon, UNSW@ADFA, Canberra  
P.C.M. Gubbens, T.U. Delft  
M. Russina & E. Kemner, Helmholtz-Zentrum Berlin

Date(s) of Experiment

13/05/2008 – 17/05/2008

Date of Report: 15/12/2008

The objective of these inelastic neutron scattering (INS) measurements was to characterise the crystal field (CF) interaction at the Er site of the intermetallic,  $\text{ErCr}_2\text{Si}_2$ . Additional data were also able to be recorded for the isostructural compound  $\text{ErMn}_2\text{Si}_2$ . Masses of 8.5 g and 7 g, respectively, of finely ground specimen material were packed into the 50 mm diameter x 1 mm cavities of rigid, aluminium holders and INS spectra were recorded with  $E_i = 18.6$  meV ( $\lambda_i = 2.1$  Å) over a range of temperatures (Fig. 1 and Fig. 2). Additional spectra were recorded for an  $\text{YCr}_2\text{Si}_2$  reference sample, the empty cell and a vanadium standard sample (1 mm thick). The local point symmetry at the rare earth site is tetragonal  $D_{4d}$  ( $4/mmm$ ) which requires a CF Hamiltonian with 5 CF parameters. It is our experience that the characterisation of the CF

interaction is best achieved through self-consistent interpretation of experimental data for a combination of measurement techniques. To this end, we have already recorded temperature-dependent specific heat and nuclear quadrupole interaction ( $^{169}\text{Tm}$ -Mössbauer spectroscopy) data for isostructural  $\text{TmCr}_2\text{Si}_2$  and  $\text{TmMn}_2\text{Si}_2$ . In the interim, we expected that CF parameters derived from an INS investigation reported elsewhere for  $\text{HoCr}_2\text{Si}_2$  [1] would provide a useful starting point. This approach proved reasonably successful for the CF interpretation of our  $^{169}\text{Tm}$ -Mössbauer spectroscopy data for  $\text{TmCr}_2\text{Si}_2$  [2]. In Fig. 3, simulated spectra are compared with the 11 K spectra reported here for  $\text{ErCr}_2\text{Si}_2$  and  $\text{ErMn}_2\text{Si}_2$ . The degree of disagreement is unexpected and throws some doubt on the earlier CF interpretations. This work is continuing.

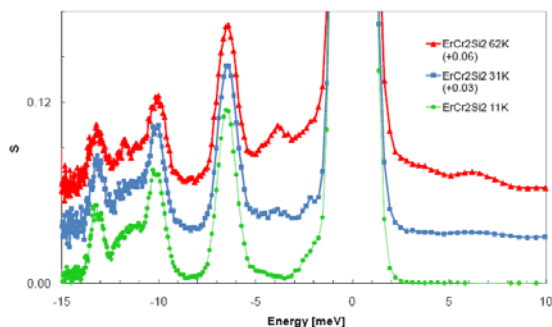


Fig. 1: INS spectra for  $\text{ErCr}_2\text{Si}_2$

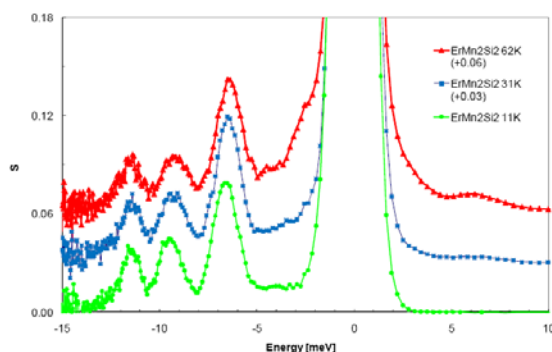


Fig. 2: INS spectra for  $\text{ErMn}_2\text{Si}_2$

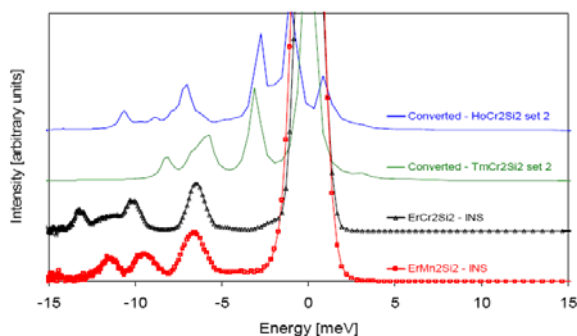


Fig. 3: Comparison with simulated spectra at 11 K

[1] O. Moze, M. Hofmann, J. M. Cadogan, K. H. J. Buschow and D. H. Ryan, *Eur. Phys. J. B* **36** (2003) 511-518.

[2] B. Saensunon, G. A. Stewart and K. Nishimuro, *J. Alloys Compd.* (in press)

	<b>EXPERIMENTAL REPORT</b> <b>INS studies of crystal field in RPdIn (R=Ce, Nd) compounds.</b>	Proposal N° PHY-03-589 Instrument <b>V3</b> Local Contact Z. Izaola
	Principal Proposer: Łukasz Gondek, AGH University of Science and Technology Experimental Team: Zunbeltz Izaola, BENSC Margarita Russina, BENSC J. Czub, Jagiellonian University	Date(s) of Experiment 06/08/2008 – 10/08/2008

Date of Report: 21/05/2008

The RPdIn compounds exhibit interesting magnetic properties, which have been widely investigated in the past. The proposed experiment on NdPdIn sample was aimed to determine the crystal field levels scheme using the INS technique. The LaPdIn sample was considered as the reference for extracting the phononic contribution.

An example of collected data is given in the figure 1. The spectrum was collected at 2.5 K. Anomalies are clearly visible at energies of 1.8, 4.2, 6.2, 9.3 meV. The energies (except the last one) are in a very good agreement with those estimated on basis of specific heat measurements. The comparison is presented in figure 2.

It is clearly visible, that the  $\text{Nd}^{3+}$  multiplet is split into five crystal field doublets. Moreover, it was shown that the ground doublet is not split due to magnetic correlations. It is interesting, that at energy gain of about 5.1 meV some anomaly is visible. The origin of this anomaly seems to be unclear at the present state of data treatment.

Figure 1. INS data for NdPdIn at 2.5 K.

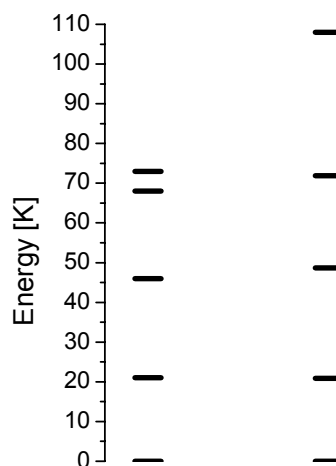
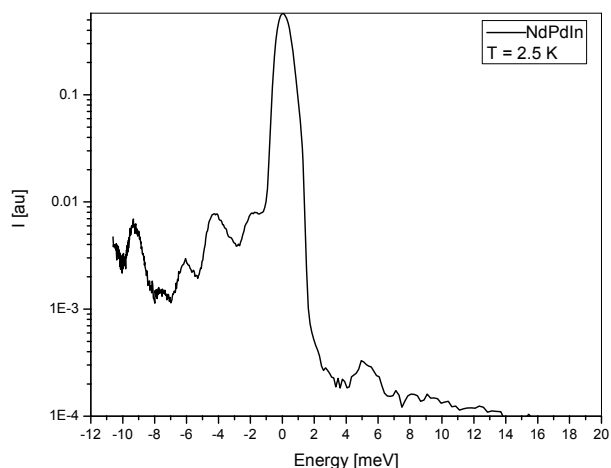


Figure 2. Comparison of crystal field splitting as derived from specific heat data (left) and INS (right).



*This research project has been supported by the European Commission under the 6<sup>th</sup> Framework Programme through the Key Action: Strengthening the European Research Infrastructures.*

*Contract n°: RII3-CT-2003-505925 (NMI 3).*



## EXPERIMENTAL REPORT

### Spin excitations in the novel two-leg spin-ladder compound $\text{BiCu}_2\text{PO}_6$

Proposal N°  
PHY-03-610-EF

Instrument **V3**

Local Contact  
Ewout Kemner

Principal Proposer: Markus Skoulatos – HZB, Berlin, Germany  
 Experimental Team: Klaus Habicht - HZB, Berlin, Germany  
 John Goff – Dept. of Physics, Royal Holloway, London, UK  
 Christoph Geibel – MPI-CPfS Dresden, Germany  
 Ramesh Nath - MPI-CPfS Dresden, Germany  
 Ewout Kemner – HZB, Berlin, Germany  
 Bella Lake – HZB, Berlin, Germany

Date(s) of Experiment

22/07/2008 – 28/07/2008

Date of Report: 15/01/2009

Spin-ladders represent important model systems in quantum magnetism since their properties lie between the classes of one-dimensional and two-dimensional magnetic systems. It is believed that a better understanding of spin-ladder systems will lead to a more complete description of 2D magnetic systems in general. In gapped ladder model systems the microscopic origin of the energy gap, multi-particle continua and bound states are theoretically extensively investigated. However, only a few gapped ladder systems have been synthesized and are available for experimental studies.

The novel two-leg spin-ladder material  $\text{BiCu}_2\text{PO}_6$  is an ideal candidate for experimental investigations. Structural studies reveal that two distorted square pyramids with a  $\text{Cu}^{2+}$  ( $S=1/2$ ) ion situated in their centers form Cu dimers [1]. Each dimer connects two others by its four corners resulting in a zigzag double chain along the b-axis. Susceptibility and specific heat measurements [1] suggest absence of long-range magnetic order and indicate that the spin gap is about 3 meV while intraladder leg coupling is  $J \sim 7$  meV ( $\sim 80$  K). The system thus provides a unique opportunity to examine the excitations in a temperature range from well above  $J$  to well below  $J$  quite conveniently. Since the measured magnetic susceptibility is significantly lower than the 2D HAF and the isolated ladder, NNN interactions along the legs might play an important role introducing some degree of frustration into the system.

Figure 1 shows the magnetic contribution of powdered  $\text{BiCu}_2\text{PO}_6$  at 3K. Data were collected at  $\lambda_i=2.4$  Å, which gives an energy transfer up to 12meV, and an energy resolution of 0.8meV at the elastic line. One can see a gap of roughly 2meV, as well as some steep dispersion around  $Q=1.1$  Å<sup>-1</sup> (as well as  $2.2$  Å<sup>-1</sup>). It seems that the signal is split into two branches, at 5 and 7meV, however it is difficult to judge from such powder datasets. Their intensities

decrease as  $Q$  increases, a signature of spin waves (expect  $I \propto 1/Q$  for magnons). This can be contrasted with  $\text{BiCu}_2\text{VO}_6$  [2] that has 3 modes at much higher energies (16, 25 and 39meV).

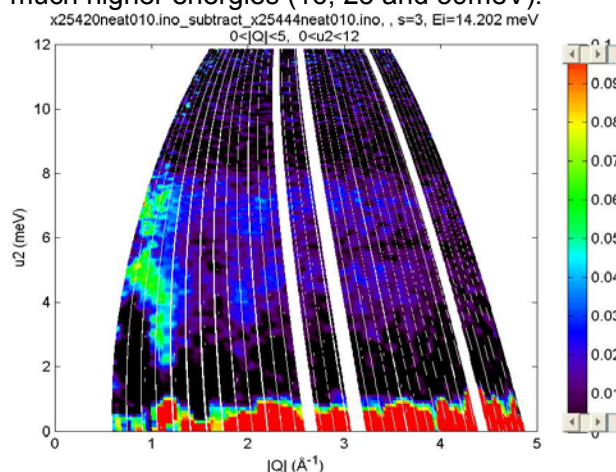


Fig. 1: Powder averaged inelastic spectrum showing the magnetic contribution in  $\text{BiCu}_2\text{PO}_6$ . 50K data have been subtracted from 3K data. Two magnon bands are visible at  $\sim 5$  and  $\sim 7$  meV.

Our data agree with the susceptibility results, since the maximum of the susceptibility (dominant interaction at 64 K = 5.5 meV) coincides with the lowest of the measured modes. Furthermore, we see the gap at about  $1.1$  Å<sup>-1</sup> (and at  $Q=2.2$  Å<sup>-1</sup>). This would correspond to the middle of the B.Z., i.e.  $\pi/d$ . Hence,  $d \approx 2.85$  Å from our data. The intradimer distance of the Cu dimers in this structure is 2.8 Å [1]. So the characteristic distance we get out from the NEAT data coincides with the proposed dimers from the structure.

A single crystal experiment would clarify the situation and give a much better picture of the exchange couplings in the system.

#### References:

- [1] B. Koteswararao *et al.*, Phys. Rev. B **76**, 052402 (2007)
- [2] T. Masuda *et al.*, Europhys. Lett., **63**, pp. 757-763 (2003)



## EXPERIMENTAL REPORT

### Spin excitations in LuVO<sub>3</sub>

Proposal N° EF/Instr. time

Instrument **V2**

Local Contact  
Klaus Habicht

Principal Proposer: Markos Skoulatos – HZB, Berlin, Germany  
 Experimental Team: Klaus Habicht – HZB, Berlin, Germany  
 Jon Goff - Dept. of Physics, Royal Holloway, London, UK  
 Le Duc Tung - Dept. of Physics, Liverpool, UK

Date(s) of Experiment

22/04/2008 – 04/05/2008

Date of Report: 18/11/2008

The perovskite orthovanadates  $RVO_3$  ( $R$ =rare earth) provide an ideal environment to study the **orbital** degree of freedom and its interplay with the **spin** and **lattice**. There are two  $t_{2g}$  electrons in  $V^{3+}$ , which adopt the high-spin configuration due to Hund's-rule coupling. One electron always occupies the  $d_{xy}$  orbital due to the orthorhombic distortion, and the other electron occupies one of the two possible states  $d_{yz}$  or  $d_{zx}$ . The orbital pseudospin is  $T=1/2$  and, orbital quantum fluctuations are expected to play an important role in the physics of  $RVO_3$ .

These compounds can exhibit either a  $G$ - or a *more exotic*  $C$ -type magnetic structure, as well as combinations of both as a function of temperature. According to the standard Goodenough-Kanamori rules, a  $G$ -type spin structure is compatible with a  $C$ -type orbital arrangement and vice versa. However, from inelastic neutron scattering studies of  $YVO_3$  [1] it was shown that this mechanism is not enough to account for the behaviour of such systems. Indeed, a more detailed and complex theory developed [2] was needed to explain the intermediate temperature  $C$ -type spin phase, in terms of pseudo-1D orbital chain formation along the crystallographic  $c$ -axis.

Following up our previous experiment conducted at IN8, ILL, we were able to get the temperature dependence of the signal at the centre of the BZ for the two phases. Figure 1 shows the inelastic spectrum at  $Q = (\frac{1}{2} \frac{1}{2} \frac{1}{2})$ , corresponding to the ordering wave-vector of the  $G$ -type spin ordering. The two previously unresolved modes are now clearly visible, one at  $\sim 3.5$  meV and the other at  $\sim 8.5$  meV. At  $T=84$  K, the magnetic excitations at this wave-vector abruptly disappear, and the system switches to a  $C$ -type phase. This can be seen in fig. 2, where the inelastic spectrum at  $Q = (\frac{1}{2} \frac{1}{2} 0)$  is shown as a function of  $T$ . The signal was more difficult to follow in this phase,

although we could clearly detect it *only* above 84 K. It also persists above 107 K, the temperature above which the sample enters into a paramagnetic spin state (although the orbitals seem to be ordered up to  $\sim 180$  K from heat capacity measurements).

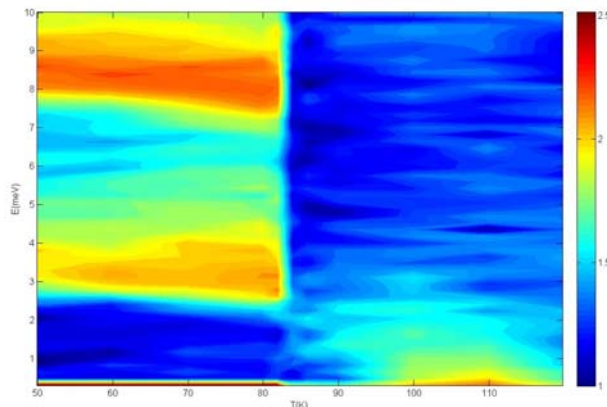


Fig. 1: Inelastic spectrum at  $Q = (\frac{1}{2} \frac{1}{2} \frac{1}{2})$  as a function of  $T$ . This corresponds to the ordering wave-vector of the  $G$ -type spin phase. Two magnon modes are visible below 84 K.

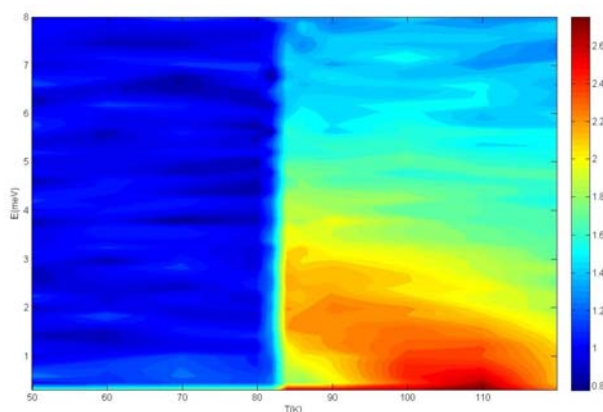


Fig. 2: The inelastic signal at  $Q = (\frac{1}{2} \frac{1}{2} 0)$  corresponds to the  $C$ -type spin ordered phase, observed at  $T > 84$  K.

#### References:

- [1] C. Ulrich *et al.*, *Phys. Rev. Lett.* **91**, 257202, (2003)
- [2] A.M. Oles *et al.*, *Phys. Rev. B* **75**, 184434, (2007)



**EXPERIMENTAL REPORT**  
**Magnetic Excitation Spectrum of the Frustrated Quantum Dimer Antiferromagnet Strontium Chromate**

Proposal N° EF  
 Instrument **V3**  
 Local Contact  
 Zunbeltz Izaola

Principal Proposer: Bella Lake, HZB  
 Experimental Team: Diana Lucia Quintero Castro, HZB  
 Elisa Wheeler, HZB  
 Magarita Russina, HZB  
 Nazmul Islam, HZB

Date(s) of Experiment  
 28/04/2008 – 04/05/2008

Date of Report: 09/01/2009

We performed an inelastic neutron scattering experiment on the time of flight spectrometer NEAT-V3, located in the Neutron Cold Guide at BENSC, Helmholtz Zentrum Berlin. The aim of this experiment was to investigate the magnetic excitation spectrum of the dimerized quantum magnet  $\text{Sr}_3\text{Cr}_2\text{O}_8$ . For this experiment we have synthesised powders of  $\text{Sr}_3\text{Cr}_2\text{O}_8$  by solid state reaction. We measured the energy dispersion as a function of the powder averaged wavevector at 2K.

The magnetic  $\text{Cr}^{5+}$  ions are arranged in hexagonal bilayers. The theory predicts that the strongest interaction is the intrabilayer interaction which couples the  $\text{Cr}^{5+}$  ions into antiferromagnetic pairs resulting in a frustrated triangular lattice of spin-1/2 dimers (see figure 1a) [1, 2].

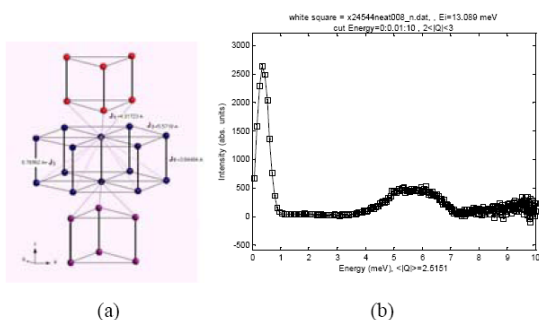


**Fig 1.** (a) Structure of  $\text{Sr}_3\text{Cr}_2\text{O}_8$  at  $T > 275\text{K}$  showing only the  $\text{Cr}^{5+}$  ions. (b) Cut along energy, with a width in  $|Q|$  between 2 and  $3 \text{ \AA}^{-1}$ , the incident energy was 13 meV.

We measured the inelastic scattering of the neutrons in the sample using three different incident energies: 8 meV, 13 meV and 20 meV.

The data show a single band of excitations centred at 5.25 meV, which have an energy gap of 3.5 meV and a bandwidth of 3.5 meV (Figure 1b).

Fitting the first moment of the data reveals that the dominant exchange constant is the

intrabilayer interaction along  $c$  as predicted by theory.

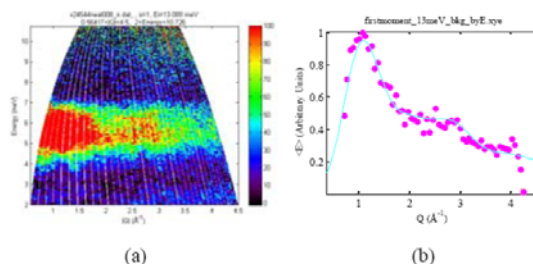


**Fig 2.** (a) Inelastic neutron magnetic scattering data of  $\text{Sr}_3\text{Cr}_2\text{O}_8$  powder as a function of energy and momentum transfer,  $E_i = 13 \text{ meV}$ . (b) Cut along powder averaged wavevector, integrating in energy around 5.8 meV. The blue line is the fitting to the first moment function [3].

With this spectrometer we got good data and after background subtraction and other corrections we were able to see the general behavior of  $\text{Sr}_3\text{Cr}_2\text{O}_8$ . Data analysis shows that the intrabilayer exchange constant was the dominant exchange. By fitting the data to the first moment function (Fig 2.b), we found that the ratio between the effective interdimer interaction and the intradimer interaction  $J'/J_0$  is 0.187 (where  $J' = 3J_1 + 6J_2$ , we considered  $J_3 = 0$  according to the theory). This ratio is agreed with the value obtained from susceptibility measurements.

**References:**

- [1] Y. Singh, D.C. Johnston *Phys. Rev. B* **76** 012407 (2007).
- [2] L.C. Chapon, C. Stock, P.G. Radaelli, C. Martin LANL preprint server <http://xxx.lanl.gov/abs/0807.0877>
- [3] M. B. Stone, I. Zaliznyak, Daniel H. Reich, and C. Broholm, *Phys. Rev. B* **64**, 144405, (2001).



## EXPERIMENTAL REPORT

### PNR study of Co/CoO exchange bias system formed by ion implantation

Proposal N°  
PHY-04-1618-LT

Instrument **V6**

Local Contact  
Anke Teichert

Principal Proposer: K. Temst – KU Leuven, B  
 Experimental Team: J. Demeter – KU Leuven, B  
 A. Teichert – HZ Berlin & KU Leuven, B  
 R. Steitz, HZ Berlin

Date(s) of Experiment

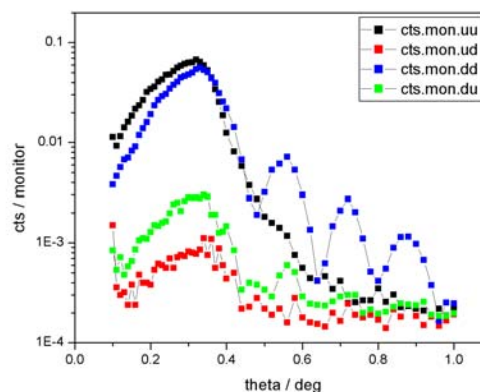
10/03/2008 – 16/03/2008

Date of Report: 09/01/2009

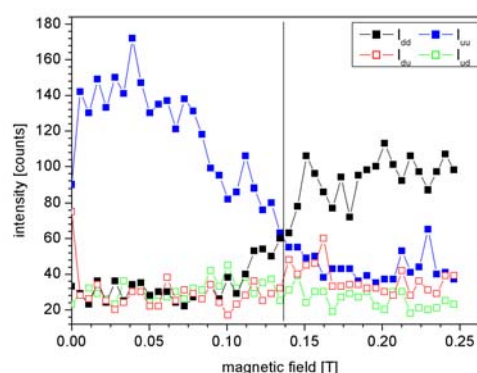
Exchange bias is an interface effect between a ferromagnetic and an antiferromagnetic material. This induces a unidirectional anisotropy in the ferromagnet after cooling below the antiferromagnet's Néel temperature while applying a magnetic field. The aim of this experiment was to study the reversal mechanism in a newly formed exchange bias system. This system is formed by the implantation of O in thin Co films. The observed exchange bias in this system can be attributed to the formation of CoO inside the Co-film. Due to its interesting magnetic properties, similar to well known exchange bias systems, on the one hand, but its clear morphological differences with these systems, a study of the magnetisation reversal mechanism is a key element in the understanding of this system.

The Co layer with a thickness of 100 nm was grown with Molecular Beam Epitaxy on an MgO substrate and capped with a thin Au layer to prevent the formation of a CoO layer by natural oxidation. The CoO was formed by the implantation of  $10^{17}$   $^{16}\text{O}$  ions /  $\text{cm}^2$  at an energy of 60 keV in this film. Vibrating Sample Magnetometry measurements were performed on the sample after cooling it from RT to a temperature of 10 K while applying a magnetic field. Besides a clear exchange bias behaviour, a training effect is observed: subsequent measurements at the same temperature show different coercive fields.

In this experiment we performed specular reflectivity measurements with spin analysis at some key field values, like saturation and coercive field, to learn more about the structural and magnetic depth profile. In figure 1 the specular reflectivity measurement of the sample in positive saturation is shown. The clear splitting between the uu- and dd- signal for certain angles offer the possibility of measuring these signals while changing the external field. These field scans were performed in all branches of the virgin and trained hysteresis loop.



In figure 2 the field scan in the virgin descending branch is shown. The crossing of the uu- and dd- signal indicates the coercive field. There is no clear increase in the spin flip signals, this indicates that this reversal is governed by domain wall nucleation and motion. All other field scans look similar, indicating that all reversals are governed by domain wall nucleation and motion. This is an interesting result since it differs strongly from the findings in Co/CoO bilayers, where a change in reversal mechanism is observed.



*In Cooperation Agreement between KU Leuven and HZB*



## EXPERIMENTAL REPORT

### Probing noncollinear spin structure in oppositely exchange-biased NiFe/FeMn/CoFe trilayers

Proposal N° PHY-04-1704

Instrument **V6**

Local Contact  
R. Steitz, A. Teichert

Principal Proposer: Ki-Yeon Kim, HANARO, KAERI, Korea  
 Experimental Team: J. -S. Lee, HANARO, KAERI, Korea  
 H. -C. Choi, Inha University, Korea  
 C. -Y. You, Inha University, Korea  
 A. Teichert, HZB, Germany  
 R. Steitz, HZB, Germany

Date(s) of Experiment

27/10/2008 – 02/11/2008

Date of Report: 15/01/2009

Ferromagnetic(F)/antiferromagnetic(AF) hetero structures exhibit the unidirectional anisotropy when they are field cooled from above a AF blocking temperature or are deposited under the applied magnetic field. The unidirectional anisotropy manifests itself as the magnetic hysteresis loop shift along field axis, that is, an exchange bias field, and increased coercivity. Compared to F/AF bilayers, F(bottom)/AF/F (top) trilayers have the advantage that the effect of the deposition order and the interaction between two F/AF interfaces on exchange bias field and magnetization reversal of the F layer can be investigated. It is generally believed that the spin structures in AF layer play a key role in establishing the exchange bias in F/AF hetero-structures.

Polarized neutron reflectivity (PNR) experiment capable of resolving the magnetization profile with a sub-nanometer depth resolution can be the most adequate solution for studying the noncollinear spin structures a spiral spin structure in exchange-biased thin films. To this end, we prepared a series of 30-nm NiFe (bottom)/FeMn/30-nm CoFe (top) trilayers with different FeMn thickness from 0 to 15 nm using magnetron sputtering technique. Magnetic field of about 300 Oe was applied along the sample plane during sample deposition. After sample growth, the oppositely and parallel exchange-biased structures were realized through a special field cooling procedure to intentionally change AF spin structure. V6 reflectometer was employed to measure the PNR of parallel and oppositely exchange-biased 30-nm NiFe/10-nm FeMn/30-nm CoFe trilayers at different magnetic hysteresis points such as magnetic saturation states and coercivities at room temperature during seven experimental days. The uu in Figure 1 means that neutrons impinging on sample have its spin polarized up and neutrons reflected from sample surface and arriving at detector have spin polarized up.

From the comparison between positive (a) and negative (c) saturations in Figure1,

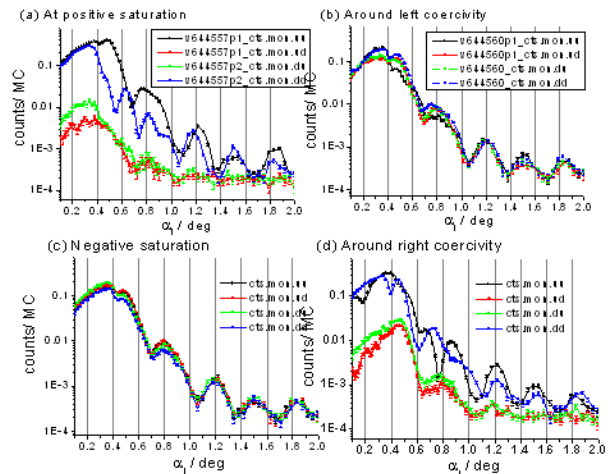


Figure 1. Nonspin flip (uu, dd) and spin flip (ud, du) neutron reflectivities of the oppositely exchange-biased 30-nm NiFe/10-nm FeMn/30-nm CoFe trilayer at different four magnetic states such as (a) positive magnetic saturation, (b) around left coercivity, (c) negative magnetic saturation, and (d) around right coercivity. uu (black line), ud (red line), du (green line), dd (blue line) in the graph.

it is interesting that nonspin flip reflectivities are very different. This indicates that FeMn spins exchange-coupled by two F layers rotate to the direction which is neither parallel nor antiparallel to the applied magnetic field. In addition, This asymmetry of nonspin flip reflectivities is observed between left (b) and right (d) coercivities in Figure 1. This means that the magnetization reversal modes are asymmetric between the descending field and ascending field branches in magnetic hysteresis loop. Although fit to the experimental data has to be done, we can infer from PNR data that the asymmetry of spin flip reflectivities between the positive and negative saturations are attributed to the noncollinear AF spin structures and the asymmetry of spin flip reflectivities between the left and right coercivities results from asymmetric magnetization reversal of the F layer.



## EXPERIMENTAL REPORT

### PRN study of epitaxial Co/CoO exchange bias system formed by ion implantation

Proposal N°  
PHY-04-1720-LT

Instrument **V6**

Local Contact  
Anke Teichert

Principal Proposer: J. Demeter – KU Leuven, B  
 Experimental Team: J. Demeter – KU Leuven, B  
 A. Schrauwen – KU Leuven, B  
 Teichert – HZ Berlin & KU Leuven, B  
 R. Steitz, HZ Berlin

Date(s) of Experiment

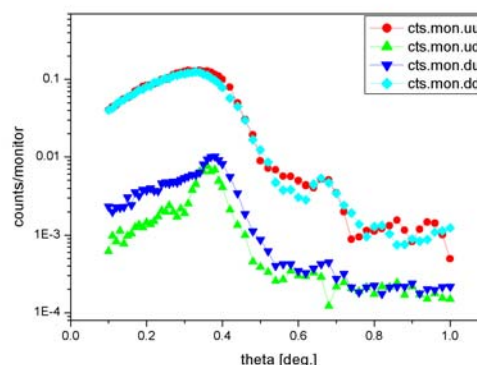
10/11/2008 – 16/11/2008

Date of Report: 09/11/2008

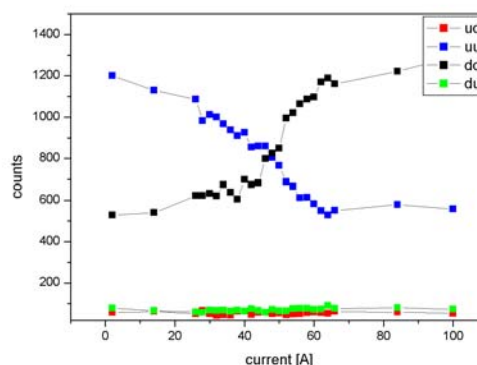
The aim of this experiment was to study the reversal mechanism in a newly formed exchange bias system. Exchange bias is an interface effect between a ferromagnetic and an antiferromagnetic material, inducing a unidirectional anisotropy in the ferromagnet. The system being studied is formed by the implantation of O in thin Co-layers, which have an epitaxial order. An earlier PNR study on a similar implanted system, but without the epitaxial ordering, showed that the magnetisation reversal was mainly occurring by domain wall nucleation and motion. The reason to study this system is to learn more about the role of epitaxial ordering on the reversal mechanism.

The sample was grown with Molecular Beam Epitaxy on Si(100), after the deposition of a Cu buffer layer. After deposition of 100 nm Co an Au capping layer was grown to prevent the formation of CoO on the surface by natural oxidation. The CoO was formed by the implantation of  $10^{17}$   $^{16}\text{O}$  ions /  $\text{cm}^2$  at an energy of 60 keV in the Co film. Epitaxial ordering was confirmed by XRD measurements and Vibrating Sample Magnetometry showed the sample had clear exchange bias properties and exhibits a training effect (change of loop width after consecutive measurements of the hysteresis loop).

In this experiment we performed specular reflectivity measurements with spin analysis at some of the important field values and magnetic field scans by measuring the different spin signals while changing the magnetic field. Figure 1 shows the specular reflectivity measurement in the first coercive field after field cooling to 10 K. The two spin flip signals are at least one order of magnitude smaller than the non spin flip signals, indicating the reversal is governed by domain wall nucleation and motion. This is confirmed by a magnetic field scan in this branch of the hysteresis loop, as shown in figure 2. The crossing of the uu- and dd- signal indicates the position of the coercive field, no increase in



spin flip signal is found there. The same type of field scans is performed in all branches of the virgin and trained hysteresis loops, all showing the same behaviour. These measurements indicate that all reversals are governed by domain wall nucleation and motion. These findings coincide with our findings in the non-epitaxially grown system, so the influence of epitaxial ordering is not immediately evident from this experiment. The behaviour is different from well known bilayer exchange bias systems where a change in reversal mechanism is found.



*In Cooperation Agreement between KU Leuven and HZB.*



## EXPERIMENTAL REPORT

### PNR study of a BiFeO<sub>3</sub> multiferroic film

Proposal N°  
PHY-04-1721-LT

Instrument **V6**

Local Contact  
Anke Teichert

Principal Proposer: K. Temst & M.J. Van Bael - KU Leuven, B  
 Experimental Team: J. Demeter - KU Leuven, B  
 A. Teichert - HZ Berlin & KU Leuven, B  
 R. Steitz - HZ Berlin

Date(s) of Experiment

08/12/2008 – 15/12/2008

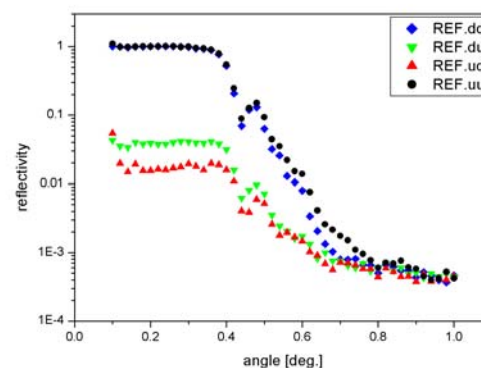
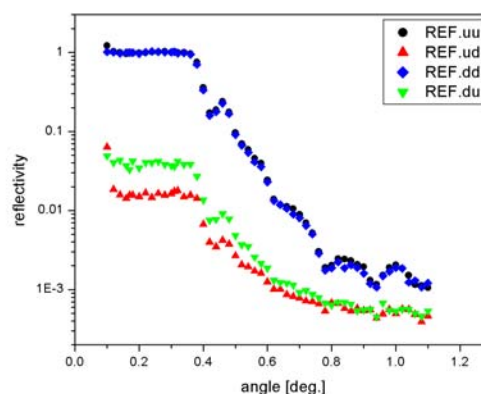
Date of Report: 09/01/2009

Lately a lot of interest arose in multiferroic materials, these are materials which exhibit simultaneous ferroelectric and magnetic ordering. These two properties can influence each other which make these materials promising for future devices. The aim of this experiment was to investigate some of the magnetic properties of a BiFeO<sub>3</sub> multiferroic film by PNR.

The film under investigation was grown (at the Universiteit Hasselt) with a powder synthesis method, this resulted in a phase-pure film with a thickness of around 100 nm. Prior to the experiment the sample was extensively characterized: structural properties were studied by XRD, XRR and SEM; electric characterizations showed ferroelectric properties; magnetic properties were studied by SQUID magnetometry. These magnetic measurements showed clear ferromagnetic properties, though rather weak, which calls for measurements with high statistics in order to be able to see the magnetic contribution.

Since the magnetic properties arise most clearly at very low temperatures, a new cryostat was implemented in the V6-setup which is able to cool the sample down to a temperature of 1.5 K. A series of reflectivity measurements were performed after cooling with or without an applied magnetic field in order to clarify the nature of the magnetism in this system. In figure 1 the reflectivity measurement in saturation, after zero field cooling to 1.5 K is shown. There is no difference in the uu- en dd- signal and the measurement looks the same as the measurement in the demagnetised state. This means that we are not able to see a magnetic contribution to the reflectivity after a zero field cooling. Subsequently the film was cooled while applying the maximum field of 0.4 T to a temperature of 12 K. This measurement is shown in figure 2. In this measurement a splitting of the uu- en dd- signal is seen at higher angles. This difference between field

and zero field cooling can indicate that the system behaves as a spin glass system.



Besides the results on the studied film, the experiment showed the successful use of a low temperature cryostat, which can cool down to a temperature of 1.5 K. This expands the experimental possibilities of the V6-instrument considerably.

*By Cooperation Agreement between KU Leuven and HZB*

	<b>EXPERIMENTAL REPORT</b>  <b>Influence of Bias voltage on structure and reflectivity of Si/ Fe multilayers</b>	Proposal N° PHY-04-1722-EF  Instrument <b>V6</b>  Local Contact A. Teichert
	Principal Proposer: A. Teichert, HZB & KU Leuven, Belgium Experimental Team: R. Steitz, HZB Th. Krist, HZB Jan-E. Hoffmann, HZB	Date(s) of Experiment  04/08/2008 – 10/08/2008

Date of Report: 14/01/2009

Recently, polarizing multilayers (MLs) attracted substantial scientific and applied interest in the last years. Focal point of many studies was the investigation of structure and the specular as well as off-specular scattering of neutrons. It was shown that high quality MLs, characterized by high reflectivity and polarization efficiency, require low interface layer thickness, roughness and high remanence.

Here, we report on the investigation on correlation between the Bias voltage, stress and structure of Si/ Fe multilayers on Si and glass substrates. The MLs with 10 bilayers have a nominal bilayer thickness of 200Å. All samples were prepared in a triode sputter machine at an argon pressure of  $0.65 \times 10^{-4}$  mbar. The Bias voltage was varied from 10 to 65V. The final stress in the layers was calculated with the Stoney formula:  $\sigma_s = (E / (1 - \nu))(d_s^2 / 6d_f)((1 / R_1) - (1 / R_0))$  where E and  $\nu$  are the elastic modules and Poisson constant,  $d_s$  and  $d_f$  the substrate and layer thickness and  $R_1$  and  $R_0$  the radii after and before the deposition. Layer structure was investigated by x-ray (XRR) and polarized neutron reflectometry (PNR) and x-ray diffractometry (XRD). PNR measurements were performed at V6 with a wavelength of 4.66Å. With a positive sensitive detector (PSD) we measured the specular and off-specular reflectivity simultaneously. The specular reflectivity gives values to the layer thickness and roughness whereas the diffuse scattering gives information about the interface morphology.

Correlation is found for Bias voltage and stress in the layers. Raise in voltage leads to linear decrease of tensile stress with a slope of  $5.5 \pm 0.7$ MPa. One can see from Fig.1 that the MLs are nearly stress-free at 60V. Further, higher voltage leads to thinner interface layers, thicker Fe layers and smaller grains. The interface layers were between 19 and 25Å, the Fe layer thickness varied between 73 and 94Å. Fig.2 shows the neutron scattering of a ML in an external magnetic field of 200 and 1030G,

respectively, prepared at 60V. The specular intensity along the line  $\alpha_i = \alpha_f$  shows the first and the second order peak which corresponds to a bilayer thickness of  $206 \pm 15$ Å. The diffuse scattering of this nearly stress-free ML reduces with stronger magnetic field. Below stress values of -120MPa we did not observe this effect. Additional diffuse streaks at the first and second order Bragg peak positions appear for compressive stress over -120MPa. X-ray rocking scans around the Bragg peaks ( $\alpha_i \neq \alpha_f$ ) revealed inhomogeneities in MLs with higher stress.

In summary, for MLs with low tensile stress diffuse scattering vanished in high magnetic field. At the same time, those were the MLs with smaller grain size.

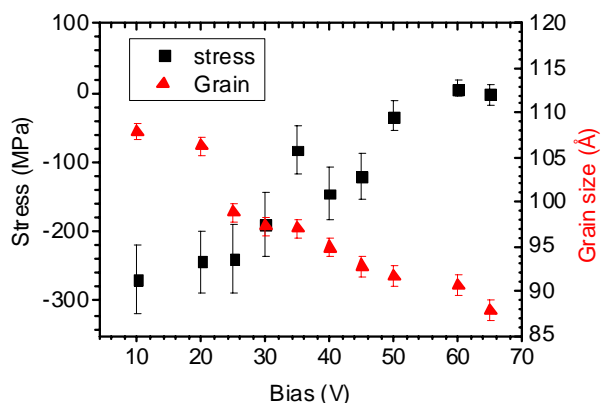


Fig. 1: Stress and grain size in ML for different Bias voltage values.

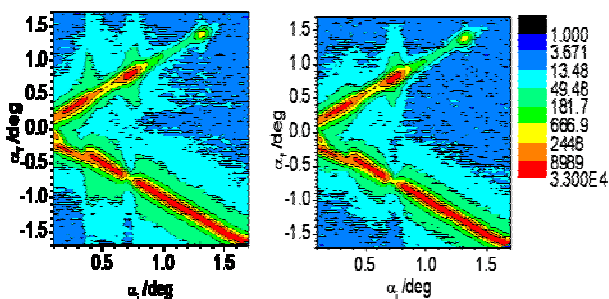


Fig. 2: Reflectivity and off-specular scattering of neutrons from a Si/ Fe ML ( $\sigma_s = 6.0 \pm 1$ MPa) at 200 and 1030G.



## Structure

Chemical Structure	111
Structural Excitations	133
Geology	140





## EXPERIMENTAL REPORT

### Structure of $(\text{PbFe}_{2/3}\text{W}_{1/3}\text{O}_3)_{1-x}-(\text{PbTiO}_3)_x$ solid solutions

Proposal N° MAT-01-2033

Instrument **E2**

Local Contact  
J.-U. Hoffmann

Principal Proposer: Alexander Naberezhnov, Ioffe PTI RAS, Russia  
Experimental Team: Alexander Naberezhnov, Ioffe PTI RAS, Russia  
J.-U. Hoffmann, HMI, Berlin

Date(s) of Experiment

15/05/2008 – 19/05/2008

Date of Report: 15/01/2008

Pure  $\text{PbFe}_{2/3}\text{W}_{1/3}\text{O}_3$  is a relaxor ferroelectric and due to iron ions undergoes the antiferromagnetic phase transition (PT) at  $T_N \approx 360$  K. The antiferromagnetic ordering with doubling of unit cell is a result of ordering of  $\text{Fe}^{3+}$  magnetic moments.  $\text{Fe}^{3+}$  ions are distributed randomly with  $\text{W}^{6+}$  ions in octahedrons of perovskite structure. It is known that in the solid solutions of relaxor ferroelectric with conventional ferroelectrics the degree of phase transition diffuseness decreases at increasing of normal ferroelectric percentage. These materials with ferroelectric and magnetic properties simultaneously are not only of fundamental interest but also of practical importance. The study of structure evolution of  $(\text{PbFe}_{2/3}\text{W}_{1/3}\text{O}_3)_{1-x}-(\text{PbTiO}_3)_x$  (PFW-PT) solid solutions gives a possibility to obtain the information about the microscopic processes resulting in modification of macroscopic properties. The most interesting concentrations are  $x = 0.2$  and  $0.3$  [1], demonstrating very unusual physical properties in vicinities of both ferroelectric and antiferromagnetic PTs. These concentrations correspond to so-called morphotropic phase boundary and demonstrate high dielectric permittivity (up to  $10^5$ ) at ambient conditions. The principle idea of proposed experiments was to study the details of temperature evolution of crystal structure, to define more exactly the phase diagram "structure-concentration" and to estimate the Neel temperatures for these solid solutions.

The principle results are:

- we have not observed rhombohedral distortions characterizing for solid solutions with small PT concentration [1] at cooling down to 140 K for both compositions (in the limits of experimental resolutions),
- the presence of tetragonal distortions in the cubic high temperature phase was confirmed up to 480 K, i.e. essentially higher than structure phase transition,
- all diffraction patterns at low temperatures can be fitted well as a mixture of high temperature cubic phase and low temperature

tetragonal phase only. The admixture of cubic phase does not exceed 20 %.

- phase diagram "structure-concentration" was specified and the temperatures of structural phase transitions were obtained,

- the temperature dependence of intensity of the antiferromagnetic peak ( $\frac{1}{2} \frac{1}{2} \frac{1}{2}$ ) was obtained for PFW80-PT20 concentration and we have estimated the Neel temperature as  $285(\pm 5)$  K. In a case of PFW70-PT30 the magnetic ordering is suppressed strongly we have observed the magnetic peak ( $\frac{1}{2} \frac{1}{2} \frac{1}{2}$ ) below 200 K at two low temperatures only.

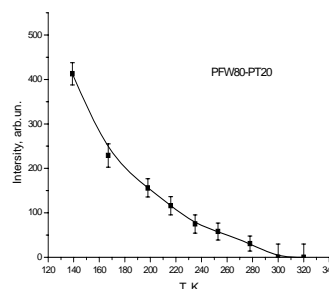


Fig 1 Temperature dependence of integral intensity of  $(\frac{1}{2} \frac{1}{2} \frac{1}{2})$  peak for PFW80-PT20

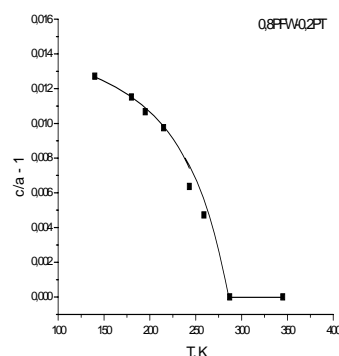


Fig.2 Temperature dependence c/a parameter for PFW80-PT20

1 Vilarinho P.M., Zhou L., Mitoseriu L., Finocchio E., Soares M.R., Baptista J.L. Morphotropic phase boundary in  $(\text{PbFe}_{2/3}\text{W}_{1/3}\text{O}_3)-(\text{PbTiO}_3)$  system // Ferroelectrics. 2002 V. 270. P. 253-258.



## EXPERIMENTAL REPORT

### Neutron scattering study on rattling in filled skutterudite compounds

Proposal N° PHY-01-2343

Instrument **E2**

Local Contact A. Hoser

Principal Proposer: K. Kaneko, ASRC, Japan Atomic Energy Agency, MPI-CPfS

Experimental Team: A. Hoser, HZ Berlin

Date(s) of Experiment

29/10/2008 – 04/11/2008

Date of Report: 15/01/2009

A large amplitude thermal vibration of a guest ion inside a rigid host cage, called 'rattling', is considered to bring characteristic physical properties and thus attracts strong interests. An effect of the rattling is discussed in terms of strong anharmonicity that leads to an appearance of off-center potential minima in some compounds. However, the presence of anharmonicity is not obvious from experimental facts. In addition, correlation between rattling ions is of strong interest but unclear as well.

Filled-skutterudite compound  $\text{PrOs}_4\text{Sb}_{12}$  is the first Pr-based heavy-fermion superconductor with  $T_{\text{sc}} = 1.85 \text{ K}$ [1], in which a Pr ion is incorporated in an over-sized Sb icosahedron cage. An importance of rattling in  $\text{PrOs}_4\text{Sb}_{12}$  was suggested from various works. In fact, the nonmagnetic singlet ground state in  $\text{PrOs}_4\text{Sb}_{12}$  suggests a novel non-magnetic mechanism for the formation of heavy quasiparticles and its superconductivity. A possible existence of off-center potential minima for Pr was also suggested from ultrasound measurements[2]. Our previous neutron diffraction study revealed that the Pr thermal motion has enormously large amplitude at room temperature, and exhibits drastic temperature dependence[3,4]. In this study, single crystal neutron diffraction experiments were carried out in order to get further insights on the rattling in  $\text{PrOs}_4\text{Sb}_{12}$  and its possible relationship with unconventional properties.

Neutron diffraction experiments were carried out on the diffractometer E2. The Ge 3 1 1 monochromator was employed to cover the wide reciprocal space. A single crystalline sample of  $\text{PrOs}_4\text{Sb}_{12}$  with the dimension of  $\sim 4 \times 4 \times 4 \text{ mm}^3$  was used in the present experiment.

We have successfully scanned over the wide reciprocal space up to  $Q = 7.7 \text{ \AA}^{-1}$  with high efficiency. Figure 1 shows the intensity map of  $\text{PrOs}_4\text{Sb}_{12}$  at the  $(h k 0)$  scattering plane measured at room temperature. The

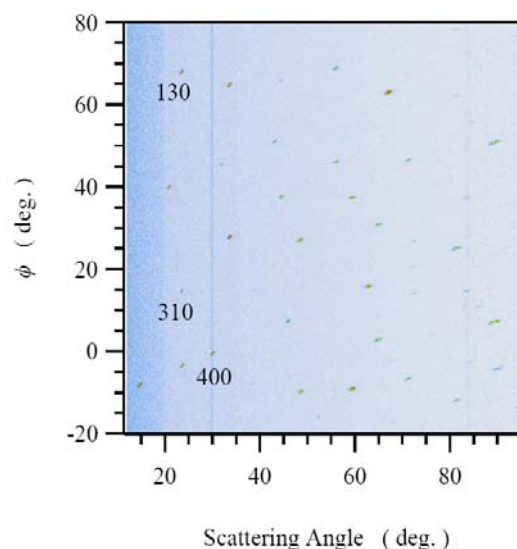


Fig. 1 The intensity map at the  $(hk0)$  scattering plane of  $\text{PrOs}_4\text{Sb}_{12}$  measured at room temperature.

intensity of nuclear Bragg peaks up to  $2\theta = 96^\circ$  was collected in this plane, in which more than 50 peaks were included. The substantial difference in the intensity between 1 3 0 and 3 1 0 reflections was observed, indicating that the present single crystal consists of the mono domain. Any trace of neither diffuse scattering nor superlattice peak was found within the present experimental accuracy. In order to visualize the rattling motion of Pr in the real space, detailed structural analysis using the maximum-entropy method is currently in progress.

#### References

- [1] M. B. Maple *et al.*, J. Phys. Soc. Jpn. **71**, Suppl. pp. 23 (2002).
- [2] K. Kaneko *et al.*, J. Phys. Soc. Jpn. **75**, 034701 (2006).
- [3] K. Kaneko *et al.*, Physica B **403**, 874 (2008).
- [4] T. Goto *et al.*, Phys. Rev. B **69**, 180511(R) (2004).



## EXPERIMENTAL REPORT

### 2<sup>nd</sup> to 3<sup>rd</sup> cross over in CFTD

Proposal N° PHY-01-2348

Instrument **E2**

Local Contact  
Andreas Hoser

Principal Proposer: Tom Fennell, University College London  
(now ILL)

Experimental Team: Andreas Hoser, HZB

Date(s) of Experiment

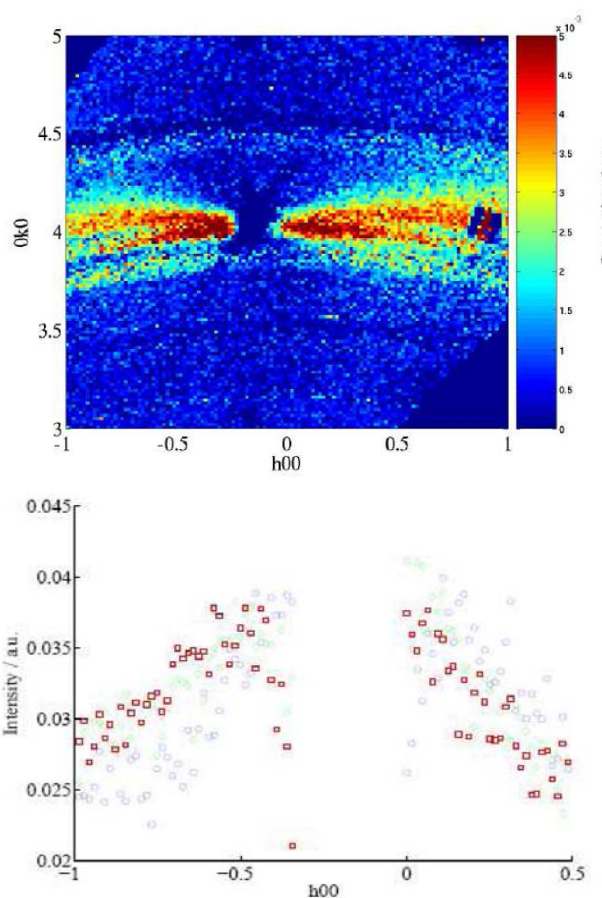
04/11/2008 – 10/11/2008

Date of Report: 14/01/2009

Copper formate tetradeuterate (CFTD) is a model 2d ice: between the copper formate layers water molecules form a two dimensional hydrogen bonded network. As with other ice like systems, there is pinch point scattering due to the specific fluctuation spectrum entailed by such a constraint. Below 245 K three dimensional antiferroelectric order is established between the layers and the cell doubles along the c-axis. In the two dimensional phase the pinch point is part of a two dimensional feature extending out of the  $hk0$  plane. We used the flatcone diffractometer E2 to assess at what temperatures this object is modulated along 001 by the onset of three dimensional correlations.

We measured a region of the scattering plane around 040 at tilts of 0, 6 8 and 10 degrees, sufficient to see the appearance of the 041/2 Bragg peak. This required two settings of the detector. We were able to measure at 270, 248 and 200 K. Unfortunately CFTD crystals dry in air, and react with aluminium. This caused some problems in getting the crystal quickly aligned, stably mounted on copper pieces and into the cryostat. More seriously a copper powder line lies very close to the 040 of CFTD. We have subtracted low temperature data to remove it. Future experiments require a low background, non-aluminium sample mount.

We found that although the scattering shifts toward the centre of the pinch point at low temperatures, even within 3 K of the transition, the diffuse scattering is essentially two dimensional.



Left: the pinch point at 040,  $\mu = 0\sigma$ . Right the intensity integrated along 0k0 at tilts of 0 (blue), 6 (green) and 8 degrees (red),  $T = 248$  K. At this temperature the scattering is shifting toward the centre of the pinch point, but remains independent of tilt, suggesting this process is still due to intra layer fluctuations.

*This research project has been supported by the European Commission under the 6<sup>th</sup> Framework Programme through the Key Action: Strengthening the European Research Infrastructures. Contract n°: RII3-CT-2003-505925 (NMI 3).*

	<b>EXPERIMENTAL REPORT</b>  <b>Crystal structure of UIrGe</b>	Proposal N° PHY-01-2184-EF  Instrument <b>E5</b>  Local Contact M. Reehuis
	Principal Proposer:      K. Prokes, HZB Experimental Team:        M. Reehuis, HZB K. Prokes, HZB	Date(s) of Experiment  10/08/2007 – 19/08/2007

Date of Report: January 2009

Magnetism in uranium-based compounds is controlled by the degree of hybridization of U 5f electron states. UIrGe belongs to orthorhombic UTX ( $T =$  transition metal and  $X =$  Si or Ge) compounds in which hybridization plays a very important role [1]. Despite of the considerable effort over the last two decades it was one of the most puzzling cases among these compounds. Bulk properties of UIrGe point to an antiferromagnetic (AF) order below 16–18K [2]. However different samples that include polycrystals and single crystals behave somewhat differently. The aim of the experiment was to verify whether single crystals prepared under a slightly different conditions by a modified Czochralski method show different structural details that might be responsible for varying physical properties.

In this report we describe a detailed structural determination of a high-quality UIrGe single crystal investigated at room temperature on E5. The wavelength used in the study was 0.89 Å produced by a copper monochromator. We have collected in total 1351 reflections in the range  $-12 \leq h \leq 8$ ,  $-7 \leq k \leq 0$  and  $-13 \leq l \leq 13$ . The full set of reflections was fitted automatically by the computer code *RACER* and the data were further corrected for the substantial absorption caused by iridium and geometrical Lorentz factor. At the end, 691 inequivalent were used in the refinement.

In the literature [1-3] it is suggested all three atoms occupy within the orthorhombic lattice with a space group *Pnma* the 4c ( $x \frac{1}{4} z$ ) Wyckoff position (however, with a distinct  $x$  and  $z$  positional parameters). Nevertheless, we have tried also couple of other crystal structure types, in particularly the disordered variant CeCu<sub>2</sub> in order to exclude possible partial mixing of Ir and Ge atoms. It became quite clear that such a mixing (if exists) is minimal. During the refinement we have varied all the positional parameters, anisotropic thermal factors and Ir and Ge occupational numbers. To account for the extinction effects we have adopted the Zachariasen model assuming a Gaussian distribution of perfect blocks (Fig. 1). The resulting

best fit with a  $R$ -factor of 3.1 % lead to a crystal structure type that is fully conform with the expected TiNiSi type of structure and in good agreement with results given in the literature [1, 2]. The refined stoichiometry is UIr<sub>0.96</sub>Ge<sub>1.01</sub>. However, it should be noted that the Ir occupancy should be taken with a caution because of relatively unprecise knowledge of the Ir scattering length that is in error of 3 % (see Table 1).

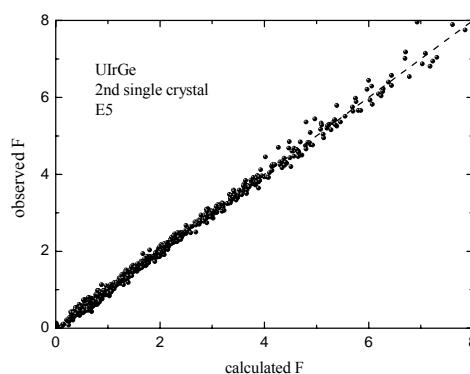


**Fig. 1.** The observed structure factors versus calculated structure factors for UIrGe in the present study.

**Table 1.** Structural parameters of UIrGe from the present study:

	$x$	$y$	$z$	$occ.$
U	-0.00660(7)	$\frac{1}{4}$	0.20225(6)	1.00
Ir	0.21850(7)	$\frac{1}{4}$	0.58715(5)	0.955(4)
Ge	0.81635(9)	$\frac{1}{4}$	0.58568(6)	1.013(5)

The obtained results are to be compared with experimental findings of a similar experiment using another crystal. These are currently under analysis.

### References

- [1] V. Sechovský and V. Havela. In: K.H.J. Buschow, Editor, *Handbook of Magnetic Materials* **Vol. 11**, North-Holland, Amsterdam (1998), p. 1 (Chapter 1).
- [2] K. Prokes, et al., *Phys. Rev. B* **60** (1999) 9532.
- [3] K. Prokes, et al., *Physica B: Condensed Matter* **350** (2004) e199.



**EXPERIMENTAL REPORT**  
**Crystal structure of YFe<sub>0.13</sub>Mn<sub>1.87</sub>O<sub>5</sub>**

Proposal N°  
PHY-01-2287-EF  
Instrument **E5**  
Local Contact  
M. Reehuis

Principal Proposer: N. Aliouane, HMI Berlin  
D. Argyriou, HMI Berlin  
A. Malyuk, HMI Berlin  
Experimental Team: N. Aliouane, HMI Berlin  
M. Reehuis, MPI Stuttgart, HMI Berlin

Date(s) of Experiment  
07/01/2008 – 27/01/2008

Date of Report: 03/02/2008

YMn<sub>2</sub>O<sub>5</sub> is a well known material that exhibits complex magnetic phase transitions [1-4]. Structural properties were reported earlier for the isotopic compounds BiMn<sub>2</sub>O<sub>5</sub> [5] and RMn<sub>2</sub>O<sub>5</sub> (Tb, Ho, Dy, ) [6]. It was shown that these compounds crystallize in the orthorhombic space group *Pbam*. In this structure type the Mn-atoms were found to be at two different Wyckoff positions *4f* (for Mn1) and *4h* (for Mn2). The Mn1-ions show distorted octahedral environments of O-atoms, while the Mn2-atoms are surrounded by five oxygen atoms forming square pyramidal environments. The Mn1- and Mn2-ions occur in the 3d<sup>3</sup>-configuration (Mn<sup>4+</sup>) and 3d<sup>4</sup>-configuration (Mn<sup>3+</sup>), respectively. In the present report we give an account on the structural properties of YFe<sub>x</sub>Mn<sub>2-x</sub>O<sub>5</sub>, where the manganese atoms are partially substituted by iron.

Single-crystal diffraction data have been collected on the four-circle diffractometer E5 using the neutron wavelength was  $\lambda = 0.8839 \text{ \AA}$  (Cu-monochromator). For the experiment we used an untwinned crystal of YFe<sub>x</sub>Mn<sub>2-x</sub>O<sub>5</sub> with dimensions  $1.7 \times 1.7 \times 4 \text{ mm}^3$ . The investigated crystal showed a large mosaic spread. Therefore the refinable mosaic parameter *g* resulted in a value very close to zero suggesting the absence of extinction. Due to the large mosaic spread we were not able to measure a large number of weak Bragg reflections with good accuracy, especially those with higher scattering angles. However, we finally could use a total number of 926 (462 unique) reflections for the crystal structure refinements. The crystal structure of this compounds could be successfully refined in the orthorhombic space group *Pbam*. Here we were able to refine 11 positional parameters of the different atoms as well as 22 anisotropic thermal parameters of the yttrium and oxygen atoms. The results are given in Tables 1 and 2. For the manganese (or iron) atoms we only refined the isotropic thermal parameters, which were constrained to be equal for both atoms in *4f* and *4h*. Furthermore, the refinement of the occupancies of these positions allowed us to find out the content of iron in this material. It was interesting to see that the position *4f* is fully occupied with manganese atoms, which occur in the 3d<sup>3</sup>-configuration (Mn<sup>4+</sup>). The iron atoms were only found to be at the position *4h*, where both transition metal ions occur in the 3+ state. Thus the Mn<sup>3+</sup>- and Fe<sup>3+</sup>-ions show

the 3d<sup>4</sup>- and 3d<sup>5</sup>-configuration, respectively. The refinement showed that 6.6 % of the manganese is substituted by iron.

Table 1. Positional parameters and occupancies of YFe<sub>0.13</sub>Mn<sub>1.87</sub>O<sub>5</sub> at 295 K. The used neutron wavelength was 0.8839 Å.

<i>a</i> = 7.2610(9) Å, <i>b</i> = 8.4786(9) Å, <i>c</i> = 5.6684(8) Å					
<i>Pbam</i>		<i>x</i>	<i>y</i>	<i>z</i>	<i>pop</i>
Y	4g	0.1373(5)	0.1706(4)	0	1.000
Mn1	4f	0	0.5	0.2503(11)	1.001(9)
Fe1	4f	0	0.5	0.2503(11)	0.001(9)
Mn2	4h	0.4164(19)	0.3517(17)	0.5	0.868(7)
Fe2	4h	0.4164(19)	0.3517(17)	0.5	0.132(7)
O1	4e	0	0	0.2660(6)	1.000
O2	4g	0.1604(7)	0.4415(6)	0	1.000
O3	4h	0.1511(7)	0.4313(5)	0.5	1.000
O4	8i	0.3932(4)	0.2055(3)	0.2470(4)	1.000

$R(F) = 0.11$ ,  $R_w(F) = 0.081$ , 926 (462 unique) reflections

Table 2. Selected bond distances (Å) and angles (°) in YFe<sub>0.13</sub>Mn<sub>1.87</sub>O<sub>5</sub> at 295 K.

	Distance / angle
Mn1(4+)-O2	1.901(6)
Mn1(4+)-O3	1.883(6)
Mn1(4+)-O4	1.908(3)
Mn2/Fe2(3+)-O1	1.926(10)
Mn2/Fe2(3+)-O3	2.041(14)
Mn2/Fe2(3+)-O4	1.903(10)
Mn1(4+)-O2-Mn1(4+)	96.5(3)
Mn1(4+)-O3-Mn1(4+)	97.5(3)
Mn1(4+)-O4-Mn2/Fe2(3+)	123.5(4)
Mn1(4+)-O3-Mn2/Fe2(3+)	130.7(2)
Mn2/Fe2(3+)-O1-Mn2/Fe2(3+)	93.0(4)

## References

- [1] A. Ikeda, K. Kohn, *Ferroelectrics* **169** (1995) 75.
- [2] Y. Noda, Y. Fukuda, H. Kimura, I. Kagomiya, S. Matumoto, K. Kohn, T. Shobu, N. Ikeda, J. Kor. Phys. Soc. **42** (2003) S1192.
- [3] S. Kobayashi, T. Osawa, H. Kimura, Y. Noda, I. Kagomiya, K. Kohn, J. Phys. Soc. Jpn. **73** (2004) 1593.
- [4] L.C. Chapon, P.G. Radaelli, G.R. Blake, S. Park, S.-W. Cheong, *Phys. Rev. Lett.* **96** (2006) 097601.
- [5] E.F. Bertaut, G. Buisson, S. Quezel-Ambrunaz, G. Quezel, *Solid State Comm.* **5** (1967) 25.
- [6] G. R. Blake, L.C. Chapon, P.G. Radaelli, S. Park, N. Hur, S.-W. Cheong, J. Rodriguez-Carvajal, *Phys. Rev. B* **71** (2005) 214402.



## EXPERIMENTAL REPORT

### Crystal structure of MgV<sub>2</sub>O<sub>4</sub>

Proposal N°  
PHY-01-2459-EF  
Instrument **E5**

Local Contact M. Reehuis

Principal Proposer: B. Lake –TU Berlin, HZ-Berlin  
E. Wheeler – HZ-Berlin  
N. Islam – HZ-Berlin  
Experimental Team: M. Reehuis, HZ-Berlin  
E. Wheeler, HZ-Berlin  
B. Lake, TU Berlin, HZ-Berlin

Date(s) of Experiment

22/07/2008 – 10/08/2008  
18/08/2008 – 28/08/2008

Date of Report: 02/01/2009

At room temperature MgV<sub>2</sub>O<sub>4</sub> was found to be Mott insulators crystallizing in the cubic normal spinel structure with the space group  $Fd\bar{3}m$  [1, 2]. This compound shows a structural phase transition to a lower symmetric tetragonal phase at about 65 K. The V<sup>3+</sup>-ions form a corner-sharing tetrahedral network and are octahedrally coordinated by six oxygen ions. Tetrahedral networks of localized spins often are governed by strong geometrical frustration and reveal fascinating ground states like a spin liquid or a spin ice.

Single crystals of MgV<sub>2</sub>O<sub>4</sub> were grown by pulling the crystals from the melt in a triarc furnace. Interestingly it could be seen that not all the prepared crystals showed the expected structural phase transition to the tetragonal phase. In order to understand these inconsistencies we have carried out single-crystal neutron diffraction experiments on the four-circle diffractometer E5. This instrument uses a Cu-monochromator selecting the neutron wavelength  $\lambda = 0.89$  Å. For the experiment we have used two high-quality single crystals of MgV<sub>2</sub>O<sub>4</sub> with sample volumes of 270 mm<sup>3</sup> (crystal 1) and 55 mm<sup>3</sup> (crystal 2), respectively. For the smaller sample we found the structural phase transition at about 60 K, whereas the larger one did not show any anomaly down to 6 K.

During the experiment we have checked the condition limiting possible reflections. For the space group  $Fd\bar{3}m$  one finds for  $hkl$ :  $h+k, h+l, k+l = 2n$  and for  $h0l, hk0, 0kl$ :  $h,k,l = 2n$ ;  $h+k, h+l, k+l = 4n$ . But surprisingly we found intensities at the forbidden positions 200, 600, 420, 820 etc., suggesting clearly the extinction rule  $h+k, h+l, k+l = 2n$  for  $h0l, hk0, 0kl$ , respectively. Thus we have carried out the structure refinements in the lower symmetric space group  $F\bar{4}3m$ , where the  $d$ -glide plane is violated. Data sets of MgV<sub>2</sub>O<sub>4</sub> have been collected for each sample (crystals 1 and 2) at room temperature with a total of 1317 (122 unique) and 933 (124 unique) reflections, respectively. In the space group  $F\bar{4}3m$  the two different Mg1 and Mg2 atoms are located at the Wyckoff positions  $4a$  (0,0,0) and  $4c$  ( $\frac{1}{4}, \frac{1}{4}, \frac{1}{4}$ ); the V-, O1- and O2-atoms at the position  $16e$ . The refinement of the overall scale factor, the positional and anisotropic thermal parameters resulted in the very satisfactory residuals  $R_F = 0.016$  ( $R_w = 0.027$ ) for crystal 1, and  $R_F = 0.020$  ( $R_w = 0.025$ ) for crystal 2, respectively. The results of the refinements are presented in Table 1. For comparison the refined parameters of MgV<sub>2</sub>O<sub>4</sub> in the higher symmetric space group  $Fd\bar{3}m$  are also listed in Table 1. For the two samples it is important to note that the refinements in  $Fd\bar{3}m$  as well in  $F\bar{4}3m$  results in the

same occupancies for all the atomic positions. Interestingly it could be found that that the V-position of crystal 1 is partially populated with 2.7% with an excess of Mg. This disordering in the structure may cause the quenching of the structural phase transition. In contrast, for the crystal 2, where this transition has been clearly observed, we found this position fully populated with vanadium. Further it is interesting to see that for both crystals no deficiency could be observed on the oxygen positions.

**Table 1**

Results of the single-crystal neutron diffraction study of MgV<sub>2</sub>O<sub>4</sub> (Crystal 1 and 2) at 295 K. For comparison the crystal structure has also been refined in the higher-symmetric space  $Fd\bar{3}m$  (for crystal 2). The thermal parameters  $U_{ij}$  (given in 100 Å<sup>2</sup>) are in the form  $\exp[-2\pi^2(U_{11} h^2 a^{*2} + \dots 2U_{13} hla^*c^*)]$ ; for symmetry reasons one finds:  $U_{11} = U_{22} = U_{33}$  (for all atoms) and  $U_{12} = U_{13} = U_{23}$  (for the O-atoms);  $U_{12} = U_{13} = U_{23} = 0$  (for the Mg-atoms). Due to the weak scattering power the positional and thermal parameters were not allow to vary. The shortest interatomic distances (in Å) as well as the O-V-O bond angle (in °) are also listed.

	MgV <sub>2</sub> O <sub>4</sub> Cr1, $F43m$	MgV <sub>2</sub> O <sub>4</sub> Cr2, $F43m$	MgV <sub>2</sub> O <sub>4</sub> Cr2, $Fd3m$
$a$ [Å]	8.4415(1)	8.4415(1)	8.4415(1)
$V$ [Å <sup>3</sup> ]	601.53(1)	601.53(1)	601.53(1)
$x$ (O1)	0.38621(9)	0.38591(7)	0.375
$x$ (O2)	0.86616(8)	0.86583(7)	0.875
$U_{11}$ (Mg1/Mg2)	0.64(2)	0.50(2)	0.50(2)
$U_{is}$ (V)	0.50	0.50	0.50
$U_{11}$ (O1 / O2)	0.64(2)	0.50(2)	0.50(2)
$U_{12}$ (O1 / O2)	-0.067(7)	-0.066(7)	-0.059(7)
$occ$ (Mg1/Mg2)	1.00	1.00	1.00
$occ$ (V)	0.973(4)	1.014(4)	1.016(4)
$occ$ (Mg3)	0.027(4)	-0.014(4)	-0.016(4)
$occ$ (O1 / O2)	0.993(13)	0.993(11)	0.993(13)
$d$ (Mg11-O2)	1.9569(7)	1.9617(6)	1.9748(4)
$d$ (Mg12-O1)	1.9916(8)	1.9872(6)	1.9748
$d$ (V-O1) ( $\times 3$ )	2.0201(8)	2.0225(6)	2.0290(4)
$d$ (V-O2) ( $\times 3$ )	2.0385(7)	2.0359(6)	2.0290
O1-V-O1 ( $\times 3$ )	84.51(3)	84.67(2)	85.10(2)
O1-V-O2 ( $\times 6$ )	94.88(3)	94.88(2)	94.90(2)
O2-V-O2 ( $\times 3$ )	85.73(3)	85.56(2)	85.10(2)

#### References

- [1] M. Onoda, H. Imai, Y. Amako, H. Nagasawa, Phys. Rev. B. **56** (1997) 3760.
- [2] O. Tchernyshyov, Phys. Rev. Lett. **93** (2004) 157206.



**EXPERIMENTAL REPORT**  
**Phase transitions of the spinel MgV<sub>2</sub>O<sub>4</sub>**

Proposal N°  
 PHY-01-2459-EF  
 Instrument **E5**

Local Contact M. Reehuis

Principal Proposer: B. Lake –TU Berlin, HZB, Berlin  
 E. Wheeler – HZB, Berlin  
 N. Islam – HZB, Berlin  
 Experimental Team: M. Reehuis – HZB, Berlin  
 E. Wheeler – HZB, Berlin  
 H.-J. Bleif – HZB, Berlin

Date(s) of Experiment

02/09/2008 – 07/09/2008  
 15/12/2008 – 21/12/2008

Date of Report: 14/01/2009

We are investigating the vanadium spinel material MgV<sub>2</sub>O<sub>4</sub> which has both spin and orbital degrees of freedom in a frustrated lattice. We want to observe and understand any ordering of the orbitals and spins and their effect upon the spin interactions.

The aim of this experiment was to investigate the structural and magnetic phase transitions of MgV<sub>2</sub>O<sub>4</sub> using crystals with slightly different compositions. In our first experiment on E9 we could clearly evidenced the presence of the two phase transitions from a powder sample. In order to investigate the phase transitions in more detail, we have measured two different crystals of MgV<sub>2</sub>O<sub>4</sub> on the four-circle diffractometer E5. We mounted each single crystal of MgV<sub>2</sub>O<sub>4</sub> on the closed-cycle refrigerator of the four circle diffractometer E5, where we could reach a base temperature of 6 K. We made measurements using incident wavelength  $\lambda = 2.4 \text{ \AA}$  (PG-monochr.).

For the first crystal of MgV<sub>2</sub>O<sub>4</sub> we could see that neither the structural nor the magnetic structure was detectable. Further experiments on E5 clearly showed that a structural disorder in the crystal leads to a quenching of both phase transitions. In contrast, for the second crystal we found a large increase in intensity of the strong reflection 004 as we went through the structural phase transition as seen in Fig. 1, probably due to the strong change of extinction (or change of mosaicity). The transition occurred between 48 K and 60 K indicating a range where both the cubic and tetragonal phase are coexisting, which has already been observed in our pervious E9 measurement. Below the Néel temperature  $T_N = 38(1) \text{ K}$  we observed the smooth increase in intensity from the magnetic Bragg reflections, as shown in Fig. 1. This shows the onset of the magnetic order of the V-moments.

To further investigate the phase coexistence and the to extract the lattice parameters of the two phases we carried out X-ray powder diffraction measurements using the Guinier geometry. A plot of the lattice parameters and the region of phase coexistence is given in Fig. 2. It has to be mentioned, that there is a temperature difference between the X-ray measurements and the neutron measurements. For the x-ray measurements it's probably difficult to measure the correct temperature, because the sample was mounted on

a plastic film and so not in good thermal contact with the thermo couple.

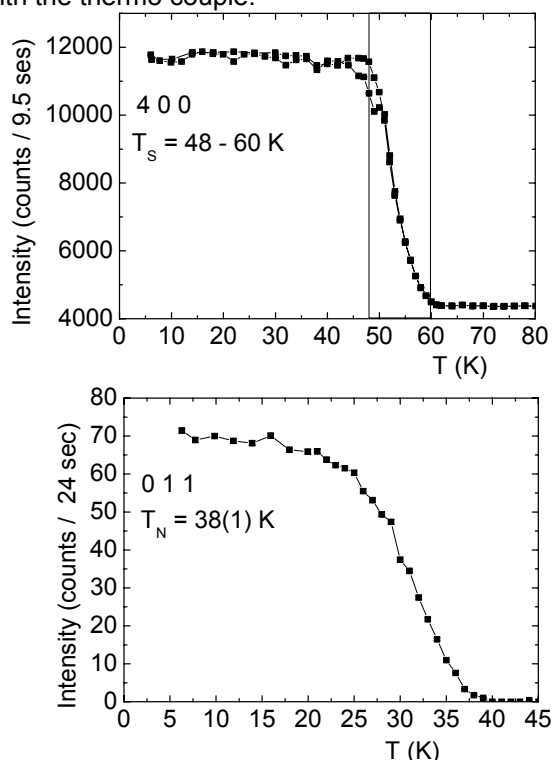


**Figure 1.** Single-crystal diffraction results: The change of intensity of the structural reflection 400 indicating the structural phase transition from the cubic to tetragonal phase transition. The magnetic reflection 110 shows the magnetic transition temperature at 37 K.

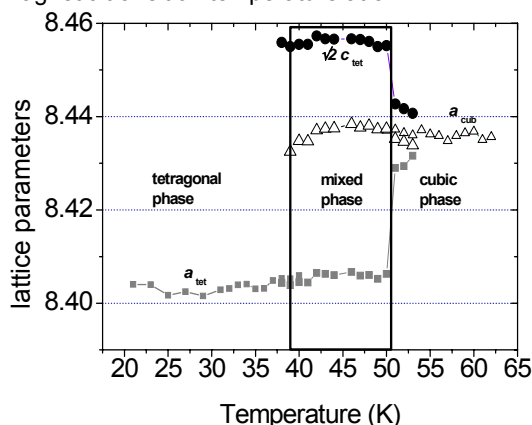


**Figure 2.** Results of the x-ray powder diffraction measurements showing the change in lattice parameters on cooling through the structural phase transition.



## EXPERIMENTAL REPORT

### Crystal structure, vacancy order and cation distribution in CuGaSe<sub>2</sub>-related semiconductors

Principal Proposer: Sebastian Lehmann - Helmholtz-Zentrum Berlin für Materialien und Energie  
 Experimental Team: David Fuertes Marrón - Instituto de Energía Solar - ETSIT, Madrid, Spain  
 Michael Tovar - Helmholtz-Zentrum Berlin für Materialien und Energie

Proposal N°s  
 MAT-01-1858  
 MAT-01-1953

Instrument **E9**

Local Contact  
 Michael Tovar

Date(s) of Experiment

07.04.-12.04.2006  
 21.11.-27.11.2006

Date of Report:

I-III-VI<sub>2</sub> Cu-containing chalcopyrites are materials of high interest in the field of thin-film photovoltaics and solar cell applications [1]. Whereas theoretical studies postulate the existence of internal stabilisation mechanisms in Cu-poor I-III-VI<sub>2</sub>s by periodic arrangement of defect pairs [2] leading to 1:3:5 and/or 1:5:8 compositions, while maintaining the chalcopyrite structure, the analysis of XRD results reported so far does not exclude other possibilities [3,4]. The experiment of the „1:1:2/1:3:5/1:5:8“ transition was aimed at the elucidation of cation distribution in „off-ideal-stoichiometric-composition“ samples of the type CuGa<sub>x</sub>Se<sub>y</sub> including single- and mixed- chalcopyrite/OVC phases of model and photovoltaic device-relevant material. The focus was set on the gallium-containing system because of relatively scarce availability of structural information about these compounds.

Sample preparation covering the compositional range from CuGaSe<sub>2</sub> to CuGa<sub>5</sub>Se<sub>8</sub> was twofold. Synthesis from the elements followed by post annealing [5] lead to polycrystalline, structural and compositional homogeneous samples. These served as references for photovoltaic relevant polycrystalline thin-film material which was synthesized by the chemical close-spaced vapour transport (CCSVT) process [6].

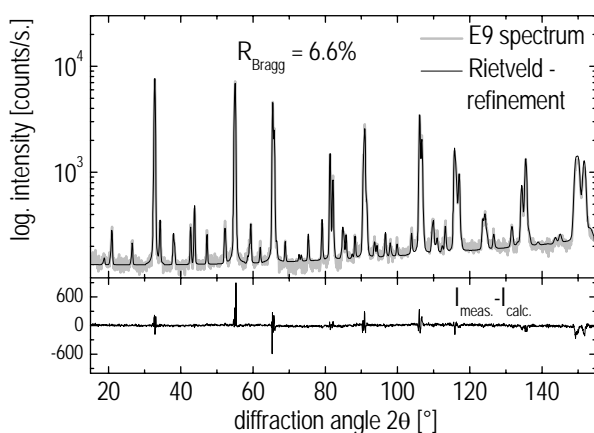


Fig. 1: Neutron diffraction measurement, Rietveld-refinement and resulting residuum for a CuGa<sub>3</sub>Se<sub>5</sub> powder sample based on a stannite-type-related structural model.

The powder samples were measured at the E9 neutron powder diffractometer followed by adjacent Rietveld-analysis. All available structural models for Cu(III)<sub>3</sub>Se<sub>5</sub>

and Cu(III)<sub>5</sub>Se<sub>8</sub> (III=In,Ga) respectively were used as input models [see 5]. As the main finding the proposal of a new structural model for the copper-poor compounds CuGa<sub>3</sub>Se<sub>5</sub> and CuGa<sub>5</sub>Se<sub>8</sub> can be stated [figs 1 and 2]. This was successfully made accessible due to the application of neutron diffraction technique resolving the different contributions of the isoelectronic species Cu<sup>+</sup> and Ga<sup>3+</sup>. Nevertheless, the proposed periodic arrangement of defect pairs [2] could neither be proved nor disproved.

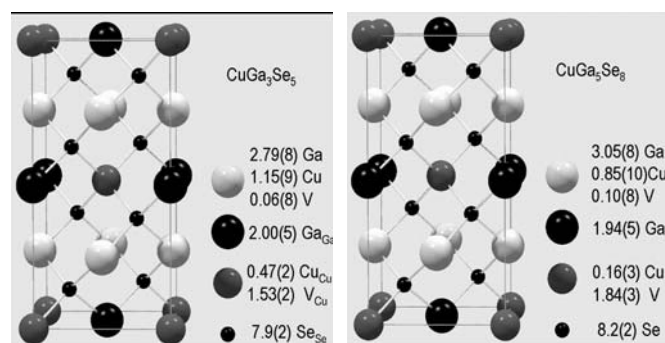


Fig. 2: New structural models proposed for CuGa<sub>3</sub>Se<sub>5</sub> (left) and CuGa<sub>5</sub>Se<sub>8</sub> (right) based on Rietveld-analysis of neutron and X-ray diffraction measurement.

Considering the CuGaSe<sub>2</sub>-Ga<sub>2</sub>Se<sub>3</sub> segment of Cu<sub>2</sub>Se-Ga<sub>2</sub>Se<sub>3</sub> pseudobinary cut of the Cu-Ga-Se phase diagram and the new structural model, three regions can be separated. Samples are single phase exhibiting the chalcopyrite structure (*sg.I42d*) in the compositional range CuGaSe<sub>2</sub>-CuGa<sub>1.5</sub>Se<sub>2.8</sub> and the new proposed stannite-type related structure (*sg.I42m*) from CuGa<sub>3</sub>Se<sub>5</sub> to CuGa<sub>5</sub>Se<sub>8</sub>. In between these regions namely CuGa<sub>1.5</sub>Se<sub>2.8</sub>- CuGa<sub>3</sub>Se<sub>5</sub> both structural phases coexist.

In order to investigate structural phase transitions measurement conditions were chosen which based on high temperature synchrotron experiments. Unfortunately in turned out that this conditions were unsuitable for the carried out E9 experiments.

- [1] Nishiwaki S. et al., Mat. Res. Soc. Symp. Proc. **763** (2003) B5.18.1.
- [2] Zhang S.B. et al., Phys. Rev. Lett. **78** (1997) 4059.
- [3] Hanada T. et al., Jpn. J. Appl. Phys. **36** (1997) L1494.
- [4] Merino J.M. et al., J. Phys. Chem. Sol. **64** (2003) 1649.
- [5] Lehmann, S. PhD thesis, Freie Universität Berlin, 2007
- [6] Rusu, M. et al., Thin Solid Films, 451-452(2006) 556-561



## EXPERIMENTAL REPORT

### Crystal structure of the $\text{CuIn}_3\text{Se}_5\text{-CuGa}_3\text{Se}_5$ solid solution series

Proposal N° PHY-01-2201

Instrument **E9**

Local Contact  
Michael Tovar

Principal Proposer: Susan Schorr - FU Berlin  
Michael Tovar, Sebastian Lehmann –  
Experimental Team: Helmholtz-Zentrum Berlin für Materialien und Energie  
José Manuel Merino, Máximo León, Josue Friedrich Universidad Autónoma de Madrid

Date(s) of Experiment

16/04/2008 – 23/04/2008

Date of Report:

The highest performance parameters among the thin film solar cell devices are provided by chalcopyrite-based structures working with  $\text{Cu}(\text{In}_{1-x}\text{Ga}_x)\text{Se}_2$  quaternary absorbers. These materials show a copper-depleted near surface region with stoichiometries close to 1:3:5 or 1:5:8 [1-3]. There is a basic need of understanding the structural properties of also the quaternary solid solution series  $\text{Cu}(\text{In}_x\text{Ga}_{1-x})_3\text{Se}_5$  and  $\text{Cu}(\text{In}_x\text{Ga}_{1-x})_5\text{Se}_8$ . These compounds of the stoichiometry  $\text{Cu}(\text{B}^{\text{III}})_3\text{Se}_5$  and  $\text{Cu}(\text{B}^{\text{III}})_5\text{Se}_8$  ( $\text{B}^{\text{III}} = \text{Ga}, \text{In}$ ) are named Ordered Vacancy Compounds [4-6], Ordered Defect Compounds [7] or Defect Compounds [8-10]. The names are due to the assumption of an ordering of vacancies, defects or no ordering. Nevertheless the knowledge about these copper-deficient phases is poor. Thereby, the system Cu-In-Se is studied superior than the Cu-Ga-Se system, but mainly based on X-ray or electron diffraction data [9-15] (except a study on  $\text{CuGa}_x\text{Se}_y$  ( $1 < x < 5$ ,  $2 < y < 8$ ) see MAT's 01-1858/1953).

From our experiments at the E9 neutron diffractometer with samples covering the full-range solid solution series  $\text{Cu}(\text{In}_x\text{Ga}_{1-x})_3\text{Se}_5$  ( $0 < x < 1$ ) we were able to extract structural parameters by Rietveld refinement, namely the space group, lattice parameters and cation distributions. For this purpose we used the Fullprof software package [16]. Adopting all so far published structural models for the so-called ordered vacancy compounds (OVCs) or related denotations for the refinements we were able to establish a stannite-type structure [ $\bar{1}42m$ ] related structural model for all members of the  $\text{Cu}(\text{In}_x\text{Ga}_{1-x})_3\text{Se}_5$  ( $0 < x < 1$ ) solid solution series which was proposed for  $\text{CuGa}_{3.5}\text{Se}_{5.8}$  in ref. [17] and for  $\text{CuIn}_3\text{Se}_5$  in ref [10]. All other models were excluded due to inconsistencies in refinement results like e.g. too high quality factors, over-occupations, anomalous high temperature factors etc..

Arising from this final structural model we have one site (8i) which is, apart from minor deficiencies (<5%), fully occupied by selenium and three cationic sites. The first of which, the 2a site, is occupied with  $\frac{3}{4}$  of vacancies and  $\frac{1}{4}$  of copper, the 2b site statistically by indium and gallium and the 4d site statistically by copper, indium and gallium. The experimentally determined scattering lengths for all corresponding lattice sites are given in figure 1 with limits for full occupation of each site for the respective elements. Additionally a composition-dependent calculated curve of these values, corresponding to statistical occupation for the respective sites 2b and 4d by indium and gallium, is also given. Despite some minor deviations from the theoretical values we found a good agreement between experimental data and

the calculated characteristics. The above mentioned deviations are most significant for the boundary composition materials  $\text{CuGa}_3\text{Se}_5$  and  $\text{CuIn}_3\text{Se}_5$  respectively and could be interpreted to stem from selenium deficiency for the first and a partial occupation of copper on the 2b site for the latter compound.

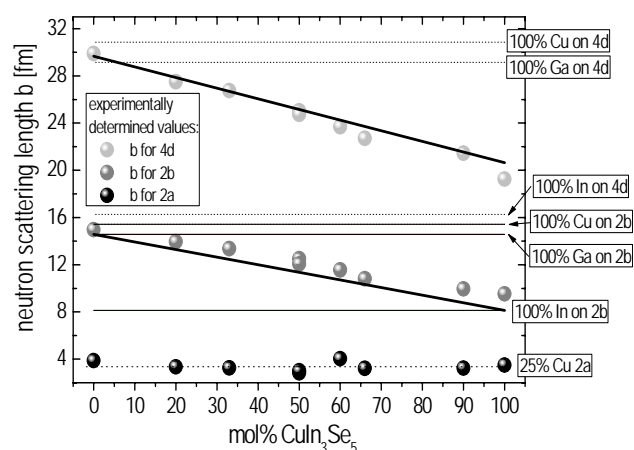


Figure 1: Composition dependent neutron scattering length for 3 cation sites 2a,b and 4d in the stannite-type related structure for the  $\text{Cu}(\text{In}_x\text{Ga}_{1-x})_3\text{Se}_5$  ( $0 < x < 1$ ) solid solution series.

Preliminary results of the  $\text{Cu}(\text{In}_x\text{Ga}_{1-x})_5\text{Se}_8$  ( $0 < x < 1$ ) solid solution series are revealing more or less identical findings as it is the case for the 1:3:5 series in terms of the structural model but of course show differences in e.g. lattice parameters and occupation factors. The evaluation of the latter series is still in progress and results will be presented later.

*This research project has been supported by the DAAD PPP-program "Acciones Integradas Hispano-Alemanas" under contract n°: "314-Al-er".*

- [1] Schmid et al. *Apl. Surf. Science* 103 (1996) 409-429
- [2] Klenk et al. *Adv. Mater.* 5 (2) (1993) 114-119
- [3] Meeder et al. *Journ. Phys. Chem. Solids* 64 (2003) 1553-1557
- [4] Bernard et al. *Physical Review B* 37 (12) (1988) 6835
- [5] Tseng et al. *Japanese Journal of Applied Physics* 65 (6) (1989) 2254
- [6] Zhang et al. *Physical Review Letters* 78 (21) (1997) 4059
- [7] Zhang et al. *Physical Review B* 57 (16) (1998) 9642
- [8] Chang et al. *Physical Review B* 68 (2003) 541081
- [9] Hanada T. et al., *Jpn. J. Appl. Phys.* 36 (1997) L1494.
- [10] Paskowicz et al. *Journal of Alloys and Compounds* 362 (2004) 241
- [11] Marin et al. *Materials Research Bulletin* 33 (7) (1998) 1057
- [12] Hönle et al. *Cryst. Res. Tech.* 23 (10/11) (1988) 1347-1354
- [13] Manoliukas et al. *Phys. Stat. Sol. (a)* 55 (1979) 709-722
- [14] Merino et al. *Phys. Rev. B* 61 (15) (2000) 10211-10215
- [15] Merino et al. *Journ. of Phys. Chem. Sol.* 64 (2003) 1649-1652
- [16] <http://www.ill.fr/pages/Science/Diff/Soft/Fp/>
- [17] S. Lehmann, PhD-Thesis, FU Berlin 2007



## EXPERIMENTAL REPORT

### Neutron Diffraction of "real" Cu/ZnO/Al<sub>2</sub>O<sub>3</sub> Catalysts for Methanol Synthesis

Proposal N° CHE-01-2202

Instrument E9

Local Contact  
Dr. M. Tovar

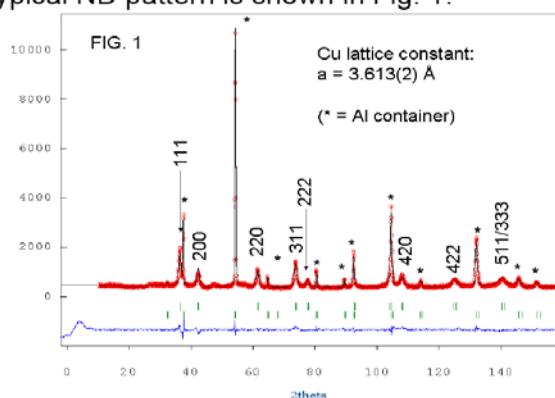
Principal Proposer: Malte Behrens, Fritz-Haber-Institut, Abteilung AC, Berlin  
 Experimental Team: Stefanie Kühl, Fritz-Haber-Institut, Abteilung AC, Berlin  
 Andreas Furche, Fritz-Haber-Institut, Abteilung AC, Berlin  
 Michael Tovar, Helmholtz-Zentrum, BENSC, Berlin  
 Dirk Wallacher, Helmholtz-Zentrum, BENSC, Berlin

Date(s) of Experiment

18/02/2008 – 21/02/2008  
 08/10/2008 – 09/10/2008  
 18/10/2008 – 22/10/2008

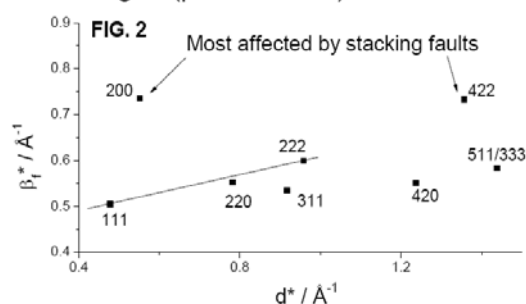
Date of Report: 13/01/2009

Industrially applied Cu/ZnO/Al<sub>2</sub>O<sub>3</sub> catalysts for methanol synthesis consist of Cu nanoparticles separated by oxide spacers. These particles are difficult to characterize by means of X-ray diffraction due to their small domain size and highly symmetric crystal structure, which allows typically only 3-4 reflections to be evaluated for a microstructural analysis at reasonable counting times. Neutron diffraction (ND) provides an alternative approach and three industrially relevant samples were activated and submitted to ND. One sample was highly active, while two samples exhibited a comparable lower activity (76 and 82% relative to the former). The Rietveld fit of a typical ND pattern is shown in Fig. 1.

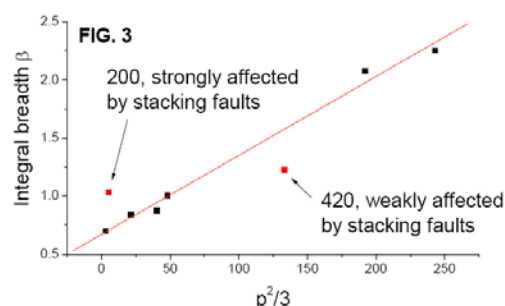


The lattice parameter of Cu and the microstructural properties of the particles can be determined on the basis of eight resolved reflections, including higher diffraction orders for the 111 line. Figure 2 is an indexed Williamson-Hall plot of the data shown in Fig. 1. The data distribution suggests presence of stacking faults in the catalyst as the lines 200 and 422, which are most affected by stacking disorder in fcc materials show the broadest profiles. All other reflections fall more or less on a horizontal line indicating the absence of anisotropy, which is in line with the spherical shape of the nanoparticles observed in TEM. A pronounced positive slope of the 111 – 222 line indicative of microstrain was only observed for the most active sample. Furthermore, this was the only sample showing indications of

paracrystallinity, which is evidenced by a straight line in the integral breadth vs.  $p^2/3$  plot shown in Fig. 3 ( $p^2 = h^2 + k^2 + l^2$ ).



Paracrystallinity is caused by the random incorporation of foreign atoms or groups in a host crystal lattice and was found e.g. in industrial ammonia synthesis catalysts.



Although no quantitative correlations of microstructure and activity have been revealed yet, these results strongly support the idea of a uniquely defective Cu lattice in active nanoparticles, which influences the surface properties and, hence, the catalytic activity of Cu. Furthermore, the applicability of ND to technical Cu catalysts in an Al sample holder setup (Al peaks marked with \* in Fig. 1) was established as a prerequisite for forthcoming in-situ experiments.

*This research project has been supported by the Federal Ministry of Education and Research of Germany (FKZ 01RI029)*

	<b>EXPERIMENTAL REPORT</b>  <b>Proton Mobility in Solid Super Proton Conductors</b>	Proposal N° CHE-01-2203 Instrument <b>E9</b>  Local Contact Dr. M. Tovar
	Principal Proposer: Prof. Dr. Dr. M. Lerch, Institute of Chemistry, TU Berlin Experimental Team: Prof. Dr. C. A. C.-Dreismann, Institute of Chemistry, TU Berlin Dr. T. Abdul-Redah, Institute of Chemistry, TU Berlin Dr. M. Tovar, HMI Dr. S. Kimber, Dr. F. Yokaichiya, HMI	Date(s) of Experiment  30/05/2008 – 03/06/2008

Date of Report: 28/07/2008

Our present research project focuses on the development and optimization of crystalline solid proton conductors as an alternative to the commonly used polymer membranes. Moreover, we focus on the fundamental understanding of solid proton conductors, e.g. the correlation between crystal structure and mobility of the ions. Promising candidates for these investigations are  $(\text{H}_3\text{O})\text{SbTeO}_6$  and  $\text{Rb}_3\text{H}(\text{SO}_4)_2$ , both super proton conductors with an outstanding proton conductivity at “low” temperatures.

We have carried out diffraction measurements at  $T = 50 \text{ K}$ ,  $295 \text{ K}$  and  $500 \text{ K}$  with both compounds, using neutron wavelength of  $1.31 \text{ \AA}$ , which is appropriate for our purposes, e.g. study of mobility and diffusion pathways of the ions from detailed analysis of the probability density function (pdf) maps after a refinement of the Debye-Waller factors.

Extensive data analysis after the measurements (being still in progress) revealed various **preliminary** striking results of considerable interest. Two of them are as follows:

(1) The comparison of the diffraction data of  $(\text{H}_3\text{O})\text{SbTeO}_6$  at the three investigated temperatures provides first evidence for the mechanism of proton mobility: The data at  $295 \text{ K}$  and  $500 \text{ K}$  (in which the material is a very good conductor) show that the motion of a H atom of  $\text{H}_3\text{O}$  is oriented towards an O-atom in the window of the  $\text{SbTeO}_6$ -cage (not through the middle of the window), whereas the O-atom shows no such preference. In contrast, at  $T = 50 \text{ K}$ , the thermal ellipsoid of H is oriented otherwise (static disorder). These findings strongly indicate that the proton mobility is **not** due to that of  $\text{H}_3\text{O}$ , but only to that of a single proton. This furthermore seems to imply that the macroscopic proton conductivity is a cooperative process, in which every single proton moving away must be replaced immediately with another one of an adjacent  $\text{H}_3\text{O}$ -unit. In addition, this material is now

investigated using QENS, INS, NCS, Solid State NMR, and Raman Spectroscopy.

(2) The diffraction data of  $\text{Rb}_3\text{H}(\text{SO}_4)_2$  reveal the following surprising feature: The H position appears **not** to be symmetric between the two O-sites constituting a “symmetric H-bond”, as one would intuitively expect. Instead, H appears to occupy one of two sites strongly outside the above O-O axis. (This result is clearly demonstrated at  $T = 295 \text{ K}$ , but further measurements must be done) Moreover, and perhaps more importantly, this finding strongly questions the validity of the main results of Ref. [D. Homouz et al., *PRL* 98, 115502 (2007)], and the claimed “first direct measurement of the proton 3D Born-Oppenheimer potential in any material”. Due to this physical context and its implications to other neutron-scattering fields (see e.g. the above reference), we intend to look into the matter in greatest detail. This system is now theoretically investigated by DFT and MD calculations in collaboration with G. Kearley, Australia.

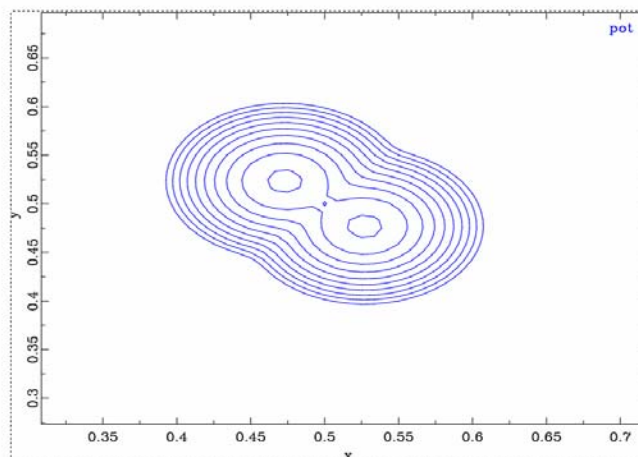


FIG: Determined potential for H in  $\text{Rb}_3\text{H}(\text{SO}_4)$  at  $T = 50 \text{ K}$  (H. Boysen). The O-O direction of the assumed “symmetric O-H-O bond” is along the x-axis; cf. D. Homouz et al., *PRL* 98, 115502 (2007)].



## EXPERIMENTAL REPORT

### In situ Neutron Powder Diffraction Study of CD<sub>4</sub> Adsorption in Cu<sub>3</sub>(1,3,5-benzenetricarboxylate)<sub>2</sub>

Proposal N° CHE-01-2205

Instrument **E9**

Local Contact M. Tovar

Principal Proposer: Prof. Dr. Stefan Kaskel, TU-Dresden  
Experimental Team: Dr. Dirk Wallacher, Experimental Environment  
Dr. Michael Tovar, Experiment Station E9  
Department of Inorganic Chemistry, Technical University Dresden

Date(s) of Experiment

23/04/2008 – 26/04/2008

Date of Report: 08/02/2009

Porous metal organic frameworks (MOFs) are a new class of porous materials. They are of great interest for gas adsorption, catalysis, and gas storage. A special interest is methane storage in MOFs for mobile applications in cars. The experiment concentrates on the *in situ* investigation of the location of adsorbed molecules of deuterio methane (methane d<sub>4</sub>) in Cu<sub>3</sub>(Btc)<sub>2</sub> (Btc = benzene-tricarboxylate) with neutron powder diffraction (see report 2007) in order to get a deeper insight into adsorption mechanisms.

1.148 g (20 mmol) Cu<sub>3</sub>(Btc)<sub>2</sub> were dried and filled in the sample cell. Neutron powder data were recorded at 77 K. Methane d<sub>4</sub> was dosed to the Cu<sub>3</sub>(Btc)<sub>2</sub> material at 77 K in four steps up to 21.1 mmol corresponding to the maximum adsorption capacity. For the maximum filling, the location of methane molecules was determined from the neutron powder data (figure 1).

Measurement details: Each measurement was carried out using the E9 neutron powder diffractometer. The scan range was 2Theta = 3 – 156°, lambda was equal to 2.816 angstrom. The measuring time was 12 h for each degree of filling. Afterwards all diagrams were equally normalized (1Mio monitor-counts) and integrated.

Figure 1 shows a section of the measured neutron diffractograms between 2Theta = 3 – 71°: bottom: pure Cu<sub>3</sub>(Btc)<sub>2</sub>; middle: Cu<sub>3</sub>(Btc)<sub>2</sub> with around 50% filling of CD<sub>4</sub>; at the top: complete filling with CD<sub>4</sub>.

The results from the Rietveld refinement of the 50% and 100% filling can be interpreted in terms of crystallographic positions that are not completely filled. The CD<sub>4</sub> molecules are filling all pores of the Cu<sub>3</sub>(Btc)<sub>2</sub>, and the main adsorption sites can be located.

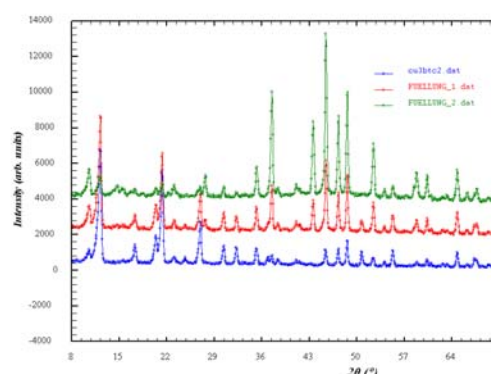


Fig 1: a section of the neutron powder diffractograms from empty Cu<sub>3</sub>(Btc)<sub>2</sub> (blue) to 100% (green) CD<sub>4</sub> sorption in Cu<sub>3</sub>(Btc)<sub>2</sub>.

Cu<sub>3</sub>(Btc)<sub>2</sub> has a bimodal pore size distribution. Two positions were identified in the smaller pore, one in the center, and one at the pore openings (Fig. 2). The larger pore shows 8 different adsorption positions and accompanies approximately 33 CD<sub>4</sub> molecules in total.

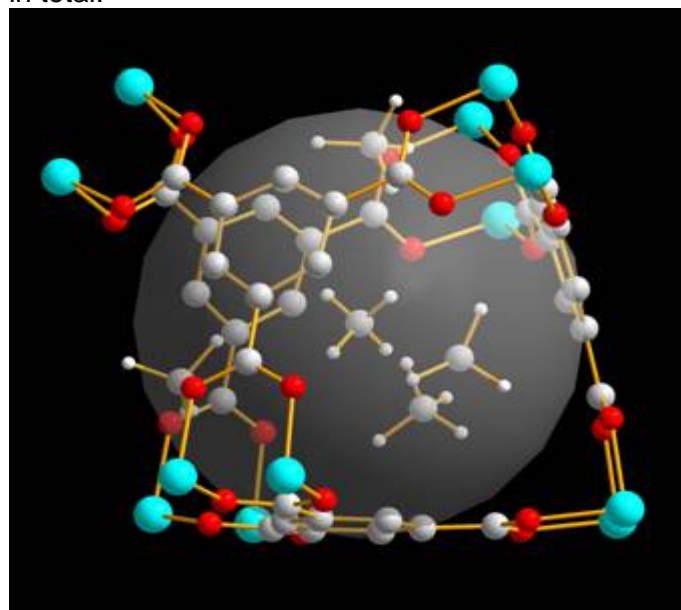


Fig 2: Location of CD<sub>4</sub> molecules in the small pore of Cu<sub>3</sub>(Btc)<sub>2</sub>.

	<b>EXPERIMENTAL REPORT</b>	Proposal N° CHE-01-2211 Instrument <b>E9</b>
	<b>Structural and order-disorder effects of water uptake in proton conducting perovskites</b>	Local Contact Simon Kimber
Principal Proposer: Niina Jalarvo, University of Oslo, FERMIO - Functional Energy Related Materials in Oslo, Norway Experimental Team: Nadir Aliouane, IFE, Institute for Energy Technology, Norway Dirk Wallacher, Helmholtz-Zentrum Berlin für Materialien und Energie GmbH Truls Norby, University of Oslo, FERMIO - Functional Energy Related Materials in Oslo, Norway	Date(s) of Experiment  13/05/2008 – 21/05/2008	

Date of Report: 15/01/2009

Protonic conductors are promising materials for a number of energy technological applications. Lately much interest has been put on oxide deficient complex perovskites, which reveal high protonic conductivity at appropriate temperatures at humid atmospheres suitable for high temperature fuel cell.

$\text{Sr}_4(\text{Sr}_2\text{Ta}_2)\text{O}_{11}$  is a member of a series of oxygen deficient complex perovskites of general formula  $\text{A}^{\text{II}}_4(\text{B}^{\text{II}}_2\text{B}^{\text{V}}_2)\text{O}_{11}\cdot v_o$  (where  $v_o$  stands for oxygen vacancy). This class of perovskites exhibits oxide ion (vacancy) conductivity in dry atmospheres and protonic conductivity in wet atmospheres. In presence of water vapour (in this case  $\text{D}_2\text{O}$ ) the perovskite will hydrate into  $\text{Sr}_4(\text{Sr}_2\text{Ta}_2)\text{O}_{11}\cdot n\text{D}_2\text{O}$  ( $0 \leq n \leq 1$ ). The water incorporation is a critical phenomenon for the proton conducting mechanism. Furthermore, it is assumed that the oxygen vacancy distribution affects strongly the charge carrier mobility. Interestingly, the hydrated oxide may exhibit order-disorder on *three* sublattices as a function of temperature and water content: the B-cation sublattice, the oxide ions and vacancies, and the deuterons.

In order to shed light into the order-disorder processes we have performed neutron powder diffraction studies at E9 spectrometer in dry and humid ( $p\text{D}_2\text{O} = 1$  bar) atmospheres between room temperature and 700 °C. The humid atmosphere was produced using the DeGAS system connected to a high temperature furnace with a Suprasil quartz tube (which has very low H content), as an insert.  $\text{D}_2\text{O}$  vapour was created outside of the furnace, by heating a small volume of  $\text{D}_2\text{O}$ , which was delivered into the DeGas system through

heated tubing to avoid condensation of the vapour.

The preliminary data analysis has been performed using GSAS and FullProf software packages. For  $\text{Sr}_4(\text{Sr}_2\text{Ta}_2)\text{O}_{11}$  the best refinements were obtained considering a cubic space group  $\text{Fm}\bar{3}m$ , with  $a = 8.3007 \text{ \AA}$ . Compared to an ordinary perovskite structure, this model contains additional “interstitial” oxygens at Wyckoff position 48g. Occupancy of these 48g positions is only about 5%, whereas there is also a slight deficiency at the octahedral oxygen sites. Furthermore, the Fourier maps reveal short-range oxygen disorder to large extent, which can be also seen at the diffraction patterns as diffuse background. Static short range disorder of the O sites complicates the structural picture of dry  $\text{Sr}_4(\text{Sr}_2\text{Ta}_2)\text{O}_{11}$ , and is also most probably responsible for the ionic transport properties of this material.

Quantitative comparison of the patterns collected for anhydrous and hydrated samples, indicates that the structure shrinks upon hydration. Refining the D sites of the  $\text{Sr}_4(\text{Sr}_2\text{Ta}_2)\text{O}_{11}\cdot n\text{D}_2\text{O}$  is a challenge and still under process.

Acknowledgements:

*This research project has been supported by the European Commission under the 6<sup>th</sup> Framework Programme through the Key Action: Strengthening the European Research Infrastructures.*

*Contract N°: RII3-CT-2003-505925 (NMI 3).*

*This work is supported by the FRINAT project 171157/V30 “Hydrogen in oxides (HYDROX)” of the Research Council of Norway.*



## EXPERIMENTAL REPORT

### High-resolution neutron diffraction study on the phase transitions in $\text{Cu}_{1-x}\text{Zn}_x\text{Fe}_2\text{O}_4$

Proposal N° MAT-01-2213

Instrument **E9**

Local Contact  
F. Yokaichiya

Principal Proposer: W. Nowicki, - AMU Poznań, Poland  
Experimental Team: W. Nowicki, - AMU Poznań  
F. Yokaichiya, - HMI, Berlin

Date(s) of Experiment

21/05/2008 – 26/05/2008

Date of Report: 28/06/2008

Ferrimagnetic cubic spinels are technically important materials, they have been extensively investigated in order to improve good soft magnetic compounds [1-3]. Modifications in the properties of copper ferrite ( $\text{CuFe}_2\text{O}_4$ ) due to the substitution of various ions have been studied by various workers [4-6]. We report new results obtained for the series of compounds  $\text{Cu}_{1-x}\text{Zn}_x\text{Fe}_2\text{O}_4$ . Neutron diffraction patterns of  $\text{CuFe}_2\text{O}_4$  and  $\text{Cu}_{0.95}\text{Zn}_{0.05}\text{Fe}_2\text{O}_4$ , recorded in the temperature range from 30°C to 500°C are shown in Fig.1 respectively. Substitution with very small quantities of  $\text{Zn}^{2+}$  ions ( $x = 0.05$  in  $\text{Cu}_{1-x}\text{Zn}_x\text{Fe}_2\text{O}_4$ ) decreases the tetragonal ( $F4_1/ddm$ ) to cubic ( $Fd3m$ ) transition temperature about 100°C (Fig.1).

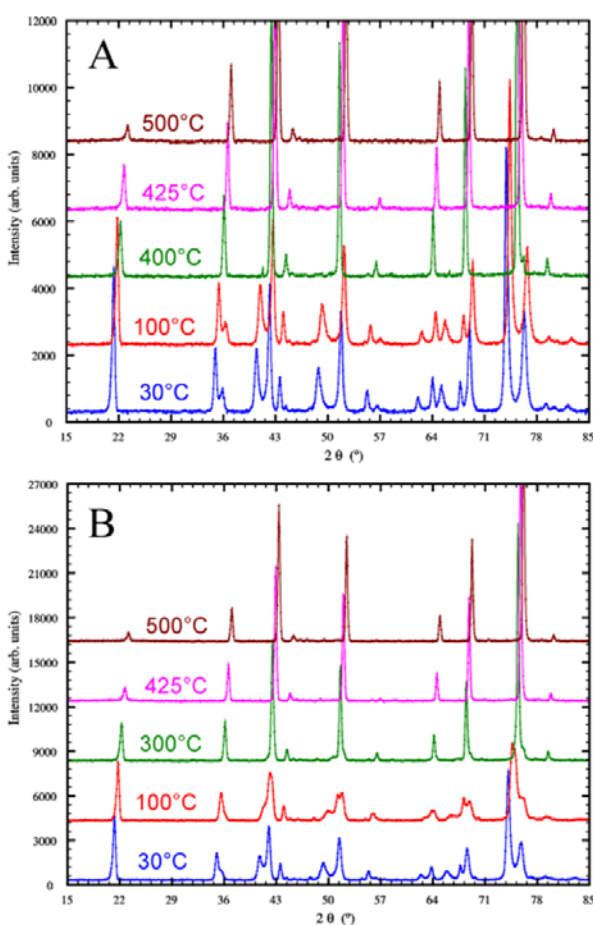


Fig.1. Neutron powder diffraction patterns recorded in the temperature range of 30°C - 500°C, for samples:  $\text{CuFe}_2\text{O}_4$  (A), and  $\text{Cu}_{0.95}\text{Zn}_{0.05}\text{Fe}_2\text{O}_4$  (B).

The elements Cu and Zn are neighbours in the periodic table, the cations  $\text{Cu}^{2+}$  and  $\text{Zn}^{2+}$  have nearly atomic form factors. Hence both cations are not distinguishable by conventional X-ray diffraction. Neutron powder diffraction is a powerful method to investigate structures containing electronic similar elements, as the different neutron scattering length of Cu and Zn. The Rietveld refinement of the  $\text{Cu}_{0.95}\text{Zn}_{0.05}\text{Fe}_2\text{O}_4$  at the 500°C temperature (about the  $T_C$ ), shows that zinc ions to occupy tetrahedral positions of cubic structure (Fig.2).

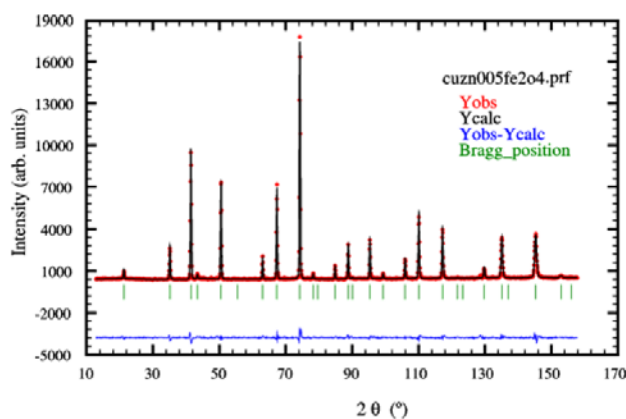


Fig.2. Neutron diffraction diagram of  $\text{CuFe}_2\text{O}_4$ , at 500°C temperature. The observed, calculated and difference profile resulting from the Rietveld analysis are shown.

Experiments were carried out at HMI, on the high-resolution neutron powder diffractometer E9 (FIREPOD). A germanium monochromator was used to give an incident neutron wavelength of 1.79801Å, and furnace HTF-2 type has been used to measurements.

#### References:

- [1] M. U. Rana, Misbah-ul-Islam, T. Abbas, Mater. Lett. **41** (1999) 52-56.
- [2] E. Prince, R. G. Treuting, Acta Cryst. **9** (1956) 1025.
- [3] R. G. Kulkarni, V. U. Patil, J. Mat. Sci. **14** (1979) 2221-2223.
- [4] S. S. Ata-Allah, F. M. Sayedahmed, M Kaiser, A. M. Hashhash, J. Mater. Sci. **40** (2005) 2923-2930.
- [5] R.G. Kulkarni, B. S. Trivedi, H.H. Josi, G.J. Baldha, J. Magn. Mater. **159** (1996) 375-380.
- [6] B.S. Boyanov, J. Thermal Anal. **44** (1995) 707-716.



## EXPERIMENTAL REPORT

### CRYSTAL STRUCTURE PHASE TRANSITIONS IN $\text{Bi}_{1-x}\text{R}_x\text{FeO}_3$ ( $\text{R}=\text{La}, \text{Nd}$ )

Proposal N° PHY-01-2216

Instrument **E9**

Local Contact  
O. Prokhnenko

Principal Proposer:

M. Kopcewicz, Institute of Electronic Materials  
Technology, Poland

Experimental Team:

D. Karpinsky JISSSP, NAS Belarus

Date(s) of Experiment

24/01/2008 – 27/01/2008

Date of Report: 10/01/2009

A crystal structure of  $\text{Bi}_{1-x}\text{Ln}_x\text{FeO}_3$  systems ( $\text{Ln}=\text{La}, \text{Nd}, \text{Eu}$ ) have been studied using neutron diffraction in a wide temperature range. A mechanism of a crystal structure phase transitions have been analyzed.

A satisfactory agreement between experimental and calculated patterns profiles for  $\text{Bi}_{0.75}\text{La}_{0.25}\text{FeO}_3$  composition has been obtained using two-phase crystal structure model in which one phase is described with the space group  $R3c$ , and another –  $Imma$  (see Figure). Chemical composition of the first phase is close to  $\text{Bi}_{0.9}\text{La}_{0.1}\text{FeO}_3$ , and of the second –  $\text{Bi}_{0.55}\text{La}_{0.45}\text{FeO}_3$ , what agrees with results of electron probe microanalysis. Fitting with other space groups of rhombic and tetragonal crystal systems does not describe satisfactorily the observed diffraction patterns. It should be noted that the use of monoclinic space group  $I2/m$  instead of  $Imma$  gave better fit, however we did not observe any additional peaks as indication of symmetry lowering down to monoclinic. Besides of perovskite phase the sample contains an insignificant quantity of impurities like  $\text{Bi}_{25}\text{FeO}_{40}$  and  $\text{Bi}_2\text{Fe}_4\text{O}_9$ . The single-phase sample  $\text{Bi}_{0.55}\text{La}_{0.45}\text{FeO}_3$  (space group  $Imma$ ) has been prepared at  $1100^\circ\text{C}$  from the starting mixture containing 2% excess of Bi ions above the stoichiometric amount.

Above mentioned results show that there is no complete solubility in the  $\text{Bi}_{1-x}\text{La}_x\text{FeO}_3$  system compounds synthesized in air. At low synthesis temperature ( $T < 850^\circ\text{C}$ ) the samples in the mentioned concentration range consist of rhombohedral  $R3c$  as well as orthorhombic  $Pnma$  and  $Imma$  phases. Whereas temperature increase leads to decomposition of rhombohedral phase and to increase of  $Imma$  orthorhombic one, however the other phases appears contain only the Bi and Fe cations.

In many aspects similar results have been obtained for  $\text{Bi}_{1-x}\text{Nd}_x\text{FeO}_3$  system. In this system the phase separation develops starting from composition  $x = 0.12$ . The crystal structure of  $x = 0.1$  sample has been successfully refined

using  $R3c$  space group. The compositions in the range  $0.15 < x < 0.23$  consist of  $R3c$ ,  $Pnma$  and  $Imma$  phases if synthesis temperature does not exceed  $820^\circ\text{C}$ . Increasing synthesis temperature, for example, for  $x = 0.18$  composition leads to a stabilization of mixed  $R3c + Imma$  phase state, however additional impurity such as  $\text{Bi}_2\text{Fe}_4\text{O}_9$  appears. We failed to obtain a single-phase sample with  $Imma$  type phase only. The single-phase  $\text{Bi}_{0.7}\text{Nd}_{0.3}\text{FeO}_3$  sample was prepared at  $950^\circ\text{C}$  during 15 hr. The unit cell of this sample is well described with a  $Pnma$  space group.

Further decrease of rare earth ionic radii leads to complete suppression of the  $Imma$  phase and narrowing of compositional range of the mixed phase state. For example we have managed to obtain rhombohedral ( $R3c$ )  $\text{Bi}_{0.92}\text{Eu}_{0.08}\text{FeO}_3$  and orthorhombic ( $Pnma$ )  $\text{Bi}_{0.8}\text{Eu}_{0.2}\text{FeO}_3$  as single phase product at synthesis temperature  $900^\circ\text{C}$  during 15 hr. In the intermediate range  $0.1 < x < 0.2$  two phases  $R3c$  and  $Pnma$  type coexist.

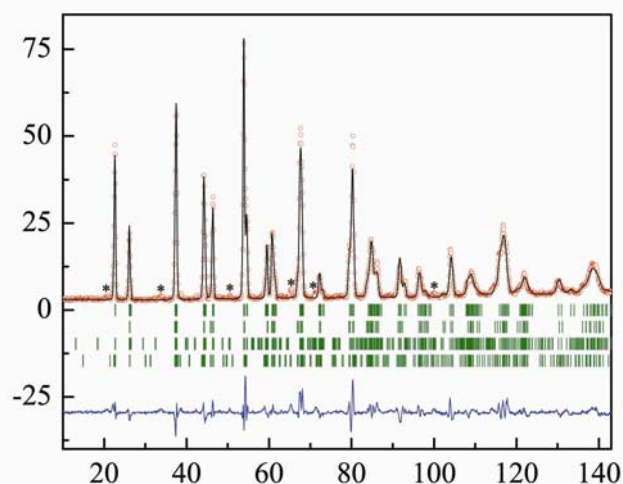


**Figure.** The observed (circles) and calculated (solid line) patterns of  $\text{Bi}_{0.75}\text{La}_{0.25}\text{FeO}_3$  compound obtained from Rietveld refinement of the NPD data at 290 K. A difference line is marked by solid line, Bragg positions – small vertical dashes. Two upper rows denote crystal phases, the lower ones – magnetic phase. A small amount of impurity phase is marked by asterisk signs.



## EXPERIMENTAL REPORT

### In-situ Neutron Diffraction Investigation of Methanol Synthesis over Cu/ZnO/Al<sub>2</sub>O<sub>3</sub> Catalysts

Proposal N° CHE-01-2357

Instrument **E9**

Local Contact  
M. Tovar, D. Wallacher

Principal Proposer: Malte Behrens, FHI, Abteilung AC, Berlin  
 Experimental Team: Raoul Naumann d'Alnoncourt, FHI, Abteilung AC, Berlin  
 Stefan Kißner, FHI, Abteilung AC, Berlin  
 Stefanie Köhl, FHI, Abteilung AC, Berlin  
 Michael Tovar, Helmholtz-Zentrum, BENSC, Berlin  
 Dirk Wallacher, Helmholtz-Zentrum, BENSC, Berlin

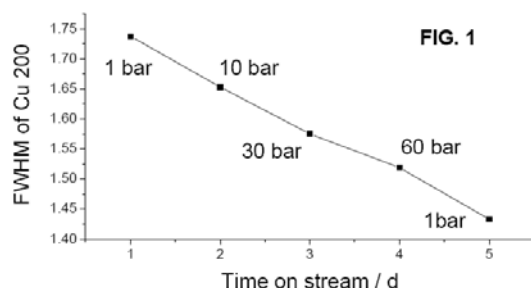
Date(s) of Experiment

03/11/2008 – 11/11/2008

Date of Report: 14/01/2009

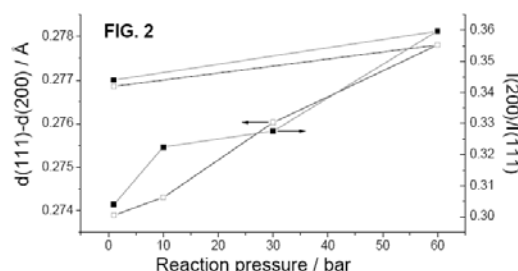
Investigation of catalysts under working conditions provides valuable information on the nature of the catalytically active sites. If the catalyst dynamically changes under reaction conditions, in-situ studies can be regarded as essential for the comprehensive understanding of a catalyst system. Such changes in morphology and Cu-ZnO interactions have been reported for the Cu/ZnO/Al<sub>2</sub>O<sub>3</sub> methanol synthesis (MS) catalyst. However, in-situ studies under realistic conditions are difficult due to the high pressure of industrial MS of ca. 60 bars and the lack of experimental probes operating at such elevated pressures.

Neutron diffraction (ND) is uniquely suitable for studies at such harsh conditions because, due to their transparency for neutrons, conventional metallic tubular reactors can be used without special windows. A plug flow reactor was designed for in-situ ND experiments to probe the structural answer of an industrially relevant Cu/ZnO/Al<sub>2</sub>O<sub>3</sub> catalyst under variations of the synthesis gas pressure at realistic conditions.



ND patterns were taken at pressures of 1, 10, 30, 60 and again 1 bar without changing the temperature (250 °C), while methanol was detected in the exhaust gas by mass spectrometry. These results constitute the first diffraction study of a MS catalyst under realistic working conditions. Unfortunately, due to a misalignment of the sophisticated catalytic setup with respect to the centre of the diffractometer caused by thermal movement of the sample stick, the wealth of information deducible from the ND patterns was restricted

and lower than expected from preparatory ex-situ experiments. In fact, only two reflections, Cu 111 and 200, could be evaluated. However, preliminary evaluation reveals severe changes of the structure and microstructure of the Cu particles as a function of reaction conditions. Some effects, like the sharpening of the 200 line (Fig. 1) are rather a function of time on stream than of pressure. Thus, sintering of Cu particles seems to be not affected by the gas atmosphere but to rather depend on thermal stress.



While sintering is irreversible, other effects were found to be at least partially reversible supporting the idea of dynamical changes in the catalyst as a function of pressure and conversion (Fig. 2). Such effects and tentative interpretations are (i) increase of the d(111)-d(200) distance (possibly related to lowering of stacking fault density), (ii) decrease of ratio of the integral intensities I(200)/I(111) (change of particle morphology). Drawing of reliable conclusions regarding the relevance of these results, however, requires deconvolution of reversible and irreversible effects and the evaluation of additional higher reflections, which will be accessible in future experiments carried out in a well-aligned setup.

*This research project has been supported by the Federal Ministry of Education and Research of Germany (FKZ 01RI0529)*



## EXPERIMENTAL REPORT

### Investigation of MoVTenb oxide catalysts for selective oxidation of propane

Proposal N° CHE-01-2358

Instrument **E9**

Local Contact  
Tovar Michael

Principal Proposer: Trunschke, Annette, Fritz Haber Institut, MPG  
 Experimental Team: Naumann, Raoul, Fritz Haber Institut, MPG  
 Kolen'ko, Yury, Fritz Haber Institut, MPG  
 Girgsdies, Frank, Fritz Haber Institut, MPG  
 Behrens, Malte, Fritz Haber Institut, MPG  
 Tovar Michael, Helmholtz Zentrum Berlin

Date(s) of Experiment

11/11/2008 – 16/11/2008

Date of Report: 15/01/2009

MoVTenb oxides are promising catalysts in selective oxidation of propane to acrylic acid. The outstanding catalytic properties are assigned to a specific orthorhombic crystalline phase denominated as M1. The present work is aimed at investigating the implication of changes in temperature and gas phase composition during propane oxidation on the crystal structure of the title mixed oxide, esp. with respect to metal site occupancy (Mo, Nb, and Te) and the oxygen sub-lattice. Phase-pure (ICSD 55097 [1]), polycrystalline M1 has been prepared from phase mixtures that have been purified by dissolution of unwanted phases. (sample ID 6059). The atomic ratio of the metals Mo:V:Te:Nb as analyzed by EDX is 62 : 17 : 6 : 15 at-%. The stoichiometry of the sub-oxide  $\text{Mo}_{1.00}\text{V}_{0.26}\text{Nb}_{0.17}\text{Te}_{0.09}\text{O}_{4.0}$  was determined by ICP-OES analysis and carrier gas-hot extraction.

$\text{CuK}\alpha$  radiation. The precise wavelength applied in the neutron diffraction experiment was obtained by refinement (Tab. 1). Data analysis has been performed using the "TOPAS" software (v.2.1, Bruker AXS). The M1 structure contains 13 crystallographic metal sites. The space group of M1 is *Pba*2. The unit cell parameters calculated based on both, the x-ray and neutron diffraction data, are in satisfying agreement. In a first step, the effect of temperature on the lattice parameters has been studied by heating the catalyst in Ar to 673 K, which is the reaction temperature generally applied in propane oxidation. An anisotropic thermal expansion has been observed reflected in slightly favored thermal expansion in the crystallographic [001] direction. The influence of changes in the redox potential of the gas phase on lattice parameters and site occupancy will be the subject of future experiments.

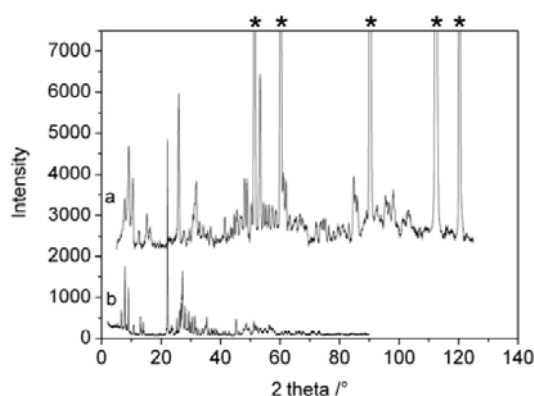


Fig. 1. Neutron powder diffraction patterns measured in a stainless steel fixed bed reactor (a) and x-ray diffraction patterns (b) of the MoVTenb oxide catalyst (reflections of the reactor wall material are indicated by \*).

In Fig. 1, the x-ray and neutron diffraction patterns of the  $\text{MoVTenbO}_x$  catalyst are compared. XRD was performed on a D8 ADVANCE diffractometer (Bruker AXS) in Bragg-Brentano Theta/Theta geometry using

Tab. 1. Lattice parameters and wavelength in the neutron diffraction experiments refined from powder diffraction (PD) data.

	X-ray PD (~293 K)	Neutron PD (~293 K)	Neutron PD (673 K)
<i>a</i> [Å]	21.1322(13)	21.135(5)	21.163(3)
<i>b</i> [Å]	26.6229(17)	26.624(6)	26.646(4)
<i>c</i> [Å]	4.01543(19)	4.0151(5)	4.0321(4)
$\lambda_n$ [Å]	—	1.796993(8)	1.796993(8)

#### References

- [1] P. DeSanto *et al.*, Z. Kristallogr. 219 (2004) 152.



## EXPERIMENTAL REPORT

### Neutron diffraction study of ultramarine-type pigments

Proposal N° CHE-01-2363

Instrument **E9**

Local Contact  
Andreas Hoser

Principal Proposer: E. Climent-Pascual, Universidad Complutense Madrid

Experimental Team: J. Hernández-Velasco, CSIC-Instituto Ciencia Materiales Madrid  
A. Hoser, BENSC, Berlin

Date(s) of Experiment

29/07/2008 – 01/08/2008

Date of Report: 14/01/2009

Ultramarines are zeolites with cubic sodalite-type structure [1], which are widely used as pigments in a variety of applications. The colour is due to the presence of polysulfide anion-radicals stabilized by the zeolite framework. The naturally occurring ultramarine (lazurite) presents deep blue color while synthetic ones are commercially available in blue, violet and pink colors. In the blue ultramarine (natural or synthetic), the blue chromophores  $S_3^-$  are located near the center of  $\beta$  cages fourfold coordinated by sodium cations forming a tetrahedron. Besides the blue chromophores, a minor proportion of the  $\beta$  cages are filled by yellow ( $S_2^-$ ), red chromophores ( $S_4$  or  $S_4^-$ ), sulfate anions and even free of anions [2]. The blue ultramarines can be prepared from different clays or zeolites heating together with a mixture of sodium carbonate, sulfur and a reducing agent under controlled atmosphere [1,2]. The violet variety requires a supplementary step in which a slow intracage oxidation of blue chromophores takes place under hydrogen chloride flow.

In this study blue (1 sample) and violet-pink (2 samples) ultramarines with different cage filling besides the chromophores, i.e. carbonate and sulfate anions, has been structurally characterized. These samples have been obtained by different synthetic routes from layered silicate (kaolin) and already synthesized sodalite (nitrite sodalite). Data were collected at 5 K and 100 K (Fig. 1), in all cases, using the E9 diffractometer equipped with a standard orange cryostat.

The obtained neutron diffraction data firstly indicate that there is no significant differences between profiles at 5 and 100 K because of the large positional disorder (Fig. 1). Currently, we are performing the Rietveld analysis of the obtained data in the space group  $I-43m$  (Fig. 2), which allow us to study with more accuracy the zeolite framework differences between the blue and violet-pink ultramarines obtained with different cage filling.

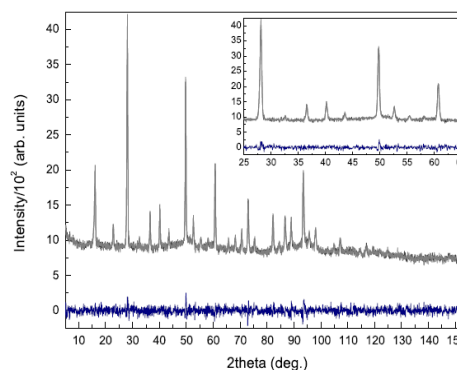


**Fig. 1:** Observed neutron profiles for pink ultramarine at 5 K (grey), 100 K (dark grey) and difference (dark blue).

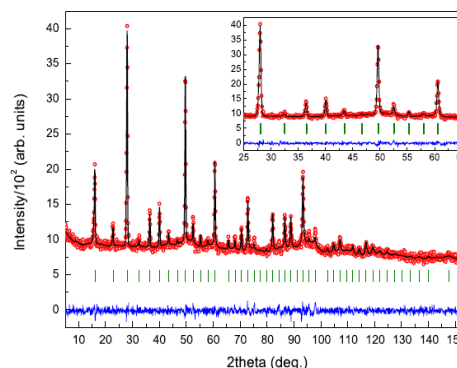


**Fig. 2:** Observed (open circles), calculated (full line) and difference (lower full line) neutron powder profiles for pink ultramarine at 100 K; the row of tick marks corresponds to the Bragg positions.

#### References:

- [1] G. Buxbaum, G. Pfaff, Industrial Inorganic Pigments, Wiley-VCH, Weinheim, 1993.
- [2] E. Climent-Pascual, R. Sáez-Puche, A. Gómez-Herrero, J. Romero de Paz, Micropor. Mesopor. Mater. 116 (2008) 344–351.

#### Acknowledgement:

This research project has been supported by the European Commission under the 6<sup>th</sup> Framework Programme through the Key Action: Strengthening the European Research Infrastructures. Contract n°: RII3-CT-2003-505925 (NMI 3).



## EXPERIMENTAL REPORT

### Structure of NaMgAl(oxalate)<sub>3</sub>·9H<sub>2</sub>O - an Extraordinary Spectral Hole-Burning Host

Proposal N° PHY-01-2377

Instrument **E9**

Local Contact  
Fabiano Yokaichiya

Principal Proposer: H Riesen, S J Campbell, School of PEMS, UNSW@ADFA;  
D Kearley, Bragg Institute, ANSTO, Australia  
S J Campbell, UNSWQADFA, Australia  
Experimental Team: D Kearley, Bragg Institute, ANSTO, Australia  
Fabiano Yokaichiya, Michael Tovar, BENSC

Date(s) of Experiment

02/10/2008 – 06/19/2008

Date of Report: 13/01/2009

We have carried out a detailed investigation of the neutron diffraction crystal structure of two deuterated samples of NaMgAl(oxalate)<sub>3</sub>·9H<sub>2</sub>O using the E9 high resolution diffractometer and ancillary equipment over the temperature range 4-200 K. These materials are of technological and scientific interest as a result of the massive increase of the spectral hole-burning efficiency obtained in the R-lines of Cr(III) in the NaMgAl(oxalate)<sub>3</sub>·9H<sub>2</sub>O host upon partial deuteration of the water molecules of crystallization [1]. The particular samples investigated were deuterated to ~50% and ~98%. These levels match outcomes of spectral hole-burning experiments carried out on oxalates deuterated to similar levels [1, 2].

While we have recently refined the X-ray crystal structure [2] no neutron diffraction based structure has so far been reported and the locations of the hydrogen and deuterium atoms are unknown. The main aims of our experiments are to determine the positions of the hydrogen/deuterium atoms and establish the nature of the hydrogen bonding. Knowledge of the exact locations of the hydrogen atoms will facilitate a better understanding of the water flips in this material, thereby allowing better scope for application of its extraordinary hole-burning properties.

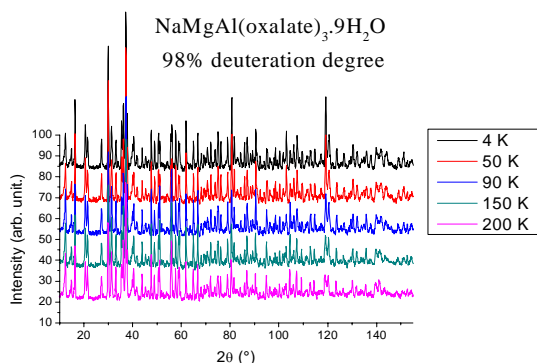


Fig 1: Representative neutron diffraction patterns for NaMgAl(oxalate)<sub>3</sub>·9H<sub>2</sub>O deuterated to ~98% from 4-200.

Initial refinements of the neutron diffraction data for the 98% deuterated oxalate are consistent with the single crystal X-ray diffraction data at 200 K which indicate that the system crystallizes in the *P3c1*

space group with nine water molecules of hydration and unit cell parameters  $a=b=16.7349(2)$  Å and  $c=12.6338(1)$  Å with  $Z=6$  [2].

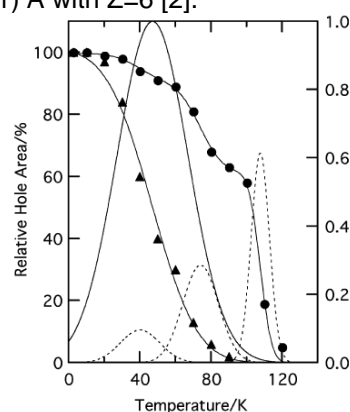


Fig. 2 Temperature-cycle hole-burning in perprotonated (triangles) and deuterated (~46%; circles) NaMgAl(oxalate)<sub>3</sub>·9H<sub>2</sub>O/Cr(III). The related gaussian distributions of the activation energies are also shown (full line perprotonated; dashed lines deuterated) [2].

Continuing refinements of our neutron diffraction patterns (4-200 K) will enable us to test our hypothesis that all oxygen atoms of the oxalate ligands are involved in hydrogen bonding with the water molecules. Based on analysis of the X-ray data we anticipate the following: six water molecules coordinated to Mg(II) form one hydrogen bond each (three with an inner and three with an outer oxygen atom of the oxalate ligands) with the remaining three water molecules possibly hydrogen bonded to the six water ligands of the magnesium(II) with each undergoing two hydrogen bonds to an inner and an outer atom of two separate oxalate ligands.

Such a scheme indicates that the water molecules are likely to be subject to three different kinds of hydrogen bonding to the oxygen atoms of the oxalate ligands. This behaviour is in accord with the observation of three Gaussian barriers in hole-burning experiments of the deuterated oxalate as shown in Fig 2 [2].

[1] H Riesen, Coordination Chemistry Reviews **250** (2006) 1737

[2] H Riesen and A D Rae, Dalton Trans (2008) 4717



## EXPERIMENTAL REPORT

### Determination of the site occupancy fractions of the Ti<sub>2</sub>AlNb-based intermetallics by NS

Proposal N° MAT-01-2378  
Instrument **E9**  
Local Contact  
Michael Tovar

Principal Proposer: B. Wu, Q. Li – Fuzhou University, China  
Experimental Team: F. Yokaichiya – BENSC, Berlin  
M. Tovar – BENSC, Berlin

Date(s) of Experiment  
18/12/2008 – 21/12/2008

Date of Report: 15/01/2009

### Introduction

The ordering behaviours of the alloying elements occupying in the sublattice (site occupy preference) is the common interesting topics in intermetallics because the mechanical properties and physical properties are affected by the ordering behaviours. Understanding the ordering behaviours help us to design the alloy composition and heat treatment condition. This neutron scattering (NS) experiments is intend to verify a general theory model, which the ordering behaviours are predicted by combine thermodynamic sublattice model and ab initio total energy calculations. Straightforwardly, we wish to measure the site occupy fractions of the alloying elements in the sublattices in Ti<sub>2</sub>AlNb-based intermetallics.

### Experiment

The Ti<sub>2</sub>AlNb-based alloy with nominal composition Ti-25Al-25Nb and Ti-22Al-27Nb were heat treatment under different conditions. The neutron scattering experiments were performed at E9 with wavelength 1.793Å.

Table 1 The composition, heat treatment condition, and the phase constituent of the alloys

No.	composition	Heat treatment	Phase
1	Ti-25Al-25Nb	1423K/1hr/WQ +973K/240hrs/WQ	O
2	Ti-25Al-25Nb	1423K/1hr/WQ +1223K/240hrs/WQ	O, B2, α <sub>2</sub>
3	Ti-25Al-25Nb	1423K/1hr/WQ +1073K/240hrs/WQ	O
4	Ti-25Al-25Nb	1423K/1hr/WQ	B2
5	Ti-22Al-27Nb	1423K/1hr/WQ +973K/240hrs/WQ	O+B2
6	Ti-22Al-27Nb	1423K/1hr/WQ	B2

O—Orthorhombic, B2—B2\_BCC, α<sub>2</sub>—D0<sub>19</sub>\_HCP

Table 2 The refined results of Sample 1#

Element	x	y	z	Occupation	s
Ti1(8g)	0.2330	0.9015	0.2500	0.797	0.42
Nb1(8g)	0.2330	0.9015	0.2500	0.203	
Al1(4c1)	0.000	0.1649	0.2500		
Ti2(4c2)	0.000	0.6353	0.2500	0.3798	
Nb2(4c2)	0.000	0.6353	0.2500	0.6202	
a	6.0617				
b	9.5963				
c	4.6714				

s: order parameter,  $s = y_{(Ti1,8g)} - y_{(Ti2,4c2)}$

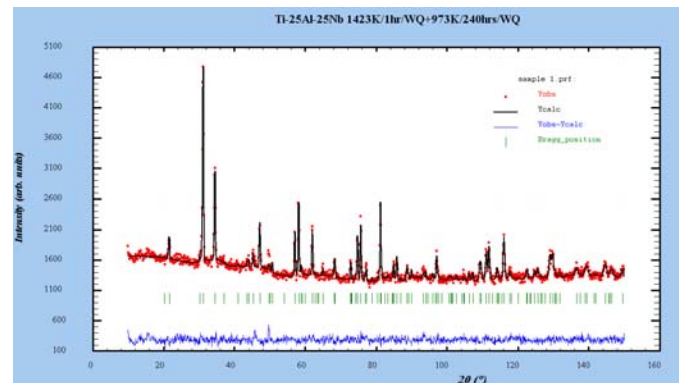


Fig. 1 The pattern of the sample 1#

### Results

The constituent phases were identified, see Table 1, and agree with the available literatures. The site fractions of Sample 1# were refined, which agree with the Neutron Scattering experiment by Mozer et al. [1] and our theoretical predictions [3], see Table 2 and Fig. 1. In the orthorhombic phase, Al atoms strongly prefer to sublattice 4c1. The site fractions of the alloys need to be further refined by using package Fullprof Suite. The coordination of the neutron scattering results with the theory model of the order-disorder transition need to be further explored.

### References:

- [1] B. Mozer, et al., *Scripta Metallurgy et Materialia*, 1990,23:2363-2368.
- [2] B. Wu, et al., *Intermetallics*, 2002,10:979-984.
- [3] B. Wu, et al., *Intermetallics*, 2008,16:42-51.
- [4] C.G. Rhodes, *Scripta Materialia*, 1998,38:681-685.



## EXPERIMENTAL REPORT

### Evidence for the formation of cross-linked chloroperoxidase in mesopores

Proposal N° CHE-04-1549

Instrument **V4**

Local Contact  
Astrid Brandt

Principal Proposer: Martin Hartmann, Institut für Physik, Universität Augsburg  
 Experimental Team: Dirk Jung, Institut für Physik, Universität Augsburg  
 Michelangelo Paradiso, Institut für Physik, Universität Augsburg  
 Dirk Wallacher, SF1, Helmholtz-Zentrum Berlin  
 Astrid Brandt, BENSC, Helmholtz-Zentrum Berlin

Date(s) of Experiment

13/03/2008 – 19/03/2008

Date of Report: 09/12/2008

#### Aim of the experiment:

The objective was to provide convincing evidence for the location of cross-linked chloroperoxidase (CPO) in the pore cavities of mesocellular foams (MCF). The enzyme was first immobilized into the support (CPO-CLEAMCF) and the catalytic behaviour of the heterogeneous biocatalyst was tested in a fixed-bed reactor. In this project, small angle neutron scattering (SANS) was introduced as a novel tool, which provides unambiguous evidence for the formation of CPO-CLEAs in the MCF mesopores.

#### Experimental conditions:

The scattering intensity was recorded in the range of  $0.06 \text{ nm}^{-1} < q < 2.12 \text{ nm}^{-1}$ . The SANS-investigations are based on the principle of „contrast matching“. The pores of the three different MCF samples (empty MCF, CPO-CLEA-MCF as prepared, CPO-CLEA-MCF after the catalytic experiment) have been filled at 280 K with condensed C5F12 by volumetric controlled gas adsorption. Then neutron scattering length densities of condensed C5F12 ( $3.43 \cdot 10^{-6} \text{ \AA}^{-2}$ ) and the MCF-silica ( $3.40 \cdot 10^{-6} \text{ \AA}^{-2}$ ) are practical identical.

#### Results and discussion:

Figure 1 shows the SANS curves of the empty sample MCF (evacuated and matched with C5F12) and the SANS curves of the matched CPO-CLEA-MCF before and after use in the fixed-bed reactor. For the latter sample the SANS pattern of the evacuated MCF without C5F12 filling is shown. The maximum at  $q =$

$0.25 \text{ nm}^{-1}$  corresponds to the (100) reflection of the simple cubic pore lattice. After filling this evacuated porous silica matrix with C5F12, the scattering intensity is reduced by more than 3 orders of magnitude, thus the matching condition

is almost perfectly fulfilled. Compared to this situation the scattering intensities of the enzyme loaded MCF do not vanish after filling the void pore spaces completely with C5F12. From these results it is obvious that the pores of this sample are partially filled with enzyme aggregates which results in a non-zero density difference. Furthermore, the experimental data show that the structural features in the scattering patterns are much sharper defined in the CPO-CLEA-MCF sample after usage in the catalytic test than in the fresh prepared CPO-CLEA-MCF-sample. During the catalytic run, these isolated (not cross-linked) molecules are obviously washed out of the support thereby leaving a more defined structure with agglomerates of CPO mainly located in the spherical cages of the support.

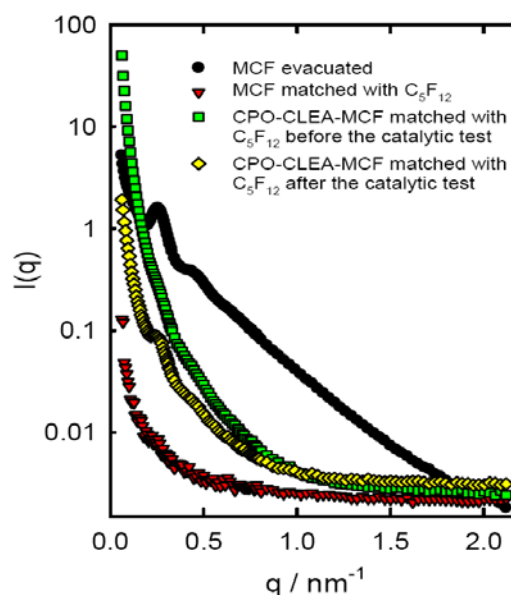


Figure 1: SANS curves of the MCF material and the CPO-CLEA-MCF matched with C5F12.

	<b>EXPERIMENTAL REPORT</b>  <b>CaFe<sub>2</sub>As<sub>2</sub> under hydrostatic pressure</b>	Proposal N° EF Instrument <b>E4</b>  Local Contact K. Prokes
	Principal Proposer: D. Argyriou, HZB Experimental Team: D. Argyriou, HZB K. Prokes, HZB S. Kimber, HZB A. Goldman, Ames Laboratory, Iowa State University, USA	Date(s) of Experiment  02/08/2008 – 10/08/2008

Date of Report: 19/01/2009

The relationship between magnetism, superconductivity and lattice instabilities in high- $T_C$  superconductors remains a hot subject in the solid state physics despite an appreciable effort. The discovery of pressure-induced superconductivity in  $\text{CaFe}_2\text{As}_2$  has opened an exciting new avenue for investigations of these effects. Similar to other members of this family of compounds [1] it undergoes at ambient pressure a transition from a non-magnetically ordered tetragonal (T) phase to an antiferromagnetic (AF) orthorhombic (O) phase below approximately 170 K. In the O phase, are the Fe moments order directed along the  $a$  axis. Neutron powder diffraction measurements under hydrostatic pressure found that for  $p > 0.35$  GPa (at  $T = 50$  K), the antiferromagnetic O phase transforms to a new, non-magnetically ordered, collapsed tetragonal (cT) structure with a dramatic decrease in both the unit cell volume (5%) and the  $c/a$  ratio (11%). The transition to the cT phase occurs in close proximity to the pressure at which superconductivity is first observed.

The single crystals of  $\text{CaFe}_2\text{As}_2$  was grown using a Sn flux. Neutron diffraction data were measured up to a pressure of 1 GPa on the E4 double axis diffractometer with  $\lambda = 2.44$  Å for the  $(hhl)T$  orientation of a 8 mg single crystal. We employed a Be-Cu clamp-type pressure cell and a 1:1 mixture of Fluorinert 77 and 70, for the pressure medium. The initial pressure was measured using a manganin pressure sensor and then monitored *in-situ* by tracking the lattice constants of NaCl crystals placed above the sample. In Fig. 1, we show the (004) reflection as a function of temperature. Here on cooling the pressure changes by  $\sim 2$  kbar from 300 to 2K from the initial pressure. At low pressures we observe the same T-O transition as we find at ambient pressure indicated by a small discontinuous expansion of the  $c$ -axis (fig. 1(a-b)). However at high pressure we can observe the new collapsed tetragonal (cT) phase that hosts superconductivity. Here the  $c$ -axis shrinks abruptly by 1 Å, an almost 10% change of the  $c$ -axis (fig. 1(d)). For intermediate pressure we

find evidence of a co-existence between the O and cT phases (fig. 1(c)) that may help explain observations of co-existence between magnetism and superconductivity. Both the T-cT and O-cT

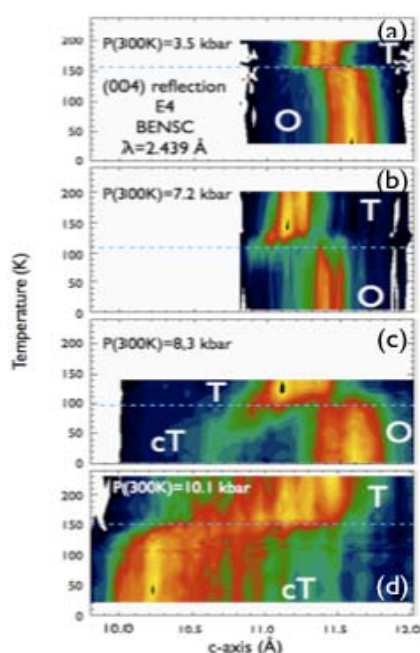


Fig 1: Temperature dependence the (004) reflection at various initial pressures measuring a 10 mg  $\text{CaFe}_2\text{As}_2$  single crystal inside a clamped pressure cell. The data are represented as two dimensional color plots with intensity shown as color.

transitions exhibit, however, significant hysteresis effects and it seems that the apparent co-existence seen in previous powder experiments [2] is a consequence of non-hydrostatic conditions. In the same measurements and others with our collaborators we also probed the magnetic order and found that the magnetism abruptly disappears as one enters the cT phase. Our results show the effect of chemical doping on the long range magnetism resembles that of pressure.

#### References

- [1] J. Zhao, et al., Phys. Rev. B **78**, 140504(R) (2008).
- [2] A. Kreyssig, et al., arXiv:0807.3032 (2008), unpublished.



## EXPERIMENTAL REPORT

### Inelastic Neutron Scattering from hydrogen clathrate-hydrates

Proposal N°  
PHY-03-483-EF

Instrument **V3**

Local Contact M. Russina

Principal Proposer: M. Russina, HMI, BENSC  
Experimental Team: Lorenzo Ulivi, CNR, Italy  
Milva Celli, CNR, Italy  
E. Kemner

Date(s) of Experiment

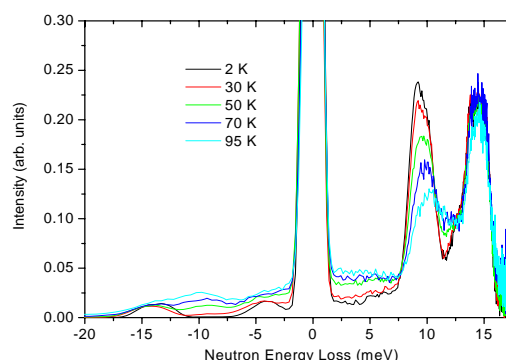
03/12/2008 – 11/12/2008

Date of Report: January 2008

Clathrate-hydrates, also known as gas hydrates, are inclusion compounds where gas molecules (e. g.  $\text{CH}_4$ , and other hydrocarbons,  $\text{CO}_2$ , and also  $\text{H}_2$ ) are trapped into a solid structure formed by  $\text{H}_2\text{O}$  molecules. The water molecules are bound in a solid lattice that forms “cages” of different size and dimension, where one or few foreign molecules are hosted. Besides being present in nature, these compounds can be prepared in laboratory and have been recently proposed as effective, safe, and economical materials for hydrogen storage. It has recently been shown that adding tetrahydrofuran (THF) to water, a ternary hydrogen clathrate can be formed, at a much lower pressure than needed for the pure  $\text{H}_2$ - $\text{H}_2\text{O}$  clathrate. Clathrates are peculiar systems for what concerns lattice dynamics, since the deeply non-harmonic motion of the guest molecules in the cages (rattling) differs from all other normal modes of the crystal, and is responsible for the anomalous thermal conductivity of these materials.

The aim of the experiment was to study the dynamics of the  $\text{H}_2$  molecules in two different hydrogen clathrates. We have measured inelastic neutron scattering spectra from three different samples, namely: 1) a deuterated tetrahydrofuran (TDF) - heavy water ( $\text{D}_2\text{O}$ ) clathrate, that has the same crystal structure of the two other clathrates examined in this study and was used as a background; 2) A TDF- $\text{D}_2\text{O}$ - $\text{H}_2$  clathrate, and 3) a sample of pure  $\text{D}_2\text{O}$ - $\text{H}_2$  clathrate. The samples were prepared in the ISC-CNR laboratory in Italy, and transported to BENSC at liquid nitrogen temperature. Due to the large incoherent neutron cross section for the proton, the measured spectra reveal strong features due to the  $\text{H}_2$  motion inside the clathrate cage. Spectra (summed over all angles) measured for the TDF- $\text{D}_2\text{O}$ - $\text{H}_2$  clathrate at five temperatures are shown in the figure, after subtraction of the (much weaker) spectra obtained for the TDF- $\text{D}_2\text{O}$  clathrate. The two

strong features visible in the energy loss side of the figure are easily assigned.



The band observed at about 14.7 meV correspond to the  $J=0 \rightarrow 1$  rotational transition of the  $\text{H}_2$  molecule, while the band around 10 meV is the fundamental transition for the rattling motion of the  $\text{H}_2$  molecule in the clathrate cage. From these measurement we derive the information that the rotational motion of the  $\text{H}_2$  molecule is almost free, since the rotational energy is very similar to that of the isolated molecule. In addition, we notice that the rattling transition has an energy which is quite high compared with the analogous in methane clathrates, due to the different mass of the molecules. The temperature behaviour puts in evidence an intensity increase on the high frequency side of the rattling transition. This is what is generally known as negative anharmonicity, and correspond to the fact that the potential for the  $\text{H}_2$  molecule rattling motion looks more like a square well than a parabola. In the analysis, the values of the transition frequencies and band intensities have been quantitatively related to the details of the interaction potential between  $\text{H}_2$  and the water molecules, with a very good agreement.



## EXPERIMENTAL REPORT

### QENS study of diffusion in Cu-Se superionic conductor

Proposal N° PHY-03-554

Instrument **V3**

Local Contact M. Russina

Principal Proposer: S. Danilkin, ANSTO, Australia  
 Experimental Team: C. Ling, University of Sydney, Australia  
 R. Macquart, University of Sydney, Australia  
 M. Russina, HMI, Berlin  
 Z. Izaola, HMI, Berlin

Date(s) of Experiment

05/02/2008 – 11/02/2008

Date of Report: 06/01/2009

Copper selenide is a mixed ionic-electronic conductor and received attention from the technological and physical point of view in particular due to a high ionic conductivity. According to [1, 2] only a fraction of Cu atoms takes part in the ionic transport in  $\text{Cu}_{2-x}\text{Se}$  compounds. The number of mobile atoms is about 1/3 - 1/8 of the total cation concentration in stoichiometric  $\text{Cu}_2\text{Se}$  and decreases with  $x$  causing the ionic conductivity to drop. This conclusion is based on the assumption that Cu mobility does not depend on composition. Therefore the QENS study is of interest because the width and intensity of quasi-elastic peak associated with Cu diffusion are directly related to Cu coefficient of self-diffusion and the number of mobile ions, respectively.

We performed measurements of the quasi-elastic broadening in  $\text{Cu}_{1.77}\text{Se}$ ,  $\text{Cu}_{1.90}\text{Se}$  and  $\text{Cu}_{1.98}\text{Se}$  compounds at 313 and 430K with NEAT time-of-flight spectrometer. Incident wavelength of 6.5 Å was chosen in order to minimise contribution from the low – energy phonons and still have sufficiently high neutron flux and resolution. Figure 1 shows the dynamic structure factor of  $\text{Cu}_{1.77}\text{Se}$  and  $\text{Cu}_{1.98}\text{Se}$  compounds measured at 313K and 430K. In ordered non-superionic  $\alpha$ -phase  $\text{Cu}_{1.98}\text{Se}$  the quasielastic component is not observed at  $T = 313\text{K}$ , however it is clearly seen in superionic  $\beta$ - $\text{Cu}_{1.98}\text{Se}$  at  $T=430\text{K}$ . By contrast the  $\text{Cu}_{1.77}\text{Se}$  compound which is superionic at ambient temperature has relatively small quasielastic component showing little difference between 313K and 430K. The analysis shows that fraction of Cu atoms which takes part in the ionic transport indeed decreases with  $x$  in general agreement with papers [1, 2], but not vanishes at  $x = 0.23$ . In contrast with data [1, 2] the self-diffusion coefficient depends on composition:  $D_i(\text{Cu}_{1.98}\text{Se}) \approx 1.7 \times D_i(\text{Cu}_{1.77}\text{Se}) \approx 6 \times 10^{-5} \text{ cm}^2/\text{s}$  at 430K.

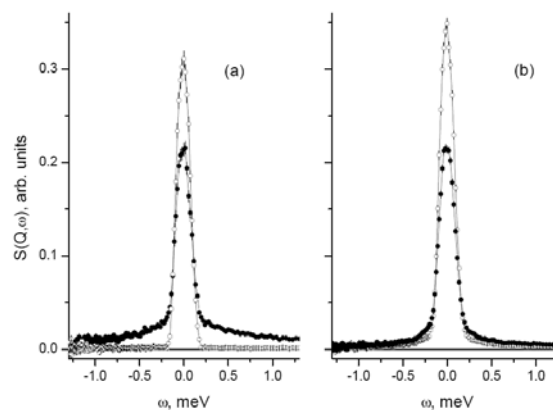


Fig. 1 Dynamic structure factor of  $\text{Cu}_{2-x}\text{Se}$  samples:

- (a)  $\alpha$ - $\text{Cu}_{1.98}\text{Se}$ :  $T = 313\text{K}$  (○);  $\beta$ - $\text{Cu}_{1.98}\text{Se}$ ,  $T=430\text{K}$  (●)  
 (b)  $\beta$ - $\text{Cu}_{1.77}\text{Se}$ :  $T = 313\text{K}$  (○);  $\beta$ - $\text{Cu}_{1.77}\text{Se}$ ,  $T=430\text{K}$  (●)

## References

- [1] R.A. Yakshibaev et al., *Sov. Phys: Solid State*, **26** (1984) 2189.  
 [2] M.A. Korzhuev, *Sov. Phys: Solid State*, **31** (1989) 1666.

## Acknowledgement

*This research project has been supported by the Access to Major Research Facilities Programme, DEST, Australia.*



## EXPERIMENTAL REPORT

### Hydrogen dynamics in complex proton conducting perovskites

Proposal N° PHY-03-588

Instrument **V3**

Local Contact  
Zunbeltz Izaola

Principal Proposer: Niina Jalarvo, University of Oslo, FERMIO - Functional Energy Related Materials in Oslo, Norway  
Experimental Team: Dirk Wallacher, Helmholtz-Zentrum Berlin für Materialien und Energie GmbH

Date(s) of Experiment

27/10/2008 – 03/11/2008

Date of Report: 15/01/2009

Materials with protonic conductivity are interesting for a number of technological energy related applications, e.g., as electrolytes in fuel cells, that can be used to deliver cleaner energy.  $\text{Sr}_4(\text{Sr}'_2\text{Ta}_2)\text{O}_{11}$  is a member in a series of oxygen deficient complex perovskites which hydrate and reveal high protonic conductivity at elevated temperatures under humid atmospheres.

To understand the proton transfer mechanism in  $\text{Sr}_4(\text{Sr}'_2\text{Ta}_2)\text{O}_{11}$ , QENS experiments were performed in a large temperature scale from 100 to 800 °C and with two energy resolutions  $\Delta E \approx 90$  and  $30 \mu\text{eV}$ . The sample was placed into a Suprasil quartz tube (very low H content), which was further connected into the DeGAS system to produce humid atmosphere ( $p_{\text{H}_2\text{O}} = 0.3$  bar) required to keep the sample hydrated. The sample size was adjusted to fill the whole beam, to avoid any possible background induced by the water vapour. Furthermore, background measurements were performed for the quartz tube, both filled with water vapour and having a vacuum inside. There was no difference between these background measurements. The quartz tube and the present water vapour did not produce any QE signal, but some weak inelastic contributions at rather high energy gain could be noted.

Measurements performed at  $\Delta E \approx 90 \mu\text{eV}$  at 100 and 200 °C did not reveal any QE contribution, and therefore a higher  $\Delta E \approx 30 \mu\text{eV}$  was employed. Using this resolution QE signal was observed between 400 and 800 °C. Above 800 °C  $\text{Sr}_4(\text{Sr}'_2\text{Ta}_2)\text{O}_{11}\text{H}_2\text{O}$  dehydrates and the QE contribution fades away.

The QENS spectra were reproduced using a so-called phenomenological model, including a contribution for the elastic peak and a Lorentzian function for the QE part. The incoherent scattering function for this model can be given as:

$$S(Q, \omega) = f [A_0(Q)\delta(\omega) + (1 - A_0(Q))L(\Delta, \omega)] \otimes R(Q, \omega) + B(Q, \omega)$$

where  $f$  is a scaling factor,  $A_0$  is the elastic incoherent structure factor,  $\delta(\omega)$  is the Dirac function,  $(1 - A_0)$  is the quasielastic incoherent structure factor,  $R(Q, \omega)$  is the resolution function and  $B(Q, \omega)$  is the background.  $L(\Delta, \omega)$  represents the QE contribution with a half-width of the half-maxima  $\Delta$ . In figure 1 is show a fit of the measured QE spectra at 500 °C, at  $\Delta E \approx 30 \mu\text{eV}$  and at  $Q = 1.25 \text{ \AA}^{-1}$ . The QE spectra are well reproduced by this model. The evolution of the QE widths as a function of  $Q$  at each temperature shows a strong  $Q$  dependency, indicating translational diffusion of protons.

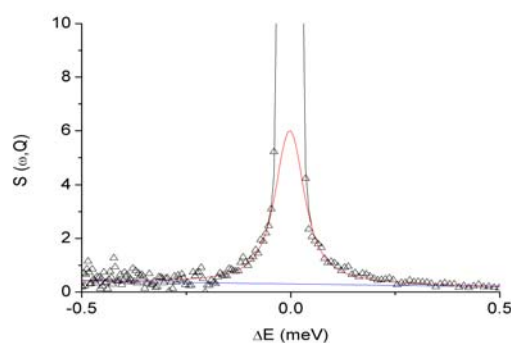


Figure 1. The QENS spectra reproduced by a phenomenological model. The triangles are the experimental points, and the solid lines the different contributions of the model.

Acknowledgements:

This research project has been supported by the European Commission under the 6<sup>th</sup> Framework Programme through the Key Action: Strengthening the European Research Infrastructures.

Contract n°: RII3-CT-2003-505925 (NMI 3).

This work is supported by the FRINAT project 171157/V30 "Hydrogen in oxides (HYDROX)" of the Research Council of Norway.



## EXPERIMENTAL REPORT

### Distinct Dynamic Behavior of Water Molecules in Hydrated Pores

Proposal N° CHE-03-596

Instrument **V3**

Local Contact  
Margarita Russina

Principal Proposer: Natalia Pérez-Heránádez, Instituto de Investigaciones Químicas (CSIC), Sevilla, Spain  
Experimental Team: Juergen Eckert, Material Research Laboratory University of California, Santa Barbara, USA  
Diego Fort, Instituto de Investigaciones Químicas (CSIC), Sevilla, Spain  
Nikolaos Tsapatsaris, Helmholtz-Zentrum Berlin für Materialien und Energie, Berlin, Germany

Date(s) of Experiment

14/10/2008 – 19/10/2008

Date of Report: 08/01/2008

Our research focuses on the role of confined water in biological processes such as ion or water transport through highly selective channels. To this end, we have synthesized a family of pore-forming compounds which incorporate water and investigated the behaviour of water behaviour with different techniques, mainly solid state NMR.

QENS experiments covering a T range from 225 to 300 K were designed in order to have access to information at a time scale faster than NMR and to attempt to distinguish between rotational and translational dynamics of the water molecules, by utilizing different instrumental energy resolution.

The experiments were carried out using 150 mg of one of our pore-forming substances sealed in gold plated sample holders of 0.2 mm depth. The first set of experiments was carried out with an energy resolution of approximately 95  $\mu\text{eV}$ , which was measured with the sample at 100 K. With this configuration we collected data at 250, 270, 290 and 300 K, and were able to observe appreciable quasielastic broadening, which showed a strong increase at higher temperatures.

We then shifted to a second configuration with an incident wavelength of 7.5Å with a resolution of approximately 45  $\mu\text{eV}$ , in an effort to differentiate between different dynamic processes possessing different widths. We collected data at four different temperatures (225, 250, 270 and 300 K). Initial analysis of the experimental data did reveal the presence of at least one more quasielastic peak with a different width, which points to the presence of a slower process.

Because of the fact that that the data analysis software was not fully functional at the time of the experiment, the analysis and fitting of the experimental spectra to models for water

dynamics was delayed. This effort is currently underway with the use of the program "Fitmo", to which remote access has been provided.

Our preliminary analysis does, however, make it clear that QENS is indeed a very useful tool for our investigations, and we therefore anticipate a continuation of our work to compare these results of water dynamics with those to be obtained on water in similar, but less confining pores.

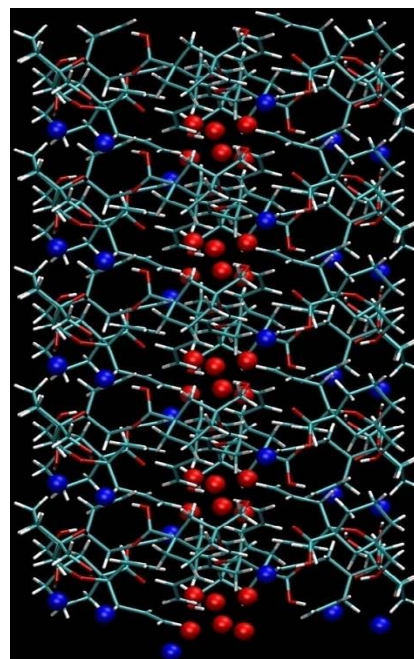


Figure: Crystal structure of the compound of interest with side view of the pore is shown. Water in the walls of the pore is represented in blue and cluster water in red.

*This research project has been supported by the European Commission under the 6<sup>th</sup> Framework Programme through the Key Action: Strengthening the European Research Infrastructures.*

*Contract n°: RII3-CT-2003-505925 (NMI 3).*



## EXPERIMENTAL REPORT

### Phason Dynamics in the Icosahedral Quasicrystal i-AlCuFe

Proposal N° PHY-03-526

Instrument **V5**

Local Contact  
Pappas, Bentley

Principal Proposer: Richard Brand, Univ. Duisburg-Essen  
 Experimental Team: Richard Brand, Univ. Duisburg-Essen  
 Catherine Pappas, HMI  
 Philip Bentley, HMI

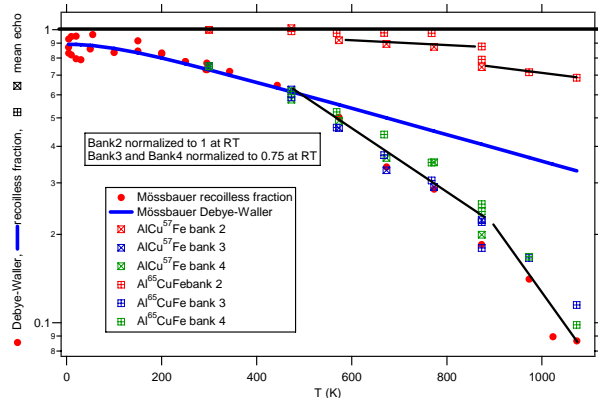
Date(s) of Experiment

26/10/2007 – 11/11/2007

Date of Report: 14/01/2008

We have continued our previous experiment (PHY-03-467) on V5 to study the high temperature phason dynamics in the icosahedral quasicrystal i-AlCuFe. Our purpose was to separate the different atomic components (especially Cu and Fe) of the phason dynamics by using changes in the scattering cross section. Three different samples were available, one with all natural isotopes, one with  $^{65}\text{Cu}$  and one with  $^{57}\text{Fe}$  respectively. The first experiment concerned mainly the sample with  $^{65}\text{Cu}$ . In the present experiment the sample with  $^{65}\text{Cu}$  and one with  $^{57}\text{Fe}$  were studied. The difference is that in the first, the copper scattering cross section is large, while in the second the iron scattering is almost absent. Thus we study mainly the contribution of copper to the atomic dynamics.

The set-up used was as follows. Bank 2 covered the range of 0.74 to 0.90 A-1, bank 3 from 1.30 to 1.43, and bank 4 from 1.71 to 1.78 A-1.



The interesting thing about these ranges is that the bank 2 is located in a region of reciprocal space where there is no significant elastic Bragg reflection from the quasicrystal. Several elastic reflections are in the range of the banks 3 and 4. Thus we can compare elastic and inelastic scattering.

To reach the high temperatures necessary for this experiment, the ILL high-temperature oven was used. This has the disadvantage that the heater is not bifilar so that a certain effect of the magnetic field generated must be compensated for. This was

achieved by measuring vitreous quartz at temperatures up to 600 K. This yields the apparent Debye Waller factor. Literature data for the measured Debye Waller factor was used to compensate.

We found that in the region of Fourier times 0.01 to 2 ns, that the echo amplitude was constant within the statistics, but decreased with increasing temperatures. We interpret this as meaning that we are sensitive to decreases in self-correlation for times shorter than 0.01 ns. Such fast processes are known to be given mainly by copper in i-AlCuFe. We normalized the average echo amplitude to that of the quartz and found that the results of bank 2 (low Q) were temperature independent and near unity up to about 600K. The results of banks 3 and 4 decreased in this region as a normal Debye Waller effect. Therefore we normalize the bank 2 data to units and those of banks 3 and 4 to the DW of quasicrystal AlCuFe measured by  $^{57}\text{Fe}$  Mössbauer spectroscopy. This yields the surprising results given in the figure. We see normal Debye behaviour up to 600K for the two banks including elastic Bragg reflections. Then there is a strong decrease which proceeds in two steps: one from 600 to about 850, and the second above this. We see the same behaviour in the data for bank 2, but here there are step decreases in the average echo intensity.

We remark as well that the data for the two samples are very similar, and that the main contribution is from copper. These results are now being analysed further. It would be interesting to follow down to shorter Fourier times to explicitly show the copper dynamics.



## EXPERIMENTAL REPORT

### Phason Dynamics in the Icosahedral Quasicrystal i-AlCuFe

Proposal N° PHY-03-600

Instrument **V5**

Local Contact  
Evgeny Moskvina

Principal Proposer: Richard Brand, Universität Duisburg-Essen  
 Experimental Team: Richard Brand, Universität Duisburg-Essen  
 Evgeny Moskvina, BENSC  
 Catherine Pappas, HMI

Date(s) of Experiment

20/08/2008 – 02/09/2008

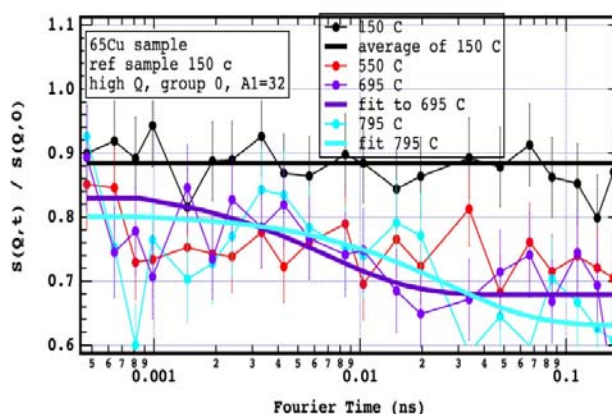
Date of Report:

We have continued our previous experiments (PHY-03-467 and PHY-03-0526) on V5 to study the high temperature phason dynamics in the icosahedral quasicrystal i-AlCuFe. Two different samples were available, one enriched in  $^{65}\text{Cu}$  and one in  $^{57}\text{Fe}$ .

In experiment PHY-03-0526 we found that in the region of Fourier times 0.01 to 2 ns, the echo amplitude was constant within the statistics, but decreased with increasing temperatures. We interpret this as meaning that we are sensitive to decreases in self-correlation for times shorter than 0.01 ns. We normalized the average echo amplitude to that of the quartz and found that the results in the low Q region were temperature independent and near unity up to about 600K. The results from higher Q range decreased in this region as a normal Debye Waller effect.

In this experiment we covered the Fourier times from 0.5 ps to 0.5 ns. We studied both the  $^{65}\text{Cu}$  isotopic sample as well as the  $^{57}\text{Fe}$  one. As before, spectra were taken up to about 1100K, using the low temperature data as normalization. Quartz data were taken at two temperatures in order to calibrate as well as check the effect of oven current on the spin echo signal.

In this experiment we were able for the first time to actually observe atomic dynamics directly. As the data reduction is not yet completed, we present here only a few examples. In the figure, we see the Q range from 1.2 to 1.6 AA $^{-1}$  at several different temperatures. The data from 150 C is clearly flat reflecting no other dynamics than lattice vibrations. The data for 695 and 795 C show clear exponential decay in the range of 0.5 to 5 ps.



The exponential decay time constant is in the range of times which we would expect from the previous MIBIMOL results (Coddens1993b,Coddens1996). The signal decays to a finite intensity. This is taken as an indication of the finite Bragg background. These data are now being analyzed and a more complete report will be submitted at a later date.

#### References:

(Coddens1993b) G. Coddens et al., Europhys. Lettr., **23**, (1993) 33.

(Coddens1996) S. Lyonnard and D. Gratias, Phys. Rev. B, **53**, (1996) 3150.



## EXPERIMENTAL REPORT

### Spectral Hole-Burning - Neutron Spin-Echo Studies of Water Flips in $\text{NaMgAl(oxalate)}_3 \cdot 9\text{H}_2\text{O}$

Proposal N° PHY-03-605

Instrument **V5**

Local Contact  
C. Pappas; S. Wellert

Principal Proposer: H Riesen, S J Campbell, School of PEMS,  
UNSW@ADFA;  
D Kearley, Bragg Institute, ANSTO, Australia  
Experimental Team: S J Campbell, UNSW@ADFA, Australia  
D Kearley, Bragg Institute, ANSTO, Australia  
Katia Pappas and Stefan Wellert, BENSC

Date(s) of Experiment

01/10/2008 – 13/10/2008

Date of Report: 09/01/2009

Using the neutron spin echo instrument V5 of BENSC and related ancillary equipment, we have investigated deuterated samples of  $\text{NaMgAl(oxalate)}_3 \cdot 9\text{H}_2\text{O}$  which exhibit remarkable spectral hole-burning properties [1]. The plan for the SPAN experiments was to delineate the dynamic effects with the aim of understanding more fully the influence of deuteration in the remarkable enhancement of the spectral hole-burning exhibited by these materials.

Previous studies suggest that the relaxation mechanism involves some motion of the water molecules, probably flipping. Neutron scattering is an ideal technique to investigate this type of motion. Our proposal was aimed at studying motion in the time range of 0.1-5 ns, this timescale having been deduced from extrapolation of NMR data. While NMR data are sensitive to motion, they give little information as to the nature of the motion or the mobile species.

We collected data at room temperature on a sample that was almost completely deuterated (~98 %). These relaxation data revealed a scatter of points with relaxation time rather than the expected decay-curve (Fig 1).

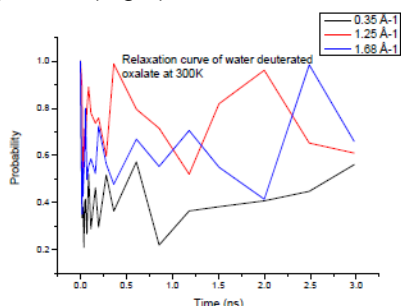


Fig. 1 Relaxation results at room temperature for  $\text{NaMgAl(oxalate)}_3 \cdot 9\text{H}_2\text{O}$  deuterated to ~ 98 %.

Similar results were obtained for other measurements in this range but without any discernable relaxation behaviour, or indeed any trends with temperature. At lower temperatures, ~200 K, any water-motion would be much slower and we therefore expected to see higher probability values at all relaxation times. While the scatter is reduced in the 200 K data (Fig 2), the actual values

are rather lower than at ~ 300 K. These findings are very difficult to understand as they infer an underlying process that is much faster at 200 K than at 300 K. We then cooled the sample to below 20 K where we would expect to see only the resolution of the instrument (value ~1) at all times, but again obtained scattered, inconclusive results.

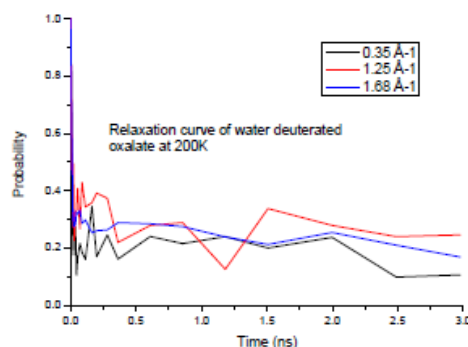


Fig. 2 Relaxation results at ~ 200 K for  $\text{NaMgAl(oxalate)}_3 \cdot 9\text{H}_2\text{O}$  deuterated to ~ 98 %.

Similar relaxation results and behaviour were obtained for a partially deuterated sample (~ 50 %). As such the entire set of results is difficult to understand in terms of relaxation of atomic positions with time. We consider the most likely explanation of our results is that the time-scale of the water motion falls outside the range of the spectrometer. Test data were therefore obtained on the V3 time-of-flight spectrometer running at high resolution. These experiments failed to reveal a quasielastic signal from the oxalate indicating that any water-motion occurs on a very long timescale and that the waters are firmly held. This would seem to militate against the waters playing a role in the rapid relaxation process – an unexpected and very interesting outcome for these experiments.

It is not unusual that NMR measurements indicate a timescale that is different from that found by neutron scattering. When this arises it usually transpires that the processes being measured by the two techniques – neutron scattering and NMR – are different.

[1] H Riesen, Coordination Chemistry Reviews **250** (2006) 1737

	<b>EXPERIMENTAL REPORT</b> <b>Cation partitioning in Zn(AlFe)2O4 spinels  as a function of temperature, by neutron  powder diffraction</b>	Proposal N° GEO-01-2035 Instrument <b>E2</b> Local Contact A. Hoser
	Principal Proposer: Prof. Dr. Alessandro Pavese, Univ. Milano. I Experimental Team: Nicoletta Marinoni, Univ. Milano, I Elena Ferrari, Univ. Milano, I A. Hoser, HZ Berlin	Date(s) of Experiment 11/11/2008 – 14/11/2008

Date of Report: January 2009

### Objectives:

In situ neutron powder diffraction (NPD) in the temperature range of 25-1100°C have been performed at E2 on synthetic and natural spinels with chemical formula Zn(Fe<sup>3+</sup>, Al)<sub>2</sub>O<sub>4</sub>. Spinel is an oxide mineral found in a wide range of geological environments, from upper mantle to crust. Their elementary cell contains 32 oxygen atoms in cubic close packing arrangement, 16 octahedrally (M) and 8 tetrahedrally (T) coordinated sites which host bi-, tri- and tetra-valent. The cation partitioning over the T- and M-sites is related to pressure and temperature. Therefore in situ determination are fundamental for understanding the thermo baric history of spinels.

The measured cation distribution has then been compared and discussed with that calculated by the maximum configuration entropy approach, for which NPD patterns have been used. The cation partitioning has finally been interpreted in the light of the configuration model of O'Neill-Navrotsky.

### Achievements/difficulties:

The cation partitioning over the T- and M-site as a function of T of the three cations (Zn, Fe<sup>3+</sup> and Al) was determined by Rietveld refinements. In particular the thermal expansion coefficients of the lattice parameters, interatomic bond lengths, Oxygen coordinate and isotropic thermal parameters were obtained from the full-profile structure refinements.

Preliminary results agree with a two-stage reaction, in which an initial exchange between Fe<sup>3+</sup> and Zn, the former leaving and the latter entering tetrahedral sites, is successively followed by a rearrangement involving Al.



## EXPERIMENTAL REPORT

### Investigation of the Al/Si distribution in sanidine

Proposal N° GEO-01-2340

Instrument **E2**

Local Contact  
Andreas Hoser

Principal Proposer: Susan Schorr, Freie Universität Berlin, FBGeowissenschaften  
 Experimental Team: Andreas Hoser, HZB für Materialien und Energie  
 Susan Schorr, Freie Universität Berlin, FBGeowissenschaften

Date(s) of Experiment

24/11/2008 – 26/11/2008

Date of Report: 19/01/2009

The feldspar sanidine is a mixture between orthoclase ( $KAlSi_3O_8$ ) and albite ( $NaAlSi_3O_8$ ). It crystallizes in a monoclinic structure based on a framework of corner-sharing  $AlO_4$  and  $SiO_4$  tetrahedra. The structure contains two symmetrically non-equivalent tetrahedral sites,  $T_1$  and  $T_2$ ; but because there are 16 T sites per unit cell and 4Al+12Si atoms to fill them, it is not possible to have an ordered Al/Si distribution in these two sites. If the Al/Si distribution is random, the structure is said to be completely disordered (high sanidine). Nevertheless applying slow annealing,  $Al^{3+}$  is expected to migrate preferentially into the  $T_1$  sites and  $Si^{4+}$  into the  $T_2$  sites in order to satisfy local electrostatical balance considerations (low sanidine).

The Al/Si distribution on the two symmetrically non-equivalent tetrahedral sites influences the kinetics of mineral reactions during the phase separation process in the orthoclase-albite system. Thus a knowledge of the Al/Si distribution in the starting material is indispensable for the further investigation of the phase separation.

Al and Si are neighbouring elements in the periodic table,  $Al^{3+}$  and  $Si^{4+}$  have the same number of electrons and therefore, nearly similar atomic scattering factors in X-ray diffraction. Otherwise the coherent neutron scattering length of Al and Si is different. Thus structural analysis by Rietveld refinement of neutron diffraction data allows the separation of isoelectrical ions like it is the case for  $Al^{3+}$  and  $Si^{4+}$ .

Neutron diffraction experiments were performed at the flat cone diffractometer E2 ( $\lambda=2.39 \text{ \AA}$ ) using two samples of natural sanidine ( $K_{0.82}Na_{0.18}AlSi_3O_8$ ), one untreated sample and the other annealed at  $1050^\circ\text{C}$ .

The neutron diffraction pattern of the untreated sample was analyzed by Rietveld refinement using the FullProf software package [1]. The structure model of orthoclase (space group

$C2/m$ ) was used as starting point for the refinement procedure. Global profile parameters including a scale factor, a  $2\theta$  zero parameter and parameters of a peak shape function (U, V, W). A Thompson-Cox-Hasings pseudo-Voigt convoluted with axial divergence asymmetry function [2] was used as peak shape function. The background was fitted using a three-parameter polynomial. The lattice parameter determined by Rietveld analysis are summarized in table 1.

The refinement of the neutron diffraction data of the annealed sample is ongoing.

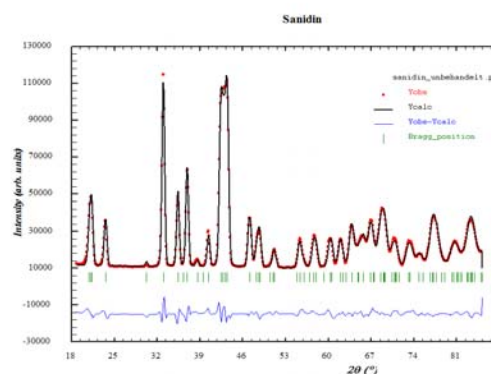


**Figure 1:** Analyzed neutron diffraction pattern of the untreated sanidine sample ( $R_{Bragg}=3.20$ ).

**Table 1:** Lattice parameter of sanidine

lattice parameter	
a [Å]	8.536 (1)
b [Å]	13.012 (2)
c [Å]	7.184 (1)
$\beta$	116.005 (2)°

Further analysis will yield more detailed results about the Al/Si distribution on the two tetrahedral sites of the orthoclase type structure.

[1] J. Rodriguez-Carjaval, Physica B 192 (1993) 55.

[2] Finger, Cox, Jephcoat, J. Appl. Cryst. 27 (1994) 892.

	<b>EXPERIMENTAL REPORT</b>  <b>Hydrogen bonds evaluation in the crystal structure of mineral catapleiite</b>	Proposal N° CHE-01-2244 Instrument <b>E5</b> Local Contact Manfred Reehuis
	Principal Proposer: Oxana Karimova Experimental Team: Manfred Reehuis	Date(s) of Experiment 14/04/2008 – 25/04/2008

Date of Report: 14/01/2009

The main goal of conducted experiment was determination of proton position in a crystal structure of mineral catapleiite. The crystal structure of catapleiite  $\text{Na}_2\text{ZrSi}_3\text{O}_9 \cdot 2\text{H}_2\text{O}$  has been studied before by X-ray diffraction. But traditional single crystal X-ray diffraction is not suitable tool for determination of proton position in a structure. The only possibility to locate hydrogen in a structure is to use single crystal neutron diffraction.

A crystal of catapleiite with dimensions 5x10x2 mm was mounted on the four-circle E5 single crystal diffractometer of the BER II reactor at the Berlin Neutron Scattering Center, Helmholtz-Center for Materials and Energy. A monochromated beam with  $\lambda=0.89491$  was attained by reflection from the (220) plane of a copper single crystal. The data were collected using an area position-sensitive ( $90 \times 90 \text{ mm}^2$ )  $^3\text{He}$ -detector. A total of 3054 reflections were collected, of which 2098 reflections were unique.

Neutron diffraction study of mineral catapleiite at BENSC resulted in successful elucidation of the structure with proton position location.

#### Acknowledgement:

This research project has been supported by the Helmholtz-Center Berlin for Materials and Energy.



## EXPERIMENTAL REPORT

### Hydration of Sm<sup>3+</sup>, Ni<sup>2+</sup> and Na<sup>+</sup> in Clay Interlayer: Quasielastic Neutron Study

Proposal N° GEO-03-547

Instrument **V3**

Local Contact  
M. Russina, E. Kemner

Principal Proposer: O. Sobolev, LGIT, CNRS&UJF, Grenoble, France  
Experimental Team: L. Charlet, LGIT, CNRS&UJF, Grenoble, France  
C. J. Cuello, ILL, Grenoble, France

Date(s) of Experiment

16/05/2008 – 19/05/2008

Date of Report: 15/01/2008

Smectite clay minerals are layer-type aluminosilicates consisting of negatively charged silicate layers held together by cations to give a stacked (crystalline) structure. Under humid conditions, the cations in the interlayer and the internal clay surfaces are hydrated. Clay minerals have been selected as the most suitable buffer material for high level radioactive waste repositories. The buffer material is expected to retard the migration of the radionuclides in case of corrosion of the waste package material.

Sm<sup>3+</sup> cation is of interest because it can be considered as a chemical analog of actinides such as Pu<sup>3+</sup> and Am<sup>3+</sup>.

In our previous experiments [1,2] we studied by means of neutron diffraction with isotopic substitution the structural parameters of the coordination of Sm<sup>3+</sup>, adsorbed in the interlayer space of the *montmorillonite*. It was found that the number of hydrogen atoms  $N_H = 5.5 \pm 2.0$  in the first coordination shell of Sm<sup>3+</sup> is equal or even slightly smaller than those of oxygen atoms  $N_O = 7.5 \pm 1.0$ . This means that not all these oxygen atoms belong to water molecules. It was supposed that the Sm<sup>3+</sup> ion binds to the clay surface via oxygen siloxane atoms, and it is probably partially hydrolyzed. However in our MD simulations and EXAFS experiments Sm<sup>3+</sup> cation was found to be localized at the middle of the clay interlayer and fully hydrated.

Quasielastic neutron scattering experiments were performed with *Na-hectorite*, *Ni-hectorite* and *Sm-hectorite* samples in order to compare the diffusion mobility of water molecules in *Sm-hectorite* with that for other interlayer cations: *strongly hydrated Ni<sup>2+</sup>* and relatively *weakly hydrated Na<sup>+</sup>*.

The incident neutron wavelength was  $\lambda_0 = 8 \text{ \AA}$ , with an elastic resolution  $\Delta \sim 30 \text{ \mu eV}$  measured by using a standard vanadium sample. Flat sample cells with 0.6 mm thickness were used, resulting in a transmission of about 94%. The sample orientation angle with respect to the incident neutron beam direction was 135°. The QENS was measured in a Q range of 0.23 – 1.33  $\text{\AA}^{-1}$ .

It was found that water mobility in *Sm – hectorite* sample is close to the water mobility in the *Ni-hectorite*. This is only possible if Sm<sup>3+</sup> ion is fully

hydrated. A compromise with the neutron diffraction data can be found, assuming that not all adsorbed Sm interacts with water molecules, probably due to precipitation.

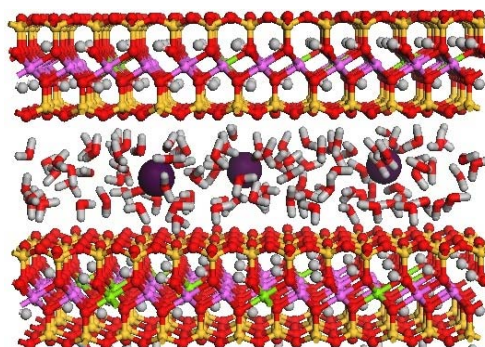


**Fig. 1** Snapshot from a molecular dynamics simulation of a hydrated smectite clay. Sm<sup>3+</sup> cations (big dark spheres) lie on the clay interlayer surrounded by water molecules.

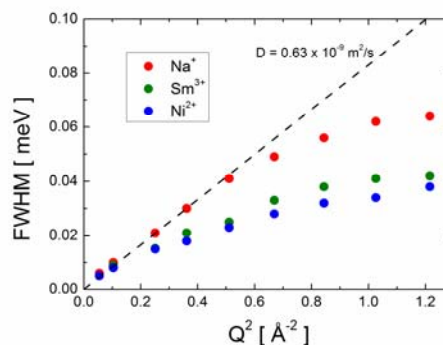


**Fig. 2** Full Width at Half Maximum of Quasielastic Scattering obtained for the *Na-hectorite* (red), *Sm-hectorite* (green) and *Ni-hectorite* (blue).

## References

- [1] Sobolev, O.; Charlet, L.; Cuello, G. J.; Gehin, A.; Brendle J.; and Geoffroy, N. *J. Phys.: Condens. Matter.* **2008**, 20, 104207
- [2] Sobolev, O.; Charlet, L.; Cuello, G.J.; Gehin, A.; Brendle, J.; *Radiochimica Acta* **2008**, 96, 1–5.

*This research project has been supported by the European Commission under the 6<sup>th</sup> Framework Programme through the Key Action: Strengthening the European Research Infrastructures.*

*Contract n°: RII3-CT-2003-505925 (NMI 3).*



## **Biology & Soft Matter**

Biology	147
Soft Matter	166





## EXPERIMENTAL REPORT

### Determination of the crystal structure of L and DL-Serine under pressure

Proposal N°  
BIO-01-2294-EF

Instrument **E6**

Local Contact  
Alexandra Buchsteiner

Principal Proposer: H.N. Bordallo, Helmholtz-Zentrum für Materialien und Energie  
Experimental Team: H.N. Bordallo, Helmholtz-Zentrum für Materialien und Energie  
Alexandra Buchsteiner, Helmholtz-Zentrum für Materialien und Energie  
Walter Kalceff, UTS, Sydney, Australia  
E.V. Boldyreva, NSU, Novosibirsk, Russia

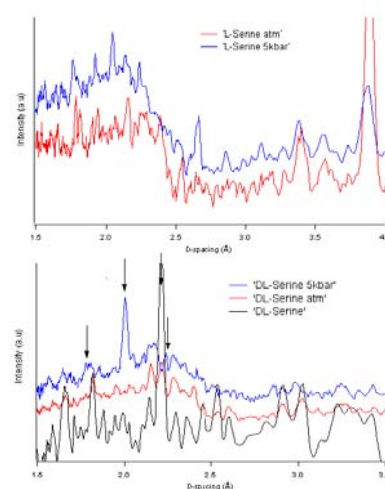
Date(s) of Experiment

22/04/2008 – 25/04/2008

Date of Report: 04/08/2008

Many biologically-active molecules are chiral, including the naturally occurring amino acids. Chirality is a property of molecules that belong to polar groups, distinguished by a unique 3D structure in which pairs of mirror image molecules are not super-imposable and are referred to as enantiomers. Amino acids crystallize in different crystal structures with different hydrogen bonding (HB) networks. In the solid state, they exist in the zwitterionic form,  $\text{NH}_3^+\text{CHR}\text{COO}^-$ , where the *R*-groups are characteristic of the particular amino acids. The  $\text{N}^+\text{-H}\dots\text{O}$  HBs contribute notably to the intermolecular interactions in these compounds. Interest in chiral (pure D or L) vs racemic (DL) amino acid forms stems from their different solid-state properties associated with the packing arrangement that leads to starkly different physical behavior. Measuring incoherent inelastic and Raman spectra over a wide temperature range, we recently identified a subtle dynamical transition (only) in L-serine near 150 K (1). Moreover, a comparative study using single crystal X-ray diffraction shows that the anisotropy of strain in L- and in DL-serine on cooling is radically different from that with increasing pressure (2). Subsequently, we performed a new inelastic neutron scattering experiment to follow the effects of pressure on the HBs in L and DLserine, observing that while in L-serine some modes harden with increasing pressure, in DLserine discontinuous changes in particular vibrational modes suggest some sort of molecular rearrangement (3). Similar behavior has been observed by Raman scattering (4). For a better understanding of our vibrational data, it is essential to determine the position of the H-atoms. Normally in biological materials this relies on costly deuteration; moreover, substitution of H for D can give rise to an increase in HB lengths and induce changes in the HB interactions due to the

Ubbelohde effect, as we have just verified (5). Instead, this problem can be tackled using neutron high flux and high-resolution powder diffractometers such E6 at HMI. A preliminary study to verify the feasibility of our proposal was performed using E6 at HMI. Results from our NPD experiments at 300K at atmospheric pressure and 5kbar are given in Fig.1. While no obvious changes, other than displacements of peak position, could be observed in L-Serine, in DL-Serine there were noticeable changes (arrows). Further studies are under way.



- 1-H.N. Bordallo, B.A. Kolesov, E.V. Boldyreva and F. Juranyi *JACS* 2007, 129, 10984
- 2-E.V. Boldyreva, E.N. Kolesnik, et al. *Z. Kristallogr.* 2006, 221, 150 & E.N. Kolesnik et al, *Doklady Phys. Chem.* 2005, 404, 169
- 3-H.N. Bordallo, E.V. Boldyreva, T. Strassle, *FOCUS* 20071237 - PSI Nov. 2007
- 4-C. Murli, R. Vasanthi and S.M. Sharma, *Chem. Phys.* 2006, 331, 77
- 5-J. M. de Souza, P. Freire, H. N. Bordallo, D.N. Argyriou, *J. Phys. Chem. B* 2007, 111, 5034



## EXPERIMENTAL REPORT

### Structural Anomalies in Valine

Proposal N°  
BIO-01-1822-EF

Instrument **E9**

Local Contact  
D. N. Argyriou

Principal Proposer: H. N. Bordallo, Helmholtz-Zentrum Berlin für  
Materialien und Energie  
Experimental Team: H. N. Bordallo, Helmholtz-Zentrum Berlin für  
Materialien und Energie  
D. N. Argyriou, Helmholtz-Zentrum Berlin für  
Materialien und Energie

Date(s) of Experiment

15/08/2007 – 19/08/2007

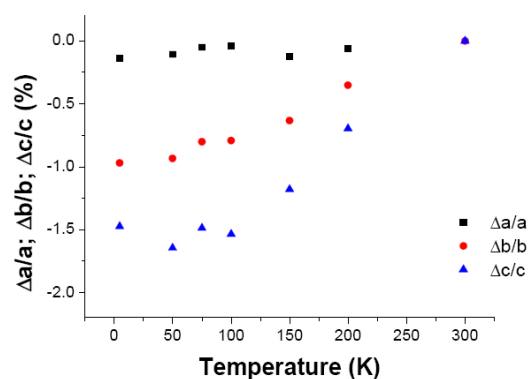
Date of Report: 03/08/2008

Valine ( $C_5H_{11}NO_2$ ) is an essential, naturally occurring amino acid, vital for human metabolism. It is needed for all muscle building, and is a necessary precursor of cholesterol. In the solid state it adopts a non centrosymmetric space group ( $P2_1$ ) and is piezoelectric. Changes in Raman spectra (1) and in the piezoelectric response at  $\sim 110$  K (2) appear to indicate a phase transition at about 120K.

The neutron powder diffraction experiments performed using E9 revealed a negative thermal expansion at about the same temperature, see Figure. However, there is no clear evidence in powder data for a change in space- group symmetry. We believe that the lattice contraction on cooling leads to changes in the hydrogen bonding network, causing rotations and twists of the zwitterions and driving the rearrangement. To get a better insight into the key role of hydrogen bonding temperature-dependent vibrational data on a large time range is being undertaken to properly study this transition.

Taking into consideration the piezoelectric response observed in the amino acids (2,3), the idea of possible phase changes appear to be of great interest. In the last years we started a careful structural study of glycine, alanine and serine. High resolution XRD and NPD on L-alanine show that while there is no change in the space group symmetry, there is an unusual increase (on cooling) of the c lattice parameter (4) – i.e., negative thermal expansion (NTE). Moreover, the evolution of the mean-square displacement obtained from QENS data on glycine (5), alanine (6) and serine (7) reveals a change in dynamic properties at about 150 K, which can be related to the reorientation of the  $NH_3$  group. In general, phase transitions such

as these can be connected to the contraction of the unit cell on cooling that leads to changes in the hydrogen-bond network, modifying the crystal symmetry through rotations and twists of the zwitterions.



1. Lima Jr., J.A., P.T.C. Freire, Sasaki, et al., J. Raman Spectrosc. 36, 1076 (2005)
2. V.V. Lemanov et al, Magnetism and Ferroelectricity 44:1840 (2002)
3. P. Langan et al, Acta Cryst. B58 :728 (2002)
4. M. Barthes, H.N. Bordallo et al European Phys. J. B 37, 375–382 (2004)
5. H.N. Bordallo, E.V. Boldyreva et al, J. Phys. Chem. B, 112, 8748 (2008)
6. de Souza J.M. Freire P.T.C. Bordallo H.N. Argyriou D.N., J. of Physical Chemistry B111,5034, (2007)
7. Bordallo, H.N., Kolesov, B.A., Boldyreva, E.V., Juranyi, F. J. Am. Chem. Soc., 129, 10984, (2007).



## EXPERIMENTAL REPORT

### Structural Organization of Photosystem II Membranes of Green Plants

Proposal N° BIO-01-2247

Instrument **V1**

Local Contact:  
Th. Hauß, S. Dante

Principal Proposer: J. Pieper, TU Berlin  
Experimental Team: J. Pieper, TU Berlin  
Th. Hauß, S. Dante, HMI Berlin  
M. Weß, G. Renger, TU Berlin

Date(s) of Experiment

21.01. – 27.01.2008

Date of Report: 19.03.08

The photosynthetic water splitting (for a review see e.g. G. Renger [1]) takes place in a multimeric membrane-bound protein complex referred to as Photosystem II (PS II).

A number of studies indicated that certain PS II redox reactions exhibit a pronounced dependence on temperature [2] and on the relative humidity of the sample [3]. Recently, we have shown that diffusive protein motions on the ps-timescale in PS II membrane fragments set on at a temperature of ~240 K and at a relative humidity (r.h.) of ~45 %, i.e. exactly the values where the PS II redox reactions are activated [4,5]. These findings suggest that the functionality of PS II is strongly correlated with the protein flexibility in PS II membrane fragments.

A deeper understanding of these effects requires information on the structural organization of PS II membrane fragments and the location of hydration water molecules.

To address this point, we carried out neutron diffraction measurements on PS II membrane fragments using the membrane diffractometer V1 (see Fig. 1). The preparation protocol was identical to that used in the preceding QENS studies. The sample was hydrated at 6 well-defined r.h.-values between 22 and 90 %. The results show a complex structure with peak positions depending on the hydration degree of the sample (see Fig. 1). Further weak, but discernible peaks are found at higher Q-values. Quite remarkable is the strong increase of the peak intensity upon r.h.-decrease from 90 to 75 %, while there is a subsequent decrease of peak intensity with decreasing r.h. below 75 %. To investigate this effect, additional experiments were carried out at a fixed r.h. of 57 % with contrast variation for the hydration water. These measurements (not shown) revealed that the structure shown in Fig. 1 is completely lost upon suppression of the water contribution to the total diffraction signal. This finding establishes that the hydration-dependent diffraction signal of PSII membrane stacks is almost entirely due to

coherent scattering originating from the hydration water molecules and that there is an ordering of these water molecules upon r.h.-decrease from 90 to 75 %. The subsequent loss of peak intensity upon a further r.h.-decrease is consistent with reduced lattice constants. A more detailed analysis is in progress.

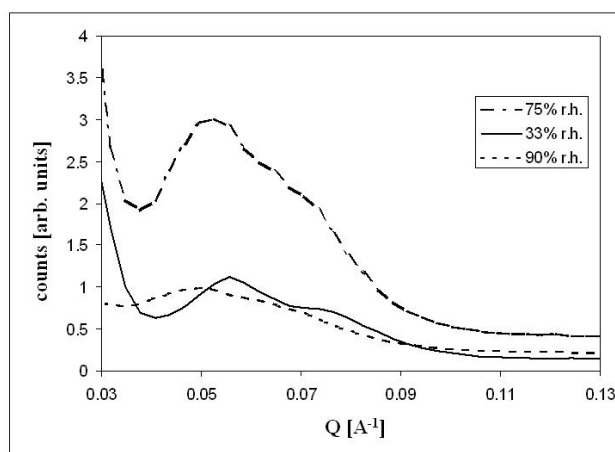


**Figure 1**

*Diffraction curves of PSII membrane fragments hydrated with D<sub>2</sub>O at r.h.-values of 33, 75 and 90 %.*

#### References:

1. G. Renger, *Biochim. Biophys. Acta* 1503 (2001) 210-228
2. Garbers, F. Reifarth, J. Kurreck, G. Renger, F. Parak, *Biochemistry* 37 (1998) 11399-11404
3. O. Kaminskaya, G. Renger, V. A. Shuvalov, *Biochemistry* 42 (2003) 8119-8132
4. Pieper, J., Hauß, T., Buchsteiner, A., Baczynski, K., Adamiak, K., Lechner, R.E., Renger, G., *Biochemistry* 46 (2007) 11398-11409
5. Pieper, J., Hauß, T., Buchsteiner, A., Renger, G., *Eur. Biophys. J.*, in press

	<b>EXPERIMENTAL REPORT</b>	Proposal N° BIO-01-2249
	<b>Role of ceramide [AP] and ceramide [EOS] in the structural assembly of stratum corneum model membrane.</b>	Instrument V1 Local Contact Th. Hauß
Principal Proposer: T. Engelbrecht – MLU, Halle (Saale), Germany Experimental Team: Annett Schroeter – MLU, Halle (Saale), Germany R. Neubert MLU, Halle (Saale), Germany Th. Hauß (HMI, Berlin).	Date(s) of Experiment: 27.08.08 – 04.09.08	

Date of Report: 13.01.2008

The human skin and its outermost layer, the stratum corneum (SC), play an important role in protecting the body against environmental influences. It is generally accepted that the barrier function of the SC is associated with its unique composition of lipids (main constituents: ceramides (CER), cholesterol (CHOL), free fatty acids (FFA)) and the special assembly. These lipids are known to develop an exceptional lamellar matrix structure, which is matter of current debates.

The focus of research effort is put on the investigation of oriented lipid model membranes on quartz slides, composed of simplistic, well defined lipid mixtures with varying ceramide components. Applying neutron diffraction as a useful tool enabled us to receive detailed information about the internal nanostructure of these model systems and to study the properties of each ceramide subclass. Our recent experiment BIO-01-2249, carried out at V1 diffractometer, dealt with the following subjects:

(i) the quaternary model systems CER[EOS]/ **D-CER[AP]**/ BA/ CHOL (23/ 10/ 33/ 33 w/w) and CER[EOS]/ **L-CER[AP]**/ BA/ CHOL (23/ 10/ 33/ 33 w/w) were investigated regarding the influence of the two diastereomers (**D**- and **L**-CER[AP], respectively) on the membrane structure, as they are known to exhibit different physicochemical properties [1]. The calculated neutron scattering length density (SLD) profiles revealed a comparable assembly of the lipid components. In both cases lamellar repeat distances of about 48.4 Å could be detected (**D**-form: 48.40 Å, **L**-AP: 48.36 Å). In contrast to other studies [2] no long periodicity phase (LPP) of 130 Å was observed, although the long-chain  $\omega$ -acylceramide CER[EOS] was present, which is regarded to be a prerequisite for the formation of the LPP. The present findings are in line with our former results (BIO-01-2140, BIO-01-2062) [3], underlining the protruding influence of the very polar and short-chain CER[AP] and confirming the

recently proposed *armature reinforcement model* [4]. It is remarkable that both systems containing the pure diastereomers of CER[AP] showed phase separation (D-CER[AP]: 3 phases, L-CER[AP]: 2 phases). In contrast, the mixture of both did not show this phase separation.

(ii) To study the amount of polar CER[AP] needed to express lipid lamellae with repeat distances of 48-49 Å, we investigated SC model membranes containing a lower ratio of 2% and 5% w/w D,L-CER[AP] (CER[EOS]/ CER[AP]/ BA/ CHOL (23/ **5**/ 38/ 33 w/w and 23/ **2**/ 41/ 33 w/w, respectively). Again the neutron SLD profiles were calculated. As expected and illustrated in Fig. 1, the assembly of the lipids corresponds in both samples. It is noticeable that even a small amount of 2% CER[AP] induces the formation of the short periodicity phase, and that the other constituents, even CER[EOS], are forced to arrange inside this super-stable structure.

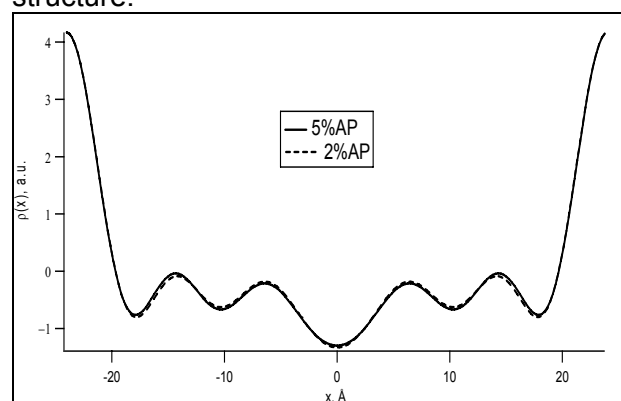


**Fig. 1:** Neutron scattering length density profile for the CER[EOS]/CER[AP]/BA/CHOL membrane with either 5% or 2% (w/w) CER[AP] at  $T=32^{\circ}\text{C}$ , 60%rH and 8% $\text{D}_2\text{O}$ .

#### References:

- [1] S. Raudenkolb, S. Wartewig and R.H. Neubert, Chem Phys Lipids 133 (2005) 89-102.
- [2] J.A. Bouwstra, G.S. Gooris, F.E. Dubbelaar, A.M. Weerheim, A.P. Ijzerman and M. Ponc, J Lipid Res 39 (1998) 186-96.
- [3] D. Kessner, M. Kiselev, S. Dante, T. Hauss, P. Lersch, S. Wartewig and R.H.H. Neubert, European Biophysics Journal with Biophysics Letters 37 (2008) 989-999.
- [4] M. Kiselev, Crystallography Reports 52 (2007) 528.



## EXPERIMENTAL REPORT

### Membrane Interactions of an Anthelmintic Drug

Proposal N° BIO-01-2251

Instrument **V1**

Local Contact

Dr. Thomas Hauß

Principal Proposer: Prof. Jeremy Bradshaw, University of Edinburgh

Experimental Team: Mr. Farid Sa'adedin, University of Edinburgh

Mr. Lijing Ke, University of Edinburgh

Dr. Thomas Hauß – HMI Berlin

Date(s) of Experiment

24/06/08 – 03/07/08

Date of Report: 15/01/2009

LS3 (LSSLLSL<sub>3</sub>) is a synthetic amphipathic peptide that lies on the hydrophobic/hydrophilic border of a phospholipid bilayer. Upon application of an applied voltage across a bilayer, the peptide 'flips' transbilayer and aggregates to form an ion channel. The channel consists of a hexamer of LS3, which has an approximate diameter of 8Å and can allow the free movement of K<sup>+</sup> and Cl<sup>-</sup> (Figure 1). Amphipathic peptides can be categorised into a particular class depending on their hydrophobicity. It is hypothesised that LS3 is classed as an apolipoprotein (A class) amphipathic peptide as evidence suggests that the peptide resides at the hydrophobic/hydrophilic interface of the membrane. Class A amphipathic peptides have been shown to stabilise lamellar formation and by the use of differential scanning calorimetry we have shown that the addition of LS3 to our phosphatidyl-ethanolamine system decreases the phase transition temperature and destabilises lamellar formation. Our investigation is to study the effect of having the peptide at a high concentration (1:50 and 1:25) molar ratio of peptide to lipid on our lipid system so we can observe:

1) How the interaction of the peptide affects lamellar stability.

2) Detailed structural information on the formation of the peptide pore by inducing at a high concentration in the bilayer.

Using a peptide to lipid concentration of 1:50 molar ratio, the neutron scattering density profile of the DOPE (cis/trans mol/mol 1:1) with LS3 peptide (deuterated leucine at position 11). The peptide density profile shows that the position of the peptide is just below the polar headgroup region of the bilayer, showing that the peptide directly acts along the hydrophobic/hydrophilic region of the membrane (Figure 2), which is in agreement to the model of peptide interaction along the membrane (Figure 1).

At higher peptide/lipid concentrations (1:25) neutron diffraction decreased at higher orders and

the presence of multiple lipid phases were observed. Analysis of the neutron diffraction is still ongoing and further work at high concentration of peptide needs to be carried out to fully investigate the mechanism of pore formation in a bilayer.

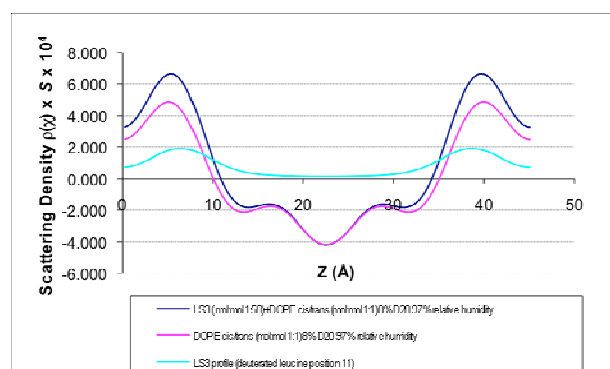
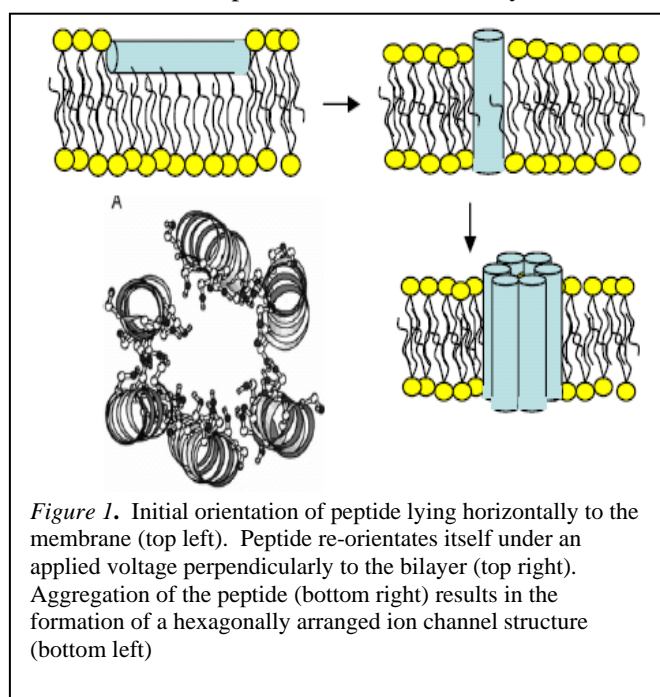


Figure 2: Neutron scattering length density profile with and without deuterated LS3.



## EXPERIMENTAL REPORT

### Mixed POPN bilayers for the confinement of ss-DNA

Proposal N° BIO-01-2253

Instrument: **V1**

Local Contact  
Thomas Hauß

Principal Proposer: Debora Berti, University of Florence and CSGI  
Experimental Team: Silvia Milani, University of Florence and CSGI  
Debora Berti, University of Florence and CSGI  
Thomas Hauß, HMI Berlin  
Sylvia Dante, HMI Berlin and IIT Genova

Date(s) of Experiment

28.05.2008 – 08.06.2008

Date of Report:

Neutron diffraction experiments have been performed on nucleolipid (POPNS) membranes to get information on possible structural variations induced by inclusion of oligonucleotides. Having a net negative charge, nucleolipids can interact with like-charged oligonucleotides through molecular recognition, due to their polar heads, constituted by nucleotides. These self-assembled systems can represent an interesting alternative to customarily used cationic lipid delivery vehicles for DNA (lipoplexes). Owing to the powder like nature of 1-palmitoyl,2-oleoyl-phosphatidyl-adenosine (POPA) membranes and considering the noteworthy structural effects of neutral lipids for lipoplexes' transfection efficiency, POPC was blended with POPA. Mixed liposomal dispersions from these lipids were prepared and de-hydrated on quartz slides for neutron diffraction experiments. Such samples were then measured with and without oligos addition to the liposomal dispersion. Two molar ratios have been taken into account, 1:1 and 2:3 POPA/POPC. The mixed membranes 1:1:2 POPA:POPU:POPC, where two complementary nucleolipids are present in the sample, were investigated as well.

All the spectra for lipid samples (without any oligonucleotides) showed up to five orders of diffraction, with a mosaicity lower than  $0.5^\circ$ , confirming the excellent quality of the lamellar stacks obtained from liposomal dispersions. Figure 1 shows the profiles obtained for 1:1 POPA:POPC mixtures for all the contrast variations used in this experiment. Thanks to the high structural quality of the samples and the data gathered in the experiment, it was possible to model the profile and to obtain several important structural parameters, such as the area per polar head and the number of water molecules. Minor differences were found out between the two investigated molar ratios. Remarkably, when complementary base oligos (50dT) were added to POPN/POPC

membranes a new lamellar phases (Figure 2) was visible, having a higher bilayer spacing with respect to the same membrane without oligos ( $54\text{\AA}$ ). Because of the similarity with the results obtained with neutral lipids and DNA bound thanks to the presence of divalent cations, the first lamellar phase (larger in terms of bilayer thickness,  $58\text{\AA}$ ) has been assigned to a novel structure constituted by oligos within the lamellae, whereas the second one (smaller in terms of bilayer thickness,  $52\text{\AA}$ ) is consistent with the presence of lamellae deprived in oligos and maybe enriched in POPC.<sup>1</sup>

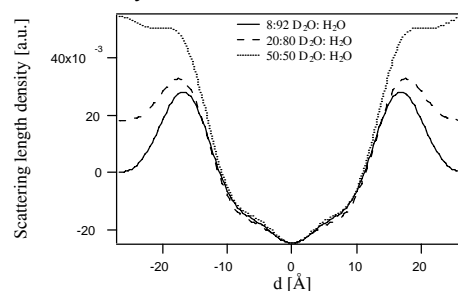


Figure 1. 1:1 POPA/POPC SLD profiles

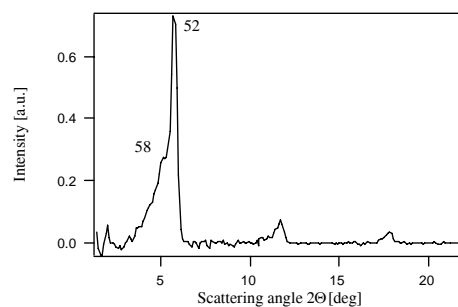


Figure 2. 1:1:1 POPA:POPC:50dT Diffraction patterns. Similar experiments have been carried out on POPG/POPC mixture where POPG is an anionic lipid as well as nucleolipids. In this case the addition of oligos does not induce any relevant structural transformations (no difference in the bilayers spacing value,  $56\text{\AA}$ ) even if a decreased mosaicity is detectable.

1) S. Milani et al, *Langmuir*, **2009**, 10.1021/la8029825

This research has been supported by the European Commission (6<sup>th</sup> Framework Programme through the Key Action: Strengthening the European Research Infrastructures. Contract n°: RII3-CT-2003-505925 (NMI 3).

	<b>EXPERIMENTAL REPORT</b>  <b>Diffraction by magnetically aligned lamellar aggregates of LHCII</b>	Proposal N° BIO-01-2254 Instrument <b>V1</b> Local Contact Thomas Hauß
	Principal Proposer: Gyözö Garab, Biological Research Center, H-6701 Szeged, Hungary Experimental Team: Gergely Nagy, Instiut Laue-Langevin, BP 156 6, FR-38042, Grenoble Cedex 9, France Thomas Hauß, Hahn-Meitner-Institut, Glienicke Strasse 100, D-14109 Berlin, Germany	Date(s) of Experiment  17/03/2008 – 20/03/2008

Date of Report:

The project aims determining the structural parameters associated with the psi-type CD signals of LHCII, the main light harvesting protein complex of plants. By studying magnetically aligned stacked lamellar aggregates of LHCII we plan to establish correlation between spectroscopic data and structural parameters. These data can then be combined with near-atomic resolution data on LHCII crystals, and will be used in model calculations for partly ordered multilamellar membrane system. Loosely stacked lamellar aggregates also posses the ability to undergo light-induced reversible reorganization with a novel, biological thermo-optic mechanism. We will make attempts to capture these reorganizations.

By using the membrane diffractometer V1 of BENSC, we performed measurements on magnetically aligned tightly stacked lamellar aggregates of LHCII. As shown by polarized fluorescence on the same sample, they can be aligned at 1.2-1.5 T. (The fluorescence polarization ratio was ~1.15, lower than the optimally attainable value, ~1.3, but suitable for measurements.) The samples, suspended in 20 mM Tricine/D2O buffer were filled in a quartz cell of 1 mm optical pathlength. In order to avoid possible problems (encountered last time using horizontal field) with the temperature controller and the gradient inside the sample compartment, we used the VM-5 Warm-bore magnet with vertical field of 2T in a tube exposed to RT. In order to match the preferentially horizontal alignment of the lamellae we had to insert diaphragms in the beam to record the diffraction in the vertical direction. Under these conditions, we were not able to recognize any evidence of the multilamellar order. A closer inspection of the magnet revealed that this might have been partly due to the very small acceptance angle

of the magnet in the vertical direction. In the remaining time, we used a pair of permanent magnets (approx 0.7 T) and an aluminium spacer of 2.2 mm thickness, and collected data using a quartz capillary of 2 mm diameter. Samples were measured with different conditions (preparation, D2O content), but with the settings mentioned above we could find sign of the lamellar order only at one sample (type IV LHCII in 100% D2O). In this case a very weak peak could be observed on a background, which could be fitted well with a power function. The equation

$$I = b + \frac{A}{w * \sqrt{\frac{\pi}{2}}} * e^{-2 * \left(\frac{q-q_0}{w}\right)^2} + Bq^{-p}$$

was fitted for the scattering curve ( $I$  in a.u.,  $q$  in  $\text{\AA}^{-1}$ ). The centre position of the peak was  $0.083\text{\AA}^{-1} \pm 0.004\text{\AA}^{-1}$  which is in accordance with our later measurement (Institut Laue Langevin, D22, 2008.10.13) where we could observe a well defined peak at  $0.083\text{\AA}^{-1}$ . Before further experiments, we plan to perform experiments with SAXS measurements on same and similar LHCII samples.

Acknowledgement:

*This research project has been supported by the European Commission under the 6th Framework Programme through the Key Action: Strengthening the European Research Infrastructures. Contract n°: RII3-CT-2003-505925 (NMI 3).*



**EXPERIMENTAL REPORT**  
**Nanostructure and hydration of  
 phospholipids/lysophospholipids multilamellar  
 membrane**

Proposal N° BIO-01-2255  
 Instrument **V1**  
 Local Contact  
 Thomas Hauß

Principal Proposer: E. Ermakova, Joint Institute for Nuclear Research  
 Experimental Team: M. A. Kiselev, Joint Institute for Nuclear Research  
 S. Dante, HMI  
 T. Hauß, HMI

Date(s) of Experiment  
 14 – 22 May 2008

Date of Report: 10 December 2008

Pure lysophospholipid (lysoMPC) and mixed DMPC/lysoMPC membranes with molar ratio 6/1 and 4/3 were characterized by neutron diffraction.

The neutron diffraction patterns from lysoMPC were recorded at  $T=20^\circ\text{C}$ , RH 57% with contrast variation 8%, 20% and 50%  $\text{D}_2\text{O}$ . Four diffraction orders (fig. 1) allows one to restore the Fourier profiles of neutron scattering length density across the bilayer and to determine the internal structure of the membrane. The signs of structural factors were evaluated as “+”, “+”, “-”, “-”.

Internal structure of the lysoMPC membrane and hydrophobic-hydrophilic boundary ( $X_{\text{HH}}$ ) have been determined from Fourier profile analysis. The repeat distance of the bilayer is 40.2 Å. The membrane thickness is  $d_{\text{m}}=31.9$  Å,  $X_{\text{HH}}=7.9$  Å. The intermembrane water space is  $d_{\text{w}}=8.4$  Å. The thickness of the polar head group region is  $d_{\text{HP}}=7.2$  Å. Phase transition was found between  $25^\circ\text{C}$  and  $30^\circ\text{C}$  at RH 57%.

Two minimum on the Fourier profiles probably reflect interdigitated position of hydrocarbon “tails” in the membrane with pure lysoMPC molecules.

Parameters of the mixed DMPC/lysoMPC membranes were determined as well (Table 1).

Table 1. Internal structure of the mixed DMPC/lysoMPC membrane at  $T=40^\circ\text{C}$  and RH=96 %.

R	d	$d_{\text{m}}$	$d_{\text{w}}$	$d_{\text{PH}}$	$X_{\text{HH}}$
6/1	49.4	39.4	10.0	8.4	14.7
4/3	48.0	38.1	9.9	8.1	11.7
DMPC	49.1	40.0	9.1	7.3	-

R – DMPC/lysoMPC molar ratio, d – repeat distance,  $d_{\text{m}}$  – membrane thickness,  $d_{\text{PH}}$  – thickness of the polar head group region,  $d_{\text{w}}$  – intermembrane water layer,  $X_{\text{HH}}$  – hydrophilic-hydrophobic boundary.

The data for pure DMPC membrane at the same condition are given for comparison in the last line of the table.

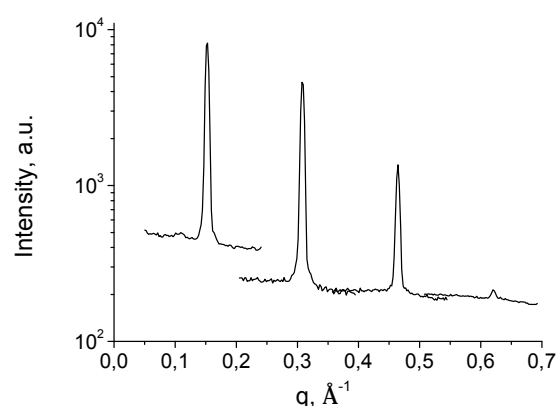


Fig.1 Neutron diffraction pattern from oriented multilamellar membrane of pure lysoMPC at  $T=20^\circ\text{C}$ , RH 57%, 8%  $\text{D}_2\text{O}$ .

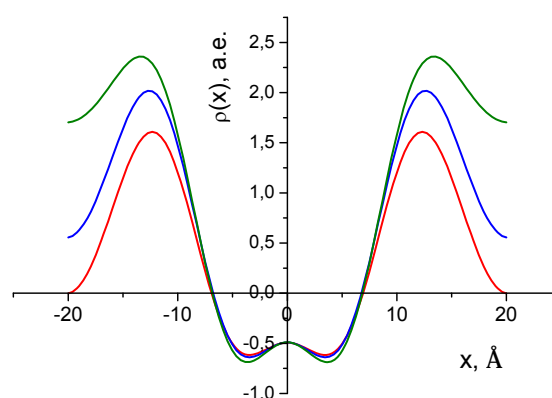


Fig. 2 Fourier profiles of lysoMPC membrane at  $T=20^\circ\text{C}$ , RH 57%, 8% (red), 20% (blue) and 50% (green)  $\text{D}_2\text{O}$ .

Our diffraction experiment demonstrates that lysoMPC molecules create lipid bilayer on the quartz substrate at specified conditions. Thus lysoDMPC has membrane-generating properties at special conditions.

The next step will be study of DMPC/lysoMPC systems in water excess by SANS.

	<b>EXPERIMENTAL REPORT</b>  <b>Amyloid aggregates in lipid membranes</b>	Proposal N° BIO-01-2420 Instrument: <b>V1</b> Local Contact Silvia Dante
	Principal Proposer: Rolando Ranieri, University of Genova Experimental Team: Rolando Ranieri, University of Genova Annalisa Relini, University of Genova Thomas Hauß, HMI Berlin	Date(s) of Experiment 24.11.2008 – 03.12.2008

Date of Report:

Amyloid aggregation is involved in several fatal diseases, such as Alzheimer's disease, Parkinson's disease and systemic amyloidoses. Increasing experimental evidences indicate that protein oligomers rather than mature fibrils are the major responsible of cytotoxic effects.

HypF-N (MW 10452 Da) is the N-terminal domain of a bacterial hydrogenase maturation factor. This protein undergoes amyloid aggregation in the presence of trifluoroethanol (TFE) and its pre-fibrillar aggregates are toxic to cultured cells. Therefore, it represents a useful model to study fibrillogenesis and the interaction of prefibrillar and fibrillar aggregates with cell membranes. The experiment Bio-01-2420 is the continuation of the previous experiment Bio-01-2064 within a project aimed to study the interaction of HypF-N and its amyloid aggregates with phospholipid membrane models. Both the experiments are based on lamellar neutron diffraction measurements carried out at BENSC V1 diffractometer and their final aim is that to reconstruct the structure of the lipid bilayer containing protein aggregates.

In the experiment Bio-01-2064 the measurements have been carried out on POPC/POPS (92:8 mol/mol) supported membranes containing native, oligomeric and fibrillar HypF-N. POPC/POPS liposomes were incubated either with HypF-N in the native state, oligomeric HypF-N obtained after 22 h aggregation or HypF-N mature fibrils obtained after 7 days. After incubation, liposomes were deposited onto quartz slides and dried. Samples were prepared using both non deuterated HypF-N and HypF-N carrying 35 deuterated glycines.

The analysis of the results showed that the structure of the lipid bilayer is strongly affected by the interaction with the protein.

Interesting qualitative information has been obtained, but we were not able to obtain the reflection number necessary to reconstruct the lipid bilayer structure.

In the experiment Bio-01-2420, to obtain reflections of higher orders, we have reduced the protein concentration in the samples by a factor of three and we have decreased the relative humidity to 85%. The samples have been prepared as in the previous experiment. Diffraction measurements have been performed on samples containing native protein and oligomers at three different contrasts (8%, 20%, and 50 % D<sub>2</sub>O) and reflections until the fifth order have been detected. Furthermore, control measurements have been performed on POPC/POPS (92:8 mol/mol). The experiment ended on Dec. 4<sup>th</sup>, 2008 and at present the data are still under analysis.

#### Acknowledgment

This research project has been supported by the European Commission under the 6th Framework Programme through the Key Action: Strengthening the European Research Infrastructures. Contract n°: RII3-CT-2003-505925 (NMI 3).

	<b>EXPERIMENTAL REPORT</b>  <b>Moving towards the understanding of each functional group in proteins</b>	Proposal N° BIO-03-557 Instrument <b>V3</b> Local Contact E. Kemner
	Principal Proposer: Elena Boldyreva, Novosibirsk State University Experimental Team: Heloisa N. Bordallo, HZ Berlin Boris Kolesov Ewout Kemner, HZ Berlin	Date(s) of Experiment 16/02/2008 – 24/02/2008

Date of Report: 15/01/2009

The unique physical characteristic of proteins is that they display flexibility over a large range of time scales, from fs (individual bond vibrations) to ps (small group fluctuations) to ns and longer (collective motions). All these motions are thermally-driven, and temperature is a potential probe for the functional role of these motions. Selective activation of a particular motion in a characteristic temperature interval is of primary importance for the protein flexibility responsible for protein function. Different classes of motions are frozen in different temperature ranges on cooling or at different pressures on squeezing. Different experimental techniques are sensitive to the motions with different relaxation times, and so can selectively detect different types of disorder. This often leads to confusion and seeming discrepancies in the conclusions on the occurrence of a phase transition based on using different experimental techniques. At the same time, this selectivity can be used on purpose, and a complementary study of a system in a wide T/P range with as many experimental techniques as possible, can be helpful to elucidate the nature of the multiple dynamic transitions in these systems.

Dynamic properties of proteins are often studied at simpler model systems – molecular crystals with selected functional groups, which can mimic important functional groups / molecular fragments of biopolymers. Acetamide group belongs to such important molecular fragments. For instance, structure and vibrational studies of *N*-methylacetamide (CH<sub>3</sub>CONHCH<sub>3</sub>, or NMA), a single amide containing methyl groups at both

extremities, has been the subject of a number of experimental and theoretical investigations<sup>1,2,3,4</sup>. Interestingly, most hydrated proteins undergo a dynamic transition in the temperature range of about 200 K–230 K which is related to an increase in the mean-squared displacement  $\langle u^2 \rangle$ , showing a behavior very similar to the one observed in the model NMA system<sup>5</sup>. A step forward is to extend this work to real-life systems in a more systematic way. As examples of more complex molecules, we selected methacetine, phenacetine, paracetamol. It is interesting and important to know, how the dynamics of molecular fragments in the acetamide group in these molecules is related to the packing of molecules in a crystal, the structure and the properties of the hydrogen bond networks.

Using NEAT at HZ Berlin we obtained surprising results that highlight how little is known about the relation dynamical response - polymorphism in paracetamol. This is of some general importance as polymorphism is of paramount importance in pharmacology. We are now processing the results and a publication should be submitted in the very near future.

<sup>1</sup> Eckert, J; Barthès, M. et al.; *J. Phys. Chem. B* **2001**, 105, 19;

<sup>2</sup> Kearley G.J; Johnson et al.; *J. Chem. Phys.* **2001**, 115, 2614;

<sup>3</sup> Mirkin, N.G., Krimmin, S.J.; *J. Mol. Struct.* **1995**, **334**, 3;

<sup>4</sup> Trabelsi, S.; Nasr, S.; Bahri, M.; Bellissent-Funel, M.-C. *J. Phys. Chem. B* **2006**, 110, 25021;

<sup>5</sup> Bordallo, H. N.; Argyriou, D. N.; Barthes, M.; Kalceff, W.; et al. *Phys. Chem. B.* **2007**; 111, 7725;



## EXPERIMENTAL REPORT

### Investigation of the hydration water and internal dynamics of biocompatible and not biocompatible polymer

Proposal N° BIO-03-582

Instrument V3

Local Contact M. Russina

Principal Proposer: D. Russo, ILL+ INFM OGG & CRS-SOFT, F  
Experimental Team: A. De Francesco, ILL+ INFM OGG & CRS-SOFT, F  
D. Russo, ILL+ INFM OGG & CRS-SOFT, F  
M. Russina, Helmholtz-Zentrum Berlin

Date(s) of Experiment

06/12/2008 – 09/12/2008

Date of Report: 15 January 2009

The objective of the present experiment was the investigation of the picosecond dynamical behavior of hydration water and polymer functionalized gold nanoparticles and biopeptides. For this we have been allocated 7+3 days beam time on NEAT spectrometer. Following an unexpected problem during the synthesis of gold nanoparticles and the lost of one day and half of beam time because of the reactor shutdown we decided to invest all the remaining days to study a common topic of the two proposals, i.e. hydration water dynamics on molecules of biological interest. Then we investigated the role of hydration water dynamics in the biocompatibility and non biocompatibility of the polymer itself.

The background of this proposal is then in the biotechnology and medical application field. Although many theoretical and experimental efforts have been devoted to this problem in the last decades, it is not yet clear the mechanism responsible for biocompatibility at a molecular level. Several classes of poly(ethylene glycol) (PEG) based polymers were recently synthesized<sup>1</sup> with a different behavior with respect to the interaction with biological material. Poly(2methoxyethylacrylate) (PMEA) showed excellent biocompatibility with platelets, white blood cells, and proteins<sup>2</sup>. In comparison to similar nonbiocompatible polymers, hydrated PMEA shows a peculiar exothermic peak in the differential scanning calorimetry (DSC) thermograph at around 230K. This peak was assigned by the authors to a particular state of water called freezing bound water, supposed to crystallize at lower temperature due to the interaction with the polymer<sup>1</sup>. Besides PMEA, another very interesting thermo sensitive polymer was recently synthesized whose ability to resist protein and cell adsorption depends on the temperature, poly[2(2ethoxyethoxy)ethyl methacrylate] (PEEA). At T=4°C no cells or proteins adsorb on the surfaces, whereas at 37°C a noticeable adsorption is reported. In order to probe the role of water in biocompatible to non biocompatible polymers we also studied the non biocompatible diblock copolymer poly(MEA2hydroxyethylmethacrylate) (PHEMA). Inelastic neutron scattering is an ideal tool to determine the dynamical properties of water. For liquid water the quasielastic response allows for a clear classification in terms of diffusivity. For solid water the density-of-states distinguishes crystalline from amorphous water and allows for a classification of the solid phases as a function of density. It is thus possible to give an unambiguous picture of the water subsystem even in complex hydrated materials.

All the polymers involved in this study were synthesized and characterized with gel permeation chromatography, H1NMR. Data of adsorption of cells, proteins, and platelets as well as DSC thermographs are already available for all the polymers here investigated.

The experiment was performed on the NEAT spectrometer, whose energy resolution (FWHM=60 eV) was well suited to our needs. We first measured the internal dynamics of PHEMA polymer hydrated in D2O, while data on the other two D2O hydrated polymers were been already collected in previous experiments at ILL. Also, the hydration water was studied by measuring the polymers hydrated with H2O. PMEA, PEEA and PHEMA had an equilibrium water content (EWC) of 5.5%, 20% and 26%, respectively. The samples have been investigated at four distinct temperatures: 200K, 263K, 277K, 310K (corresponding to temperatures before and after the exothermic peaks of bulk and freezing bound water). A scan at 20K has been also collected in order to take account of instrument resolution and to normalize the data. The sample container was an aluminium slab, of internal thickness of 0.2 mm, oriented at 135° with respect to the incident beam. By combining the data obtained with deuterated and hydrogenated water we will obtain new information on the contribution of the polymer and solvent dynamics. In Figure 1, the scattered intensities of PEEA and PHEMA hydrated with H2O are shown at different temperatures. A stronger temperature dependence is visible for the PEEA. The analysis of data is still in progress given that the experiment has been performed from 5 December to 16 December

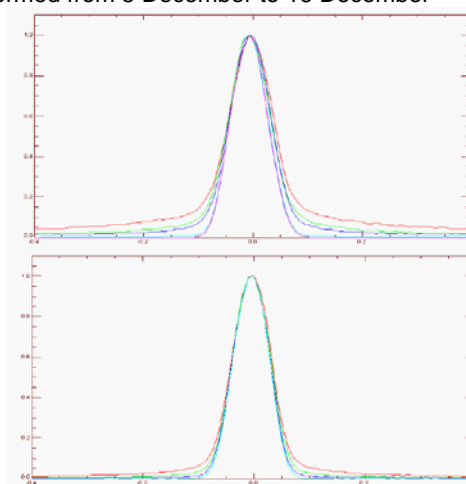


**Figure 1.** Scattered intensities vs energy transfer at scattering angle of 82deg at different temperatures. Pink, 20K (only PEEA); Cyan, 200K; Blue, 263K; Green, 277K; Red, 310K. Top: hydrated PEEA; Bottom: Hydrated PHEMA.

- 1 M. Tanaka, A. Mochizuki, *Journal of Biomedical Materials Research Part A* (2003) 64A,4,684
- 2 M. Tanaka, A. Mochizuki, N. Ishii, T. Motomura, T. Hatakeyama, *Biomacromolecules* (2002) 3, 364



**EXPERIMENTAL REPORT**  
**Concentration fluctuations and microdomain formation in lipid membranes**

Proposal N°  
 CHE-04-1635-EF  
 Instrument **V4**  
 Local Contact  
 Karsten Vogtt

Principal Proposer: Roland Winter, TU Dortmund  
 Klaus Czeslik, TU Dortmund  
 Karsten Vogtt, Hahn-Meitner-Institut Berlin  
 Experimental Team: Karsten Vogtt, Hahn-Meitner-Institut Berlin  
 Christoph Jeworrek, TU Dortmund

Date(s) of Experiment  
 11/02/2008 – 14/02/2008

Date of Report: 10/03/2008

Microdomain forming lipid mixtures, so called “raft-mixtures”, have been in the focus of recent research because of their relevance e.g. in cell trafficking and signalling. Here, multilamellar vesicles, consisting of a mixture of dioleoylphosphatidylcholin (DOPC), deuterated dipalmitoylphosphatidylcholin (DPPC-d62) and cholesterol in a ratio of 45:27:28, have been investigated as a model system in the temperature range between 5 and 48 °C. The solvent was chosen to match the average scattering length density of the lipids at 20 °C (64.5 % H<sub>2</sub>O, 35.5 % D<sub>2</sub>O) in order to probe for structural inhomogenities in the lipid bilayers.

A first data analysis exhibits a Bragg-peak at about 0.5 nm<sup>-1</sup> at low temperatures (see Fig. 1), corresponding to a distance  $d$  of about 13 nm. A small second order peak can be determined around 0.9 nm<sup>-1</sup>. With increasing temperature the former Bragg-peak disappears, presumably due to the transition from a homogenous phase into the Ld-Lo-coexistence region. Interestingly, the small second order peak prevails even at higher temperatures, suggesting persistence of residual order at lower length scale.

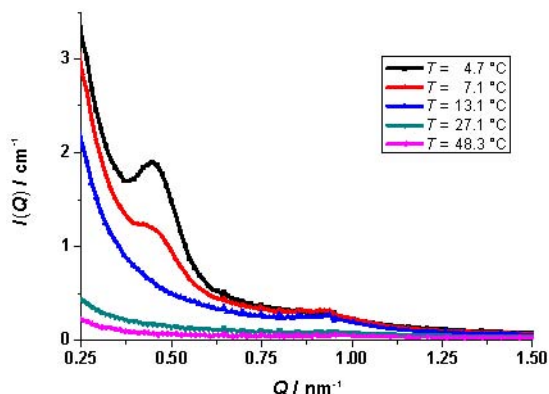


**Fig. 1:** SANS intensities of a DOPC:DPPC-d62:cholesterol (45:27:28) mixture at different temperatures  $T$ .

The fractal dimensionality  $D$  was determined by applying a linear fit to the double-logarithmic plot of the intensities  $I$  versus the momentum

transfer  $Q$  at low values.  $D$  changes slightly between 5 and 20 °C, achieving a maximum value between 9 and 11 °C

(see Fig. 2) indicating fluctuations in the lateral structure of the system.

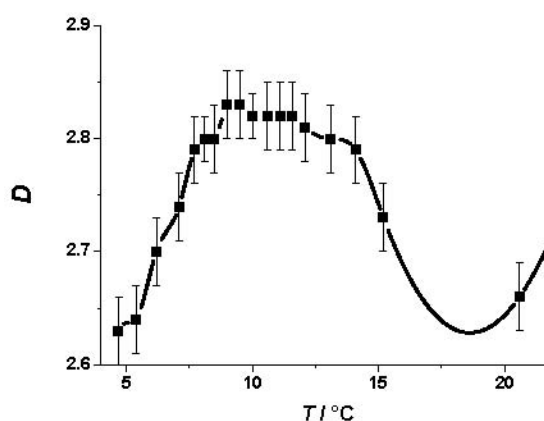


**Fig. 2:** Dimensionality  $D$  as function of temperature  $T$ , terminated from the double logarithmic plot of scattered intensity at low  $Q$ -values between 0.04 and 0.1 nm<sup>-1</sup>.

The data reveals the presence of lateral structural inhomogeneity in the examined temperature range. Long range order decreases with increasing temperature, while short range order prevails to some extent. These findings coincide with the concept of microdomain formation under the observed experimental conditions, suggesting the examined ternary mixture as a suitable model system for further studies on microdomain formation.



## EXPERIMENTAL REPORT

### Influence of Temperature and Co-solvents on the Large Scale Structure of $\beta$ -Lactoglobulin

Proposal N°  
BIO-04-1710-EF

Instrument **V4**

Local Contact  
Karsten Vogtt

Principal Proposer: Marie-Claire Bellissent-Funel, Helmholtz-Zentrum Berlin  
Experimental Team: Marie-Claire Bellissent-Funel, Helmholtz-Zentrum Berlin  
Karsten Vogtt, Helmholtz-Zentrum Berlin

Date(s) of Experiment

03/08/2008 – 08/08/2008

Date of Report: 10/11/2008

$\beta$ -Lactoglobulin, the main protein in whey, exhibits a complex structural behaviour. Depending on pH and temperature it forms monomers, dimers and higher oligomers. At high temperatures aggregation occurs, leading to large clustered objects or gel formation, depending on concentration, pH and ionic strength of the solution. In order to understand the relationship between structure and dynamics, SANS-measurements were undertaken to complete results from time-of-flight experiments (carried out on NEAT instrument at BENSC).

The SANS intensities of  $\beta$ -Lactoglobulin solutions (5, 10 and 20 mg/ml, pD 7.4) were determined at different temperatures (25, 41, 51, 56, 61, 66, 70, 75 and 81 °C). For the concentrations  $C = 5$  mg/ml and 10 mg/ml at room temperature, the data can be fitted well representing the structure of the dimeric protein using a form factor for two attached spheres with  $R_1 = R_2 = 1.72$  nm (see Fig. 1). A structure factor of Hayter-Penfold type accounts well for the interactions. With increasing temperature, SANS intensities decrease at low  $Q$ -values, owing to the dissociation of Lactoglobulin into monomers. This behaviour could be modelled treating the monomers as spheres with a radius  $R = 1.72$  nm. At  $\sim 75$  °C aggregation sets in, leading to polydisperse clusters at higher temperatures. At the initial step of aggregation (75 °C) and low concentrations (5 and 10 mg/ml), Lactoglobulin forms dimers and, presumably, tetramers. Latter ones can be fitted well with a form factor for a cylinder and exhibit a higher partial specific volume than the dimers (see Fig. 2). The size of cylinders, however, differ for the two different concentrations. The tetramers seem to be formed by the monomers, since within the accuracy of the experiment no monomeric fraction could be detected at 75 °C, although between 66 and 70 °C about one third of the dimers are dissociated.

The results obtained allow interpretation of the time-of-flight data in the protein preaggregated regime. For the data in the aggregated regime, further refinement of the applied model is necessary.

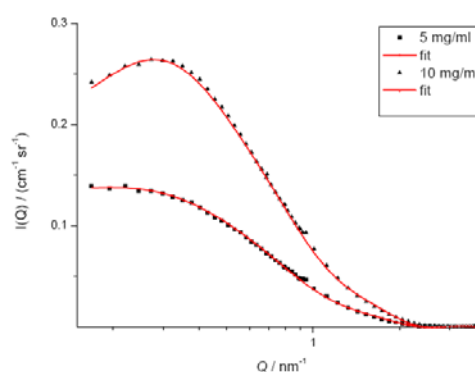


**Fig. 1:** SANS-intensities of Lactoglobulin solutions (5 and 10 mg/ml) at room temperature.

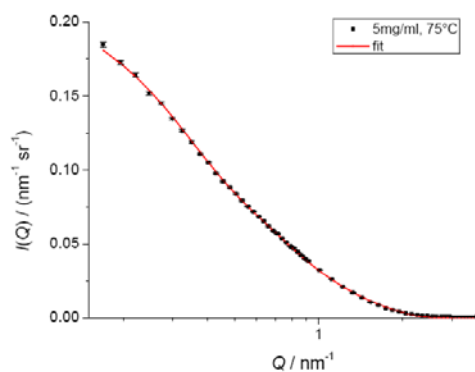


**Fig. 2:** Lactoglobulin in the preaggregated regime at 75 °C (5 mg/ml). The fit models the coexistence of dimers and cylindrical oligomers.

	<b>EXPERIMENTAL REPORT</b> <b>Contrast Matched SANS on Small Unilamellar Vesicles: The Lateral Distribution of Lipid Rafts</b>	Proposal N° BIO-04-1711-EF Instrument <b>V4</b> Local Contact Karsten Vogtt
	Principal Proposer: Karsten Vogtt, Helmholtz-Zentrum Berlin Experimental Team: Karsten Vogtt, Helmholtz-Zentrum Berlin Christoph Jeworrek, TU Dortmund	Date(s) of Experiment 08/08/2008 – 10/08/2008

Date of Report: 07/10/2008

Lipid mixtures, consisting of a lipid with high melting point and one with a low melting point, exhibit a complex phase behaviour in presence of cholesterol. One interesting feature is the presence of two liquid phases. Since lipids form structures like uni- or multilamellar vesicles in excess water, one central question addresses the spatial distribution of these phases. Especially size and location of the liquid phases on a unilamellar vesicle are of high interest, because these structures play a crucial role in biological processes like e.g. the emission of neurotransmitters in the synaptic cleft. Since vesicular lipid structures exhibit a high plasticity in biological systems, the question, whether their complex phase behaviour is linked with their biologic functional diversity, is a central question addressed to lipid science. Small, unilamellar vesicles consisting of DOPC, DPPC and cholesterol (45:27:28) were prepared. This mixture was shown to exhibit inhomogeneous spatial phase separation in a previous experiment (see: CHE-04-1635-EF). The solvent was a mixture of water and deuterium oxide, selected to match the average scattering length density of the vesicles. Under these conditions, the scattering contrast is zero, if the lipids are in a single phase, while it deviates from zero, if the lipids become unevenly distributed between different phases. Small unilamellar vesicles with a diameter of  $\sim 40$  nm were successfully prepared, with the extrusion method (see Fig. 1). SANS intensities were determined for matched unilamellar vesicles at different temperatures (Fig. 2). The intensity, but also the shape of the form factor changes with increasing temperature, suggesting changes in the distribution of lipids, but likewise in the spatial arrangement of the phases in the unilamellar vesicle. Further analysis will give a more detailed picture about the distribution of the liquid phases.

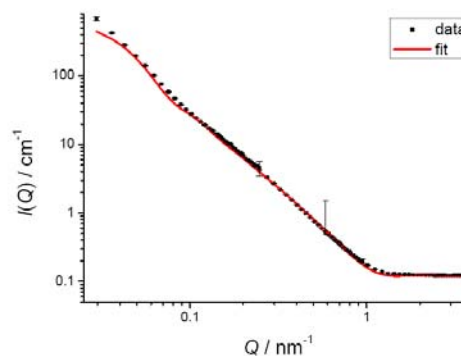


Fig. 1: SANS-intensity of unmatched unilamellar vesicles (black dots) and fit (red line) at 10.3 °C.

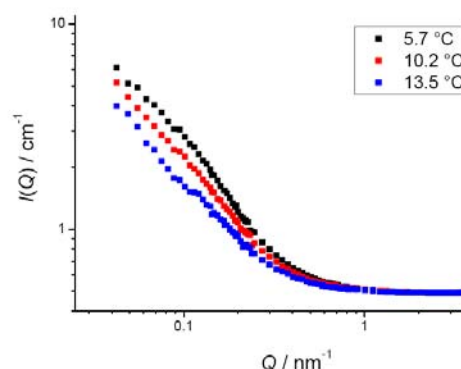


Fig. 2: SANS-intensity of matched unilamellar vesicles at different temperatures.

	<b>EXPERIMENTAL REPORT</b> <b>3-dimensional water flow imaging using cold neutron CT and D2O tracer – Studies on rose bent-neck</b>	Proposal N° BIO-04-1498 Instrument V7 Local Contact Nikolay Kardjilov
	Principal Proposer: Uzuki Matsushima, Iwate University Experimental Team: Wolfgang Graf, Humboldt-Universität zu Berlin Nikolay Kardjilov, HZB Werner B. Herppich, ATB	Date(s) of Experiment 02/06/2008 – 08/06/2008 08/11/2008 – 16/11/2008

Date of Report:

### Introduction:

The bent-neck syndrome is a widespread problem damaging millions of cut roses. The 3D water flow image will help to understand various problems related to drought stress of plant, such as bent-neck syndrome. Using cold neutron radiography and tomography with D<sub>2</sub>O tracer, water flow and structural characteristic of three cut roses (*Rosa Hybr.*) varieties were investigated to analyze bent-neck resistances.

### Materials and methods:

The cultivars 'Akito', 'Milva' and 'Red Giant', respectively, have low, middle and high bent-neck resistances. The non-destructive visualization methods cold neutron radiography (CNR) and tomography (CNCT) were used to observe in-situ water transport and structure of sample peduncles. D<sub>2</sub>O and H<sub>2</sub>O tracer were used to visualize water flow. Due to the different attenuation coefficients of D<sub>2</sub>O and H<sub>2</sub>O for cold neutrons, these two liquids can be clearly distinguished in the radiography. The experiments were performed at HZB's neutron tomography instrument CONRAD.

### Results and discussion:

From observing the D<sub>2</sub>O level in the stem at different times after the exchange, it was possible to deduce the vector of water uptake and water transport in the roses using the optical flow algorithm block matching. Figure 1 shows vector images of roses of each cultivar calculated by block matching. Water uptake of Milva was the fastest and that of Akito was the second. It was expected that the better water conductance system of Milva would improve bent-neck resistance. However, water flow of the largely bent-neck resistant Red Giant roses was the slowest.

Figure 2 shows vertical and horizontal CNCT slices of rose peduncles. Structural differences were already observed before drought stress, when only the peduncles of Akito and Milva were fully filled with water. On the other hand, intercellular space of Red Giant peduncle pith tissue was largely air filled. This indicated the

Red Giant peduncle was more mature than peduncles of Akito and Milva. Because of late the state of maturation, epidermal and xylem structures of Red Giant should be stronger than those of Akito and Milva. After drought stress, Akito and Milva lost more water through the surface due to their immature epidermis. Red Giant should be more resistant against dehydration because of the well developed plant structure, e.g. a thick cuticle was expected. Because plants of this cultivar could effectively retain water, their water uptake was lower. Also, the cylindrical structure of the peduncle was strong against bending pressure. Consequently, neutron radiography provides reliable information on the structure and the water transport processes in plants.

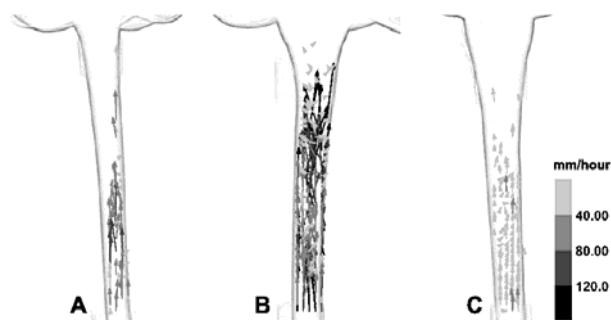


Figure 1: Vector images of water flow in peduncles of 3 rose varieties. A: Akito, B: Milva, C: Red Giant

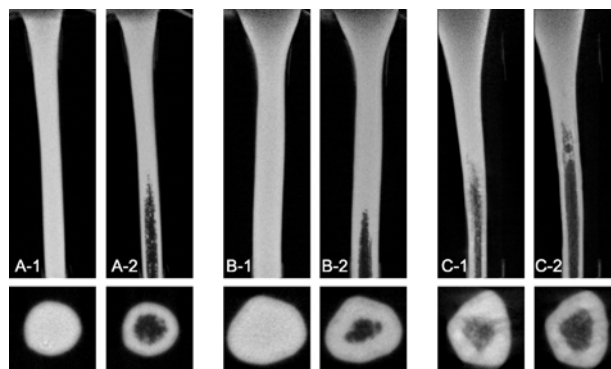
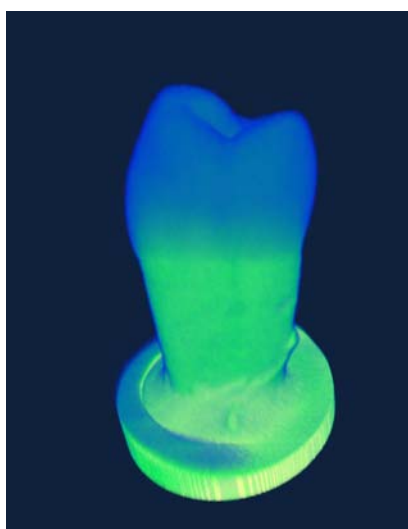


Figure 2: Vertical and horizontal CNCT slices of rose peduncles before and after drought stress. A: Akito, B: Milva, C: Red Giant The digits, 1 and 2, after capital letters indicate images before and after drought stress, respectively.

	<b>EXPERIMENTAL REPORT</b>  <b>Neutron tomography of wet teeth</b>	Proposal N° BIO-04-1533-EF  Instrument <b>V7</b>  Local Contact Nikolay Kardjilov
	Principal Proposer: Paul Zaslansky, Max-Planck Institute of Colloids and Interfaces, Golm, Potsdam Experimental Team: Nikolay Kardjilov - HMI	Date(s) of Experiment  03/12/2007 – 10/12/2007

Date of Report: January 2009

Experimental Report: Following our proposed plan, three whole wet teeth (previously stored in H<sub>2</sub>O) were immersed in-situ in D<sub>2</sub>O and tomographic series were obtained and later reconstructed (figure 1: typical 3D tooth reconstruction).



**Fig. 1**

We used an attenuation setup (no phase enhancements, distance of 25 mm between sample and imaging screen) and optimized the imaging conditions so as to be able to collect repeated measurements within the allocated beam shifts (8 sec radiography exposures, moderate resolution 200 μm thick scintillation screen). We attempted to follow the differences of scattering within the tooth regions as seen following immersion in D<sub>2</sub>O, and found that impressive changes in attenuation arose during the course of the experiment. Measurements were therefore adapted for continuous image acquisition, so as to try and follow the temporal changes occurring in the incoherent scattering images. Monte Carlo simulations (HMI) and comparison with the NIST standard attenuation cross-section calculator revealed that almost all of the attenuation in these particular samples (teeth) is due to incoherent scattering on account of neutron interactions with the hydrogen within the microstructure: Hydrogen is found in water or embedded in the protein/mineral. Hence, contributions due to the main atomic species

comprising the tooth tissues (Ca, O, N, C or P) were further neglected. Consequently we ended up with hydrogen distribution images in teeth, at different times following immersion. Due to the high sensitivity of the V7 setup, small differences in attenuation were seen and followed. This was particularly impressive in enamel, known to be highly mineralized on the outer side of the tooth containing a very low water/protein content (<5%). Enamel became transparent quite uniformly, attesting to a high permeability to water/D<sub>2</sub>O. Our experiments involved the use of whole and intact teeth. Consequently, of great concern for interpretation of our results is the rate of diffusion and exchange of hydrogen from within the microstructure. As seen in slices across the reconstructions (reproduced in figure 2), different levels of detail may be seen in the dentin at different times (near the pulp as compared to the outer rime: 1 and 5 hours rep.)

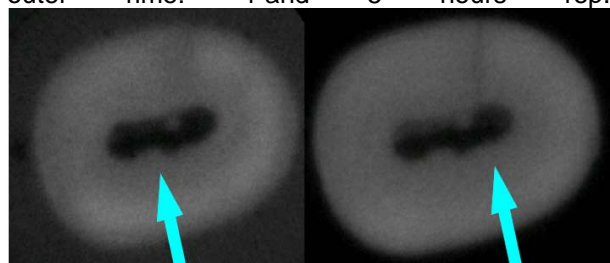


**Fig. 2**

The fact that both the absolute attenuations as well as the relative intensities vary over time raises questions as to what exactly we are observing: is this due to diffusion? Are we observing structural features, or dynamics of hydrogen exchange? These findings have highlighted the need to proceed with longer immersion measurements, to better understand the dynamics of deuteration in teeth. For this we had proposed new and longer series of measurements, that were granted to us as part of an extension allocation beamtime: BIO 04-1587.



## EXPERIMENTAL REPORT

### In-situ observation of pressure induced phase changes in cellular food materials

Proposal N° BIO-04-1586

Instrument V7

Local Contact  
Nikolay Kardjilov

Principal Proposer: Oliver Schlüter, (ATB)  
Experimental Team: Oliver Schlüter, (ATB)  
Stephan Boguslawski, (TUB)  
Nikolay Kardjilov, (HZB)

Date(s) of Experiment

14/12/2008 – 18/12/2008

Date of Report: January 2009

### Background

The application potential of cold neutron radiography was evaluated as measurement technique for the determination of pressure induced volume changes in food systems.

### Materials and Methods

High pressure experiments were performed at room temperature without temperature control using a single vessel system connected to a pressure generator (Fig. 1).

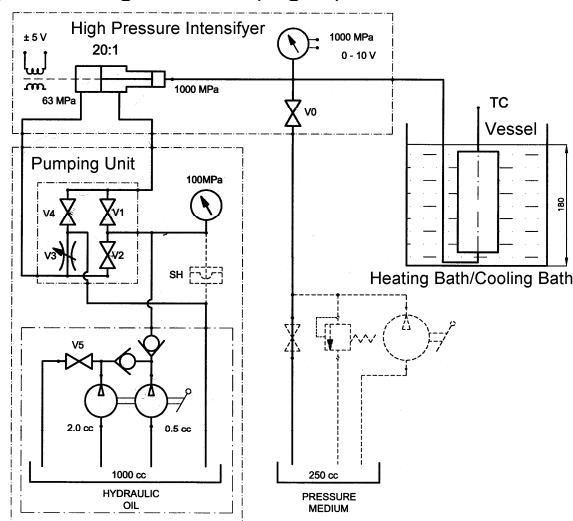


Figure 1: The schematic diagram of the high pressure apparatus.

In various experiments different food samples were inserted into the sample container with floating piston (Fig. 2). After closing the vessel stepwise pressurization (10, 50, 100, 150, 200, 250, 300, 350, 400 MPa) was performed and the pressure dependent piston movement was determined when the sample temperature reached the chamber temperature of about 25 °C. Cold neutron radiography (CNR) was conducted at V7, HMI. During the experiments, CNR images were taken every 15 seconds with an exposure time of 10 seconds.

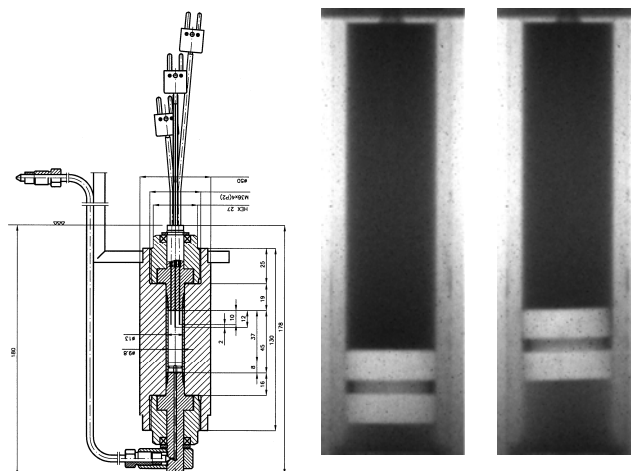


Figure 2: Sectional view of the high pressure vessel containing the upper plug with three thermocouples and a sample container with floating piston (left). Image of the piston position at 10 MPa (middle) and piston position at 400 MPa (right) using de-ionized water as reference sample.

### Results and Discussion

Using D<sub>2</sub>O as pressure transmitting medium, different liquid and multi-phase food samples (water, olive oil, cream, freeze-dried potato sample) was subjected to different pressure levels at room temperature. The kinetic of volume changes due to specific compressibilities was investigated by image analyzing procedures (Fig. 2). Liquid-gaseous phase changes were clearly identified at room temperature and the behaviour of air bubbles under high hydrostatic pressure was visualized. Determining the velocity of water flow would help to identify the different processes and mechanisms leading to an increased resistance to rehydration under high hydrostatic pressure. Design and construction of specific temperature control unit is required to detect determine pressure induced liquid-solid phase changes of water.

	<b>EXPERIMENTAL REPORT</b> <b>Role of water in human teeth: neutron tomography of in-situ dehydration and rehydration</b>	Proposal N° BIO-04-1587 Instrument V7 Local Contact Nikolay Kardjilov
	Principal Proposer: Paul Zaslansky, Max-Planck Institute of Colloids and Interfaces, Golm, Potsdam Experimental Team: Nikolay Kardjilov, André Hilger - HMI	Date(s) of Experiment 03/03/2008 – 07/03/2008 29/04/2008 – 03/05/2008

Date of Report: January 2009

Both enamel and dentin in teeth contain substantial amounts of water (~2 and 12 wt%, respectively), some of it 'free'. More than 50% of this water may be removed at low temperatures below 100 °C. Presumably water easily flows through channels in the tooth tissues, specifically through dentin known to contain many unidirectional tubules, radiating outwards from the pulp. The tubules thus entail porosity to the dentin bulk. The subtle differences in the distribution of water in the tooth is not well understood.. In our experiments in the CONRAD imaging setup on V7, we aimed on quantification of the hydrogen content in the tooth 3D structure, based on the experience gained from preliminary experiments BIO-04-1410 and specifically BIO-0401533-EF. For this purpose, we created baseline measurements of tooth hydrogen content, by creating tomograms of teeth where much of the available  $H^+$  was removed/exchanged through long (14 day) immersions in D2O and repeated exchanges of the immersion liquid every 48-72 hours. In this manner, the teeth were effectively kept wet, so as to prevent any structural damage. Our aim was to quantify the density of  $H^+$  per  $nm^3$ . We achieved this by normalization with the attenuation obtained from tomograms of pure water (imaged at different calibration distances and tested for minimization of scattering effects while maximizing object detail). To this end, and using standard reconstruction methods (Octopus V 8 suite, Ghent university) we were able to derive an effective attenuation value of  $5.12 \text{ cm}^{-1}$  for tap water. With an approximate density of  $1 \text{ gr/cc}$ , water has  $66 \text{ H}^+$  per  $nm^3$ . This was used as calibration (partially accounting for scattering effects that change the overall intensity of the radiographs of teeth) and high sensitivity maps of the density of  $H^+$  per  $nm^3$  were produced.

(Figure 1 *left*:  $H^+$  density map in a vertical slice through a reconstruction of a tooth, following immersion in D2O; *right*: similar  $H^+$  density map following tap water immersion: color coding and bar indicate density of  $H^+$  throughout the 3D structure).

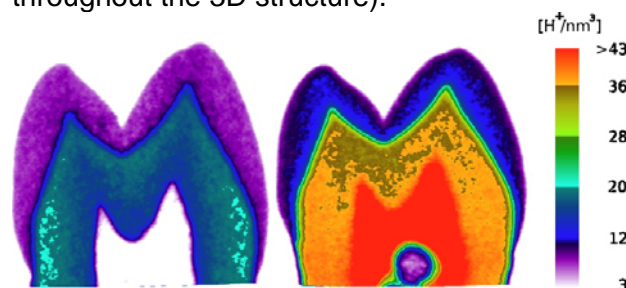


**Fig. 1** *left*: D2O tooth, *right*: Water tooth: red zone the water-filled pulp, that contains an air bubble seen on the lower part of the cavity.

Our data suggest that: a) Much water can be removed from enamel (outer top layer) and dentin (lower bulk of tooth) by  $H^+$  exchange in whole teeth. b) The low amounts of  $H^+$  in enamel in wet teeth, seen when compared to dentin or pure water, are very significant relative to those seen in the D2O exchanged tooth. Enamel is very permeable, and does not prevent water flow from reaching dentin.. c) A clear line demarcates the junction between enamel and dentin: Much  $H^+$  remains here following D2O exchange, although most of the  $H^+$  is removed. d) Significant gradients in the  $H^+$  content in dentin become visible. Such gradients do not exist in the wet state. Near enamel higher  $H^+$  levels are seen, representing areas where exchange is restricted, possibly due to higher protein content. Overall, between 20 and 32 % of the hydrogen signal may be removed, thus: much water flows through bulk dentin.

	<b>EXPERIMENTAL REPORT</b> <b>Kinetics of hemolysis of red blood cells <math>\alpha</math>-hemolysin studied by very small angle neutron scattering</b>	Proposal N° BIO-04-1581 Instrument <b>V12a</b> Local Contact Peter Walter
	Principal Proposer: Chris Garvey, ANSTO, Australia Experimental Team: Philip Kuchel, University of Sydney, Australia Peter Walter, BENSC Markus Strobl, BESNC Chris Garvey, ANSTO	Date(s) of Experiment 13/03/2008 – 20/03/2008

Date of Report: 26/01/2008

## Aim

The bacterial toxin  $\alpha$ -hemolysin is a heptameric membrane penetrating pore. The toxin is secreted as a monomer by bacteria (molecular weight of 33 kDa), and it self-assembles into a heptameric complex (~234 kDa) within the RBC membrane, creating a pore ~10 nm long, with a diameter ranging from 1.4-4.6 nm (Figure 1). The pore allows free passage of small solutes allowing a redistribution of cations, low molecular weight solutes, and intracellular proteins, and it results in osmotic stress and ultimately haemolysis. Our work here aims to understand how the protein allows the leakage of haemoglobin from the red blood cell which a globular protein 6.4 nm in diameter. Kinetic measurements of hemolysis with VSANS will give an insight into this problem.

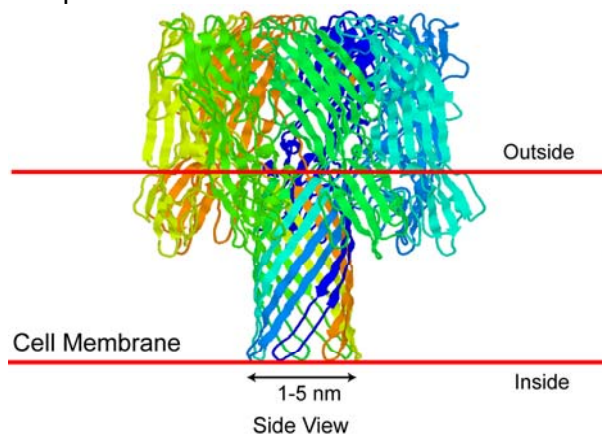


**Fig 1** Dimensions and membrane orientation of the heptameric  $\alpha$ -hemolysin pore

We have demonstrated the time resolved capacity of the linear detector of the V12a instrument to study the shape changes and lysis of actively metabolising red blood cells depleting their energy source, glucose. We have also shown it is possible to use V12a to study the kinetics of haemolysis of red blood cells by the pore forming bacterial toxin  $\alpha$ -haemolysin since the leakage of protein from

the cytoplasm to the extra-cellular solution leads to a loss of neutron scattering contrast. Previous beam time allowed us to optimise the experiment. Here we proposed to complete these measurements.

## Results

Kinetic VSANS measurements were made on the newly installed area detector of V12a on suspensions of red blood cells in 154 mM saline in  $D_2O$ . The sensitivity of this system allowed us to gather scattering curves with good statistics in 20 minutes. By contrast to previous experiments where a cell volume fraction of 60% was used, measurements were made at 70% and the problems of cell sedimentation were avoided.

The integral scattered intensity is used as a qualitative measurement of cell lysis. Contrast is due to haemoglobin concentration difference between the cell cytoplasm and the extracellular solution. In this way we can produce the familiar lysis curves which can be found by other methods in dilute suspensions but in concentrated cell suspensions which better approximate conditions in the blood stream, ~50% cell volume fraction. We have produced lysis curves for a range of  $\alpha$ -haemolysin concentrations. We find that for the lower concentrations of  $\alpha$ -haemolysin that total lysis does not occur.

## Conclusions

1. The kinetics of red blood cell lysis by the bacterial toxin  $\alpha$ -haemolysin in concentrated suspensions may be followed using very small angle neutron scattering.
2. There is no exchange of  $\alpha$ -haemolysin heptamers between red blood cells.



## EXPERIMENTAL REPORT

### Structure and Dynamics of Mesoporous Materials

Proposal N° PHY-01-2250

Instrument **V1**

Local Contact  
Thomas Hauß

Principal Proposer:

Beate Klösgen, Inst. F. Physics and Chemistry & MEMPHYS, Southern University of Denmark, DK

Experimental Team:

Nina Viola Reichhardt, Physical Chemistry 1, Lund University, Lund  
Anna Carnerup, Physical Chemistry 1, Lund University, Lund  
Thomas Hauß, Hahn-Meitner-Institute, Berlin

Date(s) of Experiment

23/05/2008 – 28/05/2008

Date of Report: 02/10/2008

The experiment done is embedded in a project on the control of diffusion by means of reversibly expanding polymers with a lower critical solution temperature (LCST) grafted onto the inner surface of pores in channels of mesoporous silica. The silica material used was two-dimensional hexagonal SBA-15 (pore size: 6 nm). Poly-N-isopropylacrylamide (PNIPAAm) was grafted by Atomic Transfer Radical Polymerization.

Aim of the neutron diffraction experiments was to acquire data on the polymer decoration structure in the mesoporous silica systems and to follow the conformational change of the polymer around the LCST.

The first experiments carried out yielded the matching point of the silica material by using D<sub>2</sub>O:H<sub>2</sub>O mixtures varying the molar ratios. The silica matching point was determined to be around 77.39% (by weight) D<sub>2</sub>O in H<sub>2</sub>O. The diffraction pattern of the silica at this condition still produced a small peak at  $q=0.07 \text{ \AA}^{-1}$  indicating that this D<sub>2</sub>O:H<sub>2</sub>O mixture is not the exact matching point of the material. It was still decided to use it for the further experiments.

The next step was the measurement of the silica material with grafted PNIPAAm.

The experiments were done at different temperatures, 25 °C, 35 °C and 45 °C.

Figure 1 shows the preliminary results, all measured at the obtained silica matching point, for silica, silica with polymerization anchor and silica with grafted PNIPAAm polymer at different temperatures.

The first data comparison showed an intensity difference between the pure silica sample at matching point and the silica with grafted PNIPAAm sample. This was taken as a confirmation that the PNIPAAm was successfully grafted and structurally follows the silica matrix which is hexagonally arranged. Furthermore it was observed that the temperature increase led to a decrease of intensity. This was taken as an

indication of the temperature induced change of polymer conformation.

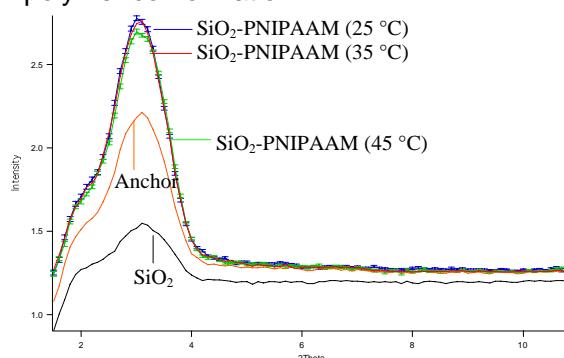


Fig. 1: Small angle diffraction data obtained on the different states of the silica system at silica matching point condition. Details see insert.

Earlier results (Jianming Zhang, *Soft Matter*, 4 (2008), 500-509) yielded a different matching point than the one determined during these experiments. Moreover, the scattering intensity at our experimentally determined matching point was too high.

A closer look exhibited the experimentally determined matching point was not correct, as a result of the sample preparation. In the experiment, silica was measured first in 100 % D<sub>2</sub>O. Thereafter portions of D<sub>2</sub>O were removed subsequently from the sample and filled up with H<sub>2</sub>O, mixed as much as could be done, and then measured. This process led to a different matching point mixture than expected. Apparently the exchange of D<sub>2</sub>O and H<sub>2</sub>O is very slow. With D<sub>2</sub>O as a start solvent, some of the surface attached hydroxyl groups of the silica get deuterated. This gives rise to an increased D<sub>2</sub>O:H<sub>2</sub>O ratio inside the pores as compared to the outside solvent composition.

The exchange of D<sub>2</sub>O against H<sub>2</sub>O is currently under investigation in further experiments, e.g. NMR experiments and TOF-TOF.

*This research project has been supported by the European Commission under the 6<sup>th</sup> Framework Programme through the Key Action: Strengthening the European Research Infrastructures.*

*Contract n°: RII3-CT-2003-505925 (NMI 3).*



## EXPERIMENTAL REPORT

### Characterization of mixed fluorocarbon and hydrocarbon surfactant crystals

Proposal N° CHE-01-2412

Instrument **V1**

Local Contact  
Thomas Hauss

Principal Proposer: Sylvain Prevost  
Experimental Team: Michael Gradzielski  
Katharina Bressel  
Sylvain Prevost

Date(s) of Experiment

07/07/2008 – 13/07/2008

Date of Report: 08/01/2009

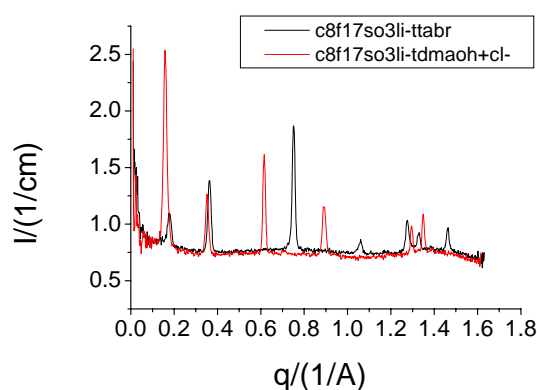
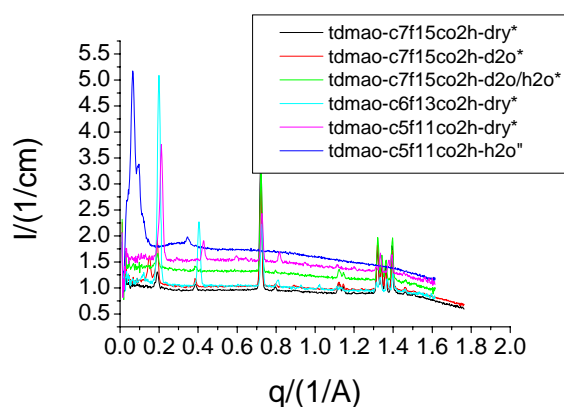
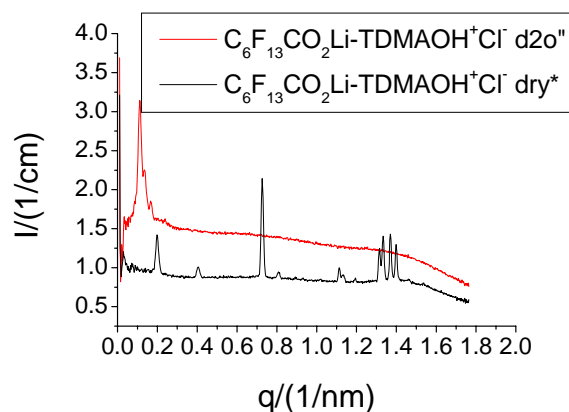
Precipitates of mixed anionic fluorocarbon and nonionic or cationic hydrocarbon surfactants were investigated with neutron diffraction on the V1 instrument at the Helmholtz-Zentrum. Our special interest was in the co-crystallisation of hydrocarbon and perfluorinated chains.

In our experiment we varied the chain length of the perfluorinated surfactant and the head group of the surfactants. Due to the high scattering contrast between hydrocarbon and fluorocarbon chains neutron diffraction should provide a lot of structure information.

All samples were prepared from mixtures of stock solutions of the surfactants. The precipitates were either examined without freeze drying (marked with ") or freeze dried (samples marked with \*) and some of the dry samples were wetted with D2O or a mixture of H2O and D2O (3,34:6,66).

The freeze-dried samples and the non-freeze-dried samples show completely different diffraction patterns. The freeze-dried samples show some singular sharp peaks in a q-range that may correspond to a length scale of the surfactant chain length and a triplet or quartet in a length scale of the distance of two head groups. These information indicate, that the crystals may have a layer-by-layer structure.

The diffraction patterns of the non-freeze-dried samples show only a broad peak or several broad peaks at low q. That means that the structures must be much larger than in the freeze-dried samples and may be the swollen form of the layer-by-layer crystalls.





## EXPERIMENTAL REPORT

### Structural anomalies in strongly supercooled confined water

Proposal N° PHY-01-2418

Instrument V1

Local Contact T. Hauss

Principal Proposer: O. Paris – MPI Golm (Abt. Biomaterialien)  
Experimental Team: M. Erko - MPI Golm (Abt. Biomaterialien)  
D. Wallacher – HZB (BENSC)  
T. Hauss – HZB (BENSC)

Date(s) of Experiment

03.11.2008 - 07.11.2008

Date of Report: 13.01.2009

The structure and dynamics of supercooled liquid water and of amorphous ice is a very active area of current research [1, 2]. In particular, there is recent theoretical [3] and experimental [4, 5] evidence for the existence of a liquid-liquid phase transition separating two water modifications of low density (LDL) and high density (HDL) liquid. Even though the coexistence line does not extend to ambient pressure, there should be a discontinuous change of thermodynamic parameters when crossing the extension of the coexistence line into the one-phase region (the so called "Widom line") [3]. Unfortunately, for bulk water the corresponding temperature region is not accessible experimentally due to the fact that water can not be supercooled into the relevant region due to homogeneous nucleation of ice. However, when confining water within narrow pores, the supercooling region is considerably extended and liquid water may be observed down to at least 150 K [5,6].

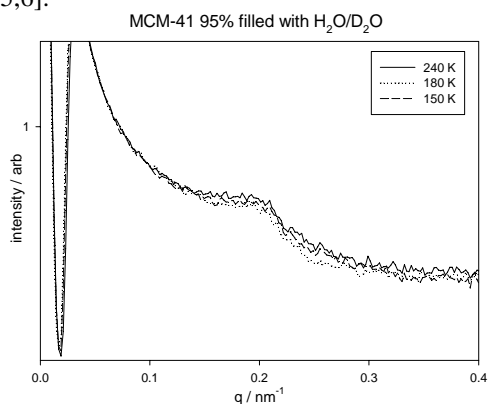


Fig. 1: SANS pattern of the 95 percent filled MCM-41 pore matrix at different temperatures.

Using the DEGAS system at the BENSC instrument V1 we have carefully filled the pores of an MCM-41 specimen via the vapour phase with a 0.6 D<sub>2</sub>O / 0.4 H<sub>2</sub>O mixture to match the silica matrix at room temperature. This has the advantage that the Bragg peaks from the pore lattice of MCM-41 at room temperature could be strongly reduced. The filling factor  $f$  was 0.95 to avoid ice nucleation outside the pores. The pore diameter of the specimen was 2.58 nm (NLDFT method), and it was shown recently that water does not freeze in this sample [6]. The change of the SANS intensity was measured while lowering the temperature from room temperature down to 150 K, providing information about mesostructural and/or density change of the confined water-mixture. The region at large scattering angles ( $14.7 \text{ nm}^{-1} - 19.6 \text{ nm}^{-1}$ ) was also measured for each temperature

step to obtain changes of the molecular water ordering, and in particular to monitor possible freezing of water at a given temperature.

The experimental SANS profiles show a weak peak at  $q \approx 0.2 \text{ nm}^{-1}$  which corresponds to the 95 percent matched (10) Bragg peak of the hexagonal ordered pores in the MCM-41 silica matrix. The data show clear changes in the SANS signal as a function of temperature (Fig. 1). We observe a minimum in the integrated (10) peak intensity around 180 K for the heating branch (Fig. 2), in accordance with the work of Liu et al. [5] who attributed this minimum to a water density minimum. The behaviour of the SANS signal during the cooling process is different, the intensity jumping between two levels for the different temperature steps (Fig. 2). This is not a measuring artifact, as neither the intensity of the primary beam, nor the intensity at large scattering angles shows such a behaviour. This surprising result needs to be reproduced with better statistics, in particular also with respect to subtle changes of the corresponding wide-angle signal at the same temperatures.

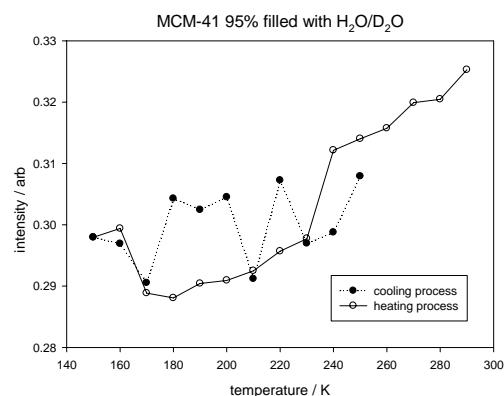


Fig. 2: Integrated (10) Bragg peak intensities of MCM-41 for cooling and heating processes.

- [1] O. Mishima, H. E. Stanley, Nature 396 (1998) 329-335.
- [2] P. G. Debenedetti, H. E. Stanley, Physics Today 56 (2003) 40-46.
- [3] L. M. Xu, P. Kumar, S. V. Buldyrev, S. H. Chen, P. H. Poole, F. Sciortino, H. E. Stanley, PNAS 102 (2005) 16558.
- [4] S. H. Chen, F. Mallamace, C. Y. Mou, M. Broccio, C. Corsaro, A. Faraone, L. Liu, PNAS 103 (2006) 12974.
- [5] D. Z. Liu, Y. Zhang, C. C. Chen, C. Y. Mou, P. H. Poole, S. H. Chen, PNAS 104 (2007) 9570-9574.
- [6] S. Jähnert, F. Vaca Chavez, G.E. Schaumann, A. Schreiber, M. Schönhoff, G.F. Findenegg, Phys. Chem. Chem. Phys. 10 (2008) 6039-6051.



## EXPERIMENTAL REPORT

### Dynamics of confined water in polysaccharide gels of pharmaceutical interest

Proposal N° BIO-03-551

Instrument **V3**

Local Contact Z. Izaola and M. Russina

Principal Proposer: Antonio Deriu, Università di Parma (Italy)  
 Experimental Team: Chiara Chiapponi, Università di Parma (Italy)  
 Ivana Finelli, Università di Roma Tor Vergata (Italy)  
 Gaio Paradossi, Università di Roma Tor Vergata (Italy)

Date(s) of Experiment

19/05/2008 – 26/05/2008

Date of Report: 15/12/2008

NEAT was used to carry out an experiment concerning the study of the dynamics in physical hydrogels based on hyaluronic acid (HYA).

This anionic polysaccharide is often used, for the rather unique viscoelastic properties, as substitute of synovial fluids in osteoarticular pathologies. A modification of the backbone with a C<sub>16</sub> alkyl chain, one every 100 saccharide residues, is sufficient to change dramatically the properties of the polysaccharide and to obtain a gel at very low polymer concentrations. The result of this modification is an injectable physical hydrogel stable at very low polymer concentration. In this experiment we have measured the hydrogels based on the derivatised form of hyaluronate, HYADD4<sup>TM</sup>, having 2 - 3 % of the amide groups grafted with a hexadecylic amide moiety and, as comparison, the unmodified polymer at the same concentrations.

We investigated both HYA aqueous solutions and HYADD4<sup>TM</sup> gels in H<sub>2</sub>O as a function of hydration: 1, 5 and 10% (w/w) at 285, 300 and 320 K.

In the framework of the jump-diffusion model, the analysis of the HWHM of HYADD4<sup>TM</sup> hydrogels and HYA aqueous solutions as a function of the scattering vector, shows that in both systems and for all investigated concentrations, the dynamics of hydration of water appears in a limited decrease of H<sub>2</sub>O diffusion coefficient of water,  $D$ , and in an increase of the residence time  $\tau_0$  with respect to the corresponding parameters of bulk water. As expected this differences, although small, increase with the polysaccharide concentration.

This effect appears at all the three temperatures probed (Figure 1).

It is interesting to note that the two systems, HYA and HYADD4<sup>TM</sup>, dramatically different on a macroscopic length scale, do not show any difference on the molecular scale probed by QENS.

In a future QENS experiment we will focus on the same systems in the presence of D<sub>2</sub>O.

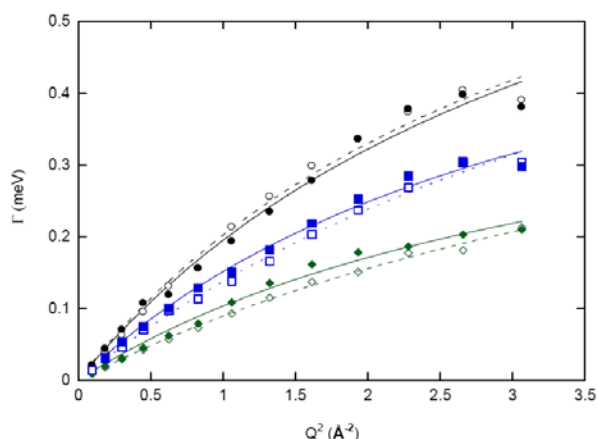


**Figure 1.** HYADD4<sup>TM</sup> hydrogels (♦) and HYA (◇) at a concentration of 10% (w/v) at 285K, HYADD4<sup>TM</sup> hydrogels (■) and HYA (□) at a concentration of 10% at 300K, HYADD4<sup>TM</sup> hydrogels (●) and HYA (○) at concentration of 10% at 320K.

HYADD4 <sup>TM</sup> 10% - T=285K	$D=1.4 \cdot 10^{-5} \text{cm}^2 \text{s}^{-1}$
HYA 10% - T=285K	$D=1.3 \cdot 10^{-5} \text{cm}^2 \text{s}^{-1}$
HYADD4 <sup>TM</sup> 10% - T=300K	$D=2.3 \cdot 10^{-5} \text{cm}^2 \text{s}^{-1}$
HYA 10% - T=300K	$D=2.1 \cdot 10^{-5} \text{cm}^2 \text{s}^{-1}$
HYADD4 <sup>TM</sup> 10% - T=320K	$D=2.7 \cdot 10^{-5} \text{cm}^2 \text{s}^{-1}$
HYA 10% - T=320K	$D=2.9 \cdot 10^{-5} \text{cm}^2 \text{s}^{-1}$

*This research project has been supported by the European Commission under the 6<sup>th</sup> Framework Programme through the Key Action: Strengthening the European Research Infrastructures.  
 Contract n°: RII3-CT-2003-505925 (NMI 3).*



## EXPERIMENTAL REPORT

### Effect of cation asymmetry in the dynamics of two room temperature ionic liquids

Proposal N° MAT-03-583

Instrument **V3**

Local Contact M. Russina

Principal Proposer: M. L. Saboungi (CRMD, CNRS Orleans, France)

Experimental Team: M. L. Saboungi (CNRS)

M. A. Gonzalez (ILL)

D. Price (CNRS)

Z. Izaola (BENSC)

M. Russina (BENSC)

Date(s) of Experiment

01/09/2008 – 07/09/2008

Date of Report:

Room-temperature ionic liquids (ILs) are defined as salts composed solely of ions with melting points below 100°C. A great interest in this class of materials has emerged during the last decade due to the interesting properties that they exhibit. In particular their use as “green” solvents replacing standard contaminant solvents constitutes a very active subject of research in the chemical industry. Another interesting property of ILs is its large tunability. This feature is derived from the possibility of combining different cations (often based on imidazolium, pyridinium, pyrrolidinium, ammonium or phosphonium derivatives) with a huge variety of anions (halides, nitrates, phosphates, etc.). As the diffusivity of cations and anions in ionic liquids are strongly coupled it is of high relevance to determine how the size and the symmetry of the cation and/or the anion affects the dynamics of a given ionic liquid. In order to determine the influence of the cation and the anion in the dynamics of ionic liquids we measured in NEAT four different ionic liquids based in the imidazolium cation: ethyl-methyl-imidazolium bromide (EMImBr), butyl-methyl-imidazolium bromide (BMImBr), EMIm-dimethylphosphate, and EMIm-dibutylphosphate. All of them were measured at at least four different temperatures between 300 and 400 K. An example of the data obtained for EMImBr at 412 K is given in Fig. 1, while the clear slowing down induced by the increase on the size of the cation when passing from EMIm to BMIm bromide is shown in Fig. 2 (note that at 300 K both of them are solid). However it seems that increasing the anion size has the opposite effect. A possible reason for this is that the ionic order becomes less pronounced. Structural work and MD simulations are being carried in order to check this. The preliminary analysis of the data indicates a complex dynamics and the existence of at least two kind of motions visible on the dynamic window of NEAT. We are currently working on the data fitting in combination with the MD simulations in order to try to obtain a coherent picture of the dynamics of those liquids.

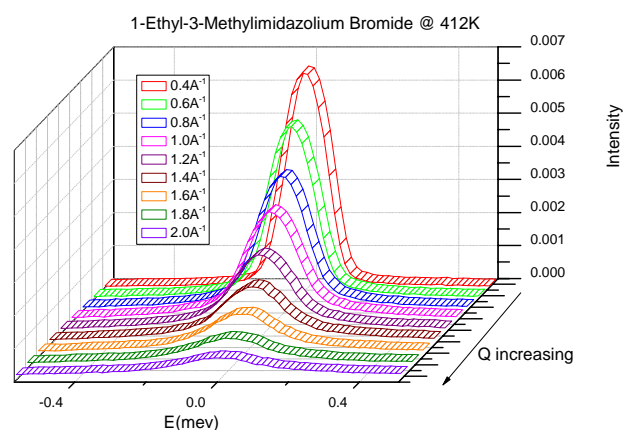


Fig. 1: Q-dependence of EMIMBr spectra

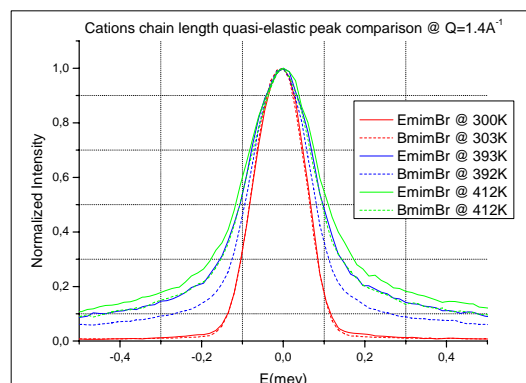


Fig. 2: Comparison of spectra for EMImBr and BMImBr at different temperatures.

*This research project has been supported by the European Commission under the 6<sup>th</sup> Framework Programme through the Key Action: Strengthening the European Research Infrastructures. Contract n°: RII3-CT-2003-505925 (NMI 3)*



## EXPERIMENTAL REPORT

### Proton Motions in Water-Saturated Plasma-Produced Membranes

Proposal N° CHE-03-591

Instrument **V3**

Local Contact  
Margarita Russina

Principal Proposer: Vanessa Peterson, Bragg Institute, ANSTO  
 Experimental Team: Gordon Kearley, Bragg Institute, ANSTO  
 Zunbeltz Izaola  
 Cormac Corr, Research School of Physics,  
 Australian National University

Date(s) of Experiment

01/07/2008 – 07/07/2008

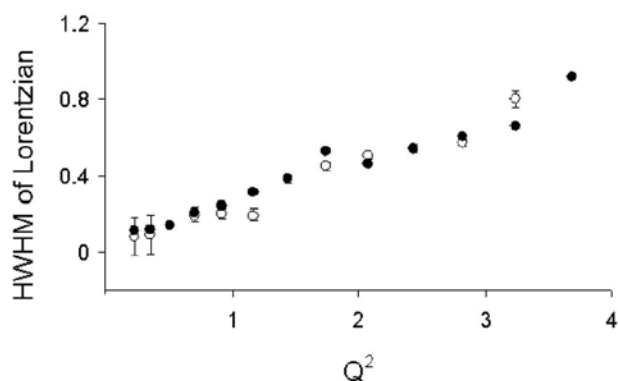
Date of Report: 09/01/2009

Polymer electrolyte membranes (PEMs) are key elements in polymer electrolyte fuel cells that allow for proton transport from the anode to the cathode. PEMs chemically similar to the commercial Nafion® have been developed using plasma techniques, allowing control of morphology and chemical composition.<sup>[1]</sup> Other advantages of this method include: a micrometric thickness allowing an easy miniaturization and strong electrode adhesion, highly cross-linked structure resulting in good chemical and thermal stability, and low permeability to organic liquids.<sup>[1]</sup>

In Nafion®, the state of water is correlated with the features of the confining polymeric environment. Consequently, water dynamics correlate with the onset and amplitude of proton conduction. QENS is an invaluable tool to the study the dynamics of confined water in Nafion®. Previous QENS studies of Nafion® show that the average dynamics of protons belonging to water molecules is revealed, even if contributions from protons that are part of the complex ionic species present in the liquid phase remain.<sup>[2]</sup>

QENS data from NEAT were collected for water saturated Nafion® 115 (~127 m) and plasma (~150 m) membranes at 300, 318, 328, and 338 K. Data were collected using 5.1 Å neutrons, giving an energy resolution of 128 eV for the  $Q$ -range 0.48–1.92 Å<sup>-1</sup>. Subtraction of data for D<sub>2</sub>O saturated membranes resulted in data from the water being conducted. Data revealed coherent scattering in the region 0.9–1.4 Å<sup>-1</sup>,<sup>[2-4]</sup> attributed to microcrystallites, noted previously to arise from lateral packing of the perfluoroethylene chains. Evidence of these crystallites was also found for the plasma-produced PEM.

$S(Q, \omega)$  were modelled using a Lorentzian convoluted with the resolution curve. In this case, the half-width at half-maximum of the Lorentzian for both the Nafion® and plasma data followed a  $DQ^2$  law.



At 300 K, a  $D$  value of  $2.2 \times 10^{-5} \text{ cm}^2 \text{ s}^{-1}$  is found for both membranes, slightly lower than for bulk water,  $2.5 \times 10^{-5} \text{ cm}^2 \text{ s}^{-1}$ , in agreement with the literature value for fully-saturated Nafion® at 300 K. This result indicates that the water diffusivity is the same in the plasma-polymerized as that in the traditional wet chemistry produced Nafion® PEM.

Traditionally, Nafion® membranes are boiled for 1 hr in 3 % H<sub>2</sub>O<sub>2</sub> and then in 0.5 M H<sub>2</sub>SO<sub>4</sub> (to remove organic and ionic impurities) before being boiled in deionised water. QENS data collected here for both for both treated and untreated Nafion® 115 revealed that water in treated Nafion is marginally more mobile

1. S. Roualdes, I. Topala *et al*, *J. Power Sources* 2006, **158**, 1270-1281.
2. A. Paciaroni, M. Casciola, *et al J. Phys. Chem. B* 2006, 110, 13769-13776
3. F. Volino, M. Pineri, *et al J Polym. Sci. Polym. Phys. Ed.* 1982, **20**, 481-496.
4. A. Pivovar, B. S. Pivovar, *J. Phys. Chem. B* 2005, **109**, 785-793



## EXPERIMENTAL REPORT

### Conformational characteristics of PHA in solution

Proposal N° BIO-04-1391

Instrument **V4**

Local Contact  
Uwe Keiderling

Principal Proposer: Rob Russell – National Deuteration Facility,  
Australian Nuclear Science and Technology  
Organisation  
Experimental Team: Seok Il Yun - ANSTO  
Rob Russell-ANSTO

Date(s) of Experiment

17/07/2007 – 22/07/2007

Date of Report: 15/12/2008

We have biosynthesised both short and medium chain length PHAs in their deuterated form (D-PHB and D-PHO) at the National Deuteration Facility (ANSTO, Australia), and these materials have been analysed by SANS in conjunction with the hydrogenated form.

Poly(3-hydroxybutyrate) (PHB) was produced from the bacterium *C. necator* in hydrogenated and deuterated form. Polymer was extracted from cell biomass and purified prior to casting as films. The various polymers were prepared in a range of dilute concentrations in chloroform prior to SANS analysis. The SANS data were fitted to the form factors for flexible or semiflexible chains using the Igor-based SANS model of NIST (National Institute of Standards and Technology, US).

flexible conformation of PHB chains in solution. The smaller contour length for PHB suggests chains might form a folded helical conformation with persistent length of 30 Å.

Sample	Mw g/mol × 10 <sup>3</sup>	A2 mol g- 2 cm <sup>3</sup>	Persistence length (Å)	Radius (Å)	Contour Length (Å)
PHB	38	0.0015	30	4.65	287
D-PHB	19	0.0016	35	4.64	689

Table 1. Characteristics of PHB and d-PHB analysed by SANS.

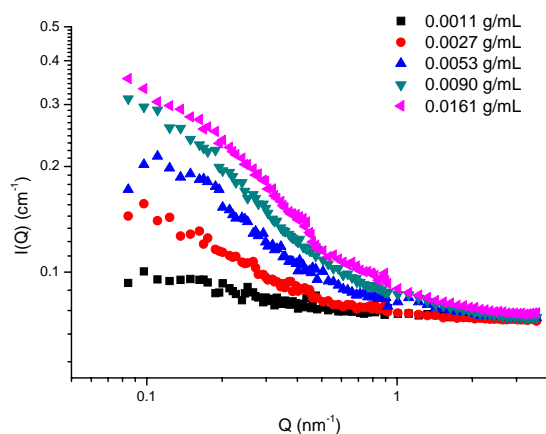


Figure 1 show the SANS data of D-PHB in chloroform as a function of polymer concentration. The molecular weight (Mw) and second virial coefficient (A2) were determined from the concentration (C) dependence of  $I(0)$  by Zimm plots. The obtained Mw and A2 for PHB and D-PHB are summarized in Table 1. The large persistent length obtained for PHB and D-PHB reflects high degree of local rigidity of the chains which contrasts with some reports in the literature showing the very

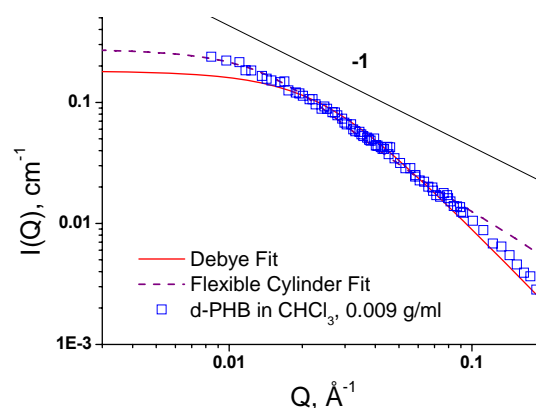


Figure 2. Comparison of the experimental data (after incoherent background subtraction) for D-PHB in chloroform, with the fits by the form factors for randomly coiled flexible chains (Debye equation) and semiflexible chains (Pederson and Schurtenberger). The PHB or D-PHB chains in dilute solutions studied in this paper had a fractal dimension close to -1 indicating that the shape of D-PHB is close to rod-like particles. Well defined molecular weight samples will be produced for more accurate modelling using SANS data.



## EXPERIMENTAL REPORT

### Desorption study mechanism in hierarchical mesoporous silica followed by C<sub>5</sub>F<sub>12</sub> in-situ SANS

Proposal N° PHY-04-1459

Instrument **V4**

Local Contact  
Astrid Brandt

Principal Proposer: B. Smarsly, University of Giessen, Germany  
 Experimental Team: S. Mascotto, University of Giessen, Germany  
 D. Wallacher, Helmholtz Zentrum Berlin, Germany  
 A. Brandt, Helmholtz Zentrum Berlin, Germany

Date(s) of Experiment

18/06/2008 – 21/06/2008

Date of Report: 18/12/2008

In general, the field of physisorption suffers from the lack of suitable independent techniques to verify theoretical models, which themselves are the basis for the determination of structural parameters. In our previous works at HZB successful results in this direction were obtained performing in-situ small-angle neutron scattering (SANS) study in mesoporous silica during C<sub>5</sub>F<sub>12</sub> adsorption at 280 K taking advantage of contrast matching between liquid C<sub>5</sub>F<sub>12</sub> and the SiO<sub>2</sub> itself. Despite the interesting outcomes by the vapour condensation in the mesopores, in-situ-SANS technique can be also successfully applied in the understanding of the pore emptying mechanism of porous solids.

The material used in this study was a hierarchical mesoporous silica (PIB-IL) containing spherical mesopores of 18 nm connected through smaller mesopores (3 nm). Furthermore, this material possesses a few additional, non-defined micropores of < 1.5 nm in size. Preliminary experiments on this sample already indicated that the small mesopores are situated between the larger ones, proving almost ideal pore hierarchy.

Until now two main theories are used in the explanation of the draining mechanism: cavitation and pore blocking. However, cavitation was only predicted, but had not been experimentally proven yet. The *pore blocking* effect (see Fig 1a) is expected to occur if the pore has access to the external surface only through a narrower neck, as in the ink-bottle pore. The wide body of the ink-bottle pore remains filled during desorption until the narrow neck empties first at a lower vapour pressure. The vapour pressure, at which a pore body empties, depends upon the size of the necks, the connectivity of the network, and the state of the neighbouring pores. By contrast, recent studies suggested that, if the neck diameter is smaller than a certain critical size (~ 5 nm) at a given experimental temperature, desorption from the pore body occurs via *cavitation* (spontaneous nucleation of a bubble). In this case the pore body can empty by diffusion, while the pore neck remains filled.

The use of the in-situ-SANS technique offered the unique chance to check the emptying mechanism.

The C<sub>5</sub>F<sub>12</sub> desorption at 280K of PIB-IL silica was followed by SANS and is presented in Fig 1b.

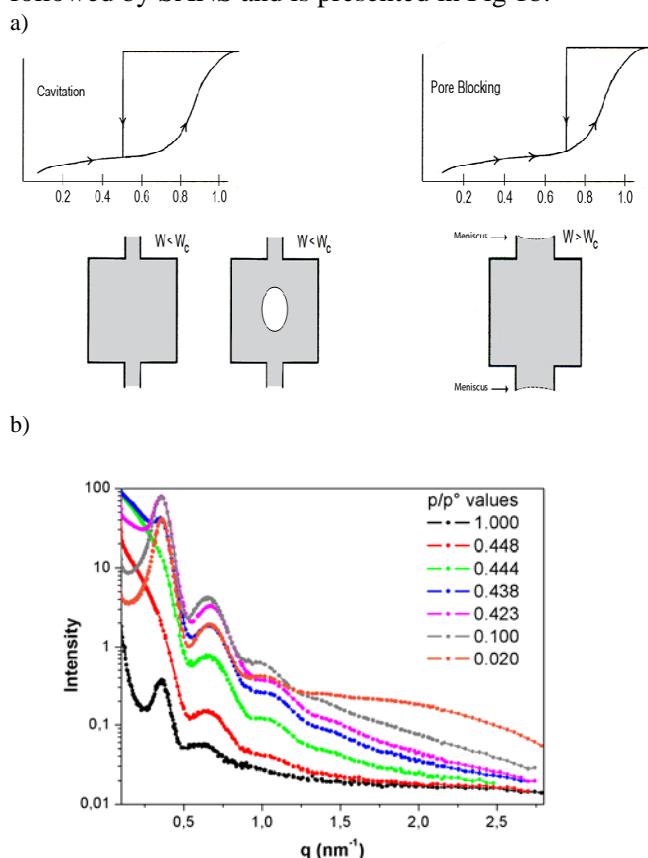


Fig 1: a) Scheme of pore emptying mechanism; b) SANS patterns during the C<sub>5</sub>F<sub>12</sub> desorption branch in PIB-IL silica.

As can be seen the progressive appearance of the Bragg peak maximum at  $q = 0.4$  nm<sup>-1</sup> reveals the emptying of the 18 nm cavities with the small mesopores still being filled. At smaller relative pressure values ( $p/p^\circ < 0.4$ ) the enhancement of the scattering intensity at  $q > 1.5$  nm<sup>-1</sup> evidences the subsequent draining of the IL mesopores and micropores. This finding is a direct proof of the *cavitation* pore emptying mechanism.



## EXPERIMENTAL REPORT

### Surface Aggregate Structure of a Binary Surfactant Mixture on Colloidal Silicas

Proposal N° CHE-04-1546

Instrument **V4**

Local Contact  
Sylvain Prévost

Principal Proposer: D. Lugo – TU Berlin  
 Experimental Team: D. Lugo – TU Berlin  
 G. H. Findenegg – TU Berlin  
 S. Prévost – HMI, Berlin

Date(s) of Experiment

09/07/2008 – 13/07/2008

Date of Report: 14/01/2009

As an extension of our earlier study of the surfactant-adsorbed layers formed by two nonionic surfactants on a colloidal silica sol ( $C_{12}E_5$  and  $\beta-C_{10}G_2$ , as the strongly and weakly adsorbing surfactant, respectively) [1], we have investigated the structures formed by a surfactant mixture containing  $C_{12}E_4$  and  $\beta-C_{12}G_2$ , which have the same chain length and a similar cmc. We expect with this mixture that  $C_{12}E_4$  will be more strongly adsorbed than  $C_{12}E_5$  as Penfold et al. [2] have found that the adsorption of  $C_nE_m$  surfactants onto silica sols increases with increasing ratio  $n/m$ . Experiments were carried out at room temperature, i.e., above  $C_{12}E_4$  cloud point.

Measurements were made using silica sols of different sizes (16, 24, and 34 nm) at several concentration (3-5 wt-%) and at pH 9 to avoid particle aggregation. For each silica size, a 1:1 mixture of surfactants was added at 5 concentrations based on  $C_{12}E_4$  adsorption value:  $1/10\Gamma_{mx}$ ,  $1/3\Gamma_{mx}$ ,  $1/2\Gamma_{mx}$ ,  $3/4\Gamma_{mx}$  and  $\Gamma_{mx}$  of  $C_{12}E_4$  (where  $\Gamma_{mx}$  is the plateau value of the adsorption isotherm of surfactant on silica). Additionally an overall concentration of 1% of the mixture was tested to see the effect of large surfactant excess. Finally, to test the effect of the molar ratio  $C_{12}E_4:\beta-C_{12}G_2$ , other ratios were prepared for the samples at  $1/2\Gamma_{mx}$  of  $C_{12}E_4$  and at 1%. Most of the samples were prepared twice, in pure  $D_2O$  (high contrast, low background) and in a mixture  $H_2O/D_2O$  to match the silica. Most of the spectra were typical for core-shell aggregates, while pure surfactants exhibited spherical to cylindrical micelles.

The SANS spectra for 24nm silica particles with 3 different  $C_{12}E_4:\beta-C_{12}G_2$  ratios at 1% are shown in Fig. 1a. At the ratios 3:1 and 1:1  $C_{12}E_4:\beta-C_{12}G_2$ , the peak at  $q \approx 0.25 \text{ nm}^{-1}$  is pronounced, which indicates that  $\beta-C_{12}G_2$  is indeed incorporated in the adsorption layer. However, at the ratio 1:3, that peak is absent indicating the formation of a different type of aggregates. One possible explanation for this behaviour is that mixed micelles of the two surfactants are

forming, i.e.,  $C_{12}E_4$  is desorbed from the silica and incorporated into the micelles of  $\beta-C_{12}G_2$ . A similar behaviour was found with the other two silicas, except for the surfactant ratio 1:1, where two phases formed. We explain this behaviour following Kaler's observations: silica particles in wormlike micelle networks act as seeds to increase junctions and therefore lead to a high viscosity and/or phase separation [3]. In the case of the sample  $1/2\Gamma_{mx}$ , the behaviour was similar (Fig 1b). These samples were prepared in a  $H_2O/D_2O$  mixture, where the silica was not matched. The peak at  $q = 0.1 \text{ nm}^{-1}$  indicates repulsive electrostatic interactions between silica beads, and the peak at  $q \approx 0.3 \text{ nm}^{-1}$  means that surfactant has been adsorbed onto the silica. At greater relative amounts of  $\beta-C_{12}G_2$  the peak at  $q \approx 0.3 \text{ nm}^{-1}$  disappears, and possibly we have the same behaviour as mentioned above. Careful modelling is on its way to quantify the equilibria between silica coatings, monomers, mixed micelles and wormlike networks.

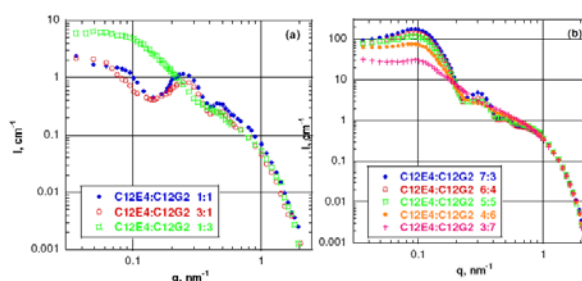


**Fig. 1:** SANS profiles from silica beads of diameter 24 nm with different concentration ratios of  $C_{12}E_4:\beta-C_{12}G_2$ : (a) 1 v.-% of surfactant mixture in a  $H_2O/D_2O$  mixture close to the contrast match point of silica; (b)  $0.5\Gamma_{mx}$  of  $C_{12}E_4$  in a  $D_2O$ -rich  $H_2O/D_2O$  mixture

- [1] G.H. Findenegg, D. Lugo, M. Karg, S. Prévost. BENSC Experimental Report 2007, CHE.04-1455  
 [2] J. Penfold et al, *J. Phys. Chem.* **1996**, *100*, 18133.  
 [3] Nettekheim F. et al., *Langmuir* **2008** *24* (15), 7718-7726



## EXPERIMENTAL REPORT

### The Role of the Water Shell and Counterion Distribution around Charged Proteins Studied by SANS

Proposal N° PHY-04-1556

Instrument **V4**

Local Contact  
Sylvain Prévost

Principal Proposer: Frank Schreiber, Uni-Tübingen  
 Experimental Team: Fajun Zhang, Uni-Tübingen  
 Luca Ianeselli, Uni-Tübingen  
 Richard Martin, University of Kent, UK  
 Sylvain Prévost, HMI, Berlin

Date(s) of Experiment

07/03/2008 – 11/03/2008

Date of Report: 14/03/2008

Stabilization of the tertiary structure as well as interactions between biopolymers in vivo strongly depends on the hydration and the surrounding ions. The protein-ion interaction and the counterion distribution as well as the hydration shell are important for tuning protein interactions in general, and thus their detailed understanding is essential for a variety of aspects in biological systems [1,2]. Recent developments have demonstrated that precise measurements using SANS with contrast variation, combined with (A)SAXS, provide one (and probably the only) way to address these issues.

In this beamtime, we have performed SANS measurements on the hydration of protein in salt solution, which has shown that detailed and complimentary structural information can be obtained even with relative low protein concentrations. In Fig.1, we show the preliminary scattering profiles of BSA solutions with three salts. In the Hofmeister series, NaCl is a neutral salt, the anion of NaSCN has a strong salting-in effect, while Na<sub>2</sub>SO<sub>4</sub> has a strong salting-out effect. In Fig.2, the SANS results for multivalent ion-bind BSA in both D<sub>2</sub>O and H<sub>2</sub>O were presented. The sample in H<sub>2</sub>O was measured only for 2 SD values (1m and 4m). Further data analysis of the salt nature effect on protein hydration by fitting the high quality data with CRYSON will be carried out imminently. Together with ASAXS measurements on the same solution, the structure of bind-ion shell around proteins can be evaluated.

[1] A. Stradner, et al. Nature 2004, 432, 492.

[2] D. I. Sevrgun et al. PNAS 1998, 95, 2267.

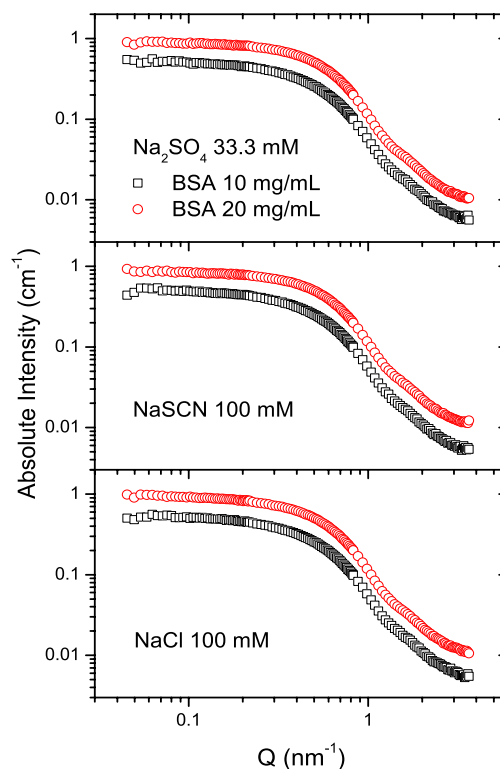


Fig. 1 Example of SANS data from BSA solutions with different salts. The whole  $Q$ -range data were merged from 3 sample-to-detector distance measurements.

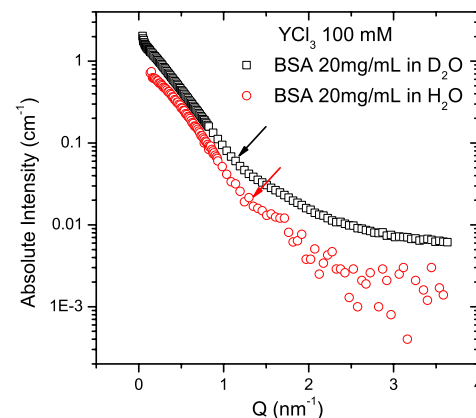


Fig. 2 SANS results of charge-inversed BSA in solution due to binding of trivalent cation (yttrium) in D<sub>2</sub>O and H<sub>2</sub>O, respectively.



## EXPERIMENTAL REPORT

### Structural investigation of phospholipid/polysaccharide nanocapsules

Proposal N° BIO-04-1568

Instrument **V4**

Local Contact  
D. Clemens

Principal Proposer: Gerelli Yuri, Physics Department, Università di Parma  
Experimental Team: Deriu Antonio, Physics Department, Università di Parma  
Barbieri Stefano, Pharmaceutical Department, Università di Parma  
Clemens Daniel, BENSC, Berlin

Date(s) of Experiment

19/05/2008 – 23/05/2008

Date of Report: 07/01/2009

In recent years nano-technologies have been used in pharmaceutical sciences to amend undesirable properties of several active compounds; in this context, nanoparticles composed of lipid material have been proposed as drug carriers. Several polysaccharides have been investigated for the stabilization of lipid membranes. Among them chitosan, a cationic polysaccharide has emerged because of its favourable biochemical characteristics, including low toxicity and high biocompatibility. In previous SANS experiments performed on D11 at the ILL we investigated the morphological and structural features of multilamellar nanoparticles obtained by direct injection of a soybean lecithin alcoholic solution into a chitosan/water solution [1]. The nanoparticle supramolecular self-organization turns out to be contemporarily driven by the aggregative behaviour of the lipid component and by the electrostatic interaction between the negatively charged fraction of the lipid material and the positively charged polysaccharide. This characterization, as a function of chitosan content in the initial chitosan/water preparation solution, is important in order to optimize the loading efficiency and to tune the drug release kinetics. In order to get more detailed structural information on these complex multi-component nanoparticles, in the present experiment we have replaced lecithin (a natural mix of phospholipids) with a controlled binary lipid mixture (98% POPC - 2% DMPS) using also perdeuterated POPC. Preliminary characterization of free-chitosan vesicles and of nanoparticles based on the new mixture were carried out by dynamic light scattering and surface charge (Z-potential) measurements. The SANS data collected at V4 were analysed in terms of a three-strip model [2]. In figure 1 we report the SANS curves for POPC/DMPS vesicles prepared with hydrogenated and perdeuterated lipids; the continuous lines show the result of a simultaneous fit of all the curves displayed. We can conclude that the particles are predominantly unilamellar; their structure, in particular the thickness of the lipid bilayers is very close to that previously measured in lecithin vesicles. Lecithin- and POPC/DMPS- vesicles have similar average size, but

the latter show a larger polydispersity of the core radius size distribution. Preliminary analyses with a modified three-strip model indicate that the addition of chitosan leads to the formation of lipid-saccharide complexes with a multi-lamellar structure: The SANS profiles are characterized by a well defined peak at  $Q \sim 0.1 \text{ \AA}^{-1}$  corresponding to a periodicity of about 60  $\text{\AA}$ . A detailed structural description of these complexes requires additional information on the bilayer structure that can be obtained from SAXS data (higher resolution and smaller length-scale probed). The SAXS data have been already obtained on ID02 (E.S.R.F. – Grenoble) and their analysis is under way.

[1] Y. Gerelli *et al.*, *Langmuir*, 24 (2008) 11378-11384.  
[2] N. Kucerka *et al.*, *PRE*, 69 (2004) 051903(9)

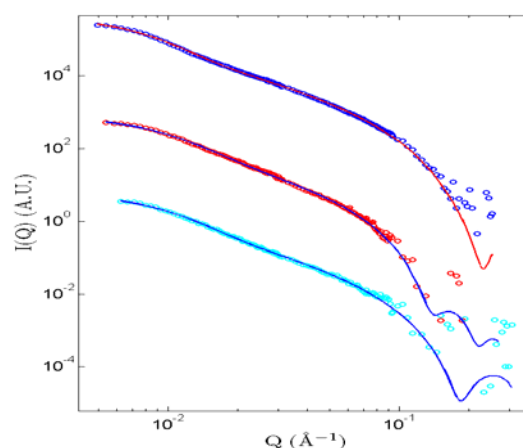


**Figure 1** SANS profiles for POPC/DMPS (blue) and D-POPC/DMPS (red) vesicles in  $D_2O$ . The lower light blue curve refers to hydrogenous POPC/DMPS in a buffer with a  $D_2O/H_2O$  mixture that matches the hydrophobic alkyl chains.

#### Acknowledgements

*This research project has been supported by the European Commission under the 6<sup>th</sup> Framework Programme through the Key Action: Strengthening the European Research Infrastructures.*

*Contract n°: RII3-CT-2003-505925 (NMI 3).*



## EXPERIMENTAL REPORT

### Phase behaviour of mixtures of anionic perfluoro surfactants and nonionic TDMAO

Proposal N°  
CHE-04-1610-EF  
Instrument **V4**  
Local Contact  
Sylvain Prevost

Principal Proposer: Michael Gradzielski  
Experimental Team: Michael Gradzielski  
Sylvain Prevost  
Katharina Bressel

Date(s) of Experiment  
06/02/2008 – 10/02/2008

Date of Report: 17/01/2009

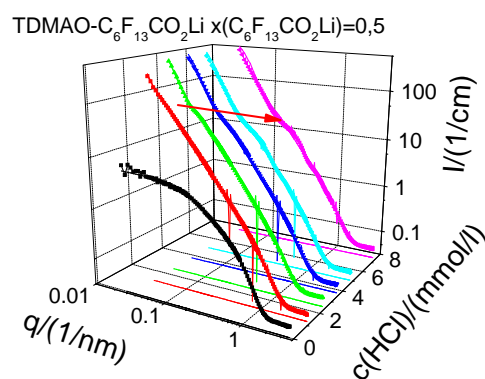
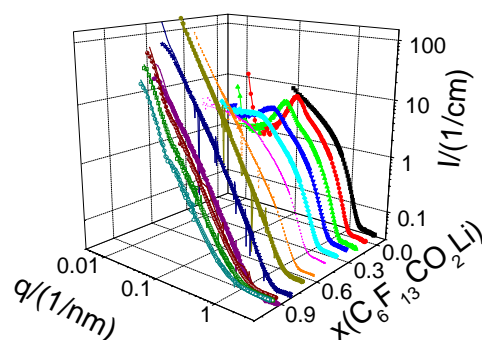
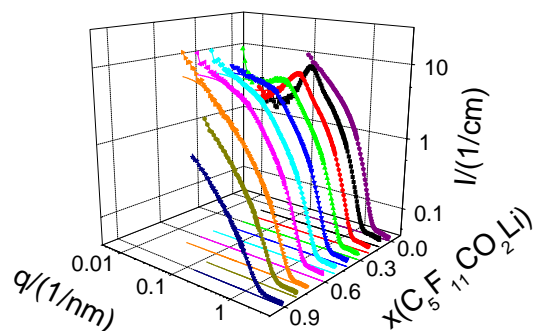
Mixtures of perfluorinated anionic surfactants and the hydrocarbon TDMAO were investigated with Small Angle Neutron Scattering to determine the phase behaviour and to characterize the size and shape of the aggregates.

Due to the attractive interactions between the anionic and the nonionic head groups and to the repulsive interactions between the perfluorinated chain and the hydrocarbon chain variation in the molar fraction of the perfluoro surfactants results in changes of the packing parameter. Protonation of the TDMAO head group results in increased attractive interaction and therefore smaller packing parameter.

All samples were prepared by mixing 50mM surfactant stock solutions so that the total surfactant concentration is 50mM.

In mixtures of  $C_5F_{11}CO_2Li$  and TDMAO ellipsoidal and wormlike micelles are formed. Increasing the molar ratio of  $C_5F_{11}CO_2Li$  leads to elongation of the micelles and transition to wormlike micelles due to the bulky perfluorinated chain.

Increasing the perfluorinated chain length results in formation of large polydispers vesicles in the  $C_6F_{13}CO_2Li$ -TDMAO phase diagram for  $x(C_6F_{13}CO_2Li)$  0,6 and a two-phase region consisting of vesicles and ellipsoidal micelles for  $0,6 > x(C_6F_{13}CO_2Li) > 0,4$ . Protonation of the TDMAO decreases the packing parameter and induces the formation of a single vesicle phase with decreasing vesicle radius with increasing HCl-concentration.



	<b>EXPERIMENTAL REPORT</b>  <b>Temperature-induced microemulsion-to-vesicle transition followed by SANS</b>	Proposal N° CHE-04-1610-EF  Instrument <b>V4</b>  Local Contact Sylvain Prévost
	Principal Proposer: Michael Gradzielski Experimental Team: Sylvain Prévost, Stanski-Lab TU Berlin + HZB Berlin Anina Barth, Stanski-Lab TU Berlin	Date(s) of Experiment  04/06/2008

Date of Report: 12/01/2008

Part of the beam time allocated to Soft Matter within the collaboration TUB – BENSC was devoted to the study of commercial-grade based microemulsions.

The aim of this experiment was to study the phase transition in the ternary system surfactant-oil-water from microemulsion to a vesicle phase. As surfactant the skin-tolerant semipolar compound tetradecyldimethyl amine oxide (TDMAO) was employed. Valerian acid methyl ester (VME) served as the apolar (oil) component.

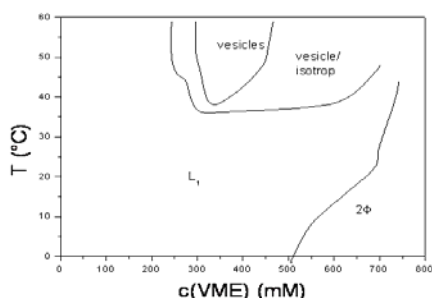


**Figure 1**

From the ternary phase diagram the appropriate ester concentration for detecting the phase transition was chosen at 325 mM VME. Due to the lower solubility of VME in D<sub>2</sub>O, which had to be used for the SANS-measurement, the sample contained 200 mM TDMAO and 273 mM VME. It was homogenized by vortexing and equilibrated at the required temperature for at least 20 min before the experiment. From former experiments the phase transition could clearly be seen because of increasing viscosity and turbidity of the sample (see table 1). Therefore 20, 25 and 43°C were chosen as experimental temperatures.

**Table 1**

	20 °C	25 °C	43 °C
273 mM VME in D <sub>2</sub> O	isotropic, clear → elongated micelles	isotropic, clear → elongated micelles	turbid, viscous → unilamellar vesicles

The SANS curves are shown on Fig. 2. At 20 and 25°C slightly elongated aggregates are seen, with relatively monodisperse radius (for a microemulsion). Increasing the temperature a pronounced peak at 31 nm appears, implying vesicles with low polydispersity.

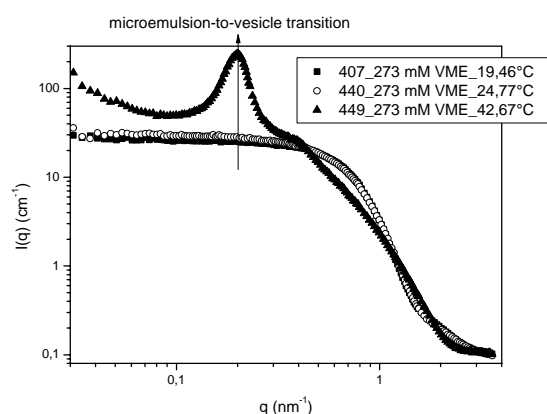


**Figure 2**

Fits indicated the presence of unilamellar vesicles, but some features of the spectra could not yet be perfectly reproduced.

Similar experiments were performed with other oils of commercial interest and demonstrated similar trends with differences related to their polarity, and more interestingly differences in the repulsions/attractions balance (fitted with a Baxter model). The origin of these differences are under study.



## EXPERIMENTAL REPORT

### Scaling-behavior of PNIPAM microgels with different crosslinker densities

Proposal N° CHE-04-1642

Instrument **V4**

Local Contact  
S. Prevost/A. Brandt

Principal Proposer: Matthias Karg – TU Berlin, Stranski Lab.  
Experimental Team: A. Brandt, HZB für Materialien und Energie GmbH  
D. Wallacher, HZB für Materialien und Energie GmbH  
S. Prevost, HZB für Materialien und Energie GmbH

Date(s) of Experiment

22/07/2008 – 25/07/2008

Date of Report: 29/07/2008

Aqueous microgels made of N-isopropylacrylamide (NIPAM) undergo a temperature-induced volume phase transition at  $T_c \approx 33^\circ\text{C}$ . Below this temperature water is considered to be a good solvent for poly-NIPAM and the particles are in a swollen state, while the solvent quality decreases rapidly reaching the phase transition temperature and the microgel collapses. The degree of swelling is strongly related to the number of crosslinks within the polymer network.

Figure 1: Sketch of microgel particles having a low (left) and a high (right) crosslinker density.

In figure 1 networks with two different crosslinker densities are illustrated. Within the reported small angle neutron scattering (SANS) experiment we focussed on poly-NIPAM microgels with three different crosslinker densities, which are 2%, 5% and 15% of the crosslinker molecule N,N'-methylenebisacrylamide (BIS).

The overall size of these spherical particles has been studied previously using dynamic light scattering, which is a well-suited technique to investigate their hydrodynamic dimensions as a function of temperature. Nevertheless, due to the rather small  $q$ -range available in a light scattering experiment the internal morphology is not accessible by this method. Hence, SANS is needed if the structure of the polymer network has to be studied. The SANS data for microgel particles can be described by a sum of a Porod decay and a Ornstein-Zernicke (OZ) contribution:

$$I(q) \propto \frac{1}{q^4} + \frac{1}{(1+q^2\xi^2)} \quad (1)$$

The magnitude  $\xi$  is a measure for the network fluctuations and a scaling-law behavior is expected:

$$\xi = \left| \frac{T - T_c}{T_c} \right|^{-\nu} \quad (2)$$

Figure 2 represents SANS curves measured within this experiment. Shown are profiles at different temperatures representing different states of swelling for the three microgels having different crosslinker densities.

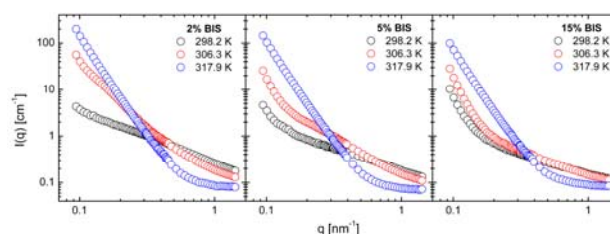


Figure 2: SANS curves for poly-NIPAM microgels at  $25^\circ\text{C}$  (swollen state),  $40^\circ\text{C}$  (collapsed state) and close to the temperature of the volume phase transition, at  $33^\circ\text{C}$ . The crosslinker density increases from left to right (2%, 5% and 15%).

During our experiment we measured SANS spectra at 17 different temperatures for each of the three samples. The special-build sample holder is shown in figure 3.



Figure 3: Sample holder consisting of a solid copper block with a Peltier element and PT 100 temperature sensors.

In the future we would like to continue with SANS experiments on the V4 instrument, since the available  $q$ -range as well as the conditions regarding sample environment are well-suited for our experiments on the internal structure of microgels.



**EXPERIMENTAL REPORT**  
**Study of the supramolecular structure of  $\mu E$**   
**used as host medium for lanthanide ion**  
**separation**

Proposal N° CHE-04-1660

Instrument **V4**

Local Contact  
Sylvain Prévost

Principal Proposer: Pierre Bauduin, ICSM CEA Marcoule, France  
 Experimental Team: Caroline Bauer, ICSM CEA Marcoule, France

Date(s) of Experiment

04/09/2008 – 07/09/2008

Date of Report: 13/12/2008

An effective strategy to co-solubilise a hydrophilic compound like water and hydrophobic compound like oil is the addition of amphiphilic molecules. The addition of co-surfactants like alcohols permits to create microemulsions ( $\mu E$ ) that are clear, isotropical and thermodynamically stable dispersions of water and oil separated by the surfactant/co-surfactant film. Special cases are bicontinuous  $\mu E$  which are in equilibrium with both water and oil excess phases (so-called Winsor III). For our purpose this equilibrated state is a powerful analytical tool to study partitioning of ions between excess aqueous phase and the  $\mu E$ . Therefore the structural characterisation of these microemulsions at various compositions is indispensable and was the aim of our SANS experiment. At first we focus on aqueous salt solutions in contact with dodecane and a non-ionic surfactant, n- $\beta$ -octylglucoside (C8G1). Classically the addition of a short chain n-alcohol like n-hexanol (C6OH) forms three-phasic systems but also the addition of an extractant molecule, like tri-n-butyl phosphate, (TBP) used in nuclear industry for lanthanide ion separation. Obtained scattering curves are shown in Figure 1.

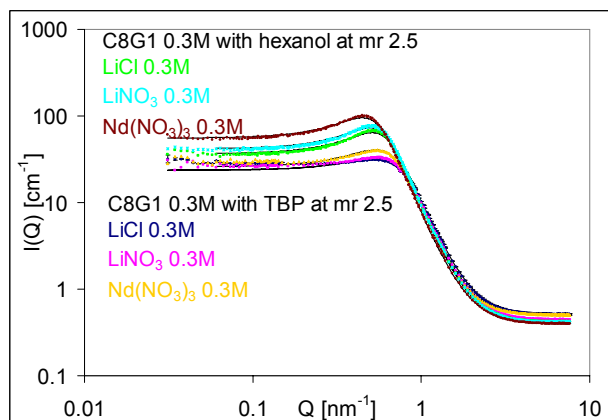


*Fig. 1 Selection of scattering functions of bicontinuous  $\mu E$  with a short chain alcohol (hexanol) or an extractant (TBP) and various salts (mr: molar ratio); Lines are the best fits*

The ratio between the cosurfactant and the surfactant was kept constant, as well as the salinity. Porod's treatment and fitting procedure with the Teubner-Strey-Model delivers useful information on the structure of these  $\mu E$ . Characteristic length scales the specific surface were taken and are shown in Table 1.

	$\Phi_w$	$\xi$	$D^*$ [nm]	$\Sigma$ [cm <sup>-1</sup> ]
C8G1 without salt (C6OH)	0.36	3.74	10.78	7.88E+05
C8G1 LiCl (C6OH)	0.37	3.85	10.94	6.74E+05
C8G1 LiNO <sub>3</sub> (C6OH)	0.35	3.94	11.28	6.25E+05
C8G1 Nd(NO <sub>3</sub> ) <sub>3</sub> (C6OH)	0.34	4.31	12.50	5.94E+05
C8G1 LiCl 0.3M TBP	0.24	2.71	9.68	8.91E+05
C8G1 LiNO <sub>3</sub> 0.3M TBP	0.25	2.87	9.80	8.35E+05
C8G1 Nd(NO <sub>3</sub> ) <sub>3</sub> 0.3M TBP	0.26	3.28	10.19	6.66E+05

*Table 1 Extracted characteristic values of the  $\mu E$  (see Fig. 1)  $\Phi_w$  volume fraction of water in the  $\mu E$ ,  $\xi$  correlation length,  $D^*$  periodicity of the domains and  $\Sigma$  specific surface*

Secondly probes were prepared with a cationic surfactant dodecyltrimethylammonium chloride (DTACI), pentanol (C5OH) as cosurfactant and salt. The scattering curves are not shown here but they are similar to those obtained with the nonionic surfactant. In order to study adsorption effects of cations at the different water oil interface only the nature of the salt was varied. We find that the cationic  $\mu E$  are less dependent on the nature of the salt than the non-ionic  $\mu E$ . Together with the findings of other analytical techniques the salt concentration of the water domains in the  $\mu E$  will be determined and interpreted in terms of specific ion adsorption.

*This research project has been supported by the European Commission under the 6<sup>th</sup> Framework Programme through the Key Action: Strengthening the European Research Infrastructures.*

*Contract n°: RII3-CT-2003-505925 (NMI 3)*



**EXPERIMENTAL REPORT**  
**Effect on the block copolymer self-assembling in water of block selective cyclodextrin addition.**

Proposal N° **CHE-04-1667**

Instrument **V4**

Local Contact  
**S. Prevost**

Principal Proposer: S. Milioto – University of Palermo  
 Experimental Team: M. Gradzielski - TU Berlin, Stranski-Lab.  
 G. Lazzara - University of Palermo  
 S. Prevost - TU Berlin, Stranski-Lab., HMI Berlin

Date(s) of Experiment

31/08/2008 – 04/09/2008

Date of Report: 06.01.2009

The pseudopolyrotaxanes formed by cyclodextrins (CDs) and polymers is an attractive issue in supramolecular chemistry because they represent models for molecular recognition and can be employed in several fields such as drug delivery. Recently, we evidenced [1] the formation of pseudopolyrotaxanes formed by native and alkylated cyclodextrins with different cavity size and amphiphilic copolymers such as poly(ethylene oxides)-poly(propylene oxides)-poly(ethylene oxides) generally indicated as  $EO_aPO_bEO_a$  where a and b are the repetitive number of EO and PO units, respectively. The SANS experiments clearly show (figure 1) that the copolymer in water forms strongly interacting spherical aggregates with a core shell architecture. The addition of a CD changes the structure of the system and its effect is strongly dependent on the CD cavity size. Namely, if one adds the hydroxypropyl- $\beta$ -cyclodextrin (HP- $\beta$ -CD) it turns out that the intensity is reduced and above a given CD concentration the intensity vs. Q trend does not show anymore an interaction peak; that is consistent with the rupturing of the copolymer aggregates. On the other hand, the hydroxypropyl- $\alpha$ -cyclodextrin (HP- $\alpha$ -CD) at the higher concentrations generates a more pronounced maximum which indicates stronger interactions (an example is given in figure 2). The different response of the copolymer aggregates to the two CDs can be ascribed to the CD cavity size and to the consequent selectivity toward the EO and PO units. In particular, the ability of HP- $\beta$ -CD to include both the EO and the PO segments renders the polymer much more hydrophilic and thereby disfavors the formation of aggregates. In the case of HP- $\alpha$ -CD, only the EO segments can be included and therefore the complexed copolymer may participate to the formation of micelles having the hydrophilic shells decorated with the CD baskets. Such a picture explains also the more pronounced maximum due to the increase of the effective

volume fraction of the aggregates as a consequence of the HP- $\alpha$ -CD addition.

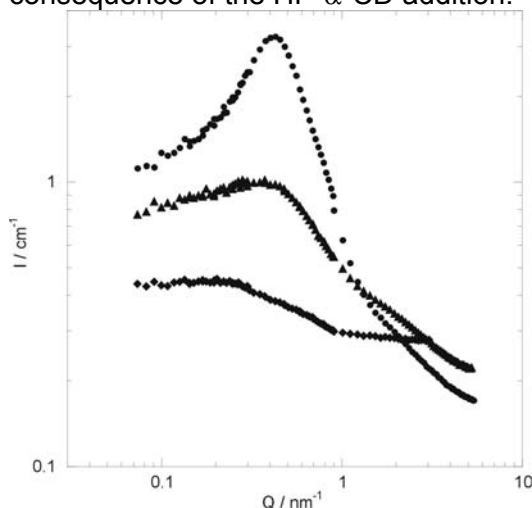


**Figure 1.** Scattering function of the  $D_2O+F88$  mixture in the absence ( $\bullet$ ) and the presence of HP- $\beta$ -CD at different concentrations: ( $\blacktriangle$ ), 5 wt.%; ( $\blacklozenge$ ), 23 wt.%.

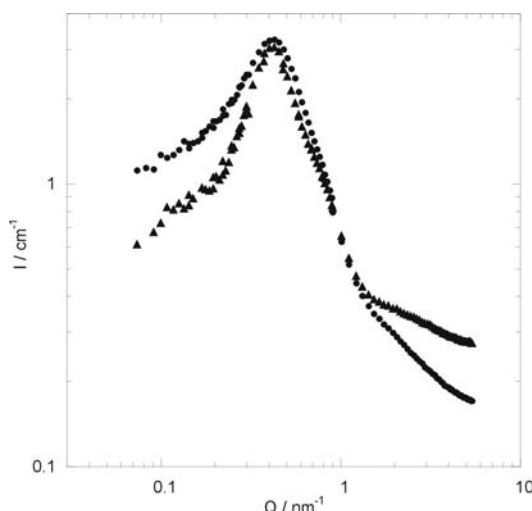


**Figure 2.** Scattering function of the  $D_2O+F88$  mixture in the absence ( $\bullet$ ) and the presence ( $\blacktriangle$ ) of HP- $\alpha$ -CD 23 wt.%.

**References**

[1] G. Lazzara and S. Milioto *J. Phys. Chem. B* **2008**, 12, 11887.

**Acknowledgements**

This research project has been supported by the European Commission under the 6th Framework Programme through the Key Action: Strengthening the European Research Area, Research Infrastructures. Contract n°: RII3-CT-2003-505925 (NMI3)



## EXPERIMENTAL REPORT

### Nanocomposites based on clay nanoparticles and block copolymer

Proposal N° CHE-04-1667

Instrument V4

Local Contact  
S. Prevost

Principal Proposer: S. Milioto – University of Palermo  
Experimental Team: M. Gradzielski - TU Berlin, Stranski-Lab.  
G. Lazzara - University of Palermo  
S. Prevost - TU Berlin, Stranski-Lab., HMI Berlin

Date(s) of Experiment

31/08/2008 – 04/09/2008

Date of Report: 06/01/2009

Nanocomposites are interesting materials characterized by nano-sized fillers and a polymeric matrix. Their physico-chemical properties may be tuned and modulated for specific purposes achieving extraordinary properties which could not be attained by normal composite materials, i.e. enhancement of mechanical properties, thermal and chemical stability, reduced flammability, material reinforcement, flame resistance, electro-optical properties, cosmetic applications, etc. Within this topic, we synthesized and characterized nanocomposites based on poly(ethylene) glycol 2000 and the tri-block copolymer  $EO_{98}PO_{67}EO_{98}$  (F127). As inorganic filler we used laponite which is a synthetic clay containing disk-like nano-platelets with a radius of 12.7 nm and a thickness of 0.9 nm. In order to explore a Q-range as wide as possible we have employed 4 different configurations at V4 instruments.

Looking at the data from F127 (figure 1), one can see a peak for the pure copolymer which is less pronounced in the nanocomposite with the 20 wt.% of laponite and disappears for higher laponite contents. Such a peak corresponds probably to a lamellar distribution of PEO and PPO with a mean spacing which increases from 14.8 nm to 21.3 nm by adding a 20 wt.% of laponite. At larger laponite concentration, the lamellar structure is not evident. In this case the  $I$  vs  $Q$  trend for  $Q > 0.1 \text{ nm}^{-1}$  is consistent with a model which assumes only the form factor of disk laponite nanoparticles dispersed in a uniform medium. The deviation at lower  $Q$  values is likely due to attractive interactions between disks and potential cluster formation. From a first analysis it comes out that a fractal law can take into account for the data at low  $Q$  and a fractal dimension of ca. 200 nm is obtained. Such a large dimension can represent the cluster of nano-platelets oriented almost in a random way.

Similar considerations in the laponite rich systems are valid for the PEG 2000/laponite nanocomposites. Of course PEG 2000 does not show any lamellar structure, but it can be observed that low amount of disk dispersed in PEG 2000 assumes a more ordered lamellar structure with a periodic distance of ca. 1.4 nm as showed by the appearance of a peak at high  $Q$  values.

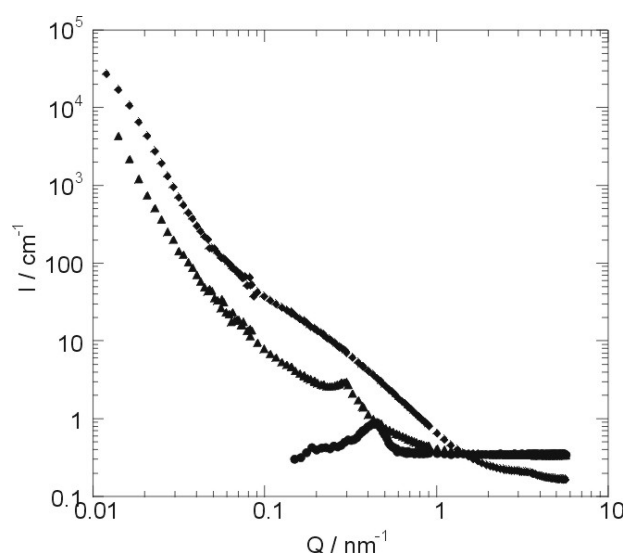


**Figure 1.** Scattering intensity of F127 as a function of the scattering vector  $q$  in the absence (●) and the presence of laponite at different concentrations: (▲), 20 wt.%; (◆), 69 wt.%.

#### Acknowledgements

This research project has been supported by the European Commission under the 6th Framework Programme through the Key Action: Strengthening the European Research Area, Research Infrastructures. Contract n°: RII3-CT-2003-505925 (NMI3)



## EXPERIMENTAL REPORT

### Micellar-Size effect on the Catalytic Hydrogenation of Dimethyl Itaconate in TX-100 Microemulsions

Proposal N°  
MAT-04-1714-LT

Instrument **V4**

Local Contact  
Sylvain Prévost

Principal Proposer: Michael Gradzielski – TU Berlin  
Experimental Team: Juan Milano – TU Berlin  
Sylvain Prévost – HZB, Berlin  
Reinhard Schomäcker – TU Berlin

Date(s) of Experiment  
28/08/2008 – 30/08/2008

Date of Report: 11/01/2009

It is well known that water in the core of reverse micelles may display deviating electrophilic and nucleophilic properties relative to “bulk water” because of strong interactions with the head groups of the surfactant, depending on the size of the droplets. Thus, the effect on reactions is often dependent on the water/surfactant molar ratio ( $\omega$ ) [1]. The present study reports the correlation between the size of reverse micelles obtained by SANS measurements, and the initial hydrogenation rate of dimethyl itaconate (DMI) with the water-soluble catalyst complex Rh-TPPTS using nonionic Triton X-100 microemulsion systems with different water content as dispersive media. The influence of the cosurfactant/surfactant mass ratio ( $\delta$ ) as a reaction parameter was studied, and additionally the effect of the catalyst was probed.

SANS spectra were recorded with different contrast conditions: microemulsions were prepared from heavy water, Triton X-100, 1-pentanol, and either hydrogenated or perdeuterated cyclohexane. The former case provide an inner look to the D<sub>2</sub>O-based core of the micelles, while in the latter case the hydrogenated interfacial film is probed. Figure 1-a presents SANS scattering curves for four Triton microemulsions with  $\omega = 20$  and different amounts  $\delta$  of pentanol contained. All the curves show the existence of noninteracting particle systems and by comparing them one could suggest that the change of maximum height that increases with decreasing  $\delta$ , points to the increasing micellar size. A slight elongation of the micelles is observed when using less cosurfactant ( $\delta = 0.75$ ), and also when adding the catalyst to the core (0.8 mmol/L of Rh, using TPPTS/Rh of 7.5)

We used the Guinier approximation to determine the hydrodynamic radius of the micelles [2], and as Figure 1-b shows, these were correlated with the Initial hydrogenation rate of the catalytic hydrogenation of DMI (2 g in 100 ml of microemulsion) in Triton X-100 microemulsions with different  $\delta$ , at 25 °C and

1.1 bar, using 20 mg of [Rh(cod)Cl]<sub>2</sub> and 357 mg of TPPTS. The tendencies are similar when changing  $\omega$  (10→15→20) for systems with different  $\delta$ , showing higher rates for systems with larger micelles.

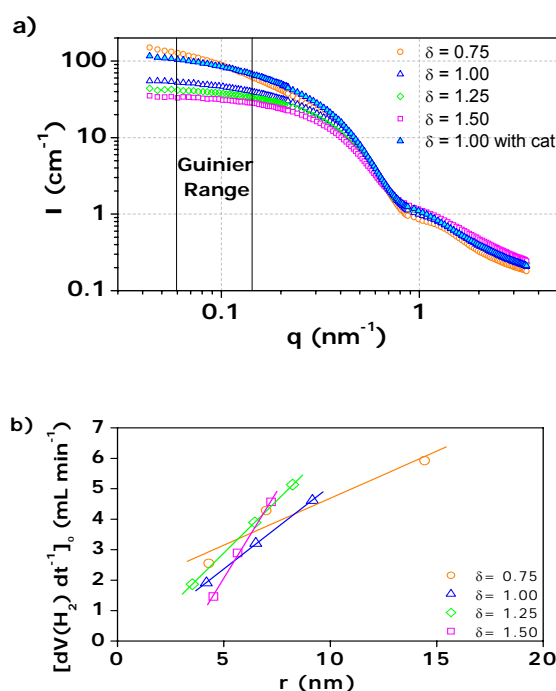


**Fig. 1:** (a) SANS spectra of Triton X-100 microemulsions with constant  $\omega = 20$  and different  $\delta$ , and influence of the water soluble catalyst complex Rh-TPPTS on the spectra. (b) Initial hydrogenation rate of the catalytic hydrogenation of DMI (2 g in 100 ml of microemulsion) as a function of the micelle hydrodynamic radius (Guinier approximation of the SANS spectra) in Triton X-100 microemulsions with different  $\delta$ , at 25 °C and 1.1 bar, using 20 mg of [Rh(cod)Cl]<sub>2</sub> and 357 mg of TPPTS.

#### References

- [1] T. Dwarz; E. Paetzold; G. Oehme. *Angew. Chem. Int. Ed.*, **2005**, *44*, 7174-7199.
- [2] K. S. Freeman, N. C. Beck Tan, S. F. Trevino, S. Kline, L. B. McGown, D. J. Kiserow, *Langmuir*, **2001**, *17*, 3912-3916.



## EXPERIMENTAL REPORT

### Structural relaxation in the ultra fragile glass former Decalin

Proposal N° PHY-03-561

Instrument **V5**

Local Contact  
Katia Pappas

Principal Proposer: Stefan Eibl, ILL Grenoble  
Experimental Team: Marie Plazanet, ILL Grenoble  
Katia Pappas, HMI Berlin  
Evgeny Moskvina, HMI Berlin

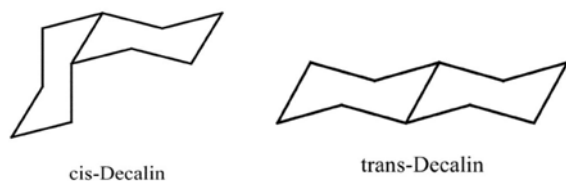
Date(s) of Experiment

11/02/2008 – 24/02/2008

Date of Report: 13/03/2008

### Scientific background

A molecular liquid can be supercooled below its melting temperature,  $T_m$ , and form a glass, an amorphous solid, at temperature  $T_g$ . The way its dynamical properties (viscosity or relaxation time  $\tau_\alpha$ ) evolves with  $T$  at atmospheric pressure above  $T_g$  provides a criterion to classify it among other liquids differing by their configuration or chemical interactions. This criterion is called fragility,  $m$ , or steepness index, as introduced by Angell in 1985; it focuses on data close to  $T_g$  showing how fast the dynamics increase approaching the structural arrest at  $T_g$ .

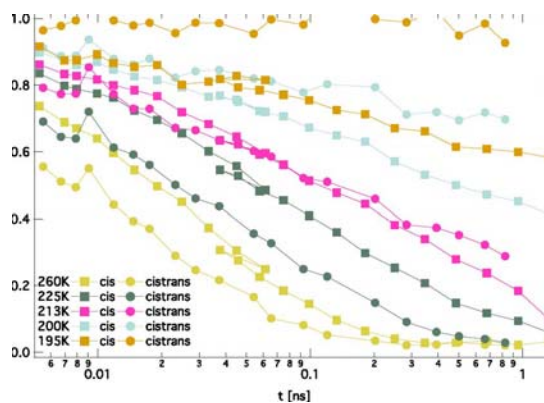


While a number of highly fragile glassformers are found for polymeric materials ( $m$  up to 200), only very few examples of molecular liquids exhibiting  $m > 100$  have been reported. Among them the mixture of cis-trans decahydronaphthalene with a mixing ratio of roughly 1:1 (cis-trans Decalin,  $T_g = 134.7\text{K}$ ) plays a central role. Based on a VTF fit of dielectric data, Richert (JCP 2002) found an  $m = 147$  for that mixture, one of the highest reported values. Based on the absence of aromatic character, an intermediate behaviour was expected and the pure cis Isomer does actually show this moderate fragility in a short  $T$ -range close to  $T_g$  (150K), with a measured fragility of  $m \sim 60$  [1]. The mixture of the two configurations, has consequently a considerable effect on the dynamical properties, mainly for a characteristic relaxation time greater than  $10^6$  s. Additionally while in most systems a relationship between the dynamical and thermodynamical properties seems to work, assuming that the fragility is also related to the way the configurational entropy decreases from  $T_m$  to  $T_g$ , Decalin does not follow it. A study on the variation of the properties versus composition is currently in progress in Orsay. The mixture of configurations appears as a new tool for studying the whole pattern of fragile liquids, without

changing the chemical nature of the liquids, or applying external parameters such as pressure or confinement. More work is required to understand this exceptional behaviour.

### Experimental results

Relaxation curves of cis-trans Decalin have been measured in the fourier time range from 5 ps to almost 1 ns. The temperatures the relaxation curves were recorded for ranged from 260 K past the melting point at 240 K covering a supercooled domain down to the structural arrest that set in at about 195 K. The temperature steps were chosen to yield reasonable resolution for the phase-changerange and assure comparability to the data collected for cis Decalin. It was so possible to study the resulting curves for cis-trans Decalin in direct comparison with the previously collected data for cis Decalin. The relaxation behaviour could be tested for cooling history dependence as it was reheated and cooled fast to a temperature that had already been recorded on slow cooling. This research project has been supported by the European Commission under the 6th Framework Programme through the Key Action: Strengthening the European Research Infrastructures. Contract n°: RII3-CT-2003-505925 (NMI 3).



Relaxation curves of cis (squares) and cis-trans (dots) Decalin at comparable temperatures. In the observed Temperature range the relaxation of cis-trans slows down more than the relaxation of pure cis



## EXPERIMENTAL REPORT

### Fast structural relaxation in the ultra fragile glass former Decalin

Proposal N° PHY-03-601

Instrument **V5**

Local Contact  
Evgeny Moskvina

Principal Proposer: Stefan Eibl, ILL Grenoble  
Experimental Team: Stefan Wellert, HMI Berlin  
Evgeny Moskvina, HMI Berlin  
Katia Pappas, HMI Berlin

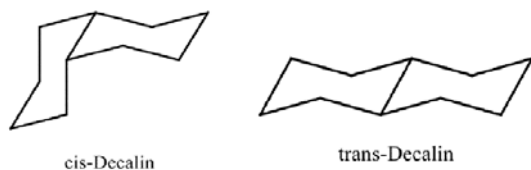
Date(s) of Experiment

21/07/2008 – 05/08/2008

Date of Report: 10/09/2008

#### Scientific background

A molecular liquid can be supercooled below its melting temperature,  $T_m$ , and form a glass, an amorphous solid, at temperature  $T_g$ . The way its dynamical properties (viscosity or relaxation time  $\tau_\alpha$ ) evolves with  $T$  at atmospheric pressure above  $T_g$  provides a criterion to classify it among other liquids differing by their configuration or chemical interactions. This criterion is called fragility,  $m$ , or steepness index, as introduced by Angell in 1985; it focuses on data close to  $T_g$  showing how fast the dynamics increase approaching the structural arrest at  $T_g$ .



While a number of highly fragile glassformers are found for polymeric materials ( $m$  up to 200), only very few examples of molecular liquids exhibiting  $m > 100$  have been reported. Among them the mixture of cis-trans decahydronaphthalene with a mixing ratio of roughly 1:1 (cis-trans Decalin,  $T_g = 134.7\text{K}$ ) plays a central role. Based on a VTF fit of dielectric data, Richert (JCP 2002) found an  $m = 147$  for that mixture, one of the highest reported values. Based on the absence of aromatic character, an intermediate behaviour was expected and the pure cis Isomer does actually show this moderate fragility in a short  $T$ -range close to  $T_g$  (150K), with a measured fragility of  $m \sim 60$  [1]. The mixture of the two configurations, has consequently a considerable effect on the dynamical properties, mainly for a characteristic relaxation time greater than  $10^{-6}$  s. Additionally while in most systems a relationship between the dynamical and thermodynamical properties seems to work, assuming that the fragility is also related to the way the configurational entropy decreases from  $T_m$  to  $T_g$ , Decalin does not follow it. A study on the variation of the properties versus composition is currently in progress in Orsay. The mixture of configurations appears as a new tool for studying the whole pattern of fragile liquids, without changing the chemical nature of the liquids, or applying external parameters such as pressure or

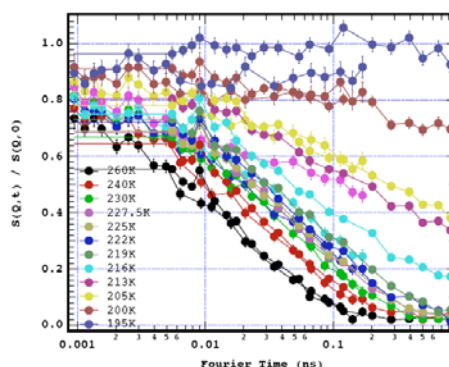
confinement. More work is required to understand this exceptional behaviour.

#### Experimental results

Relaxation curves of mixtures of cis-trans Decalin with mixing ratios of cis:trans of 1:1 and 5:3 have been measured in the fourier time range from 1 ps to almost 1 ns. The temperatures the relaxation curves were recorded for ranged from 260 K past the melting point at 240 K covering a supercooled domain down to the structural arrest that set in at about 195 K. The temperature steps were chosen to yield reasonable resolution for the phase-change-range and assure comparability to the data collected in previous experiments. It was so possible to study the substances at lower fourier times by operating the instrument at short wavelength. The agreement with previously recorded curves at higher wavelegths are good. The following graph shows curves for cis-trans Decalin at the two wavelengths measured at.

This research project has been supported by the European Commission under the 6th Framework Programme through the Key Action: Strengthening the European Research Infrastructures.

Contract n°: RII3-CT-2003-505925 (NMI 3).



Relaxation curves of cis-trans Decalin at different wavelengths but comparable temperatures. In the observed Temperature range the agreement is good and will allow more accurate data evaluation.



## EXPERIMENTAL REPORT

### Effect of cation asymmetry in the dynamics of two room temperature ionic liquids

Proposal N° MAT-03-603

Instrument **V5**

Local Contact M. Russina

Principal Proposer: M. L. Saboungi (CRMD, CNRS Orleans, France)  
Experimental Team: M. L. Saboungi (CNRS)  
B. Aoun (CNRS and ILL)  
M. A. Gonzalez (ILL)  
S. Wellert (BENSC)  
C. Pappas (BENSC)

Date(s) of Experiment

27/11/2008 – 08/12/2008

Date of Report:

Room-temperature ionic liquids (ILs) are defined as salts composed solely of ions with melting points below 100°C. A great interest in this class of materials has emerged during the last decade due to the interesting properties that they exhibit. In particular their use as “green” solvents replacing standard contaminant solvents constitutes a very active subject of research in the chemical industry. Another interesting property of ILs is its large tunability. This feature is derived from the possibility of combining different cations (often based on imidazolium, pyridinium, pyrrolidinium, ammonium or phosphonium derivatives) with a huge variety of anions (halides, nitrates, phosphates, etc.). As the diffusivity of cations and anions in ionic liquids are strongly coupled it is of high relevance to determine how the size and the symmetry of the cation and/or the anion affects the dynamics of a given ionic liquid. The goal of this experiment was to explore the dynamics of different ionic liquids on the nanosecond scale. We measured the dynamics of two ionic liquids with different cation sizes: ethyl-methyl-imidazolium bromide (EMImBr) and hexyl-methyl-imidazolium bromide (HMImBr), and a third one changing the bromide anion by a much larger anion: EMIm-dimethyl-phosphate.

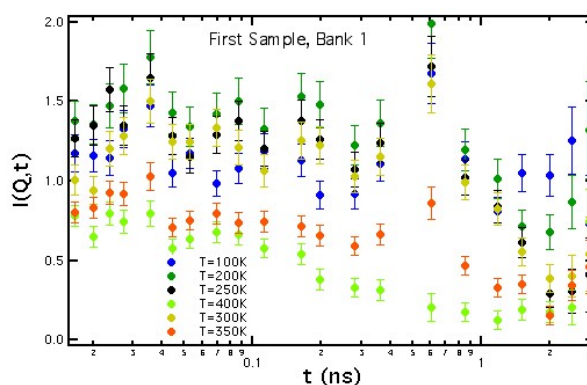


Fig. 1: EMImBr at several temperatures (first bank)

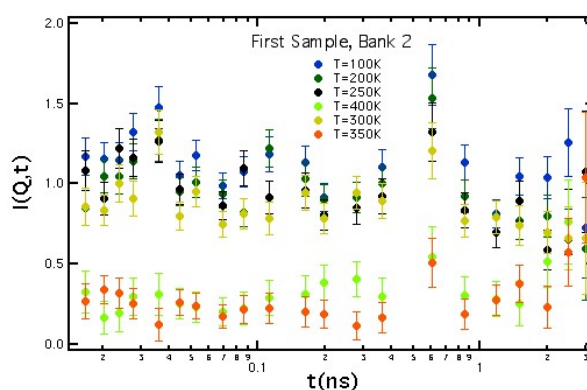


Fig. 2: EMImBr at several temperatures (second bank).

Figures 1 and 2 show the data obtained for EMImBr at different temperatures in the first and second bank of detectors. While a qualitative difference between the data corresponding to the sample on the liquid state (at 350 and 400 K) and the solid is observed, in particular on the second bank, the signal from our samples (mainly incoherent) is too low to allow us to obtain reliable conclusions about the dynamics of these ionic liquids.

*This research project has been supported by the European Commission under the 6<sup>th</sup> Framework Programme through the Key Action: Strengthening the European Research Infrastructures. Contract n°: RII3-CT-2003-505925 (NMI 3).*



## EXPERIMENTAL REPORT

### Asymmetric lipid bilayer sandwiched in polyelectrolyte multilayer films by layer-by-layer assembly

Proposal N°  
PHY-04-1531-EF

Instrument **V6**

Local Contact Ralf Köhler

Principal Proposer: Ralf Köhler  
Experimental Team: Jiangshan Chen, Rumen Krastev\*  
MPI of Colloids and Interfaces,  
Golm/Potsdam, Germany  
\*present address: NMI, Reutlingen, Germany

Date(s) of Experiment

06/07/2007 – 12/07/2007  
04/01/2008 – 07/01/2008

Date of Report: 15/01/2009

Lipid membrane on polymer cushions can be created directly via vesicle fusion. The assembly of lipid bilayer membranes alternated with polyelectrolytes (PE) has been already demonstrated<sup>1,2</sup>. The lipid membranes act as internal barriers to separate two compartments of the PEM. Usually, this structure is charge symmetric, i.e., lipid bilayer is sandwiched between the PE with the same charge because of the symmetric structure of the bilayer. The preparation of asymmetric lipid bilayer is challenging. In the present work, we show the formation of charge asymmetric lipid bilayer of DMPE between cationic PDAMDAC and anionic d-PSS.

The Si blocks used as substrates were dipped first in PEI solution (1 mg/ml, salt free) to form a precursor layer. Then the build-up process continued using the LbL procedure<sup>3</sup> by sequentially immersion into PE solutions (1 mg/mL, in 0.5 M NaCl) for 10 min. The PE cushion had the structure Si/PEI/(d-PSS/PAH)<sub>4</sub>/d-PSS/PDADMAC. PDADMAC was used as last layer to guarantee strong positive charge of the terminating layer at different pH conditions because of the independence of its charge on the pH. The lipid bilayer was prepared by incubation in lipid SUV suspension for 30 min at 60 °C and neutral pH. The deposition continued with a d-PSS layer at acidic conditions. Due to the fact that the charge of the DMPE molecule strongly depends on the pH<sup>4</sup> it was possible to "sandwich" the DMPE bilayer between a layer of the cationic PDADMAC and the anionic d-PSS through LbL self-assembly.

The neutron reflectometry experiments were performed in  $\theta/2\theta$  geometry against D<sub>2</sub>O in a home made chamber. The build-up process was followed in-situ. The reflectivity curves at different deposition steps are shown in the Figure 1a and the SLD profiles in Figure 1b.

The experimental results were confirmed by UV-spectroscopy, QCM and zeta potential measurements<sup>4</sup>.

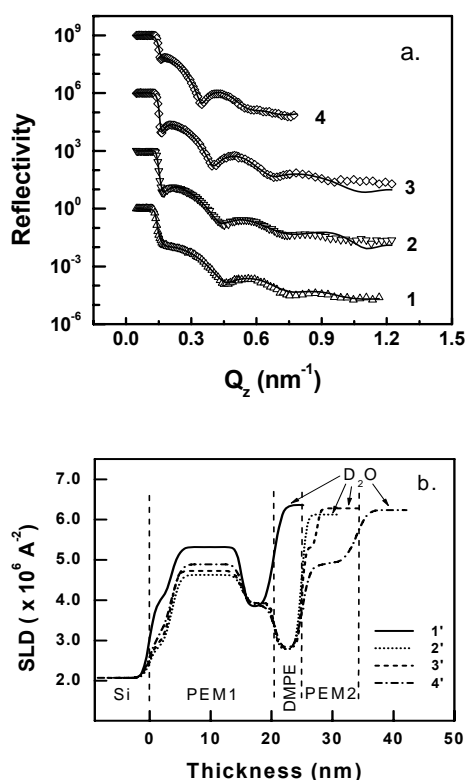


**Figure 1.** a) (a) NR curves from the samples: (1) Si/PEI/(d-PSS/PAH)<sub>4</sub>/d-PSS/PDADMAC, (2) after DMPE deposition, (3) after PSS deposition, and (4) after subsequent PDADMAC/PSS deposition. The solid lines show the best fit to the experimental data. The curves are shifted for clarity. (b) SLD profiles for the corresponding samples.

#### References:

1. C. Delajon et al *Langmuir*, 2005, **21**, 8509.
2. Z. H. An et al *Biomacromolecules*, 2006, **7**, 580.
3. G. Decher, *Science*, 1997, **277**, 1232.
4. J. Chen et al *Soft Matter* **5**, 2009, 228.

#### Abbreviations:

DMPE - 1,2-Dimyristoyl-*sn*-glycero-3-phospho ethanolamine;  
PDAMDAC - poly-(diallyl dimethylammonium chloride); d-PSS - fully deuterated poly(sodium 4-styrenesulfonate); PAH - poly(allylamine hydrochloride); PEI poly (ethylenimine).



## EXPERIMENTAL REPORT

### Polyelectrolyte based nanocomposites

Proposal N°  
PHY-04-1531-EF

Instrument **V6**

Local Contact Ralf Köhler

Principal Proposer: Ralf Köhler, HZ Berlin and MPI of Colloids and Interfaces, Wissenschaftspark Golm, 14424 Potsdam-Golm

Experimental Team: Marta Kolasinska, MPIKG, Potsdam  
Rumen Krastev, MPIKG, (present address: NMI, Reutlingen, Germany)

Date(s) of Experiment

06/07/2007 – 12/07/2007  
18/08/2008 – 23/08/2008

Date of Report: 19/01/2009

Nanometer thick polymer based materials with particles embedded in the polymer matrix possess a number of specific properties, pertaining to their structure with potential application in chemistry, (bio)sensing and material science. The properties of the obtained materials depend strongly on the inter particle distances in the matrix, with consequences for the mechanical response and optical and magnetic properties of the samples. The motivation of present studies was to generate nanoparticle/polyelectrolyte (NP/PEM) composite films with magnetite nanoparticles organized in 2D structures. The ordering of NP into 2D layers was based on the difference in the hydrophobicity of the composite sub-layers. In one case the polyelectrolyte cushion: PAH/PSS (poly(allylamine hydrochloride)/poly(sodium 4-styrenesulfonate)) included a lipid bilayer (DMPC, dimyristoylphosphatidylcholine) with a highly hydrophobic center, which was obtained by vesicle fusion and spreading [1] on the polyelectrolyte multilayer. The lipid bilayer was "sandwiched" by two hydrophilic constituents: polyelectrolyte multilayer from one side and charged nanoparticles from the other side. Due to its highly hydrophobic center, it acted as a barrier preventing hydrophilic nanoparticles from diffusion inside the PEM. As deposition of lipid bilayer and magnetite nanoparticles was proved in-situ with quartz crystal microbalance (QCM), it was studied step by step with neutron reflectometry (NR). The results obtained for adsorption of DMPC and magnetite nanoparticles on the PEM are depicted in Figure 1 as reflectometric curves and the respective scattering length density profiles. First, PEM cushion was measured against liquid D<sub>2</sub>O (black circles). Then DMPC was deposited and the sample was measured (green triangles). Next magnetite nanoparticles were adsorbed and the sample was measured again (blue squares).

When nanoparticles are deposited on the DMPC bilayer supported on PEM, they rather assemble at the lipid bilayer's surface. While analyzing the

NR data of that system, one can distinguish three separate parts in the SLD profiles. They refer to PEM, DMPC bilayer and NP, respectively. Thus, particles are arranged into a 2D layer at the surface.

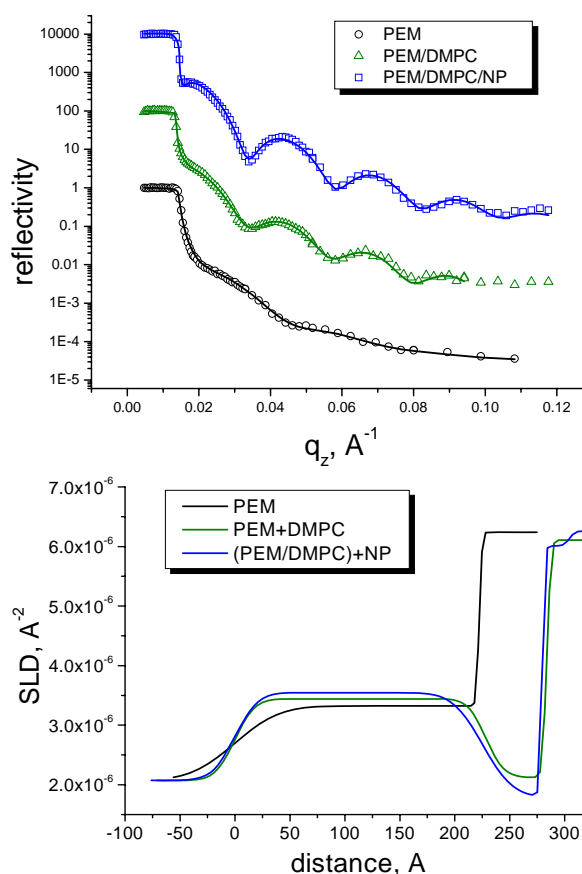


Fig. 1. NR curves and SLD profiles of DMPC deposition on PEM and NP deposition on PEM/DMPC

The obtained results confirmed our prediction that the lipid bilayer prevents nanoparticles from diffusion inside the polymer cushion.

1. C. Delajon, T. Gutberlet, R. Steitz, H. Mohwald, R. Krastev, *Langmuir*, **2005**, 21, 8509



## EXPERIMENTAL REPORT

### Water content of polyelectrolyte multilayers: Influence of type of degree of polymer charge and ion specific effects

Proposal N° CHE-04-1594

Instrument **V6**

Local Contact  
Roland Steitz

Principal Proposer: S. Doodoo, TU Berlin  
Experimental Team: S. Doodoo, TU Berlin  
R. v. Klitzing, TU Berlin  
R. Steitz, HMI Berlin

Date(s) of Experiment

14/01/2008 – 21/01/2008

Date of Report: 07/03/2008

The swelling behavior of thin polyelectrolyte multilayer (PEM) is of interest since it is assumed to be strongly correlated to sensoric and permeability for drugs. In our previous report we assumed that there are two types of water which contribute to the swelling of the multilayer; "free water" and "void water". In this report we present latest results of neutron reflectivity experiment on PEMs at the solid/liquid interface. Polyelectrolyte multilayers were prepared according to the layer by layer adsorption method [1].

The samples consisted of Si/PEI/(PSS/PDADMAC100%)<sub>6</sub>, with 0.1 M, 0.25 M NaCl, and 0.1 M NaBr salts. In addition Si/PEI/(PSS/DADMAC75%-co-NMVA25%)<sub>6</sub>, with 0.1 M, 0.25M NaCl and 0.1 M NaBr salts were prepared. The samples were measured against vacuum after H<sub>2</sub>O, vacuum after D<sub>2</sub>O, H<sub>2</sub>O liquid and D<sub>2</sub>O liquid. From Table 1, the thickness of the film increases with increasing ionic strength due to change from flat to coiled conformation [2]. PEMs prepared from NaBr salt were thicker than those prepared from NaCl due to the effect of the anions and their position in the Hofmeister Series. Cl<sup>-</sup> is smaller than Br<sup>-</sup>, with a lower polarizability and tends to have a well-ordered larger hydration shell. Therefore the polycation (PDADMAC) interacts stronger with Br<sup>-</sup> than Cl<sup>-</sup>. Consequently the charges along the polycation chain are more effectively screened in the case of Br<sup>-</sup> than in the case of Cl<sup>-</sup>, which leads to stronger coiling and larger film thickness. Table 1 shows that with decreasing degree of polymer charge the polyelectrolyte multilayer becomes thicker due to a strong coiling caused by a reduction in electrostatic repulsion along the polyelectrolyte chains [3]. From Fig. 1, the neutron reflectivity spectra, of vacuum after H<sub>2</sub>O and vacuum after D<sub>2</sub>O superimposes indicating that there is no displacement of hydration water after exposure of sample to D<sub>2</sub>O liquid. In contrast to PSS/PDADMAC in the PSS/PAH system 1 H atom is exchanged against a D atom.

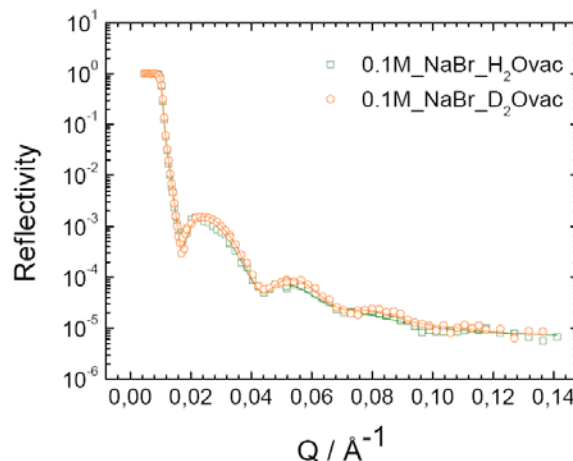


Fig.1 Neutron reflectivity against vacuum after H<sub>2</sub>O and D<sub>2</sub>O of Si/PEI/(PSS/PDADMAC100%)<sub>6</sub> at 0.1M NaBr concentration.

This leads to different reflectivity curves against vacuum after exposure to H<sub>2</sub>O and D<sub>2</sub>O [4].

Table1. Summary of thickness against preparation parameters obtained from best fit to the data.

Sample	Thickness in Å by Neutron Reflectometry			
	D <sub>2</sub> Ovac	H <sub>2</sub> Ovac	D <sub>2</sub> Oliq	H <sub>2</sub> Oliq
100%P_0.1M_NaCl		146	226	224
100%P_0.1M_NaBr	229	228	384	392
75%P_0.1M_NaCl		146	226	224
75%P_0.1M_NaBr	217	217	339	336
100%P_0.25M_NaCl		275	491	465
75%P_0.25M_NaCl	307	321	550	550

#### Reference:

- [1] G. Decher, Science 277 (1997) 1232
- [2] R. Steitz et al., Colloids and Surfaces A 163(2000) 63-70
- [3] U. Voigt et al., J. Phys. Chem B 107 (2003) 5273
- [4] S. Doodoo, J.E. Wong, R. Steitz, R. v. Klitzing in preparation

	<b>EXPERIMENTAL REPORT</b> <b>In situ - SRSANS investigations of gas condensation in mesoporous metaloxide thin films</b>	Proposal N° PHY-04-1596 Instrument <b>V6</b> Local Contact Roland Steitz
	Principal Proposer: S. Mascotto, University of Giessen, Germany Experimental Team: B. Smarsly, University of Giessen, Germany D. Wallacher, Helmholtz Zentrum Berlin, Germany R. Steitz, Helmholtz Zentrum Berlin, Germany	Date(s) of Experiment 23/06/2008 – 30/06/2008

Date of Report: 18/12/2008

Mesoporous materials in form of thin films are nowadays rising of interest because of numerous applications in the fields of sensing, catalysis and photovoltaics. The structure characterization of such systems, especially regarding the porosity and the pores accessibility, presents however many questions, which cannot be answered by the standard technique. The knowledge of such information indeed is crucial for the enhancement of the materials quality.

In our previous works at HZB the application of in-situ small-angle neutron scattering (SANS) study in mesoporous silica powders during  $C_5F_{12}$  adsorption at 280 K – taking advantage of contrast matching between liquid  $C_5F_{12}$  and the  $SiO_2$  itself – provided successful results in the determination of the morphology of the porous structure.

The concept of the in-situ-SANS technique was then applied in the present experiment to thin films materials. The only change is collection of the scattering pattern in reflection geometry (SRSANS), more suitable for a thin film analysis than the transmission.

The samples object of this study (SP2350) was a film of mesoporous silica 150 nm thick deposited on a silicon wafer by dip coating of a sol-gel solution. In Fig. 1 are presented a typical transmission SAXS pattern and AFM analysis. As can be seen the material presents a well ordered mesostructure with spherical pores of 20 – 24 nm in size. In the SAXS pattern can be recognized a Bragg peak at  $s = 0.05 \text{ nm}^{-1}$  typical of a cubic packing, while the humps at  $s = 0.9$  and  $0.15 \text{ nm}^{-1}$  belong to the form factor of a sphere.

This experiment then gave the chance for the first time to detect the accessibility of a thin film system and the connection between the pores.

In Fig.2 are shown the reflectivity pattern of SP2350 collected at different sorption state. Unlike the transmission geometry, the reflection of the neutron at V6 enables to cover a limited range of  $s$  values allowing to collect just the form factor contributes.

As can be seen the maximum decreasing of the peak is registered at 0.15  $p/p^\circ$ . For higher pressure values the sample the porous matrix is not

accessible to the  $C_5F_{12}$  flow. One possible explanation to this fact is that the connections between the pores are not enough to allow the permeation of the adsorbate. Furthermore, since the  $C_5F_{12}$  is a quite big molecule ( kinetic radius = 0.9 nm) and the connection between the spherical pores are given by micropores of  $\sim 1 \text{ nm}$ , the flow of the gas could be discouraged also by steric obstruction.

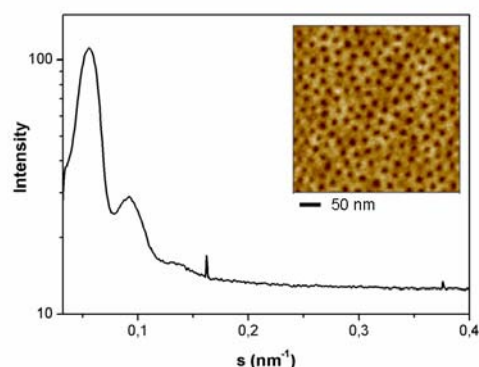


Fig 1: SAXS pattern and AFM micrograph of SP2350

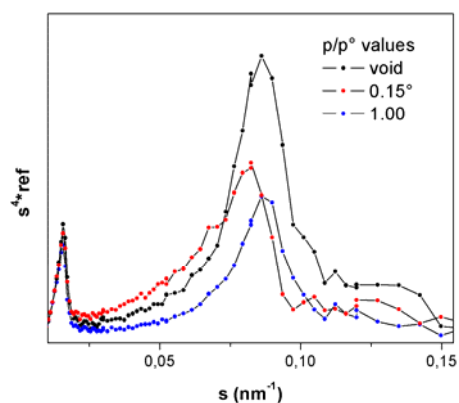


Fig.2: SRSANS pattern during  $C_5F_{12}$  sorption in SP2350



## EXPERIMENTAL REPORT

### Immobile Light Water and Proton-Deuterium Exchange in Polyelectrolyte Multilayers

Proposal N° PHY-04-1597

Instrument **V6**

Local Contact Ralf Köhler

Principal Proposer: C. A. Helm, EMAU Greifswald  
 Experimental Team: O. Ivanova, EMAU Greifswald  
 O. Soltwedel, EMAU Greifswald  
 M. Gopinadhan, EMAU Greifswald  
 R. Steitz, HMI

Date(s) of Experiment

05/02/2008 – 11/02/2008  
 30/05/2008 – 02/06/2008

Date of Report: 14/01/2009

Polyelectrolyte multilayers (PEM) are formed by sequential adsorption of oppositely charged polyelectrolytes from aqueous solutions [1]. Intramolecular forces bind water in the PEM tightly.

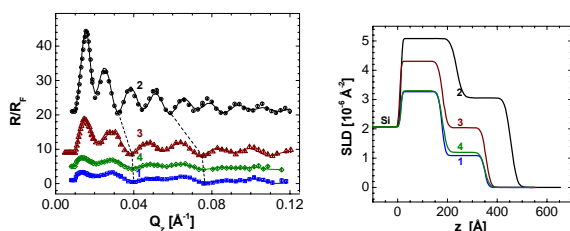


Fig. 1. Left: Normalized neutron reflectivity curves of  $d_5p_5$  PEM. It is prepared at 15°C from an aqueous solution containing 1 mol/L NaCl. The sequence of the experiments 0% RH (curve 1)  $\Rightarrow$  100% RH  $D_2O$  (curve 2)  $\Rightarrow$  0% RH (20 h drying, curve 3)  $\Rightarrow$  0% RH (after immersion for 6 h in  $H_2O$  and 20 h drying, curve 4). Straight lines are fits; dashed lines connect interference minima of the same order. Right: the corresponding scattering length density profiles.

To quantify the swelling on a molecular scale as function of the relative humidity (RH), the PEM architecture is varied. The polyanion is poly(styrenesulfonate) (PSS) and the polycation poly(allylamine hydrochloride) (PAH). PEM either consists of 10 protonated bilayers ( $p_{10}$ ), 10 deuterated bilayers ( $d_{10}$ ), or two different building blocks,  $p_5d_5$  or  $d_5p_5$  [2].

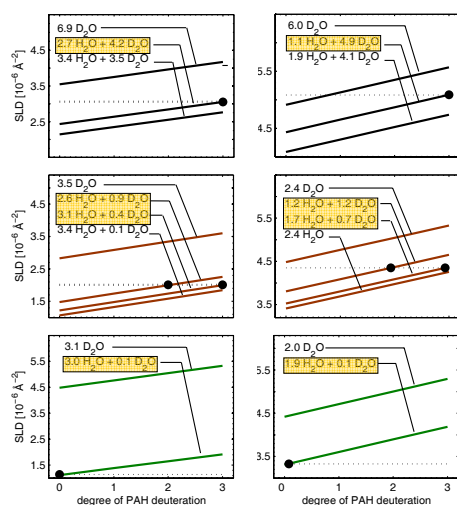


Fig. 2: Calculated  $SLD$  of the protonated (left column) and the deuterated block (right column) of the  $d_5p_5$  PEM (cf. Fig. 1). In the virgin PEM at 0%RH, the protonated block contains 3.4  $H_2O$  (deuterated block: 1.9). Top: 100 %RH  $D_2O$ , center: 0 % RH, bottom: 0% RH after immersion in  $H_2O$ . The  $x$ -axis gives the degree of PAH deuteration; the dotted lines show the measured  $SLDs$  within 10% error. The straight lines are calculated assuming different  $H_2O/D_2O$  compositions for  $n_{H_2O,swell}$  as measured by the thickness change.

The film architecture is selected to obtain as many independent parameters as possible, specifically the thickness and the scattering length density of each block. At the beginning of the experiment,  $n_{H_2O}$ , the number of water molecules per PAH/PSS monomer pair is calculated from the scattering length density  $SLD$  in a block

$$n_{H_2O} = \frac{[b_{PAH} + b_{PSS} - SLD \cdot (V_{PAH} + V_{PSS})]}{(SLD \cdot V_{H_2O} - b_{H_2O})}$$

( $b_i$  and  $V_i$  are the scattering lengths and volumes of the respective molecules or monomers, respectively). On increase of the RH, water incorporation causes the block to thicken from  $l_{dry}$  to  $l_{swell}$ .

$$n_{H_2O,swell} = \frac{[l_{swell} / l_{dry} (n_{H_2O,dry} \cdot V_{H_2O} + V_{PSS} + V_{PAH}) - (V_{PSS} + V_{PAH})]}{V_{H_2O}}$$

$n_{H_2O,swell} - n_{H_2O,dry}$  gives the number of added  $D_2O$  molecules. However, the increase of the  $SLD$  of each block (cf. Fig. 1) is too large to be explained with  $D_2O$  addition only. Proton-deuterium exchange occurs. The data indicate that three mobile protons of each bound PAH monomer are replaced by deuterium ions, yet most of the  $H_2O$  molecules found in a PEM at 0% RH remain bound at 100% RH  $D_2O$  (proton-deuterium exchange rate of an amino group is below 0.5 ms [3.]), cf. Fig. 2. On drying, the thickness of the virgin film is retrieved, yet the  $SLD$  is still larger. Clearly, the PAH monomers retain their deuterium ions. Only after immersion into  $H_2O$  the original reflectivity curve is obtained, i.e. the deuterium-proton exchange is reversed.

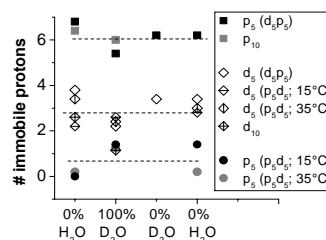


Fig. 3: Amount of protons attributed to tightly bound water molecules per monomer pair measured for the films architectures. The RH given in the  $x$ -axis follows the sequence of the experiments.

This model of proton-deuterium exchange in the PAH monomers is able to describe all investigated PEMs, cf. Fig. 3. At 0% RH the amount of bound water in the deuterated layers does not depend on the film architecture, whereas in the protonated layers it does.

#### Literature

- 1 G. Decher. *Science*, **277** (1997) 1232
- 2 O. Ivanova, O. Soltwedel, M. Gopinadhan, R. Köhler, R. Steitz, C.A. Helm, *Macromolecules* **41** (2008) 7179
- 3 K. Wüthrich, *NMR of Proteins and Nucleic Acids*; John Wiley and Sons, New York 1986



## EXPERIMENTAL REPORT

### Critical and multilayer adsorption from alkane + perfluoroalkane mixtures to chemically modified and bare silicon substrates

Proposal N° PHY-04-1601

Instrument V6

Local Contact  
Roland Steitz

Principal Proposer: A. Zarbakhsh, QM UCL, UK  
 Experimental Team: A. Zarbakhsh, QM UCL, UK  
 J. Webster, RAL ISIS, UK  
 Anke Teichert, HZB

Date(s) of Experiment

21/04/2008 – 28/04/2008

Date of Report: January 2009

Hydrocarbon-fluorocarbon interactions are of great practical importance with applications such as non-stick coatings, anti-graffiti paints and specialised lubricants and surfactants and are of academic and applied interest. Interesting adsorption behaviour occurs close to the liquid-liquid coexistence curve of a binary liquid mixture. As coexistence is approached along a path of constant composition a thick film of the preferentially adsorbed component builds up. The thickness  $l$  of this multilayer film is expected to grow as  $l \sim |T - T_0|^{-1/3}$ , where  $T_0$  is the coexistence temperature. A special situation arises when the critical solution temperature  $T_c$  is approached. In this region the behaviour of the system is governed by composition fluctuations in the bulk. Here, the thickness of the adsorbed film scales with the correlation length  $\xi$  of the bulk fluctuations, and behaves as  $l \sim \xi \sim |T - T_c|^{-0.305}$ . However, despite the similarity in the film thickness divergence, the analytical behaviour of the composition profiles is different in the two regimes. The power-law dependence of critical adsorption is well established, and  $\varphi(z) - \varphi(\text{bulk}) \sim z^{-0.52}$ , where  $\varphi$  is the volume fraction composition and  $z$  is the coordinate normal to the interface.

The major issue we proposed in this experiments was how the critical adsorption profiles and the multilayer adsorption profiles differ along path of non-critical composition, namely,  $\varphi$  (Hexane) = 0.12 as we approach the phase separation temperature  $T_{sep}$  and to determine the (slab or exponentially decaying) nature of the multilayer adsorbed film for a coupled layer and a bare silicon substrate. We studied the adsorption from mixtures of hexane-perfluorohexane to alkylated (prepared using octadecyltrichlorosilane as the coupling agent, C18) and a bare RCA cleaned, Si substrates. In this experiment we approached along paths of non-critical composition, namely  $\varphi$  (Hexane) = 0.12. The data obtained are shown in Figure 1 & 2 for C18 and RCA cleaned Si substrates. The changes in density profile can be seen from data as the phase separation temperature ( $T = -11.5$  °C) is approached. The data for the same substrate at the equimolar composition  $\varphi = 0.5$ ) is also shown for comparison.

The data are currently being analysed in depth to estimate the adsorbed amounts for both the C18 and the RCA cleaned Si and the compositional fluctuations are also being refined and determined.

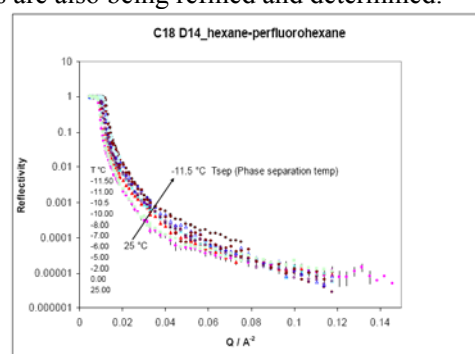


Figure 1. Reflectivity for the RCA Cleaned Si

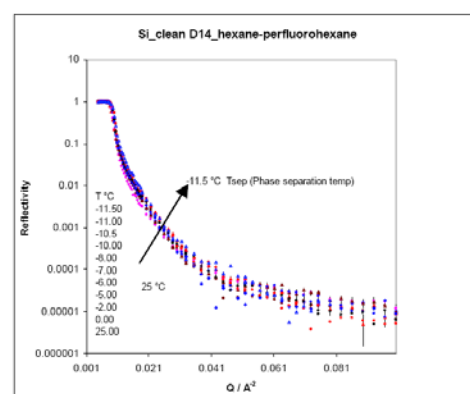


Figure 2. Reflectivity for the C18 Silicon

*This research project has been supported by the European Commission under the 6<sup>th</sup> Framework Programme through the Key Action: Strengthening the European Research Infrastructures. Contract n°: RII3-CT-2003-505925 (NMI 3).*

## References

- "Neutron reflectivity studies of critical adsorption: Behaviour of the surface scaling function" James Bowers, Ali Zarbakhsh, Hugo K. Christenson, Ian A. McLure, John R. P. Webster, Roland Steitz, *Physical Review E* 72, 041606 (2005).
- "Composition profile of a wetting film in a binary liquid mixture". James Bowers, Ali Zarbakhsh, Ian A. McLure, John R. P. Webster, Roland Steitz, Hugo K. Christenson, *J. Phys. Chem. C*, 111, 5568-5571 (2007)..

	<b>EXPERIMENTAL REPORT</b>  <b>The solid-liquid interface of sheared micellar solutions</b>	Proposal N° PHY-04-1617-EF  Instrument <b>V6</b>  Local Contact R. Steitz
	Principal Proposer: R. Steitz, HMI, M. Wolff, Ruhr-University Bochum Experimental Team: S. Gerth, University Erlangen P. Gutfreund, Ruhr-University Bochum R. Steitz, HMI	Date(s) of Experiment  21/01/2008 – 27/01/2008

Date of Report: 11/02/2008

After the successful test with a rheometer on the sample stage of the reflectometer V6 (Exp.: PHY-04-1527-EF) the aim of the present experiment was to study the reorientation of micellar crystallites in the near surface region under shear load.

For the present experiment we focused on the relaxation after stopping the shear in a 20 % solution of the Pluronic F127 in D<sub>2</sub>O. The micelles of this sample are known to form a densely packed structure close to a solid interface and Rocking curves of the first order reflection along the specular line, corresponding to the 111 reflection of a cubic dense packing, were taken along  $q_x$  for shear rates. Representative data sets for the sample in contact with different substrates are shown in figure 1. Data before and after (6-8 hours after stopping the shear) shearing the sample and at the lowest and highest shear rate are presented.

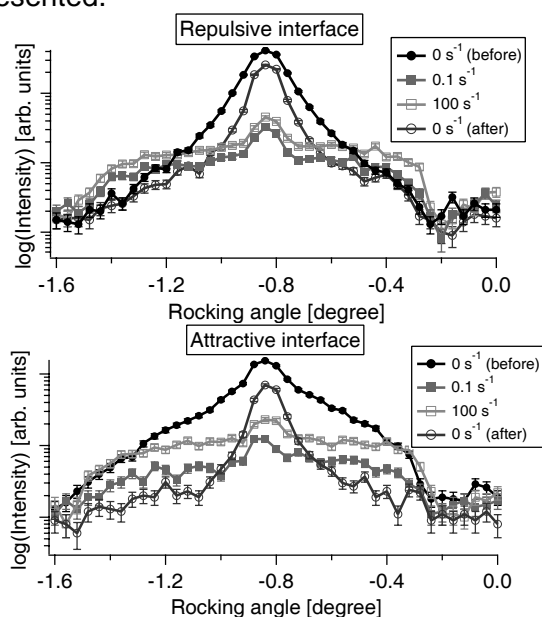


**Figure 1:** Rocking curves for the sample in contact with two differently terminated substrates (repulsive - upper panel, attractive - lower panel) taken before during and after shearing the sample.

It is clearly visible that shear has a strong influence on the line shape. A initially (without shear) narrow line representing a lateral correlation length of some  $\mu\text{m}$  becomes broadened under shear. For increasing shear rates the intensity is again slightly increased and the peak shape becomes asymmetric. After stopping the shear again a narrow resolution limited peak develops related to a well ordered crystalline structure.

In figure 2 the time dependence of the narrow peak intensity after stopping the shear is shown. The micelles rearrange on a time scale of several hours. The black and grey data points show the result of two independent measurements to test the reproducibility of the experiment and the lines correspond to an exponential fit to the data. It turns out that the relaxation of the polymer micelles is dependent on the properties of the solid substrate. For the repulsive interface we extract a relaxation time of about two hours and for the attractive one 5 hours.

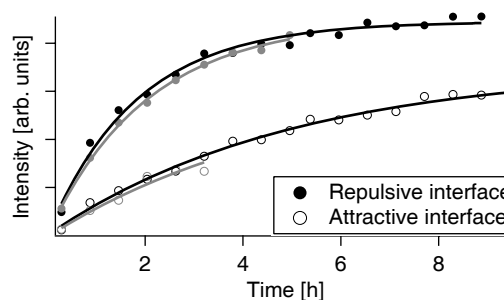


**Figure 2:** Intensity of the narrow component plotted versus time after stopping the shear taken with the sample in contact with differently terminated substrates.

Further detailed data evaluation is on the way.



## EXPERIMENTAL REPORT

### Influence of thermal treatment on thin polyelectrolyte multilayers of varying charge density

Proposal N°  
PHY-04-1622-EF  
Instrument **V6**  
Local Contact Ralf Köhler

Principal Proposer: Ralf Köhler, HMI Berlin, Glienicke Str. 100, 14109 Berlin  
 Experimental Team: Ingo Dönch, MPI KGF Potsdam, Abt. GF, Am Mühlenberg 1, 14476 Potsdam  
 André Laschewsky, Fraunhofer IAP Potsdam, Geiselbergstr.69, 14476 Potsdam  
 Andreas Fery, Uni Bayreuth, PC II, Universitätsstraße 30, 95440 Bayreuth  
 Rumen Krastev, MPI KGF Potsdam, Abt. GF, Am Mühlenberg 1, 14476 Potsdam

Date(s) of Experiment  
  
03/06/2008 – 08/06/2008

Date of Report: 15/01/2009

Polyelectrolyte (PE) multilayers (PEM) have a broad potential for appliance on, e.g., medical, and biotechnological field, and can serve as an object of matter for understanding intermolecular interactions, and self-assembling processes in general. Recently it was found that free-standing PEM organised in hollow capsules made from strong PEM undergo an irreversible change in morphology during temperature treatment in aqueous environment [1]. This change was attributed to a rearrangement of the polymer chains during heating yielding to a lower interfacial energy between water and the partially hydrophobic PE chains. Our study aims to investigate this rearrangement altering the relative strength of Columbic and van der Waals interactions in PEM. These forces are considered to be the principal interactions which are active in the PEM network. The interactions were changed using a polycation with different charge density (ChD) thus allowing for built-up of PEM with different ratio between ionic and van der Waals interactions.

Neutron reflectometry (NR) was used for examination of PEM rearrangement and respective thickness and density change upon post preparation heating of PEM. The samples were prepared from d-PSS (fully deuterated poly(sodium 4-styrenesulfonate) as polyanion and PDAMDAC (poly-(diallyl dimethyl ammonium chloride) as polycation on quartz supports using the spraying version of the LbL technique<sup>2,3</sup>. Always PEI (poly (ethylenimine) was used as a first layer.

The polycation PDADMAC, was available with different ChD, by addition of uncharged spacer units during the chain synthesis. Three probes of PDADMAC were used - 100%, 89%, and 75%. All studied samples had the structure PEI/(dPSS/PDADMAC)<sub>9</sub>. All measurements were performed in dry N<sub>2</sub> once after sample

preparation and after heating in water bath at 70°C for 1 hour.

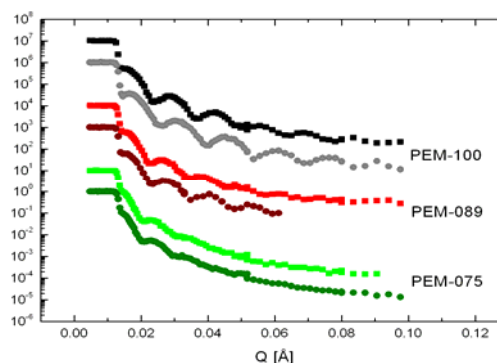


Figure 1: Reflectivity curves from PEM of different ChD before (squares) and after (circles) thermal treatment

Charge density	Thickness, nm	
	Before treatment	After treatment
100 %	47.0	42.7
89 %	51.5	48.5
75 %	60.0	60.4

Table 1: Thickness of PEM prepared from PDADMAC with different charge density before and after thermal treatment at 70°C.

The PEM thickness was found to be systematically affected by the ChD of the PEM. The changes in the film thickness upon heating are also related to the charge density of the polycation. The sample with 100% ChD, shrinks 9%, whereas the thickness of PEM with 75% charge density remains constant. The rearrangement is hindered by increasing number of random distributed spacer units in the chain.

1. K. Köhler et al. *J. Phys. Chem. B* 2005, **109**, 18250
2. G. Decher, *Science*, 1997, **277**, 1232.
3. J.B. Schlenoff et al. *Langmuir* 2000, **16**, 9968.



## EXPERIMENTAL REPORT

### Water content of polyelectrolyte multilayers: Influence of type of degree of polymer charge and ion specific effects

Proposal N° PHY-04-1698

Instrument **V6**

Local Contact  
Roland Steitz

Principal Proposer: S. Dodoo, TU Berlin  
Experimental Team: S. Dodoo, TU Berlin  
R. v. Klitzing, TU Berlin  
R. Steitz, HZ Berlin

Date(s) of Experiment

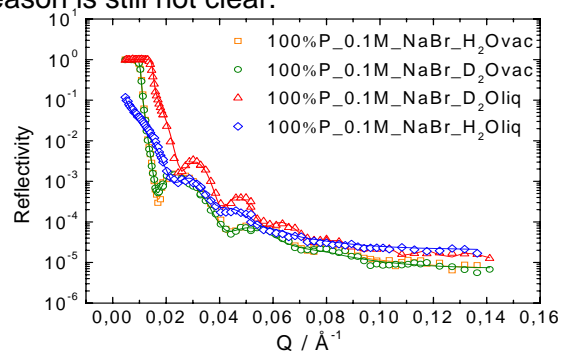
01/09/2008 – 07/09/2008

Date of Report: 19/09/2008

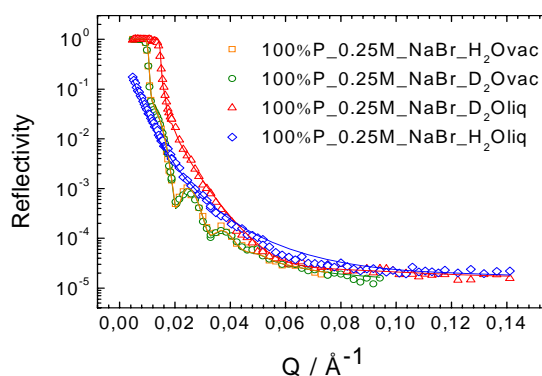
Driven by the development and miniaturization of electronic and optical devices with new properties, the modification of surfaces by the adsorption of ultrathin films has become increasingly important. In our previous report we showed the effect of the anions and their position in the Hofmeister Series on the thickness of the polyelectrolyte multilayers (PEM). In this report we present latest results of neutron reflectivity experiment on PEM at the solid/liquid interface. Polyelectrolyte multilayers were prepared according to the layer by layer adsorption method [1].

The samples consisted of Si/PEI/(PSS/PDADMAC100%)<sub>6</sub> prepared from aqueous solutions of 0.25 M NaF and 0.25 M NaBr. In addition Si/PEI/(PSS/DADMAC75%-co-NMVA25%)<sub>6</sub> prepared from aqueous solutions of 0.25 M NaF and 0.25 M NaBr. The samples were measured against vacuum after H<sub>2</sub>O, vacuum after D<sub>2</sub>O, H<sub>2</sub>O liquid and D<sub>2</sub>O liquid. Figure 1 (a) and (b), show neutron reflectivity spectra of PDADMAC100% multilayers at ionic strength of 0.1 M NaBr and 0.25 M NaBr respectively. We observed no displacement of hydration water after exposure to D<sub>2</sub>O liquid. This could be seen from the spectra of H<sub>2</sub>Ovac coinciding with D<sub>2</sub>Ovac. There was larger thickness for the higher ionic strength multilayers and subsequently higher amount of water uptake, due to increased counterions causing structural changes as the chains change from flat conformation to coiled conformation [2]. The observation was in agreement with past experiments with NaCl. In figure 1 (c), we changed to PDADMAC75% to investigate the effect of degree of charge [3]. The polyelectrolyte multilayers also showed no displacement of hydration water or replacement of H by D after exposure to D<sub>2</sub>O. The thickness of the multilayers was much thinner compared to the PDADMAC100% after adsorption of six double layers. This was an indication that the adsorption of polyelectrolyte

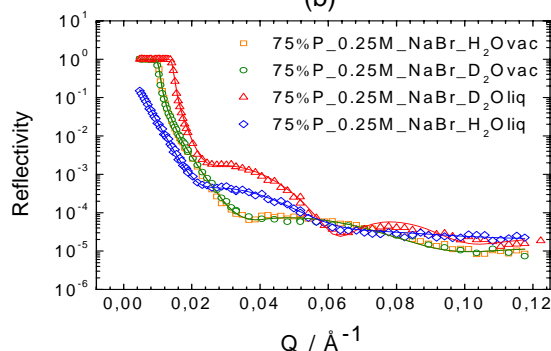
chains stop after some number of steps. The reason is still not clear.



(a)



(b)



(c)

Fig.1 NR measurements against H<sub>2</sub>Ovac, D<sub>2</sub>Ovac, D<sub>2</sub>Oliq, and H<sub>2</sub>Oliq (a) PDADMAC100% at 0.1 M NaBr, (b) PDADMAC100% at 0.25 M NaBr, (c) PDADMAC75% at 0.25 M NaBr.

#### Reference:

- [1] G. Decher, Science 277 (1997) 1232
- [2] R. Steitz et al., Colloids and Surfaces A 163(2000) 63-70
- [3] U. Voigt et al., J. Phys. Chem B 107 (2003) 5273



## EXPERIMENTAL REPORT

### Hofmeister effects on the structure of protein adsorbates

Proposal N° CHE-04-1699

Instrument **V6**

Local Contact  
Roland Steitz

Principal Proposer: Claus Czeslik, Technische Universität Dortmund, Fakultät  
Experimental Team: Florian Evers, Metin Tolan, Technische Universität Dortmund  
Roland Steitz, Ralf Köhler, Helmholtz-Zentrum Berlin

Date(s) of Experiment

25/08/2008 – 01/09/2008

Date of Report: 09/01/2009

It is well known that the folding stability of protein molecules is affected by the presence of cosolvents. Recently, we have found that non-ionic cosolvents have a pronounced effect on the degree of protein adsorption at a silica-water interface [1]. In the present study, we were interested in the effects of Hofmeister ions on the mechanism of protein adsorption. In the so-called Hofmeister series, cations and anions are arranged according to their effectiveness in precipitating globular proteins.

The protein ribonuclease A was chosen as model protein, whose affinity for adsorption at a solid surface was probed applying neutron reflectometry. Kosmotropic and chaotropic salts were added to the protein solution in advance of the adsorption experiments. In order to exclude electrostatic driving forces for protein adsorption, the solid surface was modified with a thin hydrophobic polystyrene film. In Figure 1, selected neutron reflectivity curves are shown, as obtained in the performed experiments. The neutron reflectivity curves were analyzed on the basis of a three-layer model, Si / SiO<sub>2</sub> / polystyrene / protein adsorbate / protein solution.

As can be seen in Figure 2, the adsorbed amount of ribonuclease A at a hydrophobic polystyrene film is significantly affected by the presence of salts. Moreover, the adsorbed amounts nicely follow the Hofmeister series, when considering kosmotropic or chaotropic salts alone. However, as might be unexpected, the presence of both the kosmotropic salts [(NH<sub>4</sub>)<sub>2</sub>SO<sub>4</sub>, Na<sub>2</sub>SO<sub>4</sub>] and the chaotropic salts [NaSCN, Ca(SCN)<sub>2</sub>] lowers the adsorbed protein mass. From an inspection of the corresponding scattering length density profiles, this reduction can be attributed to a decrease of the protein volume fraction in the adsorbate. The performed study is in full

agreement with earlier experiments on non-ionic cosolvents [1]. Apparently, kosmotropic cosolvents reduce the interfacial affinity of proteins by stabilizing their hydration shell and native fold, whereas chaotropic cosolvents lower hydrophobic driving forces for adsorption by increasing the solubility of hydrophobic areas on the protein surface.

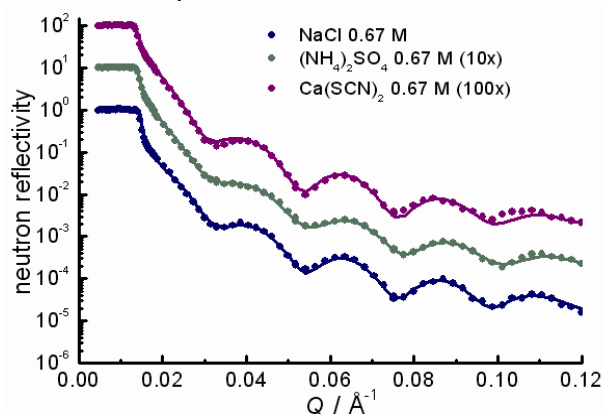


**Figure 1.** Typical neutron reflectivity curves as obtained in the experiments. The protein ribonuclease A was adsorbed at a silicon wafer, which was coated with a polystyrene film. The protein solution contained various salts selected from the Hofmeister series.

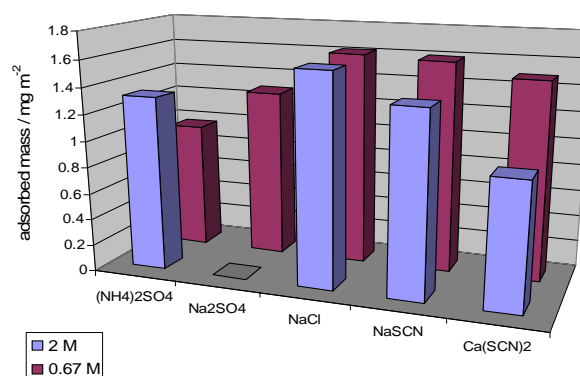


**Figure 2.** Adsorbed amounts of protein at a hydrophobic polystyrene surface in the presence of kosmotropic [(NH<sub>4</sub>)<sub>2</sub>SO<sub>4</sub>, Na<sub>2</sub>SO<sub>4</sub>] and chaotropic [NaSCN, Ca(SCN)<sub>2</sub>] salts. NaCl is used as reference.

[1] J. Koo, T. Gutberlet, C. Czeslik, J. Phys. Chem. B 112 (2008) 6292-6295.



## EXPERIMENTAL REPORT

### Water at a Hydrophobic Substrate and the Effect of Pressure, continued

Proposal N°  
PHY-04-1718-EF

Instrument **V6**

Local Contact R. Steitz

Principal Proposer: R. Steitz, Helmholtz-Zentrum, Berlin  
Experimental Team: M. Kreuzer, RKU Heidelberg  
R. Dahint, RKU Heidelberg

Date(s) of Experiment  
02/07/2008 – 07/07/2008  
01/12/2008 – 08/12/2008

Date of Report:

Recent studies of the interface of water against hydrophobic surfaces by neutron and X-ray reflectometry have revealed a depletion of water in a thin boundary layer next to the substrate [1]. In that context neutron reflectivity experiments performed on the interface of heavy water ( $D_2O$ ) against thin films of perdeuterated polystyrene (d-PS) spin-coated onto silicon blocks have revealed a non-vanishing scattering contrast at the polymer/water interface, although the two materials (d-PS and  $D_2O$ ) have closely similar scattering length densities (SLD) [2].

To observe a pressure-induced decrease in the depletion length,  $d_2$ , we managed in a first round of experiments (Proposal PHY-04-1526-EF, 2007/II) to measure two samples each at 1 and 1000 bar. The depletion length decreased by 1.6 Å and 1.0 Å, respectively, for the two samples. The depletion length represents the thickness of an equivalent vacuum layer and is a convenient measure for comparing results from different experiments and theoretical predictions. In fact, the observed change in  $d_2$  for the d-PS/ $D_2O$  interface is in qualitative agreement with molecular dynamics (MD) simulations on the interface of an alkane slab in water [3]. The latter study investigated pressure effects on the depletion length and predicts a decrease in  $d_2$  from 2.56 Å to 1.89 Å as the pressure is increased from ambient (1 bar) to a hydrostatic pressure of 1000 bar at a constant sample temperature of 300 K [3].

In the most recent experiments, we set out to repeat the predicted pressure dependence of  $d_2$  to validate the principal results achieved in 2007/II. Implementation of the Heidelberg high pressure cell and achieving full functionality of the experimental setup ( $p = 1000$  bar) proceeded without difficulties in the December experiment only. Unexpectedly, during the measurements at high pressure the films of d-PS appeared to be unstable under the extreme conditions. We managed to measure 4 samples each at 1 bar and 1000 bar, but only one film remained on the silicon substrate,

after pressure was induced. We measured a d-PS film thickness of 177 Å ( $SLD=6.17E-6$  Å<sup>-2</sup>) and one additional layer,  $d_a$ , on top of it, with  $d_a=96$  Å ( $SLD=5.82E-6$  Å<sup>-2</sup>). The SLD of the  $D_2O$  subphase was  $6.12E-6$  Å<sup>-2</sup>. Additional X-ray measurements with the same sample revealed a total layer thickness of 210 Å. When pressure was induced, we observed a decrease in the layer to  $d_a=89$  Å ( $SLD=6.09E-6$  Å<sup>-2</sup>) and a change in SLD of the  $D_2O$  subphase to  $6.38E-6$  Å<sup>-2</sup>. This result corresponds to a decrease in  $d_2$  from 4.71 Å to 4.05 Å. The pressure dependent change in  $d_2$  is in good agreement with prediction [3]. However, the absolute values of extracted layer thickness are two times larger than expected [3]. We conclude that the additional layer  $d_a$  stems from the combined system of organic contamination and a depletion of water in the boundary layer. Unfortunately, it was not possible to fit a model, where these two contributions were separated. After pressure release back to 1 bar we measured a layer thickness of  $d_a=89$  Å ( $SLD=5.83$  E-6 Å<sup>-2</sup>) with  $D_2O$  subphase SLD of  $6.16E-6$  Å<sup>-2</sup>. This corresponds to a depletion length,  $d_2$ , of 4.77 Å.

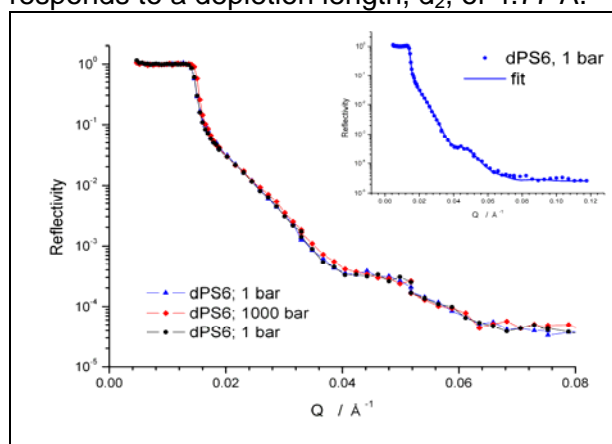


**Figure 1:** Subsequent neutron reflectivity from the solid/liquid interface of sample dPS6 against  $D_2O$ . The inset shows a fit (solid line) to the reflectivity curve at 1 bar (circles).

[1] Schwendel et al., Langmuir 2003, 19 2284

[2] Steitz et al., Langmuir 2003, 19, 2409

[3] Mamatkulov et al



## EXPERIMENTAL REPORT

### Determination of kinetics of structural growth in coagulating milk

Proposal N° PHY-04-1678

Instrument **V12a**

Local Contact M. Strobl

Principal Proposer: Ir. L.F. van Heijkamp, Delft University of Technology  
 Experimental Team: Peter Walter, HMI  
 Markus Strobl, HMI  
 Sven-Oliver Seidel, HMI  
 Robert Monka, HMI

Date(s) of Experiment

02/07/2008 – 06/07/2008

Date of Report: 09/01/2008

### Experiments

Deuterated milk samples were prepared by suspending 10% (w/w) NILAC® fat-free casein powder in D<sub>2</sub>O using 10.0 mm thick cuvettes. At time 0 hours a small amount of lactic acid (glucone-δ-lactone) was added to start the coagulation of milk into yoghurt.

The bulk structure of the milk particles was statically measured before and after gelation over periods of 1.0 and 1.5 hours respectively, and averaged afterwards to 10 minute signals. The time evolution of the structure during gelation was measured kinetically in steps of 10 minutes. All data was normalized with the sample transmission.

### Modelling

The measured data  $I_m(q_y)$  consisted of the scattered intensity, part of the direct beam and a background level. The scattered intensity was a projection of the scattering function  $I_s(q_y)$  convoluted with the resolution function  $R(q_y)$ :

$$I_m(q_y) = \int R(q_y - Q_y) \left[ \int I_s(Q) dQ_x \right] dQ_y + (1 - c_s) \cdot R(q_y) + I_b \quad (1)$$

- The resolution curve was obtained from a D<sub>2</sub>O measurement of 1 hour, averaged to 10 minute intensities and described as a sum of three Lorentzian-type functions, for negative and positive  $q_y$ -range separately.

- The scattered signal was described with an isotropic Self-Affine model:

$$I_s(q) = I_0 4\pi a^3 (2H + 1) \left[ (aq)^2 + 1 \right]^{-(H + \frac{3}{2})} \quad (2)$$

for which the analytical projection and Fourier transform are known and where the attenuation was used to express  $I_0$  as a function of integral intensities.

- The scattered fraction  $c_s = \lambda^2 \phi_v (\phi_v - 1) \Delta \rho_s^2 t \xi$ , with wavelength  $\lambda = 4.76$  Å, volume fraction  $\phi_v = 0.10$ , contrast  $\Delta \rho_s \approx 5.7 \cdot 10^{-7}$  Å<sup>-2</sup>, sample thickness  $t = 10.0$  mm and correlation length:

$$\xi = 2a\sqrt{\pi} \Gamma(H + \frac{1}{2}) / \Gamma(H) \quad (3)$$

### Results

The measured data was fit for length scale  $a$ , Hurst exponent  $H$  and scattered fraction  $c_s$ .

- The length scale changed from  $250 \pm 25$  nm to  $726 \pm 4$  nm during 8 hours, with little apparent change for the first two hours, see figure 1.
- Initial data was not sensitive to  $H$  and fitting produced some unphysical values, but after ~3 hours a constant value of  $H = -3/8$  was found.
- The scattered fraction could be calculated from  $a$  and  $H$  to reasonable agreement with the contrast as found from SESANS data.

### Conclusions

The first two hours a milk particle size of 250 nm was seen, in excellent agreement with the SESANS value for the average casein micelle diameter of  $238 \pm 24$  nm. During the next six hours the micelles coagulated into aggregates until gelation, where the typical length had increased by a factor 2.9, where a factor of 3.3 had been observed in SESANS.

Although the initial dimensionality could not be established well, static USANS measurements of milk and yoghurt were in good agreement with SESANS results. Kinetic USANS measurements yielded reliable additional information about the coagulation process.

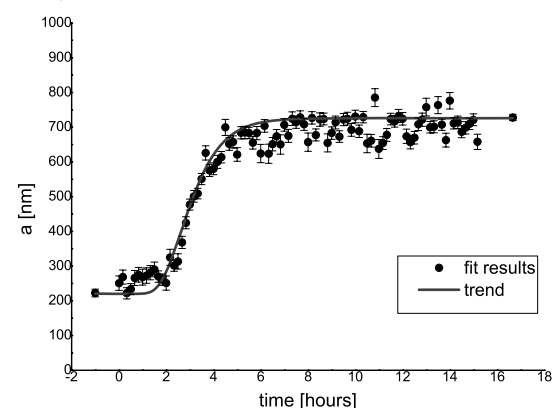


Fig. 1: Length scale change of milk to yoghurt coagulation after acidification at 0 hours.

*This research project has been supported by the European Commission under the 6<sup>th</sup> Framework Programme through the Key Action: Strengthening the European Research Infrastructures. Contract n°: RII3-CT-2003-505925 (NMI 3).*



## EXPERIMENTAL REPORT

### USANS of magnetite sphere suspensions in ferrofluids

Proposal N° PHY-04-1679

Instrument **V12a**

Local Contact  
Wolfgang Treimer

Principal Proposer: Apoorva G. Wagh, BARC, Mumbai 400085, India  
 Experimental Team: Sohrab Abbas, BARC, Mumbai 400085, India  
 Sven-Oliver Seidel, University of Applied Sciences- FB II  
 Robert Monka, University of Applied Sciences  
 Wolfgang Treimer, BENSC, HMI, Berlin

Date(s) of Experiment

05/12/2008 – 09/12/2008

Date of Report: January 2009

Trapping and controlled release of light has recently been demonstrated with a suspension of magnetite spheres in a ferrofluid [1-2]. Diffraction of linearly polarised He-Ne laser light from the ferrofluid gets extinguished for a critical magnetite sphere size ( $\sim 1 - 3 \mu\text{m}$ ), when a critical magnetic field (100–170 Oe for  $3 \mu\text{m}$ , 450–460 Oe for  $1 \mu\text{m}$ ) is applied transverse to the direction of laser polarisation. When the laser is switched off and the magnetic field is reduced, the ferrofluid releases the trapped laser light.

We explored a possible sharp variation in the agglomeration and magnetic properties of the ferrofluid systems by recording USANS spectra with unpolarised and polarised neutrons of  $4.76 \text{ \AA}$  wavelength of samples in quartz cuvettes affording 1 mm pathlength, sonicated for 20 minutes immediately prior to measurements. However, no significant variation in the USANS profiles was observed (Figs. 1-3) for 3 and  $1 \mu\text{m}$  sphere suspensions at magnetic fields ranging from 0 to 500 Oe. Further work is necessary to understand this negative result.

We thank B. Chudasama and R.V. Mehta for supplying the samples.

#### REFERENCES:

- [1] R.V. Mehta, R. Patel, R. Desai, R.V. Upadhyay and K. Parekh, Phys. Rev. Lett. **96**, 127402 (2006).  
 [2] R.V. Mehta, R. Patel and R.V. Upadhyay, Phys. Rev. B **74**, 195127 (2006).

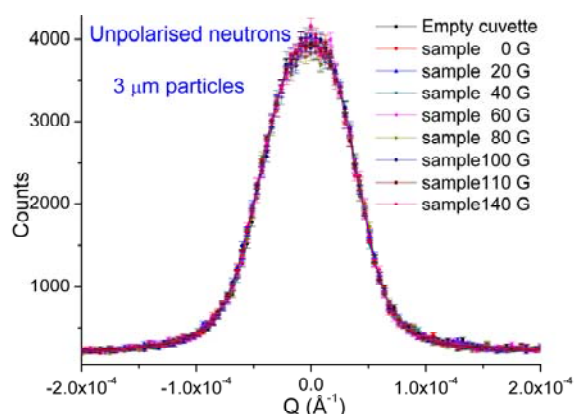


Fig.1 USANS of  $3 \mu\text{m}$  magnetite spheres' suspension in a ferrofluid.

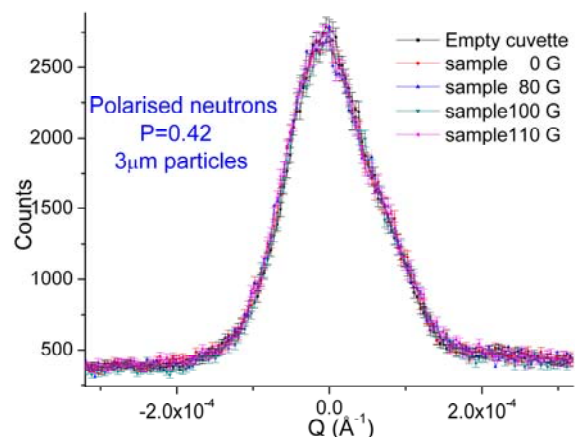


Fig.2 USANS with polarised neutrons of the same sample as in Fig.1.

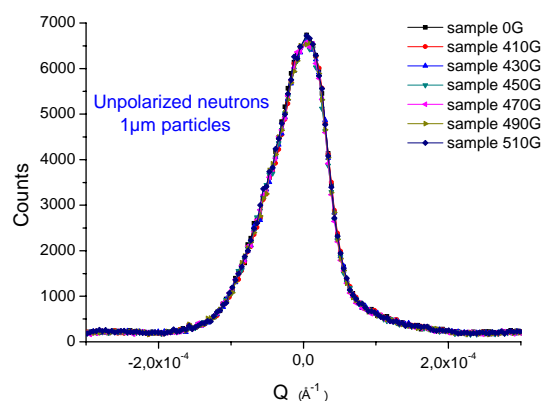


Fig.3 USANS of  $1 \mu\text{m}$  magnetite spheres' suspension in a ferrofluid.



## **Material Science**

Structures and Phases	203
Strain and Stress	230





## EXPERIMENTAL REPORT

### Hydration kinetics of cement with PCE superplasticizers

Proposal N° MAT-01-2027

Instrument **E2**

Local Contact  
J.-U. Hoffmann,  
A. Hoser

Principal Proposer: G. Kloess - Leipzig University  
Experimental Team: J.-U. Hoffmann, A. Hoser - HZB für Materialien und Energie  
S. Schorr - FU Berlin  
M. Ende - Leipzig University  
A. König - Leipzig University & MFPA Leipzig

Date(s) of Experiment

29/09/2008 – 02/10/2008  
27/10/2008 – 29/10/2008

Date of Report: 13/01/2009

The process of cement hydration is very complex and depends on several parameters. For a conventional X-ray diffraction experiment the concrete has to be grinded into a powder. Unfortunately some phases like ettringite are under suspicion to perish by stronger grinding. In a neutron diffraction experiment the concrete sample can be investigated in form of a cylindrical rod due to the much higher penetration depth of neutrons. Thus grinding of the sample can be avoided. Hence neutron scattering experiments were carried out at the E2 flat cone diffractometer using a wavelength of 2.39 Å. The concrete samples were freshly prepared and measured 1, 7 and 28 days after mixing. Different cements were used (with and without PCE superplasticizers). The probed volume provided satisfying statistics and generated homogeneous diffraction rings. Because of the high water content within the sample, the peak to background ratio is 0.1 or lower (Fig. 1) due to incoherent scattering of hydrogen. On the other hand the higher the sample diameter the better the statistics and the volume information. The cylindrical sample diameter was changed for optimization from 15 mm to 7 mm.

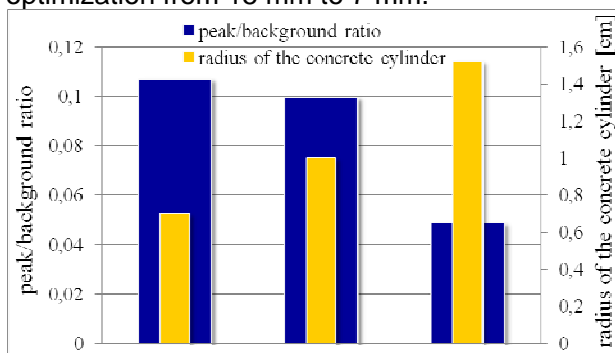


**Fig. 1:** The low peak-to-background ratio of the 001-peak of portlandite versus the sample cylinder radii used at E2.

The ratio of ettringite to portlandite was used to determine the effect of grinding (see table 1). The diffraction patterns were analyzed using Rietveld refinements. For the neutron data the background was corrected and a Gaussian peak shape assumed.

Table 1: Ratio ettringite/portlandite

	X-rays	neutrons
Ettr. / Portl.	35 : 65	70 : 30

Thus the ettringite content determined by X-ray measurements is too small which may cause misinterpretations of the hydration process.

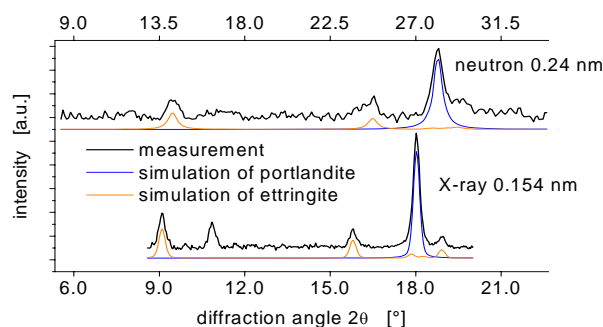


**Fig. 2:** Neutron and X-ray diffraction measurements of the same concrete. The two curves below the line of measurement show the simulations of portlandite and ettringite using Rietveld refinement.

Data from literature verify the retarding effect of superplasticizers only for the first day of the hydration process. However, still after one week of hydration we found a different slope of the background. In the sample containing PCE the background intensity is 2% higher (Fig. 3). It should be a hint for PCE supported long time storage of water. Further analysis will yield more detailed results to the influence of additives like microsilica to the kinetics of phase generation during the first 4 weeks of hydration.

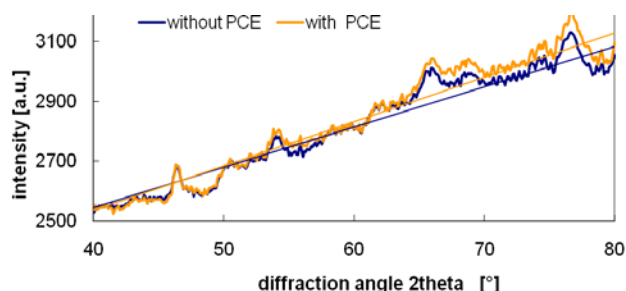


**Fig. 3:** Different slope of the background of neutron scattering in samples with and without PCE after 7 days.



## EXPERIMENTAL REPORT

### In situ neutron diffraction studies of complex aluminium hydride material at high deuterium pressure

Proposal N° MAT-01-2233

Instrument E6

Local Contact  
Alexandra Buchsteiner

Principal Proposer: Claudia Weidenthaler, MPI für Kohlenforschung, Mühlheim  
Experimental Team: André Pommerin, MPI für Kohlenforschung, Mühlheim  
Wolfgang Schmidt, MPI für Kohlenforschung, Mühlheim  
Michael Felderhoff, MPI für Kohlenforschung, Mühlheim  
Alexandra Buchsteiner, Dirk Wallacher, Helmholtz-Zentrum Berlin

Date(s) of Experiment

14/04/2008 – 22/04/2008

Date of Report: 15/01/2009

This experiment is a continuation of our first proposal (MAT-01-2138), which focussed on the developed of experimental equipment and principal conditions for studies of reversible hydrogen storage materials under non-ambient conditions, especially under high gas pressures. In 2008 we tried to apply the experimental experience to other complex aluminium hydride systems. Aim of the experiments was (a) to investigate the formation of potential metastable phases under non ambient conditions and (b) potential rehydrogenation under high hydrogen pressures. The experimental conditions applied covered the pressure range from ambient pressure up to 350 bar and a temperature range from 140 to 500 K. All compounds were prepared by high energy ball milling which is a simple method for the synthesis of complex aluminium hydrides via a metathesis reaction starting from a metal chloride and  $\text{NaAlH}_4(\text{NaAlD}_4)$ . One disadvantage is the formation of high amounts of NaCl and Al which cannot easily be removed (Eq.1).



The mechanochemical preparation of the materials might be one reason why the experiments did not succeed. The synthesis products have very small crystal sizes which results in very broad diffraction peaks. Furthermore, all samples show extremely high amorphous backgrounds. Additionally, the amount of crystalline complex aluminum hydrides formed beside NaCl and Al is not very high. As a representative example Fig.1 shows the X-ray powder pattern and the neutron diffraction pattern of a sample containing  $\text{BaAlD}_5$ , NaCl, and Al. While the reflections of the  $\text{BaAlD}_5$  are clearly visible, they are not visible in the neutron diffraction pattern. Since the scattering properties of Ba are good, this result was unexpected. One explanation could be that the size of the scattering domains is too small for neutron diffraction experiments.

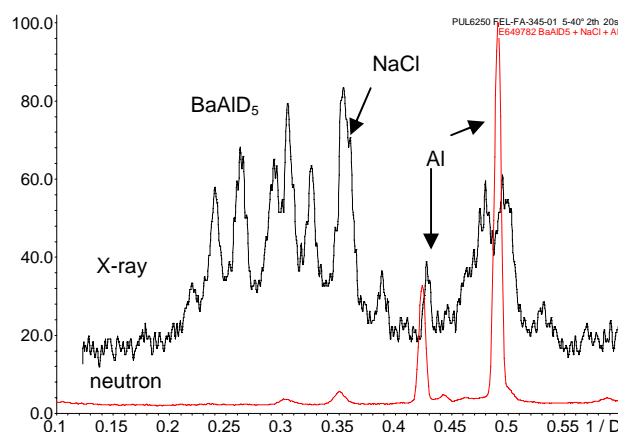


Figure 1: Comparison of the X-ray and neutron powder patterns of  $\text{BaAlD}_5$ , NaCl, and Al. Another reason could be that the contribution of the Al sample container absorbs almost completely the contribution of the sample (Fig.2).

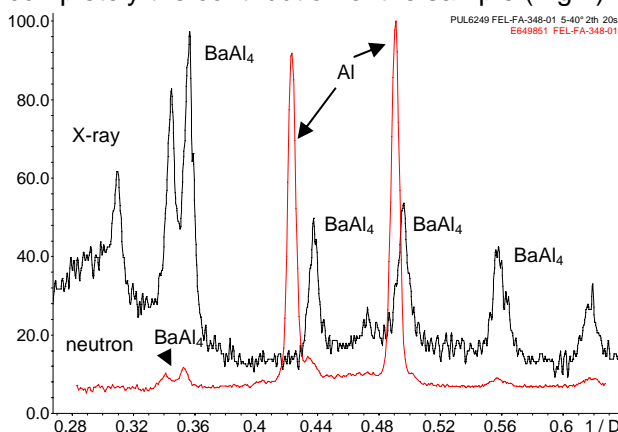


Figure 2: Comparison of the X-ray and neutron powder patterns of  $\text{BaAl}_4 + \text{BaD}_2$ . The following compounds were also investigated:  $\text{KAlD}_4$ ,  $\text{BaAl}_4 + \text{BaD}_2$ ,  $\text{BaD}_2 + \text{Al}$  but the powder patterns did not show any changes during the high pressure treatment which could be due to too short reaction times.



## EXPERIMENTAL REPORT

### On the synthesis of LiBD<sub>4</sub> via AIB<sub>2</sub>

Proposal N° MAT-01-2234

Instrument **E6**

Local Contact  
Alexandra Buchsteiner

Principal Proposer: Arndt Remhof, EMPA  
Experimental Team: Arndt Remhof, EMPA  
Florian Buchter, EMPA  
Oliver Friedrichs, EMPA  
Dirk Wallacher, BENSC

Date(s) of Experiment

27/05/2008 – 04/06/2008

Date of Report: 03/09/2008

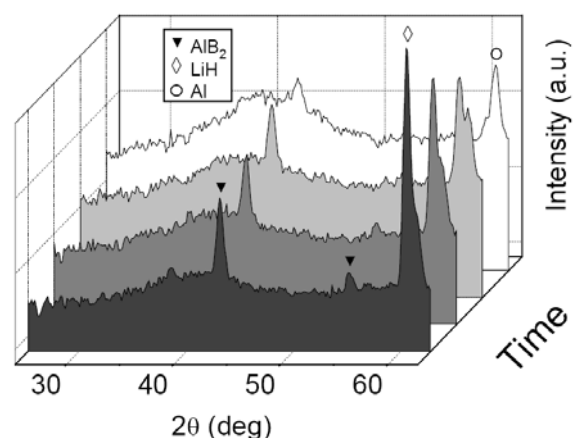
Among the alkali and earth alkali complex borohydrides LiBH<sub>4</sub> is outstanding due to its high hydrogen storage capacity and its reversibility. A main hindrance for technical applications is its high stability, leading to high desorption temperatures. Also the rather slow kinetics of the system remains a challenge.

Recently, we observed the synthesis of LiBH<sub>4</sub> from the elements at 700°C with an applied hydrogen pressure of 150 bar [1]. Pre-annealing of Li and B prior to the hydrogen exposure reduces the required temperature. With in situ neutron diffraction we observed that this involves the formation of LiB and of LiH as starting materials [2]. As a way to destabilize LiBH<sub>4</sub> the use of other B based intermetallics such as AIB<sub>2</sub> was proposed [3,4].

The main purpose of the experiment was to study the synthesis of LiBD<sub>4</sub> starting from AIB<sub>2</sub> and LiD in applied D<sub>2</sub> atmosphere at elevated temperatures and to identify the phases present during the reaction.

We first filled an Inconel sample container with a ball-milled mixture of Al<sup>11</sup>B<sub>2</sub> and LiD and placed it into the high temperature furnace (HTF), provided by BENSC. The HTF was placed onto the sample stage of the E6 instrument and the sample container was connected to the gas loading system, supplying deuterium (D<sub>2</sub>) of 50 bar. Neutron powder diffraction was carried out at an incident wavelength of 2.4 Å. During the experiments the temperature of the sample was kept constant at 450°C, and increasing pressures were applied. The deuterium uptake was monitored via the pressure drop. A diffractogram covering the whole accessible 2θ range was recorded in 6 hours. During the hydrogen uptake faster scans have been performed to monitor the nucleation and growth of new phases. The main result is depicted in the figure. AIB<sub>2</sub> and LiD as starting materials can clearly be identified. With

increasing pressure they vanish and the occurrence of elemental Al and LiBD<sub>4</sub> can be observed. As LiBD<sub>4</sub> melts at 280°C, no diffraction peak can be observed at 450°C. However, the formation of LiBD<sub>4</sub> leads to the occurrence of a broad diffuse feature, which transforms into the diffraction pattern of LiBD<sub>4</sub> at lower temperatures.



Reaction of AIB<sub>2</sub> and LiD to LiBD<sub>4</sub> and Al in D<sub>2</sub> atmosphere.

We conclude that the formation of LiBD<sub>4</sub> follows the reaction



The reaction already starts at 450°C at a pressure ≤ 25 bar, which is much lower than the required pressures observed experimentally for the direct synthesis. However, at this pressure, the reaction is rather slow. Higher pressures enhance the kinetics considerably.

[1] O. Friedrichs et al, *Acta Mater.* **56**, 949 (2008).

[2] A. Remhof et al., *Phys. Chem. Chem. Phys.*, in press.

[3] J. J. Vajo, et al., *J. Phys. Chem. B* **109** 3719 (2005).

[4] S. A. Jin et al., *Scripta Mater.* **68**, 963 (2008).



## EXPERIMENTAL REPORT

### Study of hydrogen storage in metal doped carbons by neutron diffraction

Proposal N° CHE-01-2236

Instrument **E6**

Local Contact  
A Buchsteiner

Principal Proposer: Theodore Steriotis, NCSR Demokritos - Greece  
Experimental Team: Georgia Charalambopoulou, NCSR Demokritos - Greece  
Jorge Hernandez-Velasco, Instituto de Ciencia de Materiales de Madrid, CSIC - Spain  
Dirk Wallacher, BENSC - Germany

Date(s) of Experiment

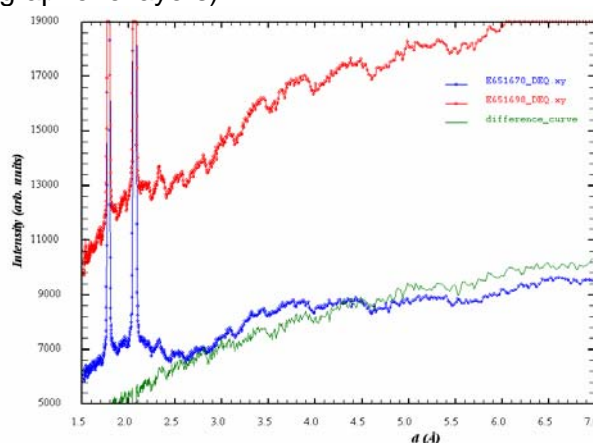
22/07/2008 – 29/07/2008

Date of Report: 16/01/2009

One of the challenges for the practical use of H<sub>2</sub> as energy carrier concerns the efficient H<sub>2</sub> storage with respect to a great number of operating requirements. Solid storage appears a promising route, but fully satisfactory materials have not been identified yet. Recently, a new family of novel carbon-metal (e.g. Ti, V, Pd, Pt) nanocomposites revealed considerable potential for hydrogen storage. Our group has developed Pd-alloy/carbon nanocomposites by doping different carbon substrates such as (a) a foam graphite-oxide-like material (which is lightweight and possesses high surface area and porosity) and (b) a novel carbonaceous material called carbon cones (composed of curved graphite sheets and flat carbon discs). Both nanocomposites have revealed remarkable hydrogen uptake at room temperature and rather low pressures. These high H<sub>2</sub> storage capacities might be attributed to a mechanism known as hydrogen spillover (H<sub>2</sub> sorption on Pd or Pt doped porous solids is considered to involve dissociative chemisorption of hydrogen followed by diffusive cascading into various adsorption sites on the carbon material).

With the experiment CHE-01-2236 we pursued to investigate the alleged spillover mechanism in Pd-alloy doped carbon foam and carbon cone systems through the combination of in-situ hydrogenation and neutron powder diffraction. Main aim of these measurements was (a) to monitor diffraction pattern changes upon loading the carbogenic materials with hydrogen (the changes at low scattering angles could be related to atomic hydrogen intercalation between graphene layers) and (b) to investigate bulk hydride formation (catalyst particles) upon hydrogenation. Both samples were loaded in a stainless steel cell, which was fixed in the beam of E6 diffractometer, and was connected to a gas handling system via a capillary. Room temperature neutron diffraction measurements of empty cell, outgassed

samples and samples loaded with different pressures of either H<sub>2</sub> or D<sub>2</sub> (up to 80 bar) were performed. However the available amount of samples (and thus the quantity of metal catalysts) was low and the catalyst phases were hardly detected in the outgassed samples. Upon hydrogenation (deuteration) a large amount of hydrogen was detected as increased background (originating from incoherent scattering), however the diffraction patterns were qualitatively identical to the pattern of unloaded sample. Since the amount of catalyst particles was very low, possible alteration (hydride formation) of their phase could not have been observed. Additionally, possible intercalation of atomic hydrogen was not observed. It should nevertheless be pointed out that some broad structures at high  $d$  (low angles) seem to appear, indicating that hydrogen is located in the bulk of the material (surface, pores) rather than within fixed positions (e.g. metal particles or in-between graphene layers).



Diffraction patterns (in  $d$ -spacing) of the carbon foam sample loaded with H<sub>2</sub> ( $p=50$  bar) (red) and unloaded (blue). Difference in green.

This research project has been supported by the European Commission under the 6<sup>th</sup> Framework Programme through the Key Action: Strengthening the European Research Infrastructures.

Contract n°: RII3-CT-2003-505925 (NMI 3).



## EXPERIMENTAL REPORT

### On the cycling behaviour of LiBD<sub>4</sub>

Proposal N° MAT-01-2395

Instrument **E6**

Local Contact  
Alexandra Buchsteiner

Principal Proposer: Arndt Remhof, EMPA  
Experimental Team: Arndt Remhof, EMPA  
Ji Woo Kim, EMPA  
Oliver Friederichs, EMPA  
Dirk Wallacher, BENSC

Date(s) of Experiment

27/08/2008 – 04/09/2008

Date of Report: 03/09/2008

The fundamental properties of a technical applicable hydrogen storage material are (i) a high storage capacity, (ii) fast sorption kinetics and (iii) a convenient working temperature. Due to its high storage capacity, LiBH<sub>4</sub> is a promising candidate for a hydrogen storage material [1]. In previous experiments we examined the synthesis of LiBH<sub>4</sub> from the elements [2] and from AlB<sub>2</sub> and LiD as starting materials [3]. To decrease the sorption temperature and to enhance the sorption kinetics, additives such as Al or MgH<sub>2</sub> have been suggested [4,5].

In the present experiment we examined the cycling behavior of LiBD<sub>4</sub> according to the reaction



Therefore, we first filled an Inconel sample container with a ball-milled mixture of Al<sup>11</sup>B<sub>2</sub> and LiD and placed it into the high temperature furnace (HTF), provided by BENSC. The HTF was placed onto the sample stage of the E6 instrument and the sample container was connected to a gas loading system. Absorption was carried out by connecting the sample container to a D<sub>2</sub> reservoir (50 bar, 1.3l) and the absorption was monitored via the pressure drop. Desorption was carried out in two different ways: (i) into a pre-evacuated reservoir (50ml) or (ii) into dynamic vacuum.

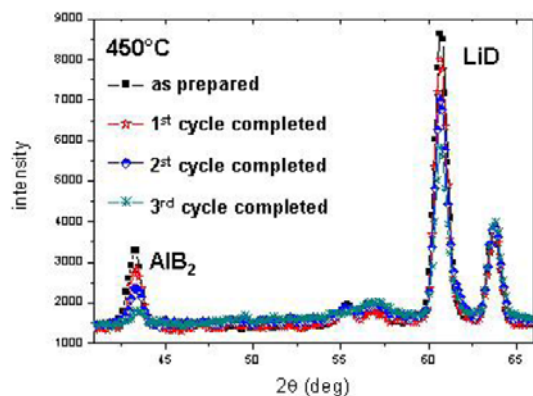


Fig. 1: Effect of deuterium cycling

The first method allows to follow the desorption via the increase in pressure and the measurement of equilibrium pressures. For the LiBD<sub>4</sub> decomposition we determined a plateau pressure of 4.3 bar at 450°C, which is in agreement with earlier measurements [6]. Three complete absorption/desorption cycles have been carried out at 450°. Figure 1 shows the decreasing hydrogen capacity of the reaction.

Desorption into dynamic vacuum at 450°C leads to the decay of LiD and to the creation of a new phase that could be identified as LiAl, as shown in figure 2.

The reaction  $2\text{LiAl} + \text{D}_2 \leftrightarrow 2\text{LiD} + 2\text{Al}$  was found to be reversible in an applied a D<sub>2</sub> atmosphere ( $p > 300$  mbar).

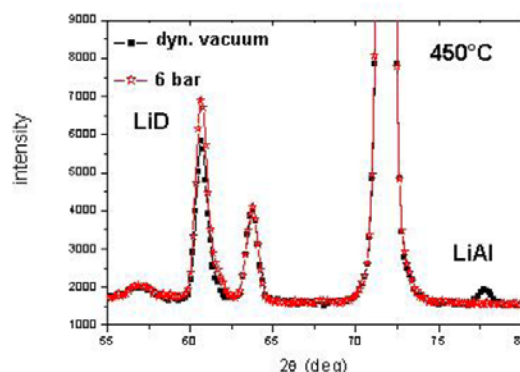


Fig. 2: LiAl forms upon desorption in dynamic vacuum

Apart from an in-situ insight into the cycling process of LiBD<sub>4</sub> and Al, we could improve the sample environment to study complete deuterium absorption/desorption cycles in reactive complex hydride systems.

- [1] A. Züttel et al., *Scripta Mater.*, **56**, 823 (2007).
- [2] A. Remhof et al., *Phys. Chem. Chem. Phys.*, in press
- [3] O. Friedrichs et al., submitted, and BENSC experimental report MAT-01-2234
- [4] J. J. Vajo, et al., *J. Phys. Chem. B* **109** 3719 (2005).
- [5] S. A. Jin et al., *Scripta Mater.* **68**, 963 (2008).
- [6] P. Maunon et al., *Phys. Chem. B.* **112**, 906 (2008).



## EXPERIMENTAL REPORT

### Effect of restricted geometry on stability of ferroelectric phase in confined KNO<sub>3</sub> and NaNO<sub>2</sub>

Proposal N° MAT-01-2117

Instrument **E9**

Local Contact  
M. Tovar

Principal Proposer: Alexander Naberezhnov, Ioffe PTI RAS, Russia

Experimental Team: Ewa Resiakiewicz-Pasek, Institute of Physics,  
Wroclaw University of Technology, Poland

Date(s) of Experiment

24/10/2007 – 02/11/2007

Date of Report: 12/01/2008

Last decades nanostructured materials attract a special attention because their properties are essentially different from those of conventional bulk materials. In particular it is known that the reduction of real physical size of particles from the microscopic down to nanoscopic scales results in a change of the majority of physical properties of confined materials (CM). One of important aspects of CM is a stability of structure as a function of spatial dimension, geometry and topology of nanoparticles. There are various methods of preparation of such ultra-dispersed substances and one of them is embedding of materials into different porous matrices: porous glasses, artificial opals, chrysotile asbestos etc. It is known that the thin-film KNO<sub>3</sub> exhibits ferroelectric properties at much lower temperatures than bulk material and ferroelectric potassium nitrate films may be used for fabrication memory devices. Potassium nitrate (KNO<sub>3</sub>) has three different structures. At low temperature the orthorhombic (Pmcn)  $\alpha$ -phase is stable. Upon heating at  $\sim 401$  K this phase transforms into the trigonal (R-3c) disordered  $\beta$ -phase. On cooling from  $\sim 473$  K  $\beta$ -KNO<sub>3</sub> undergoes a transformation to the metastable ferroelectric trigonal (R3m)  $\gamma$ -phase at  $\sim 398$  K which transforms to  $\alpha$ -KNO<sub>3</sub> at about 373 K on further cooling. It was shown that at a high cooling rate ( $\sim 15$  K/min) from 403 to 303 K the  $\gamma$ -phase was obtained as a pure phase at 303 K, but it was eventually transforms to  $\alpha$ -KNO<sub>3</sub> in 15 minutes at this temperature. At a slow cooling rate ( $\sim 0.5$  K/min) from 403 K to 303 K the  $\gamma$ -phase started to form at 391 K and transforms to  $\alpha$ -KNO<sub>3</sub> at 370 K. Both  $\alpha \rightarrow \beta$  and  $\gamma \rightarrow \alpha$  order-disorder transitions are governed by rotations of NO<sub>3</sub><sup>-</sup> groups around the c-axis. We have studied the modification of structure of KNO<sub>3</sub> confined within porous glasses with average pore diameter 320 nm in the temperature interval from RT up to 507 K at heating and on cooling down to 350 K after heating. The cooling rate from 507 K down to 410 K was  $\sim 2.7$  K/min. Principle results are:

1 – The broadening of Bragg peaks due to size effect was not registered, but we have observed

the essential broadening of elastic peaks at large Q due to stresses.

2 – On cooling in a vicinity of 385 K the coexistence of  $\gamma$  and  $\beta$ -phases in a temperature interval 5-7 K is observed and the pure  $\gamma$ -phase exists below 380 K only.

3 – The transition from  $\gamma$ -phase to  $\alpha$ -phase we have detected below 364 K, at that at 364 K the coexistence of  $\gamma$ - and  $\alpha$ -phases is observed.

These results are confirmed by measurements of dielectric response of this CM.

The second sample was sodium nitrite embedded into analogous matrices.

We have obtained the temperature dependence of order parameter  $\eta(T)$  for this CM (Fig.1).

It is easy to see that at low temperatures  $\eta(T)$  corresponds to the analogous one for the bulk, but starting from  $\sim 380$  K it deviates from  $\eta(T)_{\text{BULK}}$ , but the phase transition (PT) for CM remains the first order PT and  $T_C$  does not changed. Possibly this dependence is a results of very wide distribution of nanoparticle sizes and reflects the appearance of premelted state, which we have observed for small particles of sodium nitrite above  $T_C$  [1].

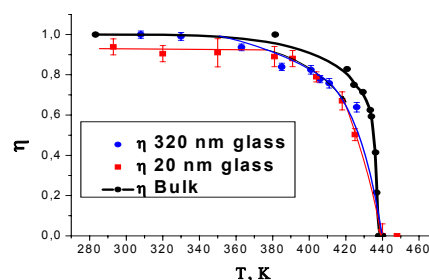


Fig. 1 Temperature dependences of order parameter for the bulk (black circles), embedded into 320 nm porous glasses (blue circles) and 20 nm porous glasses (red squares)

[1] A. Naberezhnov et al., Eur. Phys. J. E **12**, s21 (2003)

	<b>EXPERIMENTAL REPORT</b>  <b>Phase transition of shape memory NiTi wires</b>	Proposal N° MAT-01-2314-EF  Instrument <b>E9</b>  Local Contact M. Tovar
	Principal Proposer: M. Tovar Experimental Team:	Date(s) of Experiment  18/01/2008 – 23/01/2008

Date of Report: 15/01/2009

Shape memory alloys like NiTi (*"nitinol"*) get more and more impact in our daily life, i.g. as flexible glass frames, surgical instruments or as actuators in robotic systems. The memory effect bases on the crystallographic phase transition of cubic austenite to trigonal/monoclinic martensite phase. The transition takes place over a broad temperature range which depends on the composition of the alloy.

As material for studying the mechanism of the phase transition NiTi wires [1] were at disposal showing the so-called thermal shape memory effect (the wire remembers a beforehand given shape). To get information about the process on microscopic scale neutron diffraction experiments have been carried out at different temperatures and different heating and cooling conditions.

The room temperature diffractogram of the NiTi wires shows the monoclinic phase  $P2_1/m$  (martensite) reported in [2]. When heated up a phase transition to cubic phase  $Pm\bar{3}m$  (austenite) [3] starts around 300°C and is finished at 400°C (fig. 1). In this temperature region one can emboss a special shape to the wire which later on the quenched wire remembers when warmed up again.

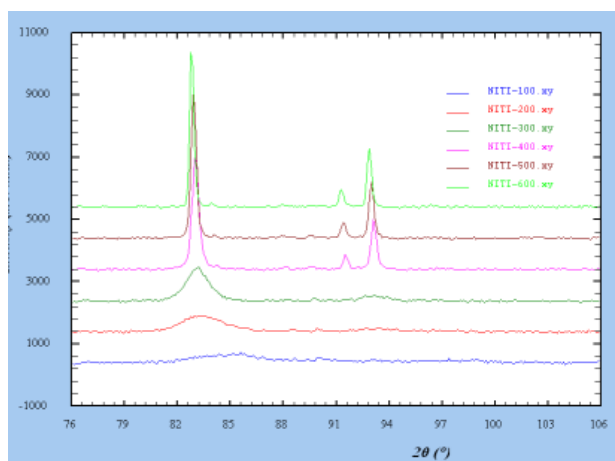


Fig. 1: Diffractogram of shape memory alloy NiTi between 100 and 600°C

The sample was further heated up to 600°C and than cooled down to room temperature. The question now was: what will be the crystallographic phases during adjacent heat (and mechanical)

treatment where the memory effect takes place? Therefore a heating run from 30° to 100°C and a cooling run back to 30°C were performed while diffraction patterns were collected every 10°.

Surprisingly the starting pattern showed a **phase mixture** of martensite/austenite phase instead of the expected pure martensite (fig. 2, blue diagram at bottom). The heating scans than reveals the phase transformation martensite-austenite at about 70°C and pure austenite phase at 90°C. In this temperature interval the thermal memory effect takes place (i.e. the wire remembers a beforehand given shape).

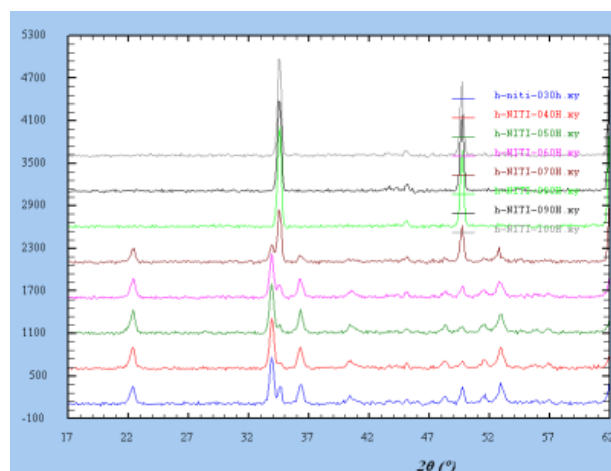


Fig. 2: Heating run of NiTi from 30 to 100°C

The adjacent cooling run from 100° down to 30°C showed that in the cooled wires the austenite phase is still present to a considerable fraction, while only slowly the martensite phase increases. This is surprising since the memory effect initially is related to a transformation from two single (pure) phases (martensite-austenite) but obviously works independently from the phase purity. Moreover it obviously just works with phase mixtures.

[1] Vendor: Memory-metalle.de

[2] Cuevas, F at al., Journal of Solid State Chemistry (2006) 179, 3295-3307

[3] Parlinski, K.; Parlinska-Wojtan, M., Physical Review, Serie 3. B – Cond. Matter (2002) 66, 064307-1-064307-8

	<b>EXPERIMENTAL REPORT</b>	Proposal N° MAT-01-2318-EF
	<b>Investigation of phase transitions of 4 mol% yttria stabilized zirconia using neutron scattering</b>	Instrument <b>E9</b> Local Contact O. Prokhnenko
Principal Proposer: V. Ryukhtin, TU Berlin and HZB, Berlin Experimental Team: R. Ochrombel – DRL, Köln O. Prokhnenko, HZB, Berlin Wiedenmann – HZB, Berlin S. Bilge – DLR, Köln	Date(s) of Experiment  14/01/2008 – 16/01/2008	

Date of Report: 15/01/2009

Partially yttria stabilized zirconia (PYSZ) is very promising ceramics material. It can be used for deposition of thermal barrier coatings (TBCs) on turbine blades (TB). This material is widely used for coating of TB by means of electron beam physical vapor deposition (EB-PVD) [1]. However, 4 mol%  $Y_2O_3$ - $ZrO_2$  TBCs show phase instability [2, 3]. Thereby, PYSZ passes a cascade of phase transitions, which is still not completely understood. This irreversible process is thermal activated. The fact of phase instability is relevant for a technical application of this as TBC-material. We employed neutron powder diffraction method in order to investigate a dynamic of phase transition in dependence of grain size in PYSZ. With high resolution and fast scanning time it is a good tool to separate several phases.

Rietveld refinement of the sample measured at room temperature is shown in Fig. 1. Analysis of this pattern has been detected cubic and monoclinic phases of  $ZrO_2$ . At temperatures higher than 900 °C a third phase – tetragonal one – become visible.

The results are needed to choose of optimal morphologies of PYSZ TBC for stabilization phase transition. This information will be used for estimation of influence of different phases in PYSZ on thermal resistivity and mechanical properties of such kind TBCs.

### References

1. J. R. Nicholls, M. J. Deakin, D. S. Rickerby Wear, Volumes 233-235, December 1999, Pages 352-361.
2. U. Schulz, J. Am. Ceram. Soc. 83 (4) 904-10 (2000).
3. G. Witz, V. Shklover, W. Streuer: Investigation of phase transition of 4mol% Yttria stabilized zirconia. J. Am. Ceram. Soc. 90 [9] 2935-40 (2007).

### Acknowledgment

*This research project has been supported by the DFG project (Wi 1151/4-1).*

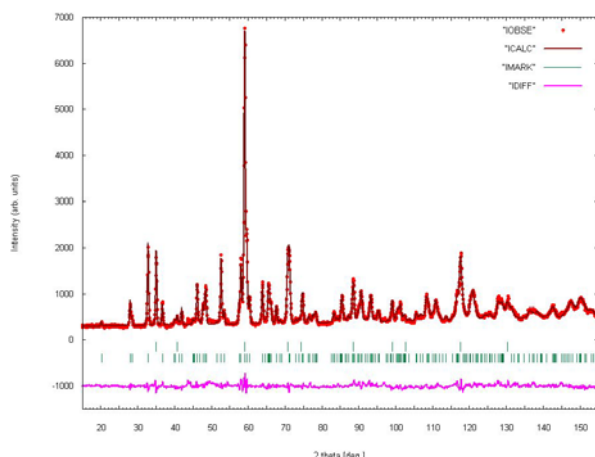


Fig. 1. Neutron PDF pattern of PYSZ powder measured at room temperature with fitted lines.

Powder diffraction instrument E9 (HZB, Berlin) with high temperature furnace (HTF) have been used for *in-situ* PDF measurements at temperatures from room temperature to 1100 °C. Neutron wavelength was defined by (511) reflection from germanium monochromator of 1.797745 Å. Studied PYSZ powder was filled in vanadium container for the measurements.

	<b>EXPERIMENTAL REPORT</b> <b>Investigation of the structural changes of the crystalline metal organic framework (MOFs) MIL-88B up</b>	Proposal N° MAT-01-2359 Instrument <b>E9</b> Local Contact Dr. Fabiano Yokaichiya
	Principal Proposer: Dr. Ralf Köhn, Ludwig-Maximilian-Universität, München Experimental Team: Camilla Scherb, Ludwig-Maximilian-Universität, München Dr. Fabiano Yokaichiya, BENSC, Berlin Dr. Dirk Wallacher, BENSC, Berlin	Date(s) of Experiment  27/10/2008 – 30/10/2008

Date of Report: 15/01/2009

## Introduction

Due to their many potential applications such as gas sorption, molecular separation, gas storage and catalysis, MOFs have been intensively studied<sup>1</sup>. Some of these MOFs show “breathing” like response<sup>2</sup> to organics and are with respect to their application as sensors of great interest. For example, the structure of MIL-88 is very flexible and the cell constants of these materials are strongly dependent on the pore content<sup>2,3</sup>. The aim of this proposal is to study *in-situ* their structural change upon changes in atmospheres.

Using the unique DEGAS equipment available at the BENSC, attached to the E9 instrument, different measurements were performed to follow the structural changes of MIL-88B during adsorption of water molecules. Due to

the large amount of powder and the relatively low diffusion of water through the filled sample cell, single steps of the structural changes during adsorption could not be obtained. We were able to record the diffraction data of the evacuated sample and the completely hydrated sample, however. (Fig 1). The comparison shows the significant change from the empty form of MIL-88B crystals **a** to the D<sub>2</sub>O filled form **b**.

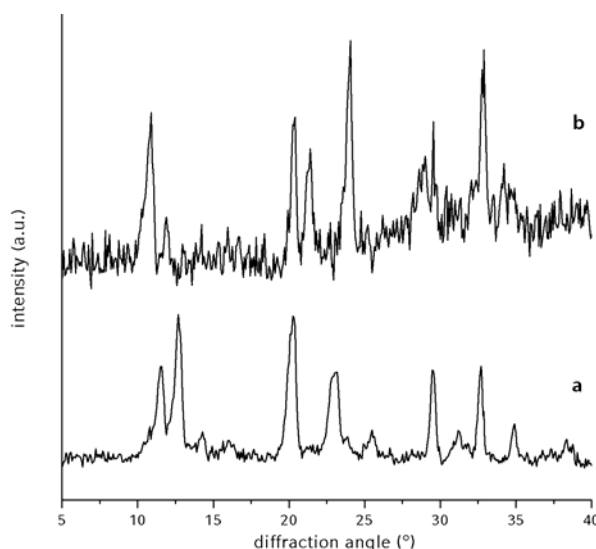


**Figure 1:** diffraction data of **a**: evacuated sample, **b**: sample exposed to liquid D<sub>2</sub>O. Scan time was different for both samples.

<sup>1</sup> a) U. Mueller, M. Schubert, F. Teich, H. Puetter, K. Schierle-Arndt, J. Pastre, *J. Mater. Chem.* **2006**, *16*, 626; b) N. W. Ockwig, O. Delgado-Friedrichs, M. O'Keeffe, O. M. Yaghi, *Acc. Chem. Res.* **2005**, *38*, 176; c) A. K. Cheetham, C. N. R. Rao, R. K. Feller, *Chem. Commun.* **2006**, 4780.

<sup>2</sup> T. Loiseau, C. Serre, C. Huguenard, G. Fink, F. Taulelle, M. Henry, T. Bataille, G. Férey, *Chem.--Eur. J.* **2004**, *10*, 1373.

<sup>3</sup> C. Mellot-Draznieks, C. Serre, S. Surble, N. Audebrand, G. Férey, *J. Am. Chem. Soc.* **2005**, *127*, 16273.



## EXPERIMENTAL REPORT

### Neutron Diffraction Studies of Polymer/Clay Nanocomposites

Proposal N° MAT-01-2252

Instrument **V1**

Local Contact  
Silva Dante/Thomas  
Hauss

Principal Proposer: F.K. Katsaros – N.C.S.R. “Demokritos”

Experimental Team: T.A. Steriotis - N.C.S.R. “Demokritos”

A.A. Sapalidis - N.C.S.R. “Demokritos”

E.P. Favvas - N.C.S.R. “Demokritos”

Date(s) of Experiment

17/06/2008 - 24/06/2008

Date of Report: 13/01/2008

The aim of this experiment was to study polymer nanocomposites using neutron membrane diffraction and to investigate thoroughly the structural changes (crystallinity, swelling, disordering and migration of clay layers) as a function of the relative humidity of the composites. V1 diffractometer was extremely well suited in this respect, not only due to its geometry but also because of the unique sample environment (in terms of controlled relative humidity) and pertinent know-how available.

Polyvinyl alcohol (Mowiol 5-88) – Bentonite nanocomposites films with clay loading of 5, 10 and 20% by weight with thickness of approximately 100 $\mu$ m were cut in 6 x 1cm rectangular shape and placed between quartz plates for the measurements.

The diffraction patterns obtained from lamellar and in-plane sample positions revealed that there is a specific orientation of bentonite plates, parallel to the film surface. This conclusion is in agreement with the results obtained from XRD measurements and gas permeability technique, in which the well organized and dispersed impermeable inorganic layers, increase the resistance in flow through the nanocomposites film, acting as gas barriers.

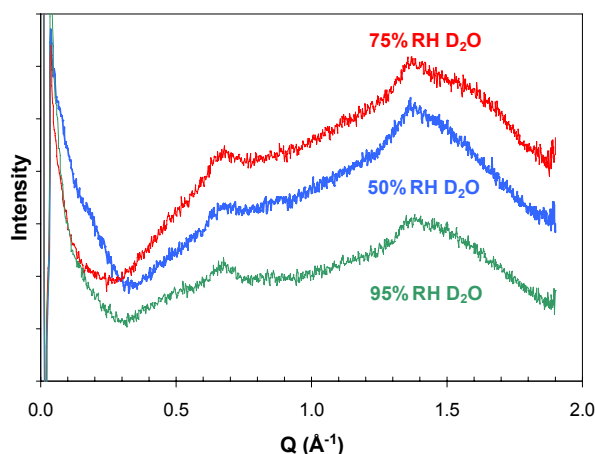


Figure 1. Neutron diffraction pattern on PVAB20 (20%wt of clay) at different D<sub>2</sub>O relative humidities

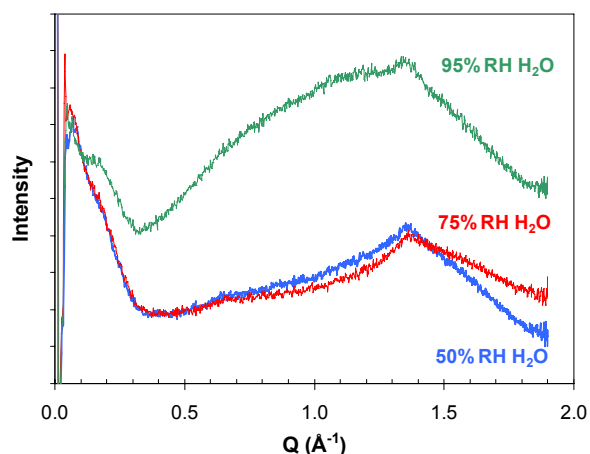


Figure 2. Neutron diffraction pattern on PVAB20 (20%wt of clay) at different H<sub>2</sub>O relative humidities

In addition, measurements on hydrated samples enabled us to enlighten specific regions of the diffraction spectra. More specifically, hydrated with H<sub>2</sub>O samples, were measured in order to monitor the structural changes as a function of the relative humidity of the composites at low Q region (inorganic rich region). On the other hand, diffraction experiments on pre-equilibrated with D<sub>2</sub>O samples revealed the structural changes in polymeric matrix, due to hydration. The obtained peak at 0.66-0.72 Å<sup>-1</sup> can be attributed to the presence of a new crystalline phase, presumably induced by the presence of the silicates.

Finally, measurements on pure PVA samples revealed a gradual dissolution of the polymer crystallites above 55% RH. At 95% RH the crystalline phase is almost disappeared. On contrary, in the case of nanocomposites, the crystallinity remains unaffected of hydration up to 95% .

#### Acknowledgements

This research project has been supported by the European Commission under the 6<sup>th</sup> Framework Programme through the Key Action: Strengthening the European Research Infrastructures. Contract n°: RII3-CT-2003-505925 (NMI 3)



## EXPERIMENTAL REPORT

### Analysis of sorption strains in SBA-15 by in-situ neutron diffraction using zero contrast water

Proposal N°  
PHY-01-2317-EF

Instrument **V1**

Local Contact T. Hauß

Principal Proposer: O. Paris – MPI Golm (Abt. Biomaterialien)  
Experimental Team: J. Prass – MPI Golm (Abt. Biomaterialien)  
D. Wallacher – HMI (SF1/BENSC)  
A. Brandt – HMI (SF1/BENSC)  
S. Dante – HMI (SF1/BENSC)

Date(s) of Experiment

13/02/2008 – 22/02/2008

Date of Report: 15/01/2008

Strains due to sorption processes are a long known effect, but it is still not clear to what extent these strains do affect the sorption process itself (1). For ordered mesoporous materials such as SBA-15 or MCM-41, diffraction methods are a powerful tool for monitoring such strains in-situ by simply measuring the shift of the Bragg reflections from the pore lattice (2). However, due to the change of the scattering contrast during sorption, slight peak shifts due to contrast effects are also possible, which might obscure the deformation of the solid pore lattice

Here we report new sorption experiments of water on SBA-15 using the DEGAS system at the V1 instrument at BENSC. To exclude contrast effects, we used a zero contrast mixture  $m(\text{D}_2\text{O})/m(\text{H}_2\text{O})=0.08/0.92$  as a sorbing fluid. The piping of DEGAS was optimized for small dead volume allowing to measure desorption branches of the isotherm with high accuracy. The different pressure regions such as bulk condensation and mesopore draining are clear and reproducible. Small-angle diffraction patterns have been measured at equilibrium conditions along the desorption branch for two independent runs. Three peaks from the 2D hexagonal lattice of SBA-15 can be easily distinguished, although they are strongly broadened as compared to X-ray measurements due to the wavelength spread and the divergence of the neutron beam. Nevertheless, strain analysis could be performed by calculation of the centroid of the first bragg peak after subtraction of a linear background and determination of the position of the primary beam for each profile. Fig. 1 summarizes calculated strains as a function of the amount of absorbed fluid. A contraction is observed between a filling factor of 0,2 and close to 1, and a distinct expansion is observed

for filling factor reaching and exceeding 1. This reproduces the contraction in the presence of menisci and the expansion due to lowered interfacial energy of the pore surface, already observed for pentane with in-situ X-ray scattering (2). The corresponding strains measured with X-rays during continuous water sorption are shown in the inset. This experiment clearly proves that these strains are not artifacts (no contrast changing due to zero contrast water), and that possible non equilibrium stages in the X-ray measurements do not influence the strain isotherms.

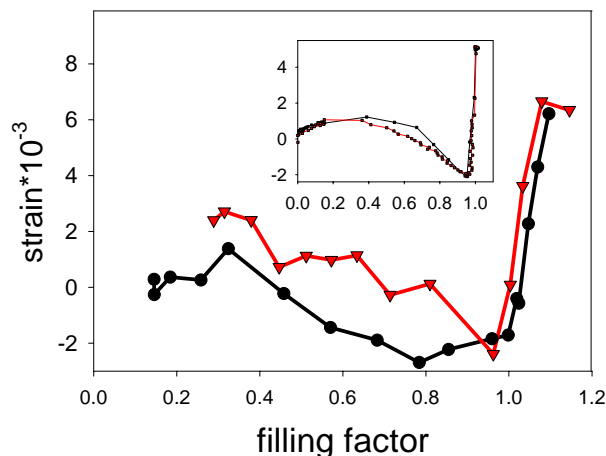


Fig. 1: Sorption strain as a function of filling factor for two subsequent desorptions of zero contrast water in SBA-15 measured with neutrons. The inset shows the corresponding data measure with XRD.

We gratefully acknowledge the financial support from the Deutsche Forschungsgemeinschaft (SFB 448).

- (1) A. Grosman, C. Ortega, *Phys. Rev. B* **78** 085433 (2008)
- (2) G. Günther, J. Prass, O. Paris, M. Schoen *Phys. Rev. Lett.* **101** 086104 (2008)



## EXPERIMENTAL REPORT

### Functional groups and pore geometry in proton-conducting mesoporous SO<sub>3</sub>H-MCM-41

Proposal N° MAT-01-2417

Instrument **V1**

Local Contact  
Astrid Brandt

Principal Proposer: Michael Wark, Leibniz University Hannover  
Experimental Team: Michael Wark, Leibniz University Hannover  
Roland Marshall, Leibniz University Hannover  
Dirk Wallacher, BENSC  
Thomas Hauss, BENSC

Date(s) of Experiment

22/07/2008 – 29/07/2008

Date of Report: 07/01/2009

During our recent stay at BENSC we studied Si-MCM-41 and three samples functionalized with SO<sub>3</sub>H groups by co-condensation synthesis reactions. The linked SO<sub>3</sub>H-groups, which are supposed to be distributed uniformly, make the material proton conducting.

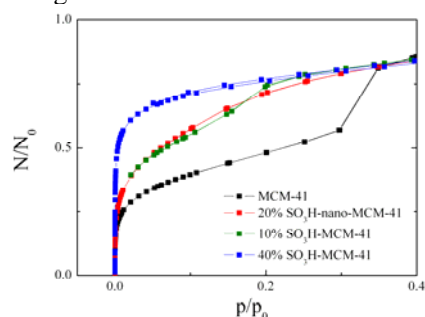


**Fig.1:** N<sub>2</sub> sorption isotherms of measured samples (micro- and mesopore region)

With increasing degree of SO<sub>3</sub>H-groups in the Si-MCM-41 samples, the ratio of micro- to mesopore volume drastically increases, leading to higher N/N<sub>0</sub> ratio in N<sub>2</sub> adsorption at low p/p<sub>0</sub> (Fig. 1).

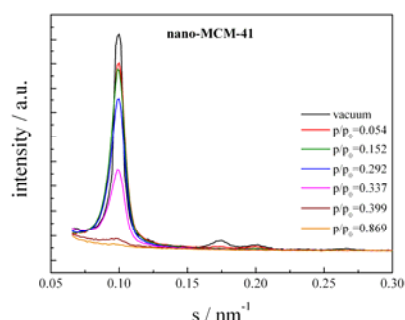


**Fig.2:** Neutron scattering patterns for nano-MCM-41

If in the pure nano-Si-MCM-41 (particle diameter: ≈ 100 nm) the pores are filled by N<sub>2</sub> adsorption, the intensity of the neutron diffraction peaks decreases (Fig.2). At low N<sub>2</sub> partial pressure (p/p<sub>0</sub> < 0.1) first the (110) reflection loses intensity, leading to a reversal of the intensity ratio of the (110) and the (200) reflection. The intensity of the (100) reflection, however, decreases significantly only when the whole mesopore channels are filled at p/p<sub>0</sub> > 0.3. This behavior confirms a model proposed for micro-/mesoporous SBA-15 basing on in-situ SAXS studies discussing as first step a growth of a liquid-like film at the walls.

Our SANS investigations showed that both, the anchored SO<sub>3</sub>H-propylsilanes as well as the adsorbed N<sub>2</sub>, decrease the neutron scattering, because both reduce the electron density contrast between the channel pores and the framework walls. If 10 % of the wall silica atoms are linked to SO<sub>3</sub>H-propyl groups again first the (110) and (200) reflections are almost disappearing indicating changes in the pore wall layer. Compared to pure Si-MCM-41, the (100) reflection decreases in intensity at much lower N<sub>2</sub> partial pressures indicating again the formation of smaller micropores (Fig. 3).

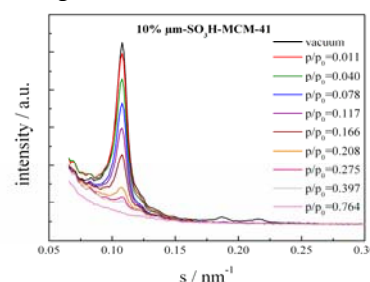


**Fig. 3:** Neutron scattering patterns for 10%μm-MCM-41

Increasing functionalization increases the relative amount of micropores further and the step at p/p<sub>0</sub> ≈ 0.3, indicating filling of mesopores, disappears (Fig. 1). Consequently, also the intensity of the (100) reflection, measured in vacuum, decreases and for 40% functionalization it is completely gone. N<sub>2</sub> adsorption in this sample reduces the background scattering at s < 0.1 indicating the filling of the remaining micropores.

In summary, by combining N<sub>2</sub> adsorption and neutron scattering we could effectively discriminate between filling of micro- and mesopores and analyze the altered pore structure which is important for the interpretation of proton conduction in the samples.

The results are included in abstracts prepared for the 21<sup>st</sup> German Zeolite Meeting March 2009 in Kiel and the Bunsentagung 2009 in Cologne.

	<b>EXPERIMENTAL REPORT</b>  <b>Understanding the Water Transport between the Gel and Capillary Pores in cement pastes</b>	Proposal N° MAT-03-520 Instrument <b>V3</b> Local Contact Kemner E.
	Principal Proposer: Alridge, Laurence, ANSTO Experimental Team: Bordallo, Heloisa N., HZB	Date(s) of Experiment 23/04/2008 – 28/04/2008

Date of Report: 15/01/2009

Portland cement reacts with water to form an amorphous paste through a chemical reaction called hydration. In concrete the formation of pastes causes the mix to harden and gain strength to form a rock-like mass. Within this process lies the key to a remarkable peculiarity of concrete: it is plastic and soft when newly mixed, strong and durable when hardened. The performance of the concrete is determined by quality of the paste. Creep and shrinkage of concrete specimens occur during the loss and gain of water from cement paste. In order to better understand the role of water in mature concrete, a series of quasi-elastic neutron scattering (QENS) experiments were carried out on cement pastes with water/cement ratio varying between 0.32 and 0.6. The samples were cured for about 28 days in sealed containers with experiments were carried out with an actual sample of Portland cement rather than with the components of cement studied by other workers. The details of this work is found in the publication H. N. Bordallo, L. P. Aldridge, A. Desmedt, Water Dynamics in Hardened Ordinary Portland Cement Paste or Concrete: From Quasielastic Neutron Scattering, The Journal of Physical Chemistry: B 110 (36) (2006) 17966-17976. QENS spectra showed behaviour that was attributed to three types of water (1) chemically bound water (2) physically bound water and (3) confined water. Furthermore it was found that when the pastes were heated at 105°C no Quasi Elastic signal was detected indicating that both the physically bound and the confined water were removed. However on re-hydration only physically bound water was found.

In a follow up to this work we investigated the QENS spectra of cement pastes that had been hydrated for at least 90 days and that had been

dehydrated by exposure to saturated solutions of LiCl (with RH of 11%).

The Powers Brownyard model of cement pastes differentiates between two types of pores capillary pores and gel pores. The larger capillary pores would be expected to primarily hold the physically bound water while the confined water would be expected to be in the smaller gel pores which may be related to the interlayer water of clays. In the present work we have attempted to optimise the measurements so that we could measure the quasi elastic spectra of water confined in the gel pores.

We have also measured the QENS spectra of re-adsorbed water as a function of time. Cement paste was first heated at ~ 105 and it was confirmed that there was no quasi-elastic scattering. Then water was added and the spectra were measured. The spectra could be interpreted as showing that at first there was only physically bound water and that it took an appreciable time (hours) for the spectra of the physically bound water to become evident.

The results are rather surprising and highlight how little is known about the position of water in cement pastes. The role of water in the pastes is critical to controlling the shrinkage of the pastes and also the transmission of ions through the pastes. This is of some environmental importance as cements are used in repositories to contain radioactive wastes and this confinement will be controlled by the movement of water in the cement pastes.

We are now processing the results and fitting the data and hope to have this work completed in the near future.



## EXPERIMENTAL REPORT

### In-situ monitoring of the deformation of nanopores due to capillary forces upon vapour sorption

Proposal N° MAT-04-706

Instrument **V4**

Local Contact  
Astrid Brandt

Principal Proposer: Gudrun Reichenauer, Bavarian Center for Applied Energy Research  
Experimental Team: Matthias Wiener, Bavarian Center for Applied Energy  
Astrid Brandt, Helmholtz-Zentrum für Materialien und Energie  
Dirk Wallacher, Helmholtz-Zentrum für Materialien und Energie

Date(s) of Experiment

18/03/2008 – 20/03/2008

Date of Report:

In-situ SANS measurements were performed to investigate the relationship between the macroscopic shrinkage of highly porous materials upon capillary condensation and the corresponding structural changes on the microscopic length scale. Earlier a linear shrinkage upon capillary condensation of up to 30 % has been identified as being responsible for a tilt of the isotherm in the range of high degree of filling (Fig.1). For this study a silica aerogel with a porosity of about 90 % and a pore size of 20 nm was exposed to the adsorptive, n-pentane that was partly deuterated to provide an adsorptive with zero scattering length density. For controlled dosing the DEGAS (volumetric sorption) setup was applied. As a consequence of the zero coherent scattering of the adsorbens, the coherent scattering patterns observed at different degrees of pentane filling directly reflect the structural changes of the silica backbone of the monolithic aerogel (shrinkage and reexpansion effects upon capillary condensation). The plot of the scattering cross section times  $q^2$  reveals the deformation of the silica skeleton. The inserts in Fig.2 indicate the structures involved on different length scales.

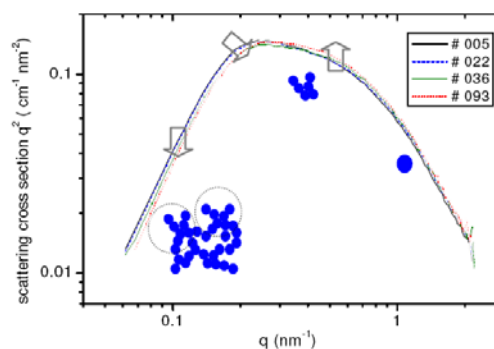


Fig.2: Scattering cross section multiplied by  $q^2$  for different degrees of pore filling upon adsorption (arrows indicate changes).

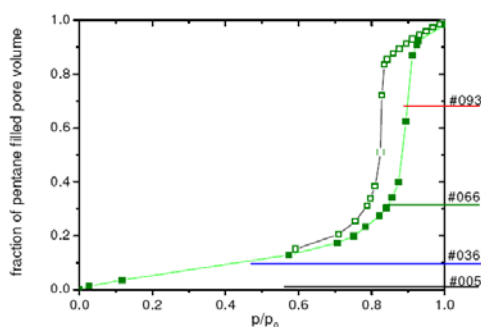


Fig.1: Pentane isotherm (from gravimetric experiment) for the monolithic silica aerogel investigated (density about 0.28 g/cm<sup>3</sup>, pore size about 20 nm). The numbers on the right indicate the positions of the isotherm at which SANS runs were performed (see Fig2.).

The graph reveals that effects are particularly pronounced in the  $q$ -range between 0.01 and 0.7 nm<sup>-1</sup> reflecting the mesopores in between the spherical network particles as well as at low  $q$ -values; the latter range provides information on the changes of the arrangement of the flake like clusters upon adsorption. The main problem encountered during the measurement was the huge amount of time (several hours) needed for dosing and equilibration of the sample in each step of the isotherm; consequently, the time granted was not sufficient to completely fill the sample and to also investigate the desorption branch. This can significantly be improved by modifying the dosing unit of DEGAS. Another option is to fill the sample with the adsorbens externally prior to the in-situ run to investigate the desorption branch of the isotherm. In this range the compression effects are expected to be about a factor of 2 larger, consistent with findings from macroscopic length changes. The direct comparison of the detailed effects on the network structure of the aerogel upon adsorption and desorption are expected to provide an important insight in the adsorption and desorption mechanisms in disordered porous systems.



## EXPERIMENTAL REPORT

### In-situ observation of diffusion in porous membrane produced from single crystal superalloy

Proposal N° MAT-04-1559

Instrument **V4**

Local Contact  
U. Keiderling

Principal Proposer: P. Strunz, NPI Řež  
Experimental Team: P. Strunz, NPI Řež  
D. Mukherji, TU Braunschweig  
U. Keiderling, BENSC  
J. Šaroun, NPI Řež

Date(s) of Experiment

23/05/2008 – 25/05/2008

Date of Report: 14/01/2009

The diffusion of liquids and gasses is an important question for the prospective applications (e.g. separation processes, catalytic substrate) of porous metallic membrane with oriented pore structure. Understanding the diffusion can help to optimize the fabrication of the membrane by selective phase dissolution. In the initial experiment, we intended to observe the kinetics of the H<sub>2</sub>O and D<sub>2</sub>O diffusion through the membrane. D<sub>2</sub>O lowers the scattering contrast when filled into the pores of the Ni<sub>3</sub>Al ( $\gamma'$ ) membrane, H<sub>2</sub>O increases it. The degree of filling of the pores and thus diffusion rate could be in principle determined when performing a time-resolved experiment.

The 0.7mm thick porous membrane (based on CMSX4 superalloy) was tested at several Q-ranges in order to select the most suitable one for the kinetics experiment. The fluid was filled in the reservoir of a special cell on one side of the porous membrane and was allowed to flow through the pores under ambient pressure. It was, however, found that the pores are occupied very quickly, already during the time between the reservoir filling and the measurement start, i.e. in the time span of less than 20s. A similar test as with water was done with silicon oil but with the same result.

After removal of D<sub>2</sub>O from the reservoir (i.e. both surfaces are on air), the evaporation of liquid from the pores occurs. Due to the enormous scattering from the freed pores, the scattering intensity increase can be clearly observed as the evaporation proceeds. It can be estimated, that 0.5  $\mu$ m depth (per surface) is emptied each minute. Although only very rough estimation of the diffusion is obtained, the data can be used for microstructural characterization of the membrane and for the determination of the scattering length density (SLD) of the porous membrane walls (originally  $\gamma'$  rafts of CMSX4 alloy).

Some of the measured and fitted V4 data are depicted in Fig. 1. The subsequent measurement at the double-bent-crystal SANS facility (NPI Řež) enabled to determine the average distance between the longitudinal pores (4770 Å; the interparticle interference maximum from Bragg-

like scattering on the ordered rafts clearly visible in Fig.1). When employing this value, the V4 SANS data can be evaluated in more detail. By combining data from both facilities, the average thickness of the rafts was found to be 2800 Å and its volume fraction 64%. Consequently, the volume fraction of pores should be around 36%. The specific interface between  $\gamma'$  phase and the pores was determined to be 49000 cm<sup>2</sup>/cm<sup>3</sup>. SLD of the  $\gamma'$  rafts was determined to be 73.0×10<sup>9</sup> cm<sup>-2</sup> (assumed SLD of the CMSX4 alloy 67.27×10<sup>9</sup> cm<sup>-2</sup>, calculated from the composition). Consequently, SLD of the  $\gamma$  matrix can be back-calculated: 57.3×10<sup>9</sup> cm<sup>-2</sup>.

The model of the pore microstructure resulting from the optimum fit is also depicted in Fig. 1.

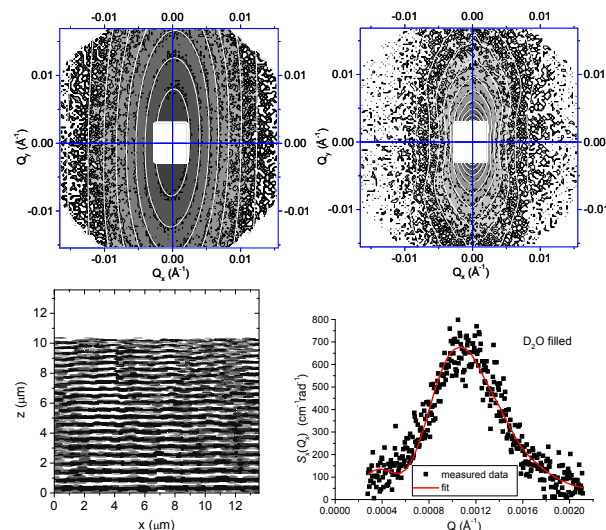


Fig. 1. Top: V4 data for unfilled (left) and D<sub>2</sub>O filled (right) membrane. Gray scale map shows measured 2D data and the white equi-intensity lines depict the fitted curve. Bottom: The projection of the 3D microstructure model fitted to the data (left) and scattering curve for D<sub>2</sub>O filled pores (right).  $S_x(Q_x)$  is the cross-section  $d\Sigma/d\Omega(Q_x, Q_y)$  integrated over the vertical angular component.

*This experiment was supported by EC under FP6 through the project RII3-CT-2003-505925 (NMI 3).*



## EXPERIMENTAL REPORT

### Characterization of porosity microstructure in PYSZ-based TBC coatings using SANS

Proposal N°  
MAT-04-1607-EF

Instrument **V4**

Local Contact  
V. Ryukhtin

Principal Proposer: V. Ryukhtin, TU Berlin and HZB  
Experimental Team: R. Ochrombel – DLR Köln  
D. Wallacher – HZB, Berlin  
Wiedenmann – HZB, Berlin  
S. Bilge – DLR Köln

Date(s) of Experiment

15/01/2008 – 18.01.2008  
14/05/2008 – 18/05/2008

Date of Report: 15/01/2009

Small-angle neutron scattering (SANS, V4) with *in-situ* high temperature furnace (HTF-1) was employed for study of porosity in turbine blade coatings (TBC) samples. Material of samples was partially (7 mol%) and fully (14mol%) stabilized by yttria zirconia (PYSZ and FYSZ respectively) which have been prepared by electron beam physical vapor deposition (EB-PVD) method [1]. The measurements have been conducted at V-4 instrument with neutron wavelength of  $\lambda=6.05 \text{ \AA}$  and sample-detector (SD) distances 1, 4 and 16 m. Temperature program was as following: room temperature, 500 °C, 700 °C, 900 °C, 1000 °C, 1100 °C, cooling down, room temperature. The samples were kept at all temperature points for 1 hour, cooling down took about 5-7 hours. In-situ thermal treatment was done in vacuum.

Fitting of the SANS data has been done using SASPROFIT software [2], with free size distribution of ellipsoidal particles. A model of prolate ellipsoids (with aspect ratio  $R/r > 1$ ) has been chosen for the simultaneous fitting of SANS data taken at sample to detector distances (SD) 1 m and 4 m. At these distances SANS instruments covers Q range which mainly corresponds to small pores and influence on scattering of very large pores (intercolumnar) is negligibly small.

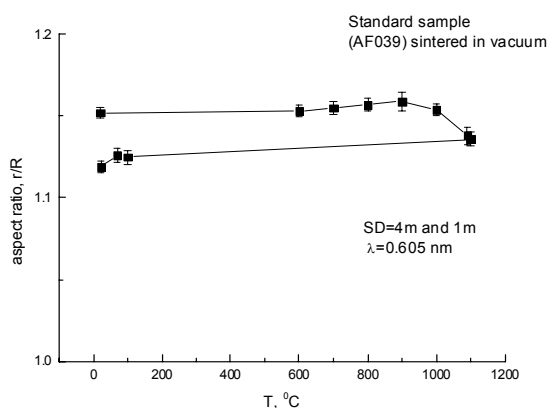


Fig. 1. Changing of pores anisotropy in standard PYSZ TBC sample during temperature treatment.

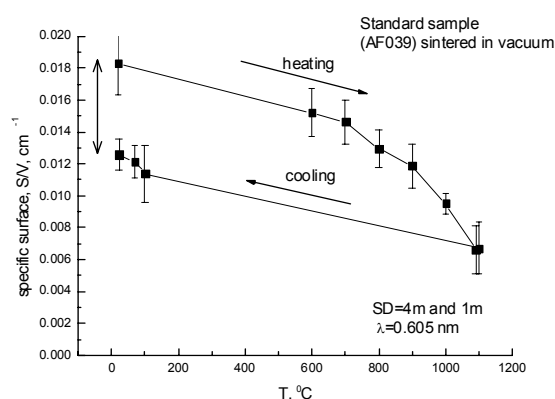


Fig. 2. Specific surface of pores in standard PYSZ sample measured by SANS in dependence on temperature.

Fitted free output parameters – overall aspect ratio and specific surface – are shown in Fig. 1 and Fig. 2 respectively for standard (rotation speed during EB-PVD was 12 rpm) PYSZ TBC. Both characteristics have irreversible dependence. The aspect ratio remains constant up to 900 °C than decreases and keeps same value during cooling down. However, specific surface has different behaviour during thermal aging – it starts to decrease from very beginning of heating. Analysis of these data permits us to describe thermal aging process and compare it for PYSZ and FYSZ TBCs.

#### References

1. J. R. Nicholls, M. J. Deakin, D. S. Rickerby Wear, Volumes 233-235, December 1999, Pages 352-361.
2. J. Šaroun, J. Appl. Cryst (2000) 33, 824-828.

*This research project has been supported by the the DFG project (Wi 1151/4-1).*



## EXPERIMENTAL REPORT

### SANS investigations of porosity structure in thermal barrier coatings

Proposal N°  
MAT-04-1712-EF  
Instrument **V4**  
Local Contact  
V. Ryukhtin

Principal Proposer: V. Ryukhtin, TU Berlin and Helmholtz Zentrum Berlin  
Experimental Team: R. Ochrombel – DLR Köln  
S. Prévost – HZB, Berlin  
A. Wiedenmann – HZB, Berlin  
S. Bilge – DLR Köln

Date(s) of Experiment

18/08/2008 – 22/08/2008

Date of Report: 15/01/2009

Small-angle neutron scattering (SANS) technique was employed for investigation of porosity in turbine blade coatings (TBC). Partially (7 mol%) and fully (14mol%) stabilized by yttria ZrO<sub>2</sub> samples (PSYZ and FYSZ respectively) have been grown by electron beam physical vapor deposition (EB-PVD) method for this measurements. We used matching liquid in order to distinguish open and close porosity contribution in scattering since the porous microstructure is rather complex in such TBCs [1]. Measurements have been carried out at neutron wavelength of  $\lambda=6.05$  Å and sample-detector (SD) distances of 1 m and 4 m. Mixture of D<sub>2</sub>O (89 wt%) and H<sub>2</sub>O (11 wt%) was used for “shadowing” of open pores since it has the same scattering length density value ( $SLD=55.5 \cdot 10^{10} \text{ cm}^{-2}$ ) as the ceramic matrix.

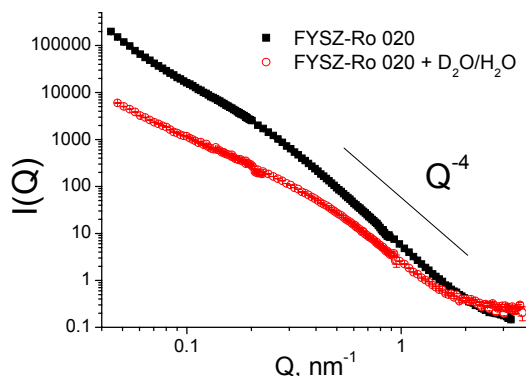


Fig. 1. SANS scattering of FYSZ TBC sample measured in air (squares) and in matching liquid (circles).

Apparent Porod constants (APC) were obtained from radial averaged SANS data measured for virgin (as-deposited) and thermally aged (100h at 1100 °C in air) PSYZ and FYSZ TBCs. The rotation speed influences porous microstructure in TBC [2]. Dependences of these APC values on rotation speed during deposition for FYSZ are shown in Fig. 2. High-Q region of SANS data

( $Q>0.5 \text{ nm}^{-1}$ ) were used for fitting. Incoherent background was included in scattering procedure for data measured in D<sub>2</sub>O/H<sub>2</sub>O.

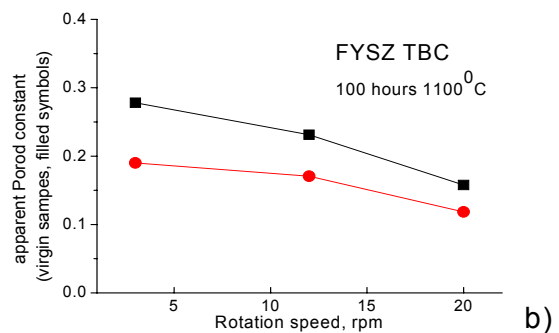
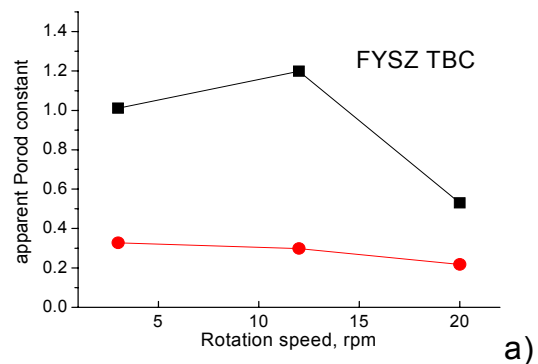


Fig. 2. Apparent Porod constants for virgin (a) and aged (b) FYSZ TBCs measured by SANS in air (squares) and in matching liquid (circles).

### References

- U. Schulz and M. Schmücker, Mater. Sci. Eng. 276 (2000), p. 1.
- U. Schulz, S.G. Terry and C.G. Levi, Materials Science and Engineering. A, Structural Materials: Properties, Microstructure and Processing 360 (2003), p. 319.

*This research project has been supported by the DFG project (Wi 1151/4-1).*

	<b>EXPERIMENTAL REPORT</b> <b>An investigation of water propagation at membrane on PEMFC using Neutron Imaging Technique</b>	Proposal N° OTH-04-1223 Instrument <b>V7</b> Local Contact N. Kardjilov
	Principal Proposer: TaeJoo Kim, KAERI, P.O.B. 105, Yuseong, DaeJeon, 305-600, Korea, +82-42-868-8521 Experimental Team: CheulMuu Sim, KAERI, P.O.B. 105, Yuseong, DaeJeon, 305-600, Korea, +82-42-868-8612 N. Kardjilov, HMI	Date(s) of Experiment  07/02/2008 – 08/02/2008

Date of Report: February 2009

The purpose of our experiments is to measure the cross-sectional water distributions within the layers of PEM fuel cells under different conditions

For these experiments, we designed and made a very simple PEMFC. The water and air are supplied into the each channel. At the initial stage, the water will only occur on local areas of GDL nearby the channel and then it may propagate into the larger area of the GDL. With conventional physical-models, it is difficult to estimate the water fraction at each layer and its propagation length accurately enough. Moreover, the water in-depth position is also important.

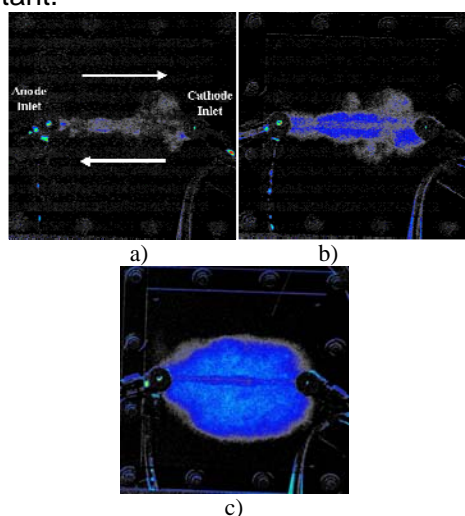


Fig. 1. Test result of horizontal case, a) before supplying, b) after 1000 sec, and c) after 5400 sec

Figs.1 and 2 are test results of horizontal and vertical cases, respectively. Black area at processed neutron image means low water and blue means high water. Although there exists some water before supplying the hydrogen and air into PEMFC as shown as Fig.1-a), the water propagation was well visualized from channel to MEA by neutron imaging technique when comparing from Figs.1-a), 1-b) to 1-c). Especially since the thickness of MEA is less than 300  $\mu\text{m}$ , the maximum thickness of water at MEA is less

than 300  $\mu\text{m}$  and the water distribution and behavior was well measured. It shows the power of neutron imaging technique.

When checking the Fig.1-c), the propagation length between higher part and lower part is different. The propagation length of lower part is bigger than that of higher part. It seems that the gravitational force might affect the water distribution and propagation. These results conform by the Fig.2-c). Since gravitational force is same between right and left part for the vertical case, the propagation length is similar.

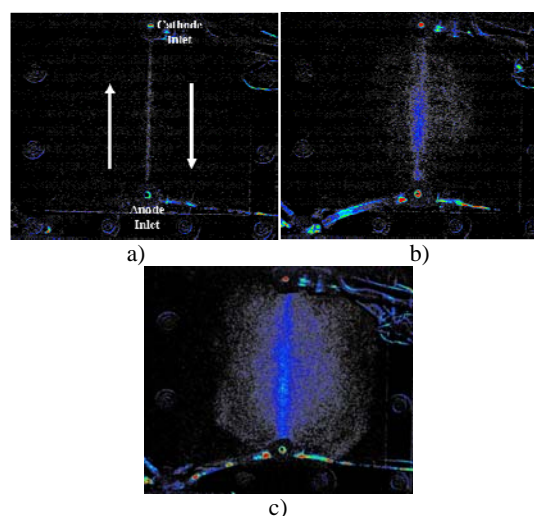


Fig. 2. Test result of vertical case, a) before supplying, b) after 1000 sec, and c) after 6300 sec

#### References

1. J. Scholta, G. Escher, W. Zhang, L. K"uppers, L. J"orissen, and W. Lehnert, " Investigation on the influence of channel geometries on PEMFC performance", *Journal of Power Sources* 155 (2006) 66–71
2. S. Shimpalee, J.W. Van Zee, "Numerical studies on rib & channel dimension of flow-field on PEMFC performance", *International Journal of Hydrogen Energy* 32 (2007) 842 – 856
3. C. Xu and T.S. Zhao, "A new flow field design for polymer electrolyte-based fuel cells", *Electrochemistry Communications* 9 (2007) 497–503



## EXPERIMENTAL REPORT

### Combined local current distribution measurements and neutron radiography of operating DMFCs

Proposal N° MAT-04-1492  
MAT-04-1588-LT  
Instrument V7  
Local Contact  
Nikolay Kardjilov

Principal Proposer: A. Schröder – Forschungszentrum Jülich GmbH, Jülich  
Experimental Team: K. Wippermann – Forschungszentrum Jülich GmbH, Jülich  
I. Manke – HZB, Berlin  
N. Kardjilov – HZB, Berlin  
André Hilger – HZB, Berlin  
J. Schloesser, S. Petrov – HZB, Berlin

Date(s) of Experiment

19/02/2008 – 22/02/2008  
23/06/2008 – 27/06/2008  
09/11/2008 – 16/11/2008

Date of Report: 08/01/2009

Both the uneven fluid distribution and the concentration decrease of the reactants over the active area along the flow field channels lead to a pronounced inhomogeneous current distribution as well as to a power loss and increased ageing of direct methanol fuel cells. With the knowledge of the local distribution and transport phenomena of CO<sub>2</sub> bubbles and water droplets at different operation modes, investigations on the improvement of cell components and design are possible.

Measurements using segmented circuit boards provide insight into the current distribution of the whole active area. To find the reason for this distribution, a further measurement technique is mandatory, detecting the CO<sub>2</sub> and water distribution. Neutron radiography has shown to be an applicable method (1, 2). As the neutron radiation is strongly attenuated by hydrogen-rich liquids and less affected by the solid cell components, areas filled with water can easily be distinguished from areas filled with CO<sub>2</sub>. Applying exposure times of about 10 s, the resolution of through-plane radiographs is up to 45 μm. A combination of neutron radiography and segmented current measurement results in an in situ correlation of the current and fluid distribution.

Measurements with different flow field geometries confirmed the suitability of the combination of these two in situ measurement techniques. The measurements were carried out during DMFC operation at varying cell currents and stoichiometric factors. Applying exposure times of 10 s, the development of CO<sub>2</sub> bubbles on the anode side and the formation of water droplets on the cathode side could be well observed.

An exemplary result shows a flooding effect: Special conditions lead to a flooding of the cathode channels with water (Fig. 1) causing a depletion of oxygen and therewith a reduction of current at the flooded areas (Fig. 2).

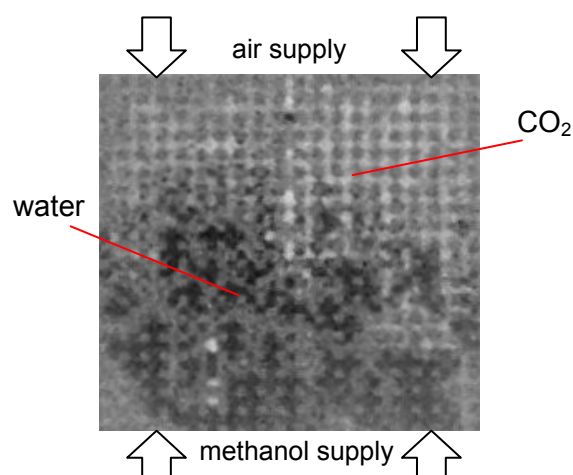


Fig. 1: Normalized neutron radiograph, 300 mA/cm<sup>2</sup>, λ<sub>air</sub> = λ<sub>methanol</sub> = 4, 70 °C

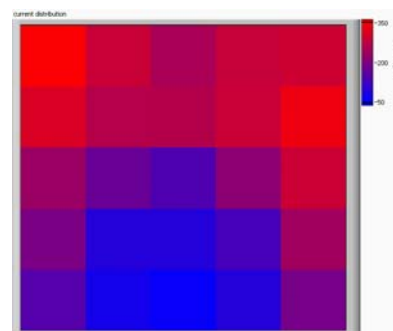


Fig. 2: Local current distribution, 300 mA/cm<sup>2</sup>, λ<sub>air</sub> = λ<sub>methanol</sub> = 4, 70 °C

#### Acknowledgement:

We gratefully acknowledge the financial support of this work by the German Federal Ministry of Education and Research (BMBF) under Grant No. 03SF0324.

#### References:

1. D. Kramer, E. Lehmann, G. Frei, P. Vontobel, A. Wokaun, G. G. Scherer, Nuclear Instruments and Methods in Physics Research A 542 (2005) 52–60
2. C. Hartnig, I. Manke, N. Kardjilov, A. Hilger, M. Grünerbel, J. Kaczerowski, J. Banhart, W. Lehnert, Journal of Power Sources, 176 (2008) 452-459



## EXPERIMENTAL REPORT

### Transmission analysis on strong absorbing boron alloyed steels

Proposal N° MAT-04-1493

Instrument **V7**

Local Contact  
Nikolay Kardjilov

Principal Proposer: Michael Zawisky, TU - ATI Wien, A  
Experimental Team: Michael Zawisky, TU - ATI Wien, A  
Eva Dyrnjaja, TU - ATI Wien, A  
Nikolay Kardjilov, HZ Berlin

Date(s) of Experiment

10/09/2007 – 11/09/2007

Date of Report: January 2009

### Objectives

The goal of the proposed experiment is the verification of enhanced neutron transmission through strong absorbing boron alloyed steels caused by hypothetical boron inhomogeneities as expected from our Monte Carlo MCNPX simulations. An intense monochromatic beam was chosen to avoid beam hardening effects and to reduce background effects.

### Achievements

The transmission measurements at V12a were successfully performed up to a thickness of 11 mm at a neutron wavelength of 0.5244 nm, and then the transmission through the boron alloyed steels reached the background limit. We found systematic deviations from the exponential transmission law, as expected from the Monte Carlo simulations. Then the measurements were repeated using a collimator in front of the samples and placing the steels directly on the scintillator screen to achieve the best spatial resolution of 200 micron. No difference in the transmission curves were found, this proves that scattering corrections are negligible in the strong absorbing steels. We also found no regions of reduced absorption in the steel. This confirms previous measurements at the Atomic Institute with thermal neutrons down to 100  $\mu\text{m}$  resolution. We could repeat transmission measurements at a wider wavelength range from 0.25 – 0.52 nm at CONRAD instrument V7. First results at 0.25 nm wavelengths are promising even at 11 mm thickness we achieved sufficient transmission above the background limit. In all measurements pronounced deviations from the exponential transmission law have been detected.

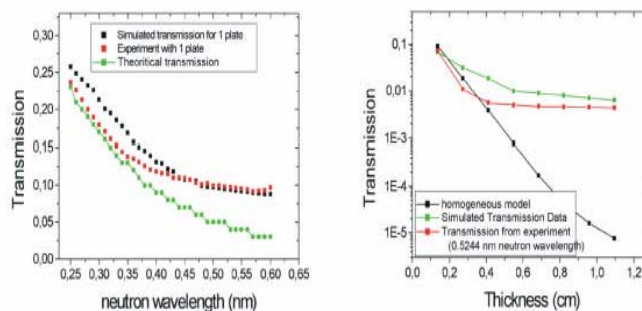


**Fig.1.** Left; the transmission values for one plate with 0.137 cm thick scanned from 0.25 to 0.6 nm neutron wavelength at CONRAD instrument compared with calculated exponential law and simulated transmission values versus given wavelength while the deviation from exponential law is clearly detected. Right; transmission of boron steel alloy plates with monochromatic neutron beam at 0.5244 nm compared with simulated model which describes inhomogeneities of boron distribution in steel matrix.

### Acknowledgement

We would like to thank M. Strobl, P. Walter, O. Seidl, N. Kardjilov for their support and assistance during our stay at HMI-Berlin.



**EXPERIMENTAL REPORT**

**Combined neutron and impedance spectroscopy measurements for water detection in a PEM fuel cell**

Proposal N° MAT-04-1588-LT
Instrument <b>V7</b>
Local Contact N. Kardjilov
Date(s) of Experiment 24/08/2008 – 30/08/2008

Principal Proposer: R. Kuhn, ZSW  
 Experimental Team: R. Kuhn, Ph. Krüger, J. Kacerowski, Ch. Hartnig, ZSW  
 A. Hilger, N. Kardjilov, I. Manke, HZB

Date of Report: January 2009

A low temperature PEM fuel cell, which is very close to a commercial one, was tested.

A long term observation has been carried out. Neutron radiography (NR) was used for the visualisation of the liquid water evolution in the cell. In parallel, an electrochemical impedance spectroscopy (EIS) over the whole cell was measured.

The cell temperature was 53°C. On cathode side the utilisation was set to 60% and the humidification temperature of the air was also constant at 35°C. On the anode side, hydrogen was humidified with 25°C and utilization was 20%.

For calculating the intensity, which is an indicator for the amount of water, the current images were divided by a dry cell image. Also a beam correction was done every 15 min.

For the interpretation of EIS data a larger variety of equivalent circuit diagrams are known which describe the performance of a PEM- fuel cell (s. fig.1). Physical meanings and values are assigned to the electrical components. The EIS measurements were done with a Zahner IM6 / EL 300 in a range from 100 mHz to 10 kHz.

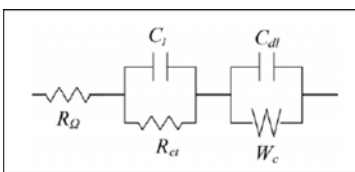


Fig 1: Simple example of an PEMFC equivalent circuit

Figure 2 shows the recorded spectra. The frequencies increase from the right to the left site. The measurement points at high frequencies give the value for the membrane resistant  $R_{\Omega}$ , which is strongly influenced by the membrane water content. On the right site of the diagrams the diffusion limitation can be derivate.

Figure 2 A gives an idea of the behaviour at different current densities. At high current densities the membrane gets wetter and wetter (decreasing of  $R_{\Omega}$ ), and the diffusion limitation increases.

Figure 2 B shows the difference between low and high humidification conditions.

In this images the global amount of water is available, but only in 2-D. This makes it difficult to differentiate between the water in the gas diffusion layer (GDL) / membrane and the water in the gas channels. The combined measurement of NR and EIS makes this possible.

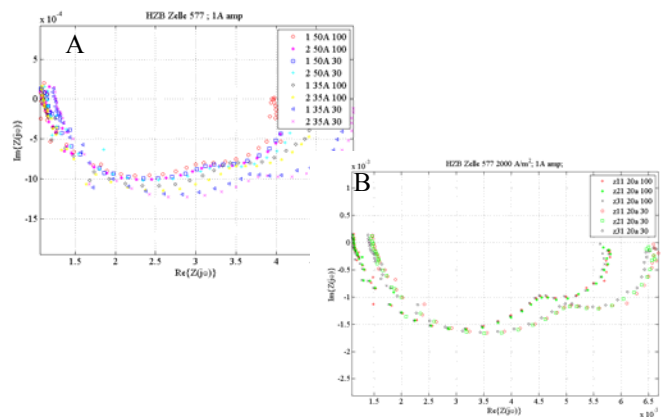


Fig 2: Results of the spectroscopy

In Figure 3 the images show the difference between 2000 and 5000 A/m². Note that the operating conditions are chosen in a way, that under ideal conditions the air outlet flow should have the same humidification and should be below 100% r. h.

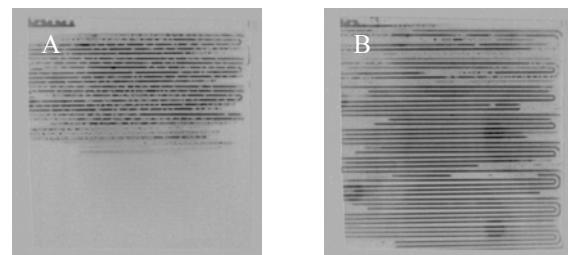


Fig. 3: 2000 A/m<sup>2</sup>                      5000 A/m<sup>2</sup>

A first result indicates that the gas flow velocity has much more on the equilibrium water content in the GDL as the current density has. One reason can be the convective entry in the GDL at higher flow rates (drying the GDL).

To insure the reproducibility the problem occurs that the experiment before us had an influence of the used beam. So a suitable compensation of this effect is under development. This will help for a much more detailed analyse of the data.



## EXPERIMENTAL REPORT

### Energy selective imaging of structural materials

Proposal N° MAT-04-1685

Instrument V7

Local Contact  
N. Kardjilov

Principal Proposer: L. Josic, Paul Scherrer Institut (PSI), NUM, NIAG, Switzerland  
 Experimental Team: N. Kardjilov, Helmholtz-Zentrum Berlin (HZB), Germany  
 A. Hilger, Helmholtz-Zentrum Berlin (HZB), Germany  
 A. Hilger, Helmholtz-Zentrum Berlin (HZB), Germany  
 M. Dawson, Helmholtz-Zentrum Berlin (HZB), Germany  
 M. Tamaki, TAMAKI Memorial Institute, Japan  
 E. Lehmann, Paul Scherrer Institut (PSI), NUM, NIAG, Switzerland

Date(s) of Experiment

24/11/2008 – 30/11/2008

Date of Report: 24/02/2009

Energy selective neutron imaging has been performed at cold neutron imaging beam line CONRAD (V7 instrument) of HZB. Samples of different structures and purposes were investigated in order to understand their scattering behavior in transmission mode with high spatial resolution.

Powders, powder mixtures and polycrystals of different materials were scanned in the broad energy range to investigate scattering cross sections and sample structures. In the Fig. 1. examples of Fe and Cu are shown together with theoretical evaluations and experimental data from the cold neutron imaging beam line ICON (PSI, CH). It can be seen that experimental data agree well in first order with theoretical predictions and deviations indicate textures in materials (the absence or suppression of the first Bragg edge). The objective of this investigation was to confirm scattering cross sections of different materials for the application in the quantitative radiography and tomography.

In welded materials energy selective neutron imaging at specific neutron energies can detect structural changes in details (Fig. 2). Measured images do not show any similarities to any other available imaging technique (e.g. optical). The objective of this part of the experiment was to investigate structural changes in industrial materials during manufacturing processes.

In the third part of the experiment the mosaicities of several single graphite monocrystals were measured. The objective of this investigation was a development of the energy selective option for the polychromatic neutron beam. It was shown that the mosaicity is conveniently given by the Gaussian function of the neutron transmission trough the crystal as a function of the angle  $\theta$  which corresponds to the neutron wavelength  $\lambda$  ( $\lambda=2d\sin\theta$ ,  $d$ -the distance between planes in the crystal). The minimum of the Gaussian function  $\theta_c$  is the rotation angle of the crystal in respect to the initial polychromatic neutron beam direction for which the corresponding wavelength  $\lambda_c$  is the most attenuated by the crystal. Using at least two crystals and changing the value  $\theta_c$

of each crystal enables an extraction of the wanted wavelength  $\lambda$  (Fig 3).

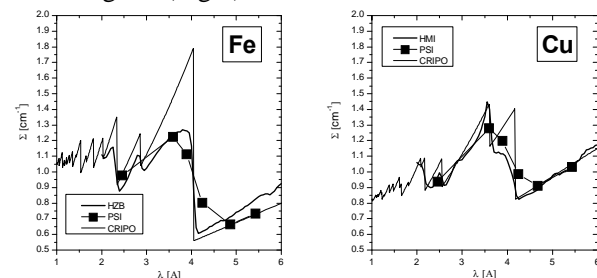


Fig 1. Comparison of the experimental data (HMI, PSI) with theoretically evaluated data (CRIPO) for Fe and Cu. The presence of textures are shown.

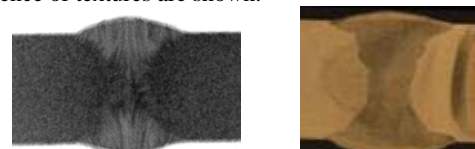


Fig 2. Left: Neutron image of X-type of weld at a single energy. Right: Optical image of the same weld. The difference in the images is clearly shown.

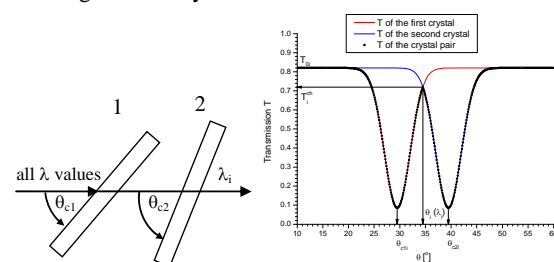


Fig 3. The principle of the extraction of the wanted wavelength  $\lambda_i$  from the initial polychromatic neutron beam. Transmissions of single crystals are given by their mosaicities (red and blue lines). The resulting transmission of the crystal pair is shown with open symbols.

*This research project has been supported by the European Commission under the 6<sup>th</sup> Framework Programme through the Key Action: Strengthening the European Research Infrastructures.*

*Contract n°: RII3-CT-2003-505925 (NMI 3).*



## EXPERIMENTAL REPORT

### Fracture of a mechanically constrained Ni-Mn-Ga single crystal after extended magnetic cycling

Proposal N°  
MAT-04-1724-EF  
Instrument **V7**  
Local Contact  
André Hilger

Principal Proposer: Markus Chmielus (HZB), Rainer Schneider (HZB), Katharina Rolfs (HZB), Peter Müllner (Boise State University)  
Experimental Team: André Hilger (HZB), Andreas Paulke (HZB), Markus Chmielus (HZB)

Date(s) of Experiment  
  
21/07/2008

Date of Report: 14/01/2009

In a previous study [1], magnetic-field-induced strain (MFIS) had been measured for a Ni-Mn-Ga single crystal in a rotating magnetic field of 0.97 T for a total of 100 million cycles. The MFIS increased from below 0.5% during the first 20,000 magneto-mechanical cycles to above 1.2% at 250,000 cycles. After a maximum MFIS of 2.1 % at 0.6 million cycles was reached, the MFIS decreased slowly and stayed nearly constant for the final 30 million cycles. After the test was stopped, cracks were found on the surface of the sample. In the present work, these cracks were examined using x-ray micro computer tomography and optical microscopy. The sample was examined for cracks with micro computer tomography (Fig. 1) and optical microscopy (Fig. 2) after it had been cycled for 100 million cycles in a 0.97 T magnetic field.

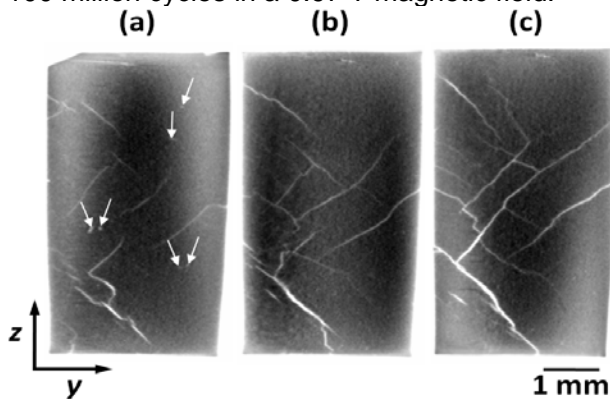


Figure 1: Micro computer tomography micrographs after 100 million magneto-mechanical cycles. Slice (a) represents a cross section close to the surface of the sample, slice (b) a cross-section in the center of the sample, and slice (c) a cross-section at the side opposite to slice (a).

In the lower and upper quarter of the sample, all cracks are found to be parallel to each other, while in the center, cracks are also seen that are perpendicular to each other. The distance between parallel cracks longer than 1 mm is 0.5 mm or more. All cracks form an angle of approximately 45° with the lateral surfaces and,

therefore, are parallel to {110}. The micro computer tomography slices reveal pores in the sub-100 μm range marked with arrows in Fig. 1 (a). However, pores do not seem to be nucleation sites of cracks. Fig. 1 (c) is a slice taken close to the surface shown in Fig. 2.

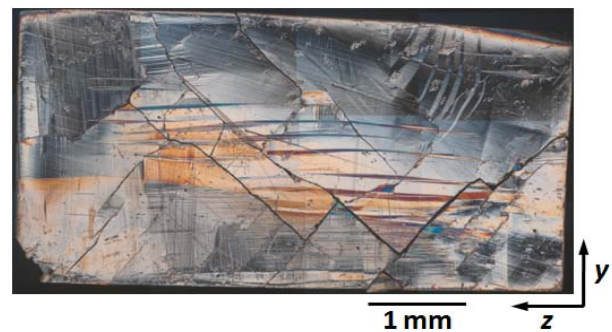


Figure 2: Optical micrograph of the surface after 100 million magneto-mechanical cycles.

Cracks are visible over the entire surface, with a higher density in the center of the sample. A static magneto-mechanical experiment (performed at Boise State University) with linear magnetic field is showing a recoverable strain increasing from less than 1% at 0.3 T to 5.9% at 1 T. These results were submitted for publication [2].

MC acknowledges funding from DFG SPP 1239 and the US Department of Energy, Office of Basic Energy Sciences Contract DEFG-02-07ER46396.

#### References

- [1] M. Chmielus et al., Training, constraints, and high-cycle magneto-mechanical properties of Ni-Mn-Ga magnetic shape-memory alloys, *Eur. Phys. J. Special Topics* **158**, 79-85 (2008).
- [2] M. Chmielus et al., magneto-mechanical properties and Fracture Of a mechanically constrained Ni-Mn-Ga Single Crystal after extended magnetic cycling, *ICOMAT 2008 Conference Proceedings*, TMS, submitted.

	<b>EXPERIMENTAL REPORT</b>	Proposal N° MAT-04-1724-EF
	<b>Influence of thermo-mechanical training of Ni-Mn-Ga single crystals on crack initialization</b>	Instrument <b>V7</b>  Local Contact André Hilger
Principal Proposer:	Markus Chmielus (HZB), Katharina Rolfs (HZB), Rainer Schneider (HZB)	Date(s) of Experiment
Experimental Team:	André Hilger (HZB) Andreas Paulke (HZB) Markus Chmielus (HZB)	21/07/2008 – 24/07/2008

Date of Report: 14/01/2009

In a previous study [1], magnetic-field-induced strain (MFIS) had been measured for a Ni-Mn-Ga single crystal in a rotating magnetic field of 0.97 T for a total of 100 million cycles. After a maximum MFIS of 2.1 % at 0.6 million cycles was reached, the MFIS decreased slowly and stayed nearly constant for the final 30 million cycles. After the test was stopped, cracks were found on the surface of the sample. In the present work, these cracks were examined using x-ray micro computer tomography [2]. In this study, the dependency of initial thermo-mechanical training was investigated on four samples. The micro computer tomography instrument uses a Hamamatsu flat panel detector and a micro focus tube with 100 kV acceleration voltage and a spot size of 7  $\mu\text{m}$ . A 200  $\mu\text{m}$  beryllium and a 1 mm aluminum filter were used to define the energy-range of the x-ray spectrum. The micro computer tomography slices reveal pores in the sub-100  $\mu\text{m}$  and 100  $\mu\text{m}$  range marked before (a) and after (b) thermo-mechanical training for all samples (sample 1 shown in Fig. 1, sample 3 in Fig. 2)

It is very interesting that no growth of cracks and no initialization of new cracks at pores, edges or other parts of the sample is visible after the thermo-mechanical training. Further investigations regarding subsequential mechanical training as well as magneto-mechanical cycling have to be performed to detect the crack initialization point of time that leads to cracks seen in [2].

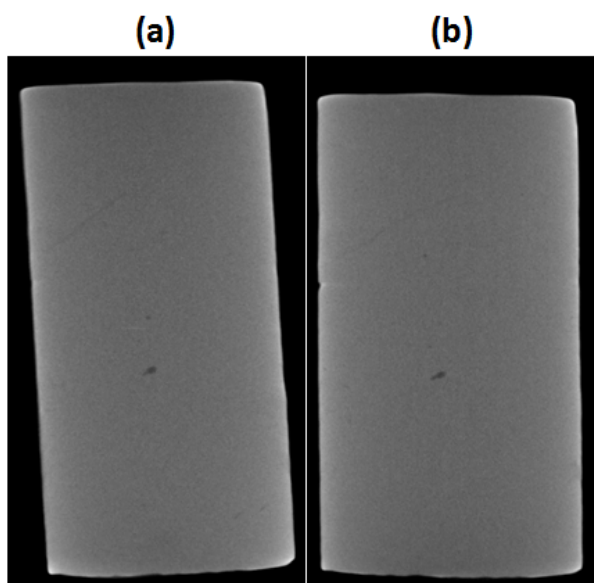


Figure 1: Micro computer tomography micrographs of sample 1 before (a) and after (b) thermo-mechanical training.

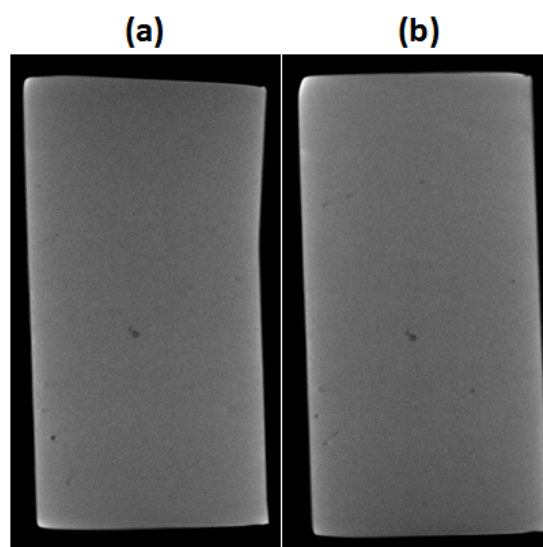


Figure 2: Micro computer tomography micrographs of sample 3 before (a) and after (b) thermo-mechanical training.

MC acknowledges funding from DFG SPP 1239.

#### References

[1] M. Chmielus et al., Training, constraints, and high-cycle magneto-mechanical properties of Ni-Mn-Ga magnetic shape-memory alloys, *Eur. Phys. J. Special Topics* **158**, 79-85 (2008).

[2] M. Chmielus et al., magneto-mechanical properties and Fracture Of a mechanically constrained Ni-Mn-Ga Single Crystal after extended magnetic cycling, *ICOMAT 2008 Conference Proceedings*, TMS, submitted



## EXPERIMENTAL REPORT

### Quantitative mapping of $\alpha$ -Fe, $\gamma$ -Fe and Fe<sub>3</sub>C phases in steels using Bragg-edge tomography

Proposal N° MAT-04-1776

Instrument V7

Local Contact  
N. Kardjilov

Principal Proposer: T. Kandemir – FH Aachen  
 Experimental Team: T. Kandemir, U. Gerling – FH Aachen  
 N. Kardjilov, A. Hilger - HZB  
 I. Manke - HZB

Date(s) of Experiment

27/06/2008 – 30/06/2008

Date of Report: 09/01/2009

The aim of this measurement was to visualize the distribution of different phases in commercial steels using Bragg-edge mapping with neutrons.

The transmission of monochromatic neutrons through a polycrystalline microstructure displays reproducible, well-defined decreases at defined wavelengths so-called Bragg-Edge phenomenon. The position of these transmission decreases corresponds to certain  $d_{hkl}$  spacing. Therefore Bragg edge mapping can be used to separate different phases in commercial steels (mat. number: 1.1730).

After generating equal starting microstructure to all samples, each sample runs through a different heat treatment inducing structural changes. Quenched bainitic and martensitic microstructures (both are containing ( $\gamma$ -Fe) Austenite), also two carbonized samples using graphite and charcoal to excite a (Fe<sub>3</sub>C) cementite phase were investigated [Fig.1].

The mapping of the phase distribution was performed using the CONRAD/V7 instrument with its option for wavelength selection. First, radiographic images of all samples and a  $\alpha$ -Fe reference sample were taken by fine-tuning the wavelength in steps from 2.0 Å to 6.0 Å. After mapping the Bragg edge positions [Fig.2] and comparing the intensities as a function of the neutron wavelength, the optimal wavelength - which produces a large intensity between (110)  $\alpha$ -Fe and (111) Austenite ( $\gamma$ -Fe)- is selected at 4,06 Å for tomography [Fig.3].

The bainitic and martensitic samples which are consisting of dendrites surrounded with Austenite in a rest matrix of  $\alpha$ -Fe were mapped and reconstructed.

A varying underground signal –caused by the near (103) Fe<sub>3</sub>C lattice plane- and the instrumental offset given by the wavelength resolution  $\Delta\lambda/\lambda$  of 3% are the limitations of the method.

#### References:

- [1] Bollenrath F., Hauk V., Müller E.H., Z Metallkd 1967;58:76.  
 [2] L. Edwards et al., ISIS Experimental Report, 2002, 12648

- [3] Martinez-Perez M.L. et al. Acta Mat. 2004 ;5303:5313  
 [4] Daymond M.R., Priesmeyer H.G. Acta Mat. 2002; 1613:1626

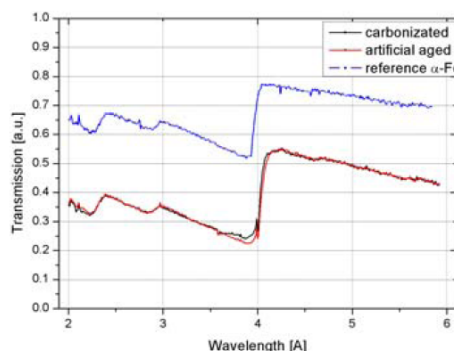


Fig. 1: Bragg-edges of reference  $\alpha$ -Fe sample (a), artificial aged martensitic sample (c) and carbonized (cementite) sample

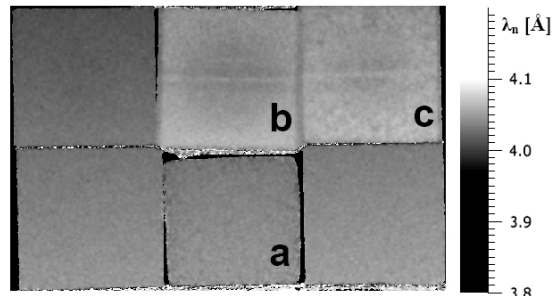


Fig. 2: Peak-position of the  $\alpha$ -Fe sample (a), bainitic sample (b) and martensitic sample (c)

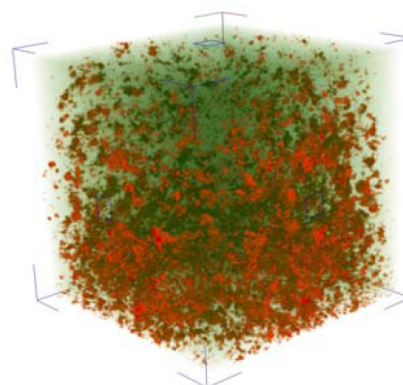


Fig.3: Tomography of martensitic sample (c) at 4,06Å.  $\gamma$ -Fe-rich phase is shown in red,  $\alpha$ -Fe-matrix in green



## EXPERIMENTAL REPORT

### Transmission analysis on strong absorbing boron alloyed steels

Proposal N° MAT-04-1480

Instrument **V12a**

Local Contact M. Strobl

Principal Proposer: Dr. Michael Zawisky; TU - ATI Wien  
 Experimental Team: M. Zawisky, TU - ATI Wien  
 E. Dyrnjaja, TU - ATI Wien  
 Markus Strobl, Helmholtz-Zentrum Berlin

Date(s) of Experiment

10/09/2007 – 12/09/2007

Date of Report: January 2009

#### Objectives

The goal of the proposed experiment is the verification of enhanced neutron transmission through strong absorbing boron alloyed steels caused by hypothetical boron inhomogeneities as expected from our Monte Carlo simulations. An intense monochromatic beam was chosen to avoid beam hardening effects and to reduce background effects.

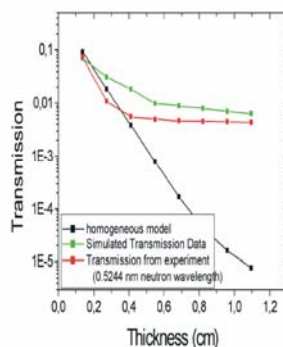
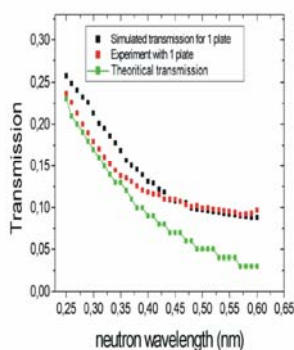
#### Achievements

The transmission measurements at V12a were successfully performed up to a thickness of 11 mm at a neutron wavelength of 0.5244 nm, and then the transmission through the boron alloyed steels reached the background limit. We found systematic deviations from the exponential transmission law, as expected from our Monte Carlo simulations. Then we repeated the measurements using a collimator in front of the samples and placing the steels directly on the scintillator screen to achieve the best spatial resolution of 200 micron. No difference in the transmission curves were found, this proves that scattering corrections are negligible in the strong absorbing steels. We also found no regions of reduced absorption in the steel. This confirms previous measurements at the Atomic Institute with thermal neutrons down to 100  $\mu\text{m}$  resolution. We could repeat transmission measurements at a wider wavelength range from 0.25 – 0.52 nm at CONRAD instrument V7. First results at 0.25 nm wavelengths are promising even at 11 mm thickness we achieved sufficient transmission above the background limit. In all measurements pronounced deviations from the exponential transmission law have been detected.

**Fig.1.** Left; the transmission values for one plate with 0.137 cm thick scanned from 0.25 to 0.6 nm neutron wavelength at CONRAD instrument compared with calculated exponential law and simulated transmission values versus given wavelength while the deviation from exponential law is clearly detected. Right; transmission of boron steel alloy plates with monochromatic neutron beam at 0.5244 nm compared with simulated model which describes inhomogeneities of boron distribution in steel matrix.

#### Acknowledgement

We would like to thank M. Strobl, P. Walter, O. Seidl, N. Kardjilov for their support and assistance during our stay at HMI-Berlin. This research project has been supported by the European Commission under the 6<sup>th</sup> Framework Programme through the Key Action: Strengthening the European Research Infrastructures. Contract N°: RII3-CT-2003-505925 (NMI 3).





## EXPERIMENTAL REPORT

### Investigation of the Fusion Relevant Material by USANS

Proposal N° MAT-04-1582

Instrument **V12a**

Local Contact  
Peter Walter

Principal Proposer: Halit Tatlisu, ATI Vienna  
Experimental Team: Peter Walter, HMI Berlin  
Markus Strobl, HMI Berlin

Date(s) of Experiment

25/04/2008 – 30/04/2008

Date of Report: 15/12/2008

Fiber reinforced ceramic matrix silicon carbide composites ( $\text{SiC}_f/\text{SiC}$ ) are ideal candidate materials for fusion reactor and high temperature structural applications because of their radiation resistance and high-temperature stability. Porosity within the  $\text{SiC}_f/\text{SiC}$  composite materials arise due to manufacturing process and can not be eliminated with any procedure. The porosity reduces most of the outstanding properties of the composites such as thermal conductivity and stability. Therefore, it is necessary to characterize the type of the porosity in the composites to increase the stability and life time under harsh environment. In this work the high temperature performances of the  $\text{SiC}_f/\text{SiC}$  composites have been investigated using ultra-small angle neutron scattering (USANS). The structure change of the composites has been resolved before and after heat treatment. Four conditions were studied to understand high temperature effect on the composites, heat-treated at 1200 °C for 5 and 8 hours, heat treated at 1700 °C for 1 hour and at 1900 °C for 1 hour.

First, one heat-untreated composite was measured. The same composite was investigated again under identical measurement condition after heat-treated at 1200 °C for 5 and 13 hours to understand the microstructure change within the composite. We observed that the microstructure of the composite was not significantly altered with increasing treatment time as seen in Figure 1. The three scattering curves are similar in the whole  $q$ -range. Subsequently, the composite was heat-treated at 1700 °C and 1900 °C for 1 hour. The scattering at the lowest  $Q$  values is related to the larger pores, and from the small pores at low  $Q$ . Figure 2 shows progressively increasing scattering from small pores at middle and high  $Q$  values with increasing heat-treatment temperature from 1200 °C to 1900 °C. As a result the heat treatment processes give rise to decrease the amount of large

pores within the composite, i.e. the population of the small pores increases with increasing temperature from 1200 to 1900 °C.

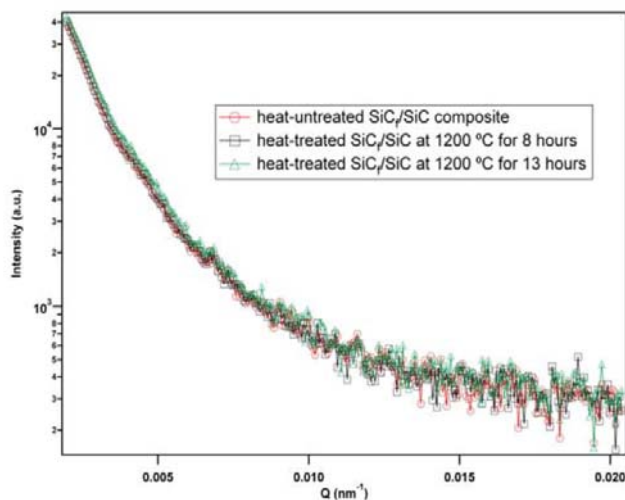


Fig. 1. The effect of the heat treatment at 1200 °C.

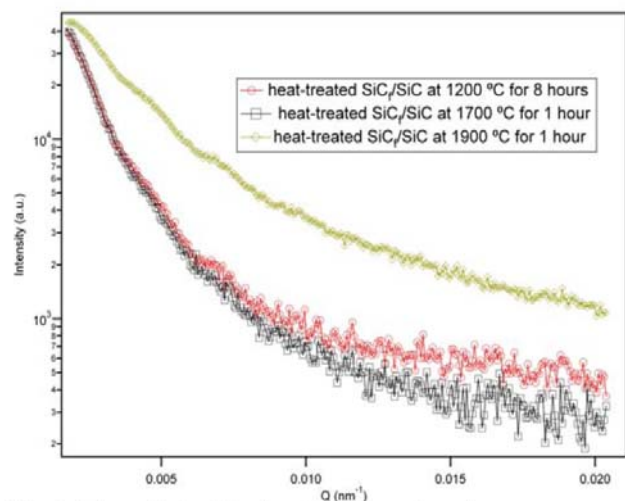


Fig. 2. The effect of the heat treatment on the scattering patterns can clearly be seen.

#### Acknowledgement

This research project has been supported by the European Commission under the 6<sup>th</sup> Framework Programme through the Key Action: Strengthening the European Research Infrastructures. Contract n°: RII3-CT-2003-505925 (NMI 3).



## EXPERIMENTAL REPORT

### Res. Stress states in machine components, Comparison of calculation, Neutron- and X-ray diffraction

Proposal N° MAT-01-1987

Instrument E3

Local Contact  
T. Poeste

Principal Proposer: Priv. Doz. Dr. Ing Thomas Hirsch  
Experimental Team: M. Sc. Jeremy Epp  
Dr. Ing Tobias Poeste  
Dr. Rainer Schneider

Date(s) of Experiment

17/06/2008 – 25/06/2008

Date of Report: 30/10/2008

In order to improve the level of knowledge concerning the causes of distortion an intensive characterization of residual stress states in parts is done by XRD. However, this method is not able to give information from the bulk without any destructive operations. Neutron diffraction method was therefore required for complementary investigations. The aims of the conducted experiments were to characterize the residual stress state in machine components for the validation of FEM calculations and additionally to receive more information on the active mechanisms responsible for the distortions.

#### Discs

This geometry is studied as a simplified model for gears. The first RS measurements were made on the machined state (turned). A grid of points along the radius of the disc and for several axial positions with a total number of 33 positions was measured in axial, radial and hoop direction. One problem occurred during the measurement of the radial component. Measurements were done through the aluminium sample holder for several positions and contrarily to our assumption; this caused a displacement of diffraction lines leading to unusable data. A reiteration of these measurements with an appropriate sample holder is necessary to conclude precisely on the residual stress state. However, it could be seen that variations of the peak positions were present along the radius, which could be due to the inhomogeneous chemical composition (presence of banded structure) or to micro RS. Complementary measurements are required to clarify these assumptions.

A hardened disc has also been measured and the results obtained may explain the origin of so called "dishing" phenomena occurring during the hardening process of these discs. As presented in Figure 1 the RS distribution is very inhomogeneous and may be correlated to the fibre flow pattern of the cross section. Complementary investigations will be necessary to confirm these results especially in measuring a spray formed disc presenting a very homogeneous macrostructure.

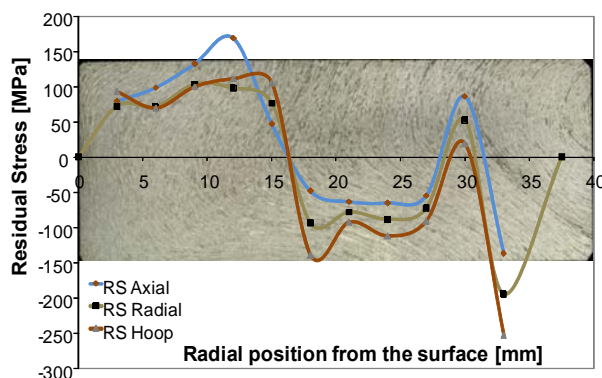


Figure 1: Residual stress measured along the radius of a hardened disc and the corresponding macrostructure

#### Rings

Cylindrical and tapered rings were measured in different material states. Results obtained for the machined state confirm the tendency already observed in previous experiments. The residual stresses produced during turning are confined in a very small surface layer of several hundred microns and the bulk of the material is not affected (almost no residual stresses are present). The RS states in retained austenite and martensite have also been measured in a hardened tapered ring but only at 4 positions. The comparison with FEM calculations will require some more measurements along the cross section.

#### Instrument

Thanks to the improvement of the E3 instrument, 500 measurements could be performed during the allocated beam time of 8 days. That is why we would like to especially thank the BENSC crew.



# EXPERIMENTAL REPORT

## Residual stresses in monofilament reinforced composites

Proposal N° MAT-01-2148

Instrument **E3**

Local Contact  
Tobias Poeste

Principal Proposer: Michael Schöbel, TU Wien  
Experimental Team: Georg Fiedler, TU Wien  
Guillermo Requena, TU Wien  
Heinz Kaminski, TU Wien

Date(s) of Experiment  
30/10/2007 – 06/11/2007  
18/02/2008 – 24/02/2008  
23/07/2008 – 24/07/2008

Date of Report: 18/08/2008

### Motivation

Monofilament reinforced composites are used as high conducting heat sink materials in novel fusion reactor systems. A low coefficient of thermal expansion is important to reduce thermal fatigue damage during operation. High conducting copper is reinforced with SiC fibers. Titanium interface coatings are developed to improve bonding quality resulting in an improved thermal stability of these systems.

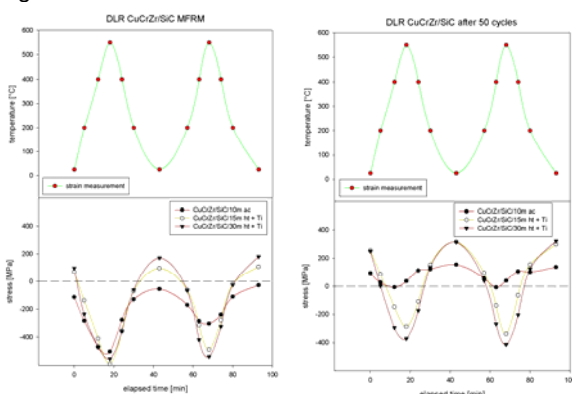
### Experiment

Residual stresses caused by a big thermal expansion mismatch between copper and the SiC fibers show the bonding quality and matrix damage during thermal cycling. In situ stress measurements were made on the E3 instrument during cycling up to its operation temperature. For this purpose cylindric CuCrZr/SiC/10-30m samples with different interfaces and fiber volume fractions were heated up to 550°C with a thermocoax and the stresses in the copper matrix were measured under similar conditions.

### Results

Compressive matrix stresses during the first two cycles in the CuCrZr of up to -500 MPa were generated (Fig.1 left). The stresses in the sample without Ti interlayer decreases after the first cycle.

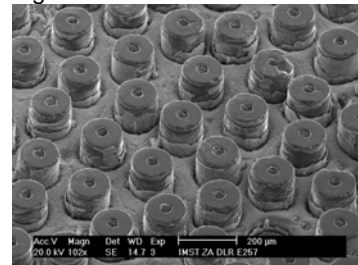
Figure.1.:



Residual stresses evaluated during 2 cycles between RT and 550°C in fiber direction. After 50 cycles on the right.

The same samples were cycled 50 times ex situ between RT and 550°C and measured under similar conditions again (Fig.1 right). The stress amplitude shows a low decrease from ~700 MPa to ~600 MPa and the mean value shifts up out of the compressive regime to almost 0.

Figure.2.:



A SEM image of extruding fibers on the sample surfaces. Fiber fragmentation in the MFRM can be expected.

During thermal cycling fiber extrusion could be investigated (Fig.2). On both ends of the samples the fibers got extruded from the surface due to fiber fragmentation during thermal cycling.

### Conclusions

High amounts of residual stresses (~600MPa) are built up in the CuCrZr matrix. The uncoated fibers show stress relaxation caused by debonding already in the second cycle. The Ti coated fibers prove thermal stability. A shift of the stress mean value during cycling is a result of plastic matrix deformation. Thermal fatigue damage is caused by debonding as well as fiber fragmentation. The residual stresses are not significantly affected by fragmentation. Complementary in situ synchrotron tomography will be made to investigate the fiber fragmentation process during cycling.

### Acknowledgement

This research project has been supported by the European Commission under the 6<sup>th</sup> Framework Programme through the Key Action: Strengthening the European Research Infrastructures.

Contract n°: RII3-CT-2003-505925 (NMI 3).

Least but not last I would like to thank Tobias Poeste and Robert Wimporoy for their professional support at the E3 instrument.

	<b>EXPERIMENTAL REPORT</b>  <b>Micro stress accumulation in multiphase superalloys</b>	Proposal N° MAT-01-2260 Instrument <b>E3</b> Local Contact Robert C. Wimpory
	Principal Proposer: J. Repper, FRM II, TU München, D-85747 Garching Experimental Team: J. Repper, FRM II, TU München, D-85747 Garching M. Hofmann (FRM II, TU München, D-85747 Garching) Robert C. Wimpory (HZB)	Date(s) of Experiment  26/05/2008 – 30/05/2008

Date of Report: July 2008

**EXPERIMENTAL.** All measurements were made on tensile test samples of IN718 as shown in Figure 1. We explored three sample sets differing in microstructure. The first set consists of samples made from ingot material of IN718 used in industry (Sample AZ). The other two sample sets consist of thermal treated ingot material. The first thermal treatment propagates the precipitation of the brittle  $\delta$ -phase (Sample 112). The second treatment (Sample 118) is equivalent to the standard treatment of IN718 also used in industry and propagates the precipitation of  $\gamma'$ - and  $\gamma''$ - phases. The measurements on all three sample states were carried out at the neutron residual stress diffractometer E3 at BENSC at HZB with a 50kN stress rig from FRM II, Garching. The wavelength was  $\lambda = 1.486 \text{ \AA}$  with a gauge size of  $4 \times 4 \times 6 \text{ mm}^3$ . Due to the restricted  $2\theta$  range of the instrument set up only four Bragg reflections of the fcc Ni-matrix ((200), (220), (311), (222)) were observable. The scattering angle coverage of the detector allowed the observation of one Bragg reflection per measurement only. Therefore, four identical test specimen for each sample state were used to investigate the behaviour of four Bragg reflections. During the in situ measurements the applied load was increased continuously with a velocity of  $v_F = 5 \text{ N/s}$ .

**RESULTS AND DISCUSSION.** The stress-strain diagrams for all reachable Bragg reflections and all three sample states could be measured. An example can be seen in figure 2. A macroscopic Young's modulus of  $E = 194 \pm 5 \text{ GPa}$  was determined for all sample sets. The microscopic Young's modulus could be determined for each crystallographic direction. The values fit well with values for the microscopic Young's moduli for a pure Nickel matrix calculated based on the Kröner model [1] using the XEC [2] program. The accumulated micro strains after a macroscopic unloading of the sample are determined. For all three sample states the reflections with the highest accumulated micro strains are the (200)

(tensile strains) and the (220) (compressive strains) reflections. This result is in accordance with literature [3]. In contrast the results for the (311) and the (222) Bragg reflections. In these cases differences in the mechanical behaviour between the different sample states could be seen.

## REFERENCES

- [1] E. Kröner: Berechnung der elastischen Konstanten des Vielkristalls aus den Konstanten des Einkristalls, Zeitschrift für Physik, Bd. 151 (1958), 504-518.
- [2] H. Wern, R. Johannes, H. Walz: Dependence of the X-ray Elastic Constants on the Diffraction Plane; Phys. Stat. Sol. (b), 206 (1998), 545-557.
- [3] T.M. Holden, R.A. Holt, A.P. Clarke: Intergranular stains in Inconel-600 and the impact on interpreting stress fields in bent steam-generator tubing, Materials Science and Engineering A, 246 (1998), 180-198.



Figure 1: Round tensile test sample with a total length of 60 mm and a gauge length diameter of 6 mm.

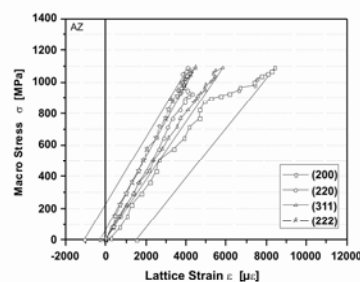


Figure 2: Stress-strain diagrams for the four investigated Bragg reflections of the Ni matrix phase of ingot material of IN718 (AZ).



## EXPERIMENTAL REPORT

### Residual Stress distribution in composite castings

Proposal N° MAT-01-2261

Instrument **E3**

Local Contact  
Robert C. Wimpory

Principal Proposer: Uwe Wasmuth, Institute of Metal Forming and Casting (UTG) TU München  
 Experimental Team: Uwe Wasmuth, (UTG)  
 Matthias Reihle, (UTG)  
 Robert C. Wimpory, (HZB)

Date(s) of Experiment

04/03/2008 – 08/03/2008

Date of Report: 20/01/2009

The requirements on cast parts especially in the automotive sector strongly have increased in recent years. Applications are e.g. engine blocks with different composite casting concepts like aluminium-magnesium [1] or cast iron-aluminium combinations. Due to different thermal expansion coefficients and cooling rates of the materials residual stress [2,3] and distortions occur during solidification. A DFG project [4] deals with the evaluation of residual stress distribution in composite casting test specimens (see fig. 1).



Fig. 1: test specimen consisting of steel insert (S235) and casted aluminium (AlSi9Cu3)

Figures 2 and 3 show the strain in submerged steel ring in the casting (strain and stress respectively). Strain measurement in the aluminium was not possible due to grain size.

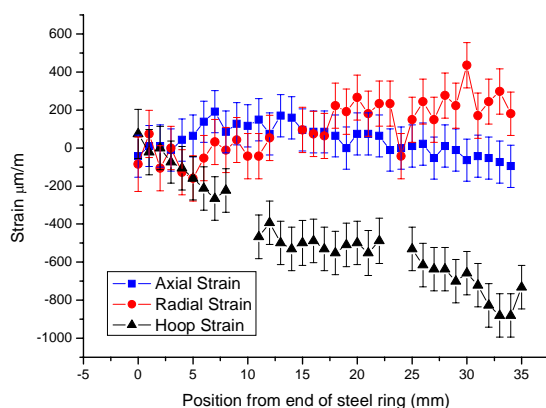


Figure 2. Strain in submerged steel ring

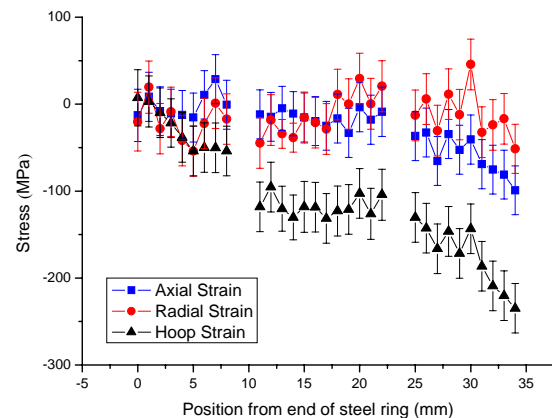


Figure 3. Stress in submerged steel ring

#### References

- [1] Gießtechnik im Motorenbau, Konstruktion, April 4-2005, S. 7-8
- [2] U. Wasmuth, M. Hofmann: Messung von Eigenspannungen in Verbundgusskurbelgehäusen mittels Neutronendiffraktometrie, VDI-Berichte Nr. 1899 (2005)
- [3] Experimental report (proposal 49 at STRESS-SPEC, FRM II), Residual stress analysis of a prototype engine block
- [4] DFG-project "Steigerung der Berechnungsgenauigkeit im Aluminium-formguss mittels Neutronen-diffraktometrie"



# EXPERIMENTAL REPORT

## Residual stresses in diamond reinforced MMC for heat sink applions

Proposal N° MAT-01-2262

Instrument **E3**

Local Contact  
Tobias Poeste

Principal Proposer: Michael Schöbel, TU Wien  
Experimental Team: Georg Fiedler, TU Wien  
Wolfgang Altendorfer, TU Wien  
Johannes Jonke, TU Wien

Date(s) of Experiment  
24/07/2008 – 28/07/2008  
02/09/2008 – 07/09/2008  
08/10/2008 – 13/10/2008

Date of Report: 14/01/2009

### Motivation

Diamond (CD) reinforced metals are investigated concerning their thermal properties to improve the performance of IGBT modules by a superior thermal management. Goal is to develop a MMC to substitute commonly used AISiC with a composite of higher thermal conductivity and a comparable low coefficient of thermal expansion.

### Experiment

In situ neutron diffraction during thermal cycling was made to evaluate the micro stress evolution during changing temperatures. Experiments similar to those on AICD (FRM2/ESRF) were made on the CuCD system at E3 on HMI.

### Results

The micro stresses in an Al/CD/60p composite with isolated particles are compared in Fig.1 (left) to an AISi7/CD/60p composite measured at the Stress Spec instrument on FRM2.

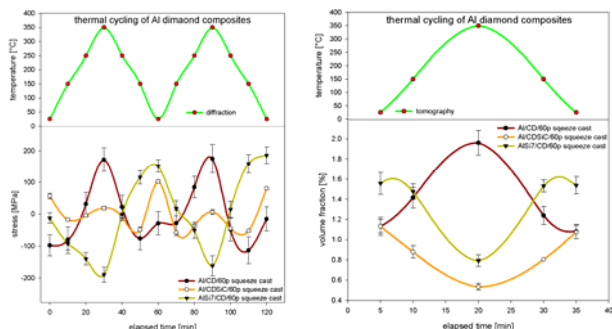


Figure 1: Compressive stresses are generated during heating in the AISi7 matrix by a connected network of CD-Si reinforcements. Tensile stresses dominate in the weakly bonded Al matrix. Changes in void volume fractions are due to stress induced matrix creep.

Tensile stresses in Al/CD/60p are generated in the sample center regions where the particle concentration is higher than close to the surface. Small micro stresses at the interfaces are superposed. Compressive stresses dominate in the AISi7 matrix. Two different types of reinforcement architectures are responsible: isolated particles in the Al/CD/60p and a system of a reinforcement network in the

AISi7/CD/60p with diamonds connected by Si bridges like in AISi7Mg/SiC/70p. Synchrotron tomography (at ID19 on ESRF) was made to determine the changes in void volume fractions by stress induced matrix creep during thermal cycling shown in Fig.1 (right).

The copper diamond system investigated on E3 showed high micro stress levels at the interfaces for good bonding superposing the macro stresses. Tension was identified during heating for weak bonding caused by macroscopic sample effects.

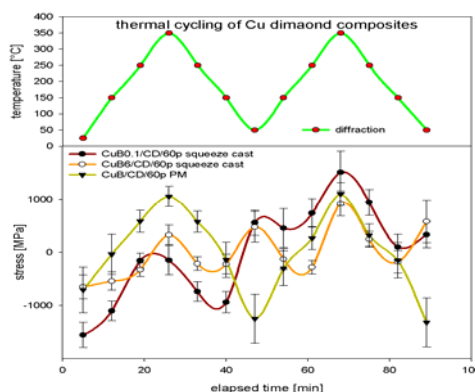


Figure 2: Weakly bonding for the PM Cu/CD is proven by dominating macro stresses. Debonding after the first cycle can be observed for the squeeze cast CuB0.1/CD by a stress shift into the tensile regime. The stresses in the good bonded CuB6/CD appear more stable.

### Conclusions

Diamond reinforced copper has promising thermal properties but the long term stability is problematic due to its reinforcement by isolated particles. The poor wettability of the diamond crystals with the copper matrix complicates the production. Boron content in the matrix was proven to increase bonding quality but does not connect the particles to a 3D network (like Si in Al). A good interface bonding alone is not sufficient to provide the thermal fatigue resistance under cycling thermal load.

### Acknowledgement

First of all I thank the good cooperation with EMPA, EPFL and IFAM who delivered the custom made MMC samples necessary for the planned neutron experiments. Least but not last I would like to thank Tobias Poeste and Robert Wimporoy for their professional support at the E3 instrument.

	<b>EXPERIMENTAL REPORT</b> <b>Residual stresses in CFC-Cu joining brazed to CuCrZr alloy for nuclear fusion technology</b>	Proposal N° MAT-01-2263 Instrument <b>E3</b> Local Contact Robert Wimpory
	Principal Proposer: Fabrizio Fiori, Univ. Politecnica delle Marche Experimental Team: Vittorio Calbucci, Politecnica delle Marche Robert Wimpory, HMI Berlin	Date(s) of Experiment 9/03/08 – 16/03/08

Date of Report: 04/04/2008

With the aim to determine the residual stresses behaviour in CFC-Cu joining brazed to CuCrZr alloy, we have been carry out the diffraction measurements with the E3 instrument on two different samples. Each of these two samples is constitute by a two layer. The first one is graphite while the other layer is a Copper-Chromium-zirconium alloy. These two layers are connected by a pure copper interface and other two interlayer of brazing alloy made by 87.75% Cu, 12% Ge and 0.12% Ni of 60  $\mu\text{m}$  thickness (fig.1). The difference between these two samples is that one of them was submitted to thermal treatment. The brazing process consists in a heat treatment at 970-980°C for 30 min (heating rate 30°C/min), a rapid cooling (>1°C/s) from this temperature to 475°C, and a isothermal treatment at 475°C for 3h and finally an isothermal treatment at 350°C for other 3h in vaccum.

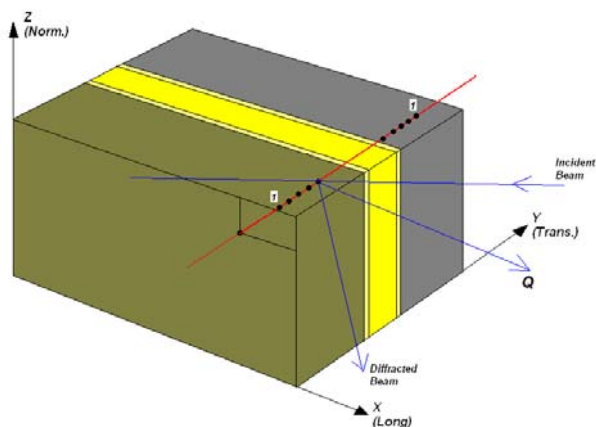


Fig. 1 - Geometry of the samples and measured points in the CuCrZr alloy. Example of transmission measurements for stress in X direction, corresponding to the Longitudinal direction for the stresses.

All the measurements have been executed with a beam wavelength of 1.486 Å and a gauge volume of 1x1x1mm<sup>3</sup>, selecting the primary and secondary slit of 1mm. Concerning the d0 value for the CuCrZr alloy we have been carry out the measurements in a CuCrZr reference sample while

for the graphite we have considered the value obtained in the point much far from the interface. The results obtained for the stress in CuCrZr alloy and graphite of the not treated sample are reported in the following graphs. To obtain the values of the stresses has been utilized the following mechanical parameters:  $E(\text{CuCrZr})=137000(\text{MPa})$  and  $\nu(\text{CuCrZr})=0,36$ . Concerning the elastic constants of CFC, the bulk ones were used because they take into account the fibre orientation, unlike the DEC for ( $\bar{1}10$ ) reflection of graphite. Starting from the values of the elastic constant of CFC for each measured direction, the values of the compliance has been obtained and than the residual stresses was calculated.

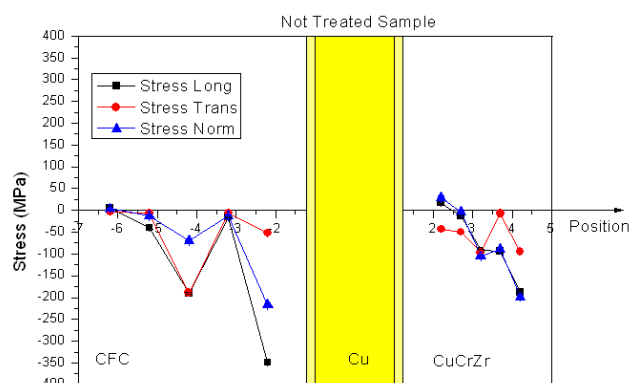


Fig 2 – Result for the stresses in the not treated sample.

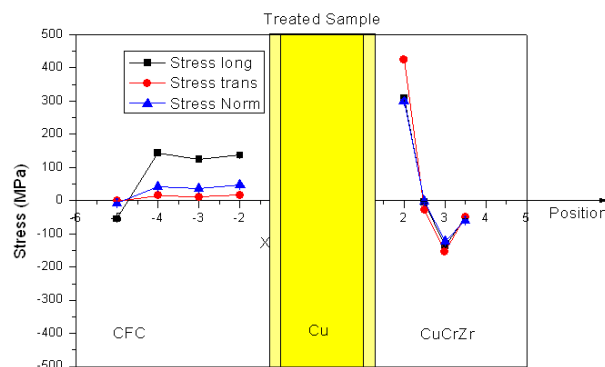


Fig 3 – Results for the stress in the treated sample



**EXPERIMENTAL REPORT**  
**Residual stress distribution: a key to understand the interfacial bonding mechanisms of high-velocity oxy-fuel (HVOF) thermally sprayed coating/substrate system**

Proposal N° MAT-01-2264  
 Instrument **E3**  
 Local Contact  
 Robert Wimpory

Principal Proposer: Manescu Adrian – Università Politecnica della Marche (UNIVPM), Ancona, Italy  
 Experimental Team: Manescu Adrian, (UNIVPM), Ancona, Italy  
 Robert Wimpory, HMI Berlin

Date(s) of Experiment  
 06/02/2008 – 12/02/2008

Date of Report: 19/01/2009

Thermal spray processes in the application of thick coatings have been essentially investigated in the perspective to form free standing components. Due to the complexity of bonding between the coating and the substrate materials, less attention has been given to create thick coatings to enable expansion of the application area of thermal sprayed products into new repair and aeronautical maintenance applications. The challenge to form a several millimetres thick coating is to control how residual stresses build up through the coating thickness, and in which extent these stresses control the adhesion mechanisms. In this framework, we analyzed at HMI Berlin on the E3 diffractometer the through thickness residual stress distribution in four specimens of Inconel sprayed coating on Inconel substrate.

The four analyzed specimens of cylindrical shape with a diameter of 30mm had different coating thicknesses: 1mm, 1.6mm, 2mm and 2.4 mm while the substrate had a thickness of 6mm. We chose the (311) Ni peak for the analysis. The specimens were measured in their centre so we assumed a radial symmetry, the measurements being performed in two orthogonal directions: the axial one (reflection) and the radial one (transmission) – Fig. 1.

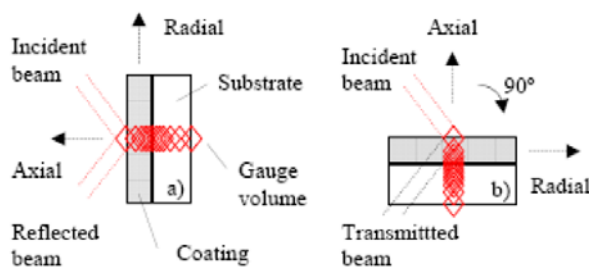


Fig. 1. Geometry of the experiment

Measurements were performed also in an annealed substrate specimen for determining

the unstrained interplanar distance for the substrate. A through thickness scan in a free standing coated specimen was used to determine the reference for the coatings. The slits we used defined a gauge volume of about  $0.5 \times 0.5 \times 5 \text{ mm}^3$  and we measured at different thicknesses through the coating and the substrate with overlapping gauge volumes, with a step of 0.1mm in the coatings and in the substrate close to the interface and higher steps in the rest of the coating – not near the interface - (0.2mm step) and in the rest of substrate (0.2 to 0.5mm steps).

The neutron diffraction (ND) measurements were performed in order to verify the stresses obtained with another method: the modified layer removal method (MLRM). In Fig. 2 we present a comparison between the stresses obtained with the two methods for one of the investigated specimens.

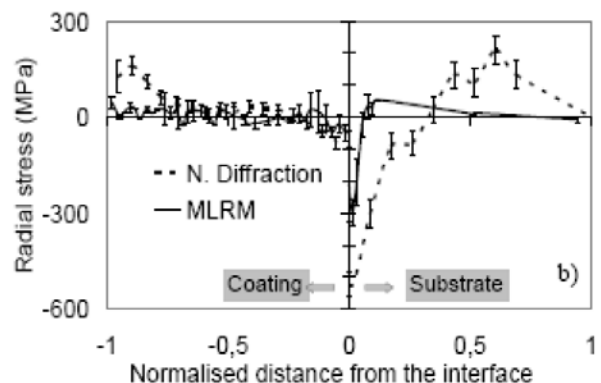


Fig. 2. Comparison between ND and MLRM

A quite good agreement was obtained for what concerns the stress trend. We also obtained that the difference in stress amplitude at the interface seems to significantly decrease when coating thickness is increased, which might be due to higher temperature due to longer spraying time.



## EXPERIMENTAL REPORT

### Stresses in built-up welding stainless steel on ferrite

Proposal N° MAT-01-2265

Instrument **E3**

Local Contact  
Robert Wimpory

Principal Proposer: Sumin V., JINR, Russia  
 Experimental Team: Wimpory R., HMI, Berlin  
 Sheverev S., JINR, Russia

Date(s) of Experiment

17/03/2008 – 20/03/2008

Date of Report: 14/05/2008

The industrial reactor VVER-1000 vessel is covered by built-up stainless steel welding for corrosion resistance. Since the vessel is made of ferritic steel the ferrite - austenite interface forms residual stresses. Tensile stresses in ferrite can lead to corrosion cracking. So it is very important to know stresses under the built-up welding.

In this investigation the residual strains were measured under interface in a template (Fig. 1) cutted from the real VVER-1000 reactor vessel. Normal residual strains perpendicular to the interface (see Fig. 1) and tangential ones were measured by E3 spectrometer. Data for normal component is presented in Fig. 2. It was assumed that two components of tangential strains (in x and y directions) are equal. So we measured residual strains only in x tangential direction (Fig. 2).

The residual stresses under the built-up welding were calculated on the basis of measured data (Fig. 3). These stresses are compressive in tangential direction which prevents fracturing in this direction. The stresses in normal direction are tensile and it can contribute to the possible exfoliation of stainless steel layer.

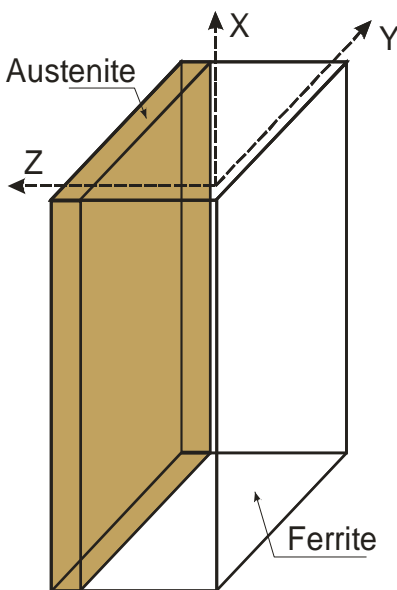


**Fig. 1:** Scheme of sample.

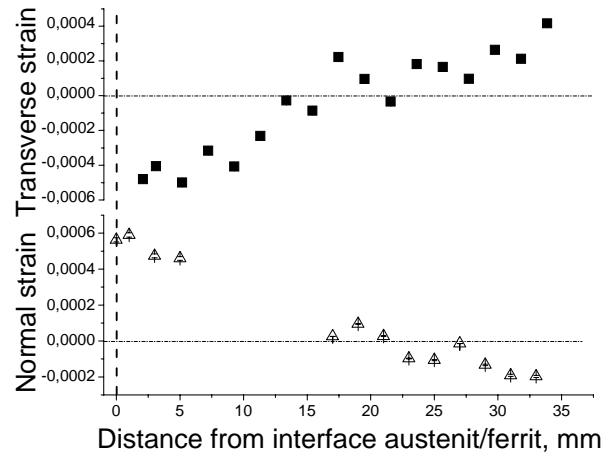


**Fig. 2:** Residual strains in normal and transverce directions.

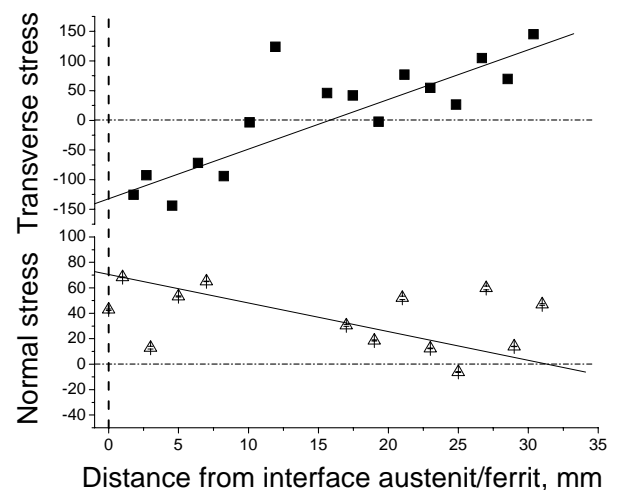


**Fig. 3:** Residual stresses in normal and transverce directions.



## EXPERIMENTAL REPORT

### Quantifying residual stress in welded CT specimens

Proposal N°  
MAT-01-2275-EF

Instrument **E3**

Local Contact  
Robert C. Wimpory

Principal Proposer: Robert C. Wimpory (HZB), Simon Kamel (Imperial College, London), Kamran Nikbin (Imperial College, London)  
Experimental Team: Robert C. Wimpory (HZB)

Date(s) of Experiment

08/03/2008 – 09/03/2008  
17/04/2008 – 20/04/2008

Date of Report: 12/01/2009

Residual stresses can have a significant effect on the structural integrity of components. They are also a key feature in welded pipe and plate components containing defects that needs to be quantified and modelled in order to improve component lifing at low temperatures.

Neutron diffraction measurements are important to validate models and hence E3 was used to perform residual strain (and hence stress) measurements for comparison.

In the example given here experimental and numerical investigations have been performed using blunt-notched compact tension C(T) specimens, of 347 stainless steel weld material, to examine the effect of tensile and compressive residual stress at the crack tip on fracture properties of the material.

The residual stress is introduced into the C(T) specimens by a tensile or compressive mechanical preload to produce, respectively, a compressive or tensile residual stress ahead of the notch (see figure 1.)



Figure 1. Blunt notch compact-tension specimens are mechanically deformed to generate residual stress (S. Kamel).

Neutron diffraction measurements are performed on the preloaded specimens, prior to introduction of a crack, and compared with predictions of the residual stress from finite element analyses of the preloaded C(T) specimens (see figure 2).

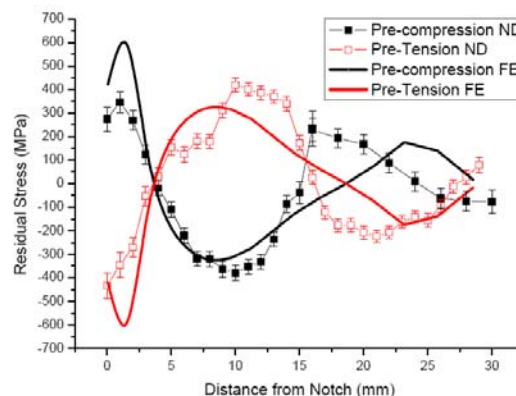


Figure 2. Comparison of Neutron Diffraction measurements (HZB) with Finite element model (Imperial College London)

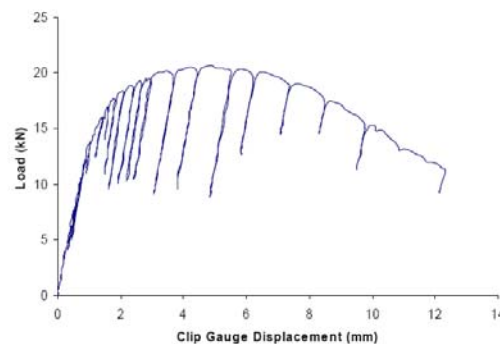


Figure 3. Load displacement curve during fracture test on as-received (non-preloaded) specimen, (Imperial College London)

Figure 3 shows a load-displacement curve for a fracture test for an as-received (non-preloaded) specimen. This indicates that this particular material is highly ductile at room temperature, which suggests that residual stress will have an insignificant effect here on the fracture loads.

Work is currently in progress to examine the effect of residual stress in C-ring specimens extracted from high strength tubing.



## EXPERIMENTAL REPORT

### Visualization of local textures using neutron diffraction

Proposal N°  
MAT-01-2277-EF

Instrument **E3**

Local Contact M. Boin

Principal Proposer: M. Boin, Helmholtz Centre Berlin  
Rainer Schneider, Helmholtz Centre Berlin  
Experimental Team: R. Wimpory, Helmholtz Centre Berlin  
T. Poeste, Helmholtz Centre Berlin  
C. Randau, TU Clausthal

Date(s) of Experiment

24/01/2008 – 27/01/2008

Date of Report: 13/01/2009

A textured Mg AZ31 sample has been investigated using neutron diffraction and Bragg edge transmission. The crystallographic orientation distribution was analysed on E3 (BER-II) as well as on STRESS-SPEC instrument (FRM-II) by the conventional diffraction method. The sample (shown in figure 1) was cut into two similar pieces to allow parallel studies using Bragg edge transmission on CONRAD (V7) [1].

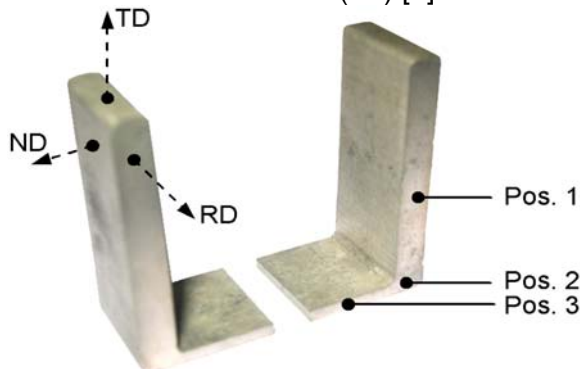


Figure 1: Extruded Mg AZ31 sample - RD, TD and ND represent the rolling, transverse and normal direction.

The extruded specimen was expected to have local texture changes around the bend. Therefore, we selected three different local positions around the bend, as indicated in figure 1, to capture the crystallographic orientation information. A Eulerian cradle supported by an integrated x-y-z-table was used to drive to the selected positions. The measured diffraction intensities have been transformed into pole figures (see figure 2) to visualise the local texture changes.

The resulting pole figures show the orientation variation depending on the local position. The first pole figure shows the basal planes being arranged perpendicular to the rolling direction (RD), which changes with position as can be seen in the second pole figure. If we rearrange the coordinate system by changing normal and transverse direction for the 3<sup>rd</sup> position (see TD and ND labelling in the last

pole figure), similarities to a cold rolling texture [2] can be seen.

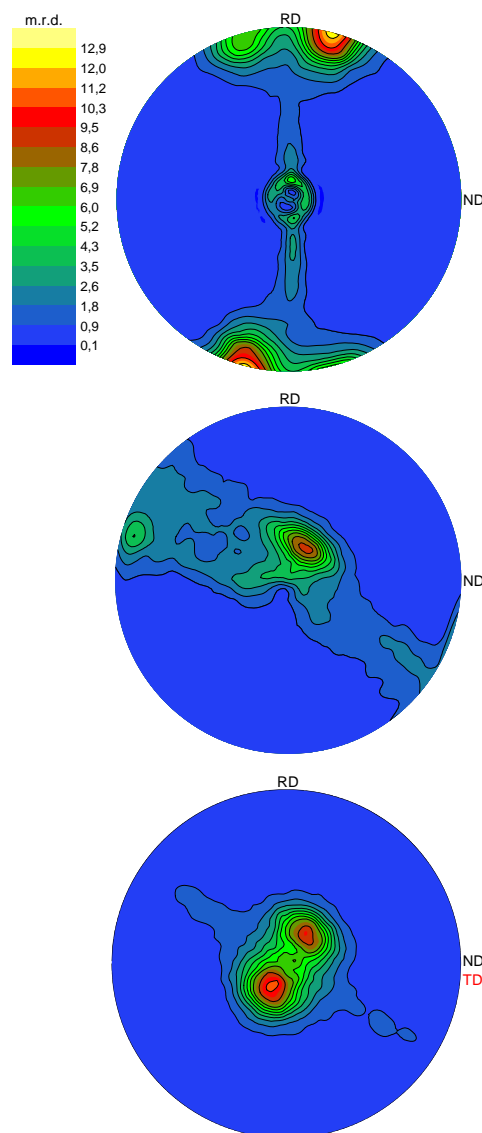


Figure 2: Pole figures of (002) reflection showing the measurement position 1, 2 and 3.

The results of this measurement providing the dataset of a sample local texture changes will be used as a reference to promote the development of the Bragg edge transmission method mentioned above.

[1] M. Boin, BENSC report, MAT-04-1633-EF

[2] A. Styczynski et al. / Scripta Materialia 50(2004) 943–947



## EXPERIMENTAL REPORT

### Residual stress states in hardened components, analysis of case hardened 20MnCr5 discs

Proposal N° MAT-01-2429

Instrument **E3**

Local Contact  
T. Poeste

Principal Proposer: Priv. Doz. Dr. Ing Thomas Hirsch  
 Experimental Team: M. Sc. Jeremy Epp  
 Dr. Ing Tobias Poeste  
 Dr. Rainer Schneider  
 Dr. Robert Wimpory

Date(s) of Experiment

24/11/2008 – 01/12/2008

Date of Report: 15/01/2009

Neutron diffraction experiments have been done on several discs made of carburizing steel 20MnCr5 after heat treatment. The aim of the investigations was to control the residual stress state of the discs after case hardening and blank hardening. The results obtained were compared to those obtained for the previous experiment (MAT 01-1987), which are presented in figure 1. These results are from a blank hardened disc which has been quenched in gas nozzle field.

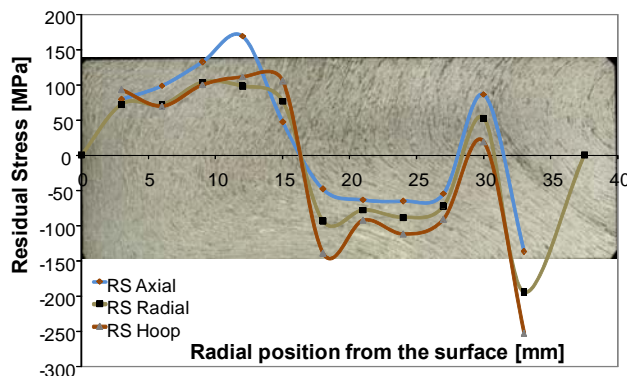


Figure 1: Residual stresses along the radius of a blank hardened disc and the corresponding macrostructure

The distribution of the residual stresses along the radius presents a strong drop 15mm from the surface. The cause of this distribution may be the inhomogeneous macrostructure obtained after forging, or the quenching process.

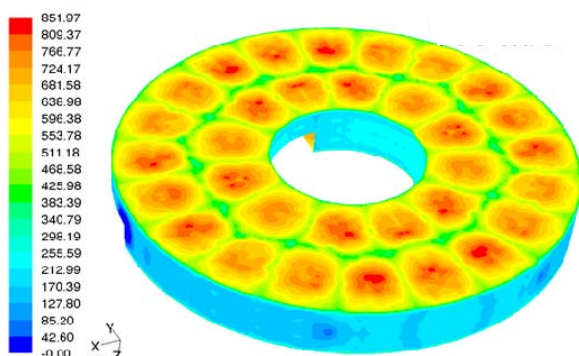


Figure 2: Heat transfer coefficients at the surface of a disc quenched in gas nozzle field

Figure 2 presents the heat transfer coefficients obtained for the quenching in gas nozzle field. Every red area corresponds to a nozzle. Strong differences in cooling rates are present between the zones, which could induce the creation of discontinuous residual stresses distribution.

Other discs which were not quenched in gas nozzle field, but with a gas streaming coming from the lateral area of the discs were investigated. Residual stress distributions presenting a drop like shown before were not found. In figure 3, the residual stress state measured along the radius of a case hardened disc is presented with the corresponding macrostructure. Only small periodic variations can be seen, but no drop. The variations may come from the chemical and microstructural inhomogeneities (banded structure), which can induce different stress-free lattice spacing.

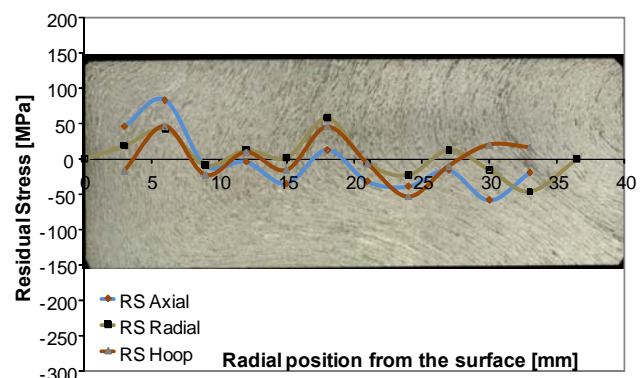


Figure 3: Residual stresses along the radius of a case hardened disc and the corresponding macrostructure

The fact that no similar residual stress state could be observed for both discs indicates that the quenching process may be the cause of the different distributions.

	<b>EXPERIMENTAL REPORT</b>  <b>Measurement of reference d0 samples for improved residual stress characterisation of Al alloys</b>	Proposal N° MAT-01-2432 Instrument <b>E3</b> Local Contact Robert Wimpory
	Principal Proposer: J.S. Robinson, University of Limerick, Ireland Experimental Team: J.S. Robinson, University of Limerick, Ireland Robert Wimpory, HZB, Berlin	Date(s) of Experiment  02/10/2008 – 08/10/2008

Date of Report: November 2008

Four high strength heat treatable aluminium alloy IDHD cores were examined on the E3 instrument at HMI between the 2nd and the 8th of October 2008. The lattice parameter variation along all 4 cores in three orthogonal directions was measured. The {311} aluminium matrix peak was used for all measurements. A gauge volume of approximately  $3 \times 3 \times 3 \text{ mm}^3$  was used for all measurements as it was found this volume gave an acceptable diffraction peak in a reasonable length of time (~800-1400 seconds).

The lattice parameter was found to vary along the length of the cores. When converted to an equivalent residual stress (assuming a constant d0) the stresses were found to vary between -100 and +100 MPa although this was dependent on the alloy type with the more quench sensitive 7075 displaying the greatest variation for edge to centre.

In addition, a Jominy end quench sample was measured with a known cooling rate variation along its length (fig. 1). Multiple measurements were made on this sample to assess the quenched end face residual stress in some detail. This will enable comparison with x-ray residual stress measurements to be made. The “pseudo” strain effect from the gauge volume emerging from the sample was also assessed for the Jominy sample to permit the “real” effect of the cooling rate on the lattice parameter to be determined close to the edge of the sample (Fig. 2).

All measurements were analysed and converted to strains and stresses at the HZB during the 6 days of beam time. There were no problems with hardware or software and the experiment was successful. It is anticipated these data will be incorporated into two journal papers to be submitted in 2009.

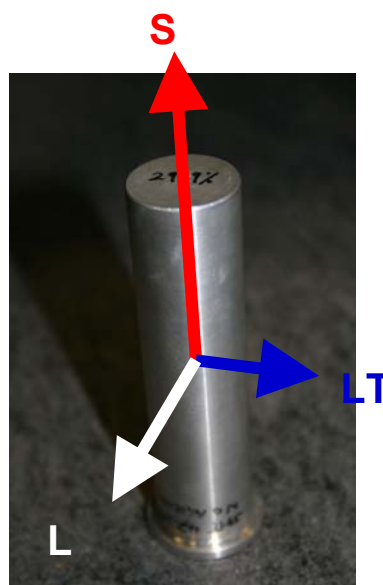


Figure 1. Jominy end quench sample

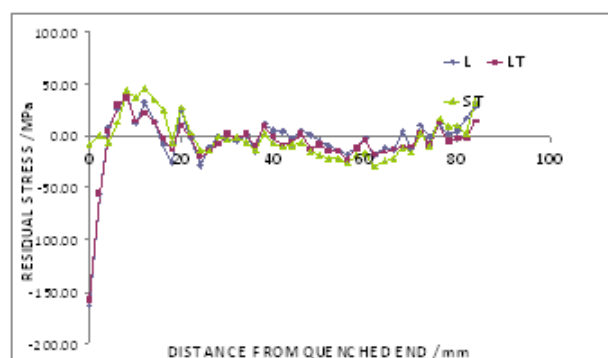


Figure 2. Variation in residual stress along the Jominy end quench sample

#### Acknowledgement

*This research project has been supported by the European Commission under the 6<sup>th</sup> Framework Programme through the Key Action: Strengthening the European Research Infrastructures.*

*Contract n°: RII3-CT-2003-505925 (NMI 3).*



## EXPERIMENTAL REPORT

### Residual strain/stress distribution in friction stir welded aluminium plates

Proposal N° MAT-01-2434

Instrument **E3**

Local Contact  
Robert Wimpory

Principal Proposer: Fabrizio Fiori, Univ. Politecnica delle Marche  
 Experimental Team: Vittorio Calbucci, Politecnica delle Marche  
 Adrian Manescu, Politecnica delle Marche  
 Robert Wimpory, HMI Berlin

Date(s) of Experiment  
 30/08/08 – 07/09/08

Date of Report: 23/09/2008

With the aim to determine the residual stresses behaviour in two different aluminium alloys plates, each of them realized by joining two plates of the same alloy by Friction Stir Weld, we carried out diffraction measurements using the E3 diffractometer. The first sample was a Al-6056 alloy while the second specimen was a Al-2139 alloy, differing from the first also for the Friction Stir weld parameter, like the pin velocity. In each sample has been considered one line in the middle of the sample and in each line 25 point were measured.

$$d_0 = \frac{(1-\nu)d_z + \nu(d_x + d_y)}{(1+\nu)}$$

To obtain the stress values we used the following mechanical parameters:  $E = 69\text{GPa}$  and  $\nu=0.35$ .

In the figure 2 below, we plotted the evolution of the stresses across the welding for the Al-6056 sample.

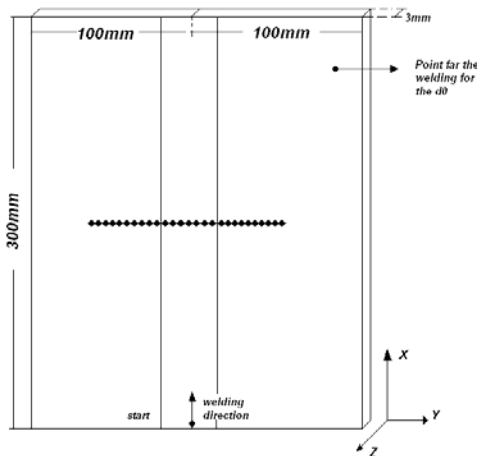


Fig. 1 - Geometry of the samples and measured points in the FSW alloy. In the picture are also reported the measured directions.

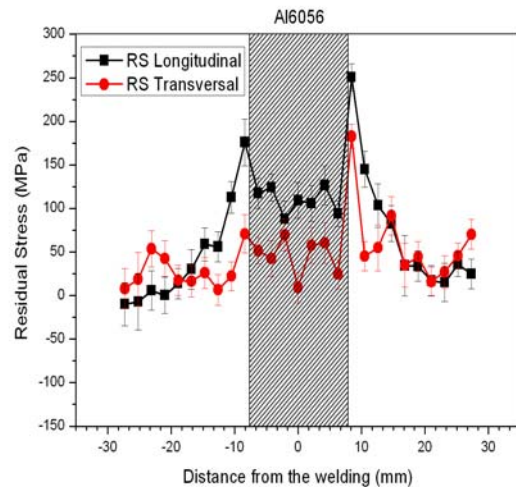


Fig 2 – Residual stresses in the Al-6056 specimen

All the measurements have been performed with a beam wavelength of  $1.486 \text{ \AA}$  and a gauge volume of  $1.5 \times 1.5 \times 1.5 \text{ mm}^3$ , selecting primary and secondary slits of  $1.5 \text{ mm}$ . As two theta, we considered the value  $2\theta = 74.6^\circ$ , which corresponds to the (311) Aluminium reflection. Assuming a biaxial stress field (due to the sample geometry), the strain/stress state was determined in the longitudinal and transversal direction, with respect to the weld seam (x and y in fig.1, respectively). The unstrained interplanar distance  $d_0$  was obtained by imposing, for each measured point, the stresses in the z direction to be zero:

The data analysis for the Al-2139 is still under evaluation.



## EXPERIMENTAL REPORT

### Strain/stress analysis in Nb<sub>3</sub>Sn/metal matrix composite superconducting cables for nuclear fusion technology

Proposal N° MAT-01-2435  
Instrument **E3**  
Local Contact  
Robert Wimpory

Principal Proposer: Adrian Manescu, Univ. Politecnica delle Marche  
Experimental Team: Vittorio Calbucci, same as above  
Robert Wimpory, HMI Berlin

Date(s) of Experiment  
30/06/08 – 07/07/08

Date of Report: 23/01/2009

The residual stress state was measured in Nb<sub>3</sub>Sn-based superconducting strands, embedded in a metal matrix to form a sort of composite cable to be used for the future ITER fusion reactor. This stress state is mainly due to the difference in thermal expansion coefficients of the various materials in the composite. The average stress in the Nb / Nb<sub>3</sub>Sn strands and in the Cu / bronze matrix has been evaluated in different spatial directions and the experimental results will be used in order to validate models developed to simulate the material performance under operating conditions in the ITER environment.

The measurements were performed on the E3 diffractometer. Two different specimens were investigated during the experiment, one having 9 strands embedded in a bronze matrix and the other having 48 strands (16 of them being empty strands – just the bronze matrix). SEM images of these two samples are reported in Fig 1.

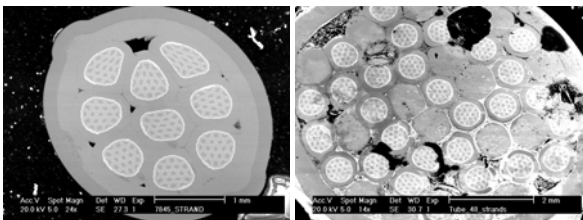


Fig. 1 – SEM images of the 9 and 48 strands specimens.

Axial symmetry was assumed due to the geometry of the specimen, so that it was sufficient to determine the interplanar distance  $d$  for only two different orientations: the axial and the radial one. The unstrained interplanar distance has been evaluated assuming the cylindrical symmetry and the existence in the wire of a longitudinal stresses induced by the extrusion treatment. In this case has been possible to use the Poisson relation  $\varepsilon_r = -\nu\varepsilon_a$  between the axial and radial strains. Solving this formula the relation for the  $d_0$  in obtained:  $d_0 = (d_r + \nu d_a) / (1 + \nu)$ .

For the 9 strands specimen the measurements were done in 2 different positions along the z axis, while for the 48 strands specimen 3 different positions were considered.

In Table 1, the residual stresses in the axial and radial directions for the two z positions in the 9 strands specimen are presented.

Material	Position	$\sigma_a$ [Mpa]	$\delta\sigma_a$ [Mpa]	$\sigma_r$ [Mpa]	$\delta\sigma_r$ [Mpa]
Bronze	z = 40	-96	11	-16	7
	z = 2	-37	7	11	6
Cu	z = 40	-42	30	215	34
	z = 2	-209	32	-166	30
Nb	z = 40	-156	16	22	17
	z = 2	-119	15	45	16
Nb <sub>3</sub> Sn	z = 40	379	21	-42	14
	z = 2	318	18	-35	12

Table 1. Residual stress in the axial and radial directions for the 9 strands specimen

These results show a relatively large difference in strain and stress values obtained in the two different sections that we analysed, especially for the Cu and bronze reflections. This might be due to the non-uniform structure of the specimen (the strands are twisted during manufacturing).

The same behaviour (even more pronounced due to a higher non-uniformity introduced by the 16 “empty” strands) was observed for the 48 strands specimens.

Moreover,  $d_0$  determination needs further analysis. An option would be to perform a measurement using the so called *sin<sup>2</sup>psi* technique that allows the evaluation of the residual stresses without the  $d_0$  value.



## EXPERIMENTAL REPORT

### Measurement of residual stress in drawn wires

Proposal N°  
MAT-01-2440-EF

Instrument **E3**

Local Contact  
Robert Wimpory

Principal Proposer: Robert C. Wimpory (HZB)  
Experimental Team: Robert C. Wimpory (HZB), Peter Tierman and Noel O'Dowd (University of Limerick)

Date(s) of Experiment

07/07/2008 – 10/07/2008  
19/12/2008 – 20/12/2008

Date of Report: 12/01/2009

One of the main advantages of producing wire or bar by the dieless drawn method, as opposed to the conventional method, is the possibility of producing parts with variable cross-section along the length by varying the drawing velocity appropriately. The aim of this measurement was to determine the residual stress distribution in bar produced by the dieless drawing method.

E3 has the advantage of having an extremely sharp gauge volume in the horizontal plane due to a new monochromator [1]. Also the optimal bending radius of the silicon 400 monochromator crystals is the same as the optimal bending radius for the suppression of the surface effect [2].

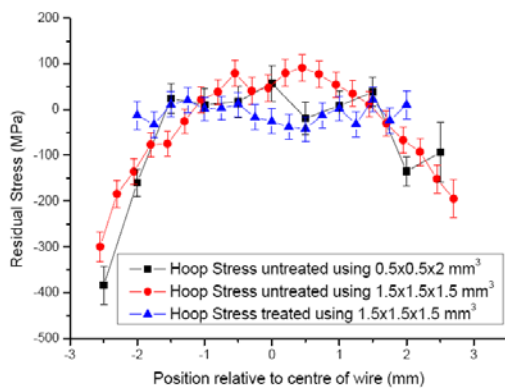


Figure 1. Hoop residual stress in the ferrite phase before (untreated) and after die-less drawing (treated).

A ferritic steel wire, drawn down to 4 mm from the original 5 mm, was examined. Figure 1 shows the residual stress in the hoop orientation (ferrite phase) along the diameter of the wire in the untreated region (before die-less drawing) and the treated region (after die-less drawing). The two measurements in the hoop direction in the untreated region were measured using two different gauge volumes to observe reproducibility and to see if the larger gauge volume was small enough to

capture the correct shape of the strain distribution in all three directions. Both measurements agree to within experiment uncertainty. The results show significant residual stress in the as-received wires particularly near the surface. However, in the drawn wires the residual stress is zero within the experimental uncertainty. Similar trends are observed for the other two principal stress directions.

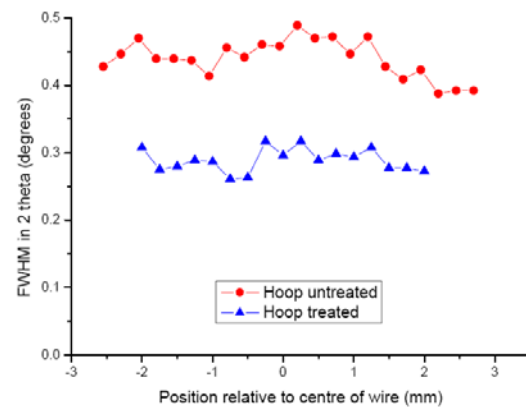


Figure 2. Hoop FWHM in the ferrite phase before (untreated) and after die-less drawing (treated).

In Fig. 2 the FWHM result is presented for the as-received and drawn wire. This result suggests that the die-less drawing anneals the sample, reducing the magnitude of the plastic strain and relieving the residual stress.

#### References

- [1] R.C. Wimpory et al, 'Efficiency Boost of the Materials Science Diffractometer E3 at BENSC: One Order of Magnitude Due to a Horizontally and Vertically Focusing Monochromator', Neutron News, Volume 19, Issue 1 January 2008, pages 16 – 19
- [2] Miroslav Vrána, P. Mikula 'Suppression of Surface Effect by Using Bent-Perfect-Crystal Monochromator in Residual Strain Scanning' Material Science Forum Vols. 490-491 (2005) pp 234-238

	<b>EXPERIMENTAL REPORT</b>  <b>Mosaic width as indicator of crystal quality during the life of Ni-Mn-Ga single crystals</b>	Proposal N° MAT-01-2442-EF  Instrument <b>E3</b>  Local Contact Robert Wimpory
	Principal Proposer: Markus Chmielus (HZB), Katharina Rolfs (HZB), Peter Müllner (Boise State University), Rainer Schneider (HZB) Experimental Team: Robert Wimpory (HZB), Tobias Poeste (HZB), Markus Chmielus (HZB)	Date(s) of Experiment  04/12/2008 – 14/12/2008

Date of Report: 14/01/2009

Magnetic shape memory alloys (MSMA's) tend to deform up to 10% in a rotating magnetic field [1]. However, this magnetic field-induced strain (MFIS) strongly depends on composition, crystal structure, crystal quality, and training. Additionally, samples with similar composition and training still show different MFIS and very different fatigue behavior. Therefore, it is of great importance to investigate the crystal quality after production, training, and magneto-mechanical cycling of the specimen. To quantify the crystal quality of a single crystal the mosaic width of structure peaks can be compared. Therefore, E3 was used to initially (not trained) analyze the structure (Fig. 1) and mosaic width of Ni-Mn-Ga MSMA. The martensite structure could be identified as 14M.

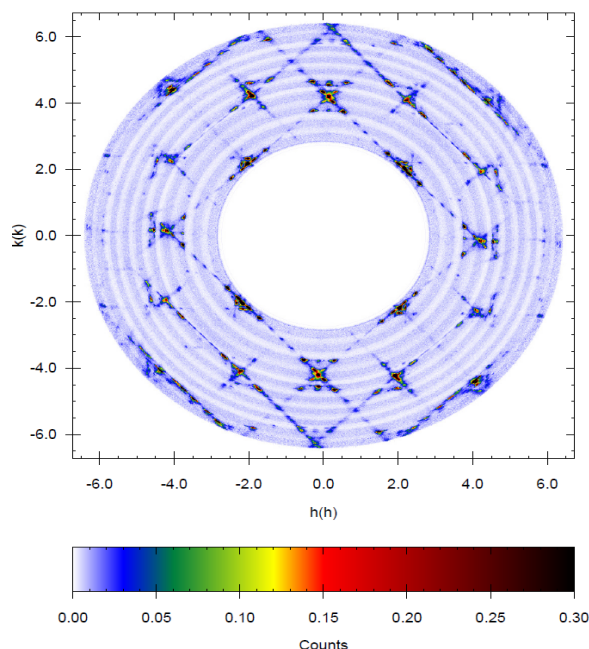


Figure 1: Neutron diffraction pattern of the specimen (self accommodated, 14M).

After the initial structure and mosaic width analysis, the sample was thermo-mechanically (TM) trained at the HZB and the mosaic width was measured again. After that, five

mechanical softening (MS) cycles followed at Boise State University, Boise, ID, USA, to reduce the twinning stress. The mosaic width was measured again at E3 and after several more compressions performed directly at E3. For a preliminary evaluation, the resolution of E3 is assumed as being  $0.28^\circ$  for the TTHS of the here evaluated (4 2 0) peak (Fig. 2).

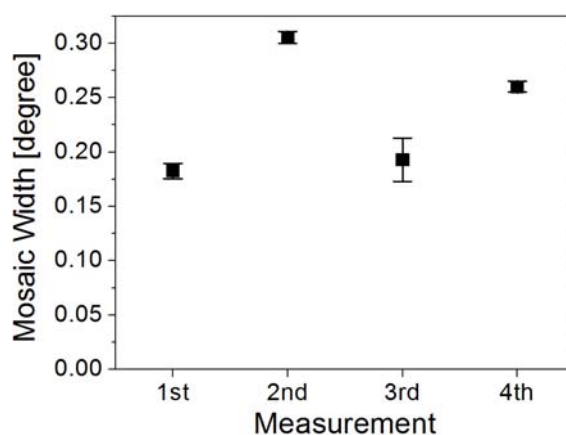


Figure 2: Preliminary evaluation of mosaic width at the initial (1<sup>st</sup>) condition, after TM training (2<sup>nd</sup>), after MS (3<sup>rd</sup>) and after additional compressions (4<sup>th</sup>).

The preliminary evaluation is inconclusive. The mosaic width of the 2<sup>nd</sup> and 4<sup>th</sup> measurement is higher than the initial mosaic width but the 3<sup>rd</sup> is again similar to the 1<sup>st</sup> measurement. Additionally, the absolute measured FWHM is very close to the resolution of E3. Twinning leads to overlapping of peaks on the detector which leads to increased errors during data analysis. This indicates a good crystal quality. MC acknowledges funding from DFG SPP 1239 and the U.S. Department of Energy, Office of Basic Energy Sciences, Contract DEFG-02-07ER46396.

#### References

[1] Sozinov, A., A.A. Likhachev, N. Lanska, and K. Ullakko, Appl Phys Lett, **80**(10), 1746-1748 (2002).



## EXPERIMENTAL REPORT

### Martensitic Structure of Co-alloyed Ni-Mn-Ga

Proposal N°  
MAT-01-2443-EF  
Instrument **E3/E7**  
Local Contact  
Robert C. Wimpory

Principal Proposer: Katharina Rolfs, Helmholtz-Zentrum Berlin für  
Materialien und Energie GmbH  
Experimental Team: Katharina Rolfs, HZB  
Robert C. Wimpory, HZB

Date(s) of Experiment  
  
02/08/2008 – 09/08/2008

Date of Report: 15/01/2009

The magnetic shape memory effect has been observed in several alloys like NiCoGa, FePd and FePt. The effect requires a high mobility of the twinboundaries in the martensitic phase as well as a high magnetic anisotropy. Ni-Mn-Ga is a material-system which exhibits both properties. Since the magnetic field induced strain in Ni-Mn-Ga is, up to now, only reported for the non-stoichiometric ferromagnetic modulated tetragonal and orthorhombic structures, exhibiting a periodicity of 10 (10M) and 14 (14M) layers, respectively, the effect is limited by the phase-transition-temperature from the martensitic modulated structure to the cubic austenitic phase and the Curie-temperature.

In order to increase both phase-transition-temperatures, Ni-Mn-Ga was alloyed with different Cobalt-contents [1]. Using the Slag remelting and Encapsulation – technique [2] single crystalline samples with 5% and 6% Cobalt have been grown successfully.

No.	Co [at- %]	Ni [at- %]	Mn [at- %]	Ga [at- %]	Mn/Ga ratio
1	6.2	44.4	28.3	21.1	1.34
2	6.2	44.9	29.1	20.1	1.45
3	4.9	45.1	30.9	19.1	1.62
4	4.9	44.7	31.7	18.7	1.70

Table 1: Composition of Ni-Co-Mn-Ga samples determined at E3 and e7

To determine the influence of Cobalt on the structural properties, the hk0 planes of several samples have been measured (see Table 1).

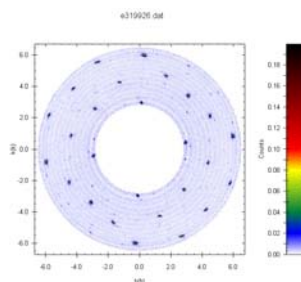


Fig1. Hk0-plane of Ni<sub>44.7</sub>Co<sub>4.9</sub>Mn<sub>31.7</sub>Ga<sub>18.7</sub>

Two different martensitic structures have been determined at roomtemperature. Samples with a lower Mn/Ga ratio show a nonmodulated tetragonal structure, which is well known from several Ni-Mn-Ga.alloys. With increasing Mn/Ga ratio, the structure changes to a nonmodulated orthorhombic structure (see Table 2). However the volumes of the unitcells are slightly bigger than in Ni-Mn-Ga due to the size of the Cobalt-atoms.

Sample	a [Å]	b [Å]	c [Å]	structure
1	6.54	5.49	5.49	tetragonal
2	6.52	5.62	5.52	orthorhombic
3	6.62	5.85	5.48	orthorhombic
4	6.29	5.73	4.79	orthorhombic
14M [10]	6.10	5.85	5.56	Pseudoorthorhombic

Table 2: Unitcellparameters of Ni-Co-Mn-Ga samples

The author appreciate the support of this work by grants of the Deutsche Forschungsgemeinschaft (SPP1239, grant No. Schn 1106/1).

[1] V. Sánchez-Alarcos J. I. Pérez-Landazábal, V. Recarte, C. Gómez-Polo, J. A. Rodríguez-Velamazán, Acta Materialia 56 (2008) 5370–5376

[2] A. Mecklenburg, S. Fiechter, H. P. Nabein, R. Schneider, DE102004018664A1 (2005)



## EXPERIMENTAL REPORT

### Residual strain-stress in anisotropic cold-rolled Zr-alloy

Proposal N° MAT-01-2266

Instrument **E7**

Local Contact  
Robert Wimpory

Principal Proposer: Sumin V., JINR, Russia  
 Experimental Team: Wimpory R., HMI Berlin  
 Sheverev S., JINR, Russia

Date(s) of Experiment

10/03/2008 – 20/03/2008

Date of Report: 14/05/2008

A common approach for strain and stress determination uses the so-called “ $\sin^2 \Psi$  method” (Christenson & Rowland [1]). When intergranular stress exists, however, the “ $d$  versus  $\sin^2 \Psi$ ” may become strongly non-linear. Also the texture contributes significantly to this non-linearity. This gets to ambiguities in determination of strain-stress tensors. Popa & Balzar [2] proposed an alternative method to accurately model diffraction line-shift in a Rietveld refinement program for all Laue symmetries without making Voigt or Reuss approximations. They defined a texture-weighted strain orientation distribution function (WSODF) and performed the spherical-harmonics analysis of this function for all crystal symmetries.

Zr-alloys with strong texture needs this method. As estimated earlier, Zr-samples have cylindrical symmetry of texture. The determination of strain tensor requires measuring only azimuthal dependence of  $d_{hkl} - d_{hkl}(\gamma)$ . Measurements were performed on E7 spectrometer.

Two studied samples have had difference in preceding handling: one (number 0) was only cold worked, another (number 1) underwent annealing at 600 °C after cold working. Measurements were carried out by revolving the sample in the plane of diffraction vector with the step of 10 degrees. Range of displacement came to 90 degrees: from the position where diffraction vector and axis of texture are parallel (0°) to the position where they are perpendicular.

Annealed Zr1 and cold worked Zr0 samples showed quite different behavior in  $d_{hkl}(\gamma)$  for all studied plains (100), (002) and (101) (Fig. 1 – 3). But in order to correctly calculate full strain tensor by method [2] we need to measure more other reflections.

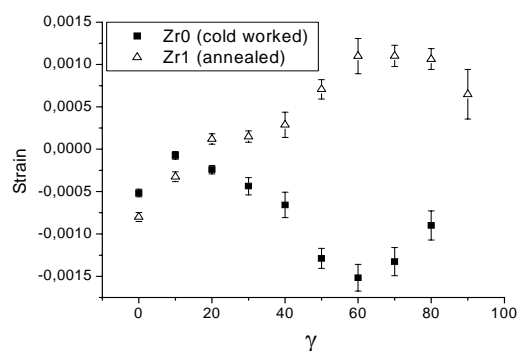


**Fig. 1:**  $d_{hkl}(\gamma)$  dependence for (100) plane.

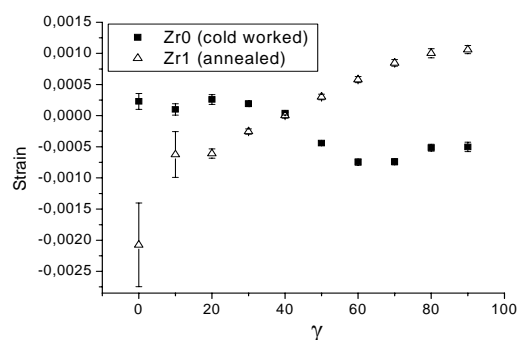


**Fig. 2:**  $d_{hkl}(\gamma)$  dependence for (101) plane.

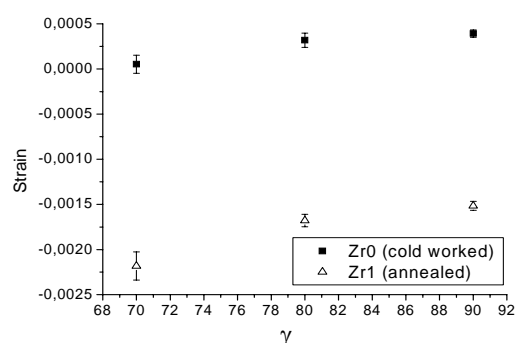


**Fig. 3:**  $d_{hkl}(\gamma)$  dependence for (002) plane.

#### References:

- [1]. Cristenson, A.L. & Rowland, E.S. (1953) *Trans. ASM*, **45**, 638-676.
- [2]. Popa, N.C. & Balzar, D. (2001) *J. Appl. Cryst.* **34**, 187-195

	<b>EXPERIMENTAL REPORT</b>  <b>TG4 Stress Relieved Specimen Measurements and grain size effect</b>	Proposal N° EF Instrument <b>E3</b>  Local Contact Robert C. Wimpory
	Principal Proposer: Robert C. Wimpory, (HZB) Experimental Team: Robert C. Wimpory, (HZB)	Date(s) of Experiment  14/11/2008 – 16/11/2008

Date of Report: 13/01/2009

The European Network on Neutron Techniques Standardization for Structural Integrity (NeT) facilitates the application of novel predominantly neutron-based techniques to structural integrity related questions applicable to processes/components relevant for nuclear power production [1]. The aim of the fourth Task Group (TG4) within NeT is to undertake 3-dimensional analyses of residual stresses in a three-pass slot weld specimen by both experimental and numerical means.

The planned weld specimens consist of a plate with a groove filled with three weld beads. A total of 12 specimens will be produced of which 7 are available for round robin measurements (4 for non-destructive, 2 for destructive, and 1 for contour measurements and d0 and comb manufacturing) [2]

The E3 measurements were the first to be made on the specimens, specimen 4-1A being a stress-relieved plate before the introduction of welding. The aim was to see if the manufacturing stresses had been indeed relaxed.

A gauge volume of  $3 \times 3 \times 3 \text{ mm}^3$  was used on the austenitic (311) reflection. It was found that the specimen was strain and hence stress free. The specimen was grainy with a typical standard deviation of 0.0125 degrees about the strain free  $2\theta$  angle compared to a fitting uncertainty of 0.008 degrees. Simulation of the grain size effect (figure 1) shows that 0.0125 corresponds to 33 grains being seen within  $\pm 1\text{SD}$  under the Bragg peak ( $\approx \pm 0.147$  degrees in this case). The probability of a grain appearing within  $\pm 1\text{SD}$  on the detector has been estimated to be 1 in 488 (for hkl 311, multiplicity 24). Therefore the grain size can be estimated to be  $\approx (\text{gauge volume}/\text{number of grains})^{0.333}$ . This is  $\approx (3000^3/488/33)^{0.333} \approx 120$  microns. This agrees well with the actual size of the grains observed [3].

It was found that rocking the specimen appeared to average things out a bit better. In this case the average fitting errors agreed better to the overall standard deviation of each data set.

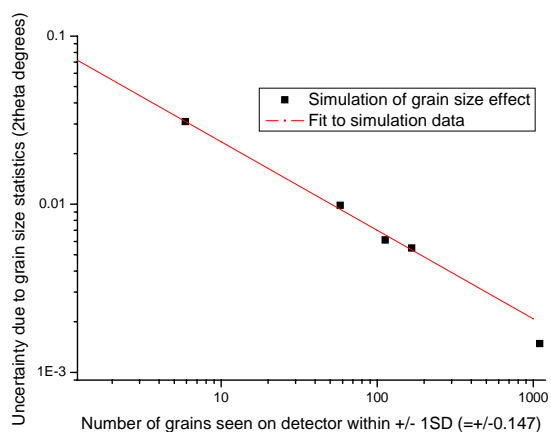


Figure 1. Simulation of grain size uncertainty on E3

#### References

- [1] R.C. Wimpory, C. Ohms, M. Hofmann, R. Schneider, A.G. Youtsos, 'Statistical Analysis of Residual Stress Determinations using Neutron Diffraction' International Journal of Pressure Vessels and Piping, doi:10.1016/j.ijpvp.2008.11.003, In press.
- [2] R.V. Martins 'NeT-Task Group 4: Three-Pass Slot Weld Specimen in Austenitic Stainless Steel Protocol for the Destructive and Non-Destructive Determination of Residual Stress in Three-Pass Slot Weld Specimens in Austenitic Stainless Steel' JRC, Petten, NL 2008.
- [3] Richard Haigh of Open University. 13<sup>th</sup> NeT NeT Steering Committee Meeting Lyon June 2008.

# **Cultural Heritage**



	<b>EXPERIMENTAL REPORT</b> <b>Identification of Hidden Object of Archaeological Interest</b>	Proposal N° ART-04-1408 Instrument V7 Local Contact N. Kardjilov
	Principal Proposer: R. Triolo, University of Palermo V. Benfante Experimental Team: R. Triolo, I. Sciacca, I. Ruffo	Date(s) of Experiment 15/03/2007 – 18/03/2007 19/05/2007 – 26/05/2007 10/04/2008 – 17/04/2008

Date of Report: June 2008

When objects of artistic or archaeological interest are studied, the fragility, the historic and even the economic value of samples analyzed must be taken into account. Neutron tomography in conjunction with other methods (i.e. neutron diffraction), seem to be a useful technique for testing objects of artistic or archaeological interest. Neutron tomography (NT) is a non invasive technique and thermal neutrons are able to penetrate thick layers of sample. Therefore, samples of greater mass than the ones allowed with other probes can be investigated. Recently at the University of Palermo (Italy) we have started a research program with the aim to obtain tomographic 3D reconstructions on a selection of ancient artillery and other objects recovered from ship wrecks in several locations close to Sicily shoreline (Sicily channel and Tyrrhenian sea). In particular some of these ship wrecks have been found near the south coast (approximately 1 mile from the shoreline) where there is, still nowadays, a very dangerous cliff (Scoglio della Bottazza). Most of the objects found belong to ships operating in the Mediterranean sea between the 4<sup>th</sup> century A.D. and the 17<sup>th</sup> century A.D.. Indeed near Scoglio della Bottazza, in shallow waters, it has been possible to spot, during a preliminary investigation, part of the artillery weapons and other arms used for self defense. The artillery parts recovered are clearly indicating that we are in presence of bulky metallic objects embedded in a thick calcareous concretion matrix (sea shells in many cases are clearly visible). Typical objects are swivel guns, long range cannons, various ammunitions and connection parts very well conserved, swords and simple parts.

We have performed measurements on a large number of small finds and on the handle of a sword for which little information was available because of the thick calcareous concretion surrounding the arm. The sword is made of three pieces (the handle and two additional pieces which should make the entire arm). Surprisingly clear images of the handle have been obtained, despite the difficulty of the experiment given the strong adsorption of the find which would have prevented the use of other probes. Even in such difficult experimental conditions Neutron Tomography (NT) has shown to be of extreme importance for obtaining the digital 3D reconstruction of the objects before the restoration work. In the following figure (Fig. 1) the reconstructed image (right) is the result of 3D reconstruction by using 2D projections (shown in the middle) taken at equidistant

rotation of the sample at 180 degrees. The original handle is also shown on the left. More data are being analysed, and more experiments are needed on the remaining pieces. Still there are many other objects that need to be recovered from the sea and the NT technique might help in building a database for identifying the correct historical frame period.

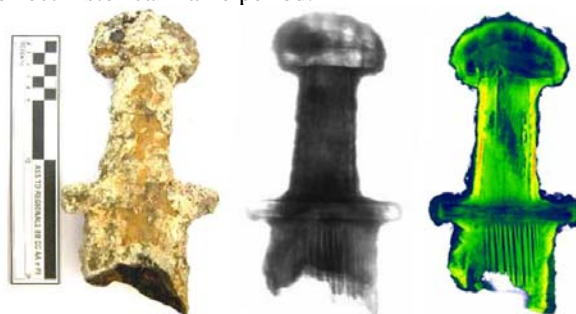


**Fig.1** Investigation of late roman sword (left) by NT technique. A two-dimensional transmission image by neutrons is shown in the middle. A single slice from the 3D-tomographic volume is shown on the right. The color scale corresponds to the presented attenuation coefficients for neutrons from blue (hollow space) to red (iron). The green part represents the distribution of diffused iron (Iron oxide).

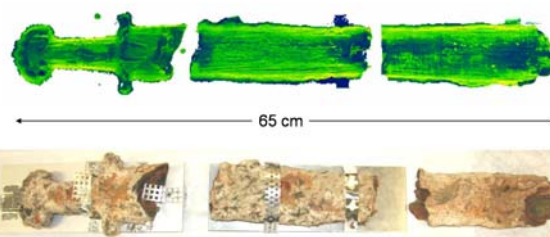


**Fig. 2** The three parts of the sword were investigated by neutron tomography. The inner structure of the preserved layers under the thick calcareous concretion matrix is clear visible.

Reference:

[1] N. Kardjilov et al, Notiziario Neutroni e Luce di Sincrotrone, vol. 13, n. 2, p. 6, 2008

	<b>EXPERIMENTAL REPORT</b> <b>Endosymbionts of fossil Echinodermata using neutron and X-ray computed tomography</b>	Proposal N° GEO-04-1489 Instrument V7 Local Contact Nikolay Kardjilov
	Principal Proposer: C. Neumann – HU Berlin Experimental Team: N. Kardjilov – HMI, Berlin A. Hilger – HMI, Berlin	Date(s) of Experiment 03/11/2007 – 06/11/2007

Date of Report: January 2008

## Introduction

Neutron and x-ray computed tomography methods were used for morphological investigation of fossil and recent traces and malformations produced by endoskeletal symbionts in the hardparts of their echinoderm hosts. The non-destructive visualization of these traces provides clues for the evolution of host-symbiont systems in deep time. Application of neutron tomography proved to gain the best results from fossil (= diagenetically altered) samples (fig. 1) whereas high-resolution micro-focus x-ray tomography achieved very good results from recent samples (fig 2). This way the advantages of the two techniques were demonstrated. X-rays provide high spatial resolution for density changes in small samples (1-2 cm) while the neutrons help to transmit bulky samples of up to 10-20 cm and provide unique contrast for hydrogenous minerals.

## Experiment

The neutron tomography experiments were performed at V7 (CONRAD) instrument using its dedicated high-resolution option providing a spatial resolution of 100  $\mu\text{m}/\text{pixel}$ .

The X-ray tomography investigations were performed at the new CT scanner having a micro-focus tube of 150 keV and beam spot size of 5  $\mu\text{m}$ . The achieved spatial resolution was between 20  $\mu\text{m}$  and 30  $\mu\text{m}$  (flat-panel detector) in dependence on the used magnification ratio provided by the cone-beam geometry.

For each sample a defined number of projection images over 360° rotation angle was used – 300-600 projections in case of neutron tomography and 600-1000 in case of X-ray method.

The obtained data were reconstructed by filtered back-projection algorithm [1] and visualized and processed by volume rendering software VG Studio Max 2.1[2].

## Results

The complementarity between X-ray and neutron tomography was proved in the first step. Best contrast was achieved in bulky fossil samples by neutron tomography when the symbiont-produced cavity in the calcitic host skeleton was filled with a silicilastic matrix (fig 1). In this case, only poor results were achieved using x-ray tomography. In contrast, high resolution x-ray tomography is more applicable measuring recent (=less dense) samples (fig. 2) where excellent results reveal details even of the ultrastructure of the host skeleton.



**Fig. 1 left:** External view of a crinoid stem (15 mm in diameter) of *Rhodocrinites* from the Early Carboniferous of England infested by the endosymbiotic coral *Cladochonus*. **right,** Neutron tomography experiments revealing coral growth modus.

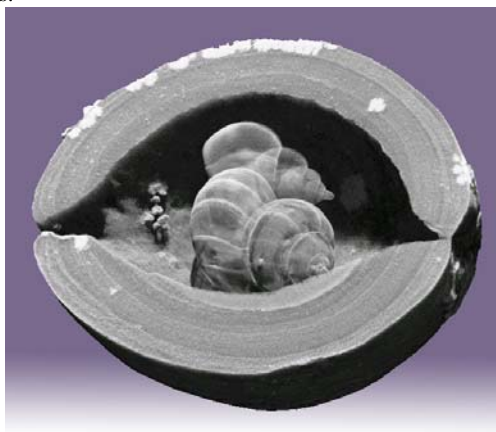


**Fig. 2** Male and female of the gall-inducing parasitic gastropod *Sabinella* sp. from West Australia. Micro x-ray tomography showing the parasites in situ in the host sea urchin spine (10 mm in diameter).

## References

- [1]. Neumann, C., Vinn, O., Kardjilov, N., Hilger, A., Manke, I. & Zabler, S. (2007): Fossil echinoderm endosymbionts: Host/symbiont interactions, new taxa, and application of neutron-, micro-, and synchrotron-computer-tomography.- *Palaeontological Association 51st Annual Meeting, Programme with Abstracts*: 47.
- [2]. Neumann, C., Kardjilov, N., Hilger, A., Manke, I. & Zabler, S. (2007): Studying fossil crinoid endosymbionts: Application of neutron-, micro- and synchrotron-computer-tomography.- *Computer Aided Visualisation in Palaeontology Meeting, London, September 13, 2007*.



## EXPERIMENTAL REPORT

### Preservation and Conservation of waterlogged wood

Proposal N° ART-04-1497

Instrument **V7**

Local Contact  
N. Kardjilov

Principal Proposer: Triolo, Roberto – University of Palermo (Italy)  
 Experimental Team: Benfante, Valerio – Univ. of Palermo (Italy)  
 Giambona, Graziella - Univ. of Palermo (Italy)  
 Ruffo, Irene - Univ. of Palermo (Italy)

Date(s) of Experiment

13/08/2008 – 19/08/2008

Date of Report: 06/01/2009

Neutron Tomography (NT) experiments have been performed on three different woods treated with different impregnating solutions. One was a fir sample (A) while the other two were different kind of Oak Chestnut samples (B and C). Neutron Radiography has been performed “in vivo” during the uptake of the solutions. For the NT experiments dry or wet samples have been equilibrated with 10% solutions of PEG 400 (solution 1), PEG 1500 (solution 2) in D<sub>2</sub>O. Solution 3 is a 1:1 mixture of solution 1 and 2.

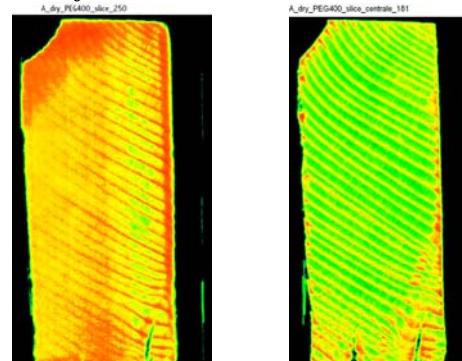
(PEG 1500). The latter has tendency to form layers on the surface of the samples. The following figure compares a surface slice and a centre slices for different samples and impregnating solutions. Further analysis is in process.

Table 1 describes the experiments performed.

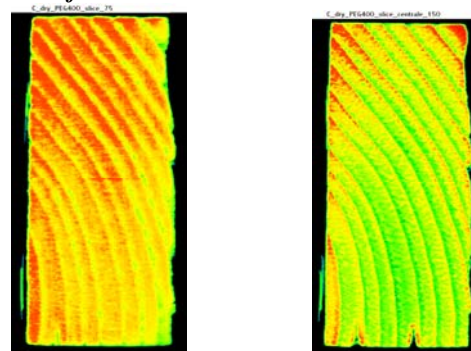
Treatment	Range of Attenuation Coefficient (cm <sup>-1</sup> )	Volume %
Dry wood A with solution 1	1.90 - 2.78	11.0
Dry wood B with solution 1	1.90 - 2.80	9.5
Dry wood C with solution 1	1.90 - 2.89	11.0
Dry wood A with solution 2	1.90 - 3.66	20.0
Dry wood B with solution 2	1.90 - 2.65	4.5
Dry wood C with solution 2	1.90 - 2.85	8.4
Sample A - Wet wood with solution 2	1.90 - 2.28	1.8
Sample B - Wet wood equilibrated with solution 2	1.90 - 2.36	1.0
Sample C - Wet wood with solution 2	1.90 - 2.37	0.6
Sample A with solution 3	1.90-2.23	1.7
Sample B with solution 3	1.90-2.27	4.0
Sample C with solution 3	1.90-2.91	22.0

From the NT data the distribution of PEG inside the samples has been obtained. By comparing surface slices with inside slices it appears evident that the low molecular weight PEG (PEG 400) penetrates deeper and more uniformly than the high molecular weight PEG

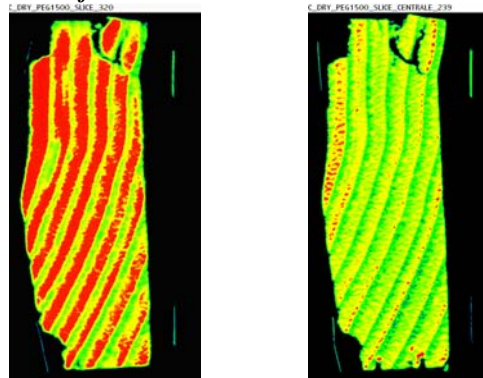
**Sample dry A equilibrated with PEG400**  
*Surface Slice*                      *Centre Slice*



**Sample dry B equilibrated with PEG400**  
*Surface Slice*                      *Centre Slice*



**Sample dry C equilibrated with PEG1500**  
*Surface Slice*                      *Centre Slice*



	<b>EXPERIMENTAL REPORT</b>	Proposal N° ART-04-1688 Instrument <b>V7</b> Local Contact N. Kardjilov
	<b>Investigating Wood Conservation Procedures by Neutron Tomography</b>	Date(s) of Experiment 19/08/2008 – 23/08/2008
Principal Proposer: Roberto Triolo – Università di Palermo (Italy) Experimental Team: Roberto Triolo – UNIPA (Italy) Irene Ruffo – ITC “L. Sturzo”–Bagheria (Italy) E. Fertitta and L. Chiappisi–UNIPA (Italy)	Date of Report: January 2009	

When buried in the ground or in water, wood is well known to decay under combined biological and chemical attack. A successful conservation strategy depends strongly upon the original wood structure and the kind of treatment. Here we report Neutron Tomography (NT) and Neutron Radiography (NR) measurements on several wood samples “naturally” and artificially deteriorated, before and after treatment with impregnating materials. In particular six Pine samples naturally deteriorated by the Brown Rot have been measured as received, then after solvent extraction and finally after equilibration with solutions of Klucel in D<sub>2</sub>O, Ethanol and Acetone and Colophony in Ethanol and Acetone. Figure 1 shows two internal sections of a wood sample before (left) and after (right) equilibration with a solution of Colophony in ethanol. From these sections the histograms derived are shown below. A clear increase of the component with high attenuation factor (the Colophony) is a consequence of the filling of the voids. Clearly, a comparison of the histograms of the different sections gives information on the efficiency of the treatment and on the penetrability of the impregnating medium.

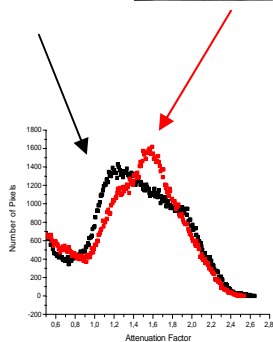
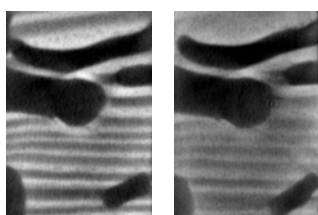


Figure 1 Dry vs. Impregnated Pine sample

Because of the smaller number of days granted with respect to the proposal request, experiments with samples “in situ” impregnated with Paraloid B72 have not been performed. Neutron Tomography data and X ray Tomography (XT) data for a Pine sample are compared in figure 2.

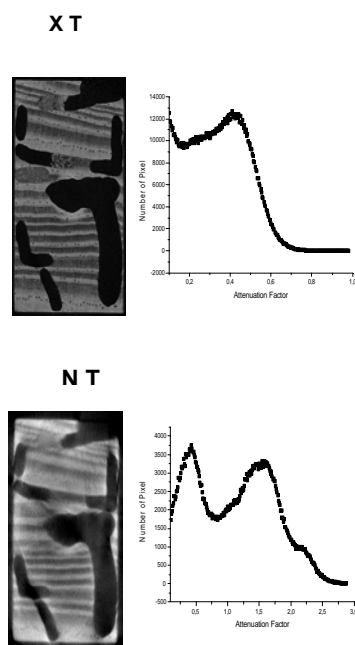


Figure 2 NT and XT on a Pine sample

Comparison of the histograms obtained from NT and XT indicates that, in this case, neutron data are richer in details (and therefore in information) than X-ray data, even if the resolution of the XT data is higher. This is due to the particularly high sensitivity of neutrons to hydrogen. Of course, the situation would be different if NT and XT data for other systems would be compared. For example, in the case of marbles, XT data are richer in details than NT. In that case the higher space resolution of the XT data gives more detailed information than NT. In our case, as most of the consolidating media are highly hydrogenated materials, NT data may play a significant role.

	<b>EXPERIMENTAL REPORT</b>  <b>Neutron autoradiographs of Paris Bordone: The two Chess Players</b>	Proposal N° ART-05-0030 Instrument <b>B8</b> Local Contact A. Denker
	Principal Proposer: C. Laurenze-Landsberg Experimental Team: C. Laurenze-Landsberg, C. Schmidt, B. Schröder-Smeibidl	Date(s) of Experiment  Nov. 2006

Date of Report: 17 December 2008

The autoradiographs of this painting reveal that Bordone altered the position of the bodies, heads and arms several times during the paintings process. In one of the earlier versions the man on the left was positioned closer to the edge of the painting; his coat covered the bench he was sitting on. The lower part of the gown seems to have extended beyond the left border of the painting. The upper left edge of the table, now covered by his elbow, was visible. Straight thin lines, visible both in the autoradiograph and in the x-ray radiograph, can be interpreted as incisions in the ground delineating the contour of this coat.

As this version is visible in the x-ray radiograph as well as in the first autoradiograph we may conclude that the colour of this coat was light brown. This fact is confirmed by the structure of the paint layer. Optical examination of the area revealed that there is an underlying brown paint layer.

In another version the man was positioned where he is today. However, his coat extended further to the left near the bench, which suggests he may have been sitting in a more bent position. The contour of the back of his gown is clarified with a thin line of paint containing copper. A tile had to be added in the now uncovered floor.

A minor adjustment was made to the position of his right arm, which was located slightly lower as his hand. Interestingly, this hand either once held the tissue now in the hand of his counterpart or maybe both gamblers were in the need of a tissue.

His head was depicted more in profile; a fact that can be observed better in the x-ray radiograph.

The figure on the right hand side also underwent subsequent changes. His shoulders were originally broader, suggesting a frontal view. Both his arms and hands were altered several times. His left arm was shown extended and directed downwards, a hand with or without tissue. His right arm was in two of the previous versions more angled and the hand also shows several revisions. In one version, the pawn was held higher and diagonal, as if he was unsure where to place it. The sleeves and collar were painted in the same copper green that has been found in the folds under the shoulder of his opponent.

In the background several changes can be observed. Important for the interpretation is the substitution of an object that appears to be a fountain on the x-ray radiograph by a group of men gambling at a table in the garden and thus repeating the theme of the painting.

The architecture was painted originally with higher and more delicate columns on a floor with smaller tiles. In the lower half of the painting Bordone had removed paint with a broad spatula.

In summary, we can state that the visual information provided by the autoradiographs and the x-ray radiograph are in accordance with the findings in other Bordone paintings. The basic contours of the figures appear to have been indicated with thin calligraphic lines. Various revisions were made before the figures had been finally positioned: the man on the left is set more in profile, whereas his opponent could be viewed more in a frontal position.

Special importance was laid on defining the two players and by accentuating the manoeuvre by which one of them will win. The viewers' attention is drawn to the meaning of the composition by the group of gamblers in the background.



Kat. N° 169 - Paris Bordone: The two Chess Players, 1550 – 55, Canvas, 112 x 181 cm



# **Fundamental Physics and Others**





## EXPERIMENTAL REPORT

### Spatial Distribution of Neutrons Scattered by Vibrating Crystals

Proposal N° PHY-01-2237

Instrument **E6**

Local Contact  
Norbert Stüßer

Principal Proposer: E. Raitman, L.A.S., Latvia  
 Experimental Team: E. Raitman, L.A.S. Latvia  
 V. Gavrilovs, L.A.S., Latvia  
 Norbert Stüßer, HMI, Berlin

Date(s) of Experiment

19/05/2008 – 26/05/2008

Date of Report:

The dynamical diffraction and inelastic scattering of neutron in perfect and bent silicon single crystals undergoing to the ultrasonic excitation were studied and the so-called Kato's profiles were observed. As preliminary calculations of the Kato's equation (taking into account ultrasonic excitation) have shown, one can expect for regime of small ultrasound waves amplitudes the fine oscillations in spatial neutron intensities distribution, and sharp increase of intensity in the Bormann triangle center for the high level ultrasonic excitation depending on the ultrasound frequency and samples thickness.

The aim of the experiments was to determine how high frequency vibrations introduced into a perfect crystal effect on the Kato's profiles in thick crystal.

The experiments were carried out on BENSC E6 diffractometer. As a sample very high quality Ge single crystal with thickness  $T=2,2$  cm was used. The intensities of diffractions for (111) reflections depending on the acoustic waves (AW) amplitudes (hf-generators voltage) were measured. The scanning was realised by using high sensitive PSD detector. The narrow forming slit with width 1.0 mm was used for higher collimation

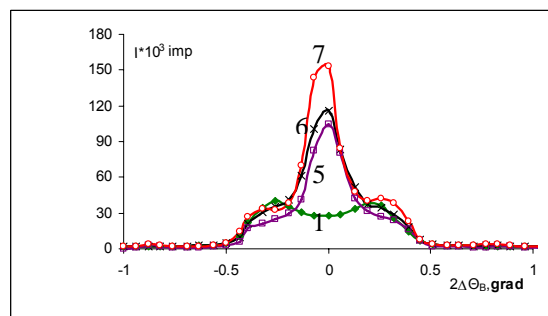
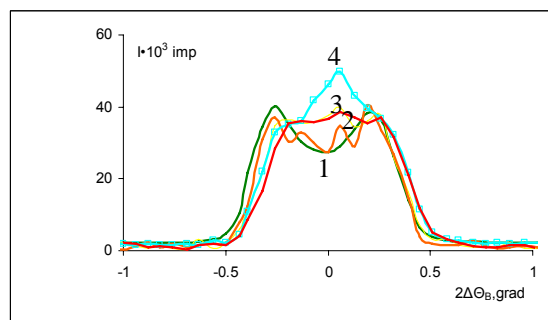
Transverse acoustic waves ( $k_s \perp H$ , where  $k_s$  is acoustic waves number) in the sample were excited by applying hf-voltage to the quarc piezo transducer ( $f_s = 39.5$  MHz) glued with salol to the sample surface. The self-resonance conditions for Ge was found by tuning to the maximum of diffraction intensity responding to the frequency changes.

The main results are shown on Fig. 1:

Fig.1. Kato's profiles for a Ge 22mm thick crystal in the  $2\Theta_B$ -space: 1- (—) - without sound, 2- (---) - with hf-generator voltage  $V_G = 0.25V$  (some oscillations (fringes) is clearly seen), 3- (—)  $V_G=0.38V$ , 4- (—)  $V_G = 1V$ , 5- (—)  $V_G = 2V$ , 6- (—)  $V_G = 3V$ , 7- (—)  $V_G = 5V$

It is shown that

- i) for relatively small AW amplitudes at least 3-4 "sound" fringes (oscillations) (curve 2) are pronounced and their sizes agrees with evaluations. The resolutions was not enough but the situation can be improved by using more narrow slits and small scanning steps.
- ii) the intensities of the Kato's profile center sharply increases with AW amplitudes growth and gain factor of 5.5 was achieved for  $V_G=5.0$  V. These results may be promising for an intensity -to- resolution governed by ultrasound monochromator creating. However, it needs further investigations.





**EXPERIMENTAL REPORT**  
**Coherent Scattering Neutron Imaging of Nickel Single Crystal**

Proposal N°  
 MAT-04-1685  
 Instrument **V7**  
 Local Contact  
 N. Kardjilov

Principal Proposer: M. B. Tamaki, (TAMAKI Memorial Institute, Japan), L. Josic (PSI)  
 Experimental Team: G. Frei, E. H. Lehmann, (PSI)  
 A. Hilger, N. Kardjilov, (HZB)

Date(s) of Experiment  
 26/11/2008 – 27/11/2008

Date of Report: January 2009

Coherent scattering of neutron wave is induced by interaction with periodic structure of materials. The phenomena observed in a single crystal may be detected by monochromatic neutron imaging. The single crystal having lattice plane distance ( $d_{BE}$ ) is applied to neutron imaging for computed tomography as shown in Fig. 1.

The coherent scattering condition may be represented by the Bragg's equation of

$$\lambda = 2 d_{BE} \sin(\phi + (90 - \theta)) \sin(90 - \zeta).$$

The relation between parameters is shown in Figure 2. When  $\phi_1$  and  $\phi_2$  satisfy Bragg condition,  $(\phi_1 + \phi_2)/2 = \phi_{BE}$  gives direction of Bragg-cut-off plane. When we find  $\zeta$  by any additional process, all the relation among wavelength, lattice plane distance and CT rotation angle can be determined.

Experiments had been conducted by using the neutron imaging facility CONRAD at HZB, which has a tunable monochromatic neutron beam. A single crystal of nickel ( $d_{BE} = 2.01\text{\AA}$ ) was used as a sample for neutron computed tomography. Rotation angular range was 180 degrees by a step of 1 degree. The 9 kinds of projection datasets were obtained in a range of neutron wavelength from 3.00Å to 4.20Å by a step of 0.15Å.

From the 9 kinds of projection datasets, all crystallographic parameters concerned to the single crystal of nickel have been evaluated as shown in Figure 3.

Further analysis of projection datasets has been intensively continuing to propose the concept and to establish the mathematical treatment for the coherent scattering CT-reconstruction as well as the conventional CT-ones.

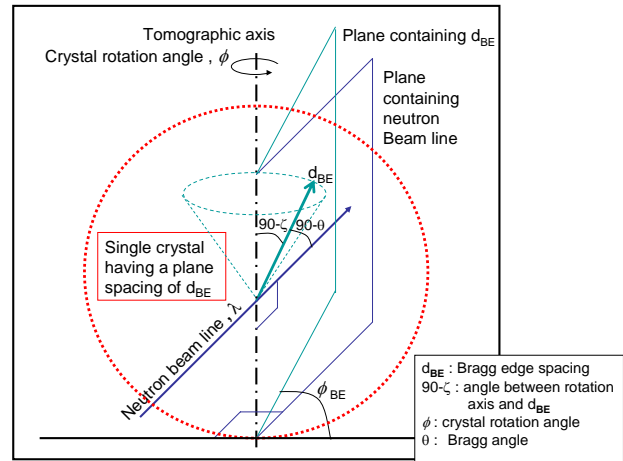


Fig. 1 Concept of coherent CT set-up for single crystal.

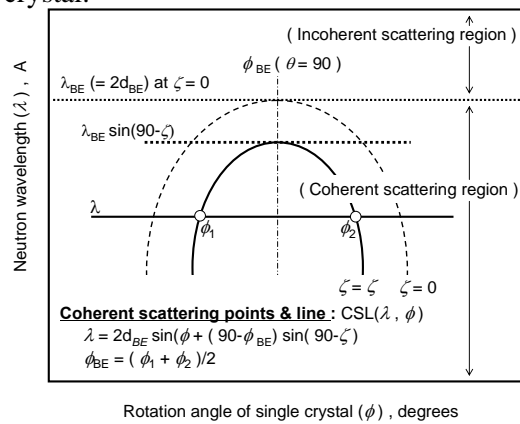


Fig. 2. Determination of coherent scattering points.

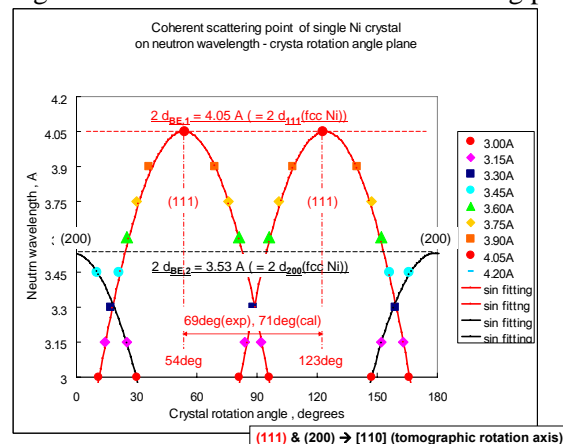


Fig.3. Results of coherent scattering parameters





# **Part II**

## **List of Publications**

<b>Theses</b>	<b>265</b>
<b>Publications</b>	<b>266</b>
<b>Conference Contributions</b>	<b>284</b>
<b>Seminar Talks</b>	<b>290</b>
<b>Posters</b>	<b>299</b>
<b>Author Index</b>	<b>309</b>



**Theses 2008**  
Examina

**PhD theses**

**2006 (supplement)**

<i>Franz, A.</i> <b>Sauerstoffdefizitäre Perowskite im System BaPbO<sub>3-x</sub> - BaSnO<sub>3</sub></b> Leipzig (2006)	E9
--	----

**2008**

<i>Bordallo, H.</i> <b>Structure et Dynamique à l'échelle Microscopique des Systèmes Incommensurables, des Oxydes à Magnéto-Résistance Géantes et des Systèmes Biologiques</b> Montpellier, Univ., Habil.-Schr. (2008)	
<i>Ianeselli, L.</i> <b>Reentrant Condensation of Proteins Induced by Multivalent Ions in Solution</b> Eberhard Karls Universität Tübingen (2008)	V4
<i>Kreitlow, J.</i> <b>Druckstudien zu strukturellen und magnetischen Eigenschaften molekularer und molekülbasierter Magnete</b> TU Braunschweig (2008)	E6
<i>Lenne, T</i> <b>Contrast variation SANS study of the phase morphology of lipid/sugar/water mixtures resulting from dehydration</b> RMIT University, Melbourne, Australia (2008)	V4
<i>Mufti, N</i> <b>Magnetic and electric response in multiferroic manganites</b> University of Groningen (2008)	E4 NMI3: 1253 NMI3: 1343
<i>Romanenko A.</i> <b>Giant elasticity of the Ni-M-Ga martensites</b> National Aviation University (Kiev, Ukraine) (2008)	E2
<i>Shirish N. Chodankar</i> <b>Structural Evolution in Different Phases of Protein Solution as Studied by Scattering</b> University of Mumbai (2008)	V4

**Publications 2008**  
BENSC Experiments and BENSC Authors

**2006 (supplement)**

<i>Kobler, U.; Hoser, A.</i> <b>Effective spin description of crystal field effects in NdAl<sub>2</sub></b> Journal of Magnetism and Magnetic Materials <b>299</b> (2006), 145 - 154	E1, E2, E6
<i>Matsushima, U.</i> <b>Efficient Photosynthesis and Auto-exhaust Resistance of Street Trees</b> NISSAN Science Foundation, 2005 (2006), 1 - 4	V7
<i>Sazonov, A.P.; Troyanchuk, I.O.; Sikolenko, V.V.</i> <b>Spin state of Cobalt ions in NdCoO<sub>3</sub></b> Crystallography Reports <b>51</b> (2006), 11 – 15	E1, E9 NMI3: 1170 NMI3: 1171
<i>Schilling, H.; Lerch, M.; Borger, A.; Becker, K.D.; Wolff, H.; Dronskowski, R.; Bredow, T.; Tovar, M.; Baetz, C.</i> <b>A new anatase-type phase in the system Mg-Ta-O-N</b> Journal of Solid State Chemistry <b>179</b> (8): 2416-2425, (2006)	
<i>Siemensmeyer, K.; Flachbart, K.; Gabani, S.; Matas, S.; Paderno, Y.; Shitsevalova, N.</i> <b>Magnetic structure of rare-earth dodecaborides</b> Journal of Solid State Chemistry, Volume <b>179</b> , 2748 (2006)	E4, V10
<i>Sikolenko, V.; Sazonov, A.; Efimov, V.V.; Efimova, E.A.; Kriventsov, V.V.; Kochubey, D.I.; Zimmermann, U.</i> <b>Phase separation in La<sub>1-x</sub>Sr<sub>x</sub>CoO<sub>3</sub> solid solutions with perovskite structure</b> Crystallography Reports <b>51</b> (2006), S67 – S75	E1, E9 NMI3: 1170 NMI3: 1171
<i>Wiedenmann, A.</i> <b>Small angle neutron scattering investigations of magnetic nanostructures</b> Chatterji, T. [Ed.] : Neutron scattering from magnetic materials. Amsterdam: Elsevier, 2006. - ISBN 0-444-51050-8 (2006), 473 - 520	V4

**2007 (supplement)**

<i>Davies, C.M.; Wimpory, R.C.; Beres, M.; Lightfoot, M.P.; Dye, D.; Oliver, E.; O'Dowd, N.P.; Bruce, G.J.; Nikbin, K.M.</i> <b>The effect of residual stress and microstructure on distortion in thin welded steel plates</b> Proceedings of the ASME Pressure Vessels and Piping Conference - 2007. Vol. <b>6</b> : Materials and Fabrication. New York: ASME, 2008. p. 851-858	
<i>Kardiljov, N.; Lo Celso, F.; Donato, D. I.; Hilger, A.; Triolo, R.</i> <b>Applied neutron tomography in modern archaeology</b> Nuovo Cimento della Società Italiana di Fisica. C, Geophysics and Space Physics <b>1</b> (2007), 79 – 83	V7 NMI3: 1252
<i>Köbler, U.; Hoser, A.</i> <b>First order spin flop transition in yttrium iron garnet (YIG)</b> Solid State Communications <b>142</b> (2007), 350 - 354	E2
<i>Köbler, U.; Hoser, A.</i> <b>The crossover from atomistic to continuous dynamic symmetry at the magnetic phase transition</b> Solid State Communications <b>142</b> (2007), 600 - 604	E2, E4, E6

<i>Köbler, U.; Hoser, A.</i> <b>Critical magnetic behaviour in one and two dimensions</b> Journal of Magnetism and Magnetic Materials <b>311</b> (2007), 523 - 529	E4, E6, V2
<i>Köbler, U.; Hoser, A.</i> <b>The impact of renormalization group theory on magnetism</b> European Physical Journal B <b>60</b> (2007), 151 - 159	E2, E6
<i>Köbler, U.; Hoser, A.; Mueller, R.M.; Fischer, K.</i> <b>Complex critical magnetic behaviour in three dimensions</b> Journal of Magnetism and Magnetic Materials <b>315</b> (2007), 12 - 25	E4, E6
<i>Koetschau, I.M.; Rodriguez-Alvarez, H.; Streeck, C.; Weber, A.; Klaus, M.; Denks, I.A.; Gibmeier, J.; Genzel, C.; Schock, H.-W.</i> <b>Pressure dependent rapid thermal processing of CuInS<sub>2</sub> thin films investigated by in-situ energy dispersive X-ray diffraction</b> Thin-film Compound Semiconductor Photovoltaics - 2007 <b>1012</b> (2007), 503	S4
<i>Kolasinska, M.; Krastev, R.; Warszynski, P.</i> <b>Characteristics of polyelectrolyte multilayers: Effect of PEI anchoring layer and posttreatment after deposition</b> Journal of Colloid and Interface Science <b>305</b> (2007), 46 - 56	V6
<i>Matsushima, U.</i> <b>Neutron Imaging for Life Science -Recent Studies-, in Japanese</b> Radioisotopes <b>56</b> (2007), 59 – 71	V7
<i>Milani, S.; Baldelli Bombelli, F.; Berti, D.; Dante, S.; Hauß, T.; Baglioni, P.</i> <b>Nucleolipid membranes: structure and molecular recognition</b> Journal of Physics: Condensed Matter <b>20</b> (2007), 104212 - 1-7	V1 NMI3: 1201
<i>Sazonov, A.P.; Troyanchuk, I.O.; Sikolenko, V.V.; Szymczak, H.; Bärner, K.</i> <b>Effect of the oxygen nonstoichiometry on the structure and magnetic properties of Nd<sub>2</sub>CoMnO<sub>6</sub>+<sub>x</sub>; double perovskites</b> Physical Status Solidi B <b>1-10</b> (2007), 200642481	E6
<i>Strobl, M.; Treimer W.; Walter, P.; Keil, S.; Manke, I.</i> <b>Magnetic field induced differential neutron phase contrast imaging</b> Applied Physics Letters 91 (2007), p. 254104/1-3	V12b
<i>Witte, U.; Schedler, R.; Stockert, O.; Loewenhaupt, M.</i> <b>The Investigation of the Crystalline Electric Field of CeCu<sub>2</sub> and CeCu<sub>6</sub></b> Journal of Low Temperature Physics <b>147</b> (3/4), 97-110 (2007)	

## 2008

<i>Abbas, S.; Wagh, A G.; Treimer, W.</i> <b>First neutron diffraction pattern from a macroscopic grating</b> Solid State Physics (India) <b>53</b> (2008), 555	V12b
<i>Abbas, S.; Wagh, A.G.</i> <b>Pancharatnam geometric phase originating from successive partial projection</b> PRAMANA: Journal of Physics <b>71</b> (2008), 1115	V12a
<i>Abbas, S.; Wagh, A.G.; Treimer, W.</i> <b>Neutron forward diffraction by single crystal prisms</b> PRAMANA: Journal of Physics <b>71</b> (2008), 1109	V12b
<i>Abou-Ras, D.; Gibmeier, J.; Nolze, G.; Gholinia, A.; Konijnenberg, P.</i> <b>On the capability of revealing the pseudosymmetry of the chalcopyrite-type crystal structure</b> Crystal Research and Technology <b>43</b> (2008), 234 - 239	

<p><i>Aliouane, N.; Prokhnenko, O.; Feyerherm, R.; Mostovoy, M.; Stremper, J.; Habicht, K.; Rule, K.C.; Dudzik, E.; Wolter, A.U.B.; Maljuk, A.; Argyriou, D.N.</i>  <b>Magnetic order and ferroelectricity in RMnO<sub>3</sub> multiferroic manganites: coupling between R- and Mn-spins</b>  <i>Journal of Physics: Condensed Matter</i> <b>20</b> (2008), 434215/1 - 12</p>	E2
<p><i>Amoretti, G.; Caciuffo, R.; Carretta, S.; Guidi, T.; Magnani, N.; Santini, P.</i>  <b>Inelastic neutron scattering investigations of molecular nanomagnets</b>  <i>Inorganica Chimica Acta</i> <b>361</b> (2008), 3771 - 3776</p>	V3
<p><i>Aynajian, P.; Keller, T.; Boeri, L.; Shapiro M.; Habicht, K.; Keimer, B.</i>  <b>Energy Gaps and Kohn Anomalies in Elemental Superconductors</b>  <i>Science</i> <b>319</b> (2008), 1509 – 1512</p>	V2
<p><i>Baldelli Bombelli, F.; Berti, D.; Milani, S.; Lagi, M.; Barbaro, P.; Karlsson, G.; Brandt, A.; Baglioni, P.</i>  <b>Collective headgroup conformational transition in twisted micellar superstructures</b>  <i>Soft Matter</i> <b>4</b> (2008), 1102 – 1113</p>	V1, V4 NMI3: 1022 NMI3: 1063
<p><i>Baranov, N. V.; Michor, H.; Hilscher, G.; Proshkin, A.; Podlesnyak, A.</i>  <b>Extra T-linear specific heat contribution induced by the f-d-exchange in Gd-Ni binary compounds</b>  <i>Journal of Physics: Condensed Matter</i> <b>20</b> (2008), 325233</p>	
<p><i>Barath, H.; Kim, M.; Cooper, S. L.; Abbamonte, P.; Fradkin, E.; Mahns, I.; Ruebhausen, M.; Aliouane, N.; Argyriou, D. N.</i>  <b>Domain fluctuations near the field-induced incommensurate-commensurate phase transition of TbMnO<sub>3</sub></b>  <i>Physical Review B: Condensed Matter</i> <b>78</b> (2008), 134407</p>	
<p><i>Bastjan, M.; Singer, S.G.; Neuber, G.; Eller, S.; Aliouane, N.; Argyriou, D.N.; Cooper, S.L.; Rubhausen, M.</i>  <b>Magneto-optical study of the spin-polarized electronic states in multiferroic TbMnO<sub>3</sub></b>  <i>Physical Review B: Condensed Matter</i> <b>77</b> (2008), 193105</p>	
<p><i>Bellouard, C.; Faure-Vincent, J.; Tiusan, C.; Montaigne, F.; Hehn, M.; Leiner, V.; Fritzsche, H.; Gierlings, M.</i>  <b>Interlayer magnetic coupling in Fe/MgO junctions characterized by vector magnetization measurements combined with polarized neutron reflectometry</b>  <i>Physical Review B: Condensed Matter</i> <b>78</b> (2008), 134429</p>	V6 IHP11: 503
<p><i>Bergner, F.; Ulbricht, A.; Hein, H.; Kammel, M.</i>  <b>Flux dependence of cluster formation in neutron-irradiated weld material</b>  <i>Journal of Physics: Condensed Matter</i> <b>20</b> (2008), 104262</p>	V4
<p><i>Biehl, R.; Hoffmann, B.; Monkenbusch, M.; Falus, P.; Prévost, S.; Merkel, R.; Richter, D.</i>  <b>Direct observation of correlated interdomain motion in alcohol dehydrogenase</b>  <i>Physical Review Letters</i> <b>101</b> (2008), 138102</p>	V4
<p><i>Bobrovskij, V.; Kazantsev, V.; Mirmelstein, A.; Mushnikov, N.; Proskurnina, N.; Voronin, V.; Pomjakushina, E.; Conder, K.; Podlesnyak, A.</i>  <b>Spontaneous and field-induced magnetic transitions in YBaCo<sub>2</sub>O<sub>5.5</sub></b>  <i>Journal of Magnetism and Magnetic Materials</i> <b>321</b> (2008), 429 - 437</p>	
<p><i>Bogach, A.; Bogomolov, L.; Glushkov, V.; Demishev, S.; Sluchanko, D.; Sluchanko, N.; Shitsevalova, N.; Levchenko, A.; Filipov, V.; Flachbart, K.; Siemensmeyer, K.</i>  <b>Bulk and Local Magnetic Susceptibility of ErB<sub>12</sub></b>  <i>Acta Physica Polonica A</i> <b>113</b> (2008), 271 - 274</p>	

<p><i>Bohnenbuck, B.; Zegkinoglou, I.; Stempffer, J.; Schüßler-Langeheine, C.; Nelson, C.S.; Leininger, Ph.; Wu, H.-H.; Schierle, E.; Lang, J.C.; Srajer, G.; Ikeda, S.I.; Yoshida, Y.; Iwata, K.; Katano, S.; Kikugawa, N.; Keimer, B.</i>  <b>Magnetic structure and orbital state of Ca<sub>3</sub>Ru<sub>2</sub>O<sub>7</sub> investigated by resonant x-ray diffraction</b>  Physical Review B <b>77</b> (2008), 224412/1 - 5</p>	
<p><i>Boiko, V.; Matas, S.; Siemensmeyer, K.</i>  <b>Preparation and orientation of solid <sup>3</sup>He crystals for neutron diffraction investigations</b>  Journal of Physics: Condensed Matter <b>20</b> (2008), 104246 - 1-6</p>	
<p><i>Bonini, M.; Lenz, S.; Falletta, E.; Ridi, F.; Carretti, E.; Fratini, E.; Wiedenmann, A.; Baglioni, P.</i>  <b>Acrylamide-Based Magnetic Nanosponges: A New Smart Nanocomposite Material</b>  Langmuir <b>24</b> (2008), 12644 – 12650</p>	V4 NMI3: 1293
<p><i>Bordallo, H.N.; Aldridge, L.P.; Churchman, G.J.; Gates, W.P.; Telling, M.T.F.; Kiefer, K.; Fouquet, P.; Seydel, T.; Kimber, S.A.J.</i>  <b>Quasi-elastic neutron scattering studies on clay interlayer-space highlighting the effect of the cation in confined water dynamics</b>  Journal of Physical Chemistry C <b>112</b> (2008), 13982 - 13991</p>	
<p><i>Bordallo, H.N.; Boldyreva, E.V.; Buchsteiner, A.; Koza, M.M.; Landsgesell, S.</i>  <b>Structure-property relationships in the crystals of the smallest amino acid: An incoherent inelastic neutron scattering study of the glycine polymorphs</b>  Journal of Physical Chemistry B <b>112</b> (2008), 8748 - 8759</p>	
<p><i>Börner, H.G.; Smarsly, B.M.; Hentschel, J.; Rank, A.; Schubert, R.; Geng, Y.; Discher, D.E.; Hellweg, T.; Brandt, A.</i>  <b>Organization of Self-Assembled Peptide-Polymer Nanofibers in Solution</b>  Macromolecules <b>41</b> (2008), 1430 – 1437</p>	V4
<p><i>Bouwman, W. G.; Plomp, J.; de Haan, V.O.; Kraan, W.H.; van Well, A.A.; Keller, T.; Habicht, K.; Rekveldt, M.T.</i>  <b>Real-space neutron scattering methods</b>  Nuclear Instruments and Methods in Physics Research A <b>586</b> (2008), 9 – 14</p>	V2
<p><i>Buchsteiner, A.; Stüßler, N.</i>  <b>Optimizations in angular dispersive neutron powder diffraction using divergent beam geometries</b>  Nuclear Instruments and Methods in Physics Research A (2008)</p>	
<p><i>Carretta, S.; Guidi, T.; Santini, P.; Amoretti, G.; Pieper, O.; Lake, B.; Slagereen, v.J.; Hallak, F. El; Wernsdorfer, W.; Mutka, H.; Russina, M.; Milios, C.J.; Brechin, E.K.</i>  <b>Breakdown of the Giant Spin Model in the Magnetic Relaxation of the Mn<sub>6</sub> Nanomagnets</b>  Physical Review Letters <b>100</b> (2008), 157203 - 1-4</p>	V3
<p><i>Chang, J.; Niedermayer, Ch.; Gilardi, R.; Christensen, N. B.; Ronnow, H. M.; McMorro, D. F.; Ay, M.; Stahn, J.; Sobolev, O.; Hiess, A.; Pailhes, S.; Baines, C.; Momono, N.; Oda, M.; Ido, M.; Mesot, J.</i>  <b>Tuning competing orders in La<sub>2</sub>-xSrxCuO<sub>4</sub> cuprate superconductors by the application of an external magnetic field</b>  Physical Review B: Condensed Matter <b>78</b> (2008), 104525 -</p>	V2

<p><i>Chernyshov, D.; Dmitriev, V.; Pomjakushina, E.; Conder, K.; Stingaciu, M.; Pomjakushin, V.; Podlesnyak, A.; Taskin, A. A.; Ando, Y.</i>  <b>Superstructure formation at the metal-insulator transition in RBaCo<sub>2</sub>O<sub>5.5</sub> (R=Nd,Tb) as seen from reciprocal space mapping</b>  Physical Review B: Condensed Matter <b>78</b> (2008), 24105</p>	
<p><i>Chmielus, M.; Chernenko, V. A.; Knowlton, W. B.; Kostorz, G.; Muellner, P.</i>  <b>Training, constraints, and high-cycle magneto-mechanical properties of Ni-Mn-Ga magnetic shape-memory alloys</b>  European Physical Journal - The Special Topics <b>158</b> (2008), 79 - 85</p>	
<p><i>Cserhádi, C.; Balogh, Z.; Csik, A.; Langer, G.A.; Erdélyi, Z.; Glodán, G.; Katona, G.L.; Beke, D.L.; Zizak, I.; Darowski, N.; Dudzik, E.; Feyerherm, R.</i>  <b>Linear growth kinetics of nanometric silicides in Co/amorphous-Si and Co/CoSi/amorphous-Si thin films</b>  Journal of Applied Physics <b>104</b> (2008), 024311/1 - 6</p>	
<p><i>Dalle-Ferrier, C.; Eibl S.; Pappas, C.; Alba-Simionesco, C.</i>  <b>Temperature dependence of three-point correlation functions of viscous liquids: the case of glycerol</b>  Journal of Physics: Condensed Matter <b>20</b> (2008), 494240/1 - 7</p>	V5
<p><i>Danilyan, G.V.; Wilpert, T.; Granz, P.; Krakhotin, V.A.; Mezei, F.; Novitsky, V.V.; Pavlov, V.S.; Russina, M.V.; Shatalov, P.B.</i>  <b>Angular correlations in emission of precession neutrons from U-235 fission induced by slow polarized neutrons</b>  Physics of Atomic Nuclei <b>71</b> (2008), 2003 - 2006</p>	V13
<p><i>Dante, S.; Hauß, Th.; Brandt, A.; Dencher, N.A.</i>  <b>Membrane fusogenic activity of the Alzheimer's peptide A<math>\beta</math>(1-42) demonstrated by small-angle neutron scattering</b>  Journal of Molecular Biology <b>376</b> (2008), 393 - 404</p>	
<p><i>Davies, C. M.; Wimpory, R.C.; Tabuchi, M.; Dean, D.W.; Nikbin, K.M.</i>  <b>The influence of specimen geometry and test times on high temperature crack growth behaviour in parent and welded 316H stainless steel</b> (2008), Proceedings of ASME Pressure Vessels and Piping Division Conference July 27-31 Chicago, Illinois, USA [Ausg. auf CD]. p. 1-9</p>	
<p><i>Dawson, M.; Kardjilov, N.; Manke, I.; Hilger, A.; Banhart, J.</i>  <b>Imaging magnetic fields with neutrons</b>  The newsletter of the British Institute of Radiology</p>	
<p><i>de la Rosa-Fox, N.; Morales-Florez, V.; Toledo-Fernandez, J. A.; Pinero, M.; Esquivias, L.; Keiderling, U.</i>  <b>SANS study of hybrid silica aerogels under "in situ" uniaxial compression</b>  J. of Sol-Gel Sci. <b>45</b> (2008), 245 – 250</p>	V4 NMI3: 1087 NMI3: 1150
<p><i>De Lisi, R.; Gradzielski, M.; Lazzara, G.; Milioto, S.; Muratore, N.; Prévost, S.</i>  <b>Aqueous Laponite Clay Dispersions in the Presence of Poly(ethylene oxide) or Poly(propylene oxide) Oligomers and their Triblock Copolymers</b>  Journal of Physical Chemistry B <b>112</b> (2008), 9328 - 9336</p>	V4 NMI3: 1300
<p><i>Denks, I. A.; Genzel, Ch.</i>  <b>Improvements in energy dispersive diffraction in respect of residual stress analysis</b>  Materials Science Forum <b>571-572</b> (2008), 189</p>	
<p><i>Desmedt, A.; Kitchin, S.; Harris, K.D.M.; Guillaume, F.; Tykwinski, R.R.; Xu, M.; Gonzalez, M.A.</i>  <b>Dynamic properties of solid ammonium cyanate</b>  Journal of Physical Chemistry C <b>512</b> (2008), 15870</p>	V3 IHP11: 424

<p><i>Dyakonov, V.; Bukhanko, F. N.; Kamenev, V. I.; Zubov, E. E.; Arciszewska, M.; Dobrowolski, W.; Mikhaylov, V.; Puzniak, R.; Wisniewski, A.; Piotrowski, K.; Varyukhin, V.; Szymczak, H.; Szytula, A.; Duraj, R.; Stüsser, N.; Arulraj, A.; Baran, S.; Penc, B.; J</i></p> <p><b>Lattice distortion effect on structure and on spin ordering of Mn ions in La<sub>1-x</sub>NdxMnO<sub>3</sub>+delta manganites</b></p> <p>Physical Review B: Condensed Matter <b>77</b> (2008), 214428</p>	E6 NMI3: 1255
<p><i>Efimova, E.; Efimov, V.; Karpinsky, D.; Kuzmin, K.; Purans, J.; Sikolenko, V.; Tiutiunnikov, S.; Troyanchuk, I.; Welter, E.; Dajac, D.; Simkin, V.; Sazonov, A.</i></p> <p><b>Short- and long-range order in La<sub>1-x</sub>SrxCoO<sub>3</sub> and La<sub>1-x</sub>BaxCoO<sub>3</sub></b></p> <p>Journal of Physics and Chemistry of Solids <b>69</b> (2008), 2187 - 2190</p>	E1, E9, V4 NMI3: 1243
<p><i>Eichelbaum, M.; Rademann, K.; Hoell, A.; Tatchev, D. M.; Weigel, W.; Stoesser, R.; Pacchioni, G.</i></p> <p><b>Photoluminescence of atomic gold and silver particles in soda-lime silicate glasses</b></p> <p>Nanotechnology <b>19</b> (2008), 135701</p>	S3
<p><i>Erko, A.; Idir, M.; Krist, Th.; Michette, A. [Eds.]</i></p> <p><b>Modern developments in X-ray and neutron optics</b></p> <p>XVI, 533 p.: 150 b/w ill., 20 b/w photos, 130 b/w graph. ill. (2008) Berlin: Springer, 2008 (Springer series in optical sciences). - ISBN 978-3-540-74560-0 XVI, 533 pages</p>	
<p><i>Fiori, F.; Calbucci, V.; Casalegno, V.; Ferraris, M.; Salvo, M.; Giuliani, A.; Manescu, A.; Rustichelli, F.</i></p> <p><b>Neutron diffraction measurement of residual stresses in CFC/Cu/CuCrZr joints for nuclear fusion technology</b></p> <p>Journal of Physics: Condensed Matter <b>20</b> (2008), 104260</p>	E3 NMI3: 1337
<p><i>Fokin, A.; Kumzerov, Y.; Koroleva, E.; Naberezhnov, A.; Smirnov, O.; Tovar, M.; Vakhrushev, S.; Glazman, M.</i></p> <p><b>Ferroelectric phase transitions in sodium nitrite nanocomposites</b></p> <p>Journal of Electroceramics (2008), 1 – 7</p>	E9
<p><i>Friedrich, F.; Sieber, I.; Klaus, M.; Genzel, Ch.; Nickel, N. H.</i></p> <p><b>Pulsed-laser deposition of ZnO thin-films on MgO substrates</b></p> <p>Physica Status Solidi <b>5</b> (2008), p. 3288-3292</p>	
<p><i>Friedrichs, O.; Kim, J. W.; Remhof, A.; Buchter, F.; Borgschulte, A.; Wallacher, D.; Cho, Y. W.; Fichtner, M.; Oh, K. H.; Züttel, A.</i></p> <p><b>The effect of Al on the hydrogen sorption mechanism of LiBH<sub>4</sub></b></p> <p>Physical Chemistry Chemical Physics <b>11</b> (2009), 1515 - 1520</p>	E6 NMI3: 1314
<p><i>Gabani, S.; Matas, S.; Priputen, P.; Flachbart, K.; Siemensmeyer, K.; Wulf, E.; Evdokimova, A.; Shitsevalova, N.</i></p> <p><b>Magnetic Structure and Phase Diagram of TmB<sub>4</sub></b></p> <p>Acta Physica Polonica A <b>113</b> (2008), 227 - 230</p>	
<p><i>Gamari-Seale, H.; Troyanchuk, I. O.; Sazonov, A. P.; Stefanopoulos, K. L.; Toebbens, D. M.</i></p> <p><b>Structure and magnetic order in La<sub>0.7</sub>Ca<sub>0.3</sub>Nn<sub>0.5</sub>Co<sub>0.5</sub>O<sub>3</sub> and La<sub>0.8</sub>Sr<sub>0.2</sub>Mn<sub>0.5</sub>Co<sub>0.5</sub>O<sub>3</sub> perovskites</b></p> <p>Physica B - Condensed Matter <b>403</b> (2008), 2924</p>	E9
<p><i>Garlea, V.O.; Zheludev, A.; Regnault, L.-P.; Chung, J.-H.; Qiu, Y.; Boehm, M.; Habicht, K.; Meissner, M.</i></p> <p><b>Excitations in a Four-Leg Antiferromagnetic Heisenberg Spin Tube</b></p> <p>Physical Review Letters <b>100</b> (2008), 037206 - 1-4</p>	V2
<p><i>Gibmeier, J.; Klaus, M.; Scholtes, B.</i></p> <p><b>In-situ investigation of the deformation behaviour of the wrought Mg base alloy AZ31 using energy dispersive synchrotron diffraction</b></p> <p>Materials Science Forum <b>571-572</b> (2008), p. 195-200</p>	

<p><i>Gibmeier, J.; Scholtes, B.</i>  <b>Instrumented Indentation Testing on Uniaxial Prestressed Steel Samples</b>  Materials Science Forum <b>571-572</b> (2008), 83 - 88</p>	
<p><i>Glavatskyy, I.; Glavatska, N.; Urubkov, I.; Hoffman, J.-U.; Bourdarot, F.</i>  <b>Crystal and magnetic structure temperature evolution in Ni-Mn-Ga magnetic shape memory martensite</b>  Materials Science and Engineering A <b>481-482</b> (2008), 298 - 301</p>	E2
<p><i>Glushkov, V.; Demishev, S.; Ignatov, M.; Khayrullin, E.; Sluchanko, N.; Shitsevalova, N.; Levchenko, A.; Filipov, V.; Flachbart, K.; Siemensmeyer, K.</i>  <b>Phonon Drag and Magnetic Anomalies of Thermopower in RB12 (R= Ho, Er, Tm, Lu)</b>  Acta Physica Polonica A <b>113</b> (2008), 275 - 278</p>	
<p><i>Goldman, A. I.; Argyriou, D. N.; Ouladdiaf, B.; Chatterji, T.; Kreyssig, A.; Nandi, S.; Ni, N.; Bud'ko, S. L.; Canfield, P. C.; McQueeney, R. J.</i>  <b>Lattice and magnetic instabilities in CaFe<sub>2</sub>As<sub>2</sub>: A single-crystal neutron diffraction study</b>  Physical Review B: Condensed Matter <b>78</b> (2008), 100506</p>	
<p><i>Gondek, L.; Arulray, A.; Baran, S.; Nenkov, K.; Penc, B.; Szytula, A.; Tomala, K.</i>  <b>Magnetic properties of Ho<sub>3-x</sub>Y<sub>x</sub>Cu<sub>4</sub>Sn<sub>4</sub> (x=0, 1, 2)</b>  Journal of Physics: Condensed Matter <b>20</b> (2008), 295205</p>	E9 NMI3: 1174
<p><i>Gondek, L.; Szytula, A.; Prokhnenko, O.</i>  <b>Complex magnetic behaviour of Ho<sub>3</sub>Cu<sub>4</sub>X<sub>4</sub> compounds (X = si and sn)</b>  Acta Physica Polonica A <b>113</b> (2008), 1179 - 1184</p>	E9 NMI3: 1174 NMI3: 1217
<p><i>Gournis, D.; Lappas, A.; Karakassides, M.A.; Többers, D.; Moukarika, A.</i>  <b>A neutron diffraction study of alkali cation migration in montmorillonites</b>  Phy Chem Minerals <b>35</b> (2008), 49 – 58</p>	E6, E9 IHP: 193 IHP: 194
<p><i>Gruyters, M.; Schmitz, D.</i>  <b>Microscopic nature of ferro- and antiferromagnetic interface coupling of uncompensated magnetic moments in exchange bias systems</b>  Physical Review Letters <b>100</b> (2008), 077205 1 - 4</p>	
<p><i>Gummel, J.; Boué, F.; Clemens, D; Cousin, F.</i>  <b>Finite size and inner structure controlled by electrostatic screening in globular complexes of proteins and polyelectrolytes</b>  Soft Matter <b>4</b> (2008), 1653 – 1664</p>	V4 IHP: 1094 IHP: 1059
<p><i>Gutberlet Th.; Klösgen B.; Krastev R.; Steitz R.</i>  <b>Neutron Reflectivity as Method to Study in-Situ Adsorption of Phospholipid Layers to Solid-Liquid Interfaces</b>  Advanced Engineering Materials <b>6</b> (2004), 832 - 836</p>	V6
<p><i>Habel, D.; Goerke, O.; Tovar, M.; Kondratenko, E.; Schubert, H.</i>  <b>Phase Relations in the System TiO<sub>2</sub>-V<sub>2</sub>O<sub>5</sub> under Oxidizing and Reducing Conditions</b>  Journal of Phase Equilibria and Diffusion <b>29</b> (2008), 482 - 487</p>	
<p><i>Hartnig, C.; Manke, I.; Kuhn, R.; Kardjilov, N.; Banhart, J.; Lehnert, W.</i>  <b>Cross-sectional insight in the water evolution and transport in polymer electrolyte fuel cells</b>  Applied Physics Letters <b>92</b> (2008), 134106 - 1-3</p>	S5

<p><i>Hartnig, Ch.; Kuhn, R.; Krüger, P.; Manke, I.; Kardjilov, N.; Goebbels, J.; Müller, B.R.; Riesemeier, H.</i></p> <p><b>Wassermanagement in Brennstoffzellen - die Bedeutung von hochauflösenden zerstörungsfreien Untersuchungsmethoden</b></p> <p>MP materials testing : materials and components, technology and application <b>50</b> (2008), 609 – 613</p>	
<p><i>Hartnig, Ch.; Manke, I.; Kardjilov, N.; Hilger, A.; Gruenerbel, M.; Kaczerowski, J.; Banhart, J.; Lehnert, W.</i></p> <p><b>Combined neutron radiography and locally resolved current density measurements of operating PEM fuel cells</b></p> <p>Journal of Power Sources <b>176</b> (2008), 452 - 459</p>	V12a
<p><i>Hollmann, O.; Steitz, R.; Czeslik, C.</i></p> <p><b>Structure and dynamics of a-lactalbumin adsorbed at a charged brush interface</b></p> <p>Physical Chemistry Chemical Physics <b>10</b> (2008), 1448 - 1456</p>	V6
<p><i>Huberman, T.; Tennant, D. A.; Cowley, R. A.; Coldea, R.; Frost, C. D.</i></p> <p><b>A study of the quantum classical crossover in the spin dynamics of the 2D S=5/2 antiferromagnet Rb<sub>2</sub>MnF<sub>4</sub>: neutron scattering, computer simulations and analytic theories</b></p> <p>Journal of Statistical Mechanics - Theory and Experiment (2008), P05017</p>	
<p><i>Imperia, P.; Kandulski, W.; Kosiorek, A.; Glaczynska, H.; Maletta, H.; Giersig, M.</i></p> <p><b>Magnetic anisotropy study of triangular-shaped Co nanostructures</b></p> <p>Journal of Magnetism and Magnetic Materials <b>320</b> (2008), 2682</p>	S1
<p><i>Ivanova, O.; Soltwedel, O.; Gopinadhan, M.; Köhler, R.; Steitz, R.; Helm, C.A.</i></p> <p><b>Strong Binding of Light Water and Proton-Deuterium Exchange in Polyelectrolyte Multilayers</b></p> <p>Macromolecules <b>41</b> (2008), 7179 – 7185</p>	V6
<p><i>Jalarvo, N.; Bordallo, H.N.; Aliouane, N.; Adams, M.A.; Pieper, J.; Argyriou, D.N.</i></p> <p><b>Dynamics of Water in Na<sub>x</sub>CoO<sub>2</sub> yH<sub>2</sub>O</b></p> <p>Journal of Physical Chemistry B <b>112</b> (2008), 703</p>	V3
<p><i>Jauch, W.; Reehuis, M.</i></p> <p><b>Electron density distribution in ferromagnetic nickel: A gamma-ray diffraction study</b></p> <p>Physical Review B <b>78</b> (2008), 235113/1 - 8</p>	E5
<p><i>Jesche, A.; Caroca-Canales, N.; Rosner, H.; Borrmann, H.; Ormeci, A.; Kasinathan, D.; Klauss, H. H.; Luetkens, H.; Khasanov, R.; Amato, A.; Hoser, A.; Kaneko, K.; Krellner, C.; Geibel, C.</i></p> <p><b>Strong coupling between magnetic and structural order parameters in SrFe<sub>2</sub>As<sub>2</sub></b></p> <p>Physical Review B: Condensed Matter <b>78</b> (2008), 180504</p>	
<p><i>Jestin, J.; Cousin, F.; Dubois, I.; Ménager, C.; Schweins, R.; Oberdisse, J.; Boué, F.</i></p> <p><b>Anisotropic reinforcement of nanocomposites tuned by magnetic orientation of the filler network</b></p> <p>Advanced Materials <b>20</b> (2008), 2533 - 2540</p>	V4 IHP: 1016
<p><i>Kaneko, K.; Hoser, A.; Caroca-Canales, N.; Jesche, A.; Krellner, C.; Stockert, O.; Geibel, C.</i></p> <p><b>Columnar magnetic structure coupled with orthorhombic distortion in the antiferromagnetic iron arsenide SrFe<sub>2</sub>As<sub>2</sub></b></p> <p>Physical Review B <b>78</b> (2008), 212502, 1 - 4</p>	V4

<p><i>Kardjilov, N.; Hilger, A.; Manke, I.; Benfante, V.; Lo Celso, F.; Triolo, R.; Ruffo, I.; Tusa, S.</i>  <b>Neutron tomography in modern archaeology</b>  Notiziario Neutroni e Luce di Sincrotrone <b>13</b> (2008), 6 - 9</p>	
<p><i>Kardjilov, N.; Hilger, A.; Manke, I.; Garcia-Moreno, F.; Banhart, J.</i>  <b>Bragg-edge imaging with neutrons</b>  MP materials testing : materials and components, technology and application <b>50</b> (2008), 569 – 571</p>	
<p><i>Kardjilov, N.; Manke, I.; Strobl, M.; Hilger, A.; Treimer, W.; Meissner, M.; Krist, T.; Banhart, J.</i>  <b>Three-dimensional imaging of magnetic fields with polarized neutrons</b>  Nature Physics <b>4</b> (2008), 399 – 403</p>	
<p><i>Kardjilov, N.; Hilger, A.; Manke, I.; Strobl, M.; Treimer, W.; Banhart, J.</i>  <b>Multifunctional Tomography Instrument with Cold Neutrons at HMI</b>  Neutron Radiography (2008), 28 – 33</p>	V7
<p><i>Kardjilov, N.; Manke, I.; Hilger, A.; Dawson, M.; Banhart, J.</i>  <b>Imaging with magnetic neutrons</b>  Advanced Materials and Processes <b>166</b> (2008), 43 - 44</p>	V7
<p><i>Karpinsky, D. V.; Troyanchuk, I. O.; Sazonov, A. P.; Savelieva, O. A.; Heinemann, A.</i>  <b>High resolution diffraction and small angle scattering neutron investigations of LaCo<sub>0.5</sub>Mn<sub>0.5</sub>O<sub>3</sub>+<math>\delta</math>: effect of oxygen content</b>  European Physical Journal B <b>60</b> (2008), 273</p>	V4
<p><i>Keiderling, U.; Wiedenmann, A.; Rupp, A.; Klenke, J.; Heil, W.</i>  <b>SANS polarization analysis at V4 SANS instrument of HMI Berlin</b>  Measurement Science and Technology <b>19</b> (2008), 034009 – 1 - 8</p>	V4
<p><i>Kessner, D.; Kiselev, M.; Dante, S.; Hauß, T.; Lersch, P.; Wartewig, S.; Neubert, R.H.H.</i>  <b>Arrangement of ceramide [EOS] in a stratum corneum lipid model matrix: new aspects revealed by neutron diffraction studies</b>  European Biophysics Journal <b>37</b>, (2008) 989-999</p>	
<p><i>Kessner, D.; Kiselev, M.A.; Hauß, T.; Dante, S.; Wartewig, S.; Neubert, R.H.</i>  <b>Localisation of partially deuterated cholesterol in quaternary SC lipid model membranes: a neutron diffraction study</b>  European Biophysics Journal <b>37</b>, (2008) 1051-1057</p>	
<p><i>Khalyavin, D. D.; Argyriou, D. N.; Amann, U.; Yaremchenko, A. A.; Kharton, V. V.</i>  <b>Low-temperature behavior of YBaCo<sub>2</sub>O<sub>5.5</sub>: Coexistence of two spin-state ordered phases</b>  Physical Review B: Condensed Matter <b>77</b> (2008), 64419</p>	E2, E9 NMI3: 1177
<p><i>Khalyavin, D. D.; Prokhnenko, O.; Stuesser, N.; Sikolenko, V.; Efimov, V.; Salak, A. N.; Yaremchenko, A. A.; Kharton, V. V.</i>  <b>Crystal and magnetic structures of NdBaCo<sub>2</sub>O<sub>5</sub>+<math>\delta</math> (<math>\delta</math> similar to 0.75): A neutron diffraction study</b>  Physical Review B: Condensed Matter <b>77</b> (2008), 174417</p>	E6, E9
<p><i>Kim, J.-H.; Ji, S.; Lee, S.-H.; Lake, B.; Yildirim, T.; Nojiri, H.; Kikuchi, H.; Habicht, K.; Qiu, Y.; Kiefer, K.</i>  <b>External magnetic field effects on a distorted kagome antiferromagnet</b>  Physical Review Letters <b>101</b> (2008), 107201/1 - 4</p>	
<p><i>Kim, T.-J.; Kardjilov, N.; Sim, C.-M.; Kim, M.-H.</i>  <b>The investigation of water discharge characteristics at PEMFC by using neutron imaging technique at CONRAD, HMI</b>  Lancaster: Destech. Publ. (2008), 425 - 431</p>	

<p><i>Kimber, S. A. J.; Argyriou, D. N.; Yokaichiya, F.; Habicht, K.; Gerischer, S.; Hansen, T.; Chatterji, T.; Klingeler, R.; Hess, C.; Behr, G.; Kondrat, A.; Büchner, B.</i></p> <p><b>Magnetic ordering and negative thermal expansion in PrFeAsO</b> Physical Review B <b>78</b>, 140503-4 (2008)</p>	
<p><i>Kipping, D.; Gähler, R.; Habicht, K.</i></p> <p><b>Small angle neutron scattering at very high time resolution: Principle and simulations of 'TISANE'</b> Physics Letters A <b>372</b> (2008), 1541 - 1546</p>	
<p><i>Kiselev, M. A.; Gutberlet, T.; Hoell, A.; Aksenov, V. L.; Lombardo, D.</i></p> <p><b>Orientation of the DMPC unilamellar vesicle system in the magnetic field: SANS study</b> Chemical Physics <b>345</b> (2008), 181</p>	V4
<p><i>Kiselev, M. A.; Zernlyanaya, E. V.; Ryabova, N. Y.; Hauss, T.; Dante, S.; Lombardo, D.</i></p> <p><b>Water distribution function across the curved lipid bilayer: SANS study</b> Chemical Physics <b>345</b> (2008), 185 – 190</p>	
<p><i>Klaus, M.; Genzel, Ch.; Holzschuh, H.</i></p> <p><b>X-Ray Residual Stress Analysis in CVD Multilayer Systems: Influence of Gradients on the Line Profile Shape and -Symmetry</b> Zeitschrift für Kristallographie <b>27</b>, 273 - 285</p>	
<p><i>Klobes, B.; Staab, T. E. M.; Dudzik, E.</i></p> <p><b>Early stages of decomposition in Al alloys investigated by X-ray absorption</b> Physica Status Solidi - Rapid Research Letters <b>2</b> (2008), 182</p>	S2
<p><i>Knabe, C.; Koch, C.; Rack, A.; Stiller, M.</i></p> <p><b>Effect of beta-tricalcium phosphate particles with varying porosity on osteogenesis after sinus floor augmentation in humans</b> Biomaterials <b>29</b> (2008), 2249</p>	
<p><i>Kovacs-Mezei, R.; Krist, T.; Revay, Z.</i></p> <p><b>Non-magnetic supermirrors produced at Mirrotron Ltd.</b> Nuclear Instruments and Methods in Physics Research Section A <b>586</b> (2008), 51 – 54</p>	V14
<p><i>Kreyssig, A.; Green, M. A.; Lee, Y.; Samolyuk, G. D.; Zajdel, P.; Lynn, J. W.; Bud'ko, S. L.; Torikachvili, M. S.; Ni, N.; Nandi, S.; Leao, J. B.; Poulton, S. J.; Argyriou, D. N.; Harmon, B. N.; McQueeney, R. J.; Canfield, P. C.; Goldman, A. I.</i></p> <p><b>Pressure-induced volume-collapsed tetragonal phase of CaFe<sub>2</sub>As<sub>2</sub> as seen via neutron scattering</b> Physical Review B: Condensed Matter <b>78</b> (2008), 184517</p>	
<p><i>Krist, T.; Teichert, A.; Kovacs-Mezei, R.; Rosta, L.</i></p> <p><b>Neutron supermirror development</b> Springer, (2008) (Springer series in optical sciences; <b>137</b>). - p. 355-370</p>	
<p><i>Krist, T.; Teichert, A.; Meltchakov, E.; Vidal, V.; Zoethout, E.; Müllender, S.; Bijkerk, F.</i></p> <p><b>Stress reduction in multilayers used for X-ray and neutron optics</b> Springer, (2008) (Springer series in optical sciences; <b>137</b>). - p. 371 - 388</p>	
<p><i>Kusmin, A.; Lechner, R.E.; Kammel, M.; Saenger, W.</i></p> <p><b>Native and Methylated Cyclodextrins with Positive and Negative Solubility Coefficients in Water Studied by SAXS and SANS</b> Journal of Physical Chemistry B <b>112</b> (2008), 12888</p>	V4
<p><i>Le, M.D.; McEwen, K.A.; Park, J-G.; Lee, S.; Iga, F.; Rule, K.C.</i></p> <p><b>Magnetic Excitations in the Ordered Phases of Praseodymium Hexaboride</b> Journal of Physics: Condensed Matter <b>20</b> (2008), 104231</p>	V2 NMI3: 1163 NMI3: 1237

<p><i>Lefmann, K.; Schober, H.; Mezei, F.</i>  <b>Simulation of a multiple-wavelength time-of-flight neutron spectrometer for a long-pulsed spallation source</b>  Measurement Science and Technology <b>19</b> (2008), 034025 - 1-12</p>	V3
<p><i>Lyphout, C.; Nylén, P.; Manescu A.; Pirling, T.</i>  <b>Residual Stresses Distribution through Thick HVOF Sprayed Inconel 718 Coatings</b>  Journal of Thermal Spray Technology <b>17</b> (2008), 1059</p>	E3 NMI3: 1291 NMI3: 1338
<p><i>Mahnke, H. -E.; Zizak, I.; Schubert-Bischoff, P.; Koteski, V.</i>  <b>Ion-beam induced nano-sized Ag-metal clusters in glass</b>  Material Science and Engineering B <b>149</b> (2008), 200 - 203</p>	
<p><i>Manescu, A; Fiori, F.; Giuliani, A.; Kardjilov, N.; Kasztovszky, Z.; Rustichelli, F.; Straumal, B.</i>  <b>Non-destructive compositional analysis of historic organ reed pipes</b>  Journal of Physics: Condensed Matter <b>20</b> (2008), 104250</p>	V7 NMI3: 1292
<p><i>Manke, I.; Hartnig, Ch.; Kardjilov, N.; Hilger, A.; Lehnert, W.; Banhart, J.</i>  <b>Neutronen-Radiographie und -Tomographie in der Brennstoffzellenforschung</b>  ZfP-Zeitung <b>Ausgabe 109</b> (2008), 35 - 39</p>	
<p><i>Manke, I.; Kardjilov, N.; Hilger, A.; Strobl, M.; Dawson, M.; Banhart, J.</i>  <b>Visualisierung dreidimensionaler magnetischer Feldverteilungen mit spin-polarisierten Neutronen</b>  MP materials testing : materials and components, technology and application <b>50</b> (2008), 572 – 579</p>	
<p><i>Manke, I.; Hartnig, C.; Kardjilov, N.; Hilger, A.; Strobl, M.; Lehnert, W.; Banhart, J.</i>  <b>Characterization of water exchange and two-phase flow in porous gas diffusion materials by hydrogen-deuterium contrast neutron radiography</b>  Applied Physics Letters <b>92</b> (2008), 244101-1 - 244101-3</p>	V7
<p><i>Manke, I.; Kardjilov, N.; Strobl, M.; Hilger, A.; Banhart, J.</i>  <b>Investigation of the skin effect in the bulk of electrical conductors with spin-polarized neutron radiography</b>  Materials Science and Engineering B <b>104</b> (2008), 076109-1 - 076109-3</p>	V7
<p><i>Matsushima, U.; Kardjilov, N.; Hilger, A.; Graf, W.; Herppich, W.B.</i>  <b>Application potential of cold neutron radiography in plant science research</b>  Journal of Applied Botany and Food Quality <b>82</b> (2008), 90 - 98</p>	
<p><i>Matsushima, U.; Kardjilov, N.; Hilger, A.; Ueno, M.; Kawamitsu, Y.; Nishizawa, T.; Herppich, W.B.</i>  <b>Visualization of water flow in tomato seedlings using neutron imaging</b>  Lancaster: Destech Publ. (2008), 358 - 362</p>	
<p><i>Milani, S.; Berti, D.; Dante, S.; Hauss, T.; Baglioni, P.</i>  <b>Intercalation of Single-Strand Oligonucleotides between Nucleolipid Anionic Membranes: A Neutron Diffraction Study</b>  Langmuir <b>25</b> (2008), 4084 – 4092</p>	
<p><i>Mueller, J; Wuttke, M; Kardjilov, N; Hilger, A</i>  <b>A burrowing, lacertid-like squamate from the eocene of Messel, Germany</b>  Journal of Vertebrate Paleontology <b>28 [Suppl.]</b> (2008), 119A</p>	
<p><i>Mufti, N.; Nugroho, A.A.; Blake, G.R.; Palstra, T.T.M.</i>  <b>Relaxor ferroelectric behavior in Ca-doped TbMnO3</b>  Physical Review B: Condensed Matter <b>78</b> (2008), 024109</p>	E4 IHP: 1253

<p><i>Mukherji, D.; Lackner, J.; Wanderka, N.; Kardjilov, N.; Näth, O.; Jäger, S.; Schmitz, F.; Rösler, J.</i>  <b>Coating of meso-porous metallic membranes with oriented channel-like fine pores by pulsed laser deposition</b>  Nanotechnology <b>19</b> (2008), 065706/1 - 8</p>	
<p><i>Mukherji, D.; Del Genovese, D.; Strunz, P.; Gilles, R.; Wiedenmann, A.; Rösler, J.</i>  <b>Microstructural characterisation of a Ni-Fe-based superalloy by in situ small-angle neutron scattering measurements</b>  Journal of Physics: Condensed Matter <b>20</b> (2008), 104220 - 1-9</p>	V4
<p><i>Nakajima, T.; Mitsuda, S.; Inami, T.; Terada, N.; Ohsumi, H.; Prokes, K.; Podlesnyak, A.</i>  <b>Identification of microscopic spin-polarization coupling in the ferroelectric phase of magnetoelectric multiferroic CuFe<sub>1-x</sub>Al<sub>x</sub>O<sub>2</sub></b>  Physical Review B: Condensed Matter <b>78</b> (2008), 024106</p>	E4
<p><i>Neov, D.; Ohms, C.; Wimpory, R.C.; Youtsos, A.G.</i>  <b>Residual stress analyses by neutron diffraction in irradiated double-V butt welded steel plates</b>  Materials Science Forum <b>571-572</b> (2008), 381 - 386</p>	
<p><i>Nyam-Ochir, L.; Ehrenberg, H.; Buchsteiner, A.; Senyshyn, A.; Fuess, H.; Sangaa, D.</i>  <b>The magnetic structures of double tungstates, NaM(WO<sub>4</sub>)<sub>2</sub>, M = Fe, Cr: examples for superexchange couplings mediated by [NaO<sub>6</sub>]-octahedra</b>  Journal of Magnetism and Magnetic Materials <b>320</b> (2008) 3251 - 3255</p>	E6
<p><i>O'Dowd, N. P.; Nikbin, K. M.; Wimpory, R.C.; Biglari, F. R.; O'Donnell, M.P.</i>  <b>Computational and experimental studies of high temperature crack initiation in the presence of residual stress</b>  Journal of Pressure Vessel Technology <b>130</b> (2008), 041403/1 - 7</p>	
<p><i>Ohira-Kawamura, S.; Shishido, H.; Kawano-Furukawa, H.; Lake, B.; Wiedenmann, A.; Kiefer, K.; Shibauchi, T.; Matsuda, Y.</i>  <b>Anomalous Flux Line Lattice in CeCoIn<sub>5</sub></b>  Journal of the Physical Society of Japan <b>77</b> (2008), 023702 – 1 - 4</p>	V4
<p><i>Ohms, C.; Martins, R.V.; Uca, O.; Youtsos, A.G.; Bouchard, P.J.; Smith, M.; Keavey, M.; Bate, S.K.; Gilles, P.; Wimpory, R.C.; Edwards, L.</i>  <b>The European Network on Neutron Techniques Standardization for Structural Integrity - NeT</b>  ASME Pressure Vessels and Piping Division Conference July 27-31, 2008, Chicago, Illinois, USA [Ausg. auf CD]. (2008), p. 1-13</p>	
<p><i>Ortore, M. G.; Sinibaldi, R.; Spinuzzi, F.; Carsughi, F.; Clemens, D.; Bonincontro, A.; Mariani, P.</i>  <b>New Insights into Urea Action on Proteins: A SANS Study of the Lysozyme Case</b>  Journal of Physical Chemistry B <b>112</b> (2008), 12881 - 12887</p>	V4
<p><i>Papaefthimiou, V.; Steitz, R.; Findenegg, G.H.</i>  <b>Schaltbare Oberfläche. Responsive Polymerschichten</b>  Chemie in unserer Zeit <b>42</b> (2008), 102 - 115</p>	
<p><i>Pappas, C.; Lelievre-Berna, E.; Bentley, P.; Bourgeat-Lami, E.; Moskvina, E.; Thomas, M.; Grigoriev, S.; Dyadkin, V.</i>  <b>Polarimetric neutron spin echo: Feasibility and first results</b>  Nuclear Instrument and Methods in Physics Research, A <b>592</b> (2008), 420 – 427</p>	
<p><i>Paul-Boncour, V.; Hoser, A.; Hense, K.; Gratz, E.; Rotter, M.; Stüßler, N.</i>  <b>Magnetic phase diagram of Ho-Ag</b>  Journal of Physics: Condensed Matter <b>20</b> (2008), 104225 - 1-5</p>	E6 IHP11: 498

<p><i>Pieper, J.; Buchsteiner, A.; Dencher, N.A.; Lechner, R.E.; Hauß, T.</i>  <b>Transient Protein Softening during the Working Cycle of a Molecular Machine</b>  <i>Physical Review Letters</i> <b>100</b> (2008), 228103 - 1 - 4</p>	V3
<p><i>Pieper, J.; Hauß, T.; Buchsteiner, A.; Renger, G.</i>  <b>The effect of hydration on protein flexibility in photosystem II of green plants studied by quasielastic neutron scattering.</b>  <i>European Biophysics Journal</i> <b>37</b> (2008) 657-663</p>	
<p><i>Podlesnyak, A.; Russina, M.; Furrer, A.; Alfonsov, A.; Vavilova, A.; Kataev, V.; Büchner, A.; Strässle, T.; Pomjakushina, A.; Conder, K.; Khomskii, D.</i>  <b>Spin-State Polarons in Lightly-Hole-Doped LaCoO<sub>3</sub></b>  <i>PRL</i> <b>101</b>, (2008) 247603</p>	
<p><i>Prokes, K.</i>  <b>Uranium Intermetallics in High Magnetic Fields: Neutron Diffraction Experiments</b>  <i>Acta Physica Polonica A</i> <b>113</b> (2008), 209 - 214</p>	
<p><i>Prokes, K.; Muñoz-Sandoval, E.; Chinchure, A.D.; Mydosh, J.A.</i>  <b>Competing magnetic structures and magnetic transitions in Er<sub>2</sub>Ni<sub>2</sub>Pb: Powder neutron diffraction measurements</b>  <i>Physical Review B</i> <b>78</b> (2008), 014425, 1 - 11</p>	
<p><i>Prokes, K.; Wand, T.; Andreev, A.V.; Meissner, M.; Honda, F.; Sechovský, V.</i>  <b>Magnetic specific heat and magnetoresistance of URhSi</b>  <i>Journal of Alloys and Compounds</i> <b>460</b> (2008), 47 - 53</p>	
<p><i>Prokes, K.; Prchal, J.; Sechovsky, V.; Andreev, A.V.</i>  <b>Magnetic Structure in UIrAl</b>  <i>Acta Physica Polonica A</i> <b>113</b> (2008), 339 - 342</p>	E4
<p><i>Prokes, K.; Sechovsky, V.; Boer, de F.R.; Andreev, A.V.</i>  <b>The field-induced magnetic structure in UIrGe</b>  <i>Journal of Physics: Condensed Matter</i> <b>20</b> (2008), 104221 - 1-3</p>	E4
<p><i>Rack, A.; Zabler, S.; Müller, B.R.; Riesemeier, H.; Weidemann, G.; Lange, A.; Goebbels, J.; Hentschel, M.; Görner, W.</i>  <b>High resolution synchrotron-based radiography and tomography using hard X-rays at the BAMline (BESSY II)</b>  <i>Nuclear Instruments and Methods in Physics Research Section A</i> <b>586</b> (2008), 327 – 344</p>	S5
<p><i>Raichle, M.; Reehuis, M.; Andre, G.; Capogna, L.; Sofin, M.; Jansen, M.; Keimer, B.</i>  <b>Incommensurate spin-density modulation in a copper oxide chain compound with commensurate charge order</b>  <i>Physical Review Letters</i> <b>101</b> (2008), 047202-1 - 047202-4</p>	E5
<p><i>Rajamathi, J.; Arulraj, A.; Ravishankar, N.; Arulraj, J.; Rajamathi, M.</i>  <b>Delamination of surfactant-intercalated brucite-like hydroxy salts of cobalt and copper and solvothermal decomposition of the resultant colloidal dispersions</b>  <i>Langmuir</i> <b>24</b> (2008), 11164 – 11168</p>	
<p><i>Rajput, P.; Gupta, A.; Meneghini, C.; Avasthi, D. K.; Darowski, N.; Zizak, I.; Erko, A.</i>  <b>Depth resolved structural study of heavy ion induced phase formation in Si/Fe/Si trilayer</b>  <i>Hyperfine Interactions</i> <b>185</b> (2008), 9 - 15</p>	
<p><i>Reehuis, M.; Ulrich, C.; Pattison, P.; Miyasaka, M.; Tokura, Y.; Keimer, B.</i>  <b>Crystal and magnetic structure of CeVO<sub>3</sub></b>  <i>European Physical Journal B</i> <b>64</b> (2008), 27 - 34</p>	E5

<p><i>Remhof, A.; Friedrichs, O.; Buchter, F.; Mauron, Ph.; Züttel, A.; Wallacher, D.</i>  <b>Solid-state synthesis of LiBD4 observed by in situ neutron diffraction</b>  Physical Chemistry Chemical Physics <b>10</b> (2008), 5859 - 5862</p>	E6
<p><i>Robinson, J.S.; Truman, C.E.; Hossain, S.; Wimpory, R.</i>  <b>Residual stress and microstructural variations in thick aluminium alloy forgings</b>  Materials Science Forum <b>571-572</b> (2008), 45 - 50</p>	
<p><i>Rogante, M.; Lebedev V.T.</i>  <b>SANS comparative investigation of Inconel 738 samples submitted to different ageing treatments</b>  Materials and Design <b>29</b> (2008), 1060 - 1065</p>	V12
<p><i>Rolfs, K.; Mecklenburg, A.; Guldbakke, J.-M.; Wimpory, R.C.; Ratz, A; Hesselbach, J; Schneider, R.</i>  <b>Crystal Quality Boosts Responsiveness of Magnetic Shape Memory Single Crystals</b>  Applied Physics Letters <b>92</b> (2008), p. 244101/1-3</p>	
<p><i>Ruegg, C.; Kiefer, K.; Thielemann, B.; McMorro, D.F.; Zapf, V.; Normand, B.; Zvonarev, M.B.; Bouillot, P.; Kollath, C.; Giamarchi, T.; Capponi, S.; Poilblanc, D.; Biner, D.; Kramer, K.W.</i>  <b>Thermodynamics of the Spin Luttinger Liquid in a Model Ladder Material</b>  Physical Review Letters <b>101</b> (2008), 247202</p>	
<p><i>Ruettinger, A.; Kiselev, M.A.; Hauss, T.; Dante, S.; Balagurov, A.M.; Neubert, R.H.</i>  <b>Fatty acid interdigitation in stratum corneum model membranes: a neutron diffraction study</b>  European Biophysics Journal <b>37</b> (2008) 759-771</p>	
<p><i>Rule, K. C.; Ehlers, G.; Stewart, J. R.; Cornelius, A. L.; Deen, P. P.; Qiu, Y.; Wiebe, C. R.; Janik, J. A.; Zhou, H. D.; Antonio, D.; Woytko, B. W.; Ruff, J. P.; Dabkowska, H. A.; Gaulin, B. D.; Gardner, J. S.</i>  <b>Polarized inelastic neutron scattering of the partially ordered Tb<sub>2</sub>Sn<sub>2</sub>O<sub>7</sub></b>  Physical Review B: Condensed Matter <b>76</b> (2008), 212405</p>	
<p><i>Rule, K.; Wolter, A.U.B.; Süllow, S.; Tennant, D.A.; Brühl, A.; Köhler, S.; Wolf, B.; Lang, M.; Schreuer, J.</i>  <b>Nature of the Spin Dynamics and 1/3 Magnetization Plateau in Azurite</b>  Physical Review Letters <b>100</b> (2008), 117202 - 1-4</p>	V2
<p><i>Rule, K.C.; Wolter, A.U.B.; Süllow, S.; Tennant, D.A.; Brühl, A.; Köhler, S.; Wolf, B.; Lang, M.; Schreuer, J.</i>  <b>Nature of the Spin Dynamics and 1/3 Magnetization Plateau in Azurite</b>  Physical Review Letters <b>100</b> (2008), 117202</p>	V2
<p><i>Salak A.N.; Vyshatko N.P.; Khalyavin D.D.; Prokhnenko O.; Ferreira V.M.</i>  <b>Low-temperature structural and dielectric phenomena in La<sub>1/3</sub>NbO<sub>3</sub> and La<sub>1/3</sub>TaO<sub>3</sub>: comparative study</b>  Applied Physics Letters <b>93</b> (2008), 162903</p>	E6, E9 NMI3: 1309
<p><i>Salak, A.N.; Prokhnenko O.; Ferreira V.M.</i>  <b>Temperature evolution of the crystal structures in La(Mg<sub>1/2</sub>Ti<sub>1/2</sub>)O<sub>3</sub> perovskite: relation to the microwave dielectric properties</b>  Journal of Physics: Condensed Matter <b>20</b> (2008) 085210</p>	E9 NMI3: 1219
<p><i>Schierle, E.; Weschke, E.; Gottberg, A.; Sollinger, W.; Heiss, W.; Springholz, G.; Kaindl, G.</i>  <b>Antiferromagnetic Order with Atomic Layer Resolution In EuTe(111) Films</b>  Physical Review Letters <b>101</b> (2008), 267202</p>	

<p><i>Schober, H.; Farhi, E.; Mezei, F.; Allenspach, P.; Andersen, K.; Bentley, P.M.; Christiansen, P.; Cubitt, B.; Heenan, R.K.; Kulda, J.; Langan, P.; Lefmann, K.; Lieutenant, K.; Monkenbusch, M.; Willendrup, P.; Saroun, J.; Tindemanns, P.; Zsigmond, G.</i></p> <p><b>Tailored instrumentation for long-pulse neutron spallation sources</b> Nuclear Instruments and Methods in Physics Research Section A <b>589</b> (2008), 34 – 46</p>	
<p><i>Schorr, S.; Wagner, G.; Tovar, M.; Sheptyakov, D.</i></p> <p><b>Comparative studies of the structure and microstructure of Zn-2x (CuBIII)(1-x)X-2 semiconductors (B-III=Ga,In; X=S,Se,Te)</b> Material Research Society Symposium Proceedings <b>1012</b> (2008), 107 - 114</p>	
<p><i>Senff, D.; Schumann, O.; Benomar, M.; Kriener, M.; Lorenz, T.; Sidis, Y.; Habicht, K.; Link, P.; Braden, M.</i></p> <p><b>Melting of magnetic correlations in charge-orbital ordered La<sub>{1/2}</sub>Sr<sub>{3/2}</sub>MnO<sub>4</sub> : Competition of ferromagnetic and antiferromagnetic states</b> Physical Review B <b>77</b> (2008), 184413/1 - 14</p>	V2
<p><i>Senff, D.; Aliouane, N.; Argyriou, D. N.; Hiess, A.; Regnault, L. P.; Link, P.; Hradil, K.; Sidis, Y.; Braden, M.</i></p> <p><b>Magnetic excitations in a cycloidal magnet: the magnon spectrum of multiferroic TbMnO<sub>3</sub></b> Journal of Physics: Condensed Matter <b>20</b> (2008), 434212</p>	
<p><i>Senff, D.; Link, P.; Aliouane, N.; Argyriou, D. N.; Braden, M.</i></p> <p><b>Field dependence of magnetic correlations through the polarization flop transition in multiferroic TbMnO<sub>3</sub>: Evidence for a magnetic memory effect</b> Physical Review B: Condensed Matter <b>77</b> (2008), 174419-1 - 17419-6</p>	
<p><i>Siemensmeyer, K.; Wulf, E.; Mikeska, H. -J.; Flachbart, K.; Gabani, S.; Mat'as, S.; Priputen, P.; Efdokimova, A.; Shitsevalova, N.</i></p> <p><b>Fractional Magnetization Plateaus and Magnetic Order in the Shastry-Sutherland Magnet TmB<sub>4</sub></b> Physical Review Letters <b>101</b> (2008), 177201</p>	E10
<p><i>Smirnov, L. S.; Wozniak, K.; Dominiak, P.; Loose, A.; Natkaniec, I.; Frontasyeva, M. V.; Pomyakushina, E. V.; Baranov, A. I.; Dolbinina, V. V.</i></p> <p><b>Refinement of the crystal structure of [Rb-x(NH<sub>4</sub>)(1-x)](3)H(SO<sub>4</sub>)(2) (x=0.11) by sincycle-crystal X-ray and neutron diffraction: I. phase II at 300 K</b> Crystallography Reports <b>53</b> (2008), 418 - 427</p>	E5
<p><i>Stremper, J.; Bohnenbuck, B.; Zegkinoglou, I.; Aliouane, N.; Landsgesell S.; Zimmermann, M. V.; Argyriou, D. N.</i></p> <p><b>Magnetic-field-induced transitions in multiferroic TbMnO<sub>3</sub> probed by resonant and nonresonant x-ray diffraction</b> Physical Review B: Condensed Matter <b>78</b> (2008), 24429-1 - 24429-11</p>	
<p><i>Strobl, M.; Hilger, A.; Kardjilov, N.; Manke, I.; Treimer, W.; Riemke, M.</i></p> <p><b>Time-of-flight spectrum measurements at the neutron imaging facility CONRAD at the Hahn-Meitner-Institute</b> Lancaster: Destech Publ., (2008), 11 - 17</p>	
<p><i>Strobl, M.; Gruenzweig, C.; Hilger, A.; Manke, I.; Kardjilov, N.; David, C.; Pfeiffer, F.</i></p> <p><b>Neutron dark-field tomography</b> Physical Review Letters <b>101</b> (2008), 123902-1 - 123902-4</p>	V7
<p><i>Strobl, M.; Staack, K.; Treimer, W.; Hilger, A.</i></p> <p><b>Quantitative neutron phase contrast tomography</b> Measurement Science and Technology <b>19</b> (2008), 034020 - 1-4</p>	V12a

<p><i>Strobl, M.; Treimer, W.; Kardjilov, N.; Hilger, A.; Zabler, S.</i>  <b>On neutron phase contrast imaging</b>  Nuclear Instruments and Methods in Physics Research Section B <b>266</b>  (2008), 181 – 186</p>	V12a
<p><i>Süllow, S.; Otop, A.; Loose, A.; Klenke, J.; Prokhnenko, O.; Feyerherm, R.; Hendriks, R.W.A.; Mydosh, J.A.; Amitsuka, H.</i>  <b>Electronic localization and 2D metallic state in UPt<sub>2</sub>Si<sub>2</sub></b>  Journal of the Physical Society of Japan <b>77</b> (2008), 024708</p>	E1, E5, E9
<p><i>Szytula, A.; Tyvanchuk, Y.; Jaworska-Golab, T.; Zarzycki, A.; Kalychak, Y.; Gondek, L.; Stüsser, N.</i>  <b>Magnetic properties of the RCuIn (R = Ce, Nd, Gd, Tb, Dy, Ho, Er) and R<sub>2</sub>CuIn<sub>3</sub> (R = Ce, Gd, Tb, Dy) compounds</b>  Chem. Met. Alloys <b>1</b> (2008), 97 – 101</p>	E6 NMI3: 1255
<p><i>Szytula, A.; Arulraj, A.; Baran, S.; Jaworska-Golab, T.; Penc, B.; Stüßer, N.; Tyvanchuk, Y.; Zarzycki, A.</i>  <b>Magnetic Structure of RCuIn (R= Nd, Tb, Ho, Er)</b>  Acta Physica Polonica A <b>113</b> (2008), 1185 - 1192</p>	E6 NMI3: 1255 NMI3: 1111
<p><i>Szytula, A.; Arulraj, A.; Baran, S.; Kaczorowski, D.; Penc, B.; Stüsser, N.</i>  <b>Magnetic properties of the compounds R<sub>2</sub>CuIn<sub>3</sub> (R=Tb,Dy,Ho,Er)</b>  Solid State Communications <b>146</b> (2008), 61 - 64</p>	E6 NMI3: 1302
<p><i>Szytula, A.; Penc, B.; Kaczorowski, D.; Arulraj, A.; Baran, S.; Stuesser, N.; Tomala, K.</i>  <b>Magnetic and electronic properties of RCoxGe<sub>2</sub> (R = Pr, Nd) compounds</b>  Journal of Alloys and Compounds <b>460</b> (2008), 120 - 124</p>	E6 NMI3: 1302
<p><i>Takahashi, N.; Shibata, K.; Sato, T.J.; Arai, M.; Mezei, F.</i>  <b>A novel time-spatial-focusing momentum-correction analyzer for the near-backscattering spectrometer DIANA at J-PARC</b>  Nuclear Instruments and Methods in Physics Research Section A <b>587</b>  (2008), 350 – 362</p>	
<p><i>Tatchev, D.</i>  <b>Structure analysis of multiphase systems by anomalous small-angle X-ray scattering</b>  Philosophical Magazine A <b>88</b> (2008), 1751 - 1772</p>	
<p><i>Teixeira, S.C.M.; Zaccai, G.; Ankner, J.; Bellissent-Funel, M.C.; Bewley, R.; Blakeley, M.P.; Coates, L.; Dahint, R.; Dalgliesh, R.; Dencher, N.A.; Dhont, J.; Fischer, P.; Forsyth, V.T.; Fragneto, G.; Frick, B.; Geue, T.; Gilles, R.; Gutberlet, T.; Haertl</i>  <b>New sources and instrumentation for neutrons in biology</b>  Chemical Physics <b>345</b> (2008) 133-151</p>	
<p><i>Tolinski, T.; Kaczorowski, D.; Kowalczyk, A.; Hoser, A.; Stuesser, N.; Talik, E.; Klimczak, L. M.</i>  <b>Neutron diffraction and magnetization measurements on CeNi<sub>4.2</sub>Mn<sub>0.8</sub> and Y<sub>0.7</sub>Ni<sub>4.2</sub>Mn<sub>0.8</sub></b>  Physical Status Solidi B <b>245</b> (2008), 1202 - 1205</p>	E6 NMI3: 1258
<p><i>Triolo, A.; Russina, O.; Fazio, B.; Triolo, R.; Di Cola, E.</i>  <b>Morphology of 1-alkyl-3-methylimidazolium hexafluorophosphate room temperature ionic liquids</b>  Chemical Physics Letters <b>457</b> (2008), 362 - 365</p>	
<p><i>Tripadus, V.; Aranghel, D.; Statescu, M.; Buchsteiner, A.</i>  <b>Molecular dynamics in DTGS (ND<sub>3</sub>) by quasielastic and inelastic neutron scattering</b>  Chemical Physics <b>353</b> (2008) 59-65</p>	

<p><i>Troyanchuk, I. O.; Bushinsky, M. V.; Karpinskii, D. V.; Mantytskaya, O. S.; Fedotova, V. V.; Prokhnenko, O. I.</i>  <b>Structural phase transitions in the Bi1-xLaxFeO3 system</b>  Journal of Experimental and Theoretical Physics Letters <b>87</b> (2008), 641 – 644</p>	E9
<p><i>Troyanchuk, I.O.; Karpinsky, D.V.; Yokaichiya, F.</i>  <b>Effect of iron doping on the magnetic structure of TbBaCo<sub>2</sub>O<sub>5.5</sub> layered perovskite</b>  Journal of Physics: Condensed Matter <b>20</b> (2008), 335228/1 - 6</p>	E9
<p><i>Troyanchuk, I.O.; Karpinsky, D.V.; Yokaichiya, F.</i>  <b>Magnetic and crystal structures of iron-ion-doped TbBaCo<sub>2</sub>O<sub>5+gamma</sub></b>  JETP Letters <b>87</b> (2008), 541 – 544</p>	E9
<p><i>Troyanchuk, I.O.; Bushinsky, M.V.; Karpinsky, D.V. et al.</i>  <b>Crystal phase transitions in Bi1-xLaFeO3 system</b>  JETP Letters <b>87</b> (2008), 738 – 742</p>	E9 IHP: 1347
<p><i>Troyanchuk, I.O.; Karpinsky, D.V.; Efimov, V.V.; Efimova, E.; Sikolenko, V.; Yusupov, R.</i>  <b>Crystal Structure and the Magnetic State of Pr<sub>0.5</sub>Sr<sub>0.5</sub>Co<sub>0.5</sub>Fe<sub>0.5</sub>O<sub>3</sub></b>  Journal of Experimental and Theoretical Physics Letters <b>87</b> (2008), 306 – 310</p>	E9
<p><i>Troyanchuk, I.O.; Bushinsky, M.V.; Karpinskii, D.V.; Mantytskaya, O.S.; Fedotova, V.V.; Prokhnenko, O.I.</i>  <b>Structural phase transitions in the Bi1-xLaxFeO3 system</b>  JETP LETTERS <b>87</b> (2008), 641 – 644</p>	E9
<p><i>Vakhrushev, S. B.; Golosovsky, I. V.; Koroleva, E. Yu.; Naberezhnov, A. A.; Okuneva, N. M.; Smirnov, O. P.; Fokin, A. V.; Tovar, M.; Glazman, M.</i>  <b>Structure and dielectric response of Na(1-x)KxNO(2) nanocomposite solid solutions</b>  Physics of the Solid State <b>50</b> (2008), 1548 - 1554</p>	E9
<p><i>Veira, J. R.; Argyriou, D. N.; Kiefer, K.; Wolter, A. U. B.; Alber, D.; Meissner, M.; Almairac, R.; Reehuis, M.; Bordallo, H. N.</i>  <b>Structural and magnetic properties of the ferroelectric magnet BaMn1-xZnxF4, a site diluted square-lattice two-dimensional Heisenberg antiferromagnet with S=5/2</b>  Physical Review B: Condensed Matter <b>78</b> (2008), 54104-1 - 54104-6</p>	E5
<p><i>Venter, A.M.; van der Watt, M.W.; Wimpory, R.C.; Schneider, R.; McGrath, P.J.; Topic, M.</i>  <b>Neutron strain investigations of laser bent samples</b>  Materials Science Forum <b>571-572</b> (2008), 63 - 68</p>	
<p><i>Voets, I.K.; de Vos, W.M.; Hofs, B.; de Keizer, A.; Cohen Stuart, M. A.; Steitz, R.; Lott, D.</i>  <b>Internal structure of a thin film of mixed polymeric micelles on a solid/liquid interface</b>  Journal of Physical Chemistry B <b>112</b> (2008), 6937 - 6945</p>	
<p><i>Wagh, A. G.</i>  <b>In the wonderland of ultra-parallel neutron beam</b>  PRAMANA: Journal of Physics <b>71</b> (2008), 797</p>	V12b
<p><i>Wagh, A. G.; Abbas, S.; Treimer, W.</i>  <b>Bragg prism monochromator and analyser for SUSANS studies,</b>  PRAMANA: Journal of Physics <b>71</b> (2008), 1171</p>	V12b
<p><i>Wagh, A. G.; Abbas, S.; Treimer, W.</i>  <b>First SUSANS spectra at wave vector transfers of 10-6Å<sup>-1</sup></b>  Solid State Physics (India) <b>53</b> (2008), 553</p>	V12b

<p>Weissbach, T.; Leisegang, T.; Kreyssig, A.; Frontzek, M.; Hoffmann, J.-U.; Souptel, D.; Koehler, A.; Behr, G.; Paufler, P.; Meyer, D. C.  <b>Intergrowth of several solid phases from the Y-Ni-B-C system in a large YNi<sub>2</sub>B<sub>2</sub>C crystal</b>  <i>Journal of Applied Crystallography</i> <b>41</b> (2008), 738 - 746</p>	E2
<p>Wiedenmann, A, Keiderling, U, Meissner, M, Wallacher, D, Gähler, R, May, R.P., Prévost, S, Klockenburg, M, Erné, B.H., Kohlbrecher, J.  <b>Low-temperature dynamics of magnetic colloids studied by time-resolved small-angle neutron scattering</b>  <i>Physical Review B</i> <b>77</b> (2008) 184417</p>	
<p>Wimpory, R.C.; Mikula, P.; Saroun, J.; Poeste, T.; Li, J.; Hofmann, M.; Schneider, R.  <b>Efficiency boost of the materials science diffractometer E3 at BENSC: One order of magnitude due to a horizontally and vertically focusing monochromator</b>  <i>Neutron News</i> <b>19</b> (1) (2008), 16 – 19</p>	
<p>Wimpory, R.C.; Ohms, C.; Hofmann, M.; Schneider, R.; Youtsos, A.G.  <b>Problems in the averaging of neutron diffraction stress data from round- robin campaigns</b>  <i>Materials Science Forum</i> <b>571-572</b> (2008), 283 - 288</p>	
<p>Witzmann, F.; Asbach, P.; Remes, K.; Hampe, O.; Hilger, A.; Paulke, A.  <b>Vertebral pathology in an ornithopod dinosaur: A hemivertebra in <i>Dysalotosaurus lettowvorbecki</i> from the Jurassic of Tanzania</b>  <i>The Anatomical Record</i> <b>291</b> (2008), 1149 - 1155</p>	
<p>Wolff, M.; Steitz, R.; Gutfreund, P.; Voss, N.; Gerth, S.; Walz, M.; Magerl, A.; Zabel, H.  <b>Shear induced relaxation of polymer micelles at the solid - liquid interface</b>  <i>Langmuir</i> <b>24</b> (2008), 11331 – 11333</p>	
<p>Zabler, S.; Rack, A.; Manke, I.; Thermann, K.; Tiedemann, J.; Harthill, N.; Riesemeier, H.  <b>High-resolution tomography of cracks, voids and micro-structure in greywacke and limestone</b>  <i>Journal of Structural Geology</i> <b>30</b> (2008), pp. 876 - 887</p>	
<p>Zaharko, O.; Mesot, J.; Salguero, L. A.; Valenti, R.; Zbiri, M.; Johnson, M.; Filinchuk, Y.; Klemke, B.; Kiefer, K.; Mys'kiv, M.; Straessle, Th.; Mutka, H.  <b>Tetrahedra system Cu(4)OCl(6)daca(4): High-temperature manifold of molecular configurations governing low-temperature properties</b>  <i>Physical Review B: Condensed Matter</i> <b>77</b> (2008), 224408-1 - 224408-11</p>	
<p>Zhou J.; Wang B.; Tong W.; Maltseva E.; Zhang G.; Krastev R.; Gao C.; Möhwald H.; Shen J.  <b>Influence of assembling pH on the stability of poly(L-glutamic acid) and poly(L-lysine) multilayers against urea treatment</b>  <i>Colloids and Surfaces B: Biointerfaces</i> <b>62</b> (2008), 250 - 257</p>	V6
<p>Zizak, I.; Darowski, N.; Klaumünzer, S.; Schumacher, G.; Gerlach, J.W.; Assmann, W.  <b>Ion-beam-induced collective rotation of nanocrystals</b>  <i>Physical Review Letters</i> <b>101</b> (2008), 065503/1 - 4</p>	
<p>Zrnik, J.; Strunz, P.; Maldini, M.; Wiedenmann, A.; Davydov, V.  <b>Small-angle neutron scattering investigatin of gamma' precipitate morphology evolution in creep-exposed single-crystal Ni-base superalloy CMSX-4</b>  <i>Journal of Physics: Condensed Matter</i> <b>20</b> (2008), 104261 – 1 - 7</p>	V4 NMI3: 1179

## Seminar and Conference Contributions 2008

### Invited Talks

#### 2005 (supplement)

<i>Brandt, A.</i> <b>BENSC User Service</b> 26th HMI Tutorial Session on Neutron Scattering, Berlin, Germany, 2/21/2005 - 2/25/2005	
<i>Brandt, A.</i> <b>ADSO-SE</b> 1st BENSC Adsorption workshop, Berlin, Germany, 9/21/2005 - 9/21/2005	

#### 2006 (supplement)

<i>Brandt, A.</i> <b>BENSC User Service</b> 29th HMI School on Neutron Scattering, Berlin, Germany, 3/3/2006 - 3/7/2006	
<i>Brandt, A.</i> <b>BENSC User Service</b> 27th HMI Tutorial Session on Neutron Scattering, Berlin, Germany, 2/27/2006 - 3/3/2006	
<i>Matsushima, U.; Kardjilov, N.; Hilger, A.; Herppich, W.B.; Nishizawa, T.; Kawamitsu, Y.</i> <b>Jyusuiwo mochiita reicyuseishi imagingniyoru tomatonaejyousanryuno kashika (Japanese)</b> nougyoukankyokougakukanrengakkai 2006nen godotaikai, Sapporo, Japan 9/11/2006 - 9/15/2006	V7

#### 2007 (supplement)

<i>Aldridge, L.; Bordallo, H.; Desmedt, A.</i> <b>Water transport in concrete using inelastic neutron scattering</b> 4th ECNS, Lund, Sweden, 6/25/2007 - 6/29/2007	V3
<i>Rüegg, C.</i> <b>Exploring novel quantum order and dynamics: Neutron scattering under extreme conditions</b> 4th ECNS, Lund, Sweden, 6/25/2007 - 6/29/2007	V2 NMI3: 1127 NMI3: 1006 IHPII: 543

#### 2008

<i>Baran, S.; Gondek, L.; Arulraj, A.; Penc, B.; Stüsser, N.; Szytula, A.</i> <b>Frustrated magnetic ordering in RTX rare earth intermetallics with the hexagonal ZrNiAl-type structure</b> 13th Int. Seminar on Neutron Scattering Investigation in Condensed Matter, Poznan; Poland, 5/8/2008 - 5/10/2008	E6 NMI3: 1303
<i>Bordallo, H.</i> <b>Natural Soil Environments: The role of cations and superparamagnetic iron oxides</b> SF1 Seminar Series, HZ Berlin, Berlin, 10/30/2008 - 10/30/2008	

<p><i>Bordallo, H.</i>  <b>Natural Soil Environments: The role of cations and superparamagnetic iron oxides</b>  Deutschen Neutronenstreutagung 2008, Garching, Germany,  9/14/2008 - 9/17/2008</p>	
<p><i>Bordallo, H.; Boldyreva, E. V.; Kolesov, B.; Landsgesell, S.; Buchsteiner, A.; Juranyi, F.; Koza, M. M.; Straessle, T.</i>  <b>Temperature and pressure effects on the reorientational dynamics of amino acids, a neutron study</b>  XXI Congress and General Assembly of the international Union of Crystallography, Osaka, Japan, 8/23/2008 - 8/31/2008</p>	
<p><i>Brandt, A.</i>  <b>BENSC User Service</b>  BENSC Day 2008, Berlin, Germany, 6/16/2008 - 6/16/2008</p>	
<p><i>Chmielus, M.</i>  <b>Influence of Surface Preparation and Training on the Properties of Magnetic Shape-Memory Alloys</b>  Seminar Talk of the Materials Science &amp; Engineering Department of Boise State University, Boise, Idaho, USA, 10/21/2008 - 10/21/2008</p>	
<p><i>Dalle-Ferrier C.; Eibl S.; Pappas C.; Alba-Simionesco Chr.</i>  <b>Temperature dependence of three point correlation functions of viscous liquids: case of glycerol</b>  7th Liquid Matter Conference, Lund, Schweden, 6/27/2008 - 7/1/2008</p>	V5
<p><i>Davies, C.; Wimpory, R.</i>  <b>Influence of Crack Growth and Specimen Sectioning on Residual Stresses</b>  VAMAS TWA31 Annual Meeting, Imperial College London,  5/19/2008 - 5/19/2008</p>	
<p><i>Denks, I.</i>  <b>Problems related to near surface residual stress analysis by means of diffraction methods - comparison of angle- and energy-dispersive techniques</b>  11th European Powder Diffraction Conference (EPDIC ), Warsaw, Poland,  9/19/2008 - 9/22/2008</p>	
<p><i>Denks, I.; Manns, T.; Genzel, Ch.; Scholtes, B.</i>  <b>An experimental approach to the problem of transforming stress distributions from the LAPLACE - into real space</b>  11 European Powder Diffraction Conference, Warsaw, Poland,  9/19/2008 - 9/22/2008</p>	
<p><i>Fery A.; Dönch, I.; Möhwald, H.; Laschewsky, A.; Ott, P.; Köhler, R.; Krastev, R.</i>  <b>Micromechanics of polyelectrolyte multilayer</b>  Kolloquium, Dresden, Germany, 4/22/2008 - 4/23/2008</p>	
<p><i>Feyerherm, R.</i>  <b>Interplay between rare earth and manganese magnetism and its effect on ferroelectricity in <math>or\text{-RMnO}_3</math></b>  Deutsche Neutronenstreutagung 2008, Garching, Germany,  9/15/2008 - 9/17/2008</p>	
<p><i>Genzel, Ch.</i>  <b>Messung innerer Spannungen in Werkstoffen und Bauteilen mit Röntgenstrahlen - Stand und Perspektiven</b>  Industrieforum 2008, DESY, Hamburg, Germany, 11/5/2008 - 11/5/2008</p>	

<p><i>Glavatskyy, I.; Glavatska, N.; Soderberg O.</i>  <b>Crystal and magnetic structure temperature evolution in Ni-Mn-Ga magnetic shape memory martensite</b>          Jim Krumhansl Symposium 2008, Osaka, Japan, 11/10/2008 - 11/15/2008</p>	E2
<p><i>Glavatskyy, I.; Glavatska, N.; Soderberg O.</i>  <b>Thermal evolution of the crystal, magnetic and electronic structure of the Ni-Mn-Ga martensites</b>          Jim Krumhansl Symposium 2008, Osaka, Japan, 11/10/2008 - 11/15/2008</p>	E2
<p><i>Hauß, T.</i>  <b>Neutron Scattering as a Probe for Biology</b>          29th Berlin School on Neutron Scattering, Berlin, 3/3/2008 - 3/7/2008</p>	
<p><i>Hauß, T.</i>  <b>Untersuchungen zur Struktur und Dynamik von biologischen Membranen mittels Neutronenstreuung.</b>          Kolloquium des Clemens-Schöpf-Institut, Darmstadt, Germany, 4/7/2008 - 4/7/2008</p>	
<p><i>Hauß, T.</i>  <b>The application of neutron scattering techniques in membrane biophysics</b>          2nd European Conference on Metallobiomics, Berlin, Germany, 12/3/2008 - 12/4/2008</p>	
<p><i>Hauß, T.; Pieper, J.; Buchsteiner, A.; Lechner, R.E.; Dencher, N.A.</i>  <b>Observation of transient modulations in protein dynamics during the photocycle of bacteriorhodopsin</b>          Biological Physics at Large Facilities, Grenoble, France, 10/19/2008 - 10/23/2008</p>	
<p><i>Hoell, A.</i>  <b>Anomalous Small Angle X-Ray Scattering and some applications in material science</b>          Bhabha Atomic Research Centre (BARC), Mumbai, India, 1/11/2008 - 1/11/2008</p>	
<p><i>Hoell, A.</i>  <b>Anomalous Small Angle X-Ray Scattering and some applications in material science</b>          Material Science Division, Kalpakkam, India, 1/7/2008 - 1/7/2008</p>	
<p><i>Hoell, A.; Haas, S.; Heinemann, A.; Tatchev, D.; Kranold, R.; Goerigk, G.; Müller, M.; Banhart, J.</i>  <b>Anomalous Small Angle X-ray Scattering and its Application to photochromic Glasses</b>          Fourth Balkan Conference on Glass Science and Technology, Varna, Bulgaria, 9/27/2008 - 10/1/2008</p>	
<p><i>Jauch, W.; Reehuis, M.</i>  <b>Charge density in ferromagnetic iron and nickel from gamma-ray diffraction</b>          5th European Charge Density Meeting, Gravedona, Italy, 6/6/2008 - 6/11/2008</p>	
<p><i>Kasyutich, O.I.; Sarua, A.; Figueiredo, W.; Tatchev, D.; Hoell, A.; Haas, S.; Schwarzacher</i>  <b>3-dimensional nano-particle arrays produced by protein crystallisation</b>          Nanoscale Phenomena and Structures in Bulk and Surface Phases, Sofia, Bulgaria, 2/26/2008 - 3/2/2008</p>	

<p><i>Lake, B.</i>  <b>Magnetic Excitations in Spin-1/2 Antiferromagnetic Spin-Chains and Ladders.</b>  SC08 Workshop on Strong Fluctuations in Low Dimensional Systems, Montauk, Long Island, USA, 9/2/2008 - 9/5/2008</p>	
<p><i>Manke, I.</i>  <b>Bildgebende Verfahren in der Brennstoffzellen-Forschung</b>  Materialwissenschaftliches Kolloquium an der Universität Darmstadt, Darmstadt, Germany, 1/21/2008 - 1/21/2008</p>	
<p><i>Nowicki, W.; Darul, J.; Yokaichiya, F.</i>  <b>Synthesis, structure and magnetic properties of Fe-doped tetragonal Li<sub>0.95</sub>Mn<sub>2.05</sub>O<sub>4</sub></b>  11th European Powder Diffraction Conference, Warsaw, Poland, 9/19/2008 - 9/22/2008</p>	E9
<p><i>Pappas, C.</i>  <b>Neutron Properties and Sources</b>  5th LANCE Neutron School 2008, Los Alamos, New Mexico, USA, 7/23/2008 - 8/1/2008</p>	
<p><i>Pappas, C.</i>  <b>Neutron Instrumentation</b>  5th Los Alamos Neutron School 2008, Los Alamos, New Mexico, USA, 7/23/2008 - 8/1/2008</p>	
<p><i>Pappas, C.</i>  <b>How much Larmor Precession affords Chirality?</b>  Neutronenseminar - TU München, Germany, 11/17/2008 - 11/17/2008</p>	
<p><i>Pappas, C.; Cywinski, R.; Pickup, R.; Farago, B.; Fouquet, P.; Falus, P.</i>  <b>Generalized approach to non-exponential relaxation</b>  International Symposium on Neutron Scattering, Atomic Research Centre, Mumbai, India, 1/15/2008 - 1/18/2008</p>	
<p><i>Pappas, C.; Lelièvre-Berna E.; Bentley P.; Moskvina E.; Farago B.; Falus P.; Krist Th.; Grigoriev S.; Dyadkin V.</i>  <b>Challenges in Neutron Spin Echo Spectroscopy</b>  Polarized Neutrons in Condensed Matter Investigations, Tokai, Japan, 9/1/2008 - 9/5/2008</p>	
<p><i>Reehuis, M.; Ulrich, C.; Fujioka, J.; Miyasaka, S.; Tokura, Y.; Keimer, B.</i>  <b>Neutron diffraction study of hole-doped vanadates Y<sub>1-x</sub>CaxVO<sub>3</sub></b>  16th International Conference on Ternary and Multinary Compounds, Berlin, Germany, 9/15/2008 - 9/19/2008</p>	E5
<p><i>Reichenauer, G.</i>  <b>Length change upon ad-/desorption in mesopores</b>  3rd BENSC Adsorption Workshop, Berlin-Wannsee, Germany, 10/1/2008 - 10/2/2008</p>	V4
<p><i>Rolfs, K.</i>  <b>Co-Doping: Tuning Ni-Mn-Ga for Actuator Application?</b>  Seminar-Vortrag TU München, Munich, Germany, 10/21/2008 - 10/21/2008</p>	
<p><i>Rolfs, K.</i>  <b>NiCoMnGa - a new smart material?</b>  SF1 - Seminar at Helmholtz-Zentrum Berlin für Materialien und Energie, HZB, Berlin, Germany, 10/23/2008 - 10/23/2008</p>	
<p><i>Rolfs, K.</i>  <b>Development of MSMA-DRIVEN actuators based on standardization of single crystal growth, treatment and quality assessment</b>  SPP 1239 Evaluation, Dresden, Germany, 3/12/2008 - 3/12/2008</p>	

<p><i>Rule, K.</i>  <b>What high magnetic fields and low temperatures have revealed to me?</b>  Invited talk, ANSTO, Sydney, Australia, ANSTO, Sydney, Australia,  6/18/2008 - 6/18/2008</p>	
<p><i>Rule, K.</i>  <b>How Frustrating! A look at recent neutron scattering results from the frustrated pyrochlores Tb<sub>2</sub>Ti<sub>2</sub>O<sub>7</sub> and Tb<sub>2</sub>Sn<sub>2</sub>O<sub>7</sub></b>  Invited talk at UNSW, University of New South Wales, Sydney, Australia,  6/17/2008 - 6/17/2008</p>	
<p><i>Rule, K.</i>  <b>How Frustrating: A look at recent neutron scattering data in the frustrated pyrochlores TbTiO and TbSnO</b>  Invited talk at LLB, Saclay, France, LLB, Saclay, France,  6/5/2008 - 6/6/2009</p>	
<p><i>Schierle, E.</i>  <b>Interplay of Dy and Mn magnetic moments in multiferroic DyMnO<sub>3</sub></b>  27th BESSY Users' Meeting, Berlin, BESSY, Germany,  12/4/2008 - 12/5/2008</p>	
<p><i>Schneider, R.</i>  <b>Neutrons and Photons in Service for Industry: 3D Structure Visualization and Characterization- Strategy to Establish the Reference for NDE and FE-Simulations</b>  Second US-China Workshop on Scientific and Industrial Applications Using Neutrons, Muons and Protons, Dongguan, Guangdong Province, China,  11/7/2008 - 11/10/2008</p>	
<p><i>Schneider, R.</i>  <b>Industrial Use of Neutrons</b>  CIAE Seminar, Beijing, China, 5/28/2008 - 6/10/2008</p>	
<p><i>Schneider, R.; Boin, M.; Kardjilov, N.; Haibel, A.</i>  <b>Tomography Techniques Using Different Probes: Neutrons and Photons</b>  Seminar CIAE, Beijing, China, 5/28/2008 - 6/10/2008</p>	
<p><i>Schneider, R.; Chmielus, M.; Rolfs, K.; Mecklenburg, A.; Guldbakke, J.-M.; Raatz, A.</i>  <b>Route to Commercial Use of MSM Actuators: Noval Crystal Growth and Treatment</b>  China Institute of Physics, Beijing, China, 6/8/2008 - 6/8/2008</p>	
<p><i>Schneider, R.; Hoffmann, J.-U.; Hohlwein, D.; Prandl, W.</i>  <b>Investigation of Short-Range Magnetic/Structural Order by Diffuse Neutron Scattering</b>  CIAE Seminar, CIAE, Beijing, China, 5/28/2008 - 6/10/2008</p>	
<p><i>Schneider, R.; Wimpory, R.; Hofmann, M.</i>  <b>Residual Stress Analysis Using Neutrons</b>  Seminar CIAE, CIAE, Beijing, China, 5/28/2008 - 6/10/2008</p>	
<p><i>Schneider, R.; Wimpory, R.; Hofmann, M.</i>  <b>Residual Stress And Texture Analysis at the Research Reactors BER-II and FRM-II</b>  PTB Seminar, PTB Berlin, Germany, 9/26/2008 - 9/26/2008</p>	
<p><i>Schneider, R.; Wimpory, R.; Hofmann, M.</i>  <b>Neutrons and Photons: A Unique Tool for the Engineer</b>  China Institute of High Energy Physics, Beijing, China, 6/6/2008 - 6/6/2008</p>	
<p><i>Schneider, R.; Wimpory, R.; Hofmann, M.</i>  <b>Neutron Instrumentation for Residual Stress Analysis: Monochromators</b>  CIAE Seminar, Beijing, China, 5/28/2008 - 6/10/2008</p>	

<p><i>Schneider, R.; Wimpory, R.; Hofmann, M.; Ohms, C.</i>  <b>STRAINET: Standardization of Interfaces to Promote International Co-Operation in Neutron Diffraction</b>          IAEA Expert Meeting, Vienna, Austria, 12/10/2008 - 12/12/2008</p>	
<p><i>Steiner, M.</i>  <b>Perspectives of extreme sample environment in neutron scattering and consequences for instrumentation</b>          International Symposium on Neutron Scattering (ISNS2008), Mumbai, India, 1/15/2008 - 1/18/2008</p>	
<p><i>Steitz, R.</i>  <b>Reflectivity &amp; GISAS</b>          Workshop zum Thema Streumethoden, SPP 1273 Kolloidverfahrenstechnik, Universität Bayreuth, Germany, 9/29/2008 - 9/30/2008</p>	
<p><i>Szytula, A.; Arulraj, A.; Baran, S.; Gondek, L.; Penc, B.</i>  <b>Magnetic properties of the hexagonal RTIn rare earth intermetallics with frustration</b>          16th Int. Conf. on Solid Compounds of Transition Elements, Dresden, Germany, 7/26/2008 - 7/31/2008</p>	<p>E6          NMI3: 1303          NMI3: 1026          NMI3: 1255          NMI3: 1348</p>
<p><i>Tatchev, D.</i>  <b>Small-Angle Scattering and Anomalous Small-Angle X-ray Scattering in Materials Science</b>          externer Vortrag an University of Aberystwyth, Aberystwyth, Wales, UK, 2/7/2008 - 2/7/2008</p>	
<p><i>Vierke, J.; Schumacher, G.; Denks, I.; Wanderka, N.; Wollgarten, M.; Banhart, J.; Zizak, I.; Pilyugin, V.P.; Balog, M.; Nagy, J.; Simancik, F.</i>  <b>Strain- and Temperature-induced Glass-to-Crystal Transformations in Al-Ni-La Glass</b>          1/9/2008 - 1/9/2008</p>	
<p><i>Wimpory, R.C and Hofmann. M.</i>  <b>Net Task group 1, 2 and 4</b>          13th NeT Steering Committee Meeting at INSA-Lyon, INSA, Lyon, France, 6/9/2008 - 6/11/2008</p>	
<p><i>Wimpory, R.C.</i>  <b>Things that you may have wondered about measuring residual stresses but were probably too shy to ask ...</b>          SF1 seminar, HZB, Berlin, Germany, 5/22/2008 - 5/22/2008</p>	
<p><i>Wimpory, R.C.</i>  <b>Around the Weld in a few minutes</b>          NUM Seminar PSI, PSI, Switzerland, 3/19/2008 - 3/19/2008</p>	

## Seminar and Conference Contributions 2008

## Talks

## 2006 (supplement)

<p><i>Matsushima, U.; Kardjilov, N.; Hilger, A.; Ueno, M.; Kawamitsu, Y.; Nishizawa, T.; Herppich, W.B.</i>  <b>8th world conference on neutron radiography</b>        8th world conference on neutron radiography, Gaithersburg, MD, USA,        10/16/2006 - 10/19/2006</p>	V7
<p><i>Sikolenko, V.; Sazonov, A.; Efimov, V.; Krivencov, V.; Darowski, N.; Vyalikh, D.</i>  <b>Neutron diffraction and synchrotron radiation studies of La<sub>1-x</sub>Sr<sub>x</sub>CoO<sub>3</sub> magnetic properties</b>        International Conference on Magnetism, Kyoto, Japan,        8/20/2006 - 8/25/2006</p>	

## 2007 (supplement)

<p><i>Berti, D.; Baldelli Bombeli, F.; Betti, F.; Milani, S.; Baglioni, P.</i>  <b>Self-assembly of nucleolipids: insights from neutron scattering</b>        ECNS, Lund, Sweden, 6/25/2007 - 6/29/2007</p>	<p>V1, V4        NMI3: 1022        NMI3: 1106        NMI3: 1207</p>
<p><i>Brandt, A.</i>  <b>DEGAS - the story so far</b>        2nd BENSC Adsorption workshop, Berlin. Germany, 2/1/2007 - 2/2/2007</p>	
<p><i>Guidi, T.; Carretta, S.; Santini, P.; Amoretti, G.; Copley, J.; Qiu, Y.; Caciuffo, R.; Hiess, A.; Timco, G.; Winpenny, R.</i>  <b>Quantum Oscillations of the total spin in a heterometallic antiferromagnetic ring: Evidence from neutron spectroscopy</b>        ECNS, Lund, Sweden, 6/25/2007 - 6/29/2007</p>	
<p><i>Iolin, E.; Rusevich, L.; Strobl, M.; Treimer, W.; Mezei, F.; Mikula, P.</i>  <b>Application of ultrasound to multi crystal neutron diffractometer</b>        ECNS, Lund, Sweden, 6/25/2007 - 6/28/2007</p>	<p>V3, V12a        IHP: 462        IHP: 570</p>
<p><i>Kessner, D.; Kiselev, M.; dante, S.; Hauß, T.; Wartewig, S.; Neubert, R.</i>  <b>New insights into the structure of the Stratum Corneum lipid model matrix by neutron diffraction</b>        ECNS, Lund, Sweden, 6/25/2007 - 6/29/2007</p>	V1
<p><i>Lefmann, K.; Schober, H.; Kleno, K.H.; Mezei, F.</i>  <b>A cold neutron chopper spectrometer for the ESS long-pulse target station</b>        ECNS, Lund, Sweden, 6/25/2007 - 6/29/2007</p>	
<p><i>Matsushima, U.; Kardjilov, N.; Herppich, W.B.; Hilger, A.</i>  <b>Visualization of water flow in small plants using neutron imaging</b>  <b>Estimation of flow rate and influence of neutron and D<sub>2</sub>O</b>        The first annual meeting of Japanese Society of Agricultural, Biological and Environmental Engineers and Scientists, Osaka, Japan,        6/25/2007 - 6/27/2007</p>	V7
<p><i>Mezei, F.</i>  <b>Continuous, short pulse and long pulse sources: the numbers behind the quantum leap in beam power</b>        ECNS, Lund, Sweden, June 2007</p>	

<p><i>Pappas, C.; Cywinski, R.; Pickup, R.</i>  <b>A novel approach to modelling non-exponential relaxation in glasses and spin-glasses</b>          ECNS, Lund, Sweden, 6/25/2007 - 6/29/2007</p>	V5
<p><i>Pieper, J.; Hauß, T.; Buchsteiner, A.; Ollivier, J.; Lechner, R.; Renger, G.</i>  <b>Time-resolved QENS studies of a native photosystem</b>          4th ECNS, Lund, Sweden, 6/25/2007 - 6/29/2007</p>	V3
<p><i>Russina, M.; Kemner, E.; Celli, M.; Ulivi, L.; Lokshin, K.; Mezei, F.</i>  <b>Semi-classical dynamics of confined molecular hydrogen in water clathrates</b>          4th ECNS, Lund, Sweden, 6/25/2007 - 6/29/2007</p>	
<p><i>Sel, Ö.; Thommes, M.; Brandt, A.; Wallacher, D.; Smarsly, B</i>  <b>Investigations of pore hierarchy in mesoporous silicas by in-situ SAXS/SANS sorption studies</b>          19. Deutsche Zeolithtagung, Leipzig, 3/7/2007 - 3/9/2007</p>	V4
<p><i>Sel, Ö.; Thommes, M.; Brandt, A.; Wallacher, D.; Smarsly, B.</i>  <b>On the nitrogen sorption mechanism in silica with hierarchical mesoporosity studied by in-situ small-angle neutron scattering</b>          9th international conference on fundamentals of adsorption, Giardini Naxos, Sicily - Italy, 5/20/2007 - 5/23/2007</p>	V4
<p><i>Siemensmeyer, K.; Wulf, E.; Flachbart, K.; Gabani, S.; Matas, S.; Priputen, Shitsevalova, N.</i>  <b>Neutron diffraction study of a Shastry Sutherland magnet in the plateau regime</b>          ECNS, Lund, Sweden, 6/25/2007 - 6/29/2007</p>	
<p><i>Sitepu, H.; Garbe, U.; Brokmeier, H.-G.; Law, R.</i>  <b>Quantitative texture analysis of deformed natural quartz vein from Torridon area in NW Scotland with neutron diffraction</b>          ECNS, Lund, Sweden, 6/25/2007 - 6/29/2007</p>	
<p><i>Thielemann, B.; Rüegg, Ch.; Ronnow, H.M.; Mesot, J.; McMorrow, D.F.; Krämer, K.W.; Gvasaliya, S.; Habicht, K.; Boehm, M</i>  <b>Continuous spin-excitation spectrum in a novel spin ladder</b>          ECNS, Lund, Sweden, 6/25/2007 - 6/29/2007</p>	V2 NMI3: 1127
<p><i>Treimer, W.; Kardjilov, N.; Hilger, A.; Manke, I.; Strobl, M.</i>  <b>Radiography with polarised neutrons</b>          ECNS, Lund, Sweden, 6/25/2007 - 6/29/2007</p>	
<p><i>Triolo, A.; Russina, M.; O.; Di Cola, E.; Perroud, O.</i>  <b>Morphology of homo- and block-polymers in environmentally responsible room temperature ionic liquids: a combined SANS and SAXS study</b>          ECNS, Lund, Sweden, 6/25/2007 - 6/29/2007</p>	V4 NMI3: 1208 NMI3: 1176
<p><i>von Klitzing, R.; Steitz, R.; Wong, J.</i>  <b>Kinetics of water uptake and release of polyelectrolyte multilayers</b>          4th ECNS, Lund, Sweden, 6/25/2007 - 6/29/2007</p>	
<p><i>Wallacher, D.</i>  <b>DEGAS today</b>          2nd BENSC Adsorption workshop, Berlin, Germany, 2/1/2007 - 2/2/2007</p>	
<p><i>Wiedenmann, A.</i>  <b>Low temperature dynamics of magnetic colloids studied by time-resolved Small Angle Neutron Scattering (SANS)</b>          Inter. Conf. Magnetic Fluids, Kosice, Slovakia, 7/23/2007 - 7/27/2007</p>	V4

<p><i>Wiedenmann, A.</i>  <b>Small Angle Neutron Scattering: A non-destructive nano-analytical technique</b>  Workshop on Research Reactor Utilization, Sao Paulo, Brasil, 12/3/2007 - 12/6/2007</p>	
<b>2008</b>	
<p><i>Balanda, M.; Baran, S.; Arulraj, A.; Penc, B.; Szytula, A.</i>  <b>Magnetic properties of TbNi<sub>1-x</sub>AuxIn compounds</b>  The European Conference PHYSICS OF MAGNETISM 2008, Poznan, Poland, 6/24/2008 – 6/27/2008</p>	E6 NMI3: 1348
<p><i>Boin, M.; Kardjilov, N.; Schneider, R.; Edwards, L.</i>  <b>Strain and Texture Analysis using Bragg Edge transmission</b>  NEUWAVE (workshop on NEUtron WAVElength dependent IMAGING), Garching, Munich, Germany, 4/21/2008 - 4/24/2008</p>	
<p><i>Bordallo, H.; De Souza, J.; De Tarso, P.; Argyriou, D.</i>  <b>Structural Isotopic Effects in the smallest chiral amino acid: Observation of a structural phase transition in fully deuterated alanine.</b>  2008 APS March Meeting, New Orleans, Louisiana, USA, 3/10/2008 - 3/14/2008</p>	
<p><i>Buchsteiner, A.; Stüßer, N.</i>  <b>Optimizations in neutron powder diffraction by using divergent beam geometries in angular dispersive techniques</b>  11th European Powder Diffraction Conference, Warsaw, Poland 9/19/2008 - 9/22/2008</p>	
<p><i>Darowski, N.</i>  <b>Magnetism in thin film multilayers - a depth-selective study with x-ray magnetic circular dichroism</b>  Colloquium of the Institute of Ion Beam Physics and Material Research, Research Center Rossendorf FZD, Rossendorf, 5/19/2008 - 5/19/2008</p>	
<p><i>Darowski, N.</i>  <b>Reorientation transition in Fe/Pt multilayers studied by means of depth-selective x-ray magnetic dichroism</b>  72ste Frühjahrstagung der Deutschen Physikalischen Gesellschaft, Berlin, 2/25/2008 - 2/29/2008</p>	
<p><i>Dawson, M.; Kardjilov, N.; Hilger, A.; Manke, I.; Banhart, J.</i>  <b>Neutron imaging at HMI</b>  NeuWave Imaging, Garching, Germany, 4/20/2008 - 4/24/2008</p>	
<p><i>Dorbandt, I.; Zehl, G.; Bogdanoff, P.; Wippermann, K.; Haas, S.; Hoell, A.; Wollgarten, M.; Fiechter, S.</i>  <b>Preparation strategies and structural characterization of selenium modified ruthenium nano-particles as cathode catalyst for PEM fuel cells.</b>  213th ECS Meeting, Phoenix (AZ,) USA, 2008 5/18/2008 - 5/22/2008</p>	
<p><i>Flemming, S.A.; James, J. A.; Schneider, R.; Wimpory, R. C.; Hofmann, M.; Schobert, M.; Randau, C.; Holstein, F.; Weiss, T.</i>  <b>The Open Inspire Architecture for Control, Data Reduction and Analysis</b>  NOBUGS 2008 Conference  November 3-5, 2008 at ANSTO, Sydney, Australia, 11/3/2008 - 11/5/2008</p>	

<p><i>Haas, S.; Heinemann, A.; Kranold, R.; Tatchev, D.; Goerigk, G.; Müller, M.; Hoell, A.</i></p> <p><b>Nanostructure of silver-free photochromic glasses studied by anomalous small angle X-ray scattering</b></p> <p>IUCr2008 - XXI Congress and General Assembly of the International Union of Crystallography, Osaka, Japan, 8/23/2008 - 8/31/2008</p>	
<p><i>Hartnig, Ch.; Lehnert, W.; Manke, I.; Banhart, J.</i></p> <p><b>In situ observation of liquid water evolution and transport in PEM fuel cell</b></p> <p>European Fuel Cell Technology and Applications, Rome, Italy, 12/11/2008 - 12/14/2008</p>	
<p><i>Hauß, T.; Pieper, J.; Buchsteiner, A.; Lechner, R.E.; Dencher, N.A.</i></p> <p><b>Real-time monitoring of modulations in the protein dynamics during the photocycle of bacteriorhodopsin by quasielastic neutron scattering</b></p> <p>13th International Conference on Retinal Proteins, Barcelona, Spain, 6/15/2008 - 6/20/2008</p>	
<p><i>Hilger, A.; Kardjilov, N.; Manke, I.; Strobl, M.; Banhart, J.</i></p> <p><b>Investigation of magnetic fields at the neutron radiography station CONRAD at HMI</b></p> <p>Workshop on NEUtron WAVElength dependend IMAGING (NEUWAVE IMAGING), München, Germany, 4/20/2008 - 4/24/2008</p>	
<p><i>Hoell, A.</i></p> <p><b>Anomale Röntgenkleinwinkelstreuung und ihre Anwendung auf Glas und Glaskeramik</b></p> <p>Fachausschuss der DGG: Physik und Chemie des Glases innterhalb der Deutschen Glastechnischen Gesellschaft, Würzburg, Germany, 3/13/2008 - 3/13/2008</p>	
<p><i>Kardjilov, N.; Hilger, A.; Manke, I.; Banhart, J.</i></p> <p><b>The role of monochromatic beams in neutron imaging techniques</b></p> <p>Workshop on NEUtron WAVElength dependend IMAGING (NEUWAVE IMAGING), München, Germany, 4/20/2008 - 4/24/2008</p>	
<p><i>Kardjilov, N.; Hilger, A.; Manke, I.; Strobl, M.; Dawson, M.; Banhart, J.</i></p> <p><b>New trends in neutron imaging</b></p> <p>The Sixth International Topical Meeting on Neutron Radiography, Kobe, Japan, 9/14/2008 - 9/18/2008</p>	
<p><i>Keiderling, U.; Wiedenmann, A.; Rupp, A.; Klenke, J.; Heil, W.; Jullien, D.; Petoukhov, A. K.; Lelievre-Berna, E.; Andersen, K. H.</i></p> <p><b>Magic Box and Fast Decaying Cell - Two Methods of SANS Polarization Analysis with 3He at the V4 SANS Instrument of Helmholtz Center Berlin</b></p> <p>Polarised Neutrons In Condensed Matter Investigations PNCMI 2008, Tokai, Japan, 9/1/2008 - 9/5/2008</p>	
<p><i>Klaus, M.; Genzel, Ch.; Holzschuh, H.</i></p> <p><b>Residual Stress Depth Profiling in Complex Hard Coating Systems by X-ray Diffraction</b></p> <p>International Conference on Metallurgical Coatings and Thin Films, San Diego, USA, 4/28/2008 - 5/2/2008</p>	
<p><i>Klaus, M.; Reimers, W.; Genzel, Ch.</i></p> <p><b>Application of Energy-Dispersive Diffraction to the Analysis of Highly Inhomogeneous Residual Stress Fields in Thin Film Structures</b></p> <p>8th International Conference on Residual Stresses, Denver, USA, 8/4/2008 - 8/8/2008</p>	

<p><i>Köhler, R.; Dönch, I.; Ott, P.; Laschevsky, A.; Krastev, R.</i>  <b>Swelling of ultra thin polyelectrolyte multilayers of different charge density in water vapour</b>          DPG Frühjahrskonferenz 2008, Berlin, 2/25/2008 - 2/29/2008</p>	
<p><i>Manke, I.; Hilger, A.; Kardjilov, N.; Schloesser, J.; Petrov, S.; Hartnig, Ch.; Wippermann, K.; Schröder, A.; Sanders, T.; Krüger, P., Kuhn, R.; Wanderka, N.; Banhart, J.</i>  <b>Entwicklungen am HZB: Detektorentwicklung, Bildanalyse, FIB-Tomographie</b>          2nd RunPEM Workshop, Berlin, Germany 11/10/2008 - 11/10/2008</p>	
<p><i>Manke, I.; Kardjilov, N.; Hilger, A.; Strobl, M.; Banhart, J.</i>  <b>Applications of neutron imaging in science and technology</b>          Workshop on NEUtron WAVElength dependend IMAGING (NEUWAVE IMAGING), München, Germany, 4/20/2008 - 4/24/2008</p>	
<p><i>Manke, I.; Hilger, A.; Kardjilov, N.; Schloesser, J.; Petrov, S.; Hartnig, Ch.; Wippermann, K.; Schröder, A.; Sanders, T.; Krüger, P., Kuhn, R.; Wanderka, N.; Banhart, J.</i>  <b>Entwicklungen am HZB: Detektorentwicklung, Bildanalyse, FIB-Tomographie</b>          2nd RunPEM Workshop, Berlin, Germany 11/10/2008 - 11/10/2008</p>	
<p><i>Manke, I.; Kardjilov, N.; Hilger, A.; Strobl, M.; Banhart, J.</i>  <b>Applications of neutron imaging in science and technology</b>          Workshop on NEUtron WAVElength dependend IMAGING (NEUWAVE IMAGING), München, Germany, 4/20/2008 - 4/24/2008</p>	
<p><i>Matsushima, U.</i>  <b>Chyuseishi imagingno nougakuhenou ouyou - jyusui tracerwo mochiita syokubutunai mizudouno kashika -</b>          KURRI 2007 Chyuseishi radiography senmonkenkyuukai, Kumatori, 2/26/2008 - 2/27/2008</p>	V7
<p><i>Matsushima, U.; Graf, W.; Zabler, S.; Kardjilov, N.; Herppich, W.B.</i>  <b>Application of cold neutron and synchrotron X-ray imaging to investigate rose bent neck syndrome</b>          International symposium on postharvest quality of ornamental plants, Aarhus, Denmark, 8/11/2008 - 8/14/2008</p>	
<p><i>Matsushima, U.; Herppich, W.B.; Kardjilov, N.; Graf, W.; Hilger, A.; Manke, I.</i>  <b>Estimation of water flow velocity in small plants using cold neutron imaging with D2O tracer</b>          International Topical Meeting on Neutron Radiography (ITMNR), Kobe, Japan, 9/14/2008 - 9/18/2008</p>	
<p><i>Matsushima, U.; Kardjilov, N.; Graf, W.; Hilger, A.; Herppich, W.B.</i>  <b>Water distribution analysis in plants using cold neutron radiography - Calculation of D2O tracer vectors -</b>          17th Annual Meeting of Bioimaging Society, Chiba University, Japan, 10/30/2008 - 11/1/2008</p>	
<p><i>Matsushima, U.; Kardjilov, N.; Herppich, W.B.</i>  <b>Efficient Photosynthesis and Auto-exhaust Resistance in Street Trees - In Japanese</b>          the 67th annual meeting of Japanese Society of Agricultural Machinery, Miyazaki, Japan, 3/27/2008 - 3/30/2008</p>	V7
<p><i>Matsushima, U.; Kardjilov, N.; Hilger, A.; Herppich, W.B.</i>  <b>In-situ visualization of water flow in seedling using neutron radiography</b>          Symposium on Horticulture in Europe (SHE2008), Vienna, Austria, 2/17/2008 - 2/20/2008</p>	

<p><i>Matsushima, U.; Kardjilov, N.; Hilger, A.; Herppich, W.B.</i>  <b>In-situ Visualization of Water Flow in Seedlings-Application of Cold Neutron Radiography with D2O Tracer and the Influences for Plants</b>  International Conference on Agricultural Engineering &amp; Industry Exhibiton, Hersonissos, Greece, 6/23/2008 – 6/25/2008</p>	
<p><i>Matsushima, U.; Kardjilov, N.; Hilger, A.; Manke, I.; Shono, H.; Herppich, W.B.</i>  <b>Visualization of water usage and photosynthetic activity of street trees exposed to 2ppm of SO<sub>2</sub> - a combined evaluation by cold neutron and chlorophyll fluorescence imaging</b>  International Topical Meeting on Neutron Radiography (ITMNR), Kobe, Japan, 9/14/2008 - 9/18/2008</p>	
<p><i>Matsushima, U.; Kardjilov, N.; Hilger, A.; Shono, H.; Herppich, W.B.</i>  <b>An Application of cold Neutron and Chlorophyll Fluorescence Imaging for Studies an Auto-Exhaust Resistance in Street Trees</b>  International Conference on Agricultural Engineering &amp; Industry Exhibition, Hersonissos, Greece, 6/23/2008 – 6/25/2008</p>	
<p><i>Matsushima, U.; Kardjilov, N.; Kawabata, Y.; Sim, C. M.; Herppch, W. B.</i>  <b>Observation of water flow in vegetable seedlings using neutron Radiography, in Japanese Chyuseishi raigraphy oyobi jysui tracer demiru yasainaeno mizuidou, in Japanese</b>  the 42th KURRI usermeeting, Kumatori, 1/24/2008 - 1/25/2008</p>	V7
<p><i>Mechler, S.; Schumacher, G.; Zizak, I.; Macht, M.-P.; Wanderka, N.</i>  <b>Are metallic glasses destabilized, frustrated quasicrystals?</b>  RQ 13, Dresden, Germany, 8/24/2008 - 8/29/2008</p>	
<p><i>Morris, D.J.P.; Roger, M.; Goff, J.; Tennant, D.A.; Gutmann, M.J.; Prabhakaran, D.; Hoffmann, J.-U.; Feyerherm, R.; Dudzik, E.;</i>  <b>Sodium ordering and the control of electrons in Sodium Cobaltate</b>  British Crystallography Association annual conference, York University, York, U.K., 4/8/2008 - 4/10/2008</p>	
<p><i>Morris, D.J.P.; Roger, M.; Tennant, D.A.; Gutmann, M.J.; Goff, J.P.; Prabhakaran, D.; Hoffmann, J.-U.; Feyerherm, R.; Dudzik, E.; Kiefer, K.</i>  <b>Sodium Ordering Phase Transition in Sodium Cobaltate</b>  APS March Meeting, New Orleans, USA, 3/10/2008 - 3/14/2008</p>	
<p><i>Nowicki, W</i>  <b>Complementarity of neutron and x-ray diffraction techniques for the structure solution in quarternary Li-Mn-Fe oxides</b>  50th Annual Meeting of the Polish Crystallographic Society, Wroclaw, Poland, 6/26/2008 – 6/28/2008</p>	E9 IHP: 1345
<p><i>Papaefthimiou, V.; Günther, J.-U.; Helm, C. A.; Förster, S.; Findenegg, G. H., and Steitz, R.;</i>  <b>Reversible activation of a polyelectrolyte brush</b>  72st Annual Meeting and DPG-Spring Meeting of the Divison Condensed Matter, Berlin, 2/25/2008 - 2/29/2008</p>	
<p><i>Pappas, C.; Lelievre-Berna, E.; Bentley, P.; Moskvina, E.; Farago B.; Falus P.; , Grigoriev, S.; Dyadkin, V.</i>  <b>Polarimetric Neutron Spin Echo Spectroscopy</b>  21st Congress of the International Union of Crystallography, Osaka, Japan, 8/23/2008 - 8/31/2008</p>	
<p><i>Pappas, C., Lelievre-Berna, E., Bentley, P.M., Moskvina, E., Grigoriev, S., Dyadkin, V.</i>  <b>Polarimetric Neutron Spin Echo Spectroscopy</b>  Deutsche Neutronenstreutagung 2008, Garching, Deutschland, 9/15/2008 - 9/17/2008</p>	

<p><i>Pappas, C.; Lelièvre-Berna, E.; Bentley, P.; Moskvin, E.; Farago, B.; Falus, P.; Grigoriev, S.; Dyadkin, V.</i>  <b>Polarimetric Neutron Spin Echo : Feasibility and first Results</b>  NMI3 General Meeting, Ajaccio, Corsica, France, 6/25/2008 - 6/27/2008</p>	
<p><i>Pappas, C.; Lelièvre-Berna, E.; Bentley, P.; Moskvin, E.; Farago, B.; Falus, P.; Grigoriev, S.; Dyadkin, V.</i>  <b>Polarimetric Neutron Spin Echo : Feasibility and first Results</b>  American Conference on Neutron Scattering, Santa Fe, New Mexico, USA, 5/11/2008 - 5/15/2008</p>	
<p><i>Reichenauer, G.</i>  <b>Length change upon adsorption - Breathing of porous samples</b>  International Symposium on the Characterization of Porous Solids (COPS-VIII), Edinburgh, UK, 6/11/2008 - 6/13/2008</p>	V4
<p><i>Rolfs, K.; Mecklenburg, A.; Guldbakke, J.-M.; Chmielus, M.; Alliouane, N.; Brown, J.P.; Schneider, R.</i>  <b>Co-doping: Tuning Ni-Mn-Ga for Actuator Application?</b>  CIMTEC2008, Acireale, Italy, 6/8/2008 - 6/13/2008</p>	
<p><i>Rupp, A.</i>  <b>3He-NSF project at HMI</b>  Final NMI3 General Meeting, Ajaccio, France, 6/25/2008 - 6/28/2008</p>	
<p><i>Russell RA; Yun SI; Holden PJ; FosterLJR</i>  <b>Chain conformation of PHA polymers in solution</b>  7th AINSE/ANBUG Neutron Scattering Symposium, ANSTO, Lucas Heights, Australia, 12/8/2008 - 12/10/2008</p>	V4
<p><i>Schneider, R.; Chmielus, M.; Rolfs, K.; Mecklenburg, A.; Guldbakke, J.-M.; Raatz, A.</i>  <b>Neutrons - A Unique and Essential Tool on the Way to the Commercial Use of Novel Smart Materials</b>  MSE Nürnberg 2008, Nuremberg, Germany, 9/1/2008 - 9/4/2008</p>	
<p><i>Schröder, A.; Wippermann, K.; Mergel, J.; Lehnert, W.; Sanders, T.; Manke, I.; Hilger, A.; Kardjilov, N.; Petrov, S.; Hartnig, C.</i>  <b>Investigation of the current and fluid distribution in a direct methanol fuel cell by electrochemical methods and neutron radiography</b>  Ulm Electro-Chemical Talks, Ulm, Germany, 6/10/2008 - 6/12/2008</p>	
<p><i>Steitz, R.</i>  <b>Thin films and interfaces as seen by neutrons and X-rays</b>  Seminarvortrag Institut für Physik, AG Photobiophysik, Prof. Dr. Beate Röder, Humboldt-Universität zu Berlin, 12/8/2008 - 12/8/2008</p>	
<p><i>Steitz, R.; Papaefthimiou, V.; Günther, J.-U.; Helm, C. A.; Förster, S.; Findenegg, G. H.</i>  <b>Reversible activation of a polyelectrolyte brush</b>  AVS 55th International Symposium, Boston, MA, USA, 10/19/2008 - 10/24/2008</p>	
<p><i>Stöber, S.; Prokhnenko O.; Schorr S.; Döring T.; Pöllmann H.</i>  <b>Synthesis and crystal chemistry of manganese containing perovskites: phases with brownmillerite structures</b>  Calcium Aluminate Cements, Avignon, France 6/30/2008 - 7/2/2008</p>	
<p><i>Strobl, M.</i>  <b>Linking neutron imaging and scattering: An overview of recent developments in neutron imaging</b>  Seminar, TU Delft, Holland, 3/5/2008 - 3/5/2008</p>	
<p><i>Strobl, M.; Hilger, A.; Kardjilov, N.; Manke, I.</i>  <b>Monochromatic neutrons and phase contrast from matter and magnetic fields</b>  NEUwave Meeting, TUM, Germany 4/21/2008 - 4/24/2008</p>	

<p><i>Strobl, M.; Hilger, A.; Kardjilov, N.; Manke, I.</i>  <b>Nuclear and magnetic phase contrast imaging with neutrons</b>  ITMNR, Kobe, Japan, 9/15/2008 – 9/19/2008</p>	
<p><i>Strobl, M.; Kardjilov, N.; Hilger, A.; Manke, I.; Treimer, W.; Jericha, E.; Badurek, G.</i>  <b>Imaging with polarised neutrons</b>  PNCMI 2008, Tokai, Japan, 9/1/2008 - 9/5/2008</p>	
<p><i>Strobl, M.; Steitz, R.; Dahint, R.; Grunze, M.</i>  <b>BioRef a time-of-flight reflectometer at Hahn-Meitner Institute Berlin</b>  IUCr 2008, Osaka, Japan, 8/24/2008 - 8/30/2008</p>	
<p><i>Strunz, P.; Gilles, R.; Mukherji, D.; Hofmann, M.; del Genovese, D.; Roesler, J.; Hoelzel, M.; Davydov, V.</i>  <b>Scattering contrast dependence on thermal expansion coefficient difference of phases in two phase system</b>  Deutsche Neutronenstreutagung 2008, Garching, Germany, 9/15/2008 - 9/17/2008</p>	V4
<p><i>Süllow, S.</i>  <b>Ground state properties of the 1D distorted diamond chain azurite, Cu<sub>3</sub>(CO<sub>3</sub>)<sub>2</sub>(OH)<sub>2</sub></b>  12. International Conference on Highly Frustrated Magnetism 2008, Braunschweig, Germany 9/7/2008 - 9/12/2008</p>	E1, E2, V2
<p><i>Süllow, S.</i>  <b>Ground state and spin excitations in the 1D distorted diamond chain azurite, Cu<sub>3</sub>(CO<sub>3</sub>)<sub>2</sub>(OH)<sub>2</sub></b>  11. International Symposium on Strongly Correlated Electron Systems SCES 08, Buzios, Brazil, 8/17/2008 - 8/22/2008</p>	E1, E2, V2
<p><i>Tatchev, D.; Hoell, A.; Eichelbaum, M.; Rademann, K.</i>  <b>In situ SAXS-Study of the Formation of Gold Nano-particles in Soda-lime-silicate Glass</b>  XII.th Research Workshop Nucleation Theory and Application, Dubna, Russia, 4/12/2008 – 4/20/2008</p>	
<p><i>Tatchev, D.; Hoell, A.; Eichelbaum, M.; Rademann, K.</i>  <b>In situ SAXS-Study of the formation of gold nano-particles in soda-lime-silicate glasses</b>  Fourth Balkan Conference on Glass Science and Technology, Varna, Bulgarien, 9/27/2008 - 10/1/2008</p>	
<p><i>Tatchev, D.; Hoell, A.; Eichelbaum, M.; Rademann, K.</i>  <b>Small angle X-ray scattering study of the formation of gold nanoparticles in glass</b>  Nanoscale Phenomena and Structures in Bulk and Surface Phases, Sofia, Bulgaria, 2/26/2008 - 3/2/2008</p>	
<p><i>Tolinski, T.; Kowalczyk, A.; Hoser, A.; Stüßler, N.; Talik, E.; Klimczak, M.; Kaczorowski, D.</i>  <b>Neutron diffraction, magnetic, transport and thermodynamic studies on (CeNi<sub>4.2</sub>Mn<sub>0.8</sub>, Y<sub>0.7</sub>Ni<sub>4.2</sub>Mn<sub>0.8</sub>) and CeCo<sub>1-x</sub>Cu<sub>x</sub>Al<sub>4</sub> compounds</b>  Strongly correlated electron systems: preparation, basic research and applications, Karpacz, Poland, 10/17/2008 - 10/19/2008</p>	E6 NMI3: 1305 NMI3: 1258
<p><i>Uestuener, K.; Katter, M.; Blank, R.; Benedikt, D.; Bahrndt, J.; Gaupp, A.; Klemke, B.; Grüner, F.; Weingartner, R.</i>  <b>Sintered (Pr,Nd)-Fe-B Permanent Magnets with (BH)<sub>max</sub> of 520 kJ/m<sup>3</sup> at 85 K for Cryogenic Applications</b>  20th international Workshop on Rare Earth Permanent Magnets and their Applications, Crete, Greece, 9/8/2008 - 9/10/2008</p>	

<p><i>Vierke, J.; Schumacher, G.; Denks, I.; Wanderka, N.; Wollgarten, M.; Banhart, J.; Zizak, I.; Pilyugin, V.P.; Balog, M.; Nagy, J.; Simancik, F.</i>  <b>Strain- and Temperature-induced Glass-to-Crystal Transformations in Al-Ni-La Glass</b>          DPG Frühjahrstagung 2008, Berlin, Germany, 2/25/2008 - 2/29/2008</p>	
<p><i>Wimpory, R.C.</i>  <b>TG4 Stress Relieved Specimen measurements</b>          14th NeT Steering Committee Meeting and 5th NeT Enlargement &amp; Integration Workshop, Petten,, JRC, Petten, The Netherlands, 12/1/2008 - 12/3/2008</p>	
<p><i>Wimpory, R.C.</i>  <b>Using neutrons for non destructive testing at the surface</b>          14th NeT Steering Committee Meeting and 5th NeT Enlargement &amp; Integration Workshop, Petten, JRC, Petten, The Netherlands, 12/1/2008 - 12/3/2008</p>	
<p><i>Wollgarten, M.; Haas, S.; Tatchev, D.; Hoell, A.; Banhart, J.</i>  <b>Investigation of the microstructure during devitrification of amorphous Al88Sm12</b>          13th Int. Conference on Rapidly Quenched &amp; Metastable Materials, Dresden, Germany, 8/24/2008 - 8/29/2008</p>	

## Seminars and Conference Contributions 2008

### Posters

#### 2005 (supplement)

<i>Brandt, A.; Michaelsen, R.</i> <b>HMI instruments@BESSY &amp; BENSC future plans</b> ICNS 2005, Sydney, Australia, 11/27/2005 - 12/2/2005	
<i>Brandt, A.; Michaelsen, R.</i> <b>Performance of HMI-BENSC</b> ICNS 2005, Sydney, 11/27/2005 - 12/2/2005	
<i>Brandt, A.; Michaelsen, R.</i> <b>Neutrons for the international scientific community</b> ICNS 2005, Sydney, Australia, 11/27/2005 - 12/2/2005	

#### 2006 (supplement)

<i>Brandt, A.; Graf, H.A.</i> <b>Neutrons for the scientific community</b> Deutsche Neutronenstreutagung SNI 2006, Hamburg, Germany, 10/4/2006 - 10/6/2006	
<i>Brandt, A.; Graf, H.A.</i> <b>Polarized neutrons for the international scientific community</b> PNCMI 2006, Berlin, Germany, 9/25/2006 - 9/28/2006	
<i>Brandt, A.; Graf, H.A.</i> <b>HMI-BENSC sample environment</b> Deutsche Neutronenstreutagung SNI 2006, Hamburg, Germany, 10/4/2006 - 10/6/2006	
<i>Brandt, A.; Graf, H.A.</i> <b>HMI-BENSC Instruments</b> Deutsche Neutronenstreutagung SNI2006, Hamburg, Germany, 10/4/2006 - 10/6/2006	

#### 2007 (supplement)

<i>Aman, U.; Ritter, C.; Pfrommer, A.; Hohlwein, D.; Ihringer, J.</i> <b>Magnetic and structural phase transitions in Mn-site substituted electron-doped Manganites</b> ECNS, Lund, Sweden, 6/25/2007 - 6/29/2007	E2
<i>Argyriou, D.</i> <b>Enhanced multiferroic polarization by induced Dy spin-order in multiferroic DyMnO<sub>3</sub></b> ECNS, Lund, Sweden, 6/25/2007 - 6/29/2007	E9
<i>Argyriou, D.; Feyerherm, R.; Dudzik, E.; Landsgesell, S.; Chapon, L.C.; Prokhnenko, O.</i> <b>Melting of incommensurate-ferroelectric phase with magnetic field in multiferroic TbMO<sub>3</sub></b> ECNS, Lund, Sweden, 6/25/2007 - 6/29/2007	V2

<p><i>Baldelli Bombelli, F.; Berti, D.; Betti, F.; Brandt, A.; Baglioni, P.</i>  <b>Small angle neutron scattering investigation of the self-assembling behaviour of Di-C12P-nucleosides in solution</b>  ECNS, Lund, Sweden, 6/25/2007 - 6/29/2007</p>	<p>V4  NMI3: 1022  NMI3: 1106</p>
<p><i>Bentley, P.; Andersen, K.</i>  <b>Particle swarms applied to the design of novel and complex focussing guide systems</b>  ECNS, Lund, Sweden, 6/25/2007 - 6/29/2007</p>	
<p><i>Beran, P.; Bellido, N.; Hernandez-Velasco, J.; Ritter, C.; Frontera, C.; Garcia-Munoz, L.</i>  <b>Evolution of phase separation and single-domain structural and magnetic properties in Pr<sub>0.5</sub>Ca<sub>0.5</sub>Mn<sub>1-x</sub>Ni<sub>x</sub>O<sub>3</sub></b>  ECNS, Lund, Sweden, 6/25/2007 - 9/25/2007</p>	<p>E2  NMI3: 1051</p>
<p><i>Betti, F.; Baldelli Bombelli, F.; Berti, D.; Brandt, A.; Baglioni, P.</i>  <b>The reverse system cyclohexane/POPNI/Lecithin/water: structural investigation for inclusion of single chain oligo nucleotide</b>  ECNS, Lund, Sweden, 6/25/2007 - 6/29/2007</p>	<p>V4  NMI3: 1106  NMI3: 1207</p>
<p><i>Boin, M.; Kardjilov, N.; Haibel, A.; Edwards, L.; Schneider, R.</i>  <b>Vector tomography methods for 3D imaging of stress and texture distributions based on Bragg-edge neutron tomography experiments</b>  ECNS, Lund, Sweden, 6/25/2007 - 6/29/2007</p>	<p>E3</p>
<p><i>Bonini, M.; Fratini, E.; Neto, C.; Wiedenmann, A.; Baglioni, P.</i>  <b>Spontaneous chain-like assembly of magnetic nanoparticles revealed by small angle scattering</b>  ECNS, Lund, Sweden, 6/25/2007 - 6/29/2007</p>	<p>V4  IHPII: 515</p>
<p><i>Bonini, M.; Fratini, E.; Neto, C.; Wiedenmann, A.; Baglioni, P.</i>  <b>Spontaneous chain-like assembly of magnetic nanoparticles revealed by small angle scattering</b>  ECNS, Lund, Sweden, 6/25/2007 - 6/29/2007</p>	<p>V4  NMI3: 1021</p>
<p><i>Bordallo, H.; Freire, P.T.C.; De Souza, J.; Argyriou, D.</i>  <b>Observation of a structural transition induced by isotopic effect in the smallest chiral amino acid</b>  ECNS, Lund, Sweden, 6/25/2007 - 6/29/2007</p>	<p>E9, V3</p>
<p><i>Borga, A.; Kmmmerling, G.; Thielmann, C.; Gebauer, B.</i>  <b>DETNI front-end board system prototypes</b>  ECNS, Lund, Sweden, 6/25/2007 - 6/29/2007</p>	
<p><i>Boue, F.; Gummel, J.; Cousin, F.</i>  <b>SANS measurements of the form factor of a chain complexed inside a mixed system</b>  ECNS, Lund, Sweden, 6/25/2007 - 6/29/2007</p>	<p>V4  NMI3: 1018  NMI3: 1092</p>
<p><i>Brandt, A.; Graf, H.A.</i>  <b>BENSC User operation</b>  ECNS, Lund, Sweden, 6/25/2007 - 6/29/2007</p>	
<p><i>Buchsteiner, A.; Stüsser, N.</i>  <b>Optimizations in neutron powder diffraction by using divergent beam geometries in angular dispersive techniques</b>  ECNS, Lund, Sweden, 6/25/2007 - 6/29/2007</p>	
<p><i>Campbell, S.; Wand, J.; Dou, S.X.; Avdeev, M.; Studer, A.J.; Hoffmann, M.; Hoelzel, M.</i>  <b>Magnetic structures of Pr<sub>0.5</sub>Y<sub>0.5</sub>Mn<sub>2</sub>Ge<sub>2</sub></b>  ECNS, Lund, Sweden, 25.06.2007, 6/25/2007 - 6/29/2007</p>	
<p><i>Casinini, F.; Petrillo, C.; Sacchetti, F.; Alimov, S.S.; Gebauer, B.</i>  <b>Development of a high-resolution silicon micro-strip neutron detector in DETNI</b>  ECNS, Lund, Sweden, 6/25/2007 - 6/29/2007</p>	

<p><i>Cousin, F.; Gummel, J.; Boue, F.</i>  <b>Counterions release from electrostatic complexes of polyelectrolytes and proteins of opposite charge: a direct measurement by SANS</b>  ECNS, Lund, Sweden, 6/25/2007 - 6/29/2007</p>	<p>V4  NMI3: 1018  NMI3: 1092</p>
<p><i>Dabrowski, W.; Brogna, A.; Buzzetti, S.; Fiutowski, T.; Gebauer, B.; Schmidt, C.; Soltviet, H.K.; Szczygiel, R.; Trunk, U.; Wiacek, P.</i>  <b>MSGCROC - a novel application specific intergated circuit for readout of two-dimensionl position sensitive gas microstrip neutron detectors</b>  ECNS, Lund, Sweden, 6/25/2007 - 6/29/2007</p>	
<p><i>Dante, S.; Hauß, T.; Brandt, A.; Dencher, N.</i>  <b>Fusogenic activity of beta-Amyloid peptide detected by SANS on lipid unilamellar vesicels</b>  ECNS, Lund, Sweden, 6/25/2007 - 6/29/2007</p>	<p>V4</p>
<p><i>Desmedt, A.; Harris, K.D.M.; Tykwinski, R.; Guillaume, F.; Mereau, R.; Gonzalez, M.A.</i>  <b>Solid state transformation of Ammonium Cyanate into Urea: A QENS invenstigation of the Ammonium dynamics</b>  ECNS, Lund, Sweden, 6/25/2007 - 6/29/2007</p>	<p>V3  IHP: 454</p>
<p><i>Desmedt, A.; Pefoute, E.; Soetens, J.-C.; Prager, M.; Mancois, F.; Russina, M.</i>  <b>Dynamics in Clathrate Hydrates by combining MD and QENS</b>  ECNS, Lund, Sweden, 6/25/2007 - 6/29/2007</p>	<p>V3  NMI3: 1159</p>
<p><i>Duc Le, T.; McEwen, K.; Park, J.-G.; Lee, S.; Iga, F.; Rule, K.</i>  <b>Magnetic excitations in the ordered phases of Praseodymium Hexaboride</b>  ECNS, Lund, Sweden, 6/25/2007 - 6/29/2007</p>	<p>V2  NMI3: 1163</p>
<p><i>Farago, B.; Raitman, E.; Gavrilov, V.; Aksenov, V.; Nikitenko, Y.; Fritzsche, H.</i>  <b>Neutron scattering by acoustic wave in solids studied with diffraction, NSE and reflectometry methods</b>  ECNS, Lund, Sweden, 6/25/2007 - 6/29/2007</p>	<p>V6  IHP: 463  IHP: 571</p>
<p><i>Fiori, F.; Calbucci, V.; Giuliani, A.; Manescu, A.; Casalegno, V.; Ferraris, M.; Rustichelli, F.</i>  <b>Residual stresses induced by brazing and thermal cycling in CFC/Cu/Cu alloy joints for nuclear fusion technology</b>  ECNS, Lund, Sweden, 6/25/2007 - 6/29/2007</p>	<p>E3  NMI3: 1202</p>
<p><i>Flachbart, K.; Siemensmeier, K.; Gabani, S.; Matas, S.; Priputen, P.; Shitsevalova, K.; Wulf, E.</i>  <b>Inelastic neutron diffraction on geometrically frustrated antiferromagnetic HoB12</b>  ECNS, Lund, Sweden, 6/25/2007 - 6/29/2007</p>	<p>E10</p>
<p><i>Fouquet, P.; Bentley, P.; Farago, B.; Pappas, C.; Mezei, F.</i>  <b>The wide angle spin echo spectrometer project WASP at ILL</b>  ECNS, Lund, Sweden, 6/25/2007 - 6/29/2007</p>	
<p><i>Garcia-Munoz, J.L.; Frontera, C.; Bellido, N.; Hernandez-Velasco, J.; Beran, P.; Ritter, C.</i>  <b>Phase separation and magnetic disorder in Ti substituted Pr<sub>0.5</sub>Ca<sub>0.5</sub>Mn<sub>1-x</sub>Ti<sub>x</sub>O<sub>3</sub> manganite</b>  ECNS, Lund, Sweden, 6/25/2007 - 6/29/2007</p>	<p>E2  NMI3: 1051</p>
<p><i>Gebauer, B.; Alimov, S.S.; Borga, A.; Brogna, A.; Buzzetti, S.; Casinini, F.; Dabrowski, W.; Fiutkowski, T.; Kemmerling, G.; Klein, M.</i>  <b>Development of very high rate and resolution neutron detectors in DETNI</b>  ECNS, Lund, Sweden, 6/25/2007 - 6/29/2007</p>	
<p><i>Giuliani, A.; Giuliani, A.; Fiori, F.; Gysens, J.; Manescu, A.; Rustichelli, F.</i>  <b>Analysis of neutron diffraction profiels in bronze archaeological statuettes produced by solid waste wax casting</b>  ECNS, Lund, Sweden, 6/25/2007 - 6/29/2007</p>	<p>V7  NMI3: 1166</p>

<i>Herrero-Albillos, J.</i> <b>Short-range magnetic correlations in the paramagnetic phase of ErCo<sub>2</sub></b> ECNS, Lund, Sweden, 6/25/2007 - 6/29/2007	V4 NMI3: 1053 NMI3: 1088
<i>Hoffmann, J.-U.; Amann, U.; Ihringer, J.; Schreiber, F.</i> <b>The next generation of flat-cone diffraction</b> ECNS, Lund, Sweden, 6/25/2007 - 6/29/2007	E2
<i>Iolin, E.; Rusevich, L.; Strobl, M.; Treimer, W.; Mezei, F.</i> <b>Cold neutron scattering by ultrasound in silicon. Suppression of the ultrasound contribution to the Debey-Waller factor effect</b> ECNS, Lund, Sweden, 6/25/2007 - 6/29/2007	V12b NMI3: 1070
<i>Kali, G.; Santa, Z.; Rosta, L.; Bleif, H.-J.</i> <b>High resolution TOF powder diffractometer at the Budapest research reactor</b> ECNS, Lund, Sweden, 6/25/2007 - 6/29/2007	
<i>Kiselev, M.; Zemlyanaya, E.; Ryabova, N.; Balagurov, A.; Aksenov, V.; Dante, S.; Hauß, T.; Neubert, R.</i> <b>Significance of the fully extended conformation of ceramide molecules in the nanostructure organization of Stratum Corneum</b> ECNS, Lund, Sweden, 6/25/2007 - 6/29/2007	V1
<i>Kloesgen, B.; Bruun, S.; Hansen, S.; Stachura, M.; Wodzinska, K.; Steitz, R.; Nylander, T.</i> <b>Intrinsic depletion or not: More on the interfacial wetting of polystyrene by water</b> ECNS, Lund, Sweden, 6/25/2007 - 6/29/2007	V6 NMI3: 1185
<i>Köbler, I.; Hoser, A.</i> <b>Unexpected field dependence of the transverse magnetization in Yttrium Iron Garnet (YIG)</b> ECNS, Lund, Sweden, 6/25/2007 - 6/29/2007	E6
<i>Köhler, R.</i> <b>Water uptake in polyelectrolyte multi layers studied by neutron reflectometry</b> ECNS, Lund, Sweden, 6/25/2007 - 6/29/2007	V6
<i>Kolasinska, M.; Krastev, R.; Warszynki, P.</i> <b>Layer by layer deposition technique. Dipping vs. spraying</b> ECNS, Lund, Sweden, 6/25/2007 - 6/28/2007	V6
<i>Kreyssig, A.; Frontzek, M.; Doerr, M.; Schneidewind, A.; Hoffmann, J.-H.; Kim, J.-W.; Tan, L.; Goldman, A.I.; Loewenhaupt, M.</i> <b>Interplay of crystal-electric field, RKKY interaction and frustration in R<sub>2</sub>PdSi<sub>3</sub></b> ECNS, Lund, Sweden, 6/25/2007 - 6/29/2007	E2
<i>Lechner, R.; Pieper, J.; Hauß, T.; Buchsteiner, A.; Dencher, N.; Ollivier, J.</i> <b>Dynamics of a proton pump: Theoretical aspects of a time resolved QENS experiment</b> ECNS, Lund, Sweden, 6/25/2007 - 6/29/2007	V3
<i>LoCelso, F.; Benfante, V.; Kardjilov, N.; Hilfer, A.; Tusa, S.; Triolo, R.</i> <b>Identification of hidden object of archaeological interest</b> ECNS, Lund, Sweden, 6/25/2007 - 6/29/2007	V7 NMI3: 1214
<i>LoCelso, F.; Benfante, V.; Triolo, R.; Kardjilov, N.; Hilger, A.; Keiderling, U.; Ruffo, I.; Festa, G.; Filabozzi, A.</i> <b>Application of neutron techniques on marbles of archaeological interest</b> ECNS, Lund, Sweden, 6/25/2007 - 6/29/2007	V4, V7, V12a NMI3: 1136
<i>Manescu, A.; Fiori, Giuliani, A.; Kasztovszky, Z.; Rustichelli, F.; Straumal, B.</i> <b>Non-destructive compositional analysis of historic organs reed pipes</b> ECNS, Lund, Sweden, 6/25/2007 - 6/29/2007	V7 NMI3: 1213

<p><i>Matsushima, U.; Kardjilov, N.; Zabler, S.; Graf, W.; Hilger, A.; Manke, I.; Herppich, W. B.</i>  <b>Chyuseishi oyobi synchrotron X-sen imaging niyoru barakiribana kakeibuno hihakaikansatsu. In Japanese</b>  The first annual meeting of Japanese Society of Agricultural, Biological and Environmental Engineers and Scientists, Osaka, Japan, 6/25/2007 - 6/27/2007</p>	V7
<p><i>Matsushima, U.; Graf, W.; Kardjilov, N.; Zabler, S.; Herppich, W.B.</i>  <b>Investigation of rose bent neck syndrome using neutron and synchrotron X-ray imaging</b>  DGG und des BHGL, Erfurt, Germany, 2/21/2007 - 2/24/2007</p>	V7
<p><i>Meissner, M.; Kiefer, K.; Wallacher, D.</i>  <b>Sample environment at BENSC: New developments on magnetic field and temperature</b>  ECNS, Lund, Sweden, 6/25/2007 - 6/29/2007</p>	
<p><i>Mindur, B.; Fiutkowski, T.; Gebauer, B.; Schulz, C.; Wiacek, P.</i>  <b>Gigabit ethernet readout interface for DETNI</b>  ECNS, Lund, Sweden, 6/25/2007 - 6/29/2007</p>	
<p><i>Mindur, B.; Fiutkowski, T.; Gebauer, B.; Schulz, C.; Wiacek, P.</i>  <b>Data acquisition, monitoring and control software for DETNI</b>  ECNS, Lund, Sweden, 6/25/2007 - 6/29/2007</p>	
<p><i>Nefeodova, E.; Tiden, N.; Siemensmeyer, K.; Buchsteiner, A.; Lazukov, V.; Alekseev, P.; Shitsevalova, N</i>  <b>Magnetic response in paramagnetic and antiferromagnetic phases of PrB6</b>  ECNS, Lund, Sweden, 6/25/2007 - 6/29/2007</p>	V3
<p><i>Pappas, C.; Bentley, P.M.; Kischnik, R.; Granz, P.; Moskvinn, E.; Geza, Z.; Clemens, D.; Mezei, F.</i>  <b>The wide angle NSE spectrometer SPAN in the new guide hall of BENSC</b>  ECNS, Lund, Sweden, 6/25/2007 - 6/29/2007</p>	
<p><i>Paul-Boncour, V.; Hoser, A.; Hense, K.; Gratz, E.; Stüsser, N.</i>  <b>Magnetic phase diagram of HoAg</b>  ECNS, Lund, Sweden, 6/25/2007 - 6/29/2007</p>	E1, E6 IHPII: 498 IHPII: 545
<p><i>Pieper, O.; van Slageren, J.; Guidi, T.; Lake, B.; Mutka, H.; Buchsteiner, A.; Russina, M.; Milios, C.J.; Brechin, E.K.; Julia, A.</i>  <b>Inelastic neutron scattering studies of two MN(+3)-based single molecule magnets</b>  ECNS, Lund, Sweden, 6/25/2007 - 6/29/2007</p>	V3
<p><i>Prager, M.; Desmedt, A.; Press, W.; Allgaier, J.; Russina, M.; Unruh, T.; Natkaniec, I.; Pawlukojc, A.</i>  <b>Rotational potentials and dynamics of methyl groups and whole guest molecules in Methyl Halide Hydrates</b>  ECNS, Lund, Sweden, 6/25/2007 - 6/29/2007</p>	V3
<p><i>Prokes, K.; Mydosh, J.; Munoz-Sandoval, E.; Chinchure, A.D.</i>  <b>Richness of magnetic phases in Er<sub>2</sub>Ni<sub>2</sub>Pb</b>  ECNS, Lund, Sweden, 6/25/2007 - 6/29/2007</p>	E4
<p><i>Prokes, K.; Sechovsky, V.; Bruck, E.H.; Andreev, A.V.; DeBoer, F.R.</i>  <b>The field-induced magnetic structure in UIrGe</b>  ECNS, Lund, Sweden, 6/25/2007 - 6/29/2007</p>	
<p><i>Prokhnenko, O.; Feyerherm, R.; Dudzik, E.; Landsgesell, S.; Aliouane, N.; Chapon, L.C.; Argyriou, D.</i>  <b>Magnetic ordering in DyMnO<sub>3</sub> and its relation to ferroelectric polarization</b>  ECNS, Lund, Sweden, 6/25/2007 - 6/29/2007</p>	E9, S2
<p><i>Raitmans, E.; Gavrilov, V.; Myasishev, D.</i>  <b>Neutron scattering by acoustic waves in perfect and bent silicon crystals</b>  ECNS, Lund, Sweden, 6/25/2007 - 6/29/2007</p>	V6 IHP: 571

<p><i>Repper, J.</i>  <b>Analysis of residual stress distributions of IN 718 discs via neutron diffraction</b>  ECNS, Lund, Sweden, 6/25/2007 - 6/29/2007</p>	
<p><i>Russina, M.</i>  <b>The advantages and disadvantages of multi-slits shoppers systems for TOF spectrometers</b>  ECNS, Lund, Sweden, 6/25/2007 - 6/29/2007</p>	
<p><i>Russina, M.; Kemner, E.; Celli, M.; Ulivi, L.; Mezei, F.</i>  <b>Non-equilibrium behaviour of bulk and confined hydrogen</b>  ECNS, Lund, Sweden, 6/25/2007 - 6/29/2007</p>	V3
<p><i>Saensunon, B.; Stewart, G. A.; Gubbens, P. C. M.; Hutchison, W. D.; Buchsteiner, A.;</i>  <b>The crystal field parameters for Er<sup>3+</sup> in ErNiAl<sub>4</sub></b>  Sixth AINSE/ANBUG Neutron Scattering Symposium (AANSS 2007), Lucas Heights, 12/4/2007 - 12/6/2007</p>	V3
<p><i>Saroun, J.; Strobl, M.</i>  <b>Round robin test of double crystal SANS diffractometers</b>  ECNS, Lund, Sweden, 6/25/2007 - 6/29/2007</p>	V12
<p><i>Schneider, R.; Mecklenburg, A.; Rolfs, K.; Michaelsen, R.; Mezei, F.</i>  <b>Neutrons - a unique and essential tool on the way of the commercial use of novel smart materials</b>  ECNS, Lund, Sweden, 6/25/2007 - 6/29/2007</p>	
<p><i>Sechovsky, V.; Prokes, K.; Syshchenko, O.</i>  <b>Antiferromagnetic phases in Er<sub>6</sub>Ni<sub>2</sub>Sn</b>  ECNS, Lund, Sweden, 6/25/2007 - 6/29/2007</p>	E6
<p><i>Siemesmeier, K.; Boyko, V.</i>  <b>Preparation and orientation of solid <sup>3</sup>He crystals for neutron diffraction investigations</b>  ECNS, Lund, Sweden, 6/25/2007 - 6/29/2007</p>	E10
<p><i>Sitepu, H.</i>  <b>Combined neutron and synchrotron structural refinement of two-stage (cubic--&gt;trigonal--&gt;monoclinic) martensitic phase transformations in textured Ti<sub>50.75</sub>Ni<sub>47.75</sub>Fe<sub>1.50</sub> and Ni-Fe rich Ni<sub>50.7</sub>Ti<sub>49.3</sub> alloys</b>  ECNS, Lund, Sweden, 6/25/2007 - 6/29/2007</p>	E9
<p><i>Strobl, M.; Staack, K.; Treimer, W.</i>  <b>Quantitative neutron phase contrast tomography</b>  ECNS, Lund, Sweden, 6/25/2007 - 6/29/2007</p>	V12
<p><i>Stüsser, N.; Sadykov, R.; Hoser, A.</i>  <b>Pressure dependence of the magnetic spiral in CsCuCl</b>  ECNS, Lund, Sweden, 6/25/2007 - 6/29/2007</p>	E6
<p><i>Teichert, A.; Steitz, R.; Krist, T.</i>  <b>Diffuse scattering from polarizing supermirrors</b>  ECNS, Lund, Sweden, 6/25/2007 - 6/29/2007</p>	V6
<p><i>Tennant, A.</i>  <b>An extreme high field magnet for neutron scattering</b>  ECNS, Lund, Sweden, 6/25/2007 - 6/29/2007</p>	
<p><i>Tolinski, T.; Hoser, A.; Stüsser, N.; Falkowski, M.; Kowalczyk, A.</i>  <b>Evolution of the magnetic structure in R-Ni-M compounds (R = rare earth; M = Al, Cu, Si)</b>  ECNS, Lund, Sweden, 6/25/2007 - 6/29/2007</p>	E6 NMI3: 1258
<p><i>Triolo, A.; Russina, O.; Di Cola, E.; Perroud, O.; Bleif, H.-J.; King, S.</i>  <b>Morphology of macromolecules room temperature ionic liquids</b>  ECNS, Lund, Sweden, 6/25/2007 - 6/29/2007</p>	V4 NMI3: 1208

<p><i>Triolo, A.; Russina, O.; Gonzalez, M.-A.; Grimm, H.</i>  <b>Relaxation processes in room temperature ionic liquids</b>          ECNS, Lund, Sweden, 6/25/2007 - 6/29/2007</p>	V3
<p><i>Ulrich, C.; Reehuis, M.; Khaliullin, G.; Damlijanovic, V.; Maljuk, A.; Ivanov, A.; Schmalzl, K.; Niedermayer, Ch.; Hradil, K.; Keimer, B.</i>  <b>Spin wave dispersion in the helical spin ordererd system SrFeO3 and CaFeO3</b>          ECNS, Lund, Sweden, 6/25/2007 - 6/29/2007</p>	
<p><i>Wallacher, D.; Brandt, A.</i>  <b>Combined neutron scattering and in-situ gas adsorption experiments under controlled PVT-conditions</b>          9th international conference on fundamentals of adsorption, Giardini Naxos, Sicily - Italy, 5/20/2007 - 5/25/2007</p>	
<p><i>Wallacher, D.; Brandt, A.; Meissner, M.</i>  <b>DEGAS: Dedicated sample environment for combined gas adsorption and scattering experiments</b>          19. Deutsche Zeolithtagung, Leipzig, 3/7/2007 - 3/9/2007</p>	
<p><i>Wallacher, D.; Brandt, A.; Meissner, M.</i>  <b>Combined neutron scattering and in-situ gas adsorption experiments under controlled pVT-conditions</b>          ECNS, Lund, Sweden, 6/25/2007 - 6/29/2007</p>	
<p><i>Wallacher, D.; Brandt, A.; Smarsly, B.; Sel, Ö.; Thommes, M.</i>  <b>On the nitrogen sorption mechanism in silica with hierachical mesoporosity studied by in-situ small angle neutron scattering</b>          ECNS, Lund, Sweden, 6/25/2007 - 6/29/2007</p>	V4
<p><i>Wimpory, R.; Davies, C.M.; Schneider, R.; ODowd, N.P.</i>  <b>Quantifying teh effects of creep relaxation and prior creep damage by using measuremenst of welded fracture mechanics specimens using neutron diffraction</b>          ECNS, Lund, Sweden, 6/25/2007 - 6/29/2007</p>	E3
<p><i>Zvorykina, O.; Filimonov, A.; Naberezhnov, A.; Vakhrushev, S.; Tovar, M.</i>  <b>Neutron diffraction study of confinde solid solutions NaNO2</b>          ECNS, Lund, Sweden, 6/25/2007 - 6/29/2007</p>	E9

## 2008

<p><i>Baran, S.; Arulraj, A.; Kaczorowski, D.; Penc, B.; Szytula, A.</i>  <b>Magnetic ordering and magnetic properties of ErAuxNi1-xIn (0&lt;=x&lt;=1) solid solution</b>          16th Int. Conf. on Solid Compounds of Transition Elements, Dresden, Germany, 7/26/2008 - 7/31/2008</p>	E6 NMI3: 1303
<p><i>Bordallo, H. N.; Boldyreva, E. V.; Buchsteiner, A.; Koza, M. M.; Landsgesell, S.</i>  <b>Structure-Property Relationships in the Crystals of the Smallest Amino Acid: An Incoherent Inelastic Neutron Scattering Study of the Glycine Polymorphs</b>          50 Years of Neutron Science in Berlin, Berlin, Germany, 7/14/2008 - 7/15/2008</p>	
<p><i>Bordallo, H.; Boldyreva, E.; Buchsteiner, A.; Koza, M.M.; Landsgesell, S.</i>  <b>Structure-Property Relationships in the Crystals of the Smallest Amino Acid: An Inelastic Neutron Scattering Study of the Glycine Polymorphs as a Function of Temperature and Pressure</b>          Deutsche Neutronenstreutagung 2008, Garching, Germany, 9/15/2008 - 9/17/2008</p>	

<p><i>Brandt, A.; Wallacher, D.; Meissner, M.</i>  <b>DEGAS@HMI: Scattering experiments under controlled gas pressure</b>  20. Deutsche Zeolithtagung, Halle, Germany, 3/5/2008 - 3/7/2008</p>	
<p><i>Chmielus, M.; Carpenter, D.; Geleynse, A.; Hagler, M.; Schneider, R.; Müllner, P.</i>  <b>Numerical simulation of twin-twin interaction in magnetic shape-memory alloys</b>  Materials Research Society, Spring 2008 Meeting, Symposium Z, San Francisco, USA, 3/24/2008 - 3/28/2008</p>	
<p><i>Chmielus, M.; Chernenko, V.A.; Hilger, A.; Kostorz, G.; Müllner, P.; Schneider, R.</i>  <b>Magneto-mechanical properties and fracture of a mechanically constrained Ni-Mn-Ga single crystal after extended magnetic cycling</b>  ICOMAT 2008, Santa Fe, New Mexico, USA, 6/29/2008 - 7/5/2008</p>	
<p><i>Dawson, M.; Hilger, A.; Kardjilov, N.; Manke, I.; Strobl, M.; Grünzweig, C.; Pfeiffer, F.; David, C.; Banhart, J.</i>  <b>Interferometric imaging with neutrons</b>  ITMNR-6, Kobe, Japan, 9/14/2008 - 9/18/2008</p>	
<p><i>Dyakov, V.; Kamenev, V.; Zubov, E.; Arciszewska, M.; Kravchenko, Z.; Dobrowolski, W.; Mikhaylov, V.; Puniak, R.; Winiewski, A.; Szytula, A.; Stüsser, N.; Szymczak, H.</i>  <b>Low temperature magnetic ordering in La<sub>1-x</sub>(Pr,Nd)<sub>x</sub>MnO<sub>3</sub> manganites</b>  25th Int. Conf. on Low Temperature Physics, Amsterdam, Netherlands, 8/6/2008 - 8/13/2008</p>	E6 NMI3: 1255
<p><i>Favre Buivin, F.; O. Sobolev, L. Charlet, E. Kemner, M. Russina</i>  <b>Water - clay interaction. Quasielastic neutron scattering study</b>  Deutsche Neutronenstreutagung 2008, Munich, Germany</p>	V3 IHP: 1282
<p><i>Graf, H.A.</i>  <b>Das neue Helmholtz-Zentrum Berlin</b>  DGK 2008, Erlangen, Germany, 3/3/2008 - 3/6/2008</p>	
<p><i>Hoell, A.; Heinemann, A.; Haas, S.; Tatchev, D.; Kranold, R.; Müller, M.; Goerigk, G.</i>  <b>Nano-structure and chemical composition of a silver-free photochromic glass analysed by ASAXS</b>  HASLAB user's meeting 2008, Hamburg, Germany, 1/25/2008 - 1/25/2008</p>	
<p><i>Jericha, E.; Badurek, G.; Hilger, A.; Kardjilov, N.; Manke, I.; Strobl, M.</i>  <b>First experimental test of tensorial neutron tomography</b>  Deutsche Neutronenstreutagung, Garching, Germany, 9/15/2008 - 9/17/2008</p>	
<p><i>Jung, D.; Paradiso, M.; Wallacher, D.; Brandt, A.; Hartmann, M.</i>  <b>Cross-linked Enzyme Aggregates in Mesoporous Materials</b>  2nd EUCHEMS Chemistry Congress, Turin, Italy, 9/16/2008 - 9/20/2008</p>	V4
<p><i>Kamel, S.; Wimpory, R.C.; O'Dowd, N.; Nikbin, K.</i>  <b>Constraint effects on fracture under compressive and tensile residual stresses in fracture mechanics specimens</b>  Deutsche Neutronenstreutagung 2008, TUM, Garching, Germany, 9/15/2008 - 9/17/2008</p>	
<p><i>Keiderling, U.; Wiedenmann, A.; Rupp, A.; Klenke, J.; Heil, W.; Jullien, D.; Petoukhov, A.K.; Lelievre-Berna, E.; Andersen, K.H.</i>  <b>Magic box and fast decaying cell - two methods of SANS polarization analysis with <sup>3</sup>He at the V4 SANS instrument of Helmholtz Center Berlin</b>  Deutsche Neutronenstreutagung, Munich, Germany, 9/15/2008 - 9/17/2008</p>	
<p><i>Kiefer, K.; Klemke, B.</i>  <b>In-situ Sample Orientation for Neutron Scattering at Dilution Temperatures</b>  Deutsche Neutronenstreutagung 2008, Munich, Germany, 9/14/2008 - 9/17/2008</p>	

<p><i>Kreuzer, M.; Kaltofen, T.; Steitz, R.; Dahint, R.;</i>  <b>Lubrication in model joints - a study on shear dependence</b>  Deutsche Neutronenstreutagung 2008, TU München, Germany. 9/14/2008 - 9/17/2008</p>	
<p><i>Krist Th.; Pappas C.; Teichert A.; Fehr C.; Clemens D.; Steichele E.; Mezei F.</i>  <b>New Polarizing Guide for Neutron Wavelengths above 2.5 Å</b>  Polarized Neutrons in Condensed Matter Investigations, Tokai, Japan, 9/1/2008 - 9/5/2008</p>	
<p><i>Lake, B.</i>  <b>Structural and Magnetic properties of Ca-Cu<sub>2</sub>O<sub>3</sub></b>  XXI Congress and Assembly of the International Union of Crystallography. Organised by IUCr2008, Osaka, Japan, 8/23/2008 - 8/31/2008</p>	
<p><i>Lake, B.</i>  <b>Inelastic Neutron Scattering Studies of Mn<sup>3+</sup>-Based Single Molecular Magnets Poster</b>  50 Years of Neutrons in Berlin, HZ Berlin, Germany, 7/14/2008 - 7/15/2008</p>	
<p><i>Matsushima, U.; Kardjиков, N.; Hilger, A.; Herppch, W. B.</i>  <b>In-situ Visualization of Water Flow in Seedling Using Neutron Radiography</b>  The First Symposium on Horticulture in Europe "SHE 2008", Vienna, Austria, 2/17/2008 - 2/20/2008</p>	V7
<p><i>Mukherji, D.; Strunz, P.; Gilles, R.; Roesler, J.</i>  <b>Microstructural Stability of Co-Re alloys at 1000°C measured by in-situ SANS</b>  Deutsche Neutronenstreutagung 2008, Garching, Germany, 9/15/2008 - 9/17/2008</p>	V4 NMI3: 1271
<p><i>Nowicki, W</i>  <b>Complementarity of neutron and X-ray diffraction techniques for the structure solution in quaternary Li-Mn-Fe oxides</b>  50<sup>th</sup> Polish Crystallographic Meeting, Wroclaw, Poland, 6/26/2008 - 6/28/2008</p>	E9 NMI3: 1304 NMI3: 1257 NMI3: 1218
<p><i>Nowicki, W.; Darul, J.; Yokaichiya, F.</i>  <b>Synthesis, structure and magnetic properties of Fe-doped tetragonal Li<sub>0.95</sub>Mn<sub>2.05</sub>O<sub>4</sub></b>  11th European Powder Diffraction Conference, Warsaw, Poland, 9/19/2008 - 9/22/2008</p>	E9 NMI3: 1304 NMI3: 1345
<p><i>Rossner, H.H.; Schmitz, D.; Weschke, E.</i>  <b>Bayes-Turchin analysis of L-edge EXAFS in Cr monolayers</b>  BESSY user meeting, Wilhelm-Conrad-Röntgen-Campus, Berlin-Adlershof, Germany, 12/4/2008 - 12/5/2008</p>	
<p><i>Russell, R.A.; Yun S.I.; Holden, P.J.; Foster, L.J.R.</i>  <b>Chain conformation of biopolymers in solution.</b>  International Symposium on Biological Polyesters, Auckland, New Zealand, 11/23/2008 - 11/26/2008</p>	V4
<p><i>Schierle, E.; Schmitz, D.; Springholz, G.; Weschke, E.</i>  <b>Magnetic phase transitions at interfaces studied by resonant magnetic soft x-ray scattering.</b>  DPG Frühjahrstagung des Arbeitskreises Festkörperphysik, Berlin, Germany, 2/25/2008 - 2/29/2008</p>	
<p><i>Schierle, E.; Soltwisch V.; Schmitz, D.; Feyerherm, R.; Argyriou, D.; Weschke, E.</i>  <b>Resonant soft x-ray scattering from DyMnO<sub>3</sub></b>  DPG Frühjahrstagung des Arbeitskreises Festkörperphysik, Berlin, Germany 2/25/2008 - 2/29/2008</p>	

<p><i>Seregin, M.S.; Naberezhnov, A.A.; Dyadkina, E.A.; Hoffman, J.-U.; Filimonov, A.V.</i></p> <p><b>Temperature evolution of structure of multiferroic solid solution (1-x)PbFe<sub>2/3</sub>W<sub>1/3</sub>- (x)PbTiO<sub>3</sub></b></p> <p>XX Workshop on Applications of Neutron Scattering in Study of Condensed Matter, Gatchina, Russia, 10/13/2008 - 10/19/2008</p>	E2, E9
<p><i>Soltwisch, V.; Schierle, E.; Weschke, E.; Geck, J.; Hawthorn, D.; Wadati, H.; Wu, H.-H.; Dürr, H.A.; Wizen, N.; Büchner, B.; Ribeiro, P.; Sawatzky, G.A.; Fink, J.</i></p> <p><b>Doping dependence of charge order in La<sub>1.8-x</sub>Eu<sub>0.2</sub>Sr<sub>x</sub>CuO<sub>4</sub> studied by resonant soft X-Ray diffraction</b></p> <p>BESSY User Meeting, Berlin, Germany, 12/4/2008 - 12/5/2008</p>	
<p><i>Steitz, R.; Papaefthimiou, V.; Günther, J.-U.; Helm, C. A.; Findenegg, G. H.</i></p> <p><b>Reversible activation of a polyelectrolyte brush: Responsive monolayers</b></p> <p>Deutsche Neutronenstreutagung 2008, TU München, Germany, 9/14/2008 - 9/17/2008</p>	
<p><i>Teichert, A.; Krist, T.; Steitz, R.</i></p> <p><b>Diffuse scattering from polarizing supermirrors</b></p> <p>Deutsche Neutronenstreutagung 2008, TU München, Germany, 9/14/2008 - 9/17/2008</p>	
<p><i>Teichert, A.; Steitz, R.; Fleischmann, C.; Temst, K.;</i></p> <p><b>PNR reflectometry on Fe/CoO films</b></p> <p>Deutsche Neutronenstreutagung 2008, TU München, Germany, 9/14/2008 - 9/17/2008</p>	
<p><i>Tolinski, T.; Kowalczyk, A.; Kaczorowski, D.; Tran, V.H.; Hoser, A.; Stüßer N.</i></p> <p><b>Magnetic, thermodynamic and transport measurements on CeCoAl<sub>4</sub> and CeNiAl<sub>4</sub></b></p> <p>38èmes Journées des Actinides, Wroclaw, Poland, 4/12/2008 - 4/15/2008</p>	E6 NMI3 : 1305
<p><i>Wimpory, R.C.; Poeste, T.; Boin, M.; Flemming, S.; Schneider, R.</i></p> <p><b>E3: Versatile Strain Scanning and Stress Determination</b></p> <p>50 Years of Neutron Science in Berlin, Berlin, 7/14/2008 - 7/15/2008</p>	
<p><i>Wimpory, R.C.; Poeste, T.; Boin, M.; Flemming, S.; Denks I.; Genzel, C.; Schneider R.</i></p> <p><b>Bridging the gap between synchrotrons and neutrons in non destructive testing at the surface</b></p> <p>Deutsche Neutronenstreutagung 2008, TUM Garching, Germany, 9/15/2008 - 9/17/2008</p>	
<p><i>Zaslansky, P.; Kardjilov N.; Fratzl, P.</i></p> <p><b>The water distribution in teeth: clues for a mechanical role?</b></p> <p>Gordon conference on Biomineralization, Colby-Sawyer College, New London, NH, USA, 7/18/2008 -</p>	V7

# **AUTHOR INDEX**



# AUTHOR INDEX

Author	Page	Author	Page	Author	Page
<b>A</b>					
Abbas, S.	199	Celli, M.	133	Favvas, E. P.	212
Abdoul-Redah, T.	121	Charalambopoulou, G.	206	Felderhoff, M.	204
Aldridge, L.	215	Charlet, L.	143	Fennell, T.	113
Aliouane, N.	46, 115, 123	Chen, J.	187	Fernandez-Baca, J.	85
Altendorfer, W.	234	Cheng, Z. X.	71	Ferrari, E.	140
Amitesh, P.	4	Chiappisi, L.	254	Fertitta, E.	254
Anderson, K.	13	Chiapponi, C.	169	Fery, A.	194
Aoun, B.	186	Chmielus, M.	225, 226, 245	Fiebig, M.	42
Argyriou, D.	46, 115, 132, 148	Choi, H. C.	104	Fiedler, G.	231, 234
Arulraj, A.	62, 67, 70	Clemens, D.	176	Findenegg, G. H.	174
Aynajian, P.	93	Climent-Pascual, E.	128	Finelli, I.	169
<b>B</b>					
Badurek, G.	9	Coldea, R.	38	Fiori, F.	235, 242
Baran, S.	62, 67, 68	Corr, C.	171	Forgan, E. M.	80
Barbieri, S.	176	Cuello, C. J.	143	Fort, D.	136
Barth, A.	178	Czeslik, C.	158, 196	Frei, G.	260
Bauduin, P.	180	Czub, J.	69, 99	Friederichs, O.	205, 207
Bauer, C.	180	<b>D</b>			
Behr, G.	80	Dahint, R.	197	Friedrich, J.	119
Behrens, M.	120, 126, 127	Danilkin, S.	134	Frontzek, M.	43
Bellissent-Funel, M. C.	159	Dante, S.	149, 152, 154, 213	Fuertes-Marrón, D.	118
Benfante, V.	251, 253	Dawson, M.	5, 7, 8, 10, 12, 13, 224	Fujioka, J.	53, 54, 55, 56, 57
Bentley, P.	137	De Francesco, A.	157	Furche, A.	120
Berti, D.	152	Demeter, J.	103, 105, 106	Furukawa, H.	79
Beul, N.	23, 24	Denks, I.	15	<b>G</b>	
Bilge, S.	210, 218, 219	Deriu, A.	169, 176	Garab, G.	153
Blake, G.	48	Doodoo, S.	189, 195	Garvey, C.	165
Bleif, H. J.	28, 117	Dönch, I.	194	Gavrilovs, V.	259
Boguslawski, S.	163	Dou, S.	64	Geibel, C.	100
Boin, M.	11, 239	Dreismann, C. A. C.	121	Genzel, C.	15
Boldyreva, E. V.	147, 156	Dyadkin, V.	81, 82	Gerelli, Y.	176
Böni, P.	80	Dyrnjaja, E.	222, 228	Gerischer, S.	38, 47, 89, 92
Bordallo, H. N.	147, 148, 156, 215	<b>E</b>			
Bordenave, F.	13	Ebrahimi, O.	6, 21, 22, 23, 24, 25, 29, 30	Gerling, U.	227
Bradshaw, J.	151	Eckert, J.	136	Gerth, S.	193
Brand, R.	137, 138	Efimov, V.	35	Giambona, G.	253
Brandt, A.	131, 173, 179, 213, 216	Eibl, S.	184, 185	Gibson, C.	37, 88
Bressel, K.	167, 177	Eisenhardt, S.	90	Girgsdies, F.	127
Buchsteiner, A.	63, 147, 204	U. H.		Glavatskyy, I.	45
Buchter, F.	205	Ende, M.	203	Goff, J.	100, 101
<b>C</b>					
Calbucci, V.	235, 242, 243	Engelbrecht, T.	150	Goldman, A.	132
Campbell, S. J.	70, 129, 139	Epp, J.	230, 240	Golosovskiy, I.	39
Carnerup, A.	166	Erko, M.	168	Gondek, Ł.	40, 69, 97, 99
		Ermakova, E.	154	Gonzalez, M. A.	170, 186
		Evers, F.	196	Gopinadhan, M.	191
				Gradzielski, M.	167, 177, 178, 181, 182, 183
				Graf, W.	161
				Grigoriev, S.	81
				Grohol, D.	33
				Gruenzweig, C.	6
				Gubbens, P. C. M.	98

# AUTHOR INDEX

Author	Page	Author	Page	Author	Page
Gubkin, A.	60				
Guidi, T.	96				
Gutfreund, P.	193				
<b>H</b>					
Habicht, K.	3, 87, 89, 90, 93, 95, 100, 101				
Harrison, A.	76				
Hartmann, M.	131				
Hartnig, C.	223				
Hauß, T.	149, 150, 151, 152, 153, 154, 155, 166, 168, 214				
Heldt, G.	26				
Helm, C. A.	191				
Hernández-Velasco, J.	128, 206				
Herppich, W. B.	161				
Hilger, A.	5, 6, 7, 8, 9, 10, 12, 13, 14, 18, 19, 20, 27, 164, 221, 223, 224, 225, 226, 227, 252, 260				
Hill, A.	76				
Hirsch, T.	230, 240				
Hoffmann, J. E.	26, 107				
Hoffmann, J. U.	37, 38, 39, 40, 41, 42, 43, 44, 45, 111, 203				
Hofmann, M.	70, 232				
Hondo, S.	91				
Hoser, A.	43, 61, 66, 68, 95, 112, 113, 128, 140, 141, 203				
<b>I</b>					
Ianeselli, L.	175				
Inamdar, M.	49				
Islam, N.	77, 94, 102, 116, 117				
Ivanova, O.	191				
Izaola, Z.	97, 99, 134, 170, 171				
<b>J</b>					
Jain, A.	72				
Jalarvo, N.	123, 135				
Jericha, E.	9				
Jeworrek, C.	158, 160				
Jonke, J.	234				
Josic, L.	224, 260				
Julian, D.	13				
Jung, D.	131				
<b>K</b>					
Kacerowski, J.	223				
Kaczorowski, D.	59				
Kalceff, W.	147				
Kamarad, J.	46, 51				
Kamel, S.	238				
Kaminski, H.	231				
Kandemir, T.	27, 227				
Kaneko, K.	89, 91, 112				
Karakas, N.	29, 30				
Kardjilov, N.	5, 6, 7, 8, 9, 10, 11, 12, 13, 14, 19, 20, 27, 161, 162, 163, 164, 220, 221, 222, 223, 224, 227, 252, 260				
Karg, M.	179				
Karimova, O.	142				
Karpinsky, D.	125				
Kaskel, S.	122				
Katsaros, F. K.	212				
Kawamura, S.	79				
Ke, L.	151				
Kearley, D.	129, 139				
Kearley, G.	171				
Keiderling, U.	17, 78, 217				
Keimer, B.	53, 54, 55, 56, 57				
Keller, T.	93				
Kemke, B.	38				
Kemner, E.	98, 100, 133, 156				
Kiefer, K.	38, 44, 47, 68, 87, 89				
Kim, J. W.	207				
Kim, K. Y.	104				
Kim, T. J.	220				
Kimber, S.	75, 121, 132				
Kiselev, M. A.	154				
Kißner, S.	126				
Kloess, G.	203				
Klösgen, B.	166				
Köbler, U.	95				
Kofu, M.	92				
Köhler, R.	187, 188, 194, 196				
Köhn, R.	211				
Kolasinska, M.	188				
Kolen'ko, Y.	127				
König, A.	203				
Kopcewicz, M.	125				
Kolesov, B.	156				
Krastev, R.	187, 188, 194				
Kreuzer, M.	197				
Krist, T.	26, 107				
Krüger, P.	223				
Kuchel, P.	165				
Kühl, S.	120, 126				
Kuhn, R.	223				
<b>L</b>					
Lake, B.	77, 79, 92, 94, 96, 100, 102, 116, 117				
Larsen, J.	90				
Laschewsky, A.	194				
Laurenze-Landsberg, C.	255				
Laver, M.	80				
Lawrence, S.	44				
Lazzara, G.	181, 182				
Le, M. D.	84				
Lee, J. S.	104				
Lee, S. H.	92				
Lee, Y. S.	33				
Lefmann, K.	90				
Lehmann, E.	260				
Lehmann, S.	118, 119, 224				
Leon, M.	119				
Lerch, M.	121				
Li, Q.	130				
Ling, C.	134				
Lopez-Ortega, A.	73				
Lorenz, W.	34, 74				
Lugo, D.	174				
<b>M</b>					
Macquart, R.	134				
Malyuk, A.	115				
Manescu, A.	236, 242, 243				
Manke, I.	5, 6, 7, 8, 9, 10, 12, 13, 14, 19, 20, 27, 221, 223, 227				
Marinoni, N.	140				
Marshall, R.	214				
Martin, R.	175				
Mascotto, S.	173, 190				
Masuda, T.	91				
Matan, K.	33				
Matsuda, Y.	79				
Matsushima, U.	161				
McEwen, K. A.	84				
Meier, D.	42				
Merino, J. M.	119				

# AUTHOR INDEX

Author	Page	Author	Page	Author	Page
Mihalik, M.	51, 65	Peterson, V.	171	Rule, K.	84, 85, 87, 88, 91, 92
Milani, S.	152	Petrov, S.	221	Russell, R.	172
Milano, J.	183	Pfleiderer, C.	80	Russina, M.	97, 98, 99, 102, 133, 134, 157, 170
Milioto, S.	181, 182	Pieper, J.	149	Russo, D.	157
Mitsuda, S.	47, 50	Pieper, O.	96	Ryukhtin, V.	210, 218, 219
Miyasaka, S.	53, 54, 55, 56, 57	Pirogov, A.	60		
Monka, R.	21, 22, 198, 199	Piyadov, V.	82	<b>S</b>	
Morris, J.	58	Plazanet, M.	184	Sa'adedin, F.	151
Moskvin, E.	81, 82, 138, 184, 185	Podlesnyak, A.	50	Saboungi, M. L.	170, 186
Mufti, N.	48	Poeste, T.	230, 239, 240, 245	Saensunon, B.	98
Mühlbauer, S.	78, 80	Pommerin, A.	204	Sainctavit, P.	35
Mukherji, D.	217	Prass, J.	213	Salazar-Alvarez, G.	73
Mulders, A.	44	Prévost, S.	17, 167, 174, 175, 177, 178, 179, 181, 182, 183, 219	Sampathkumaran, E. V.	72
Müllner, P.	225, 245	Price, D.	170	Sapalidis, A. A.	212
<b>N</b>		Prokes, K.	36, 46, 47, 49, 50, 51, 52, 83, 114, 132	Šaroun, J.	217
Naberezhnov, A.	111, 208	Prokhnenko, O.	40, 46, 74, 210	Schedler, R.	34
Nagy, G.	153	<b>Q</b>		Scherb, C.	211
Nakajima, T.	47, 50	Quintero Castro, D. L.	94, 102	Schloesser, J.	221
Nath, R.	100	<b>R</b>		Schlüter, O.	163
Naumann, R.	126, 127	Raitman, E.	259	Schmidt, C.	255
Neubert, R.	150	Randau, C.	239	Schmidt, W.	204
Neumann, C.	252	Ranieri, R.	155	Schneider, R.	225, 226, 230, 239, 240, 245
Nigam, R.	64	Rayaprol, S.	72	Schöbel, M.	231, 234
Nikbin, K.	238	Reehuis, M.	53, 54, 55, 56, 57, 58, 59, 77, 90, 114, 115, 116, 117, 142,	Schomäcker, R.	183
Nogues, J.	73	Reichenauer, G.	216	Schorr, S.	119, 141, 203
Norby, T.	123	Reichardt, N. V.	166	Schrauwen, A.	105
Nowicki, W.	124	Reihle, M.	233	Schreiber, F.	175
<b>O</b>		Relini, A.	155	Schröder, A.	221
O'Dowd, N.	244	Remhof, A.	205, 207	Schröder- Schmeibidl, B.	255
Ochrombel, R.	210, 218, 219	Renger, G.	149	Schroeter, A.	150
Orendáč, M.	63	Repper, J.	232	Schulze Grachtrup, D.	36
Orendáčová, A.	63	Requena, G.	231	Sciacca, I.	251
<b>P</b>		Resiakievicz-Pasek, E.	208	Sechovský, V.	51
Pan, A.	64	Riesen, H.	129, 139	Seidel, S. O.	18, 21, 22, 23, 24, 25, 29, 30, 198, 199
Pappas, C.	18, 137, 138, 139, 184, 185, 186	Riyadi, S.	48	Sheverev, S.	237, 247
Paradiso, M.	131	Robinson, J. S.	241	Shibauchi, T.	79
Paradossi, G.	169	Rolfs, K.	225, 226, 245, 246	Shishido, H.	79
Paris, O.	168, 213	Rudorf, E.	24	Siemensmeyer, K.	63
Pascut, G. L.	38	Ruffo, I.	251, 253, 254	Sikolenko, V.	33, 35
Paul-Boncour, V.	61, 66			Sim, C. M.	220
Paulke, A.	225, 226			Skoulatos, M.	58, 87, 89, 100, 101
Pavese, A.	140			Smarsly, B.	173, 190
Penc, B.	62, 67, 68			Sobolev, O.	143
Penumadu, D.	20			Soitwedel, O.	191
Pérez-Hernández, N.	136				

# AUTHOR INDEX

Author	Page	Author	Page
Sort, J.	73	Vestergaard	75
Stein, W. D.	34, 43, 74	Jensen, N.	
Steitz, R.	4, 103, 104, 105, 106, 107, 189, 190, 191, 193, 195, 196, 197	Vogtt, K.	158, 159, 160
<b>T</b>			
Steriotis, T. A.	206, 212		
Steward, G. A.	98		
Stockert, O.	41, 89		
Strobl, M.	5, 6, 8, 9, 13, 14, 18, 19, 20, 23, 24, 27, 28, 165, 198, 228, 229		
Strunz, P.	217		
Stüßer, N.	36, 61, 64, 65, 66, 69, 70, 72, 259		
Süllow, S.	36, 37, 88		
Sumin, V.	237, 247		
Szlawaska, M.	59		
Tamaki, M.	224, 260		
Tatlisu, H.	229		
Teichert, A.	103, 104, 105, 106, 107, 192		
Temst, K.	103, 106		
Tierman, P.	244		
Tokura, Y.	53, 54, 55, 56, 57		
Tolan, M.	196		
Tovar, M.	73, 76, 118, 119, 120, 121, 122, 126, 127, 129, 130, 209		
Treimer, W.	21, 22, 23, 24, 25, 29, 30, 199		
Triolo, R.	251, 253, 254		
Trunschke, A.	127		
Tsapatsaris, N.	136		
Tung, L. D.	101		
<b>U</b>			
Ulivi, L.	133		
Ulrich, C.	53, 54, 55, 56, 57		
<b>V</b>			
v. Klitzing, R.	189, 195		
Vakhrushev, S.	39		
van Bael, M. J.	106		
van Heijkamp, L. F.	198		
van Slageren, J.	96		
Venter, A.	16		
<b>W</b>			
Wagh, A. G.	199		
Wallacher, D.	8, 120, 122, 123, 126, 131, 135, 168, 173, 179, 190, 204, 205, 206, 207, 211, 213, 214, 216, 218		
Walter, P.	165, 198, 229		
Wang, J. L.	70, 71		
Wang, X. L.	71		
Wark, M.	214		
Wasmuth, U.	233		
Webster, J.	192		
Weidenthaler, C.	204		
Wellert, P.	18		
Wellert, S.	139, 185, 186		
Weß, M.	149		
Wheeler, E.	77, 94, 102, 116, 117		
Wiedenmann, A.	78, 80, 210, 218, 219		
Wiener, M.	216		
Wimporly, R.	15, 16, 232, 233, 235, 236, 237, 238, 239, 240, 241, 242, 243, 244, 245, 246, 247, 248		
Winter, R.	158		
Wippermann, K.	221		
Wolff, M.	193		
Wu, B.	130		
<b>Y</b>			
Yamano, M.	47		
Ye, F.	85		
Yokaichiya, F.	73, 121, 124, 129, 130, 211		
You, C. Y.	104		
Yun, I. S.	172		
Yusuf, S. M.	72		
<b>Z</b>			
Zarbakhsh, A.	192		
Zaslansky, P.	162, 164		
Zawisky, M.	222, 228		
Zhang, F.	175		